

AD-A283 719



DOT/FAA/RD-93/31,I

Research and Development
Service
Washington, DC 20591

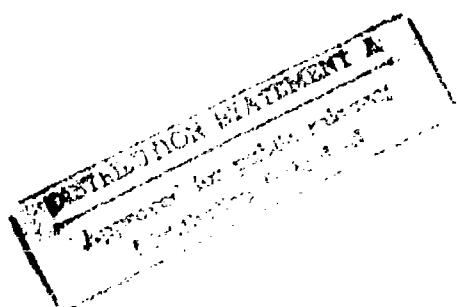
**Rotorwash Analysis
Handbook**

**Volume I - Development
and Analysis**

Samuel W. Ferguson
EMA
800 Muirfield Drive
Mansfield, TX 76063

June 1994

Final Report



This document is available to the
public through the National
Technical Information Service,
Springfield, VA 22161

94-26706



US Department of Transportation
Federal Aviation Administration

94 8 22 094

NOTICE

This document is disseminated under the sponsorship of the U.S. Department of Transportation in the interest of information exchange. The United States Government assumes no liability for the contents or use thereof.



U.S. Department
of Transportation

Federal Aviation
Administration

800 Independence Ave. S.W.
Washington, D.C. 20591

JUN 12 1994

Dear Colleague:

Enclosed is a copy of the two volume report **FAA/RD-93/31, Rotorwash Analysis Handbook**. The Federal Aviation Administration (FAA) is publishing this document and the associated computer software in order to provide a tool for analyzing rotorwash and preventing rotorwash-induced accidents and incidents.

The majority of civil helicopters are light in weight and it is rare for them to cause a rotorwash-related mishap. As civil rotorcraft increase in weight, however, they are capable of generating greater rotorwash. Anticipating the introduction of large helicopters (such as the EH-101 and the Sikorsky S-92) and the tiltrotor, the FAA has been studying how to prevent rotorwash-related mishaps.

Rotorwash is a complex phenomenon and there is much about it that is not yet fully understood. This document provides a summary of virtually all work done on this issue by various U.S. government agencies. It also documents a computer program developed using all the available flight data. This model was used in the design of the Dallas Vertiport. We recommend its use in the design of other facilities.

Providing an adequate safety margin through facility design will mitigate the need to achieve that safety margin by operational restrictions. Thus, the use of this computer model should lead to the development of safer, more efficient rotorcraft landing facilities.

Richard A. Weiss
Manager, Vertical Flight Program Office

Enclosure

Accession For	
MSIS	Serial <input checked="" type="checkbox"/>
Disc 5.25	<input type="checkbox"/>
Unknown	<input type="checkbox"/>
Job Application	<input type="checkbox"/>
Date	
Comments	
Filing Location	
File Number	
A-1	

Technical Report Documentation Page

1. Report No. DOT/FAA/RD-93-31, I	2. Government Accession No.	3. Recipient's Catalog No.						

TABLE OF CONTENTS - VOLUME I

	Page
1.0 Introduction	1
1.1 ROTWASH Software	3
2.0 Development of Rotorcraft Downwash Flow Field Models	5
2.1 The Wall Jet	6
2.1.1 Full-Scale Rotorcraft Wall Jet Characteristics	10
2.1.2 Wall Jet Profile Similarity	20
2.1.3 Determination of Fundamental Scaling Parameters	23
2.1.4 Scaling Parameter Modifications for Rotorcraft Application	27
2.1.5 Extrapolation into the Transition Region	28
2.1.6 Extension of Theory to the Twin Rotor Interaction Plane	31
2.1.7 Addition of a Boundary Layer to the Interaction Plane	36
2.1.8 Nonsteady Flow and Peak Velocity Effects	36
2.1.9 The Effect of Wind on the Wall Jet Velocity Profile	39
2.1.10 Oblique Impingement of Rotorwash with the Ground Plane	42
2.2 The Ground Vortex	49
2.3 The Forward Flight Wake	57
2.4 Concluding Remarks	61
3.0 Validation of Rotorcraft Downwash Flow Field Models	63
3.1 CH-53E Helicopter Velocity Profile Correlation	66
3.2 XV-15 Tiltrotor Velocity Profile Correlation	90
3.3 MV-22 Tiltrotor Velocity Profile Correlation	107
3.4 CL-84 Tiltrotor Velocity Profile Correlation	115
3.5 SH-60B Helicopter Velocity Profile Correlation	127
3.6 Correlation of the Ambient Wind, Ground Vortex, and Forward Flight Models	127
4.0 Development of a Mishap Analysis Methodology	141
4.1 Managing the Mishap Analysis Effort	141
4.2 Identification of Mishaps for Analysis	142
4.3 Mathematical Modeling of Mishaps	146
4.4 Evaluation of Mishap Analysis Results	147
5.0 Analysis of Rotorwash Related Hazards	149
5.1 Rotorwash Overturning Force and Moment Effects on Personnel	150
5.1.1 Background and Literature References	150
5.1.2 Mathematical Modeling of Personnel	153
5.1.3 Quantitative Validation with Experimental Data	157
5.1.4 Qualitative Evaluation of Experimental Data	165
5.1.5 Overturning Force and Moment Limits for Civilian Operations	174

	<u>Page</u>
5.1.6 Evaluation of Various Types of Rotorcraft Configurations	176
5.1.7 Potential Overturning Force and Moment Hazards Due to Rotor Generated Trailing Vortices	177
5.1.8 Summary of Personnel-Related Overturning Force and Moment Hazards	179
5.2 Rotorwash Effects on Other Nearby Rotorcraft	180
5.2.1 Review of Mishap Data	181
5.2.2 Analysis Methodology	182
5.2.3 Analysis Procedure	183
5.2.4 Analysis of Door and Cowling Related Mishaps .	187
5.2.5 Analysis of Rotor Blade/Tailboom Strike Mishaps	198
5.2.6 Evaluation of Rotorwash Hazards to Other Hovering or Taxiing Rotorcraft	201
5.2.7 Conclusions from Analysis of Door/Cowling and Rotor Blade/Tailboom Strike-Related Mishaps .	202
5.3 Rotorwash Effects on Fixed-Wing Aircraft	204
5.3.1 Mishaps Involving Fixed-Wing Aircraft with Engines Running	204
5.3.2 Mishaps Involving Fixed-Wing Aircraft with Engines Turned Off	207
5.3.3 Analytical Model for Overturning Fixed-Wing Aircraft	208
5.3.4 Conclusions from the Analysis of Fixed-Wing Overturning Related Mishaps	214
5.4 Trailing Wake Vortex Effects on Fixed-Wing Aircraft and Rotorcraft	214
5.5 Rotorwash Effects on Structures	222
5.5.1 Literature Review of Peak Velocity Profile Effects on Structures	222
5.5.2 Damage to Light Structures	233
5.5.3 Summary of Analysis Results	234
5.6 Rotorwash Effects on Ground Vehicles	235
5.6.1 Mishaps Involving Camper Shells and Automobile Sunscreens	235
5.6.2 Mishaps Involving Motorcycles	236
5.6.3 Conclusions from an Analysis of Mishaps Involving Ground Vehicles	240
5.7 Rotorwash Hazards Involving Entrained Objects and Debris	241
5.7.1 Historical Data	241
5.7.2 Energy Based Analysis Methodology	242
5.7.3 Available Test Data	248
5.7.4 Evaluation of Example Configurations Using Energy Methodology	249
5.7.5 Mishaps Involving Oil Drums	253
5.7.5.1 Analytical Model of Mishaps Involving Oil Drums	254
5.7.5.2 Analysis of Mishaps Involving Oil Drums	255
5.7.5.3 Conclusions for Mishaps Involving Oil Drums	257

	<u>Page</u>
5.7.6 Conclusions	258
5.8 Rotorwash-Generated Particulate Clouds	258
5.8.1 Mathematical Modeling of Particulate Clouds	259
5.8.2 Validation of the Particulate Cloud Model	264
5.8.3 Safety Concerns Associated with Particulate Clouds	270
5.8.4 Conclusions from an Analysis of Particulate Clouds	273
6.0 Rotorwash Analysis Examples - Scenario Definition	275
6.1 Definition of the Vertiport	275
6.2 Definition of the Design Classes of Rotorcraft	277
7.0 Rotorwash Analysis Examples - "How To" Applications	281
7.1 Velocity/Dynamic Pressure Profile Curves	281
7.2 Personnel Overturning Forces and Moments	294
7.3 Loadings on Ground Structures	305
7.4 Potential Effects on Parked Rotorcraft	306
7.5 Overturning Moments on Light Fixed-Wing Aircraft	310
7.6 Entrained Objects and Debris	310
7.7 Particulate Clouds	311
7.8 Ground Vortex Strength	312
7.9 Wake Vortex Strength	314
8.0 Conclusions and Recommendations	317
List of References	319
List of Acronyms	327

TABLE OF CONTENTS - VOLUME II

Appendix A Rotorcraft Design Data in ROTWASH Format	A-1
Appendix B Sikorsky CH-53E Helicopter and Rotorwash Data	B-1
Appendix C A Collection of References Providing Information or Further Insight into the Rotorwash Hazard Analysis Problem	C-1
Appendix D ROTWASH User's Guide	D-1
Appendix E ROTWASH Program Fortran 77 Listings	E-1

LIST OF FIGURES

	<u>Page</u>
Figure 1 Rotorwash Flow Fields of Single- and Twin-Rotor Configurations Operating in Close Proximity to the Ground	7
Figure 2 Cross Section of a Rotorwash Flow Field Impinging on the Ground	8
Figure 3 XV-15 Rotorwash Flow Field Streamline Characteristics in the Vertical Plane Along the 270-Degree Azimuth at a 12-Foot Wheel Height	11
Figure 4 XV-15 Rotorwash Flow Field Streamline Characteristics in the Vertical Plane Along the 0-Degree Azimuth at a 12-Foot Wheel Height	12
Figure 5 Time Series Strip Charts of XV-15 Downwash Wind Velocity Magnitudes	13
Figure 6 Power Spectral Density of the Bell XV-15 Time Series Presented in Figure 5	14
Figure 7 CH-53E Rotorwash Flow Field Streamline Characteristics in the Vertical Plane Along the 270-Degree Azimuth at a 20-Foot Wheel Height	15
Figure 8 Time Series Strip Charts of CH-53E Rotorwash Wind Velocity Magnitudes	16
Figure 9 Power Spectral Density of the CH-53E Time Series Presented in Figure 8	17
Figure 10 CH-53E Mean and Peak Velocity Profiles at a DFRC of 69 Feet and a Rotor Height of 37 Feet	18
Figure 11 XV-15 Mean and Peak Velocity Profiles at a DAIP of 34.8 Feet and a Rotor Height of 37.5 Feet	19
Figure 12 Non-dimensional Wall Jet Vertical Velocity Profile .	22
Figure 13 Measurements of Dynamic Pressure Decay with Equivalent Distance from the Jet Source	26
Figure 14 Measured Velocities Below a Hovering Rotor in Ground Effect	29
Figure 15 Conceptual Representation of the Flow Field Along the Interaction Plane	32
Figure 16 Comparison of Theoretical Flow Direction in the Interaction Plane with Test Data	33
Figure 17 Geometry Definition for Modeling of the Interaction Plane Flow Field	34
Figure 18 Correction Factor for Determining Velocities Within the Interaction Plane Velocity Profile	35
Figure 19 Empirically Derived Equations used in the Calculation of the Single-Rotor and Interaction Plane Peak Velocity Profiles	39
Figure 20 CH-53E Rotorwash Velocities as a Function of Rotor Height Above Ground and Gross Weight for Ambient Winds of up to 9 Knots	41
Figure 21 Rotorwash Flow Field Characteristics for a Rotor Tip Path Plane Parallel to the Ground	44

	<u>Page</u>
Figure 22 Rotorwash Flow Field Characteristics for a Rotor Tip Path Plane that is Tilted Forward with Respect to a Plane Parallel to the Ground	45
Figure 23 Three-View Drawing of the Bell UH-1H	47
Figure 24 UH-1H Rotorwash Characteristics at Radial Distances of 50, 100, and 150 Feet for Tip Path Plane Angles of 0 and 20 Degrees	48
Figure 25 Ground Vortex Structural Characteristics	50
Figure 26 Fairings for Ground Vortex Positional Constants	53
Figure 27 Boundaries for Recirculation and Ground Vortex Flow Regimes	53
Figure 28 Calculated Ground Vortex Circulation Strength	54
Figure 29 Horseshoe Vortex Geometry for Calculation of Ground Vortex Hazard Potential	56
Figure 30 Horseshoe Vortex Geometry for Calculation of Forward Flight Wake Hazard Potential	59
Figure 31 Three-View Drawing of the Sikorsky CH-53E	67
Figure 32 CH-53E Flight Test Data Measurement Locations	69
Figure 33 CH-53E Mean/Peak Velocity Profile Correlation at Eight 270-Degree Radial Stations at an Average Gross Weight of 70,000 Pounds and a Rotor Height of 37 Feet	71
Figure 34 CH-53E Mean/Peak Velocity Profile Correlation at Eight 270-Degree Radial Stations at an Average Gross Weight of 70,000 Pounds and a Rotor Height of 77 Feet	75
Figure 35 CH-53E Mean/Peak Velocity Profile Correlation at Eight 270-Degree Radial Stations at an Average Gross Weight of 70,000 Pounds and a Rotor Height of 117 Feet	79
Figure 36 CH-53E Mean/Peak Velocity Profile Correlation at 59.3 and 118.5 Feet Along the 270-Degree Azimuth at an Average Gross Weight of 56,000 Pounds and a Rotor Height of 37 Feet	84
Figure 37 CH-53E Mean/Peak Velocity Profile Correlation at 59.3 and 118.5 Feet Along the 270-Degree Azimuth at an Average Gross Weight of 56,000 Pounds and a Rotor Height of 77 Feet	85
Figure 38 CH-53E Mean/Peak Velocity Profile Correlation at 59.3 and 118.5 Feet Along the 270-Degree Azimuth at an Average Gross Weight of 56,000 Pounds and a Rotor Height of 117 Feet	86
Figure 39 CH-53E Mean/Peak Velocity Profile Correlation at 59.3 and 118.5 Feet Along the 270-Degree Azimuth at an Average Gross Weight of 45,000 Pounds and a Rotor Height of 37 Feet	87
Figure 40 CH-53E Mean/Peak Velocity Profile Correlation at 59.3 and 118.5 Feet Along the 270-Degree Azimuth at an Average Gross Weight of 45,000 Pounds and a Rotor Height of 77 Feet	88
Figure 41 CH-53E Mean/Peak Velocity Profile Correlation at 59.3 and 118.5 Feet Along the 270-Degree Azimuth at an Average Gross Weight of 45,000 Pounds and a Rotor Height of 117 Feet	89

	<u>Page</u>
Figure 42 Three-View Drawing of the Bell XV-15	91
Figure 43 XV-15 Flight Test Data Measurement Locations	92
Figure 44 XV-15 Mean/Peak Velocity Profile Correlation Along the 270-Degree Azimuth Radial at an Average Gross Weight of 12,475 Pounds and a Rotor Height of 37.5 Feet	93
Figure 45 XV-15 Downwash Flow Field Velocity Vectors in the Vertical Plane at a 25-Foot Wheel Height Along the 270-Degree Azimuth	98
Figure 46 XV-15 Mean/Peak Velocity Profile Correlation Along the 270-Degree Azimuth Radial at Three Rotor Heights for an Average Gross Weight between 12,475 and 12,555 Pounds	99
Figure 47 XV-15 Mean/Peak Velocity Profile Correlation Along the 0-Degree Azimuth Radial at an Average Gross Weight of 12,475 Pounds and a Rotor Height of 37.5 Feet	101
Figure 48 XV-15 Mean/Peak Velocity Profile Correlation Along the 180-Degree Azimuth Radial at an Average Gross Weight of 12,475 Pounds and a Rotor Height of 37.5 Feet	104
Figure 49 XV-15 Mean/Peak Velocity Profile Correlation Along the 0-Degree Azimuth Radial at Three Rotor Heights for an Average Gross Weight between 12,475 and 12,555 Pounds	108
Figure 50 XV-15 Mean/Peak Velocity Profile Correlation Along the 180-Degree Azimuth Radial at Three Rotor Heights for an Average Gross Weight between 12,475 and 12,555 Pounds	110
Figure 51 Three-View Drawing of the Bell-Boeing MV-22	112
Figure 52 MV-22 Mean/Peak Velocity Profile Correlation at 57 Feet Along the 0-Degree Azimuth Radial at Three Rotor Heights for an Average Gross Weight of 40,300 Pounds	113
Figure 53 Three-View Drawing of the Canadair CL-84	116
Figure 54 CL-84 Mean Velocity Profile Correlation Along the 270-Degree Azimuth Radial at an Average Gross Weight of 11,540 Pounds and a Rotor Height of 55.2 Feet	117
Figure 55 CL-84 Mean Velocity Profile Correlation Along the 0- and 180-Degree Azimuth Radials at an Average Gross Weight of 11,540 Pounds and a Rotor Height of 55.2 Feet	120
Figure 56 CL-84 Mean Velocity Profile Correlation Along the 270-Degree Azimuth Radial at an Average Gross Weight of 11,270 Pounds and a Rotor Height of 40.2 Feet	123
Figure 57 CL-84 Mean Velocity Profile Correlation Along the 0- and 180-Degree Azimuth Radials at an Average Gross Weight of 11,270 Pounds and a Rotor Height of 40.2 Feet	125
Figure 58 Three-View Drawing of the SH-60B	128

Figure 59 SH-60B Mean/Peak Velocity Profile Correlation Along the 0-Degree Azimuth Radial at a Wheel Height of 37.3 Feet	129
Figure 60 SH-60B Mean/Peak Velocity Profile Correlation Along the 0-Degree Azimuth Radial at a Wheel Height of 27.3 Feet	130
Figure 61 Correlation of Calculated and Measured UH-1H 5-Meter Wake-Vortex Strength at Age 20 Seconds (Approximate) as a Function of Airspeed	131
Figure 62 Correlation of Calculated and Measured CH-54 5-Meter Wake-Vortex Strength at Age 20 Seconds (Approximate) as a Function of Airspeed	132
Figure 63 Correlation of Calculated and Measured S-76 5-Meter Wake Vortex Strength as a Function of Airspeed	135
Figure 64 Correlation of Calculated and Measured UH-60 5-Meter Wake Vortex Strength as a Function of Airspeed	135
Figure 65 Correlation of Calculated and Measured CH-53E 5-Meter Wake Vortex Strength as a Function of Airspeed	136
Figure 66 UH-1H Wake-Vortex Profile at Age 59 Seconds	137
Figure 67 CH-54 Wake-Vortex Profile at Age 28 Seconds	138
Figure 68 Example of CH-54 Wake-Vortex Strength as a Function of Time	139
Figure 69 Analysis Methodology Flow Chart	143
Figure 70 Capabilities of Test Subjects To Move About With Horizontal Restraint Loads Applied at 3-Feet AGL	154
Figure 71 Graphical Definition of Overturning Force and Moment Calculation Procedure	156
Figure 72 Naval Air Test Center "Standardized" Human Profile for Rotorwash Applications	158
Figure 73 Correlation of CH-53E Horizontal Outwash Forces as a Function of Distance from the Rotor Center During Hover at 45,000 Pounds Gross Weight	160
Figure 74 Correlation of CH-53E Horizontal Outwash Forces as a Function of Distance from the Rotor Center During Hover at 56,000 Pounds Gross Weight	160
Figure 75 Correlation of CH-53E Horizontal Outwash Forces as a Function of Distance from the Rotor Center During Hover at 70,000 Pounds Gross Weight	161
Figure 76 Correlation of CH-53E Horizontal Outwash Forces as a Function of Hover Height at 45,000 Pounds Gross Weight for Two Ambient Wind Conditions	162
Figure 77 Correlation of CH-53E Horizontal Outwash Forces as a Function of Hover Height at 56,000 Pounds Gross Weight for Two Ambient Wind Conditions	162
Figure 78 Correlation of XV-15 Horizontal Outwash Forces at 270 Degrees During Hover for a Rotor Height of 37.5 Feet and a 12,475 Pound Average Gross Weight	163
Figure 79 Correlation of XV-15 Horizontal Outwash Forces at 0 Degrees During Hover for a Rotor Height of 37.5 Feet and a 12,475 Pound Average Gross Weight	163

	<u>Page</u>
Figure 80 Correlation of XV-15 Horizontal Outwash Forces at 180 Degrees During Hover for a Rotor Height of 37.5 Feet and a 12,475 Pound Average Gross Weight	164
Figure 81 Correlation of S-61 (SH-3) Peak Horizontal Outwash Forces During Hover at Rotor Heights of 57 and 77 Feet	166
Figure 82 Correlation of S-61 (SH-3) Peak Horizontal Outwash Moments During Hover at Rotor Heights of 57 and 77 Feet	167
Figure 83 Comparison of CH-53E and RH-53D Horizontal Outwash Forces on Test Subjects as a Function of Distance from the Rotor Center During Hover at a Rotor Height of 37 Feet	169
Figure 84 Qualitative Walk Through Evaluation of the XV-15 Rotorwash Flow Field at Rotor Hover Heights of 37.5 and 62.5 Feet	171
Figure 85 Regions of Overturning Force Generated by the XV-15 on Ground Personnel	172
Figure 86 Summary of Quantitative and Qualitative Data on Limiting Values of Overturning Force and Moment	175
Figure 87 Extrapolation of Experimentally Measured Overturning Force Data to Lighter Weight Classes of Personnel	176
Figure 88 Bell UH-1H Prediction Chart for Door/Access Panel and Rotor Blade/Tailboom Strike Mishaps	185
Figure 89 Rotorwash Velocity Profile Locations Plotted in the Development of the UH-1H Analysis Chart Presented as Figure 88	186
Figure 90 Estimated Threshold Rotorwash Velocity Ranges for the Mishaps Involving Door and Cowling Damage to Helicopters	188
Figure 91 Typical Hover Rotorwash Flow Pattern Characteristics With and Without Wind	189
Figure 92 Estimated Threshold Rotorwash Velocity Mean Values and Ranges for all Helicopter Mishaps Involving Door and Cowling Damage	196
Figure 93 Estimated Threshold Rotorwash Velocity Mean Values and Ranges Used in the Final Analysis of Mishaps Involving Door and Cowling Damage	197
Figure 94 Measured UH-1H Rotorwash Flight Test Data from the Indianapolis Heliport	199
Figure 95 First Estimate Separation Distances Required to Avoid Rotor Blade/Tailboom Strike Mishaps	200
Figure 96 Measured CH-53E Peak Profile Velocities as a Function of Distance from the Rotor Center at a Height of 3 Feet for a Hover Wheel Height of 20 Feet	206
Figure 97 Forces Modeled to Study the Overturning of Light Fixed-Wing Aircraft	208
Figure 98 Minimum Airspeed/Angle-of-Attack Requirements for the Overturning of Light Fixed-Wing Aircraft	211
Figure 99 CH-53E Rotorwash Velocity Streamlines	212

	<u>Page</u>
Figure 100 Vortex Probing Techniques	217
Figure 101 T-34C Upsets in the Wake of a UH-1H Helicopter	218
Figure 102 T-34C Upsets in the Wake of a UH-60 Helicopter	218
Figure 103 T-34C Upsets in the Wake of a CH-47D Helicopter	219
Figure 104 T-34C Upsets in the Wake of a CH-53E Helicopter	220
Figure 105 Probe Test Separation Distances	221
Figure 106 Rotorcraft Generated Pressure Distributions Recommended for Structural Design as a Function of Radial Offset	224
Figure 107 Uniform Building Code Wind Loads	225
Figure 108 Artists Overhead Sketches of the Dallas Vertiport	228
Figure 109 V-22 Rotorwash Flight Test Data Converted from Units of Knots to psf for Structural Design Purposes	229
Figure 110 Test Locations for Rotorcraft Models on the Dallas Vertiport	230
Figure 111 Pressure Tap Locations for Rotorwash Test of the Dallas Vertiport	232
Figure 112 Estimated Threshold Overturning Velocities for a Small Harley-Davidson Motorcycle as a Function of Drag Coefficient and Applied Moment Arm Length	239
Figure 113 Variation of Particle Terminal Velocity with Particle Diameter	245
Figure 114 Entrained Particle Velocity Ratio as a Function of Size Parameter	246
Figure 115 Peak Dynamic Pressure as a Function of Radial Distance for the Three Example Rotorcraft Configurations	248
Figure 116 Maximum Particle Velocity and Weight Limits for Eye Protection	250
Figure 117 Minimum Particle Energy Required for Penetration Through Aircraft Skin	251
Figure 118 55-Gallon Oil Drum Overturning Moments	254
Figure 119 Generic Velocity Profile Creating the Moment Required to Overturn a 55-Gallon Oil Drum	256
Figure 120 Schematic Representation of Particulate Cloud Geometry	260
Figure 121 Approximate Values for the Terrain Erosion Factor (K_T) as Identified in the Literature	262
Figure 122 Logarithmic Spiral Representation of Vortex Rollup . .	263
Figure 123 Ground Sample Particle Size Distribution	266
Figure 124 Dust Cloud Size and Shape for the H-21 Helicopter . .	268
Figure 125 H-21 Particle Cloud Boundary Comparison for Particles Ranging from 0.5 mm to 2.0 mm	269
Figure 126 A Conceptual Design for a Full-Service Elevated Vertiport	276
Figure 127 Relationship of Rotor Disk Loading to Rotor Radius . .	278
Figure 128 Vertiport Design Data for Example 7.1	283
Figure 129 HT Configuration Peak Velocity and Dynamic Pressure Versus IPLANE Distance	285
Figure 130 HT Configuration Peak Velocity and Dynamic Pressure Profiles at an IPLANE Distance of 57 Feet	286

	<u>Page</u>
Figure 131 HT Configuration Velocity and Dynamic Pressure Profile Printout at an IPLANE Distance of 50 Feet	287
Figure 132 HT Configuration Peak Velocity and Dynamic Pressure Profiles at an IPLANE Distance of 50 Feet	288
Figure 133 H Configuration Peak Velocity and Dynamic Pressure Versus DFRC Distance	290
Figure 134 H Configuration Velocity and Dynamic Pressure Profile Printout at a DFRC Distance of 65 Feet	291
Figure 135 H Configuration Peak Velocity and Dynamic Pressure Profiles at a DFRC Distance of 65 Feet	292
Figure 136 SM Configuration Peak Velocity Versus Height Above Ground Level	295
Figure 137 SM Configuration Peak Dynamic Pressure Versus Height Above Ground Level	298
Figure 138 SM Configuration Peak Overturning Force and Moment Versus Distance from the Center of the Rotor	302
Figure 139 H Configuration Peak Overturning Force and Moment Versus Distance From the Center of the Rotor	304
Figure 140 SM Configuration Peak Velocity and Dynamic Pressure Versus Distance From the Center of the Rotor	308
Figure 141 Vertiport Design Data for Example 7.4	309
Figure 142 Ground Vortex Position Calculations	315
Figure 143 Ground Vortex Velocity Field Characteristics	316

LIST OF TABLES

	<u>Page</u>
Table 1 Known Sources of Outwash Profile Flight Test Data for Rotorcraft	64
Table 2 ROTWASH Program Input Data Requirements	68
Table 3 Evaluation Matrix for CH-53E Flight Test/Mathematical Model Data Correlation	70
Table 4 Evaluation Matrix for XV-15 Flight Test/Mathematical Model Data Correlation	96
Table 5 Evaluation Matrix for CL-84 Flight Test/Mathematical Model Data Correlation	119
Table 6 Height and Weight of Subjects Used in Dynamic Force Evaluation	153
Table 7 Projected Areas Used In Calculation of Human Overturning Forces for CH-53E, XV-15, and MV-22 Flight Test Data	159
Table 8 Personnel Limitations in XV-15 Flow Field Regions . .	173
Table 9 Force and Moment Guidelines for Civilian Operations .	174
Table 10 Trailing Vortex and Ground Vortex Velocity Profile Effects on Ground Personnel	178
Table 11 Mishap Reports Involving Rotorwash Induced Damage to Other Rotorcraft	181
Table 12 UH-1H Input Data for the Rotwash Analysis Program .	184
Table 13 Annual Percentage Frequency of Wind by Speed Groups and the Mean Wind	191
Table 14 Input Data Values for Modeled Fixed-Wing Aircraft .	211
Table 15 Probe Test Separation Distances	216
Table 16 Largest Peak and Mean Pressure Magnitudes Induced by Rotorcraft	231
Table 17 Estimated Sikorsky S-76 Peak Rotorwash Velocities at 1.0 and 3.5 Feet AGL	240
Table 18 Characteristics of an Arbitrary Collection of Hazardous Objects Found in the Heliport Environment .	244
Table 19 Calculated Values for Particle Size Parameter, Velocity, Energy, and Energy-to-Impact Area Ratio for an Arbitrary Collection of Objects	247
Table 20 Input Data for H-21, CH-53E, and XV-15 Correlation Cases	266
Table 21 Results of Dust Ingestion by Various V/STOL Engines for a 5-Percent Reduction in Normal Rated Power . .	272
Table 22 Critical Rotorcraft Size Classes for "How To" Design and Analysis Options	279
Table 23 Suggested Force and Moment Limits on Personnel . .	301
Table 24 Water Spray Cloud Sizes Generated by HT, H, and SM Class Rotorcraft	313

1.0 INTRODUCTION

When rotorcraft are flown in confined areas and in close proximity to personnel, structures, equipment, or other rotary- or fixed-wing aircraft, the potential exists for rotorwash-related mishaps. Prevention of these types of mishaps has historically been almost totally the responsibility of the rotorcraft pilot. In most instances, the pilot has been provided with only minimal help and guidance in carrying out this responsibility. Also, in those cases where planners and designers have attempted to minimize these types of mishaps through heliport design decisions and operational guidelines, they have discovered that little guidance existed in the literature.

In response to requests for guidance on the subject of rotorwash, the Federal Aviation Administration (FAA) initiated a program in 1985 to develop a rotorwash analysis methodology. The goals of this research effort are to better understand, mathematically model, predict with analysis, and develop techniques and design guidance for avoidance of many of the more important types of rotorwash-related mishaps. The first written report from this research effort "Analysis and Recommendation of Separation Requirements for Rotorcraft Operation at Airports and Heliports" (reference 1) was completed in 1986. This first study focused on the development of a rotorwash analysis methodology. This methodology was implemented in a FORTRAN 77 computer program for use on IBM PC or PC-compatible computers running the DOS operating system. The FAA was not in complete agreement with all the conclusions and recommendations contained in reference 1. As a consequence, this document has never been published as an official FAA report and has effectively been superseded by several subsequently published reports.

In 1989, the FAA identified the need for an analysis of the rotorwash characteristics of 11 tiltrotor and tiltwing aircraft configurations. The results of this study are documented in DOT/FAA/RD-90/16, "Evaluation of Rotorwash Characteristics for Tiltrotor and Tiltwing Aircraft in Hovering Flight" (reference 2). An analysis of rotorwash-related mishaps was then completed in 1991 as DOT/FAA/RD-90/17, "Analysis of Rotorwash Effects in Helicopter Mishaps" (reference 3). An improved analysis methodology (the ROTWASH methodology) and its companion FORTRAN 77 computer program were developed as an outgrowth of these additional research efforts. This version of the FORTRAN 77 code (version 2.0) is documented in reference 4 as DOT/FAA/RD-90/25, "Rotorwash Computer Model - User's Guide."

Both during and subsequent to the work completed in references 2 through 4, additional rotorwash-related work was conducted by other unrelated groups of researchers. The U.S. Navy acquired limited full-scale rotorwash data on the Bell/Boeing MV-22 (reference 5), and the FAA acquired full-scale rotorwash data on

several types of helicopters (references 6 through 10). A joint FAA/U.S. Navy program was conducted to evaluate the characteristics of several rotorwash sensors, and limited data on the SH-60B were obtained (reference 11). Model-scale data were acquired for the first time in a vertiport design effort for both rotorcraft and terminal structures (reference 12).

Additional understanding was also gained with respect to how full-scale rotorwash data should be used in validating analysis tools. Further improvements were also made to the ROTWASH analysis methodology itself. Rotorwash mathematical modeling approaches that are different than those used in the ROTWASH program were investigated by two different groups. The first effort, described in reference 13, focused on development of design charts for downwash analysis of many types of vertical takeoff and landing (VTOL) aircraft. An extensive literature survey is included as an appendix to the report. Mathematical modeling work by Velkoff, described in reference 14, investigates several unique modifications to some of the basic rotorwash research work that was conducted in the 1950s and 1960s. These insightful modifications focus on improvements to the calculation of rotor mass flow characteristics and the resultant mean velocity profile as the wall jet expands. Unfortunately, this work is yet to be completed, and its influence toward improving the ROTWASH analysis methodology must await release of a future version of the program.

As a result of all the work completed since 1986, it was decided in early 1992 that a complete revision of the now outdated reference 1 was long overdue. This decision was deemed necessary because reference 1 contained almost all of the available mathematical model documentation for the ROTWASH computer program and the majority of all flight test and model data that were used to validate the mathematical models. Numerous requests were also being received for reference 1 by heliport planners and designers working with the FAA's heliport design advisory circular (reference 15). Therefore, it was decided that it would be appropriate to include numerous "How To" examples in any revision to reference 1. These examples would be structured as reference material for designers and researchers who made rotorwash related calculations by hand or through use of the ROTWASH computer program.

The presentation of technical information in this report is divided into three major groupings. The first grouping comprises sections 2 and 3. These sections document analytical mathematical models that have been developed to investigate rotorcraft downwash flow fields, as well as correlation with flight and model test data. The second major group, sections 4 and 5, is devoted to development of a hazard analysis methodology and to mathematical modeling and analysis of many of the more common types of rotorwash-related hazards. The last of the three groups, sections 6 and 7, documents the capabilities and

limitations of the latest version of the ROTWASH analysis methodology (version 2.1) through use of "How To" examples that are presented in the context of a design exercise for a hypothetical vertiport. Section 8 provides recommendations for future work required to remove some of the technical limitations discussed in sections 2 through 7.

Appendices to this report contain a rotorcraft data summary, correlation of ROTWASH output with additional flight test data not contained in section 3, a comprehensive bibliography of rotorwash-related documents, a FORTRAN 77 listing of version 2.1 of the ROTWASH computer code, and an updated user's guide replacing reference 4.

These appendices and the technical sections contained in this report should be considered as revisions to and replacements for previous work documented in references 1, 3, and 4. Therefore, this report and reference 2 are the only reports required to support use of all versions of the ROTWASH analysis methodology and computer program through version 2.1.

1.1 ROTWASH SOFTWARE

A disc copy of the ROTWASH software is provided in a sleeve inside the back cover of volume II of this report. Single copies of the software and of this report may be obtained from the following address while supplies last:

Robert D. Smith
Federal Aviation Administration
Vertical Flight Program Office, ARD-30
800 Independence Avenue SW
Washington DC 20591

On the disc are a variety of file names. Interested users should first read the file named README.DOC. This file will provide basic instructions on how to run the program, how to compile subroutines and, how to link programs. Be aware that there is one executable file for IBM PC compatible computers with a math coprocessor and a second executable file for IBM PC compatibles without a math coprocessor.

2.0 DEVELOPMENT OF ROTORCRAFT DOWNWASH FLOW FIELD MODELS

This section describes the approach, methods, and working equations required to implement three different rotor-induced downwash/outwash flow field models. These "rotorwash" models were originally developed and documented in reference 1. The three models are designed to be used as predictive tools in determining, classifying, and estimating downwash and wake hazard characteristics as influenced by flight regime and rotorcraft configuration. The models are also developed with emphasis toward rotorcraft operations in close proximity to the ground. This mode of operation results in prominent rotor wake flow field characteristics that are known to present the greatest hazard potential.

The most important type of rotorwash flow field, the radial wall jet, develops when rotorcraft hover near the ground. The downwash wake from the rotor strikes the ground and subsequently flows outward along the ground. This outward flow can result in ground surface erosion, rotor wake recirculation, and rotorcraft foreign object damage (FOD), as well as debris and wind hazards to personnel, equipment, structures, and adjacent rotorcraft or aircraft. Two or more radial wall jets can also combine along planes of symmetry for multi-rotor helicopters, tiltrotors, and tiltwing aircraft to produce extremely powerful wall jet-like flow fields that have a significant upwash velocity component associated with the usual horizontal flow across the ground. Models for both of these types of flow fields are developed and validated extensively in this report.

The ground vortex flow field generated by single main-rotor helicopters is the second type of flow field model that is developed in this report. This type of flow field develops only during hover in the presence of low speed ambient wind conditions or during very low speed rotorcraft operations in extremely close proximity to the ground. Unfortunately, the ground vortex phenomenon has received little attention as a potential rotorwash hazard source, and very little information is available to validate this model. However, recent studies are used to guide the estimation of ground vortex strength, position, and probability of occurrence. Using these references, a horseshoe vortex model is implemented that can be used to estimate local flow field characteristics, as influenced by the ground vortex, and potential hazards.

The third type of rotorwash model is developed to investigate higher forward airspeeds where rotor disk edge vortices combine to generate trailing vortex flow field structures. These trailing vortex structures are similar to the ones formed by fixed-wing aircraft. As a result of the similarity, the model is developed through analogy using many traditional fixed-wing methods.

Flight test and scale-model data are provided for use in validation of the developed mathematical models wherever possible. In situations where it is appropriate, validation data are presented in this section. Otherwise, validation data and discussions of results are contained in section 3.0.

2.1 THE WALL JET

The rotorwash flow field structure that has the greatest potential for creating hazards in close proximity to the ground is the wall jet. This flow field structure, sketched in figure 1, is created when high velocity downwash exits the plane of the rotor, impinges on the ground, changes direction by 90 degrees, and then accelerates radially outward. The maximum value of outward velocity is reached at a distance of approximately one rotor diameter from the rotor's axis of rotation. At this location, the static pressure in the flow has recovered to the atmospheric value. This location is defined as the beginning of the radial wall jet. At all locations beyond the start of the wall jet, the velocity in the wall jet profile decreases exponentially with increasing distance. For multi-rotor configurations (tandem helicopter, tiltrotor, and tiltwing), the flow fields produced by each rotor interact with one another along lines of symmetry to result in the formation of interaction plane jets. These wall jet-like structures produce even stronger and more pronounced outwash effects. These flow fields also develop a significant upwash velocity component as the air mass expands out across the ground plane.

The rotorcraft-generated flow field that results in creation of a wall jet is similar to the much less complex free jet that impinges on a ground plane. This more extensively studied type of flow field is generally subdivided into three regions. These regions are defined in figure 2 in a cross-sectional drawing. Region I is the free jet itself and extends from the exit nozzle of the propulsive device to a point above the ground plane at which the flow becomes influenced by the presence of the ground. The turning region, Region II, begins at the location that the flow changes principal direction from vertical to horizontal. Static pressure is relieved from a maximum at a stagnation point on the ground at the impinging jet centerline to ambient as the radial outwash flow develops. Region III, the wall jet region, begins at the location where static pressure has returned to ambient pressure and the flow streamlines are parallel to the ground plane (r_j). The static pressure remains essentially constant in this region as the flow moves radially outward until the velocity of the flow is dissipated.

A significant number of the wall jet analysis methods that have been reviewed for development of the ROTWASH analysis methodology follow the notable treatment of a uniform impinging jet that was developed by Glauert (reference 16). Glauert established that the velocity profiles at any radial station in the developed wall

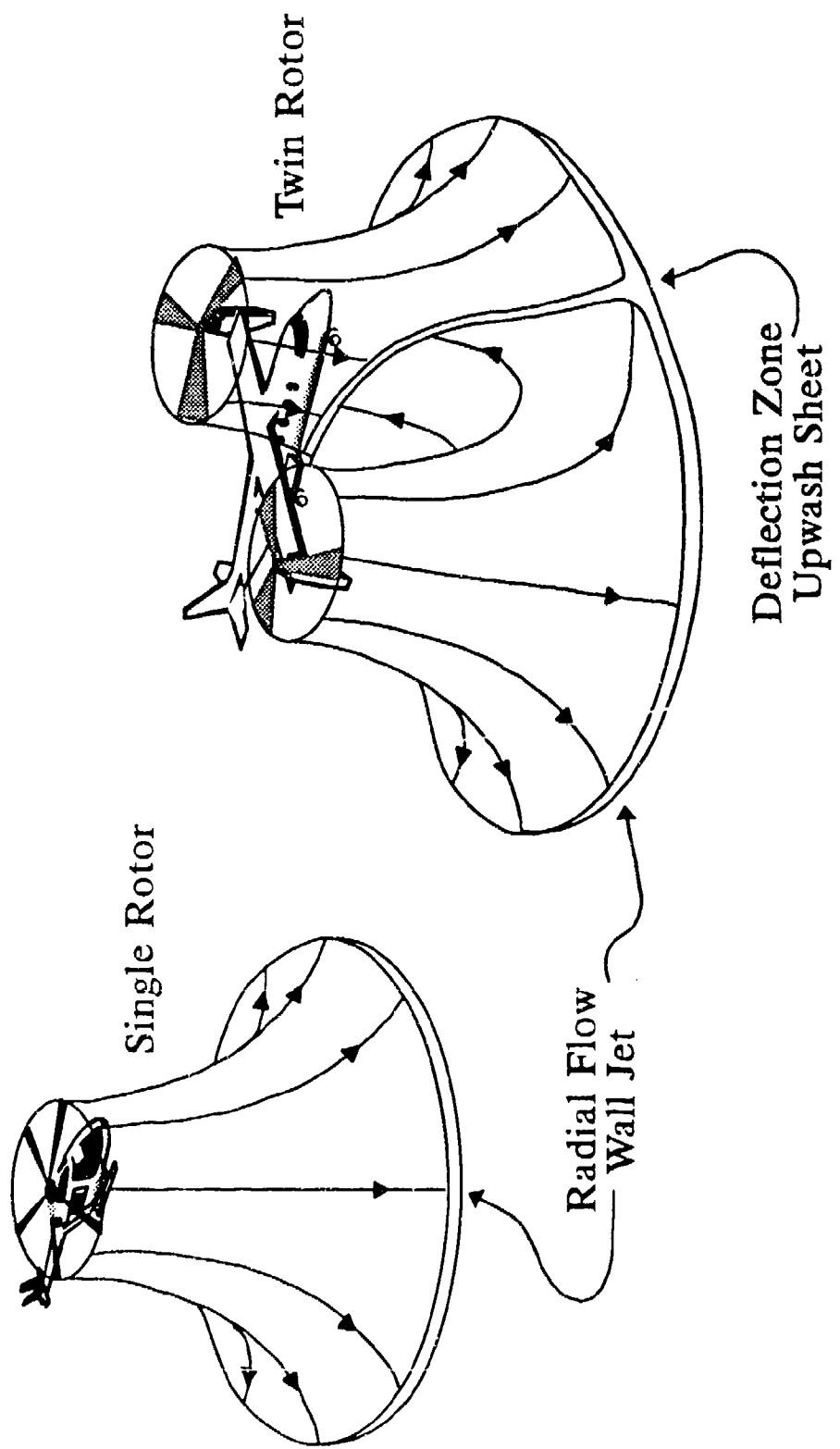


FIGURE 1 ROTORWASH FLOW FIELDS OF SINGLE- AND TWIN-ROTOR CONFIGURATIONS OPERATING IN CLOSE PROXIMITY TO THE GROUND

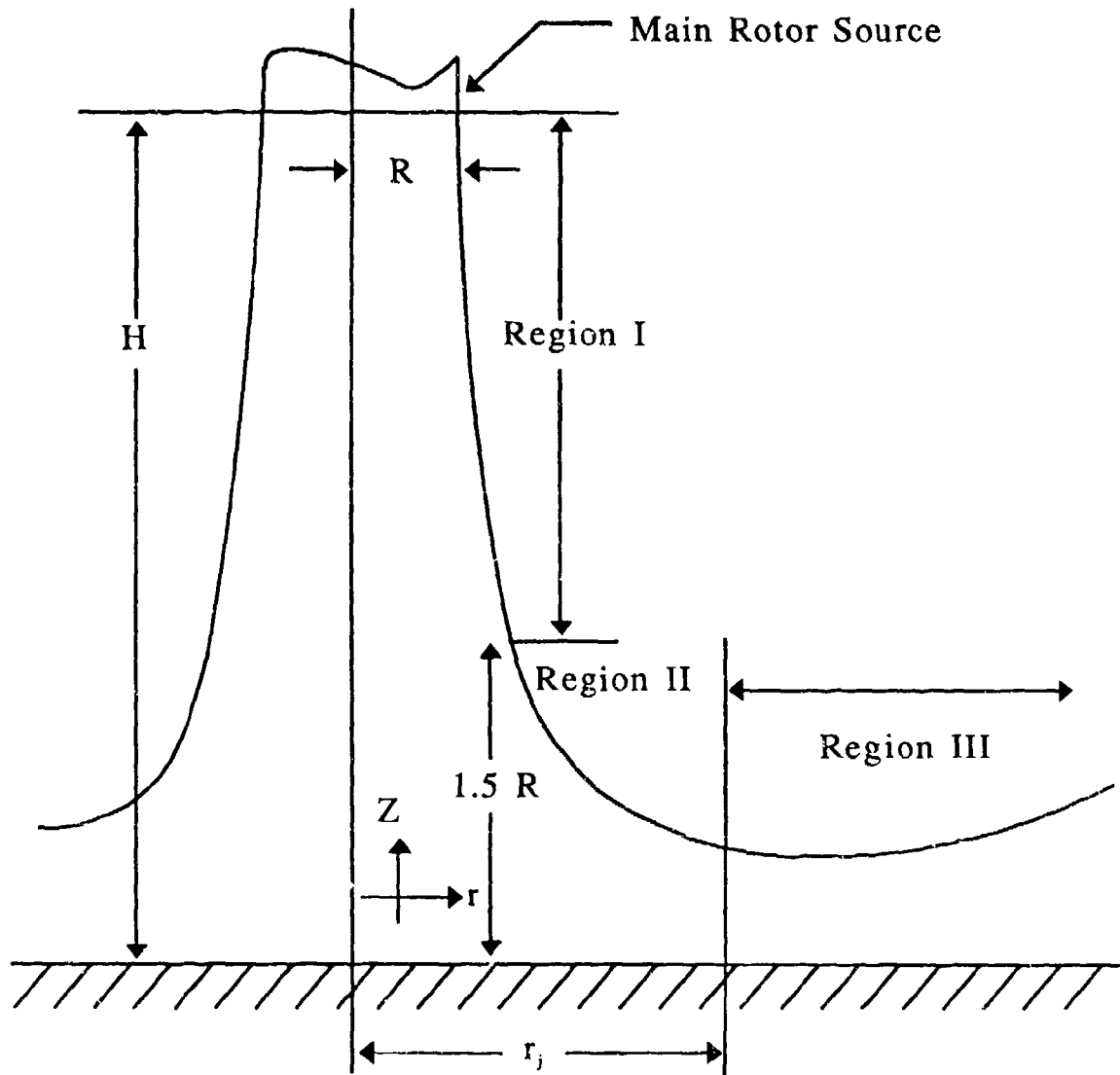


FIGURE 2 CROSS SECTION OF A ROTORWASH FLOW FIELD IMPINGING ON THE GROUND

jet region are affinely related, a fact that has been verified experimentally. More recently, interest in vertical/short takeoff and landing (V/STOL) aircraft operations has focused on quantification of the important parameters that cause ground erosion, recirculation, and equipment and personnel hazards. Hohler (reference 17) presents a wealth of experimental data and analytical approaches that, in combination, can provide a nominal solution to general downwash flow field parameters when assuming a jet nozzle source. Hohler also points out unique considerations for helping to take into account the effects of a rotor or propeller downwash source. Several examples are provided using a chart method for rapidly estimating the general magnitude of certain outwash parameters.

Migdal, et al., (reference 18) provides further analytical detail and experimental verification in a downwash flow field study that focuses on the two-jet impingement configuration and its associated upwash deflection along the interaction plane. Based on conservation of mass principles and the use of a single-jet model as a building block, semi-empirical models for each of the main flow regions of the single-jet model are coupled together. These models simulate the combined flow field of two jets and provide representative estimates for experimentally measured ground-pressure distributions. The treatment of the transitional region in this analysis is very complete; however, it is dependent upon certain assumptions with respect to the uniform jet source model.

In the process of solving a rotorwash flow field problem, the previously identified references provide valuable guidance through their respective analytical and physical descriptions of the behavior of flow-field components. However, the focus of these references is on jet sources, and the simplifying assumptions made in many instances remove the detail required to quantify hazard-avoidance criteria for rotorcraft. In particular, the models are strongly tied to decay models for a uniform free-jet source and are generally concerned with impingement cases where the jet height above ground divided by the jet diameter is large (or out-of-ground effect).

Although derived through experimental and analytical consideration of jets, a series of investigations, performed by Cornell Aeronautical Laboratories, Canadair Ltd., and Dynasciences Corporation (references 19 through 22), were identified that better address application of the jet flow field analogy to quantification of the rotorcraft downwash/outwash environment. These investigations also apply the results to quantification of associated surface erosion and dust cloud formation (or brown out) problems. Therefore, the wall jet model developed in the following sections generally parallels the Dynasciences model development (references 21 and 22) with certain clarifications. References 17 and 18 are also used to provide guidance in the extrapolation of the mathematical model

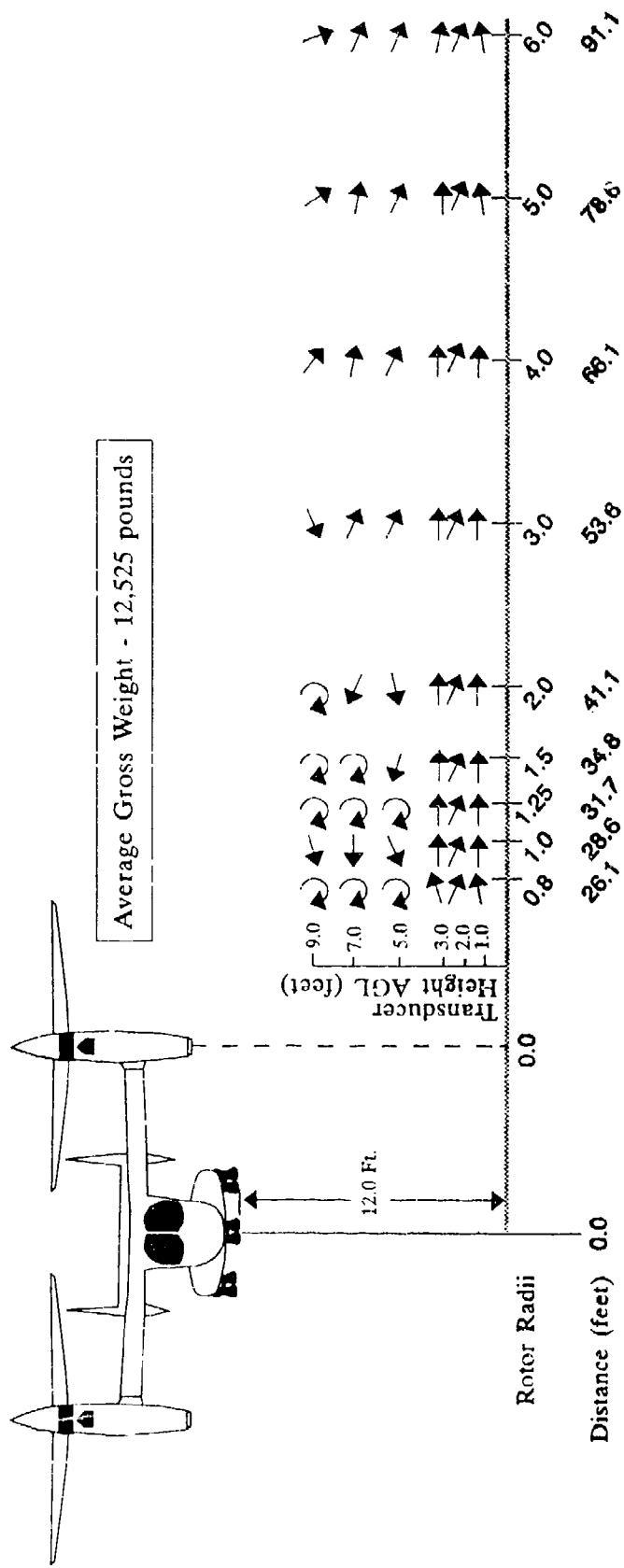
from the initial wall jet boundary back into the transition region.

2.1.1 Full-Scale Rotorcraft Wall Jet Characteristics

The usefulness of any mathematical model for predictive purposes is directly related to its ability to predict test cases accurately. This is particularly true when a very complex problem has to be analyzed based on a simplified mathematical description of the problem. Therefore, before mathematical models and their inherent simplifications are developed for the rotorwash-generated wall jet, it is important to the reader's perspective to examine the inherent characteristics of measured full-scale wall jets.

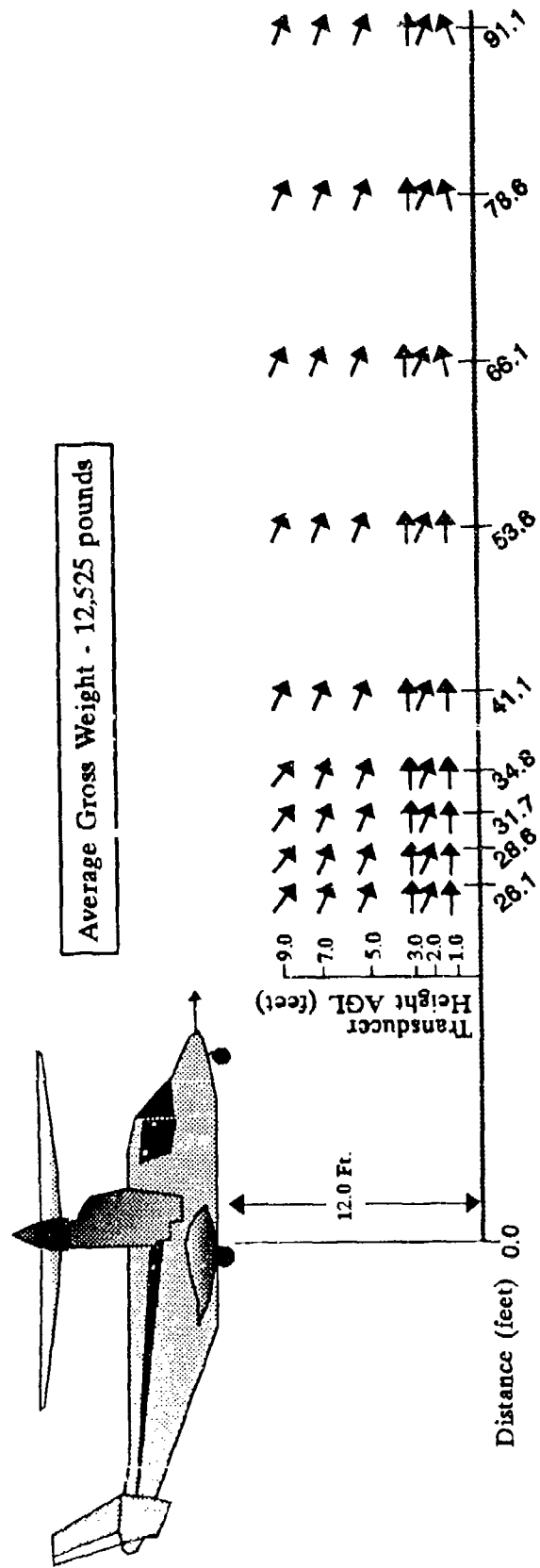
A rotorwash-generated flow field across the ground plane can be characterized as an unsteady or stochastic yet periodic flow field. Figures 3 and 4 provide examples of Bell XV-15 tiltrotor streamline data from reference 23 that generally describe the direction of the rotorwash flow field in close proximity to the XV-15. Along the 270 degree azimuth with respect to the nose of the tiltrotor (figure 3), data indicate an outward yet mostly horizontal flow up to between 5 and 7 feet above ground level (AGL), depending on the distance from the rotor. However, at heights of 5 to 9 feet AGL in close proximity to the rotor (prior to the start of the wall jet at 1.5 to 2.0 rotor radii), the flow field contains vorticity and can even be reversed toward the rotor. Along the centerline or 0-degree azimuth (figure 4), the interaction plane flow is always outward and horizontal along the ground. From a frequency perspective, the XV-15 flow field is characterized in reference 23 as being "composed of strong low frequency periodic components". However, upon analysis of eight different power spectra, the same frequency components are not always found present. Examples of a velocity time history at 2 feet AGL and its associated power spectral density characteristics are presented in figures 5 and 6, respectively (reproduced from reference 23). Frequency components vary from 0.2 to 29.5 Hz, with the majority of the energy being below 1.3 Hz. Typically, peak velocity pulses occur at 3- to 6-second intervals with an "average to peak to trough to average" duration of 0.5 to 0.6 seconds. These frequency characteristics are different than those that have been previously measured on helicopters in that the peak pulse does not continue over the full duration of the 3- to 6-second interval. Extreme peak to trough velocities for data in figure 5 vary from as high as 58 to as low as 8 knots.

Characteristics for the Sikorsky CH-53E helicopter have been measured and documented in reference 24. Examples of flow streamline, velocity time histories at 3 and 5 feet AGL, and associated power spectral density data are presented in figures 7



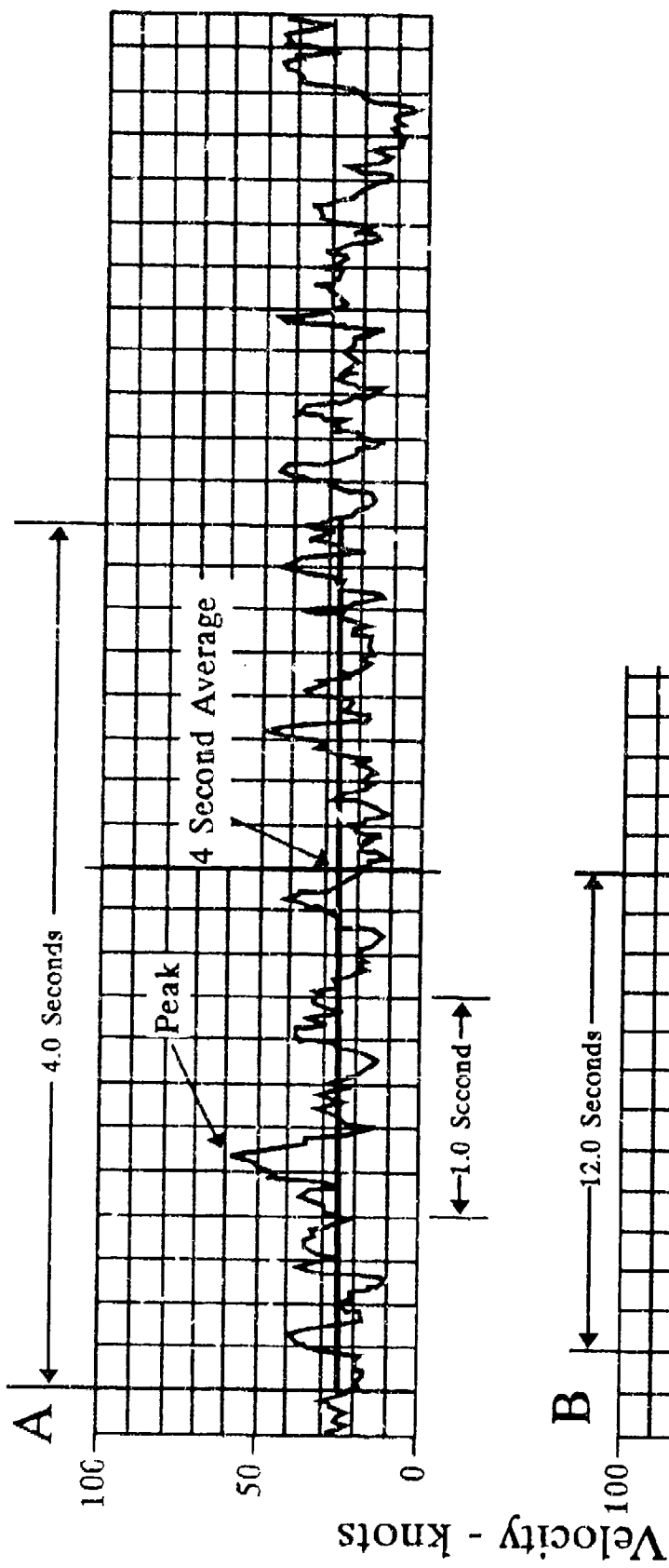
Source: Reference 23.

FIGURE 3 XV-15 ROTORWASH FLOW FIELD STREAMLINE CHARACTERISTICS IN THE VERTICAL PLANE ALONG THE 270 DEGREE AZIMUTH AT A 12 FOOT WHEEL HEIGHT



Source: Reference 23.

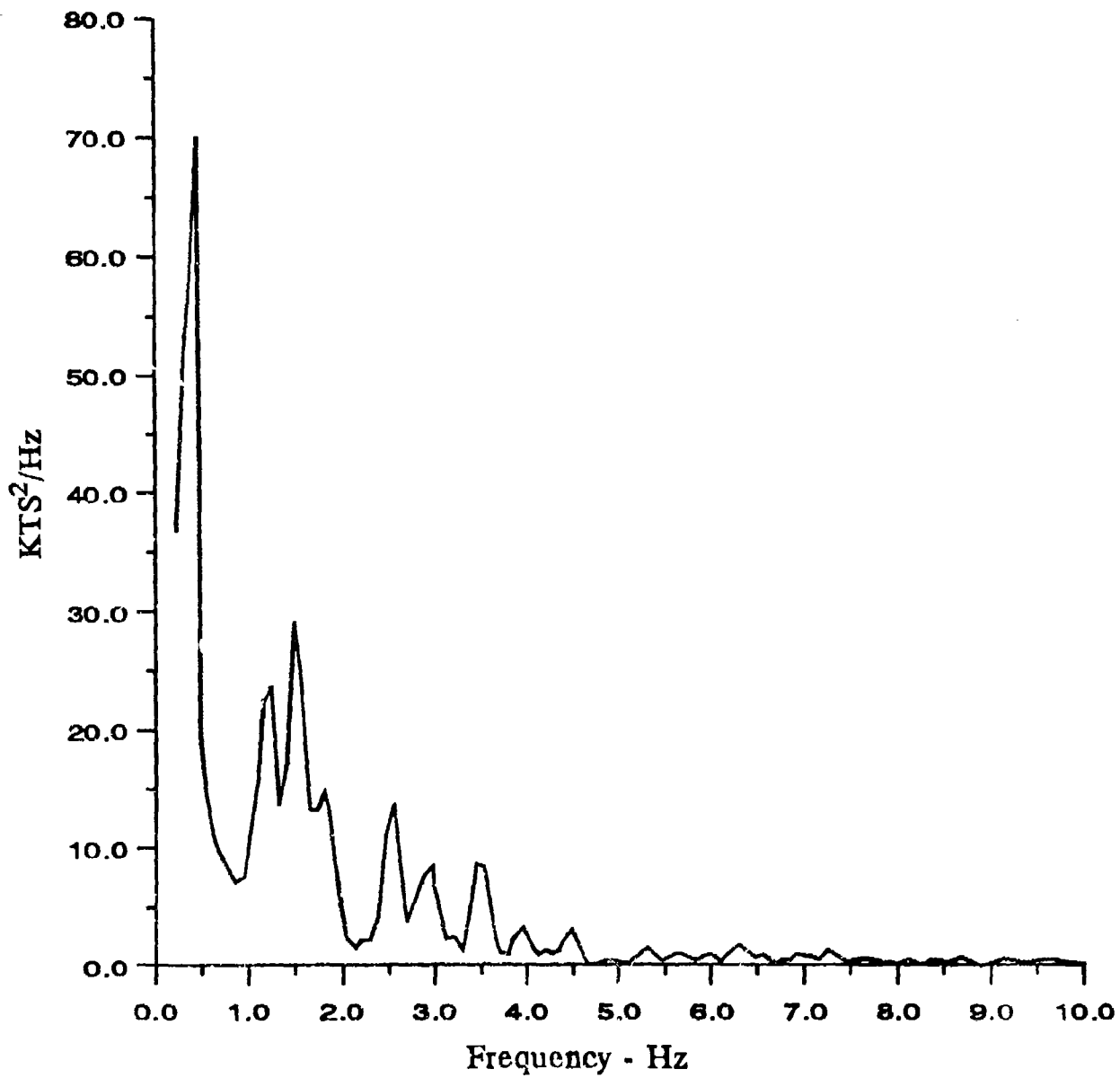
FIGURE 4 XV-15 ROTORWASH FLOW FIELD STREAMLINE CHARACTERISTICS IN THE VERTICAL PLANE ALONG THE 0-DEGREE AZIMUTH AT A 12-FOOT WHEEL HEIGHT



Note: Charts A and B represent horizontal velocity measured at 2 feet AGL along the 270° azimuth while hovering at a wheel height of 12 feet.

Source: Reference 23.

FIGURE 5 TIME SERIES STRIP CHARTS OF XV-15 DOWNWASH WIND VELOCITY MAGNITUDES



Source: Reference 23

FIGURE 6 POWER SPECTRAL DENSITY OF THE BELL XV-15 TIME SERIES PRESENTED IN FIGURE 5

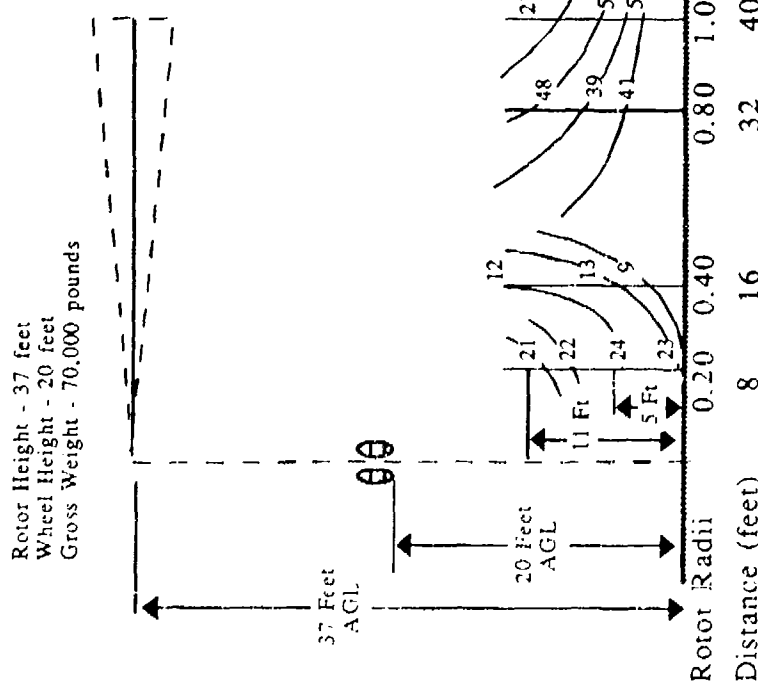
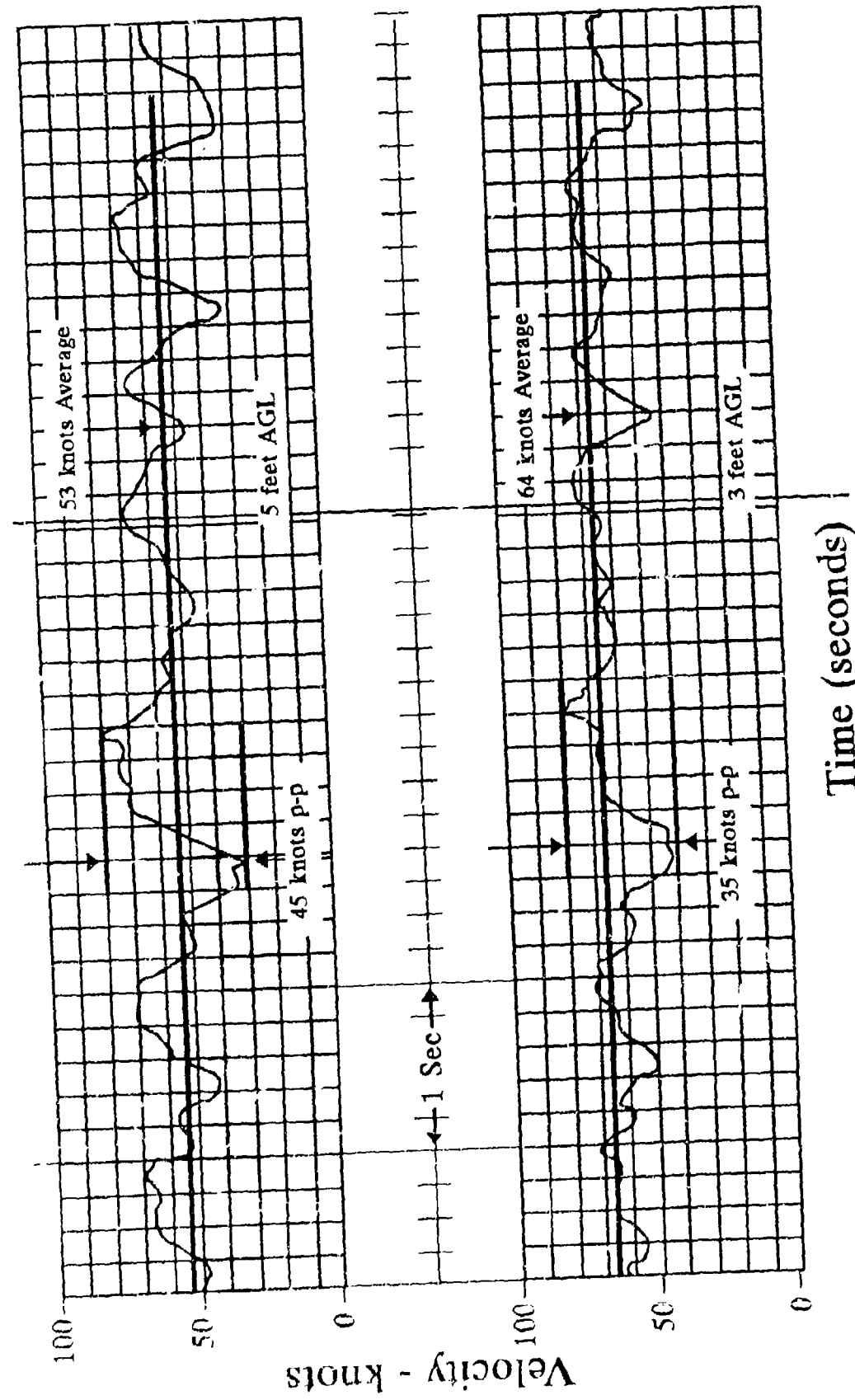


FIGURE 7 CH-53E ROTORWASH FLOW FIELD STREAMLINE CHARACTERISTICS IN THE VERTICAL PLANE ALONG THE 270-DEGREE AZIMUTH AT A 20-FOOT WHEEL HEIGHT

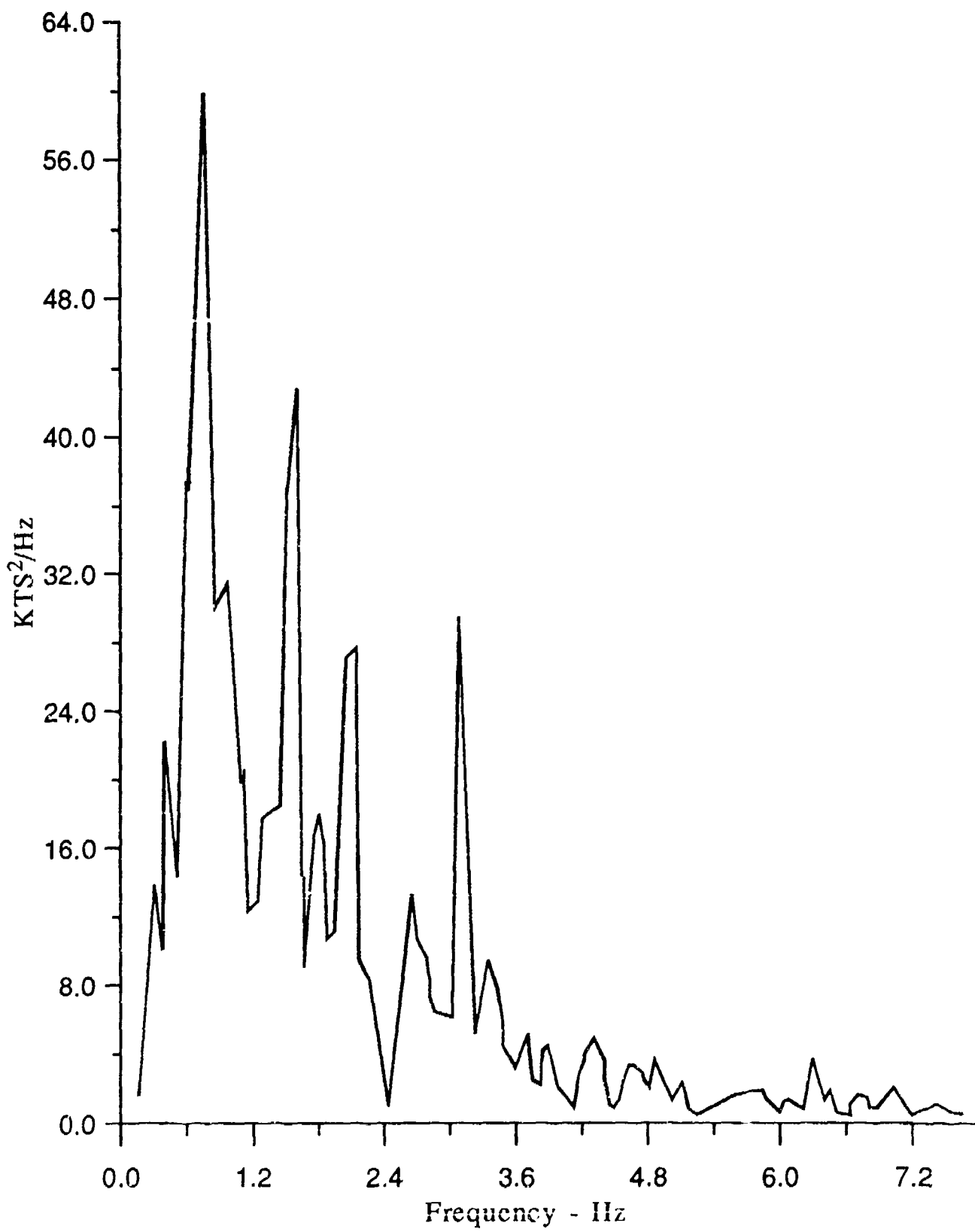
Source: Reference 24.



Note: Charts represent horizontal velocity measured at 3 and 5 feet AGL along the 270 azimuth while hovering at a wheel height of 26 feet.

Source: Reference 24.

FIGURE 8 TIME SERIES STRIP CHARTS OF CH-53E ROTORWASH WIND VELOCITY MAGNITUDES



Source: Reference 24.

FIGURE 9 POWER SPECTRAL DENSITY OF THE CH-53E TIME SERIES
PRESENTED IN FIGURE 8

through 9, respectively. Streamline data (figure 7) at 70,000 pounds gross weight and a rotor height of 37 feet indicate that the flow field becomes fully horizontal at distances in excess of 69 to 79 feet. Depending on rotor height, the major frequency component is found to vary from 0.7 to 1.5 Hz. This frequency appears to be slightly greater than that of the XV-15. Peak to trough velocity in the example varies by as much as 35 to 45 knots.

When peak velocity and statistical mean velocity measurements are obtained at several heights AGL, velocity profiles can be constructed. These velocity profiles, as measured at several distances from the center of the rotor, describe the wave front or shape of the wall jet as it expands. Typical CH-53E mean and peak velocity profiles at a distance from rotor center (DFRC) of 69 feet are presented in figure 10. Similar XV-15 profiles, at a

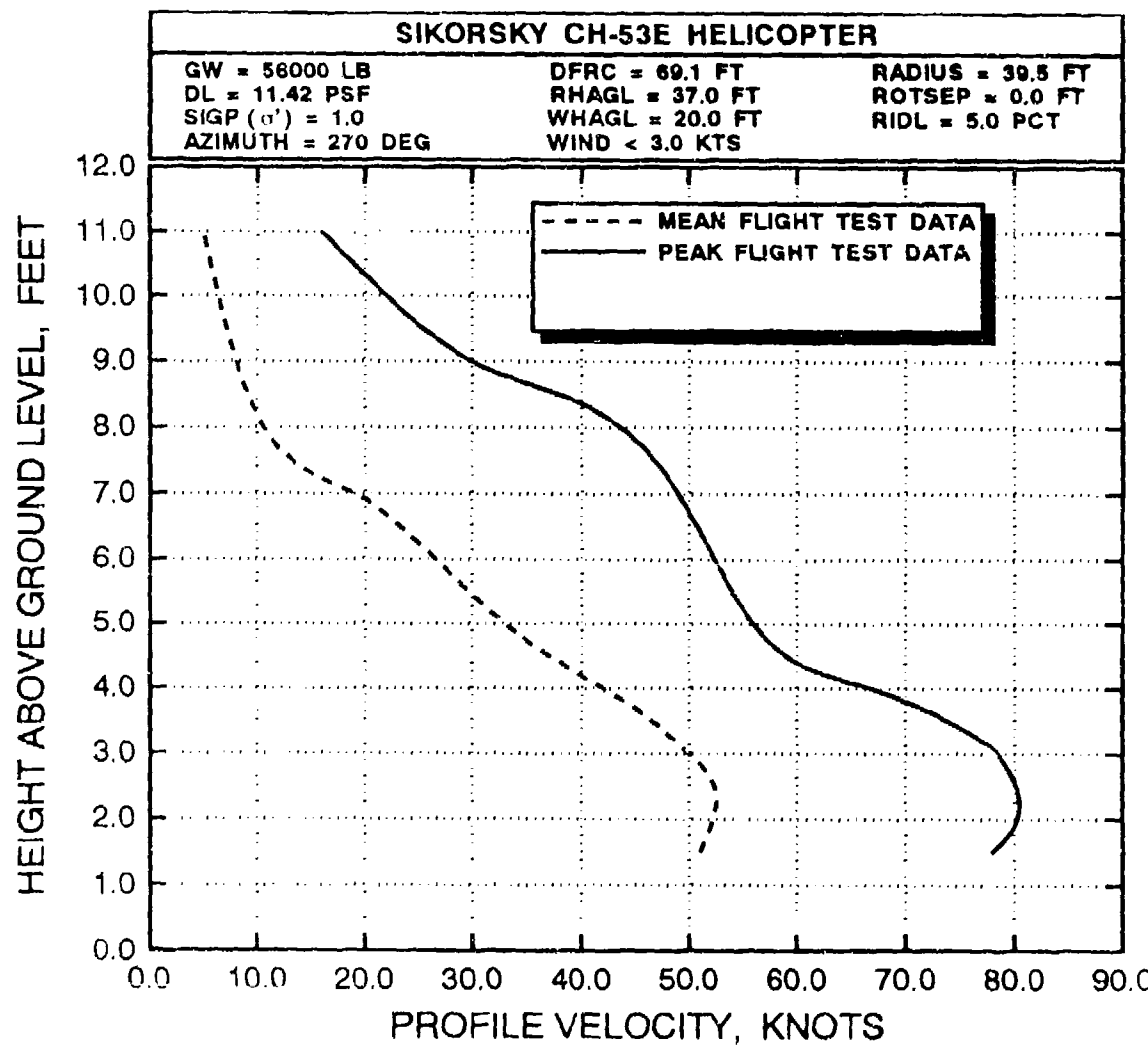


FIGURE 10 CH-53E MEAN AND PEAK VELOCITY PROFILES AT A DFRC OF 69 FEET AND A ROTOR HEIGHT OF 37 FEET

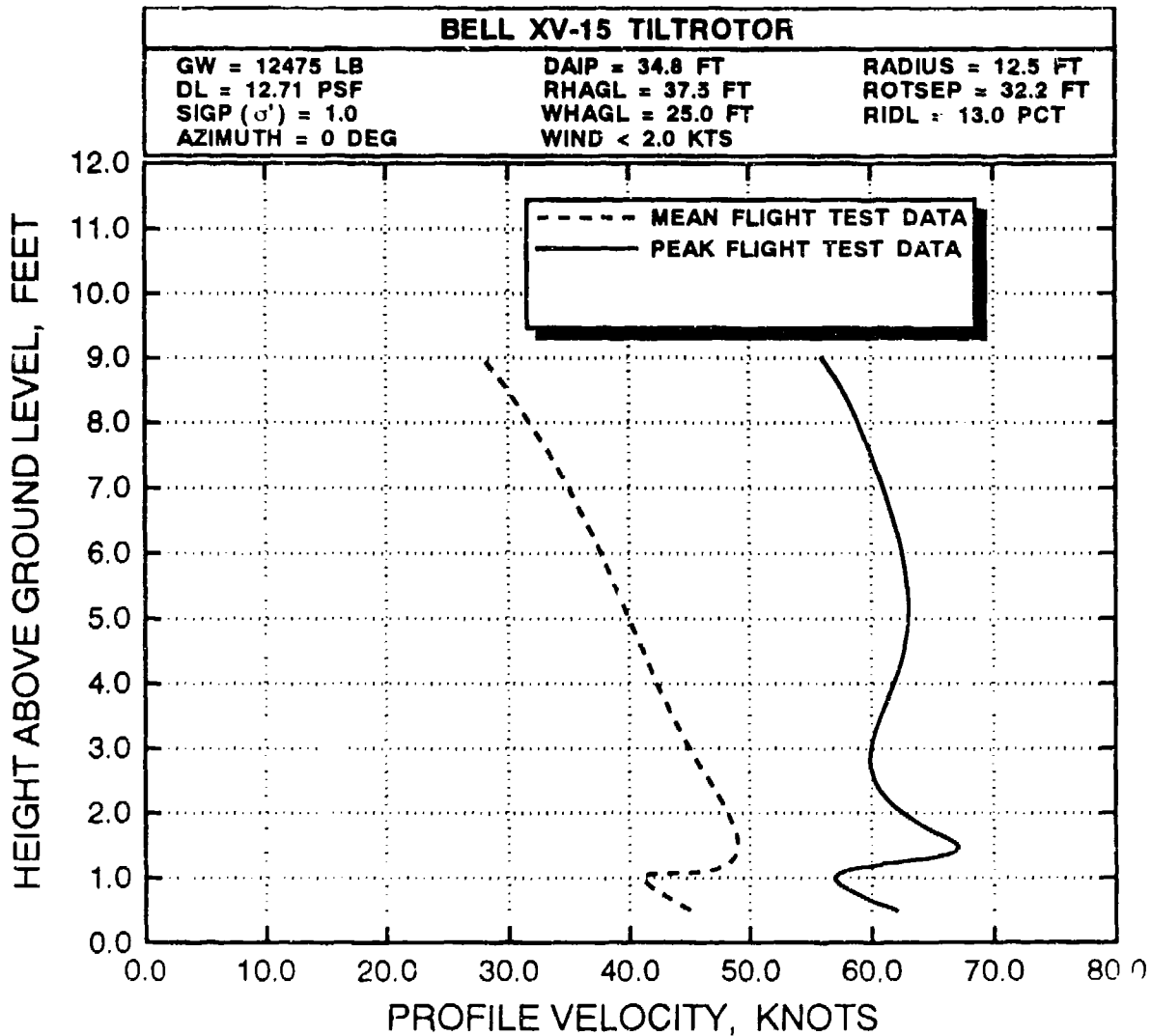


FIGURE 11 XV-15 MEAN AND PEAK VELOCITY PROFILES AT A DAIP OF 34.8 FEET AND A ROTOR HEIGHT OF 37.5 FEET

distance of 34.8 feet along the 0-degree azimuth interaction plane (DAIP), are presented in figure 11. In general, most velocity profiles have similar characteristics, in that peak velocity along the profile is always close to the ground and profile velocities rapidly decrease with increasing profile height above the peak velocity position. Exceptions to these characteristics generally occur only along the interaction plane and at distances greater than four to five times the radius of the rotor from the center of the rotor. In these cases, the peak profile velocity tends to be less pronounced and the decrease in velocity with increasing height is less rapid. Therefore, these profiles tend to have a more constant velocity or wall-like profile. A more detailed discussion on these different types of profiles is presented in the following sections.

As can be seen by the data presented in figures 3 through 11, the rotor-generated wall jet, measured in flight test, is clearly an unsteady and turbulent flow field structure. Researchers in several reports have openly acknowledged the fact that the acquisition of rotorwash flight test data is not, in general, a highly repeatable process. Factors contributing to this unsteady nature are numerous. They include the effects of vorticity in the rotor flow field and flow up through the center of the rotor, as well as small changes in ambient winds, rotorcraft pitch and roll attitude, and rotor height above ground level (RHAGL). The effects of additional unsteady secondary flows into the primary rotorwash flow field, such as turboshaft engine exhaust and tail rotor downwash (or sidewash), are also known to significantly affect wall jet profiles. These factors must be kept clearly in perspective as mathematical models are developed and validated. Otherwise, it is very easy to develop unreasonable expectations. These factors also increase the importance of emphasizing statistical concepts with respect to mathematical model validation. Only through correlation with significant quantities of flight test and scale-model data can one be sure that proposed mathematical models are reasonably valid.

2.1.2 Wall Jet Profile Similarity

The wall jet, as mathematically modeled in the ROTWASH analysis approach, is fundamentally based upon momentum theory and steady flow principles. Mathematical models are initially used to calculate several fundamental wall jet growth and decay characteristics based on rotorcraft configuration. These characteristics are combined with other theoretically and empirically derived models to calculate a steady mean velocity profile like those presented in figures 10 and 11. This velocity profile is based upon steady flow principles originally developed by Glauert and others. Empirical equations are then applied to the mean profile to account for the periodic nature of the rotor-generated wall jet and enable calculation of a corresponding peak velocity profile.

Figure 12 defines the profile shape of a fully developed wall jet, as defined by Glauert in reference 16. The velocity profile at any radial position is similar when scaled to its maximum velocity (u_m) and the vertical coordinate (z_h) at which the profile velocity is one-half its maximum. The profile is actually composed of two matched solutions to the governing viscous flows of an inner and outer layer; however, no simple, explicit, analytical representations are directly available. To circumvent this problem and facilitate simulation of the wall jet, distribution functions have been assumed, as used by Midgal, et al., in reference 18.

The inner layer is represented by the familiar turbulent boundary layer shape function

$$u/u_m = (z/z_m)^{1/7} \quad (1)$$

The outer shear layer transitions the wall jet flow to the surrounding quiescent flow field. This shear layer distribution is

$$u/u_m = (1 - [(z - z_m) / (z_b - z_m)]^{n_s})^2 \quad (2)$$

The height of the outer (or upper) boundary point (z_b) and the maximum velocity point (z_m) are determined from the ratios

$$z_b/z_h = 2.8 \quad (3)$$

and

$$z_m/z_h = 0.1944 \quad (\text{Version 2.0}) \quad (4a)$$

$$z_m/z_h = 0.28 \quad (\text{Version 2.1}) \quad (4b)$$

The latter constant (equation 4a) is the limit value for the fully developed wall jet, taken from reference 18, and is in agreement with Glauert's result for a uniform free-jet source (reference 16). This value has been used in all versions of the ROTWASH analysis methodology through version 2.0 of the software. However, due to periodicity and turbulence in the rotor-generated wall jet, this constant has recently been determined for low disk loading rotorcraft to be approximately 0.28, as defined by equation 4b. This value results in significantly improved correlation with rotorcraft flight test data and is almost identical to the value recommended by Canadair researchers (0.284) in reference 20. Glauert's work in reference 16 also indicates that turbulence increases this value; however, no alternative value is suggested for rotorcraft-related applications. In conclusion, given the values for the scaling parameters u_m and z_h , a detailed velocity profile can be constructed since the shear layer exponent (n_s) is calculated to satisfy the ratios of the profile boundary and the maximum velocity point to the half-velocity point. The determination of scaling parameters then becomes the major task in calculating wall jet characteristics.

The analytical procedure for calculating the wall jet region is developed in reference 19. This reference also establishes numerical values for a number of constants from experimental data for both uniform and nonuniform jets. References 21, 22, and 25

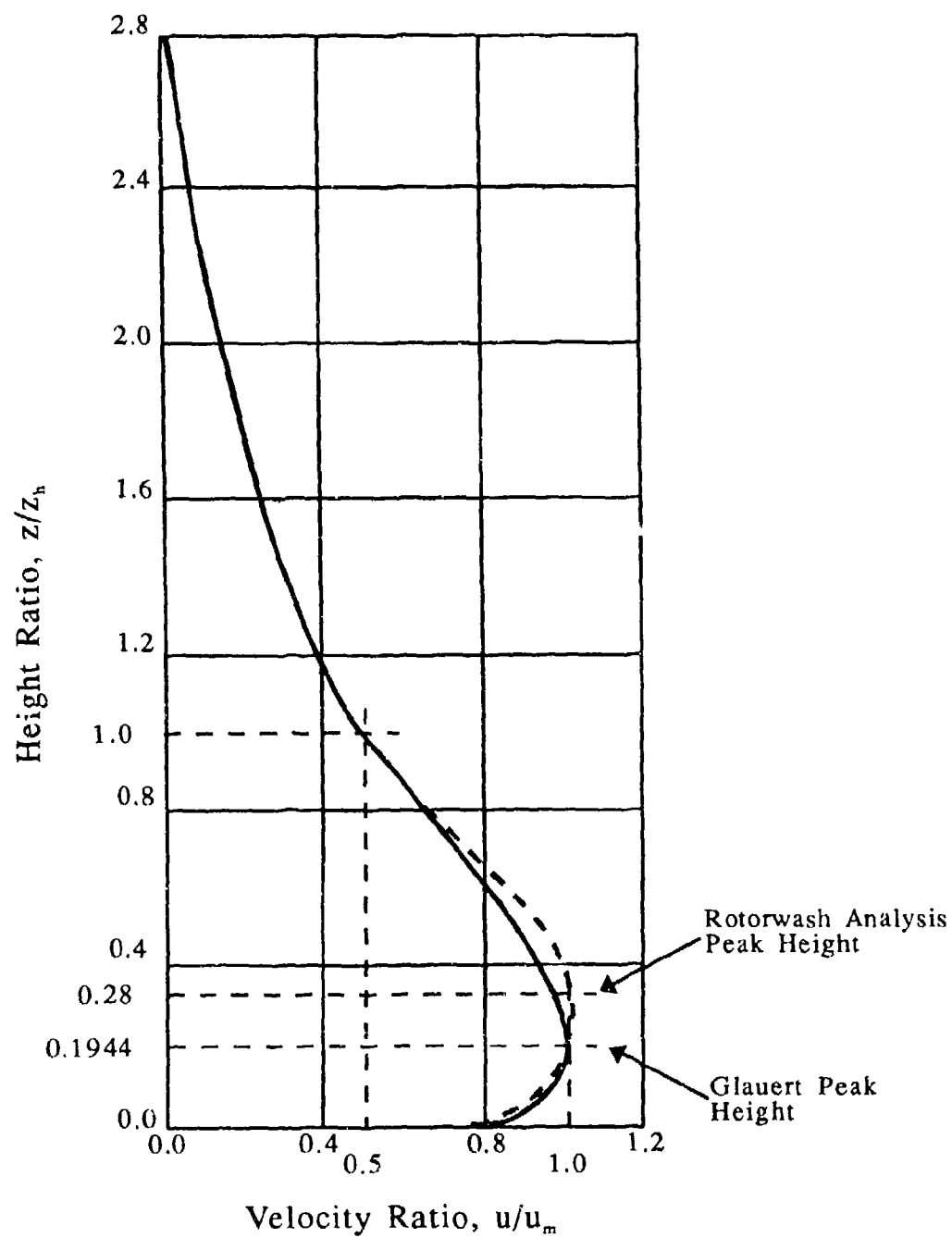


FIGURE 12 NON-DIMENSIONAL WALL JET VERTICAL VELOCITY PROFILE

extend the method to lower disk loading rotors by substituting mathematical modeling that provides for dynamic pressure decay of rotor-induced velocity in place of modeling for free-jet decay. Reference 22 also provides a good summary of the calculation procedure; however, several important typographical errors were made in presentation of the working equations in the final report. These errors will be noted as appropriate in this report.

2.1.3 Determination of Fundamental Scaling Parameters

The "fundamental" scaling parameters as they apply to the wall jet are based on theoretical as well as experimental results. These equations are developed and presented in this section as they were developed without modification in reference 1 (or all versions of the ROTWASH methodology through version 2.0). With the development of version 2.1, several improvements have been made to the fundamental equations to improve correlation for rotorcraft application, in contrast to the more fundamental uniform and nonuniform jet application. These modifications are discussed in section 2.1.4, because it is important that the original work remain documented for future reference.

Based on the work in references 21 and 22, the maximum radial velocity in the wall jet is obtained from the equation

$$u_m/\bar{U}_M = C_u (r/R)^{-1.143} \quad (\text{Version 2.0}) (5a)$$

where \bar{U}_M is the mean momentum velocity at the jet nozzle exit or, analogously, the mean velocity of the fully accelerated rotor slipstream. Similarly, the height of the half-velocity point in the outer shear layer is

$$z_h/R = C_y (r/R)^{0.028} \quad (\text{Version 2.0}) (6a)$$

The constants in these two equations are determined by the characteristics of the wall jet at its initial radius as non-dimensionalized by the rotor radius (R). From considerations of the radial mass flow and momentum flux, as calibrated by experimental data, reference 19 derives the wall jet starting half-velocity point as

$$(z_h/R)_j = 0.654 / [(u_m/\bar{U}_M)_j]^2 (r/R)_j \quad (\text{Version 2.0}) (7a)$$

This equation is also presented as equation 15 in reference 22; however, in the typing of this report, the exponent on the very

significant velocity-squared term in the denominator of the right-hand side was omitted. (The omission was verified by checking the cited references in reference 22.)

It can be further assumed that the maximum radial velocity at the start of the wall jet is equal to the maximum axial velocity in an equivalent free jet at a distance from the free-jet nozzle exit given by

$$t/R = H/R + [(r/R)_j - 1.0] \quad (8)$$

This assumption is discussed and justified with experimental findings in reference 21. However, for a rotor, the slipstream acceleration and the resulting wake contraction must also be included. Therefore, t/R must be adjusted to reflect the annular area of the rotor slipstream at which the fully developed rotor downwash velocity occurs. The slipstream contraction ratio, calculated from momentum theory, is used to account for this effect. Therefore, the effective slipstream diameter is expressed as

$$t/D_e = 0.707 (t/R) \quad (9)$$

The starting value for u_m can now be determined interactively as follows. First, a value of 2.0 is assumed for $(r/R)_j$, the initial wall jet radius. The equivalent free jet length and then t/D_e are calculated for the assumed value. As a function of t/D_e , the test data in figure 8 of reference 22 are used to obtain a decay function for dynamic pressure and thus the velocity at the start of the wall jet. This dynamic pressure decay function is represented by the following two equations.

$$(q_s)_{\max}/q_n = 1.0 - 0.025(t/D_e)^2 \text{ where } t/D_e \leq 4 \quad (\text{Version 2.0}) \quad (10a)$$

$$(q_s)_{\max}/q_n = 2.4/(t/D_e) \text{ where } t/D_e > 4 \quad (\text{Version 2.0}) \quad (11a)$$

This decay function is compared to the test data of reference 22 in figure 13 by the dash-dot-dot line. Thus, with the value for t/D_e , the decayed dynamic pressure is used to estimate a starting maximum velocity calculated from equation 12

$$u_m/U_N = [(q_s)_{\max}/q_n]^{0.5} \quad (12)$$

where U_N is the induced velocity of a fully developed rotor slipstream. This value is taken from momentum theory as an average over the rotor disk and is expressed as a function of disk loading and ambient atmospheric density as

$$U_N = [2(DL)/\rho_A]^{0.5} \quad (13)$$

Next, the average induced velocity at the rotor disk (\bar{U}) is calculated. The influence of ground effect is represented as

$$\bar{U} = k_g \bar{U}_{OGK} \\ = k_g (U_N/2) \quad (14)$$

where k_g is the ground effect-induced velocity correction factor.

$$k_g = 1.0 - 0.9e^{-2(H/R)} \quad (15)$$

An improved estimate of the starting radial position of the wall jet is then finally calculated from

$$(r/R)_j = 2.5081 (\bar{U}/u_m)^{0.486} \quad (\text{Version 2.0}) \quad (16a)$$

This equation, derived from a procedure presented in reference 19, is equation 21 in reference 22. This improved estimate for the value of $(r/R)_j$ is again used to calculate the equivalent length t/D_e . The above process is then repeated until $(r/R)_j$ is satisfactorily converged.

Using the final calculated values of $(r/R)_j$, \bar{U} , and u_m , the mean momentum velocity \bar{U}_M is calculated, shown in references 19 and 22 as

$$\bar{U}_M = (0.3586 [(r/R)_j]^{0.885} u_m \bar{U}^{0.14})^{0.88} \quad (\text{Version 2.0}) \quad (17a)$$

This equation is presented in reference 22 as equation 22 with a typographical error in the leading constant (typed as 0.385). From reference 19, it is easily determined that this constant should be $0.52/1.45 = 0.3586$, as shown above in equation 17a.

With each of the required input parameters now calculated, the half-velocity point at the start of the wall jet can be calculated using equation 7. The values for $(z_h)_j$ and $(u_m)_j$ can

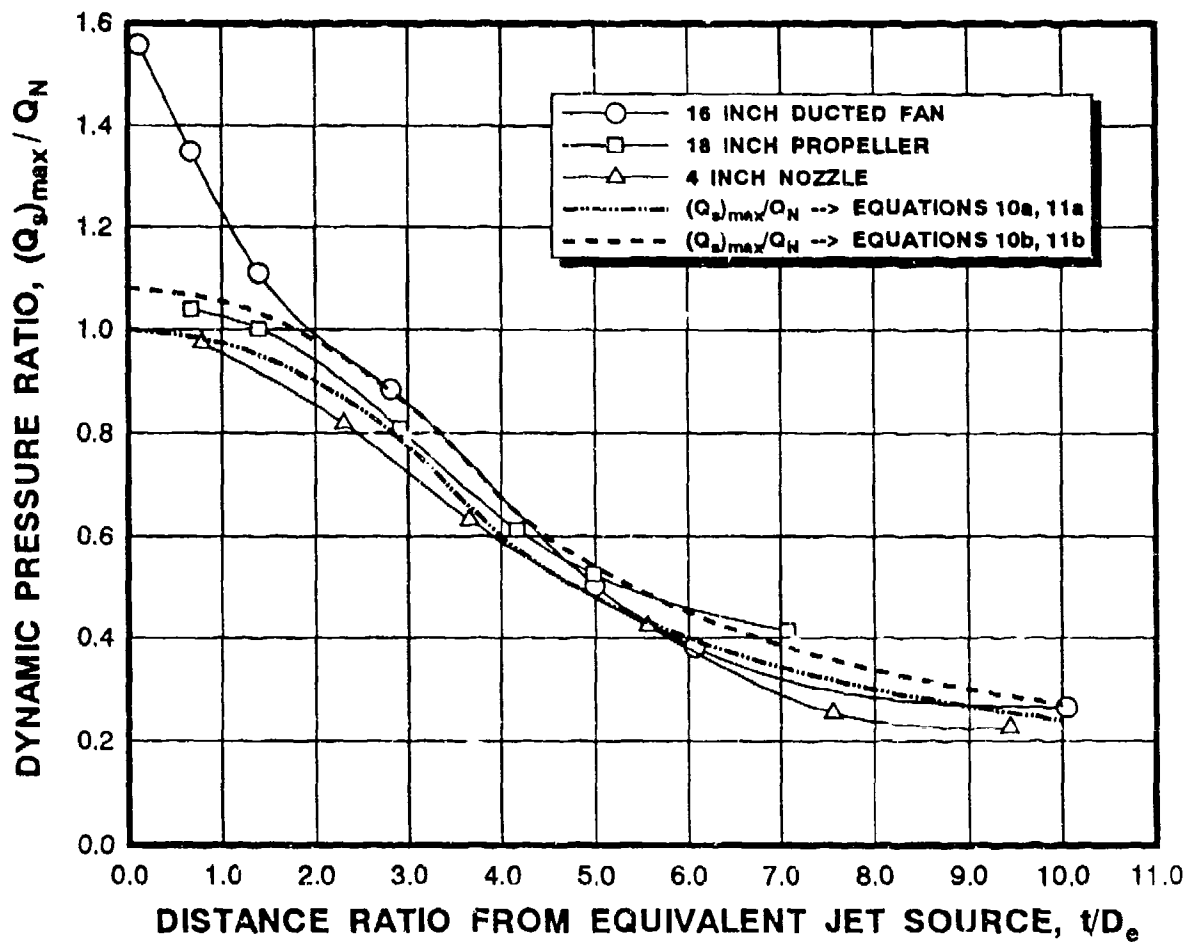


FIGURE 13 MEASUREMENTS OF DYNAMIC PRESSURE DECAY
WITH EQUIVALENT DISTANCE FROM THE JET SOURCE

then be used to obtain values for the wall jet growth function constants that are expressed as equations 18a and 19a.

$$C_u = (u_m/\bar{U}_N)_j [(x/R)_j]^{1.143} \quad (Version\ 2.0) \quad (18a)$$

$$C_y = (z_h/R)_j [(x/R)_j]^{-1.028} \quad (Version\ 2.0) \quad (19a)$$

The wall jet region is now fully defined for $(r/R) \geq (r/R)_j$ and requires only that the rotor disk loading and height above ground level be specified.

2.1.4 Scaling Parameter Modifications for Rotorcraft Application

Modifications to fundamental scaling parameters that improve correlation with rotorcraft test data have been incorporated in version 2.1 of the ROTWASH methodology. These modifications have been made for several reasons. In some cases, additional research has been identified, as was the case in the decision to modify the profile maximum velocity height, equation 4b. In other cases, the empirical adjustment of factors or exponents simply results in a better match to available test data. In each instance, these modifications are documented and referenced with the corresponding equation that is replaced in the previous section. This insures that all future modifications will benefit from a documented audit trail.

Based on the work in references 21 and 22, the maximum radial velocity in the wall jet (a mean velocity) and the height of the half-velocity point are obtained from equations 5a and 6a. However, correlation efforts conducted using rotorcraft test data indicate that these uniform jet-related equations can be simplified for the more oscillatory rotorcraft flow field. The simplifications that have been made are to the exponents of the (r/R) term in both instances. In the maximum velocity equation, the exponent is changed from -1.143 to simply -1.0 (equation 5b). In the half-velocity point equation, the exponent is changed from 1.028 to 1.0 (equation 6b). These exponents must also be adjusted in the equations for calculation of the constants C_u and C_y at the start of the wall jet (equations 18b and 19b).

$$u_m/\bar{U}_M = C_u (r/R)^{-1.0} \quad (\text{Version 2.1}) (5b)$$

$$z_h/R = C_y (r/R)^{1.0} \quad (\text{Version 2.1}) (6b)$$

$$C_u = (u_m/\bar{U}_M)_j [(r/R)_j]^{-1.0} \quad (\text{Version 2.1}) (18b)$$

$$C_y = (z_h/R)_j [(r/R)_j]^{-1.0} \quad (\text{Version 2.1}) (19b)$$

Unfortunately, neither of these two exponent changes can be justified as a result of additional theoretical or experimental knowledge. Therefore, it should not be unexpected if at some future date additional research reveals that other improved

values for these exponents exist (i.e., the yet-to-be completed work by Velkoff, reference 14). Recommendations for additional rotorcraft-related research work of this type have been made to both NASA and the academic community.

A second modification has been made to the dynamic pressure decay function equations, as represented in equations 10b and 11b. This modification is based on recently discovered data, also documented and provided by Kuhn, in reference 26. These data justify a shift in the decay function for rotorcraft to the one plotted in figure 13 by the short dashed line.

$$(q_s)_{\max}/q_N = 1.08 - 0.025(t/D_e)^2 \text{ where } t/D_e \leq 3.5 \quad (\text{Version 2.1}) \quad (10b)$$

$$(q_s)_{\max}/q_N = 2.7/(t/D_e) \text{ where } t/D_e > 3.5 \quad (\text{Version 2.1}) \quad (11b)$$

Other minor modifications to the equations used in version 2.0 have been made by rounding off several empirical constants and exponents to two significant figures. These minor adjustments more accurately reflect a believable accuracy for the values and simplify the theoretical/empirical basis of the ROTWASH methodology. These minor adjustments are easily identified in equations 7b, 16b, and 17b when compared with the original equations presented in the previous section.

$$(z_b/R)_j = 0.65/([(u_m/\bar{U}_M)_j]^2(r/R)_j) \quad (\text{Version 2.1}) \quad (7b)$$

$$(r/R)_j = 2.5(\bar{U}/u_m)^{0.5} \quad (\text{Version 2.1}) \quad (16b)$$

$$\bar{U}_M = (0.36[(r/R)_j^{0.88}u_m\bar{U}^{0.14}])^{0.88} \quad (\text{Version 2.1}) \quad (17b)$$

2.1.5 Extrapolation into the Transition Region

The transition region is defined in this study to extend from the rotor axis to the starting point of the wall jet. The flow in this region is highly dependent upon details associated with a rotor's radial induced velocity distribution, as well as the presence of the airframe, propulsive system exhaust plumes, and the induced velocity of any anti-torque devices. Figure 14 (from reference 27) illustrates the complex streamline patterns beneath a rotor in ground effect. Of particular interest is the clearly

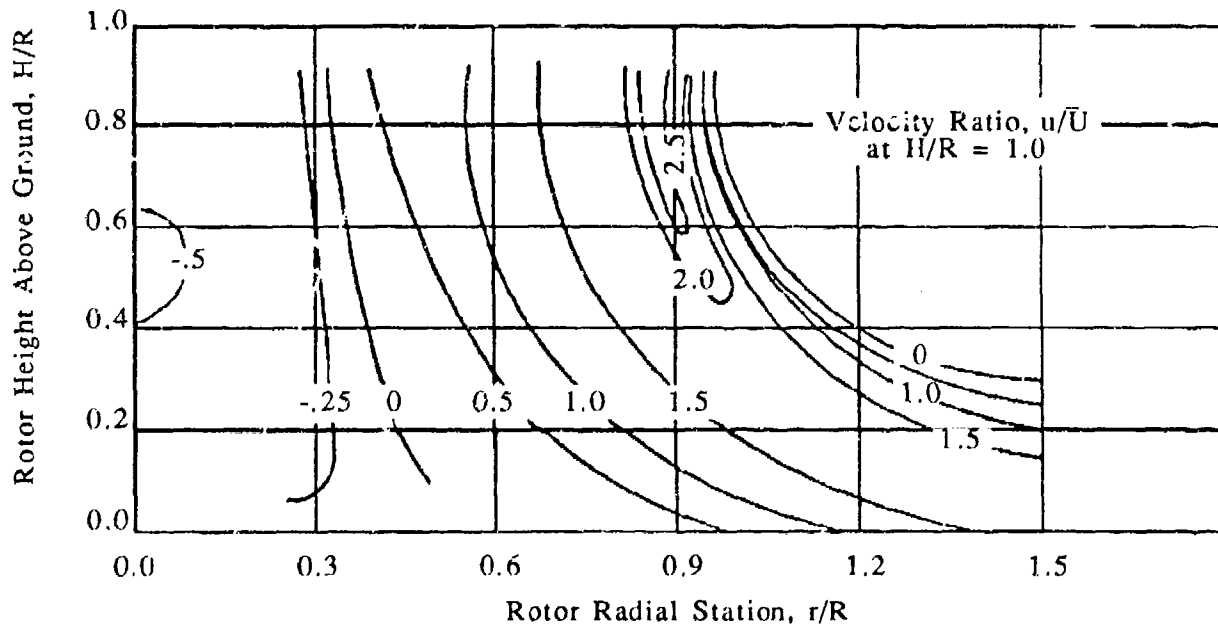


FIGURE 14 MEASURED VELOCITIES BELOW A HOVERING ROTOR IN GROUND EFFECT

defined region of recirculation near unit radius and a probable upwash zone near the center of rotation (permitted by the rotor blade root cut-out). The apparent splitting of the streamlines suggests an annular stagnation line on the ground plane at approximately mid-radius. In spite of this complexity, the developing outward flow of the region must be addressed due to its hazard potential. This is particularly true with regard to personnel movement close to a rotorcraft.

The mathematical modeling approach that has been developed to extrapolate the starting wall jet profile characteristics back into the transition region is guided by experimentally obtained data. A major assumption is made that the impinging rotor flow stagnates on the ground at the ground intersection with the rotor rotational axis. The maximum horizontal radial velocity component, u_m , is then allowed to grow as a function of the square-root of $(r/R)/(r/R)_j$ out to the start of the wall jet (which is at the iteratively computed $(r/R)_j$ location, equation 16).

$$u_m = (u_m)_j [(r/R) / (r/R)_j]^{0.5} \quad 0 < (r/R) < (r/R)_j \quad (20)$$

The point along the developing velocity profile where the maximum velocity occurs has been treated in a similar manner to the maximum velocity in previous ROTWASH versions. However, correlation results for positions equal to approximately 0.8 times the rotor radius (or $(r/R) = 0.8$) to the location where the wall jet begins indicate that a fixed value yields the best results. This value is represented by equation 21

$$z_m/R = 0.33(z_h/R) \quad (21)$$

where z_h is the calculated half-velocity height along the profile. Any further refinement to this modeling approach requires detailed knowledge of the ground pressure distribution and could also turn out to be highly configuration dependent.

The profile one-half velocity height in the transition region is defined based upon an experimental observation that the horizontal component of impinging flow senses the ground as a function of the square-root of the rotor height (H/R). At low ground effect heights, the impinging flow begins to slow and thus spread, initiating the outward transition. It is important to note the phrase "horizontal component" in the first sentence, because the actual flow field is clearly not always predominantly horizontal (figure 14). Therefore, the velocity values calculated in this region must be carefully used and not misinterpreted as total or streamline velocities. Likewise, the modeling of the square-root function should only be interpreted as an experimentally observed characteristic of the horizontal velocity component in this region. One would not necessarily expect to observe this simple relationship if a significantly more detailed model were to be developed.

To retain similarity with the fully developed wall jet, the half-velocity point of the transition shear layer is taken initially as

$$(z_h/R)_o = (H/R)^{0.5}/2.5 \quad (22)$$

Then, to transition smoothly to the developed wall jet, a near quadratic variation of z_h/R is developed based on correlation.

$$z_h/R = [((z_h/R)_o - (z_h/R)_j] / (r/R)_j^2 [(r/R) - (r/R)_j]^{1.5} + (z_h/R)_j \quad (23)$$

The boundary variation can then be calculated similar to the developed wall jet from the ratio

$$z_b/R = 2.5(z_h/R) \quad (24)$$

where 2.5 is used for improved correlation instead of 2.8 as proposed by Glauert (equation 3).

This completes the analytical description of the transition region model. The primary advantage of the approach is that it allows for rapid calculation of mean velocity profile characteristics once the starting wall jet characteristics are defined. Although necessarily simplified, this representation does yield correlation results that reasonably predict measured flight test data, as will be shown in section 3 of this report.

2.1.6 Extension of Theory to the Twin Rotor Interaction Plane

The single-rotor induced velocity impingement model described in the previous sections can also be used as a building block for simulation of twin-rotor configurations. The individual slipstreams of both tandem and side-by-side rotor configurations exhibit isolated single-rotor characteristics as well as "interaction" effects along the vertical plane of symmetry between the two rotors. This interaction plane (IPLANE) is formed when transition and wall jet regions from each rotor collide and form a stagnation line along the ground plane. Along with the expected radial or horizontal flow component, an upward velocity component or deflection zone is also formed as the flow field expands outward. Each of these flow field components is sketched in figure 1.

Velocity and directional flow characteristics along the interaction plane are influenced by the airframe and previously discussed parameters such as rotor height above ground. For side-by-side rotorcraft, such as the tiltrotor, the airframe constrains formation of an upwash component. For tandem rotor configurations, the airframe is oriented laterally to the interaction plane and offers little resistance to the formation of an upwash component. The mathematical model used in the ROTWASH analysis that describes formation of the interaction plane is obtained from reference 22. This formulation neglects all airframe influences. Therefore, adjustments have been made to coefficients in the model to conservatively predict the more critical tiltrotor and tiltwing configurations. Correlation of results with flight test data for both of these configurations is presented in section 3.

The interaction plane mathematical model is developed by considering the plane to be a thin vertical wall through which no mass flow can pass. As the radial flow from each rotor meets the wall, it is deflected up the wall at the same angle as if the flow continued along the ground. This concept is sketched in figure 15. The concept is generally supported by data from

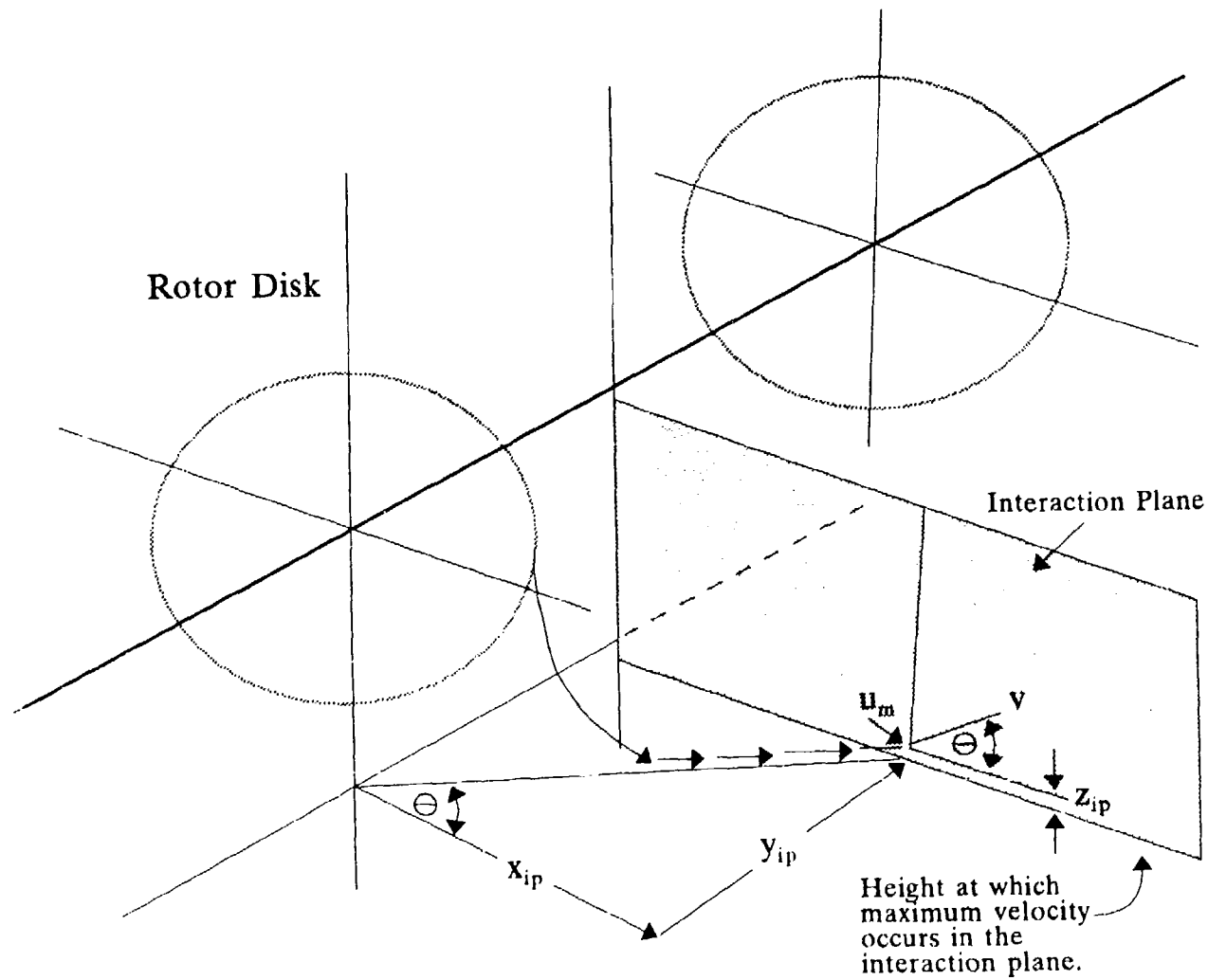


FIGURE 15 CONCEPTUAL REPRESENTATION OF THE FLOW FIELD ALONG THE INTERACTION PLANE

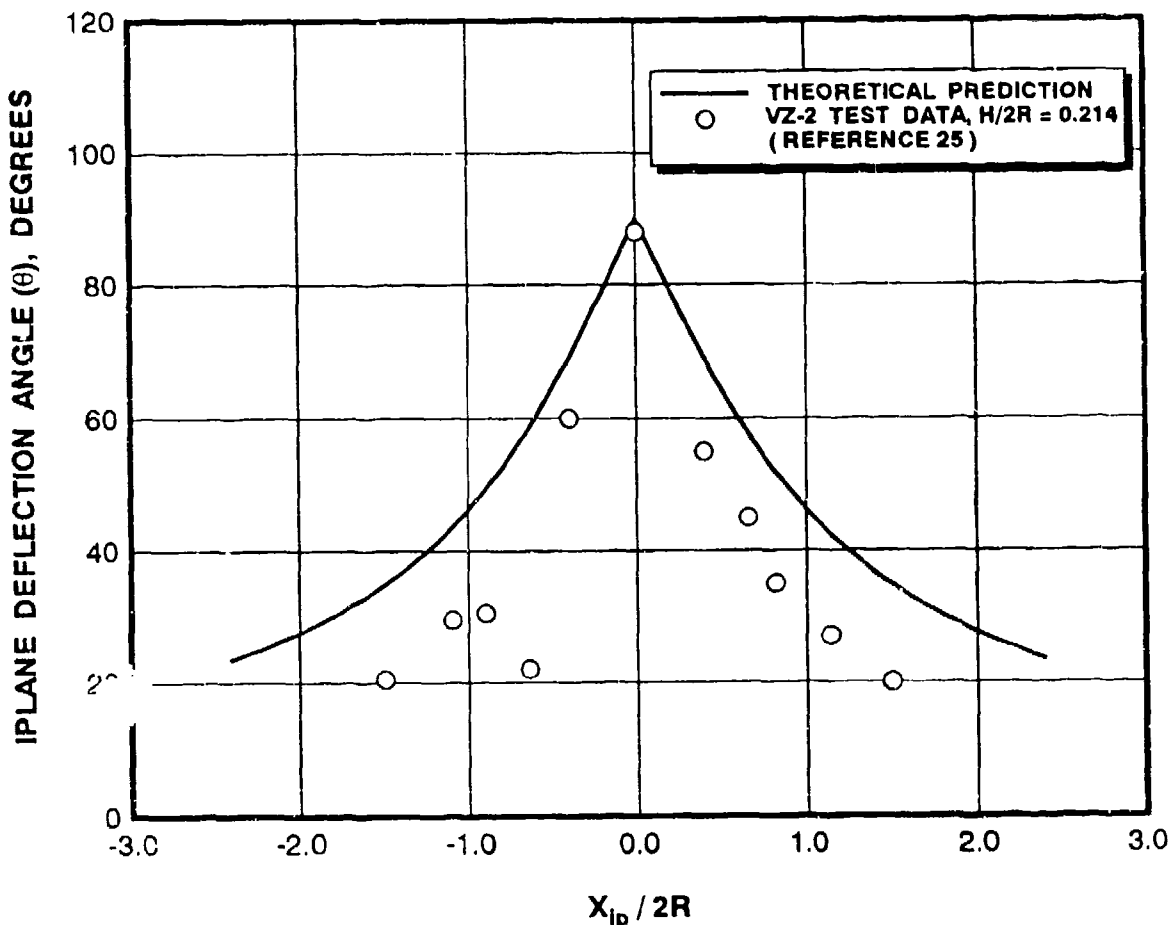
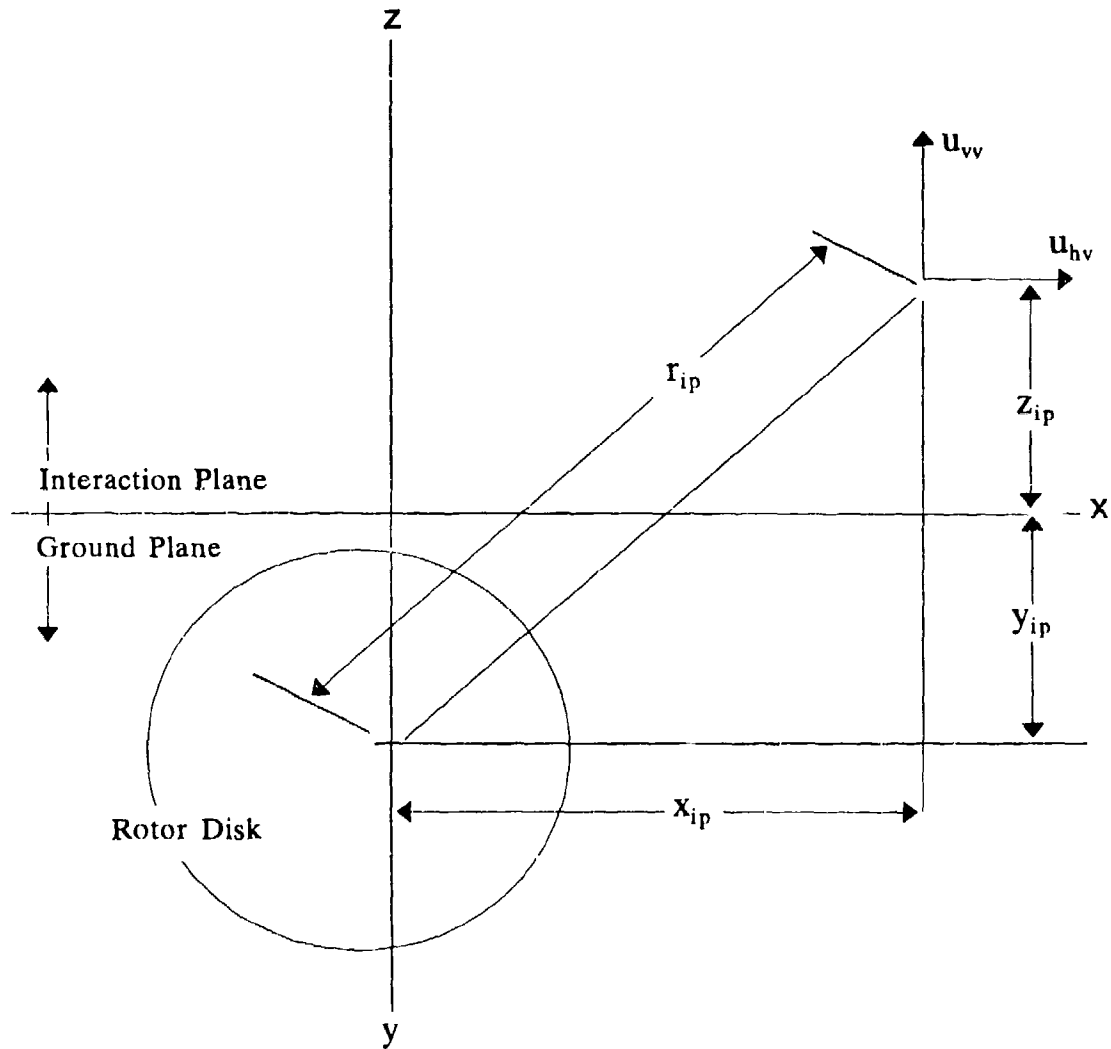


FIGURE 16 COMPARISON OF THEORETICAL FLOW DIRECTION
IN THE INTERACTION PLANE WITH TEST DATA

references 25 and 28 that are presented in figure 16 for the tiltwing VZ-2. The theoretically predicted deflection angles (θ) are somewhat higher than measured angles; however, it must again be noted that airframe effects are not accounted for in the theory.

The velocity at any point on the interaction plane is initially calculated the same as the isolated radial flow at a total distance equal to the radius along the ground from the rotor axis to the interaction plane, plus the length of the run up the plane. The geometry of this problem is illustrated in figure 17. The resulting vertical profile at any station along the interaction plane reflects only the maximum radial velocities of the colliding flows. Near the rotor, this results in an almost constant horizontal component of velocity throughout the velocity profile. However, test data cited in reference 22 indicate that the velocity along the interaction plane is considerably greater



**FIGURE 17 GEOMETRY DEFINITION FOR MODELING
OF THE INTERACTION PLANE FLOW FIELD**

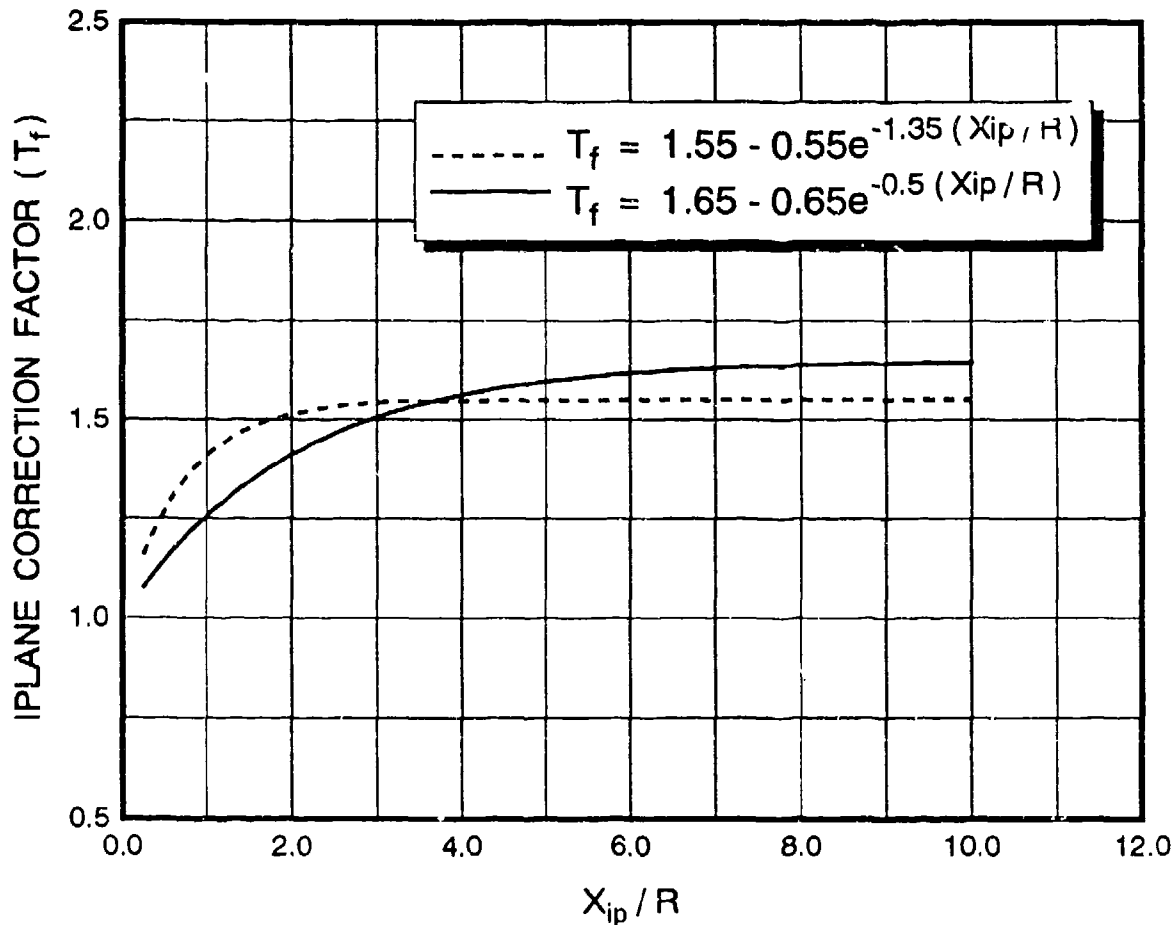


FIGURE 18 CORRECTION FACTOR FOR DETERMINING VELOCITIES WITHIN THE INTERACTION PLANE VELOCITY PROFILE

than that of just one rotor by itself. Therefore, the individual rotor contributions are somehow additive, providing a higher dynamic pressure than suggested by the concept above. Figure 18 from reference 22 graphically presents a correction factor that is analytically represented by

$$T_f = 1.55 - 0.55e^{-1.35X_{ip}/R} \quad (\text{Version 2.0}) \quad (25a)$$

This equation has been modified for version 2.1 to better correlate with tiltrotor and tiltwing flight test data by changing the constants to those of equation 25b.

$$T_f = 1.65 - 0.65e^{-0.5X_{ip}/R} \quad (\text{Version 2.1}) \quad (25b)$$

With the correction factor and the geometry as described, the horizontal and vertical velocity components, respectively, along the interaction plane are

$$U_{hv} = T_f u_m (x_{ip}/r_{ip}) \quad (26)$$

$$U_{vv} = T_f u_m [(Y_{ip} + z_{ip})/r_{ip}] \quad (27)$$

where u_m is the maximum radial velocity calculated for a single rotor at the total distance from the rotor axis (r_{ip}).

2.1.7 Addition of a Boundary Layer to the Interaction Plane

The interaction plane mathematical model calculates a full velocity profile all the way to the ground. This is because the velocity profile is built from the maximum wall jet velocity for each equivalent radius. To more realistically model the interaction plane flow, a modification is provided that adds a boundary layer shape to the bottom of the velocity profile. The assumption is made that the shape of the velocity profile at the interaction plane's base radius, as represented by equation 28, should be similar in structure to the radial (or single rotor) profile boundary layer.

$$r_{ip} = (x_{ip}^2 + y_{ip}^2)^{0.5} \quad (28)$$

This radius is used to calculate the parameters of the initial radial profile that becomes the base ($z_{ip} = 0$) of the interaction plane profile. This calculation identifies the base profile's maximum velocity vertical position (z_m) using equation 4. In constructing the interaction plane profile, if $z_{ip} > z_m$, the procedure described above is used without modification. However, for $z_{ip} \leq z_m$, a 1/7th power law turbulent boundary layer distribution

$$u_{ip}/u_m = (z_{ip}/z_m)^{1/7} \quad (29)$$

is substituted (similar to the wall jet). For this purpose, u_m is understood to be the interaction plane velocity at z_m . This modified velocity distribution is then resolved into horizontal and vertical components as is done for values of $z_{ip} > z_m$.

2.1.8 Nonsteady Flow and Peak Velocity Effects

The mathematical models developed in the previous sections are for steady flow and therefore simulate a nominal or mean flow

state. Experimental measurements of rotorcraft wall jet flows, and indeed all rotorcraft induced velocity fields, clearly show the flow fields to be quite unsteady in nature. The data presented in figures 3 through 11 provide examples of the unsteadiness in XV-15 and CH-53E flow fields. Rigorous methods for direct calculation of these types of unsteady flows as a function of time are next to impossible to derive due to the broad range of parameters that influence the problem (i.e., ambient wind, tail rotor, and engine exhaust secondary flows). Therefore, practical solutions to these types of problems are often empirically derived.

The mathematical modeling approach that has been developed to account for peak velocity profile effects, as specifically related to a rotorwash hazard analysis, is based on an empirical curve fit of flight test data. The database utilizes data from the CH-53E helicopter and both the XV-15 and MV-22 tiltrotors as documented in references 5, 23, and 24. Additional data of very limited usefulness were also identified in reference 29 for the XCH-42 (or HLH) rotor on a test stand. In reducing these flight test data, several data reduction approaches and equation formats were investigated to obtain a practical empirical model for calculation of the peak velocity profile. The procedure and curve fit format chosen for use was selected primarily because it resulted in the best correlation of calculated data with flight test data. If additional flight test data become available in the future, it could possibly be demonstrated that a different curve fit format might be more technically desirable for calculation of the peak velocity profile.

The first step in the flight test data reduction approach (or procedure) involved the tabulation of mean and peak profile velocities at both the max- and half-velocity heights above ground level (HAGL). These two height-related parameters were chosen because they are the two fundamental parameters used in calculation of the Glauert profile model. The peak to mean velocity ratio at both of these heights was then calculated and tabulated. These ratios were then plotted as a function of rotor height and distance from the rotor center (DFRC) or distance along the interaction plane (DAIP). Each of these three distance-related values was divided by the rotor radius (R) to nondimensionalize the data before they were plotted. Upon completion of the empirically derived graphs, simple least squares regression curve fits (with limiting features) were obtained for both the single- and twin-rotor data. All data that were curve fit for the single main rotor configuration were obtained along the 270-degree azimuth (out the left side of the helicopter). Data along this worst case azimuth included tail rotor downwash and engine exhaust effects.

The empirical equations generated from the flight test data were then used in the ROTWASH analysis to generate predicted peak velocity profile data for correlation with flight test data.

Following an evaluation of the results, the coefficients of the empirical equations were iteratively adjusted and re-evaluated in a very time-consuming process to obtain the best overall correlation results. The goal of this iterative process was to optimize the correlation for all three rotorcraft at the most critical locations of interest with respect to rotorwash-generated hazards. For example, correlation quality at distances very close to and extremely far away from the tip of the rotor was slightly sacrificed when improved correlation could be obtained just beyond the starting point of the wall jet. The equation coefficients obtained in the final iteration of this development process are the ones used in ROTWASH version 2.1 software.

The empirical equations describing the peak velocity (V_{pk}) at a specified height along the profile as a function of the calculated mean velocity (V_{mn}) are presented as equations 30 through 32 and are plotted in figure 19. Equations 30 and 31 are used for single-rotor (SR) helicopters and all twin-rotor radial azimuths that are not along the interaction plane (i.e., out the left or right wing of a tiltrotor). Along the interaction plane (IPLANE), equation 32 is used to calculate the peak velocity as a function of the calculated mean velocity. Each of the functions is limited such that the peak velocity can never be less than 1.2 times the associated mean velocity.

SR Peak/Mean Velocity Ratio @ Max Velocity Height

$$V_{pk}/V_{mn} = 1.047 + 0.374(r/R) - 0.0423(r/R)^2$$

Limit: If $V_{pk}/V_{mn} \leq 1.2$ Then $V_{pk}/V_{mn} = 1.2$ (30)

SR Peak/Mean Velocity Ratio @ 1/2 Velocity Height

$$V_{pk}/V_{mn} = 1.481 + 0.569(r/R) - 0.0693(r/R)^2$$

Limit: If $V_{pk}/V_{mn} \leq 1.2$ Then $V_{pk}/V_{mn} = 1.2$ (31)

IPLANE Peak/Mean Velocity Ratio @ All Velocity Heights

$$V_{pk}/V_{mn} = 0.713 + 0.304(x_{ip}/R) - 0.0185(x_{ip}/R)^2$$

Limit: If $V_{pk}/V_{mn} \leq 1.2$ Then $V_{pk}/V_{mn} = 1.2$ (32)

Single-rotor peak velocity values not at the maximum or 1/2 velocity heights are interpolated in several different ways using equations 30 and 31. If the point of interest along the profile is between the maximum and 1/2 velocity heights ($z_m < z < z_h$), the peak to mean velocity ratio is obtained by calculating both peak velocity ratios and linearly interpolating between the

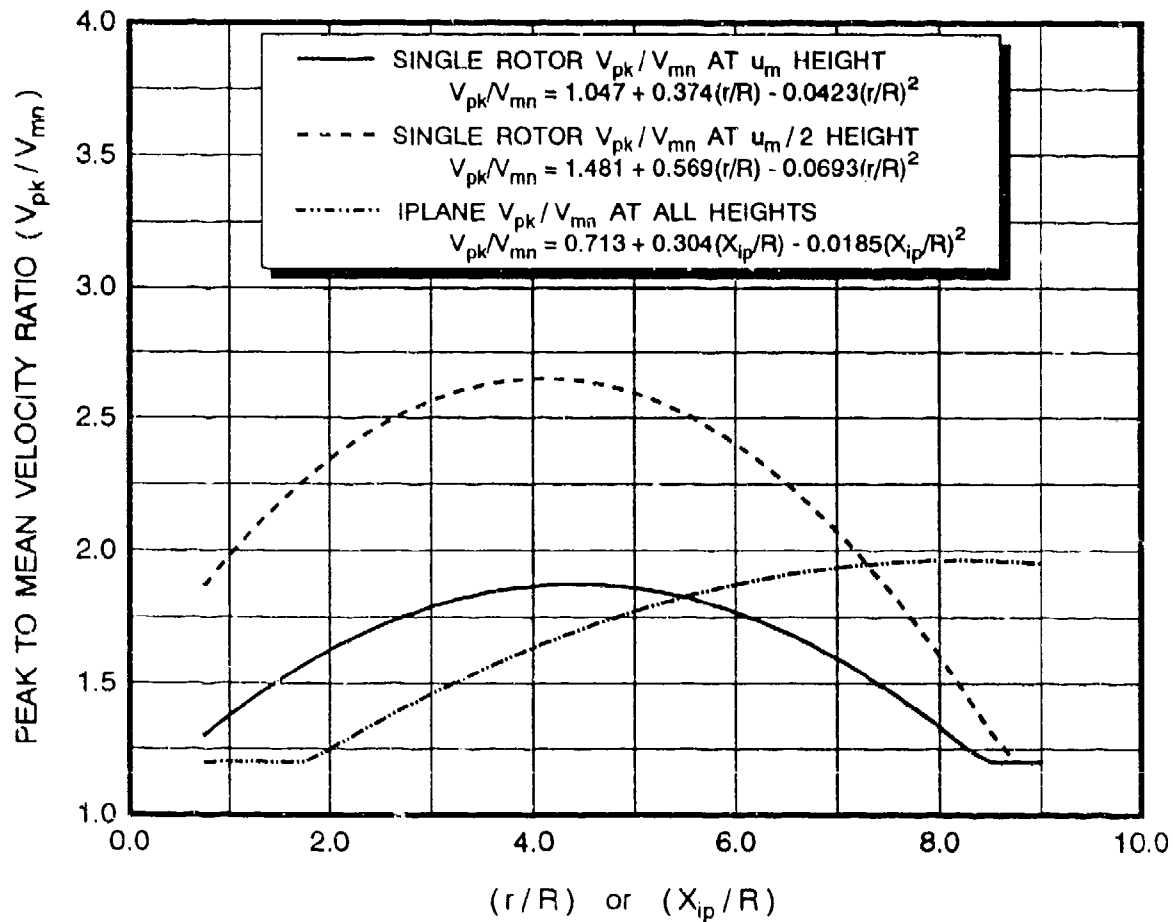


FIGURE 19 EMPIRICALLY DERIVED EQUATIONS USED IN THE CALCULATION OF THE SINGLE-ROTOR AND INTERACTION PLANE PEAK VELOCITY PROFILES

values as a function of the height. This interpolated velocity ratio is then used along with the calculated mean velocity to calculate the peak velocity. If the height of the point of interest is below the maximum velocity height ($z < z_m$), the maximum mean velocity (u_m) is calculated; the boundary layer function of equation 1 is applied; and the V_{pk}/V_{mn} ratio from equation 30 is applied. If the height of interest is greater than the 1/2 velocity height ($z_h < z$), the one-half height peak to mean ratio is calculated and multiplied by the factor (z/z_h) to obtain the peak to mean ratio for the specified height. Along the interaction plane, equation 32 is always applied directly. Therefore, no interpolation is required.

2.1.9 The Effect of Wind on the Wall Jet Velocity Profile

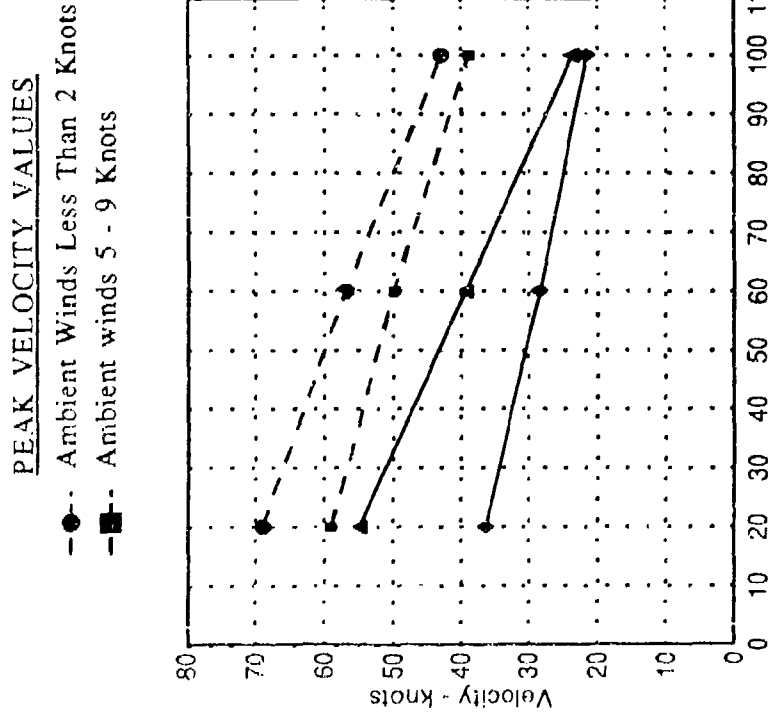
An important step to be taken in bridging the gap between the mathematical models developed in this and previous sections for the wall jet (for a zero wind hover condition) and the ground vortex (the next section) is development of a mathematical model

for prediction of ambient wind effects on outwash profile velocities. The upper operating limit for use of a wind effects mathematical model is approximately 10 knots. At ambient wind velocities greater than 10 knots, the model of the ground vortex becomes the more appropriate analysis tool. In developing the ambient wind model, a review of the database revealed that only a very limited amount of experimentally derived data were available to aid development and correlation of the model. Therefore, the mathematical modeling approach that was chosen is conservative and simple in formulation. References that provide at least some limited data on the effects of wind include one scale model test (reference 30) and four flight test experiments (references 23, 24, 29, 31, and 32).

When first considering the effect of ambient wind, one would expect distortion of the velocity profile through a reduction in the magnitude of profile velocities on the upwind side and an increase in the magnitudes on the downwind side by the velocity of the wind. This effect is generally observed to be valid as a first approximation. However, upon further investigation, this quick rationalization can be deemed flawed in that the wind will also require a forward tilting of the rotor tip path plane. This effect tends to further decrease the profile velocities as measured on the upwind side and increase the profile velocities on the downwind side.

Measured SH-3 test data in references 31 and 32 indicate that, for prevailing winds in the 2- to 4-knot range, the effect of wind on a helicopter is additive; in other words, the upwind side profile velocities are reduced by the ambient wind velocity, and the downwind side profile velocities are increased by the same value. XV-15 peak velocity profile data documented in reference 23 indicate that along the lateral axis (non-interaction plane) the effect of wind results in a significant increase in the spread or the pulsating nature of the measured peak velocity profiles on both the upwind and downwind sides. However, it is extremely hard to tell whether or not the variation in the upwind and downwind velocity profiles may or may not be equivalent to the simple vectorial addition or subtraction of the ambient wind velocity. It is also noted in the text of reference 23 that a limited investigation and measurement of the effect of a 6- to 8-knot wind along the longitudinal axis (or interaction plane) of the XV-15 seemed to have little effect on the velocity profiles.

The most interesting wind-affected data are documented in reference 24. Unfortunately, these CH-53E data are only measured on the less hazardous upwind side of the rotor. Wind velocities during the evaluation varied between 5 and 9 knots, and the data were measured at three rotor heights above the ground (37, 77, and 117 feet). As can be observed for the two gross weights of 45,000 and 56,000 pounds in figure 20, the reduction in mean and peak profile velocities appears to be also a function of rotor

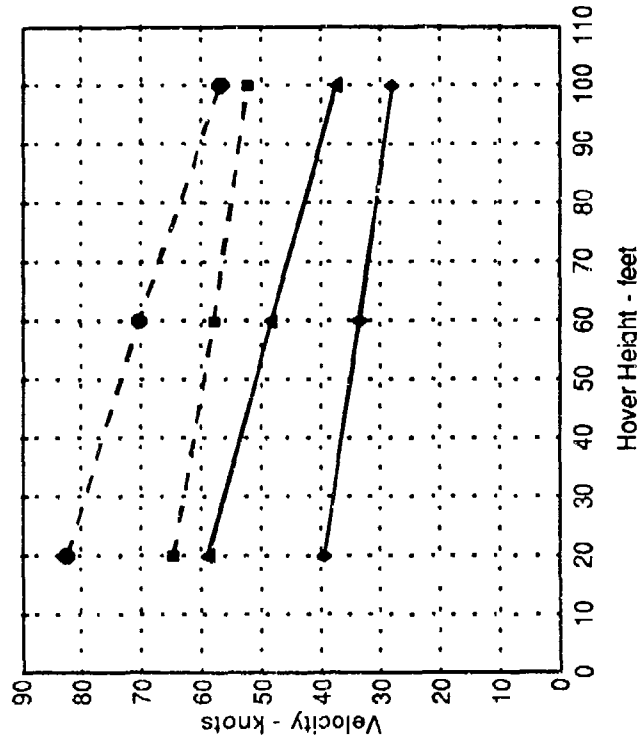


Maximum downwash velocities measured at an ambient upwind position as a function of hover height at 45,000 pounds gross weight.

Source: Reference 24.

MEAN VELOCITY VALUES

Ambient Winds Less Than 2 Knots
Ambient winds 5 - 9 Knots



Maximum downwash velocities measured at an ambient upwind position as a function of hover height at 56,000 pounds gross weight.

FIGURE 20 CH-53E ROTORWASH VELOCITIES AS A FUNCTION OF ROTOR HEIGHT ABOVE GROUND AND GROSS WEIGHT FOR AMBIENT WINDS OF UP TO 9 KNOTS

height above the ground. At the very low rotor height of 37 feet, the measured mean velocity is reduced by almost a factor of two times the ambient wind velocity. At the higher rotor height (117 feet), the reduction in mean velocity appears to equal approximately the measured ambient wind velocity. Comments reported in reference 24 from personnel that walked through the flow field strongly support this measured finding. A recommendation is also made that all U.S. Navy and Marine personnel be notified that approaches should always be made to the CH-53E from an upwind position.

Based on the data from the discussed references, a simple mathematical model has been developed to approximate the effects of ambient wind. This model is based on the conservative assumption that for rotor height to radius ratios (H/R) up to 1.0, upwind profile velocities are reduced by two times the ambient wind velocity and downwind velocities are increased by two times the ambient wind velocity. This factor is reduced as rotor height is increased. At a H/R ratio of 3.0, the factor is linearly reduced to a value of 1.0. Mathematically, this effect is represented as

$$k_{wind} = -0.5(H/R) + 2.5 \quad (33)$$

where k_{wind} is limited to never being less than a value of unity.

In summary, while the discussed approach is not extremely well-founded in experimental validation, it is nevertheless a reasonably conservative approach to take based on available test data for wind velocities of less than 10 knots. At wind velocities greater than 10 knots, the proposed mathematical correction should not be considered valid unless data obtained in the future indicate otherwise. At velocities greater than 10 knots, rotor induced velocities start to become dramatically reduced in magnitude. The subsequent formation of either a ground vortex or trailing vortices results in a rotorwash flow field that has characteristics significantly different than that of the wall jet.

2.1.10 Oblique Impingement of Rotorwash with the Ground Plane

The analysis methodology presented in sections 2.1.2 through 2.1.9 has been based upon an assumption (that is acceptable in most scenarios) that the hovering rotor is contained within a plane parallel to the surface of the ground. Two scenarios where this assumption does not apply are the initial segment of a departure from hover and the final segment of a deceleration to hover where zero forward velocity is obtained. During these very short intervals of time, the pilot is commanding a rotor thrust level in excess of that required to hover. This is because the tip path plane of the rotor is tilted in such a way as to either

command an increase in forward airspeed (a departure from hover to forward flight) or a decrease in airspeed (a flare to a hover from forward flight). A third scenario where the assumption does not apply involves analyses of hovering tiltwing aircraft where the wing is tilted either forward or aft of the vertical. In these situations, the pitch propeller or fan is used to trim out the pitching moment generated by the tilted wing. In contrast, hovering tiltrotor aircraft always have the plane of the rotor parallel to the ground because pitching moments cannot be trimmed out. If the nacelle angle is varied, the pitch attitude must also vary.

Since the methodology developed in sections 2.1.2 through 2.1.9 is not formulated to analyze scenarios involving tilted rotor tip path planes near hover, an effort was initiated in 1989 to develop a simple model for this effect. Technical aspects of this effort were first documented in reference 4. The technical approach used in the modification is generally based upon work documented in reference 20. The basis for the mathematical model includes limited experimental results that are referenced in the memorandum. Unfortunately, no effort was made to document any correlation of results with the mentioned experimental data. The mathematical modeling approach is graphically described through the use of figures 1, 21, and 22. A hovering helicopter (figure 21) at a given gross weight, rotor radius of R feet, and rotor height of H feet generates a mean-induced velocity v_i or dynamic pressure q_A across the rotor disk. If the plane of the rotor is parallel to the ground, the stream tube of air is turned 90 degrees upon impact with the ground and a circular wall jet flowfield forms at position $(r/R)_j$. A three-dimensional view of this process is shown in figure 1. As the horizontal position of the wall jet is increased to a value of $(r/R) > (r/R)_j$, the peak velocity u_m in the wall jet slowly decays. If the rotor tip path plane is tilted slightly, the effect depicted in figure 22 must be modeled. In this scenario, assuming the center of the rotor is in the same position, the impingement point of the stream tube moves further aft as the rotor tip path plane is tilted further forward. This shift of the impingement point also increases the distance $(r/R)_j$, the location where the wall jet begins. Therefore, for any fixed distance $(r/R) > (r/R)_j$, the maximum profile velocity u_m is increased when the tilt angle is increased.

The modifications required to improve the section 2.1.2 through 2.1.9 mathematical model are easy to implement. The user first defines the angle that the tip path plane will be tilted. This angle, ϕ , is then used to calculate the shift in the impingement point of the mean value of the rotor downwash. The corrected length to the impingement point, H_ϕ , is:

$$H_\phi = H/\cos\phi \quad (34)$$

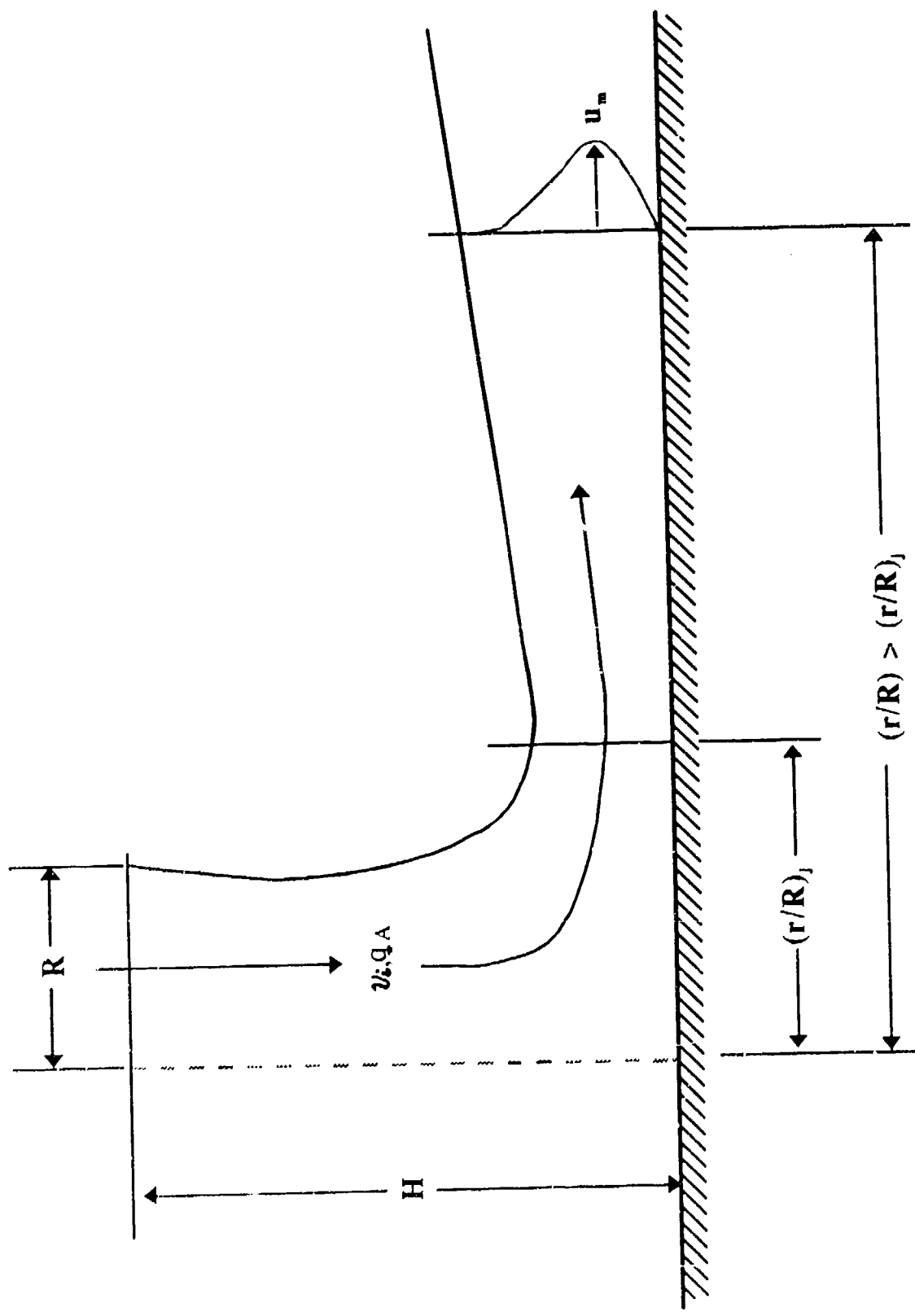


FIGURE 21 ROTORWASH FLOW FIELD CHARACTERISTICS FOR A ROTOR TIP PATH PLANE PARALLEL TO THE GROUND

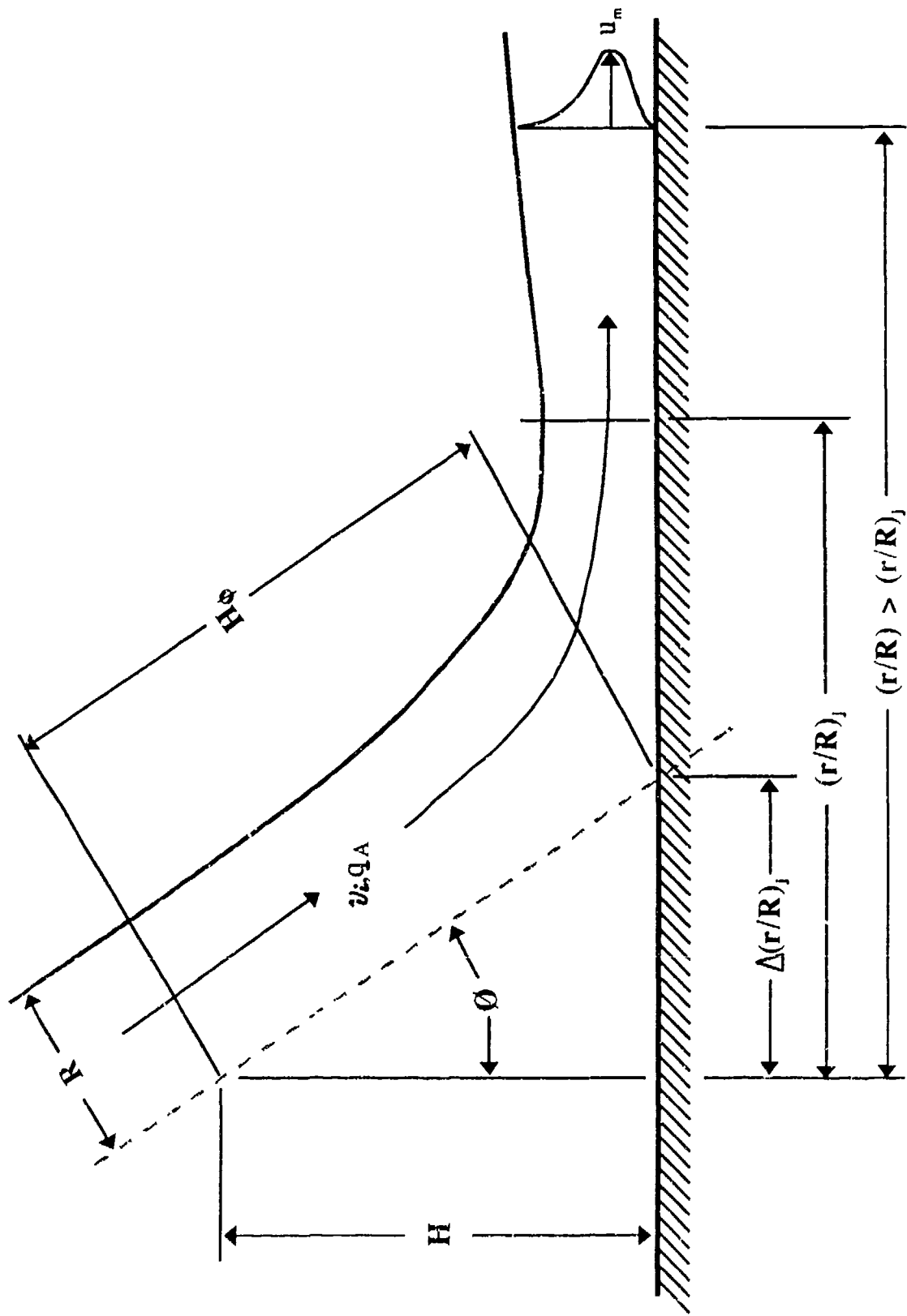


FIGURE 22 ROTORWASH FLOW FIELD CHARACTERISTICS FOR A ROTOR TIP PATH PLANE THAT IS TILTED FORWARD WITH RESPECT TO A PLANE PARALLEL TO THE GROUND

and the horizontal shift in the location of the point is:

$$\Delta (r/R)_j = H(\tan\phi) \quad (35)$$

Analytically, the effect of the parameter H_ϕ is the same as a change in the altitude of the rotor above ground level when the tip path plane is not tilted. The effect of the parameter $\Delta (r/R)_j$ is to shift the location of the formation (and strength) of the wall jet further away from the rotor.

Two practical constraints exist with respect to the use of the tilted tip path plane mathematical model improvements. The first of these constraints is related to a lack of available test data for correlation with the model. At some as yet undetermined impingement angle, the wall jet flowfield will cease to form as a circular (three dimensional) flowfield. At this angle the mathematical model, as described in sections 2.1.2 through 2.1.9, will cease to be valid. Since this critical value is presently unknown, it is recommended that tilt angles greater than 30 degrees be avoided until flight test data become available for correlation. This recommendation is not based on any particular body of data, only experience in the analysis of rotorcraft.

A second constraint on the model exists due to the fact that the model is not designed for use in the analysis of dynamic maneuvers such as a takeoff. The model may be used only during very specific portions of these maneuvers where airspeed is essentially zero (the steady flow assumptions of the model are assumed to be valid if the output data are viewed as snapshots of conditions generated during the maneuver). Also, the model must be used with caution because dynamic flight test data are not yet available for correlation. The segment of the takeoff maneuver that can be analyzed is the initial pushover from hover. At this point in the maneuver, airspeed is still essentially zero and the tip path plane is tilted forward to accelerate the helicopter. This phase of the maneuver also requires an increase in rotor thrust above that required to hover in order to avoid ground contact. Therefore, the user must know something about the gross weight of the rotorcraft and the thrust-power relationships involved to make practical use of the model for this portion of the takeoff maneuver. During a landing, the final phase of the flare maneuver at close to zero airspeed can also be analyzed. During this phase of the maneuver, the rotor is tilted back very close to its maximum position and the thrust level used to maintain altitude while decelerating is at its maximum.

The effect of adding the tilted rotor tip path plane improvements are demonstrated through an example using a Bell UH-1H. A three-view diagram of this helicopter is presented in figure 23. The gross weight of the UH-1H in the example is 9,500 pounds, and the height of the rotor above ground level is 40 feet. Results from

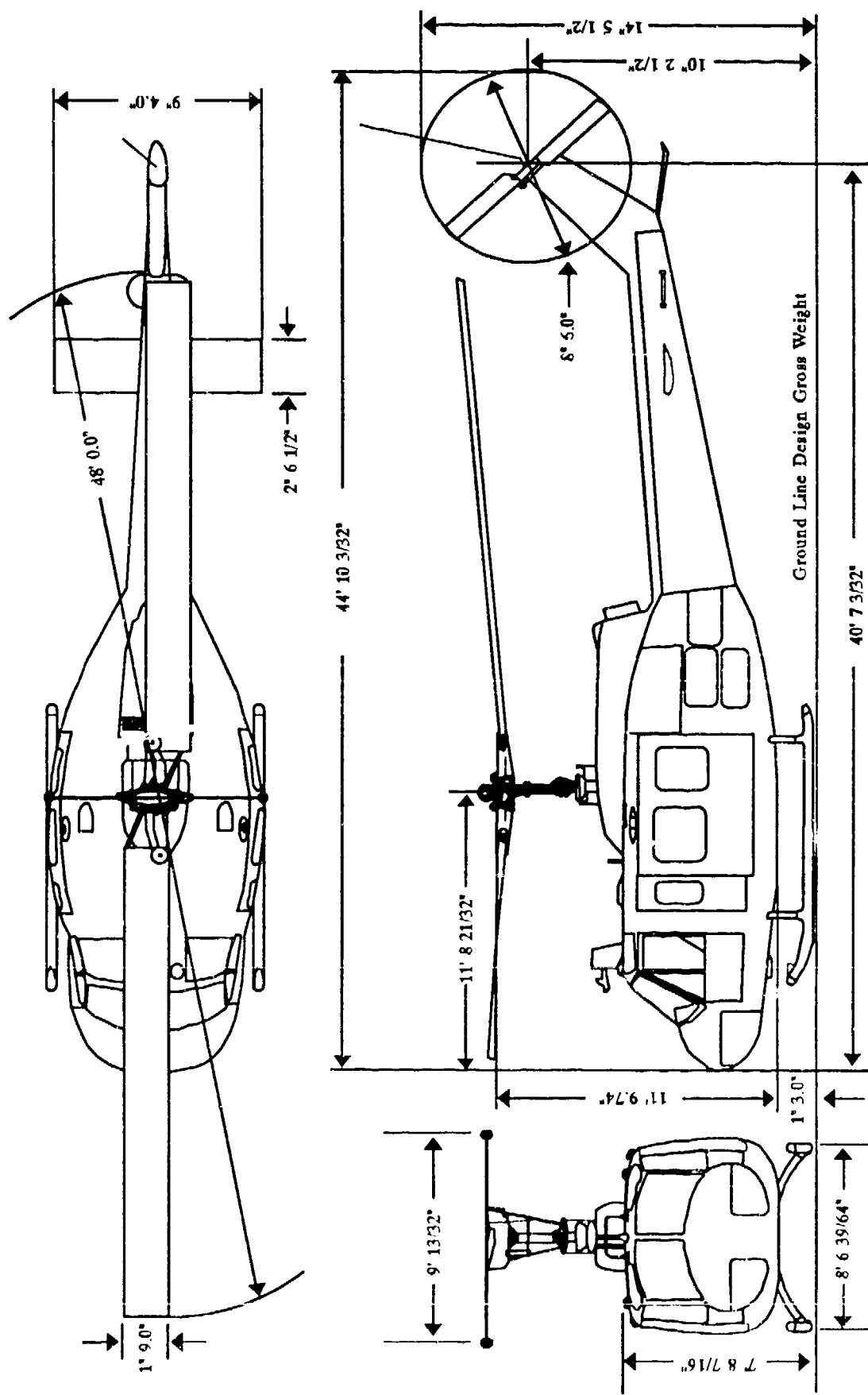


FIGURE 23 THREE-VIEW OF A BELL UH-1H UTILITY HELICOPTER

calculations for hover and the initiation of a takeoff with a 20-degree forward tilt of the tip path plane are presented in figure 24. The hover rotorwash profile characteristics are depicted by the solid lines and are provided at distances of 50, 100, and 150 feet from the center of the rotor. Peak profile

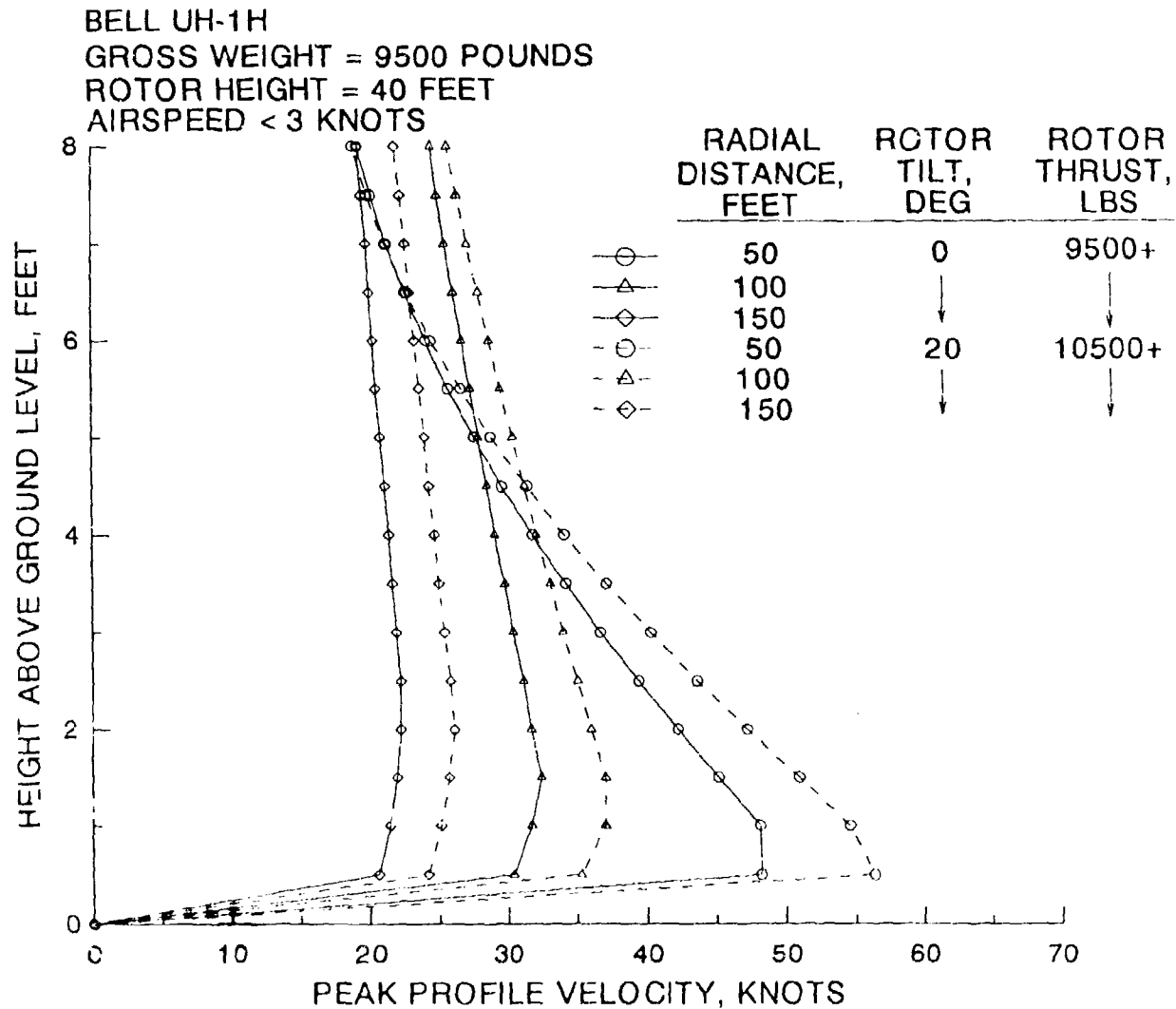


FIGURE 24 UH-1H ROTORWASH CHARACTERISTICS AT RADIAL DISTANCES OF 50, 100, AND 150 FEET FOR TIP PATH PLANE ANGLES OF 0 AND 20 DEGREES

velocities vary from approximately 48 knots at 0.5 feet above the ground to 22 knots at 2 feet for the 50- and 150-feet radial positions, respectively. If the UH-1H accelerates from hover at a tip path plane of 20 degrees, the pilot must increase thrust (through the collective stick) to approximately 10,500 pounds to maintain at least a constant altitude above the ground. Calculated results at the instant the rotor "stabilizes" at the 20-degree position are represented by the dashed lines. Peak profile velocities at the 50- and 150-feet radial positions are increased by approximately 9 and 4 knots, respectively.

2.2 THE GROUND VORTEX

The second major flow field structure that has the potential to produce a rotorwash hazard is the ground vortex. This aerodynamic phenomena forms beneath the upwind edge of the rotor disk when operating at very low rotor advance ratios in ground effect. Situations where the ground vortex may pose a hazard occur at low ambient wind conditions for hovering rotorcraft (i.e., position hold over a point on the ground) or to rotorcraft engaged in low-speed air-taxi.

The ground vortex formation mechanism is simply conceived by superimposing the wind velocity with the wall jet flow, as schematically shown in figure 25. Three-dimensionally, the ground vortex laterally wraps from the upwind position in a smooth arc, finally trailing downwind along both edges of the rotor disk to form a characteristic horseshoe pattern.

Although the occurrence of the ground vortex is well known, the main focus of the majority of studies to date has primarily been on its adverse effects on rotorcraft performance and handling qualities. Experimentally obtained ground vortex data are very limited (almost exclusively flow visualization) and analytical approaches to quantification of flow field structural features (most of which are very sophisticated) are only now being proposed. Experimental research that has been ongoing at both Princeton and Penn State University provides the best guidance for hazard analysis applications.

Curtiss (references 33 and 34) has used model rotors and the Princeton Long Track Facility to generate experimentally the ground vortex and to measure the vortex's effect on rotor moment characteristics. Sun (reference 35), in conjunction with Curtiss, has also recently used the facility to quantify the occurrence and position of the vortex as a function of rotor height above the ground, translational speed, and collective pitch. Although the range of configurations and parameters measured in this experiment are limited, the data do identify several key trends that can be used to aid in the development of a simplified ground vortex hazard model. At Penn State,

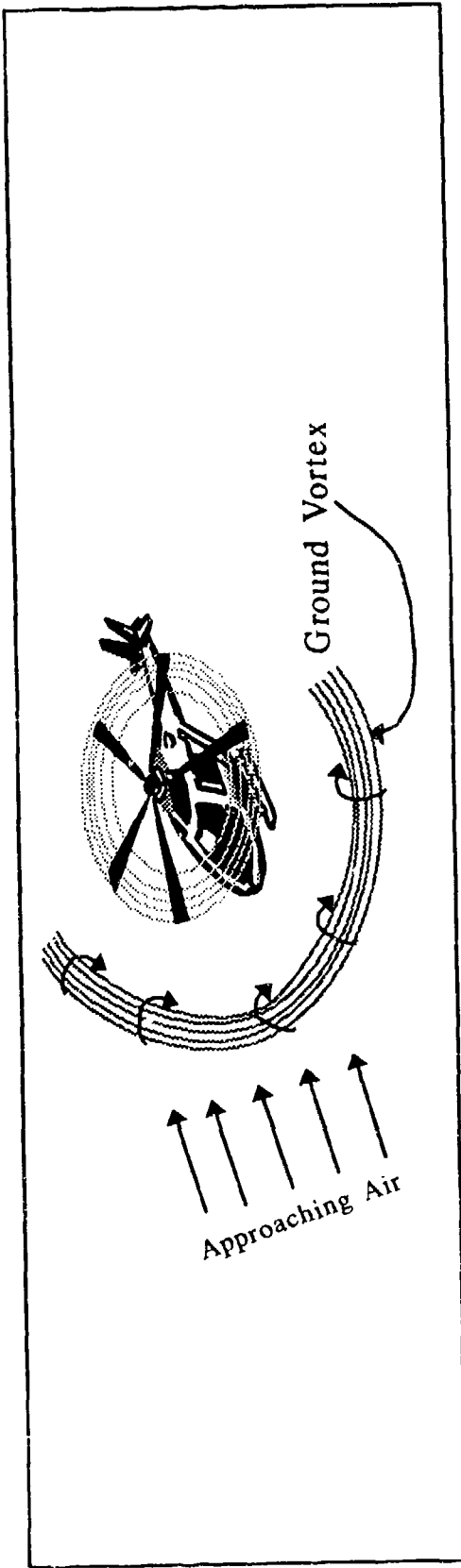
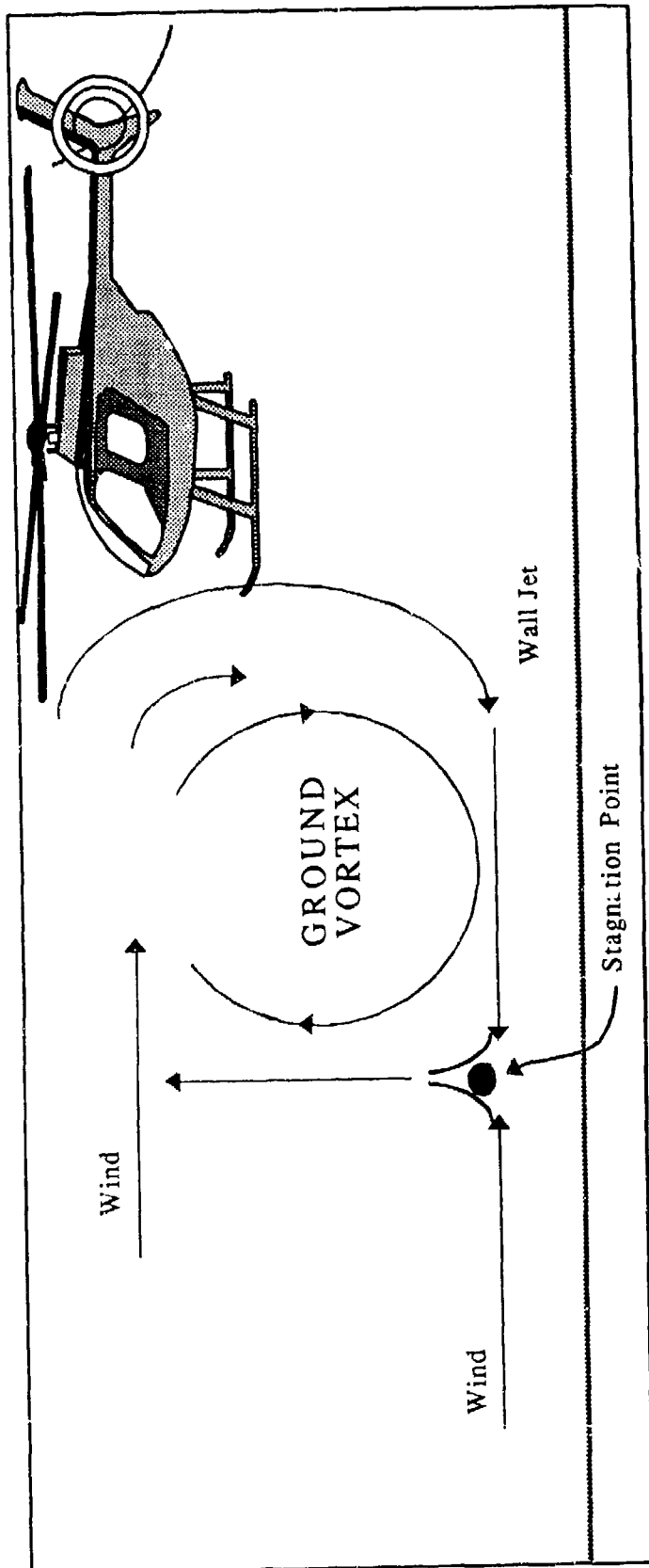


FIGURE 25 GROUND VORTEX STRUCTURAL CHARACTERISTICS

references 36 and 37, Cimbala has utilized a free jet and a ground board in a wind tunnel to investigate both vortex position and frequency content.

Any ground vortex mathematical model must, as a minimum, predict the occurrence of the vortex, its general shape and structure, and the behavior of its position as a function of rotor operating conditions. Using smoke flow visualization, Sun has mapped ground vortex position and identified some of its basic behaviors. This information is applied in this research effort to a simple horseshoe vortex system for hazard analysis purposes.

The experimental data and data trends that aid in prediction of ground vortex position were measured by Sun in terms of the center of recirculation. This vortex position is located forward of the rotor (upwind) in the longitudinal plane of symmetry. The identified trends indicate a systematic behavior with rotor advance ratio (μ) and thrust coefficient (C_T). When plotting the horizontal position of the vortex $(x_g/R)^{0.5}$ as a function of μ/C_T or constant rotor height above ground divided by rotor diameter (H/D), straight line characteristics such as

$$(x_g/R)^{0.5} = C_1 + C_2(\mu/C_T) \quad (36)$$

do approximate the data. The constants C_1 and C_2 are functions of H/D . Trends for the constants are developed from the unfaired data of figures 4.20(a), (b), and (c) of reference 35. With some liberty in setting the lower limits, these trends are

$$C_1 = 1.0 + 1.2086(H/D)^{0.4374} \quad (37)$$

$$C_2 = -0.2786(H/D)^{0.6757} \quad (38)$$

Figure 26 presents these fairings as compared to the actual values chosen from the fairings of Sun's data. The height above ground of the vortex position is observed to vary approximately linearly with rotor advance ratio. Available data do not indicate any significant trends for (z_g/R) with H/D (figures 4.20(d), (e), and (f) of reference 35). The fairing developed for this parameter is

$$(z_g/R) = -10.0\mu + 0.6 \quad (39)$$

The remaining data left to be specified for identifying both vortex occurrence and location are the H/D and μ ranges within

which the ground vortex will occur, as well as the strength of the vortex.

Sun's ground vortex data, consistent with other research data, indicate that the advance ratios where the recirculating flow leads to vortex formation and where the vortex is blown back to disappear beneath the rotor, can be specified as a function of the ratio of the free airspeed to the average flow velocity through the rotor. This parameter (μ^*) is defined as

$$\mu^* = V_f / v_i \quad (40)$$

where V_f is the translational airspeed and, for the low advance ratios of interest, v_i is approximated as the value for hover-induced velocity. Hover-induced velocity is estimated as

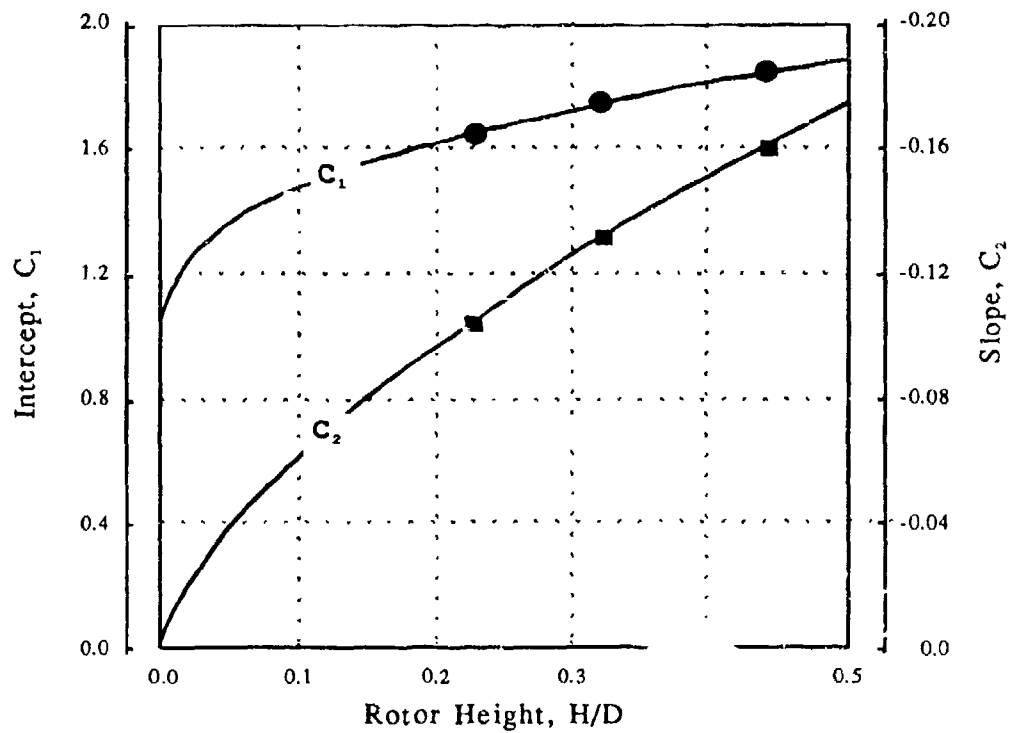
$$v_i = \Omega R (C_T / 2)^{0.5} \quad (41)$$

Figure 27, reproduced from reference 35, documents ground vortex formation boundaries as a function of H/D and μ^* . This information can be used to estimate the probability of occurrence of the ground vortex state for hazard prediction purposes.

Guidelines for determining ground vortex strength are very difficult to establish, because systematic experimental measurements of the ground vortex velocity field and its associated strength have not been made. Sun has performed simplified free wake calculations by assuming ground vortex position (from his measurements) and iterating the vortex strength to achieve positional equilibrium. These results, presented in figure 28, indicate well-behaved trends; however, the calculations are only for one thrust coefficient. Therefore, caution must be exercised if extrapolations are made. To obtain a value for ground vortex strength (Γ_g), Sun's data must be multiplied by a factor that accounts for the data in figure 28 in a non-dimensional manner. This factor, the tip vortex strength, is

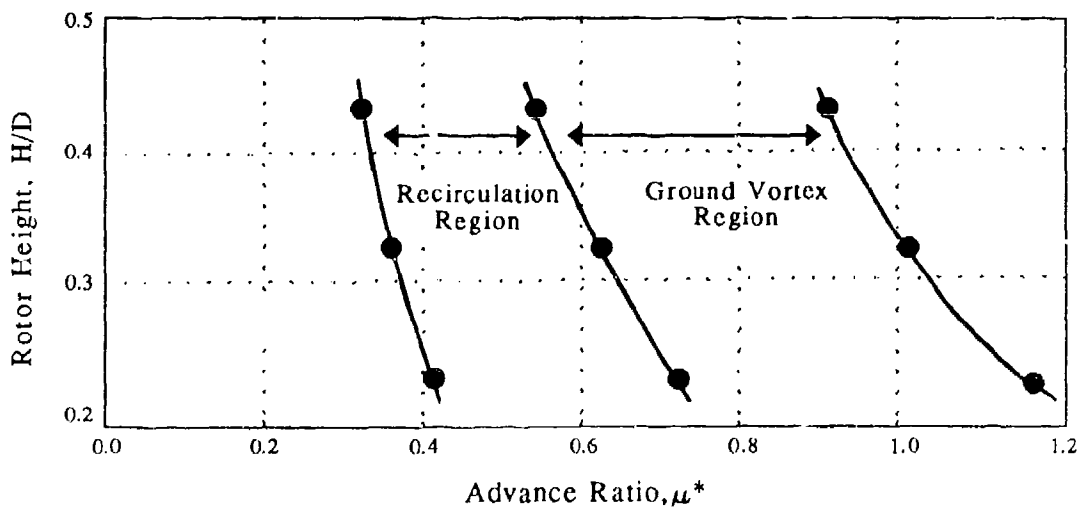
$$\Gamma_{tip} = 2\pi\Omega R^2 C_T / B \quad (42)$$

where B is the number of rotor blades.



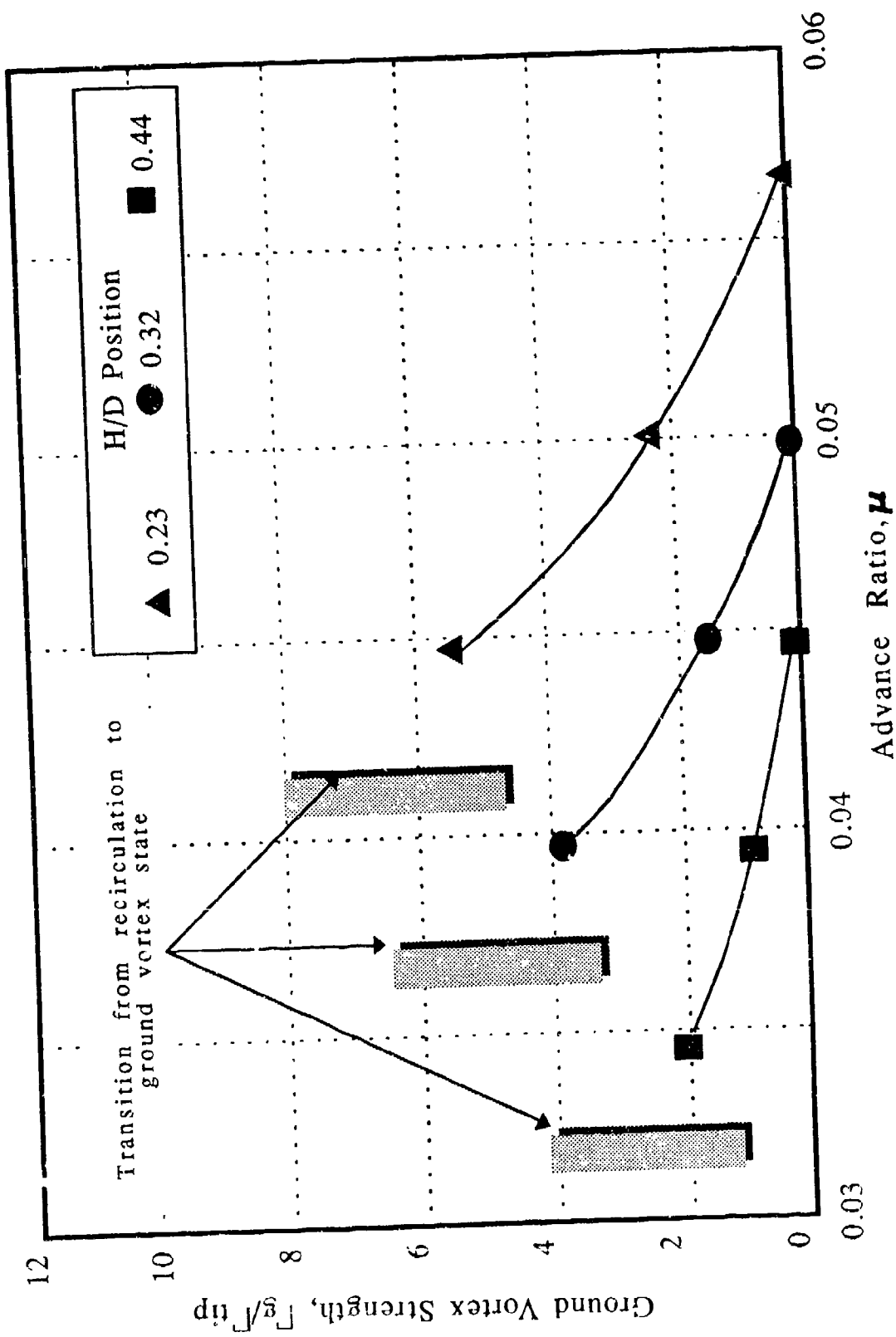
Source: Reference 35.

FIGURE 26 FAIRINGS FOR GROUND VORTEX POSITIONAL CONSTANTS



Source: Reference 35.

FIGURE 27 BOUNDARIES FOR RECIRCULATION AND GROUND VORTEX FLOW REGIMES



Source: Reference 35.

FIGURE 28 CALCULATED GROUND VORTEX CIRCULATION STRENGTH

Using the previously discussed information, though limited in scope, it should be possible to estimate realistically the limiting, or worst case hazard potential. Following establishment of a reasonably accurate prediction for occurrence of the ground vortex, the described positioning data are used to set up the horseshoe vortex geometry described in figure 29. The right-handed coordinate system is oriented such that the z-axis is positive from the system origin at the ground through the rotor disc at the center of rotation, the x-axis is positive aft (downwind), and the y-axis is positive right. Subsequent to an estimate of vortex strength (Γ_g), the induced velocity field due to the vortex and its image system (needed to enforce the condition of no flow through the ground plane) can be calculated using the Biot-Savart law.

Implementation of the Biot-Savart law in Cartesian coordinates is used to calculate the contributions of each straight line element of the ground vortex model. An element is considered to run from point "a" to point "b" such that the direction from "a" to "b" is consistent with the right-hand rule in view of the circulation sense. Point "c" is where the velocity is calculated. With the definitions

$$A = (x_a - x_c)^2 + (y_a - y_c)^2 + (z_a - z_c)^2 \quad (43)$$

$$B = 2 [(x_a - x_b)(x_c - x_a) + (y_a - y_b)(y_c - y_a) + (z_a - z_b)(z_c - z_a)] \quad (44)$$

$$C = (x_a - x_b)^2 + (y_a - y_b)^2 + (z_a - z_b)^2 \quad (45)$$

$$Q = 4AC - B^2 \quad (46)$$

then the magnitude of the velocity induced at point "c" per unit vortex strength is

$$|\bar{Q}| = [1/(2\pi Q)] [2C + B] / (A + B + C)^{0.5} - B/A^{0.5} \quad (47)$$

for $Q \neq 0$. If $Q = 0$, then point "c" is collinear with "a" and "b," and the velocity induced is zero. If the vortex element is semi-infinite in length, i.e., the trailing element of the horseshoe vortex from point "a" that passes through point "b," the velocity magnitude becomes

$$|\bar{Q}| = [1/(2\pi Q)] (2C^{0.5} - B/A^{0.5}) \quad (48)$$

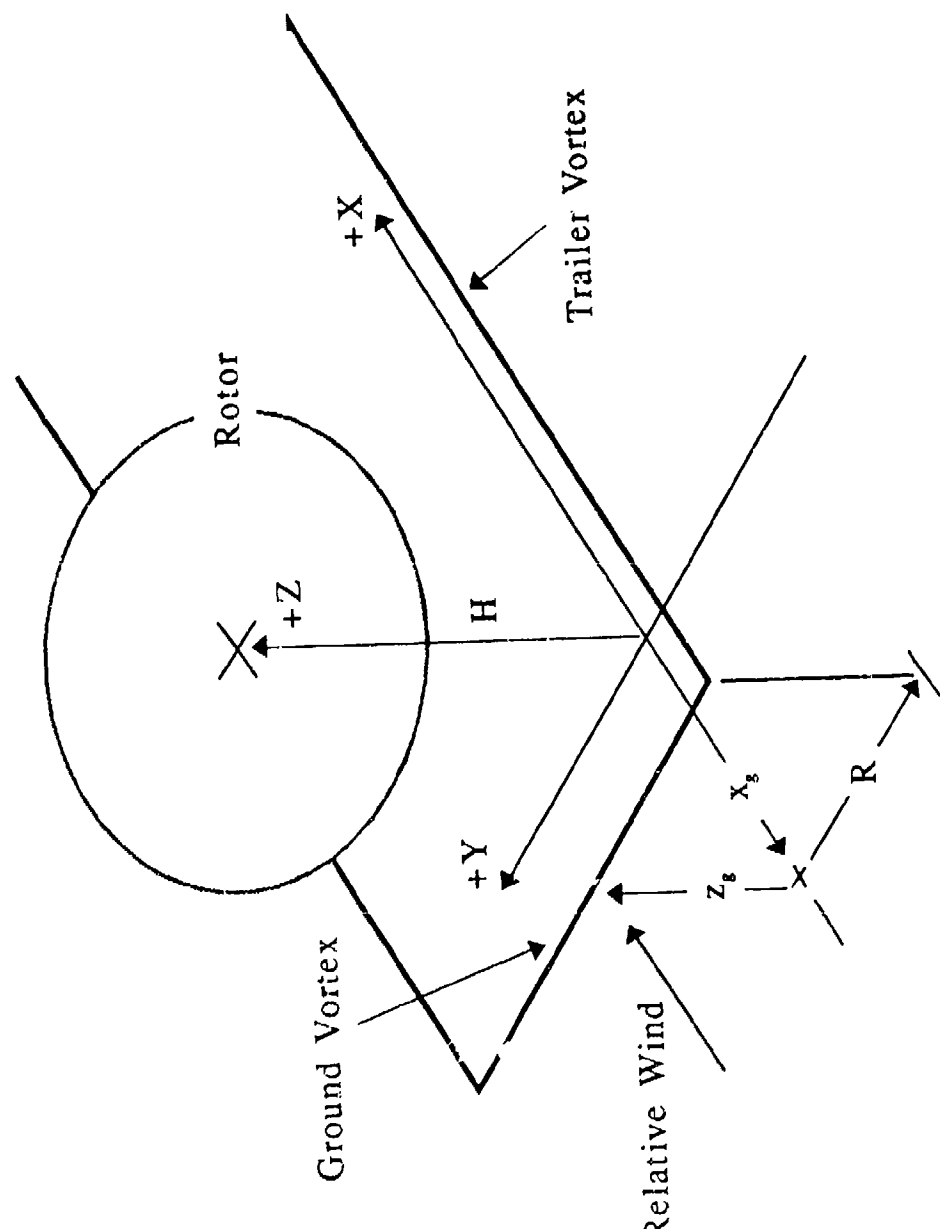


FIGURE 29 HORSESHOE VORTEX GEOMETRY FOR CALCULATION OF GROUND VORTEX HAZARD POTENTIAL

with the same consideration on the value Q . The total velocity is the product of $|\bar{q}|$ and the vortex strength. The Cartesian vector components of the induced velocity are obtained by multiplying the velocity magnitude by the appropriate direction cosines which, from the defined element geometry, are

$$c_x = (y_c - y_b) z_a + (y_a - y_c) z_b + (y_b - y_a) z_c \quad (49)$$

$$c_y = (z_c - z_b) x_a + (z_a - z_c) x_b + (z_b - z_a) x_c \quad (50)$$

$$c_z = (x_c - x_b) y_a + (x_a - x_c) y_b + (x_b - x_a) y_c \quad (51)$$

This formulation is easily applied to the geometry of the ground vortex system for each of the three straight line elements in turn. The summation of each element's contribution is then used to obtain the total vector velocity at the field point of interest. Since the formulation is for a potential vortex, the velocity must be limited for distances approaching the line of action of any of the vortex elements. This can be done by assuming a solid body rotational core for the ground vortex. Without data to estimate the core radius, a value equal to the vortex height above ground is suggested.

In summary, it is recommended that the heretofore described ground vortex model be used only for estimation of worst case hazard potential scenarios. Until further experimental data are obtained and a more detailed correlation of results is conducted, results from this mathematical model must be presumed suspect. Therefore, the model is best considered developmental at this point in time.

2.3 THE FORWARD FLIGHT WAKE

When a rotorcraft's translational airspeed (or the combination of air and wind speed) exceeds the airspeed at which the ground vortex is blown back and under the rotor, the rotorcraft will begin to develop a trailing vortex wake structure much like a fixed-wing aircraft. This velocity field can be estimated using the horseshoe vortex system and the Biot-Savart formulation as described in the previous section. However, a simpler geometry system positioned by the location of the rotor disk itself can be utilized as shown in figure 30. The span of the horseshoe is the rotor diameter ($2R$), and the settling angle of the trailing vortices is based on the approximation that they will initially descend at roughly one-half the mean rotor induced velocity (v_i). The descent angle accounts for the fact that the velocity field (and thus the wake transport) is less at the edges of the trailed wake than at the wake's mid-span.

If the idealized geometry of figure 30 is accepted as adequate for estimating the order of magnitude of the velocity field's potential for creating a hazard, the problem reduces to one of relating the strength of the horseshoe vortex system to simple rotorcraft parameters (which can be found in most introductory helicopter aerodynamic textbooks, i.e., references 38 and 39). Neglecting any rotor tip path plane inclination, the rotor induced velocity is expressed in terms of the dimensionless inflow parameter λ , where

$$\lambda = v_i / \Omega R \quad (52)$$

and the advance ratio μ , which is

$$\mu = V_f / \Omega R \quad (53)$$

In equation 53, V_f is the translational airspeed of the rotor (or rotorcraft). The mean value of induced velocity (or inflow) through the rotor can be derived from momentum theory to be

$$\lambda = \frac{C_T / 2}{(\lambda^2 + \mu^2)^{0.5}} \quad (54)$$

Thus, knowing the thrust coefficient (C_T), the advance ratio (μ), and the inflow ratio (λ), v_i can be calculated from equations 52 and 54 (where $v_i = \Omega R \lambda$) by using an iterative calculation technique.

The settling angle of the trailing vortices is defined from the horizontal and vertical velocities in terms of μ and λ . The angle χ , as measured from the horizontal using the previously discussed assumptions, is

$$\chi = [\tan^{-1}(\lambda/\mu)]/2 \quad (55)$$

Consistent with the horseshoe vortex model, the rotor is now viewed as a simple wing. Considering the strength of the horseshoe vortex to be uniform everywhere along its length, or equivalently assuming the span loading of the wing to be uniform, the strength (Γ_w) as based on gross weight (GW) is

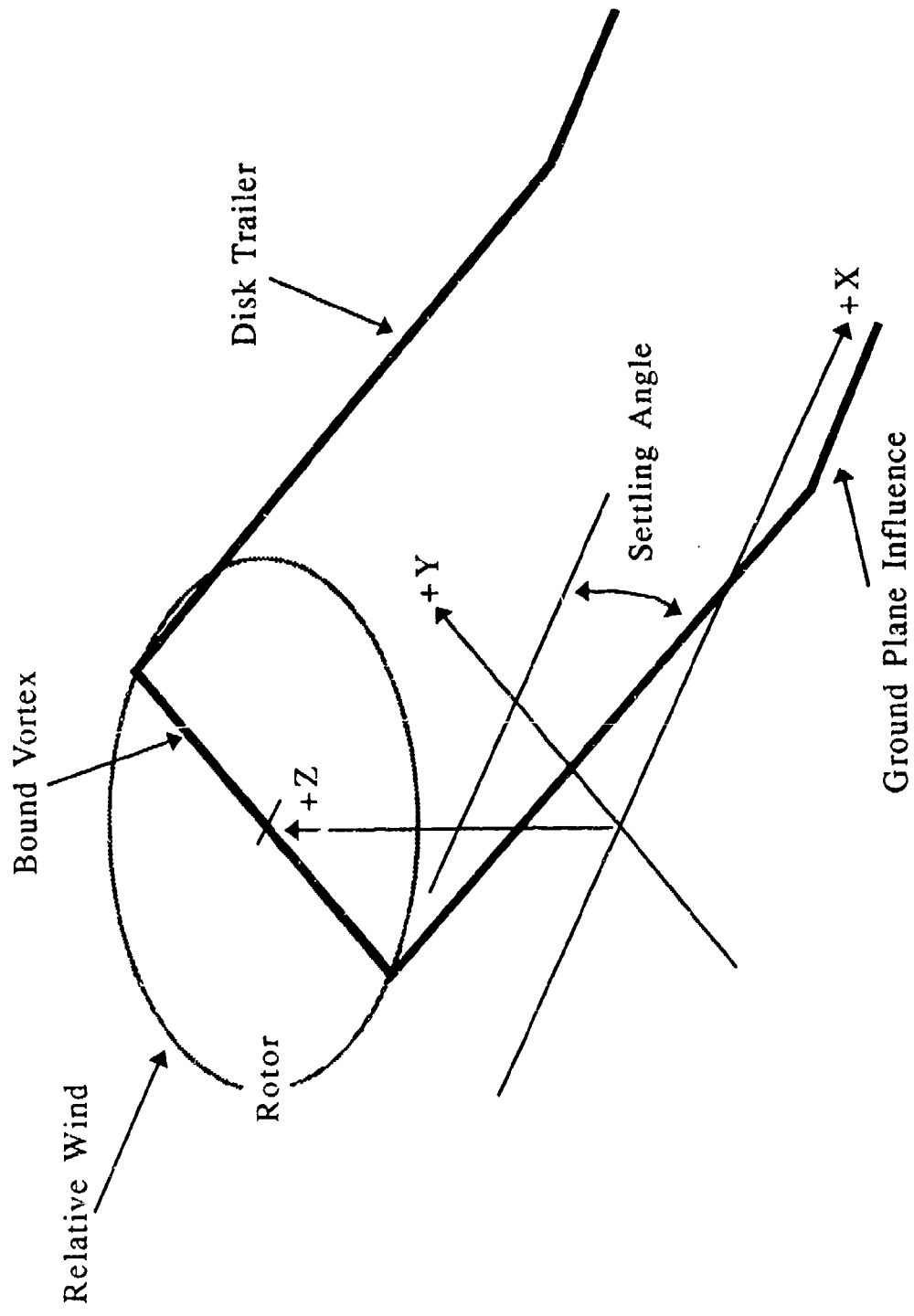


FIGURE 30 HORSESHOE VORTEX GEOMETRY FOR CALCULATION OF FORWARD FLIGHT WAKE HAZARD POTENTIAL

$$\Gamma_w = GW / (2\rho V_f R) \quad (56)$$

Substituting the definition of thrust coefficient,

$$C_T = T / [\rho \pi R^2 (\Omega R)^2] \quad (57)$$

and assuming that rotor thrust (T) is approximately equal to rotorcraft gross weight (GW), the vortex strength is

$$\Gamma_{wp} = \frac{\pi R (\Omega R)^2 C_T}{2 V_f K_e} \quad (58)$$

where K_e is an empirically determined efficiency factor analogous to Oswald's efficiency factor in the induced drag equation for fixed-wing aircraft. This factor accounts for the fact that lift distribution across the rotor is not the ideal elliptical distribution. For single main rotor helicopters, this value has been determined to be approximately 0.625 from work related to that presented in reference 10. Γ_w is washed out at very low airspeeds as a simple linear function when the settling angle exceeds approximately 8.0 degrees. At settling angles greater than this value, experimental data confirm that vorticity in the wake has difficulty forming two distinct trailers. The washout function is represented by equation 59 and its influence occurs at airspeeds typically less than 45 knots.

$$\Gamma_w = \Gamma_{wp} (1.0 - (\chi - 8.0) (0.065)) \quad (59)$$

In conclusion, the final model is equivalent to requiring the horseshoe vortex system to produce a value of downwash at the center of the rotor disk equal to the mean value over the disk as required by momentum theory and then corrected for lift distribution and low airspeed effects.

The induced velocity in the flow field can now be estimated using the defined geometry, calculated strength, and the Biot-Savart law as presented in the previous section. As for the ground vortex model, an image system must be included. Another consideration is to provide for turning of the trailers if their descent angle is large enough to cause them to impinge the ground in the near field. At low translational airspeeds, where descent angles are calculated with the ROTWASH mathematical model to be greater than 20 degrees, the trailing wake structure will in all

probability not yet be fully formed. Therefore, care must be exercised in applying the model at very low rotor translational airspeeds.

Flight test results, presented in section 3, demonstrate that the detailed rotor wake structure does organize itself rapidly into two distinct trailers containing the bulk of the system vorticity. A more complete model of this process would need to account for the development history of the trailers, their non-potential radial strength distributions, the development of a viscous core region, and the rate of decay of the trailers for increasing distances aft of the generating rotorcraft. These refinements are not included in the present mathematical model.

2.4 CONCLUDING REMARKS

In conclusion, it must be noted that the simplified models for the ground vortex and the disc edge trailing vortices are specifically developed and implemented for use with a single main rotor configuration. Application to twin-rotor configurations (either side-by-side or tandem) is possible but highly dependent on the characteristics of the particular configuration. For instance, the degree of rotor overlap and the angle of the translational velocity relative to the plane connecting the dual rotor shafts will influence whether or not the rotors can be treated independently, as a single rotor, or must be treated as a much more complex model.

The final test of the validity of each of the models presented in section 2 is based on each model's ability to correctly predict flight test or model test results. A description of that effort is presented in the next section.

3.0 VALIDATION OF ROTORCRAFT DOWNWASH FLOW FIELD MODELS

The usefulness of any predictive methodology or mathematical model is directly related to its ability to predict test cases accurately. This statement is particularly true when a complex problem is analyzed using a methodology that must be based on a simplified mathematical description of the problem. The prediction of rotorwash flow field characteristics is an example of this type of problem. Therefore, rotorwash flow field mathematical models described in section 2 have been validated extensively using most available helicopter, tiltrotor, and tiltwing flight test and model data from numerous sources. However, as a result of space limitations, documentation of the correlation effort with flight test data is primarily limited to five specific types of rotorcraft: the Sikorsky CH-53E and SH-60B helicopters, the Bell XV-15 and Bell/Boeing MV-22 tiltrotors, and the Canadair CL-84 tiltwing. These specific rotorcraft have been chosen for documentation for two primary reasons: (1) flight test data for these five rotorcraft are of higher quality than data from all other known sources, and (2) there are more data available for these specific rotorcraft than most of the other types of rotorcraft for which data are known to exist. Table 1 provides a summary of the known-to-be-available sources of rotor outwash profile flight test data, the types of rotorcraft for which the data are available, and a subjective or relative ranking of the quality of the data sources in comparison with one another. This subjective comparison is based upon factors such as the type of sensor used to measure the rotorwash flow field characteristics, the methods of data reduction employed, the quantity of data, and comments from the experimenters as to the quality of the data that are documented.

During the process of correlating the mathematically predicted rotor outwash profile characteristics with flight test data, it was discovered that two general guidelines should be followed when evaluating the quality of all correlation results (Mr. D.J. Harris, author of five of the flight test data reports listed in table 1, was most influential in helping to establish these guidelines). The most important guideline is that all fundamental mathematical modeling features of the ROTWASH analysis approach (which is based on steady flow momentum theory assumptions) and all improvements made to that approach be adopted only upon completion of correlation with as broad a database as possible. This guideline results from the acknowledgement by several researchers and data sources that the acquisition of rotorwash flight test data is not, in general, a highly repeatable process due to the unsteady nature of the rotorwash flow field environment. As discussed in section 2.1, the dynamics of the flow field are extremely susceptible to the effects of small changes in ambient wind conditions, rotorcraft attitude, and rotor height above ground level (RHAGL). The effects of additional unsteady secondary flows into the primary rotorwash flow field, such as turboshaft engine exhaust and tail

TABLE 1 KNOWN SOURCES OF OUTWASH PROFILE FLIGHT TEST DATA FOR ROTORCRAFT

RANK*	REFERENCE LIST NUMBER	TYPE OF ROTORCRAFT	GENERAL COMMENT
1	24	Sikorsky CH-53E, RH-53D	Mean and peak velocity profile data were acquired, reduced, and documented using the ion-beam deflection anemometer and statistical methods. Both main rotor thrust and the helicopter position were maintained constant during testing through the use of a load cell and a tether line from the ground to the cargo hook. A large number of test configurations were evaluated.
2	23	Bell XV-15 (Tiltrotor)	Mean and peak velocity profile data were acquired, reduced, and documented using the ion-beam deflection anemometer and statistical methods. Gross weight was allowed to vary some during testing.
3	5	Bell/Boeing MV-22 (Tiltrotor)	Mean and peak velocity profile data were acquired, reduced, and documented using the ion-beam deflection anemometer and statistical methods. Only three wheel heights at one interaction plane station were evaluated.
4	11 (reference 78 also provides extensive new data)	SH-60B	Mean and peak velocity profile data were acquired, reduced, and documented using both the ion-beam deflection and cup and vane mechanical anemometers simultaneously. This was primarily a sensor evaluation experiment. Data were acquired at two radial locations for one height AGL only.
5	40,31,32	Canadair CL-84 (Tiltwing)	Only mean velocity profile data were acquired, reduced, and documented using the ion-beam anemometer and statistical methods (reference 40). Other mean velocity data were acquired as a function of numerous variables using a mechanical anemometer (references 31 and 32).
6	29	HLH Rotor (XCH-62A)	Mean and limited peak velocity profile data were acquired, reduced, and documented using the ion-beam deflection anemometer and statistical methods. The rotor was only evaluated at one height above the ground, because the evaluation was conducted on a rotor test stand.

* Order of rank is based on a subjective quality comparison.

TABLE 1 KNOWN SOURCES OF OUTWASH PROFILE FLIGHT TEST DATA
FOR ROTORCRAFT (Continued)

RANK*	REFERENCE LIST NUMBER	TYPE OF ROTORCRAFT	GENERAL COMMENT
7	30, 31, 41	SH-3	Only mean velocity profile data were acquired. Statistical methods were not used in data reduction. Velocity sensors are incapable of measurement to the same level of accuracy as the ion-beam deflection anemometer. Data from reference 41, while being of possibly higher quality, were very limited in quantity.
8	42	OH-58A, OH-6A, AH-1G, UH-1H, UH-1M, CH-47, CH-54	Only mean velocity profile data were acquired. Profiles measured do not have expected profile shape. Profiles decay inconsistently with an increase in distance. Statistical methods were not used in data reduction. Mechanical velocity sensors are incapable of measurement to the same level of accuracy as the ion-beam deflection anemometer. Atmospheric conditions were unreported. Data were acquired at different locations.
9	6, 7, 8, 9	B206, B206L, B222, R22, A109, MD500, AS-350, AS-355, UH-1, S-76, BO-105, BK-117, AS-365, B212/412, B214ST, AS-330	Data were of limited usefulness because only mean velocity data were obtained at one height above ground level; no statistical data reduction process was used; and the sensor was a mechanical type with a very poor frequency response.
10	43, 44, 45	H-13, H-21, H-34, H-37, UH-1A, CH-47, CH-54	Data were of very limited usefulness due to the data reduction process, use of a mechanical sensor, and the age and format of data presentation.

* Order of rank is based on a subjective quality comparison.

rotor downwash (or sidewash), is also known to significantly affect rotorwash velocity profiles. Examples of the differences in magnitude between measured flight test mean and peak velocity profiles for both the CH-53E and the XV-15 were previously presented in figures 10 and 11 of section 2.1.1. This unsteady

effect was also observed in the time history and power spectral density graphs of outwash velocity at specific heights above ground level (HAGL) as were presented in figures 3 through 9.

The second guideline that was suggested and accepted was that no attempt should be made to model the peak velocity profile directly. This statement did not mean that the modeling of the peak velocity profile was not important to the development of a rotorwash hazard analysis methodology and the subsequent definition of separation guidelines. However, it acknowledges the reality of the extremely complex process by which the peak velocity profile is generated and then measured for analysis. Therefore, in the mathematical model development process, as was discussed in section 2.1.8, peak velocity profiles were developed by using empirically derived equations.

3.1 CH-53E HELICOPTER VELOCITY PROFILE CORRELATION

The Sikorsky CH-53E helicopter is the largest heavy-lift helicopter developed in the western world and can lift payloads up to approximately 32,000 pounds. A three-view profile of this helicopter is presented in figure 31. CH-53E specific input data parameters required to execute the ROTWASH analysis program are defined in table 2. The correlation of predicted rotorwash characteristics with flight test data was conducted using the data documented in reference 24. All of these flight test data were obtained at what is considered to be the worst case azimuth for the CH-53E. This azimuth is the 270-degree radial (to the pilot's left). It is important to note from the three-view drawing that the canted tail rotor and two of the three engine exhausts are considered to be highly influential secondary flows when profile measurements are made along the 270-degree azimuth. The eight stations along this radial that data were measured are diagramed in figure 32. Ambient winds during testing were measured at less than 3.5 knots. Variations in CH-53E gross weight (GW) and rotor height above ground level (RHAGL) that were evaluated are 45,000, 56,000, and 70,000 pounds and 37, 77, and 117 feet, respectively. This test matrix is presented in a more comprehensive format in table 3, along with each corresponding figure number for the comparison of flight test data with the calculated ROTWASH data.

Correlation of flight test and calculated data for the 70,000 pound gross weight configuration is presented in figures 33 through 35 at rotor heights above ground level of 37, 77, and 117 feet, respectively. Data presented in these figures generally indicate that the calculated mean velocity profile is slightly less in magnitude than the measured flight test profile at all three rotor heights. However, empirical equations that were developed to estimate the peak velocity profile generally result in a calculated profile being very close to or slightly less in magnitude than the flight test data. The radial stations

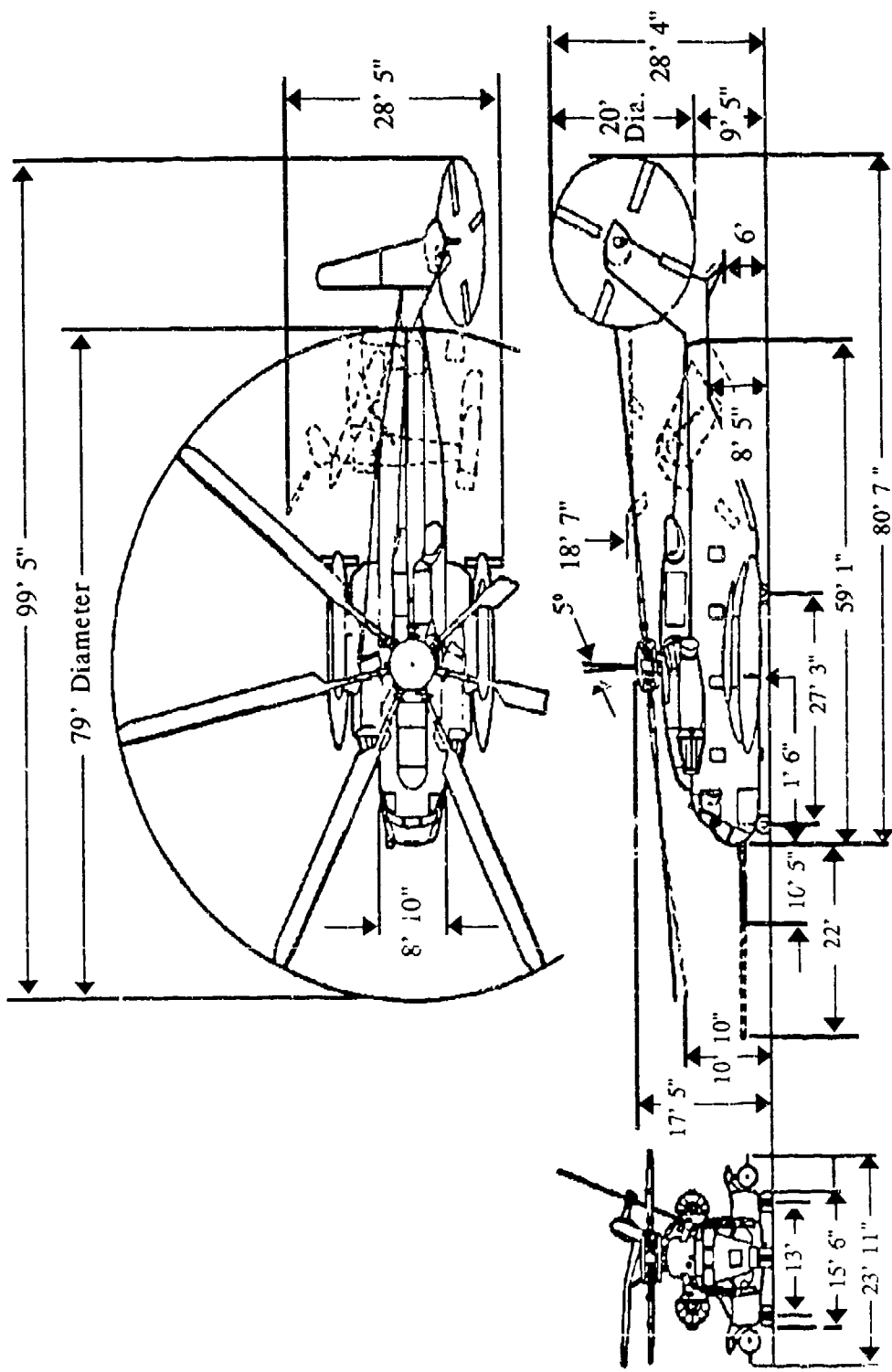


FIGURE 31 THREE-VIEW DRAWING OF THE SIKORSKY CH-53E

TABLE 2 ROTWASH PROGRAM INPUT DATA REQUIREMENTS

Rotorcraft Parameters	CH-53E	XV-15	MV-22	CL-84	SH-60B
Number of Rotors	1	2	2	2	1
Distance Between Twin Rotors (feet)	-	32.2	46.6	20.6	-
Rotor Radius (feet)	39.5	12.5	19.0	7.0	26.85
Gross Weight (pounds) (Maximum During Testing)	70,000	13,100	40,300	11,540	20,050
Download Factor (Percent of Gross Weight)	5.0	13.0	13.0	2.5	3.0
Wheel to Rotor Height (feet)	17.0	12.5	21.0	15.2	12.3

with the poorest correlation at all gross weights are generally inside, or almost inside, the radius of the rotor. Highly accurate prediction of velocity profiles in this transition region is probably not possible with this mathematical modeling approach (refer to section 2.1.5). This is because the mathematical model has to assume a generalized profile shape due to the aforementioned impracticality of modeling the influences of injected masses of air from secondary flows (such as engine exhaust, tail rotor downwash, nonlinear induced velocity distribution across the rotor disk, and the loss of mass flow due to recirculation of a percentage of the downwash velocity back up through the center of the main rotor). It is also important to note that any statistical comparison of results is somewhat meaningless due to the nature of the acquired data. For example, the flight test peak velocity profile is composed of the peak velocities measured at each height above ground over a long period of time. Therefore, this profile does not represent an "average" peak velocity profile at any one specific point in time.

Correlation also indicates that at almost all rotor heights and station positions (except for the 177.8-foot station), the calculated profile maximum velocity height is less than the almost constant value of 3 feet indicated from the flight test data. Since flight test data were measured at only two heights in the boundary layer region (approximately 1.5 and 3.0 feet), it is believed that the profile shape faired to the flight test data may not be particularly accurate due to the lack of sufficient data to interpolate the true shape of the boundary layer. Theory and experimental results clearly indicate that as the outwash flow slows down and travels further from the center of the rotor, the boundary layer becomes thicker and the maximum velocity

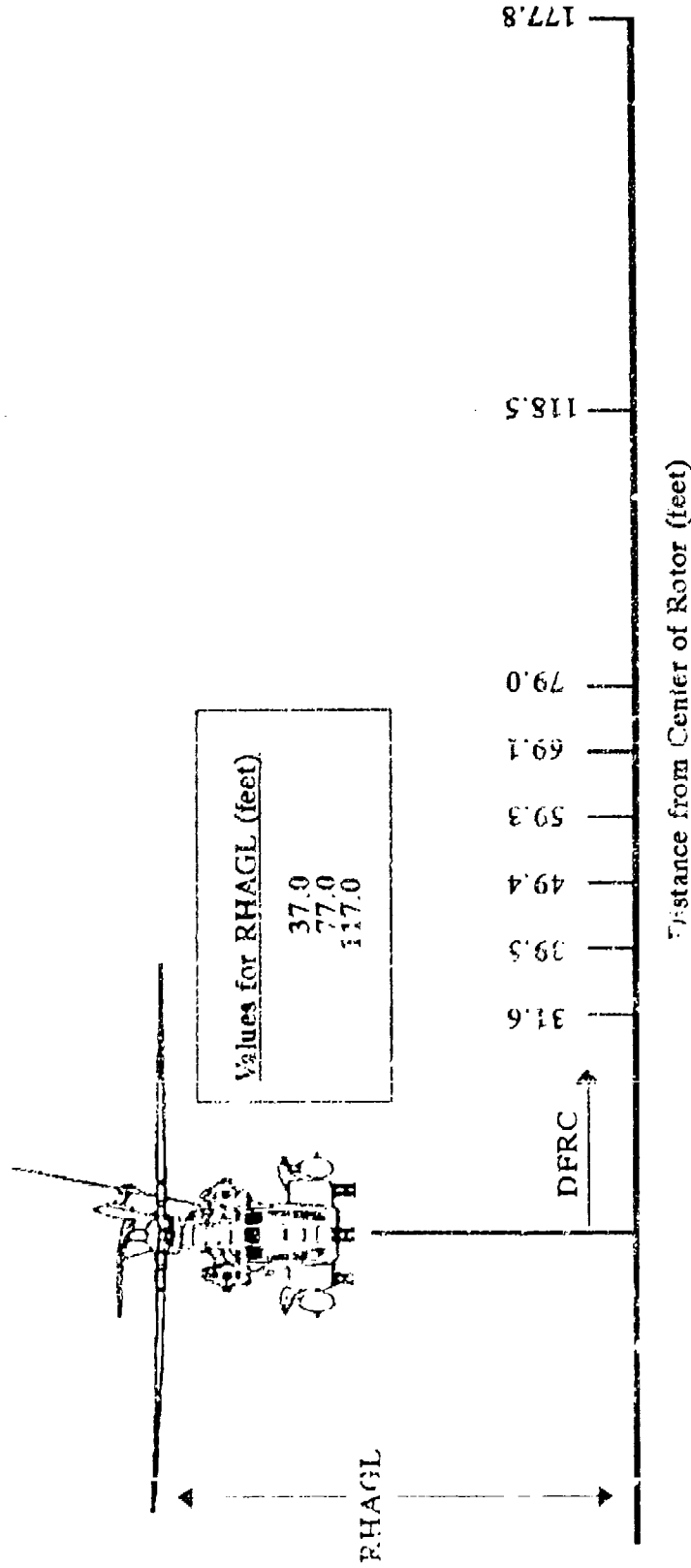


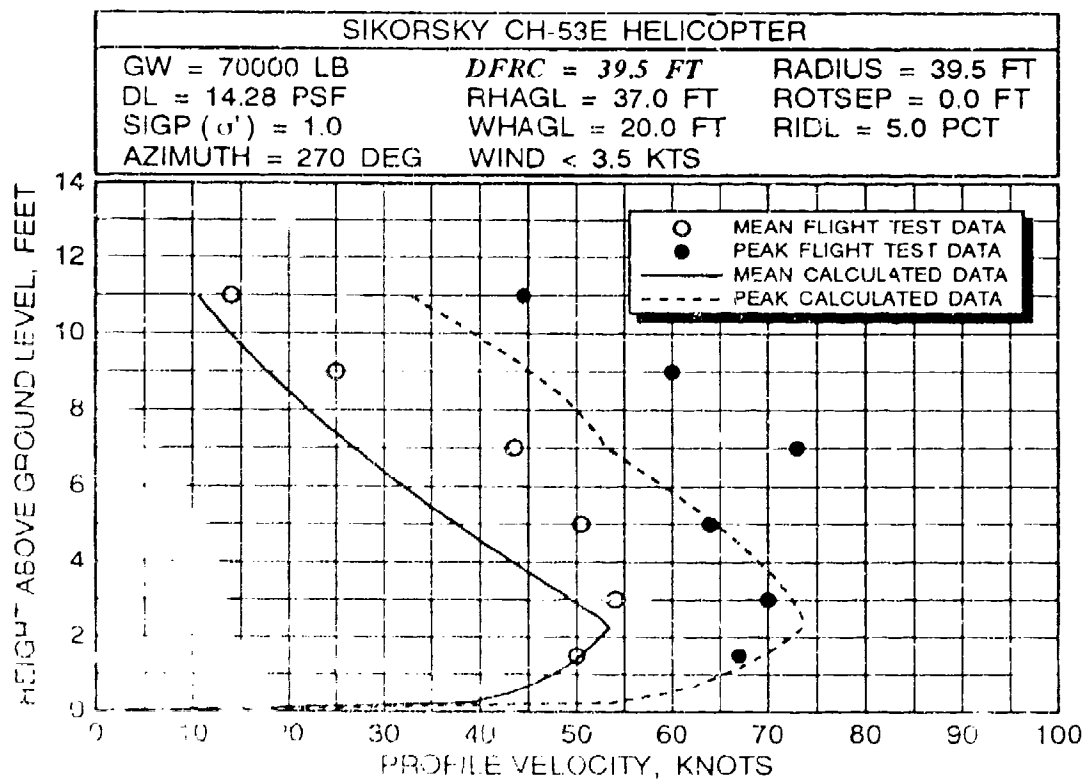
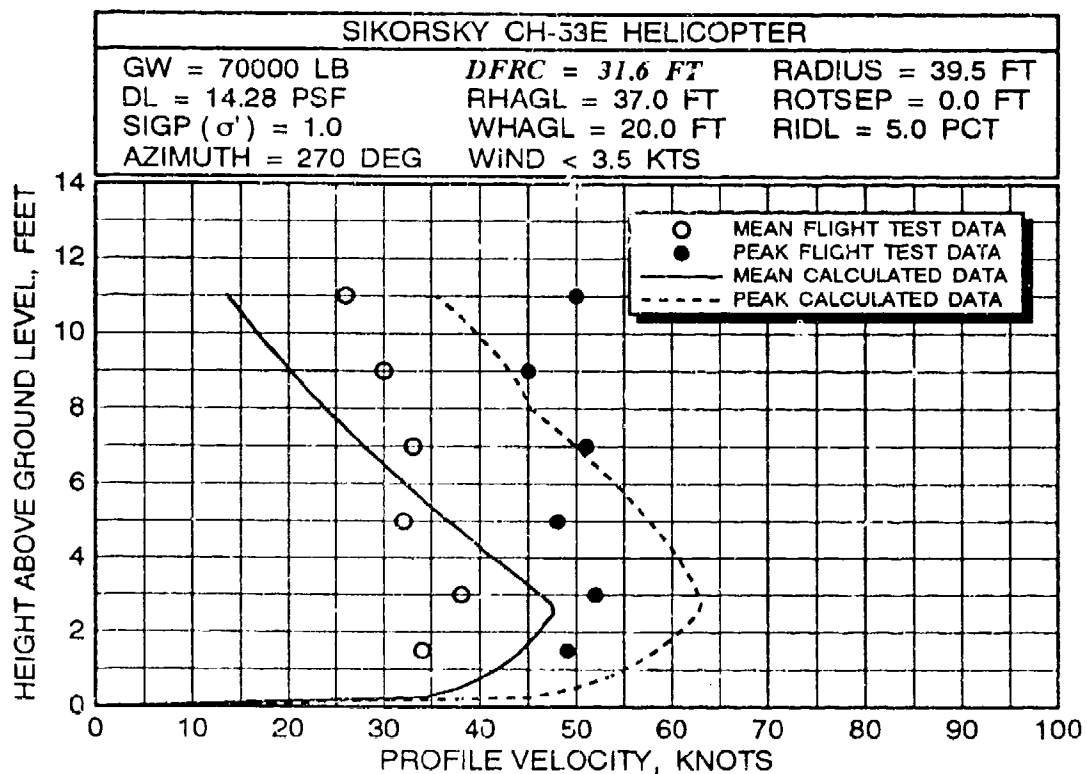
FIGURE 32 CH-53E FLIGHT TEST DATA MEASUREMENT LOCATIONS

TABLE 3 EVALUATION MATRIX FOR CH-53E FLIGHT TEST/MATHEMATICAL MODEL DATA CORRELATION

FIGURE NUMBER	GROSS WEIGHT (lb)	DISK LOADING, (lb \cdot ft 2)	ROTOR HEIGHT (feet)	DISTANCE FROM ROTOR CENTER (DFRC) ¹ (feet)
33, B2	70,000	14.28	37.0	31.6, 39.5, 49.4, 59.3, 69.1, 79.0, 118.5, 177.8
34, B3	70,000	14.28	77.0	31.6, 39.5, 49.4, 59.3, 69.1, 79.0, 118.5, 177.9
35, B4	70,000	14.28	117.0	31.6, 39.5, 49.4, 59.3, 69.1, 79.0, 118.5, 177.8
36	56,000	11.42	37.0	59.3, 118.5
B5	56,000	11.42	37.0	31.6, 39.5, 49.4, 59.3, 69.1, 79.0, 118.5, 177.8
37	56,000	11.42	77.0	59.3, 118.5
B6	56,000	11.42	77.0	31.6, 39.5, 49.4, 59.3, 69.1, 79.0, 118.5, 177.8
38	56,000	11.42	117.0	59.3, 118.5
B7	56,000	11.42	117.0	31.6, 39.5, 49.4, 59.3, 69.1, 79.0, 118.5, 177.8
39	45,000	9.18	37.0	59.3, 118.5
B8	45,000	9.18	37.0	31.6, 39.5, 49.4, 59.3, 69.1, 79.0, 118.5, 177.8
40	45,000	9.18	77.0	59.3, 118.5
B9	45,000	9.18	77.0	31.6, 39.5, 49.4, 59.3, 69.1, 79.0, 118.5, 177.8
41	45,000	9.18	117.0	59.3, 118.5
B10	45,000	9.18	117.0	31.6, 39.5, 49.4, 59.3, 69.1, 79.0, 118.5, 177.8

NOTES:

- 1) The values of DFRC are only applicable along the 270-degree azimuth (Secondary flows make this the worst-case azimuth).
- 2) Ambient winds varied between 0 and 3.5 knots.
- 3) Atmospheric density ratio was assumed equal to 1.0 since pressure altitude (which was near sea level) was not documented in reference 24. Ambient temperature was measured from 39 to 45 degrees Fahrenheit during testing.



Y CURVE 33 CH-53 MEAN/PEAK VELOCITY PROFILE CORRELATION AT EIGHT 27 DEGREES AZIMUTH STATIONS AT AN AVERAGE GROSS WEIGHT OF 70,000 LB NDB AND A ROTOR HEIGHT OF 37 FEET

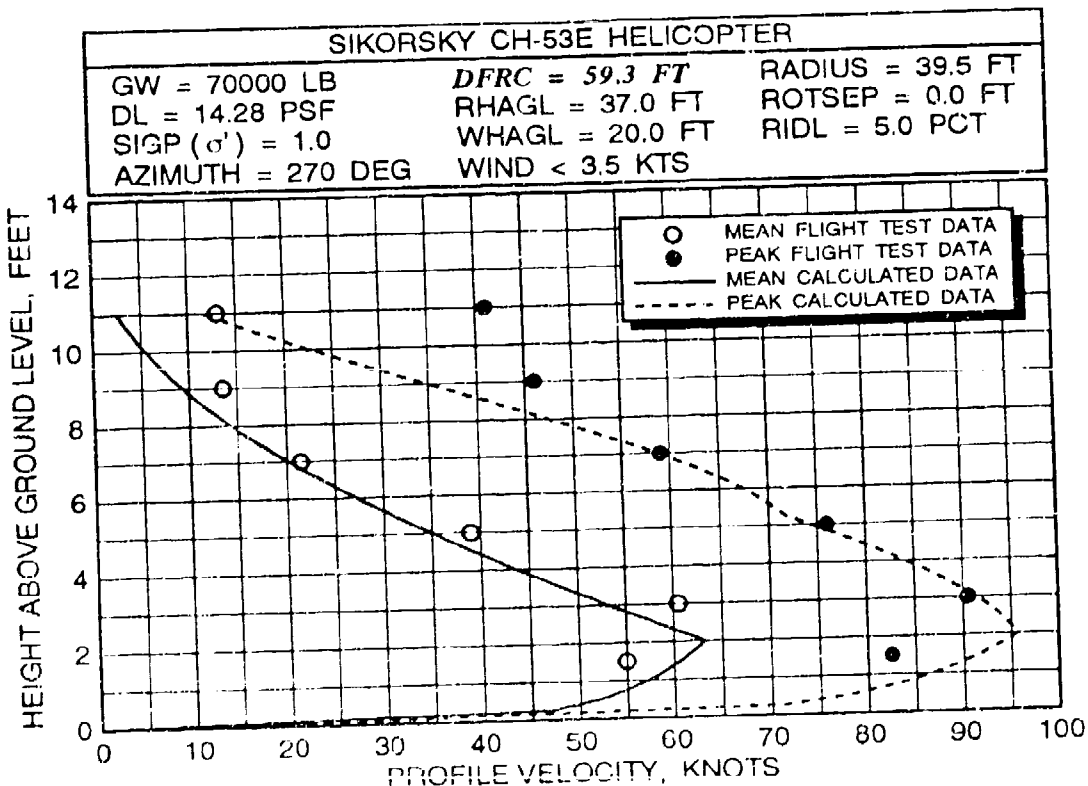
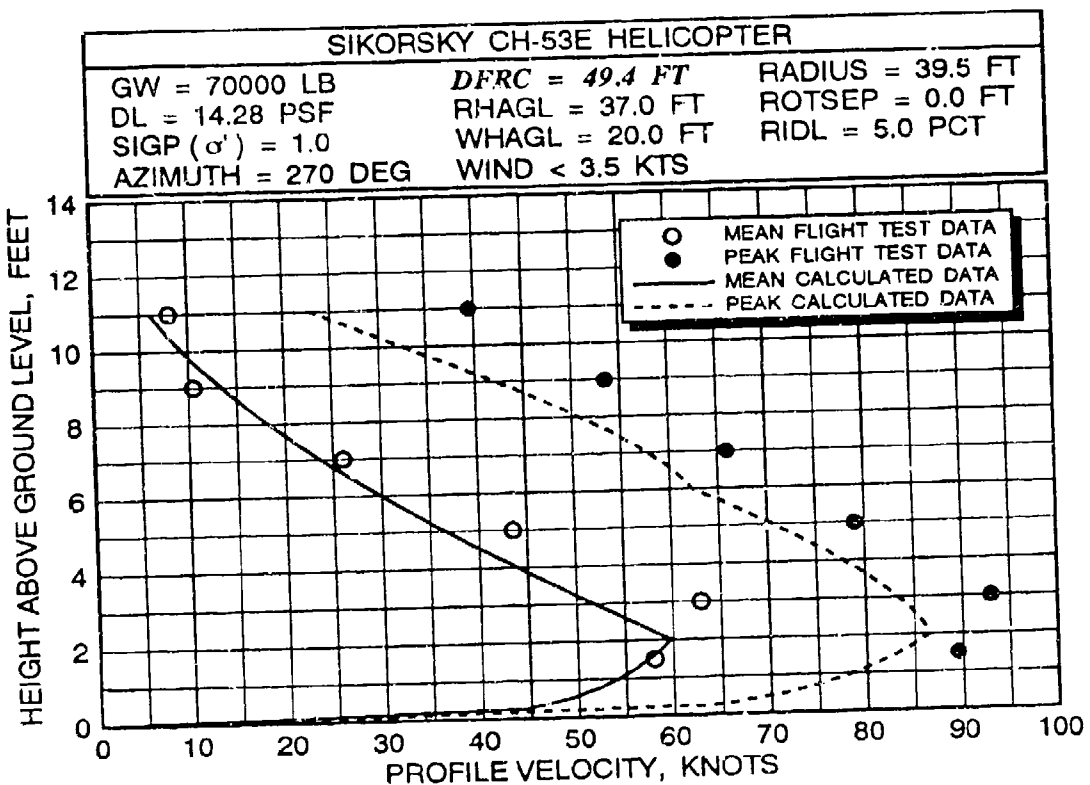


FIGURE 33 CH-53E MEAN/PEAK VELOCITY PROFILE CORRELATION AT EIGHT 270- DEGREE RADIAL STATIONS AT AN AVERAGE GROSS WEIGHT OF 70,000 POUNDS AND A ROTOR HEIGHT OF 37 FEET (continued)

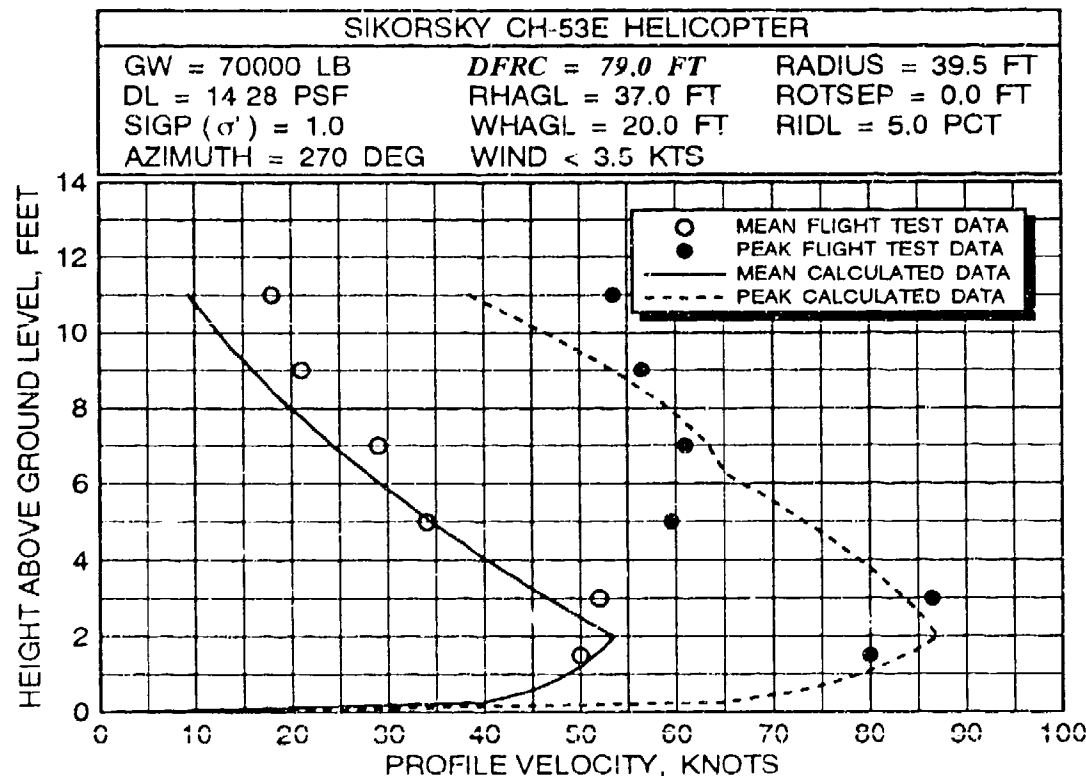
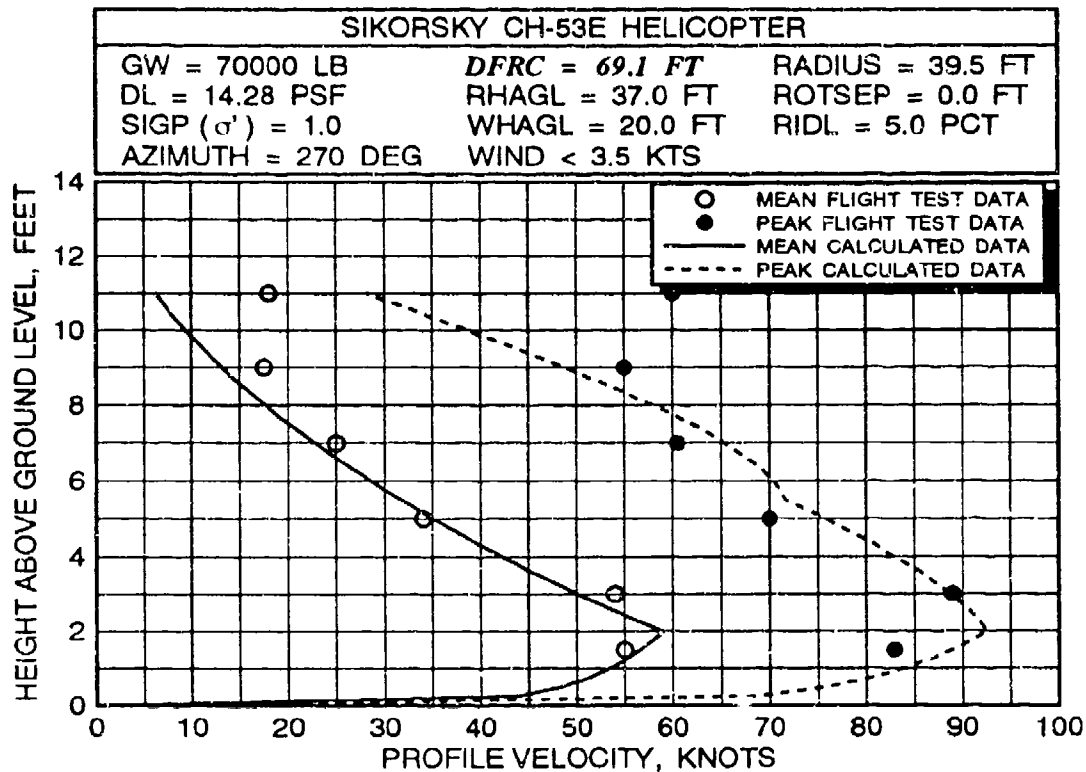


FIGURE 33 CH-53E MEAN/PEAK VELOCITY PROFILE CORRELATION AT EIGHT 270- DEGREE RADIAL STATIONS AT AN AVERAGE GROSS WEIGHT OF 70,000 POUNDS AND A ROTOR HEIGHT OF 37 FEET (continued)

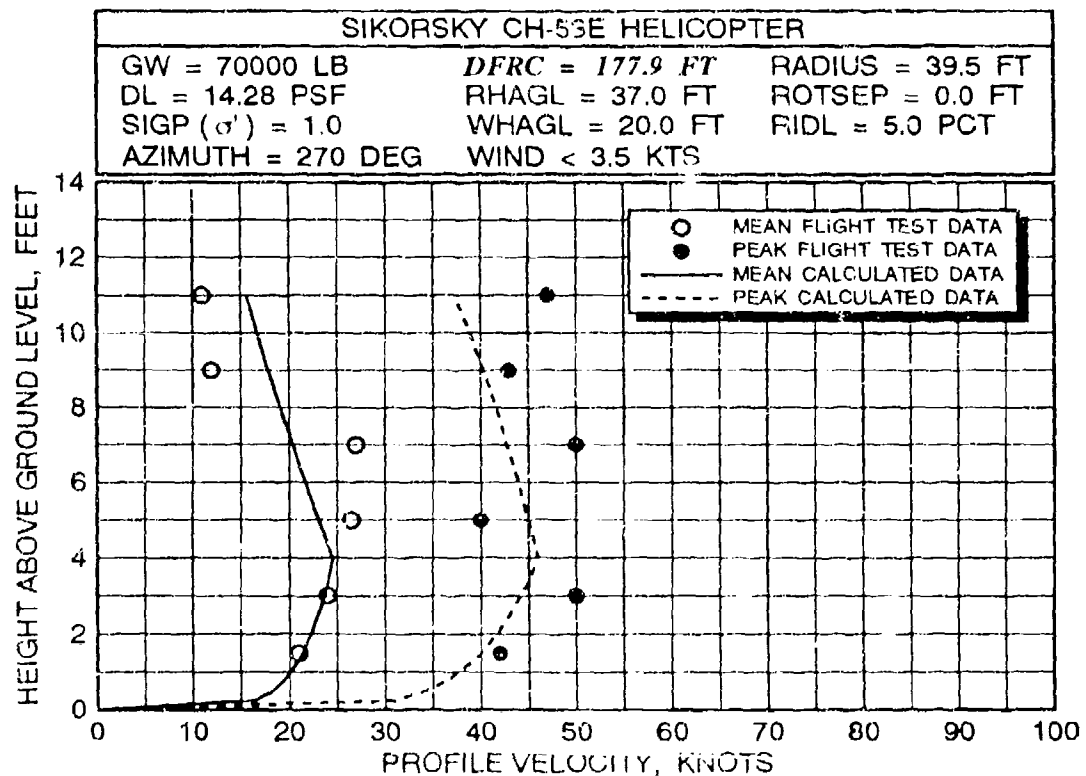
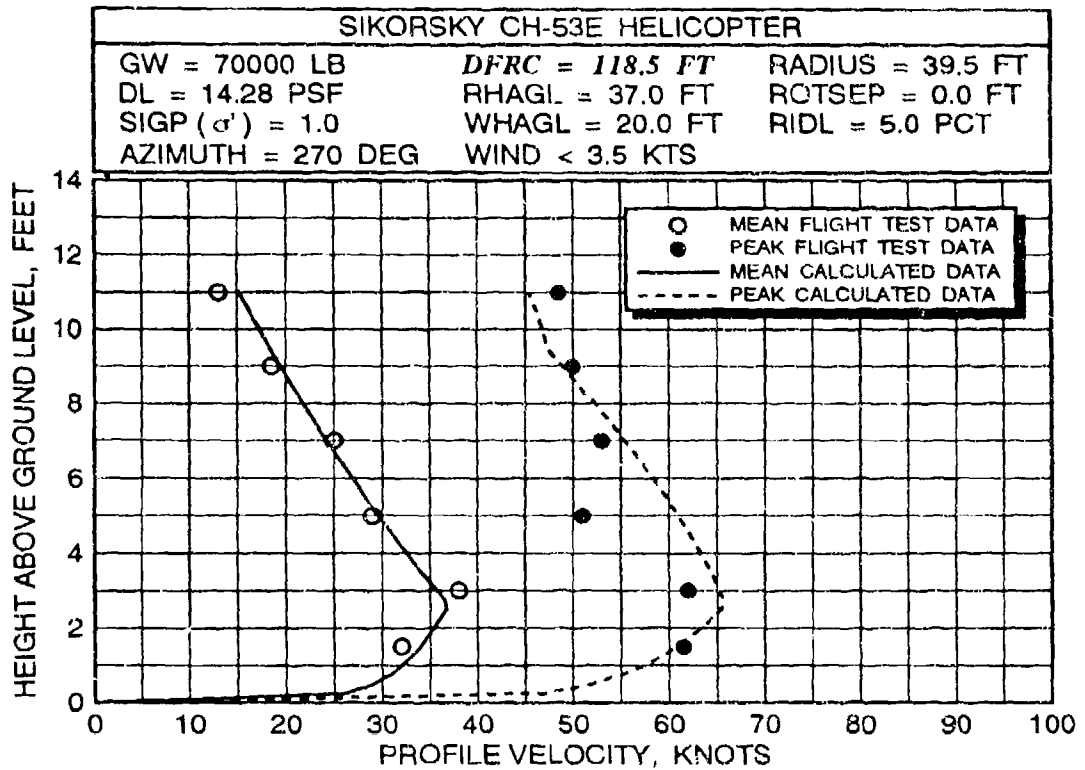


FIGURE 33 CH-53E MEAN/PEAK VELOCITY PROFILE CORRELATION AT EIGHT 270- DEGREE RADIAL STATIONS AT AN AVERAGE GROSS WEIGHT OF 70,000 POUNDS AND A ROTOR HEIGHT OF 37 FEET (continued)

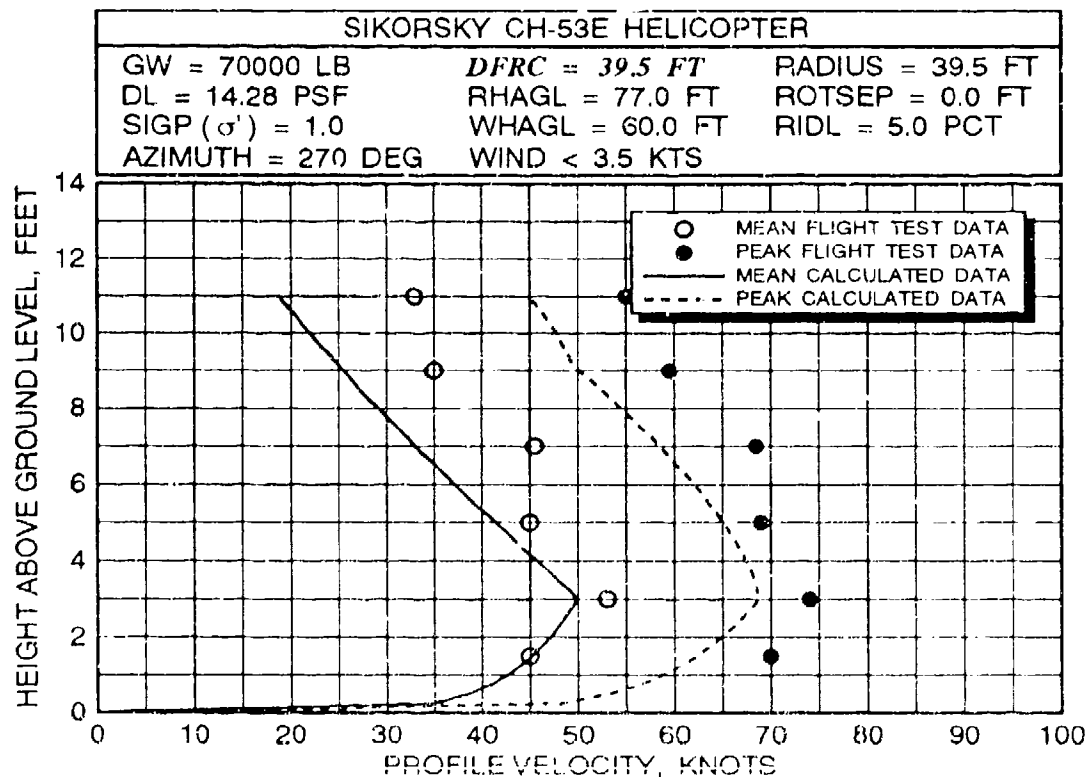
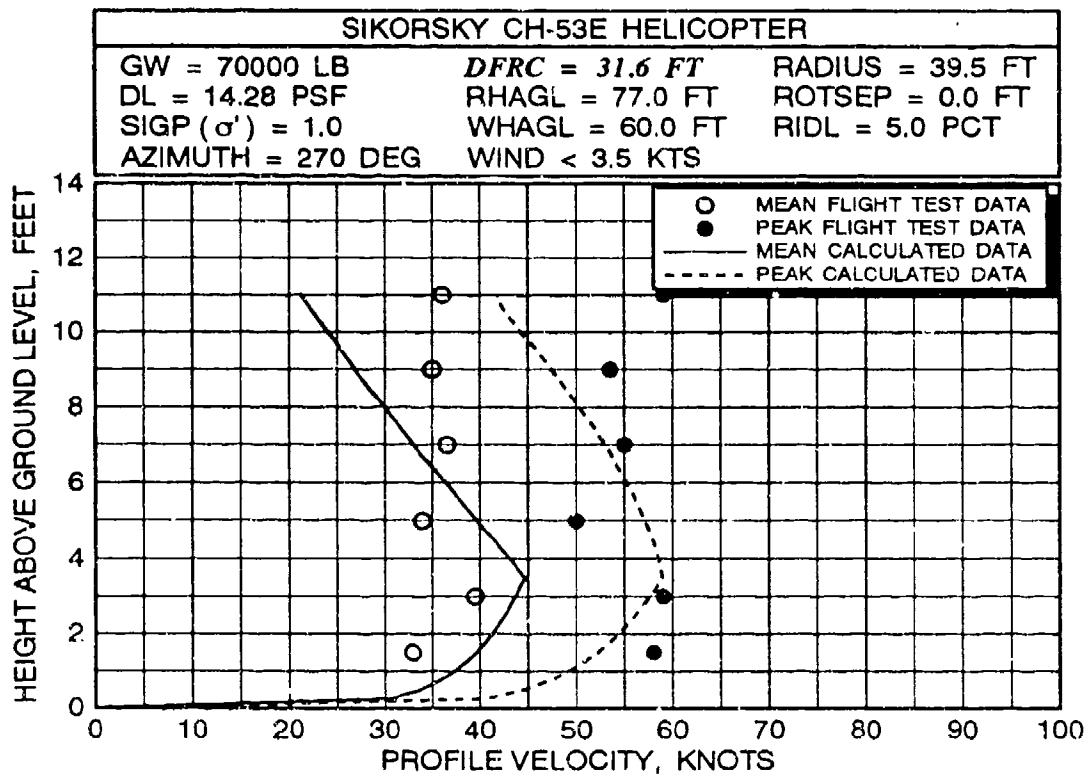


FIGURE 34 CH-53E MEAN/PEAK VELOCITY PROFILE CORRELATION AT EIGHT 270- DEGREE RADIAL STATIONS AT AN AVERAGE GROSS WEIGHT OF 70,000 POUNDS AND A ROTOR HEIGHT OF 77 FEET

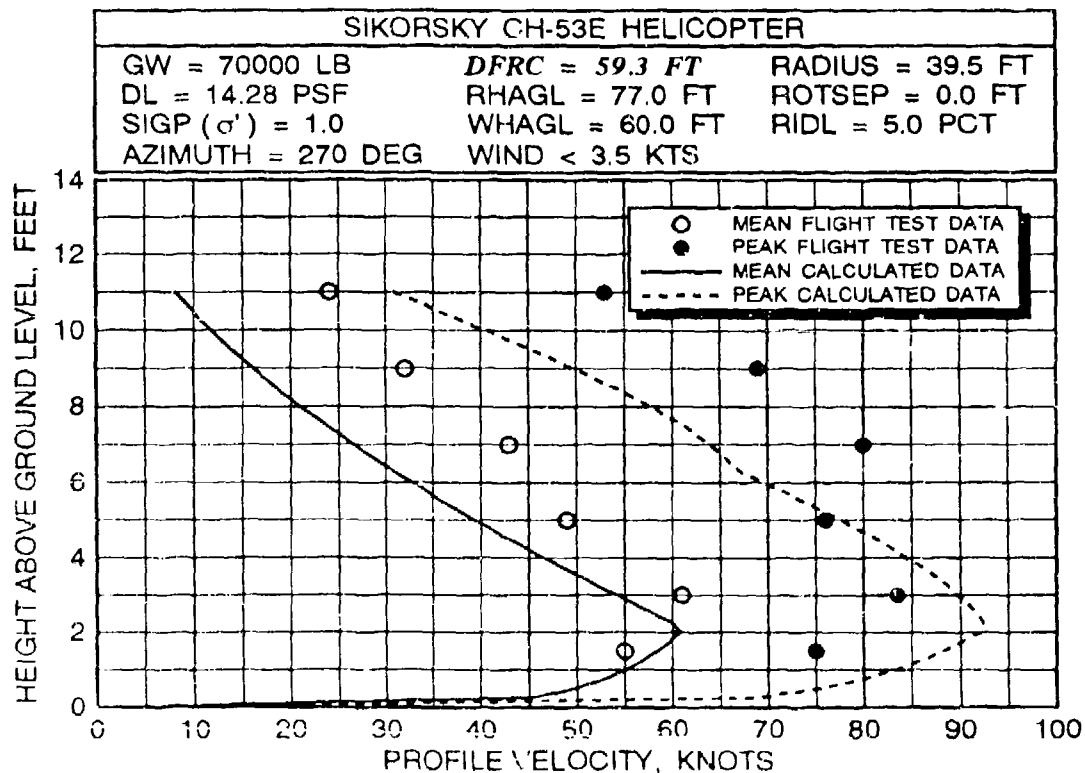
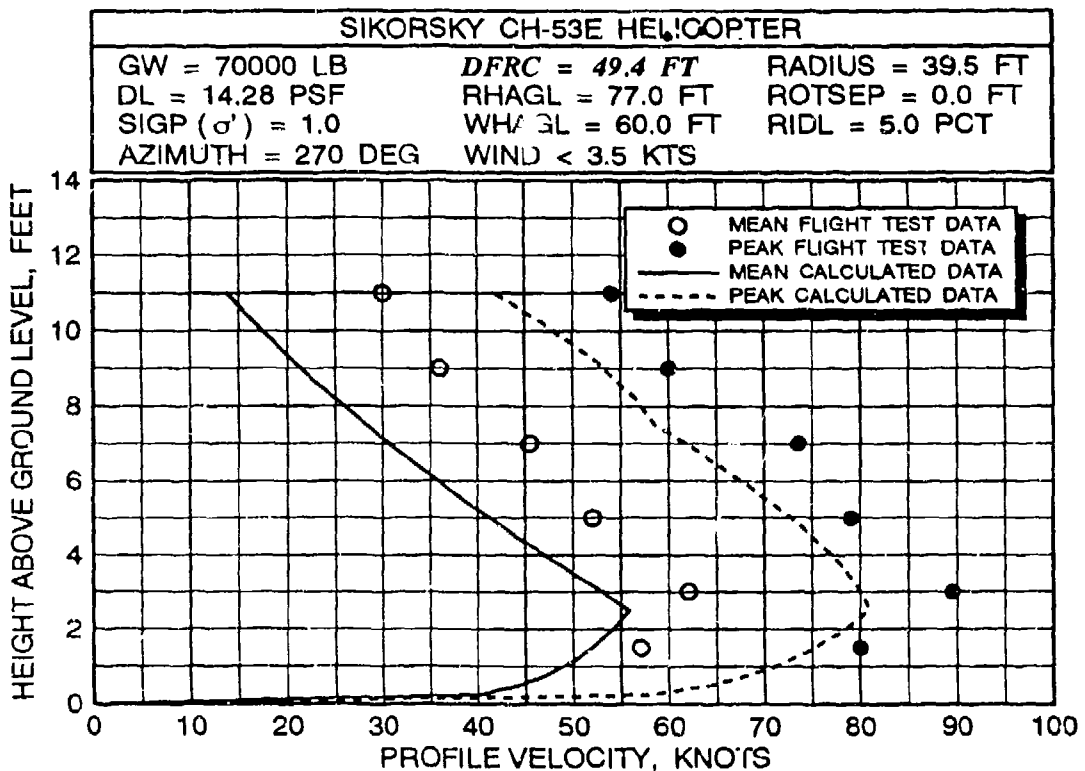


FIGURE 34 CH-53E MEAN/PEAK VELOCITY PROFILE CORRELATION AT EIGHT 270- DEGREE RADIAL STATIONS AT AN AVERAGE GROSS WEIGHT OF 70,000 POUNDS AND A ROTOR HEIGHT OF 77 FEET (continued)

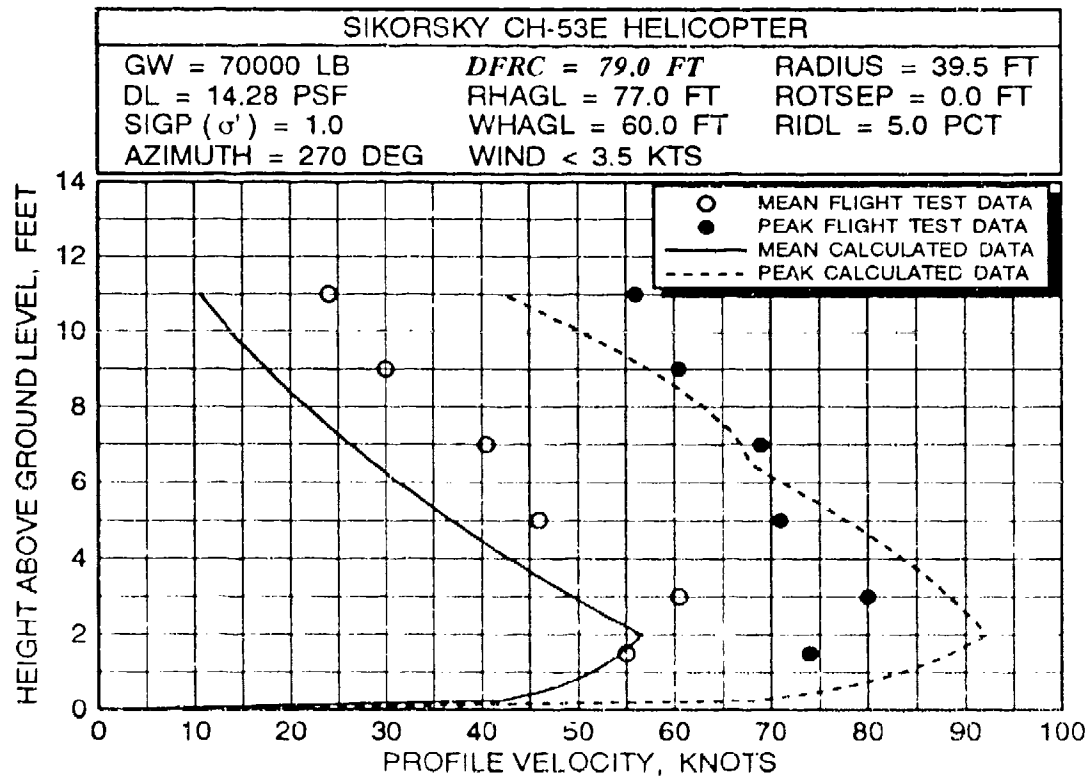
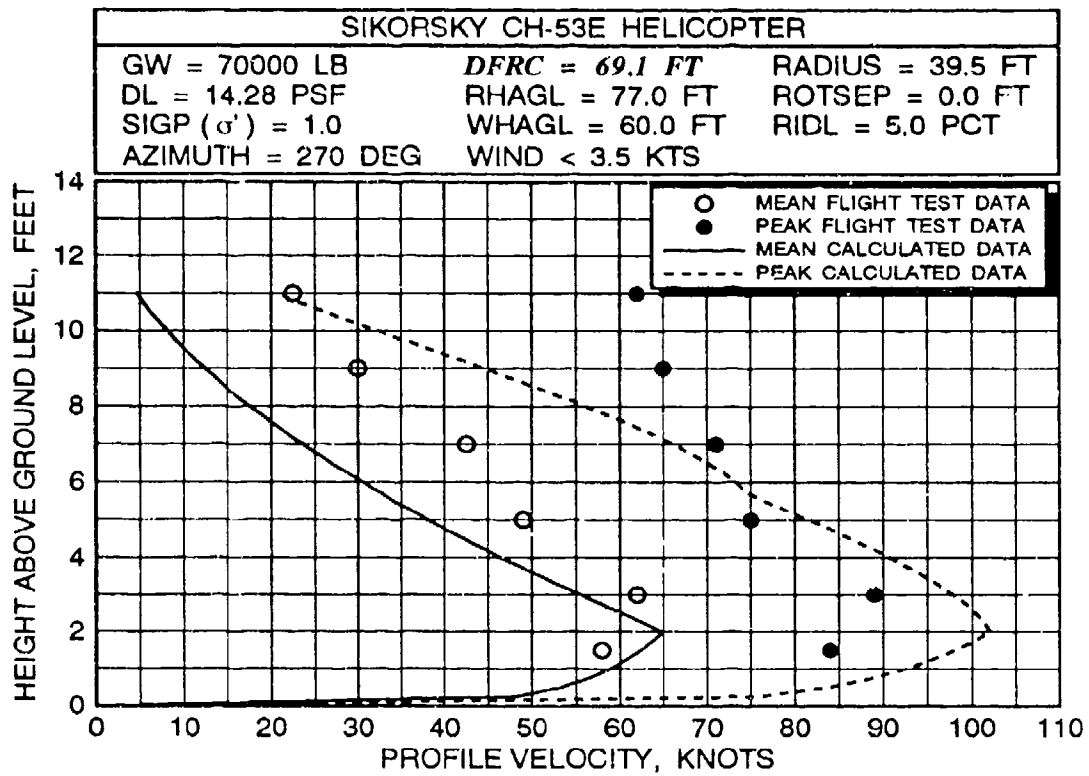


FIGURE 34 CH-53E MEAN/PEAK VELOCITY PROFILE CORRELATION AT EIGHT 270- DEGREE RADIAL STATIONS AT AN AVERAGE GROSS WEIGHT OF 70,000 POUNDS AND A ROTOR HEIGHT OF 77 FEET (continued)

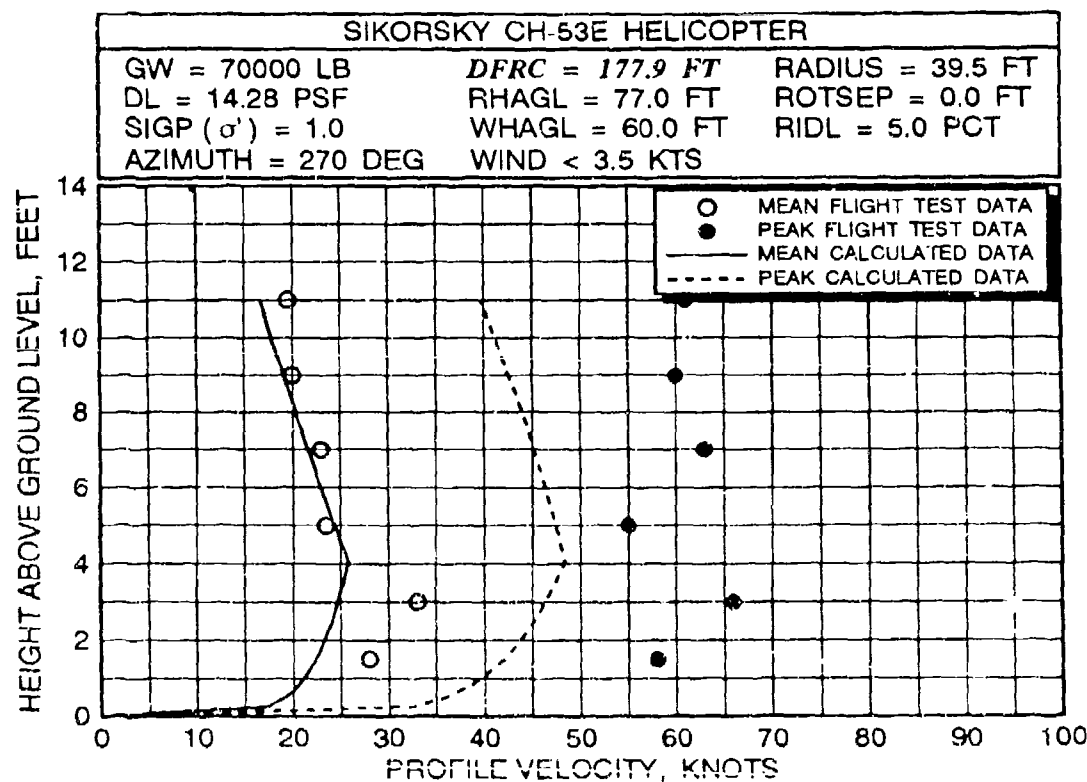
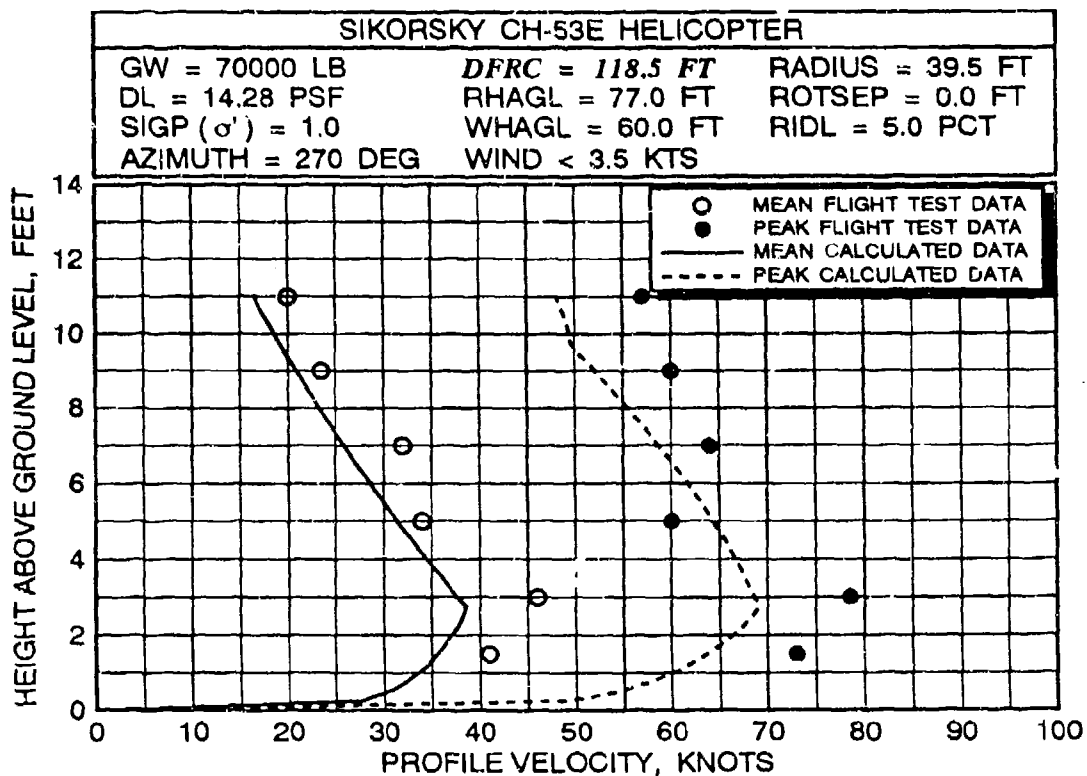


FIGURE 34 CH-53E MEAN/PEAK VELOCITY PROFILE CORRELATION AT EIGHT 270- DEGREE RADIAL STATIONS AT AN AVERAGE GROSS WEIGHT OF 70,000 POUNDS AND A ROTOR HEIGHT OF 77 FEET (continued)

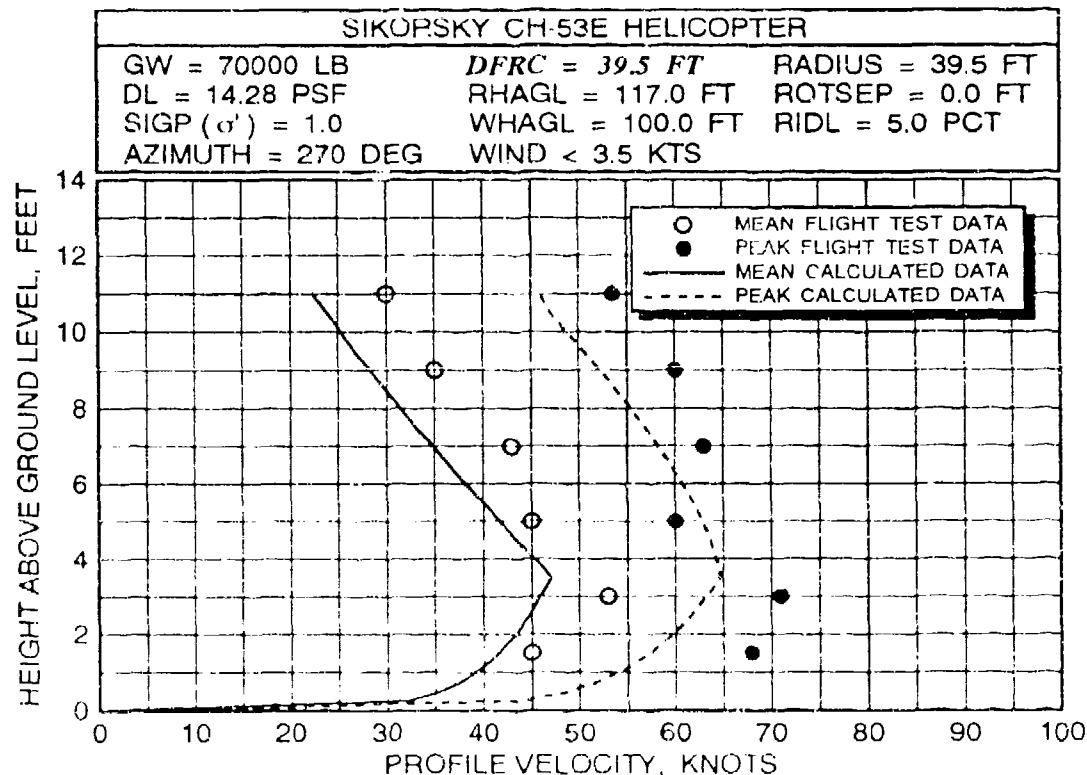
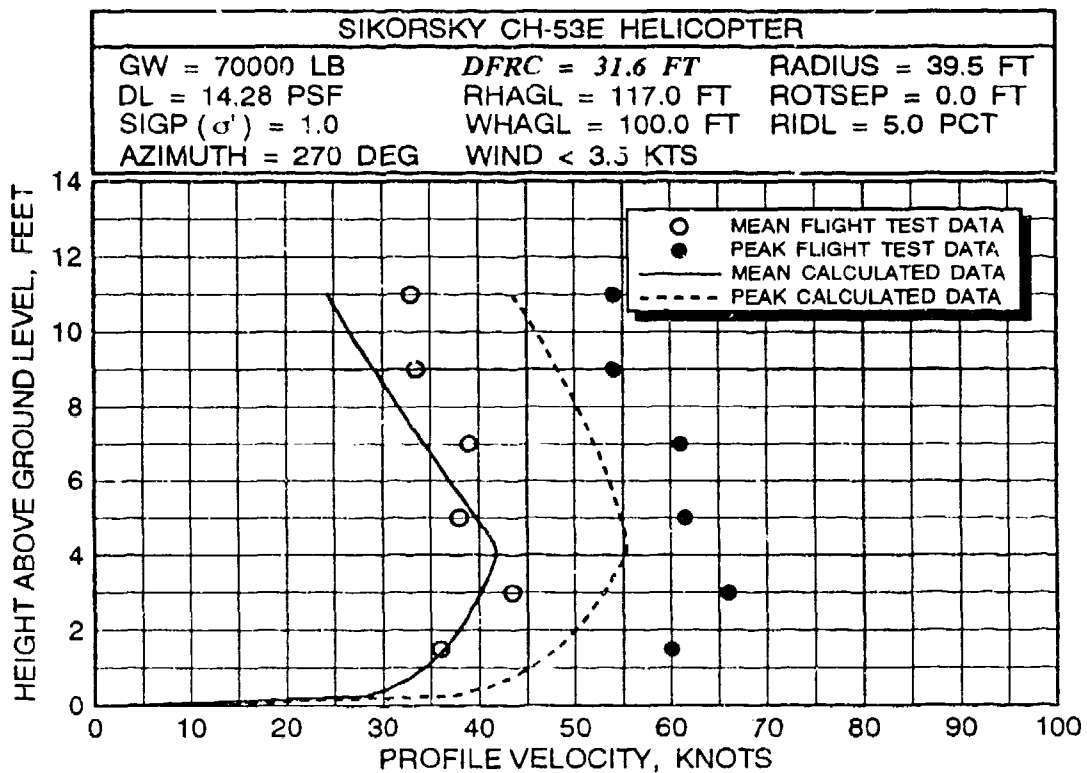


FIGURE 35 CH-53E MEAN/PEAK VELOCITY PROFILE CORRELATION AT EIGHT 270- DEGREE RADIAL STATIONS AT AN AVERAGE GROSS WEIGHT OF 70,000 POUNDS AND A ROTOR HEIGHT OF 117 FEET

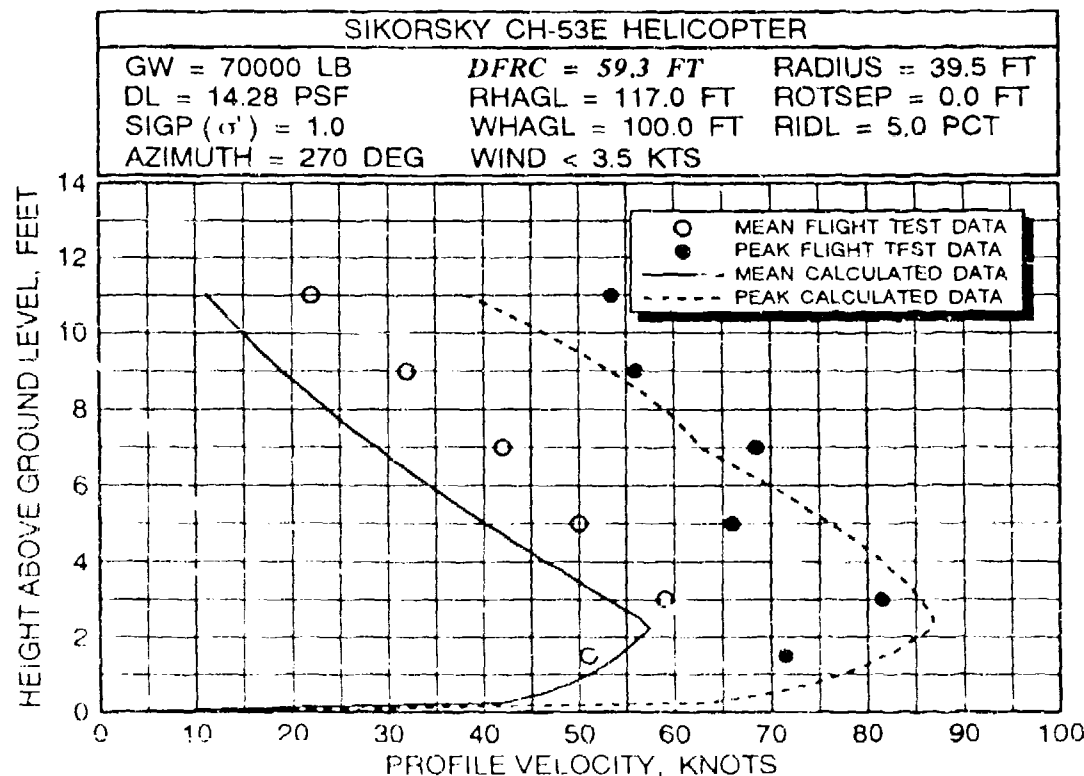
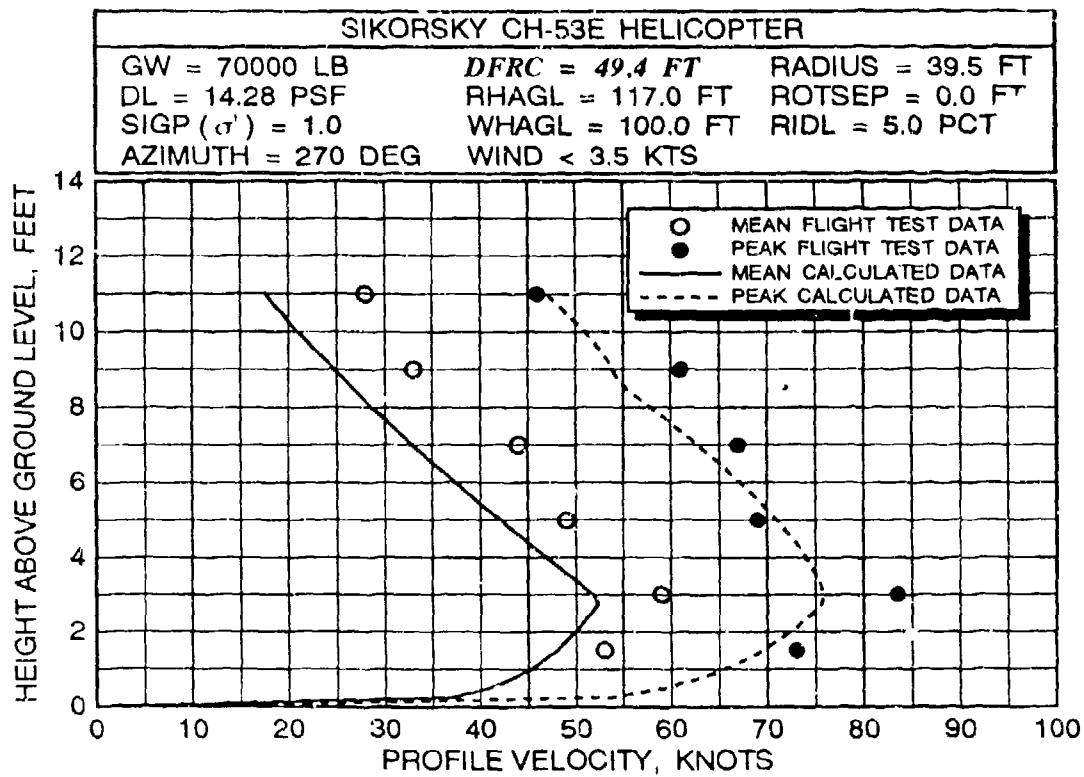


FIGURE 35 CH-53E MEAN/PEAK VELOCITY PROFILE CORRELATION AT EIGHT 270- DEGREE RADIAL STATIONS AT AN AVERAGE GROSS WEIGHT OF 70,000 POUNDS AND A ROTOR HEIGHT OF 117 FEET (continued)

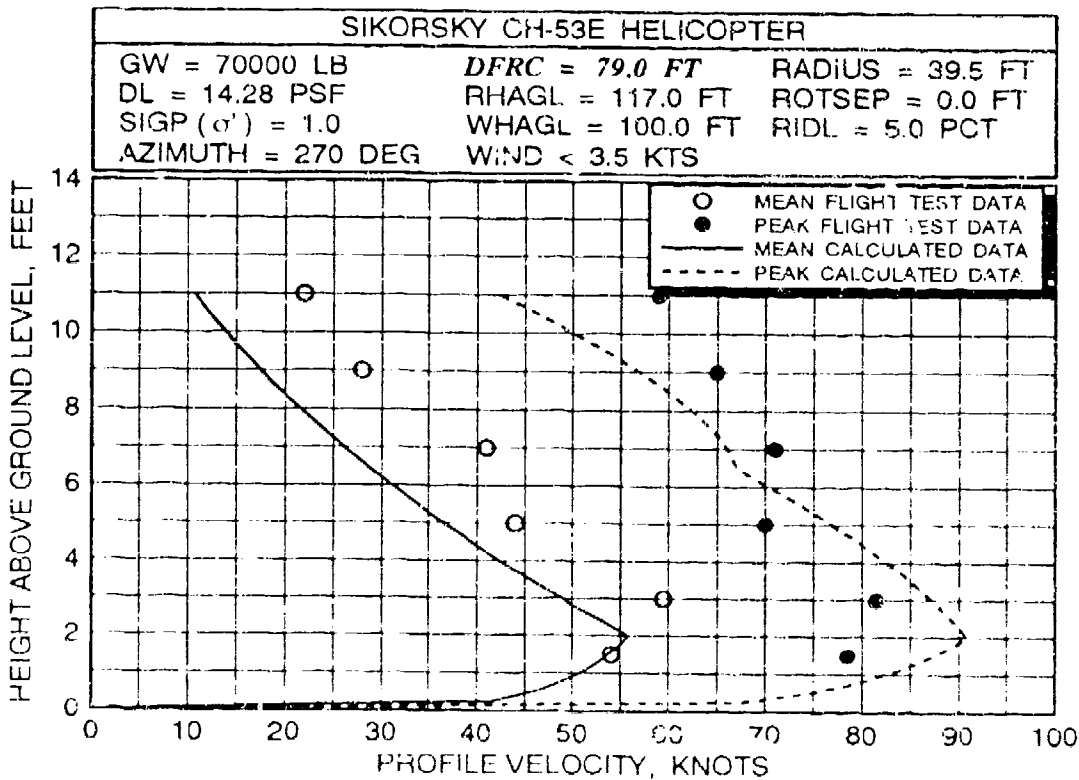
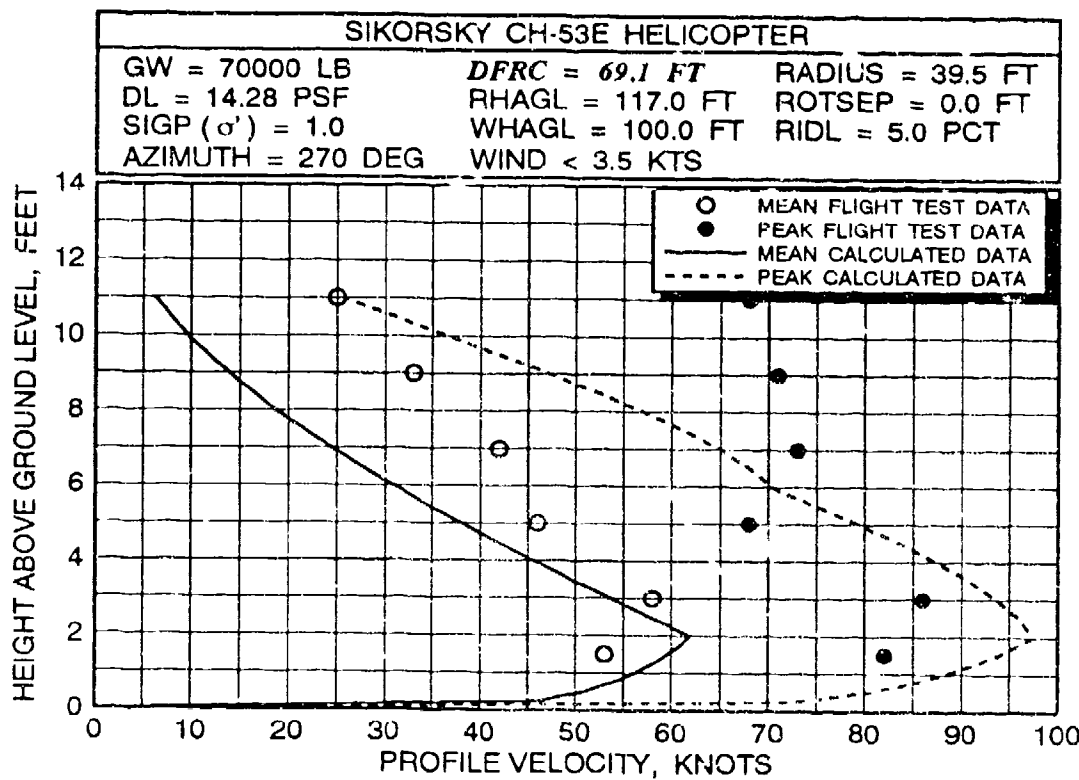


FIGURE 35 CH-53E MEAN/PEAK VELOCITY PROFILE CORRELATION AT EIGHT 270- DEGREE RADIAL STATIONS AT AN AVERAGE GROSS WEIGHT OF 70,000 POUNDS AND A ROTOR HEIGHT OF 117 FEET (continued)

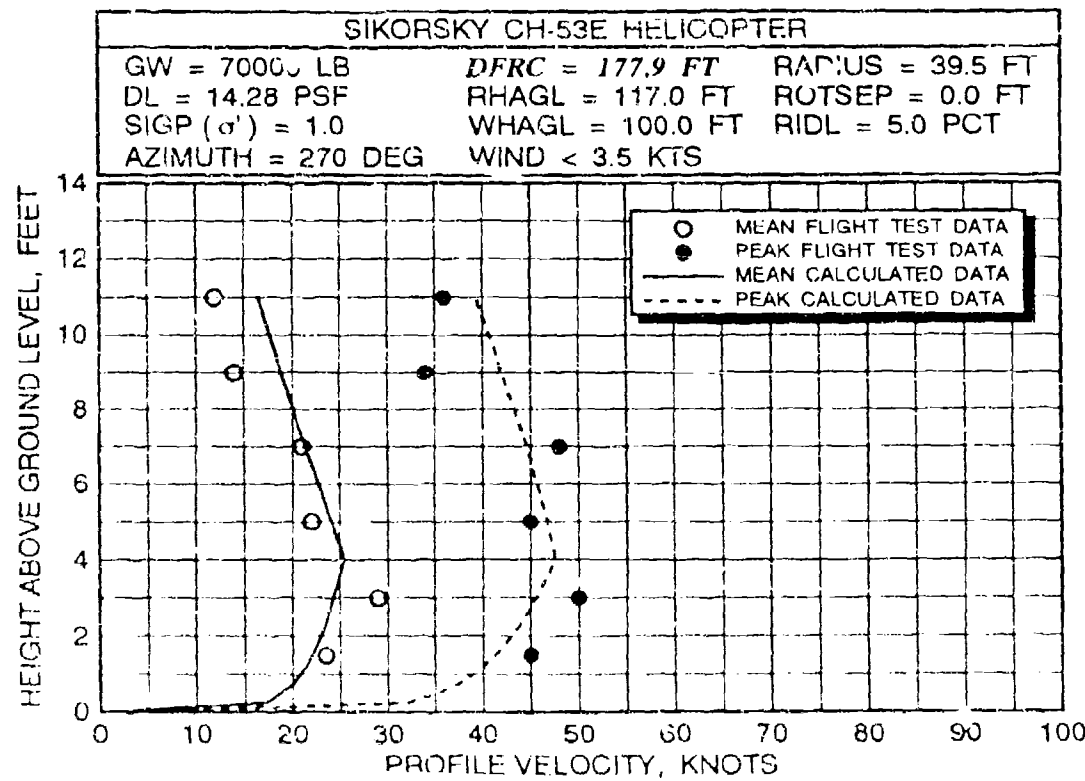
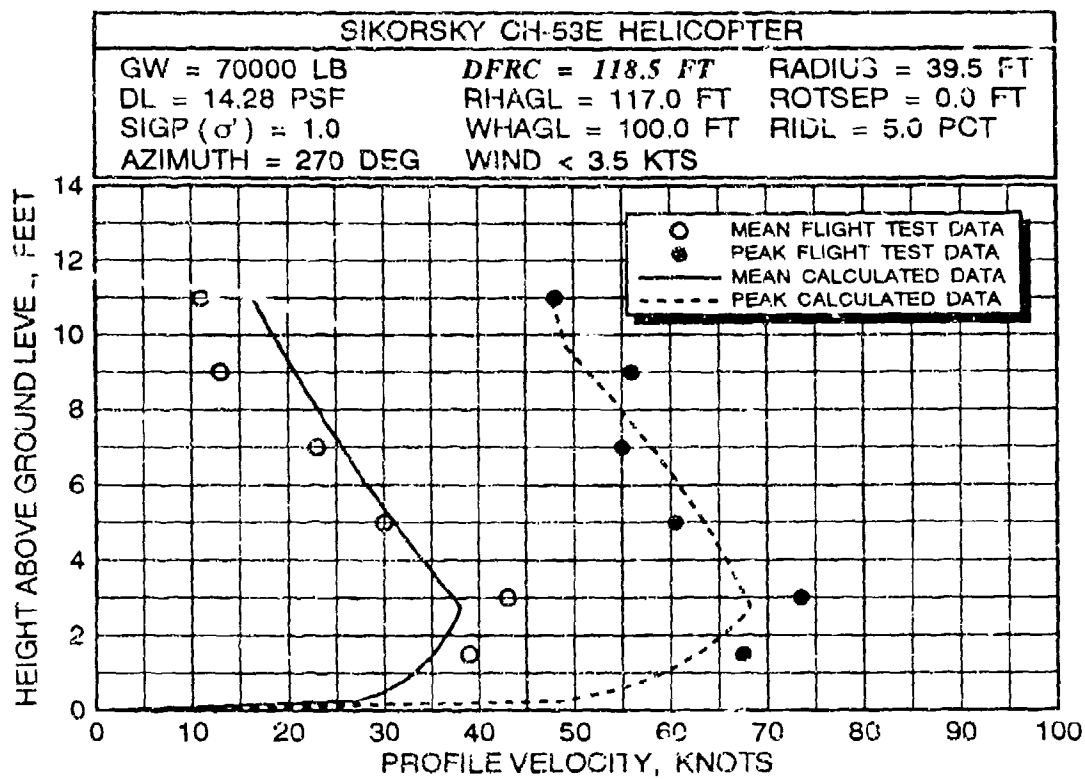


FIGURE 35 CH-53E MEAN/PEAK VELOCITY PROFILE CORRELATION AT EIGHT 270- DEGREE RADIAL STATIONS AT AN AVERAGE GROSS WEIGHT OF 70,000 POUNDS AND A ROTOR HEIGHT OF 117 FEET (continued)

height increases. Overall, even with the noted discrepancies, the quality of the correlation for this particular gross weight appears to be quite good.

A comparison and a correlation of the effect of gross weight on CH-53E mean and peak velocity profiles at stations of 59.3 and 118.5 feet is presented in figures 36 through 41. In figures 36 through 38, data at 56,000 pounds are documented to compare with the previously presented data at 70,000 pounds for all three rotor heights. Data at 45,000 pounds, in figures 39 through 41, are also provided for comparison with the data at 56,000 and 70,000 pounds.

The comparison of these selected radial stations for a variation in gross weight reveals similar results to those presented for the 70,000-pound gross weight configuration. A major exception to this statement appears in the correlation of the 117-feet RHAGL cases at both the 45,000 and 56,000 pound gross weights. In these configurations there appears to be an overprediction of the flight test peak velocity profile data. An expanded correlation of the flight test and calculated data at each of the radial stations, rotor heights above ground, and gross weights (as listed in table 3) is presented in appendix B for the interested reader.

Overall, at worst, the correlation of CH-53E flight test and calculated data indicates an extremely good duplication of trends. Many of the compared mean and peak velocity profiles are predicted quite accurately by the mathematical model. In contrast, while some of the other mean and peak velocity profiles are not predicted as accurately as would be desired, the particular trends affecting the quality of the correlation are usually not consistent among the various gross weight and rotor height perturbations. Therefore, it is hard to identify any specific weakness in the mathematical model formulation. Also, poor correlation in some instances is probably attributable to unknowns with respect to the acquired flight test data, i.e., variations in reported winds, gross weight, rotor height, and helicopter position compared to the general values documented in reference 24. The major weakness contributing to any failure to correlate in greater detail is simply the lack of a complete understanding of the very complicated unsteady flow field processes involved (which are modeled using a theoretically and experimentally derived steady flow field model). Also, as discussed earlier, since the mean velocity profile is primarily utilized to scale the more important hazard-related peak velocity profile, an extremely accurate prediction of the mean profile, while certainly desirable, should not be considered critical to a rotorwash hazard analysis.

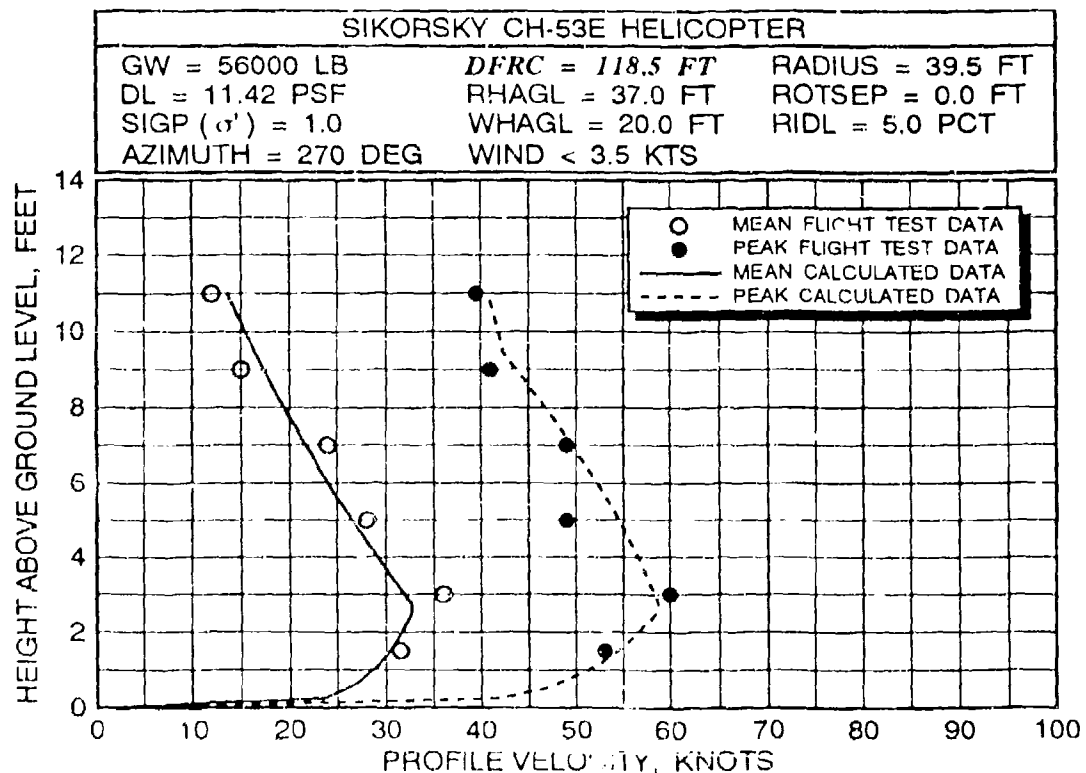
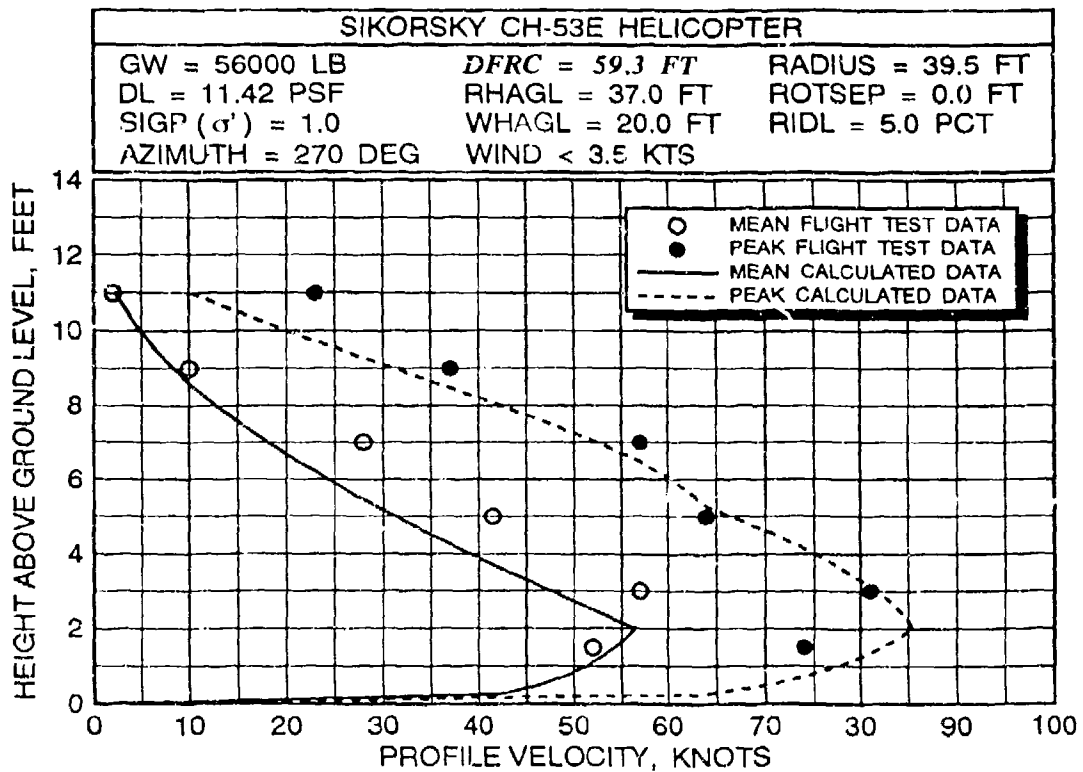


FIGURE 36 CH-53E MEAN/PEAK VELOCITY PROFILE CORRELATION AT 59.3 AND 118.5 FEET ALONG THE 270-DEGREE AZIMUTH AT AN AVERAGE GROSS WEIGHT OF 56,000 POUNDS AND A ROTOR HEIGHT OF 37 FEET

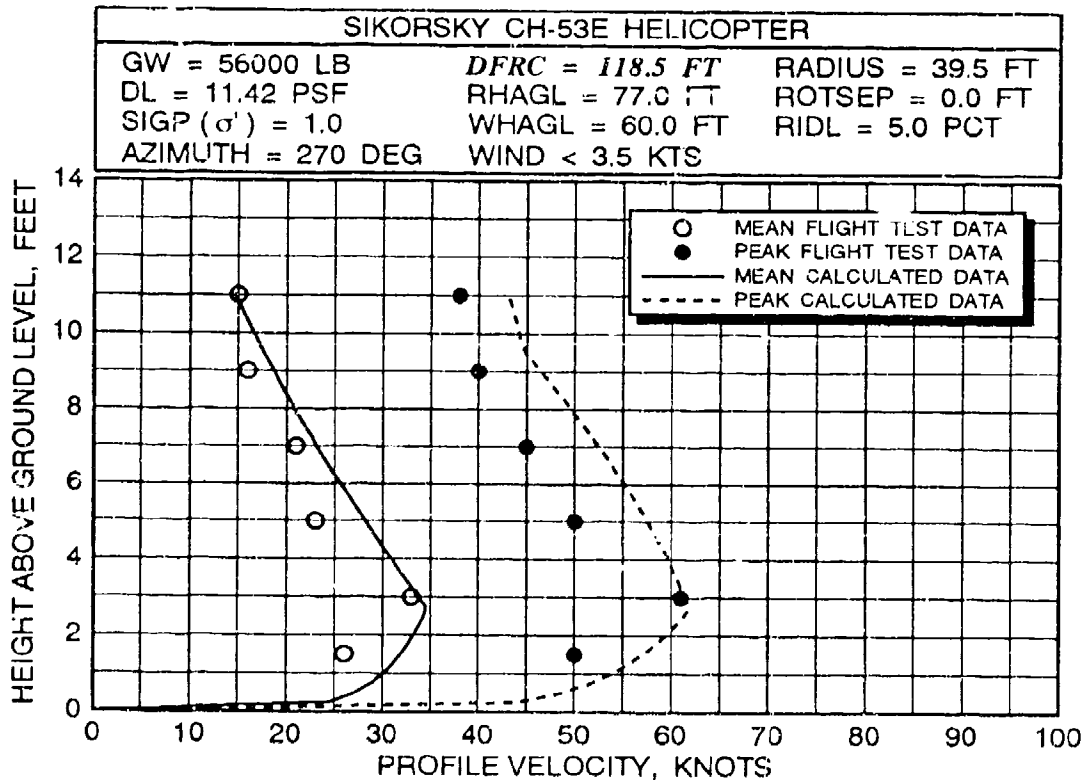
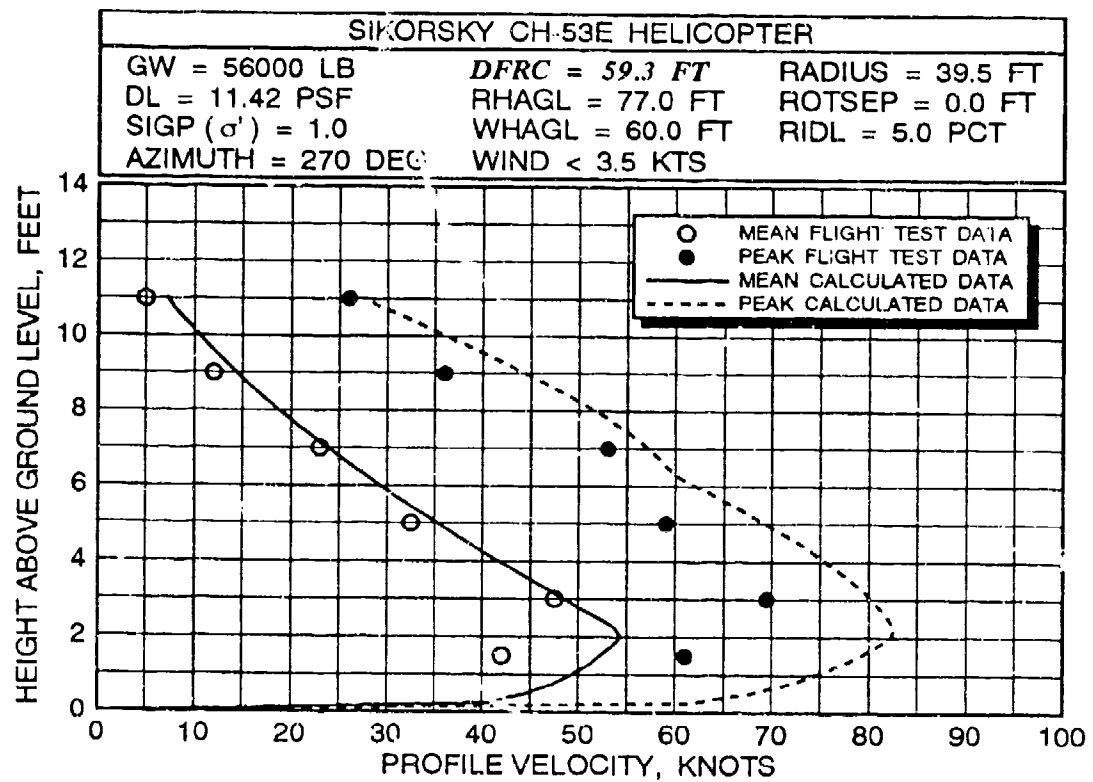


FIGURE 37 CH-53E MEAN/PEAK VELOCITY PROFILE CORRELATION AT 59.3 AND 118.5 FEET ALONG THE 270-DEGREE AZIMUTH AT AN AVERAGE GROSS WEIGHT OF 56,000 POUNDS AND A ROTOR HEIGHT OF 77 FEET

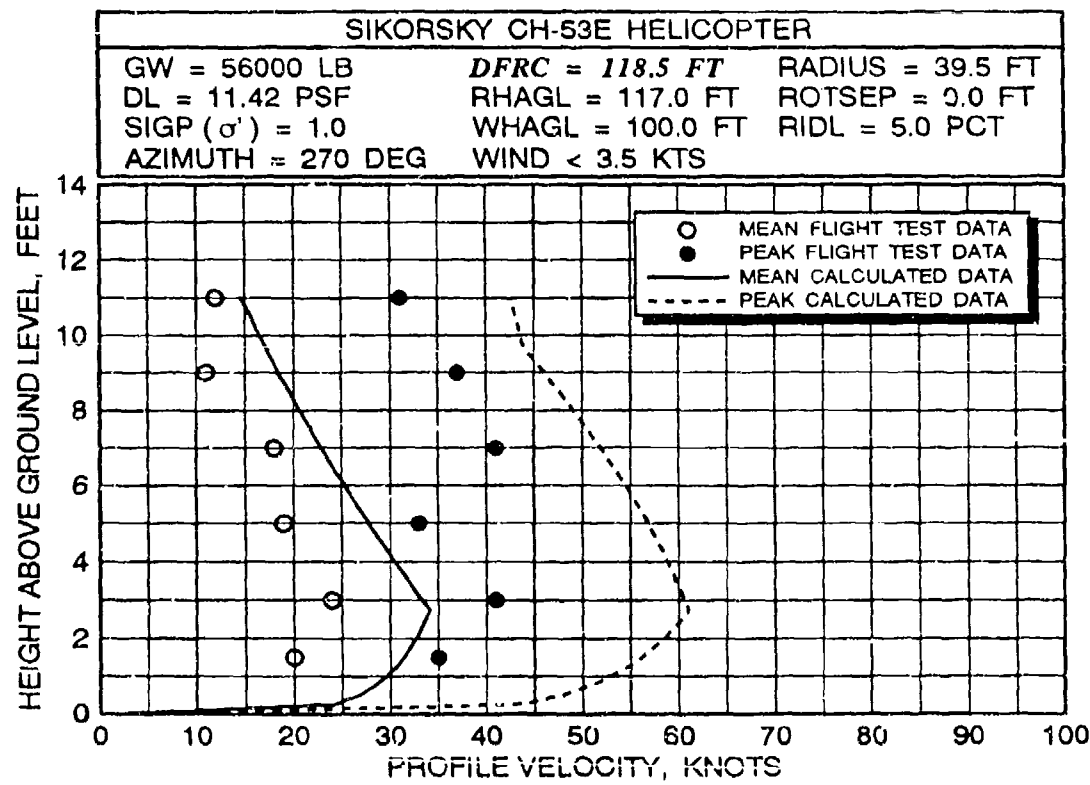
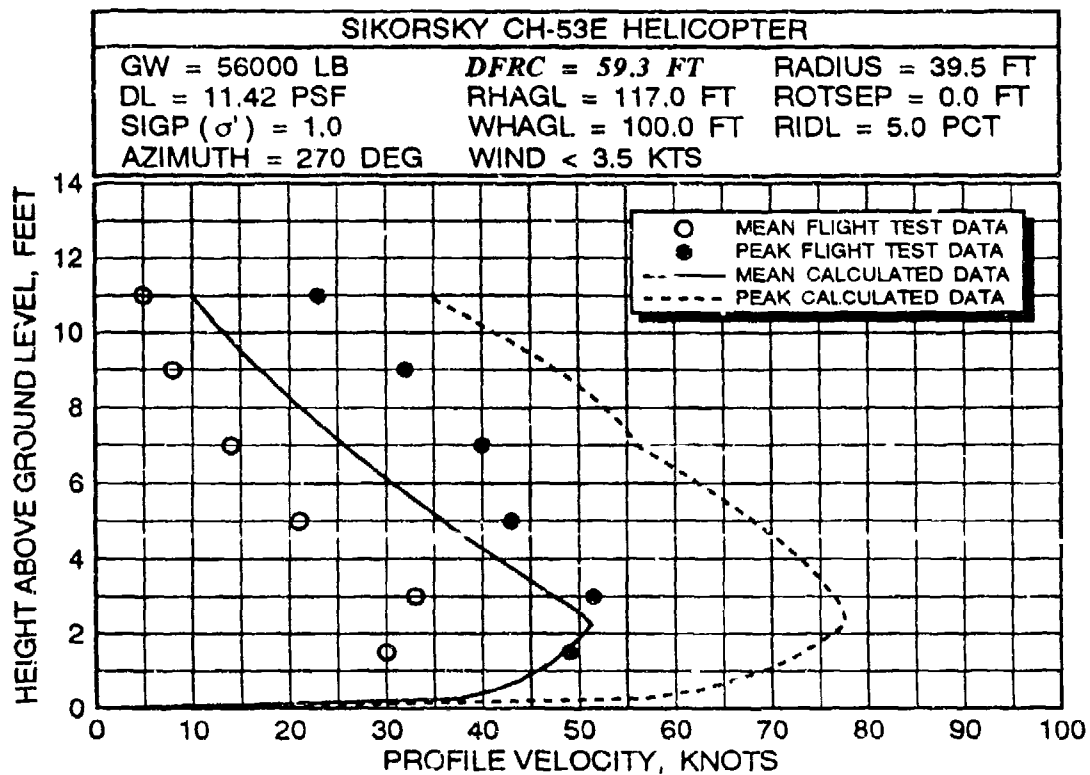


FIGURE 38 CH-53E MEAN/PEAK VELOCITY PROFILE CORRELATION AT 59.3 AND 118.5 FEET ALONG THE 270-DEGREE AZIMUTH AT AN AVERAGE GROSS WEIGHT OF 56,000 POUNDS AND A ROTOR HEIGHT OF 117 FEET

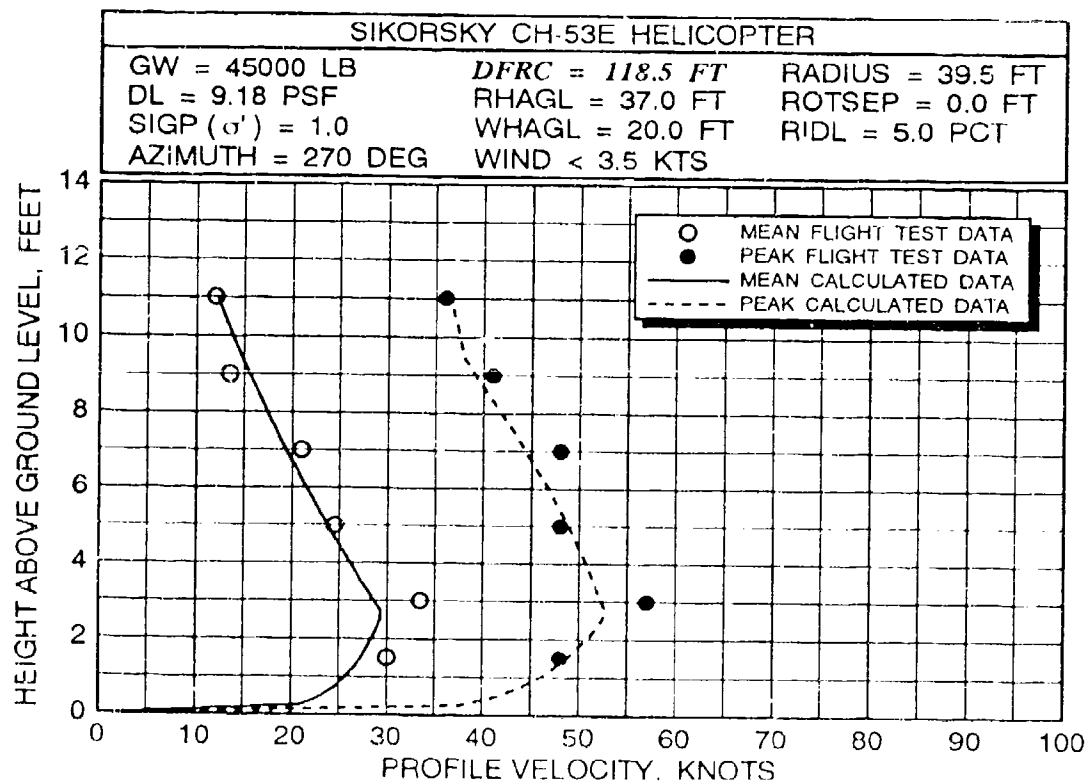
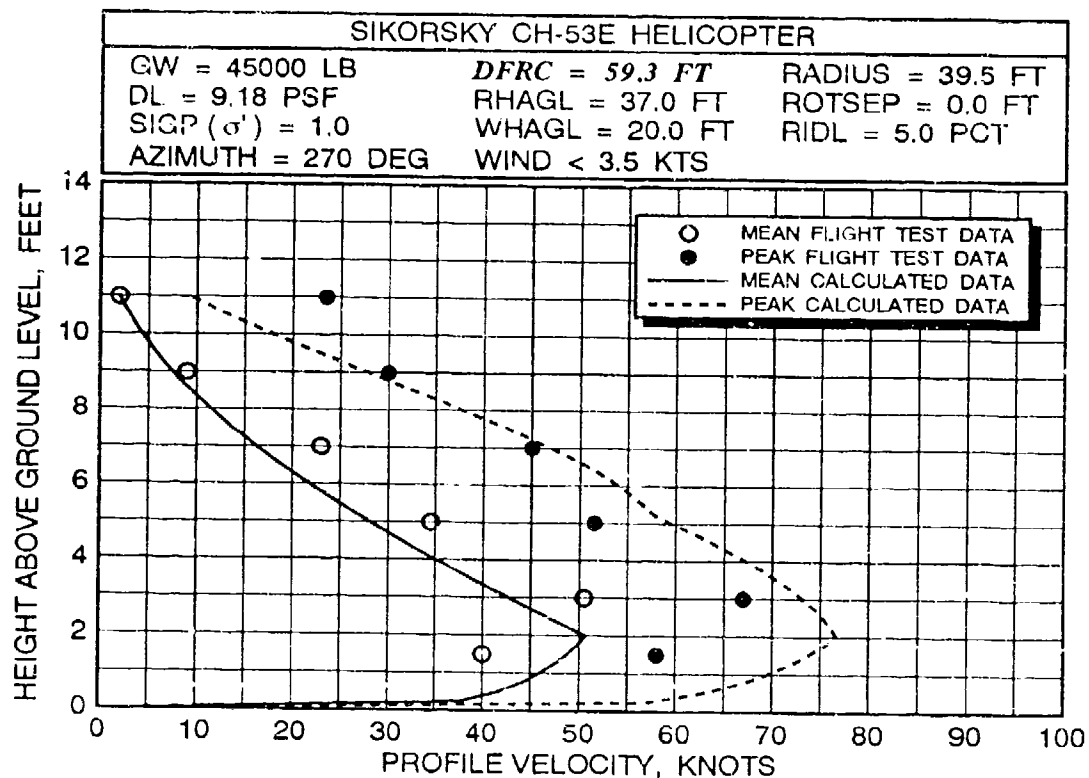


FIGURE 39 CH-53E MEAN/PEAK VELOCITY PROFILE CORRELATION AT 59.3 AND 118.5 FEET ALONG THE 270-DEGREE AZIMUTH AT AN AVERAGE GROSS WEIGHT OF 45,000 POUNDS AND A ROTOR HEIGHT OF 37 FEET

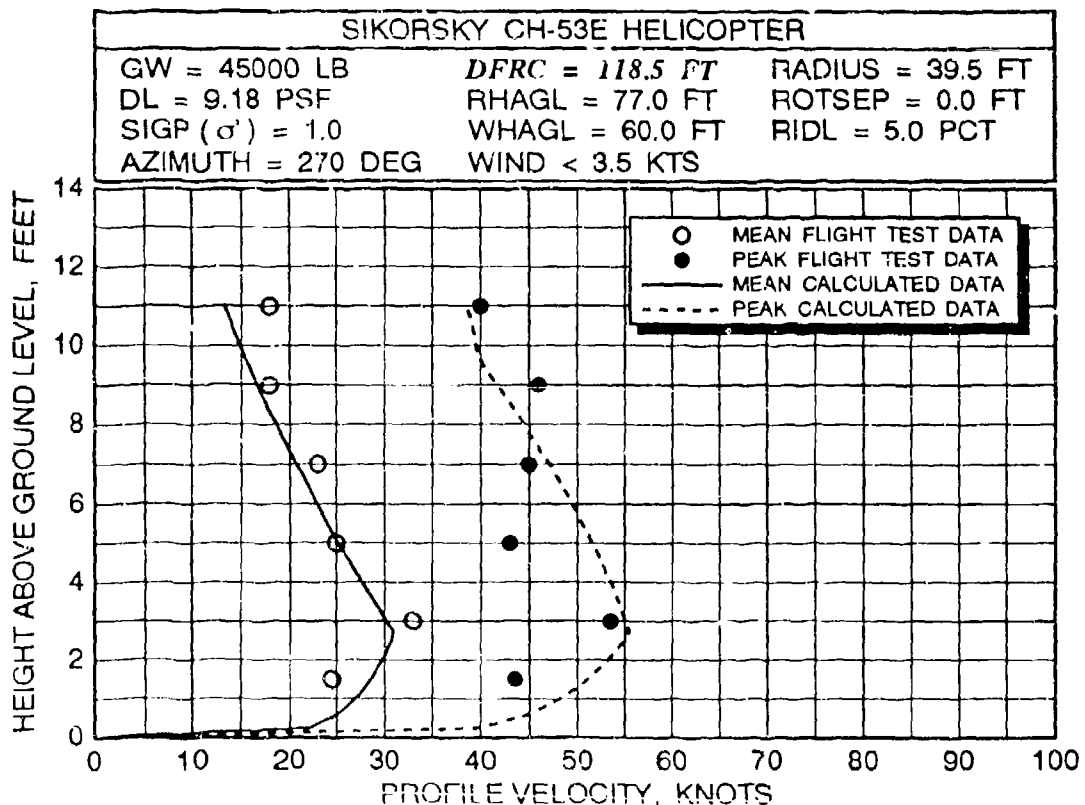
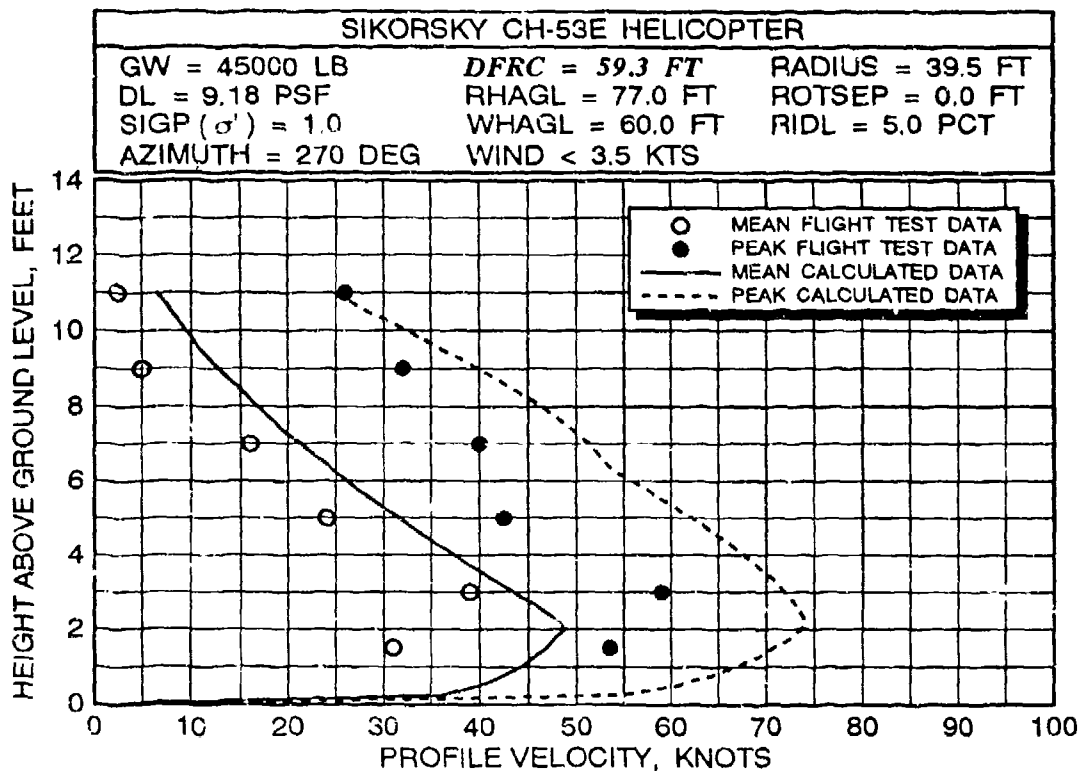


FIGURE 40 CH-53E MEAN/PEAK VELOCITY PROFILE CORRELATION AT 59.3 AND 118.5 FEET ALONG THE 270-DEGREE AZIMUTH AT AN AVERAGE GROSS WEIGHT OF 45,000 POUNDS AND A ROTOR HEIGHT OF 77 FEET

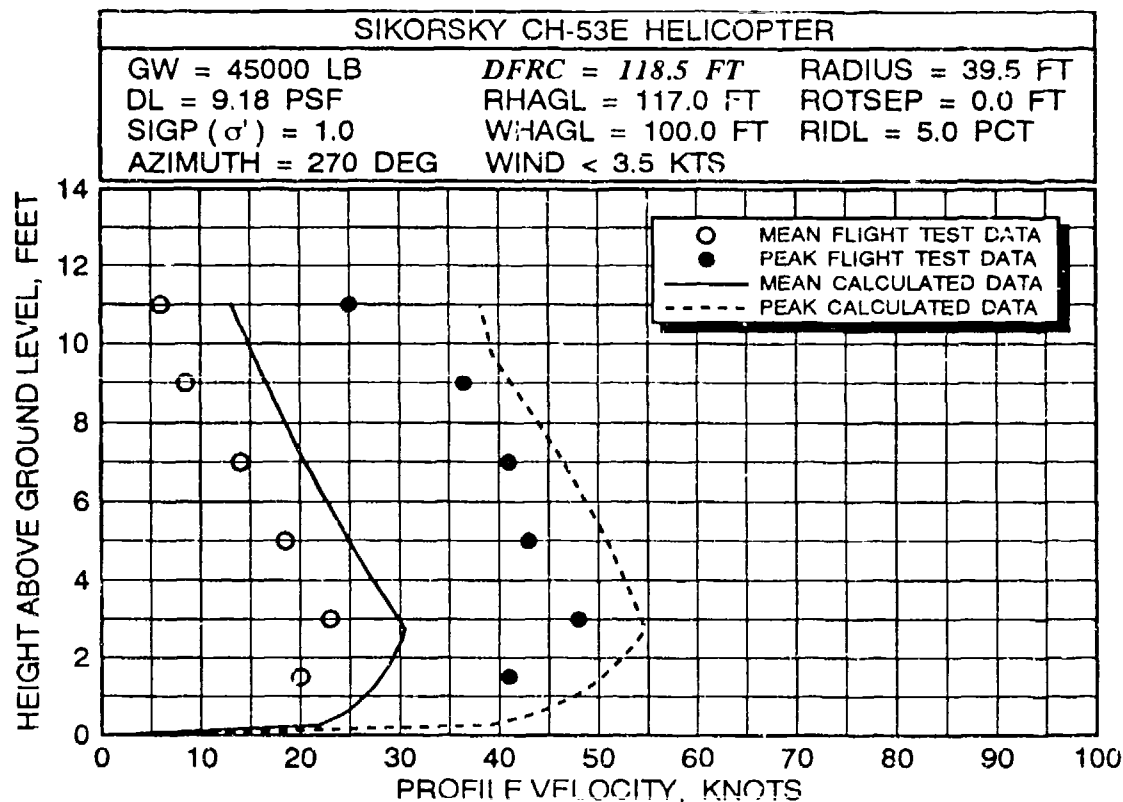
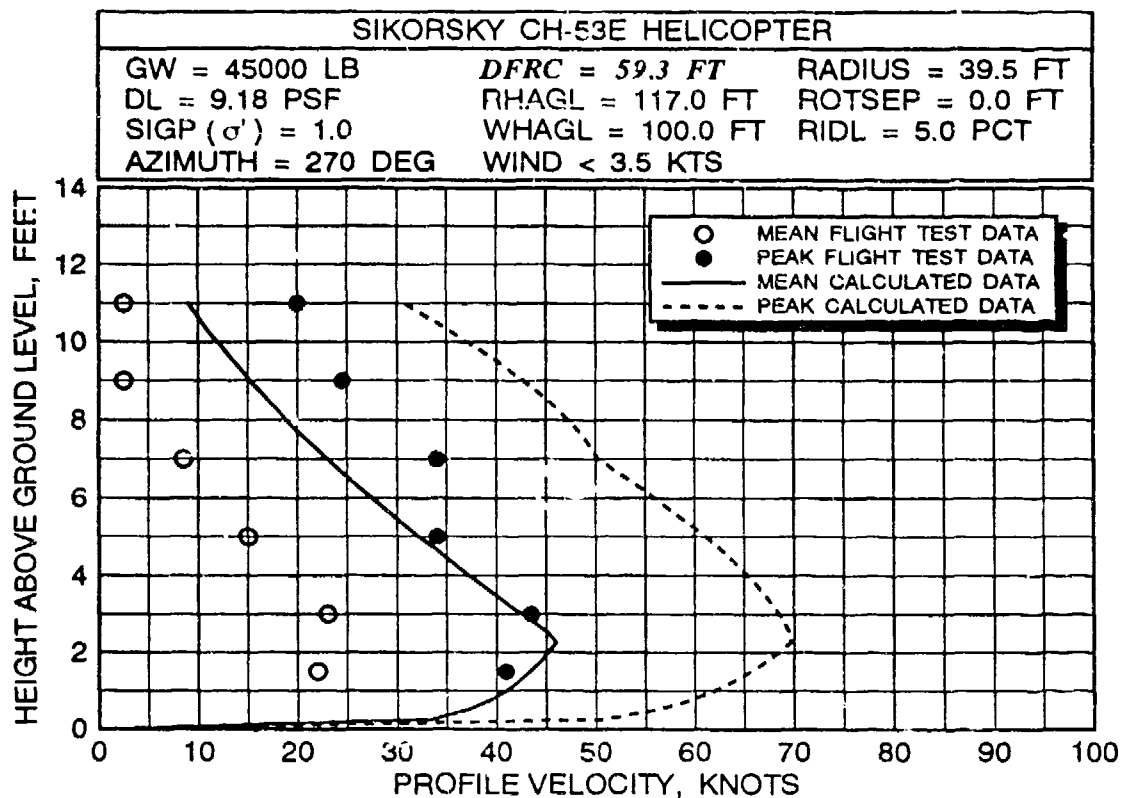


FIGURE 41 CH-53E MEAN/PEAK VELOCITY PROFILE CORRELATION AT 59.3 AND 118.5 FEET ALONG THE 270-DEGREE AZIMUTH AT AN AVERAGE GROSS WEIGHT OF 45,000 POUNDS AND A ROTOR HEIGHT OF 117 FEET

3.2 XV-15 TILTROTOR VELOCITY PROFILE CORRELATION

Correlation with the Bell XV-15 tiltrotor was conducted using flight test data documented in reference 23. This aircraft is an experimental two-seat concept demonstrator vehicle that was initially flown in 1977. The gross weight range for vertical takeoff typically varies between approximately 12,000 and 13,800 pounds. A three-view profile of the XV-15 is presented in figure 42. XV-15 specific input data parameters that are required to execute the ROTWASH analysis program were defined previously in table 2 (see page 68). The flight test data presented in reference 23 were obtained at azimuths of 0, 180, and 270 degrees (or forward, rearward, and to the left side of the pilot, respectively). Six stations were evaluated along each of these radials. These station positions are defined with respect to the XV-15 in figure 43. Ambient winds measured during the tests were below 2 knots. Data were also obtained at the radial station of 15.6 feet for 14.5, 37.5, and 62.5-feet RHAGL. Significant variations in gross weight were not evaluated. A test matrix for the XV-15, similar to the one presented for the CH-53E in table 3, is presented in table 4.

Correlation of calculated data with flight test data along the 270-degree radial position (the non-interaction plane) as a function of distance from the center of the left rotor is presented in figure 44.

These data are for a gross weight of approximately 12,475 pounds at a rotor height of 37.5 feet (wheel height of 25 feet). In a majority of the comparisons, the correlation results indicate that the ROTWASH analysis methodology predicts XV-15 mean and peak velocities (from 0 to 9-feet HAGL) to within 5 knots of measured flight test data. The poorest correlation occurs for the middle two test positions, DFRC values of 25 and 37.5 feet, with respect to peak velocity correlation. Since the peak velocity profile is based upon an empirical curve, this correlation could be easily improved. However, this would mean using a different fit than is used with CH-53E data. Since so little XV-15 data exist, it is believed that this decision would be better made at some future date. Unfortunately, any statistical comparison of these results is somewhat meaningless due to the nature of the acquired data, as was noted in the CH-53E discussion. Also, as noted with the CH-53E, the height of the maximum velocity along the mean profile, except in the far field, is underpredicted using the ROTWASH analysis methodology. This deficiency has been eliminated in plotted results by specifying a minimum boundary layer thickness of approximately 1.5 feet using a newly incorporated option provided in version 2.1 of the ROTWASH software.

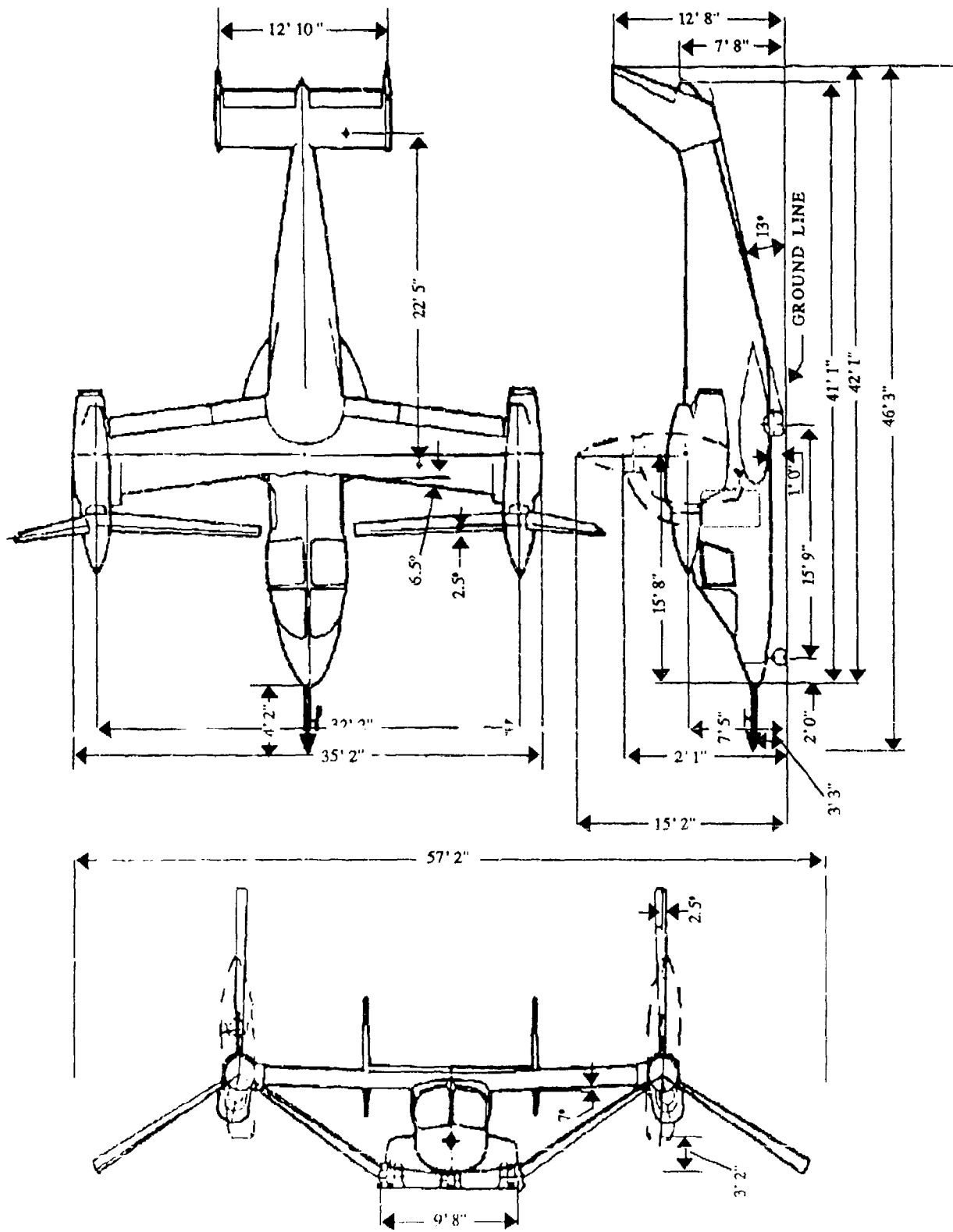


FIGURE 42 THREE-VIEW DRAWING OF THE BELL XV-15

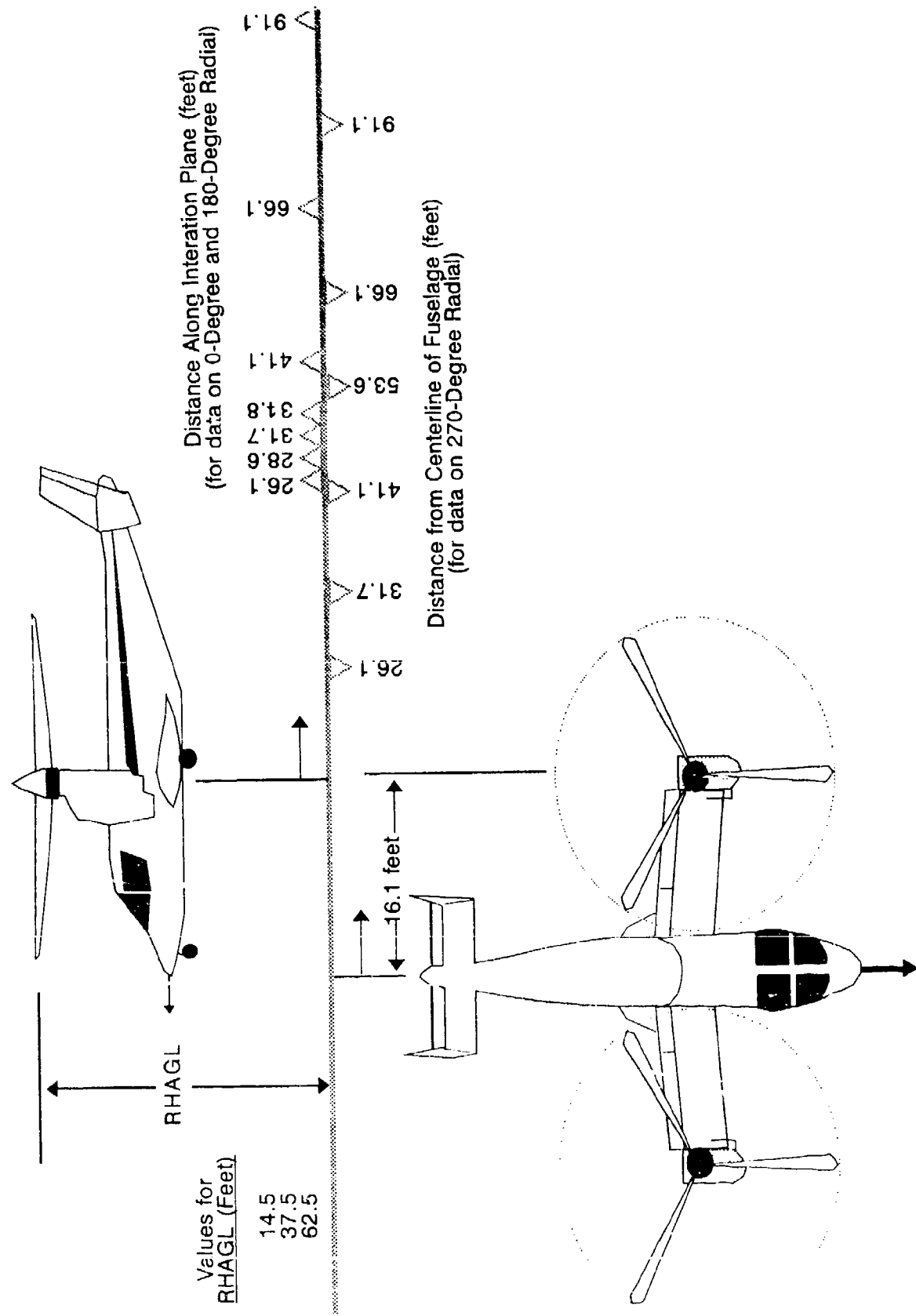


FIGURE 43 XV-15 FLIGHT TEST DATA MEASUREMENT LOCATIONS

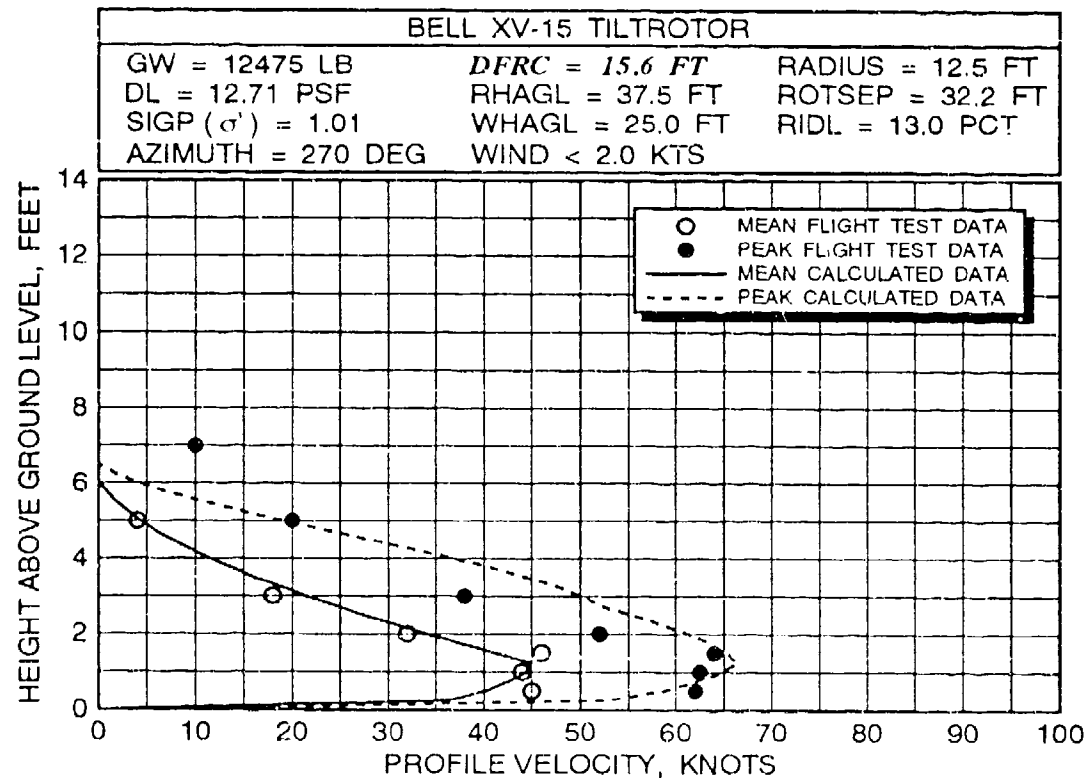
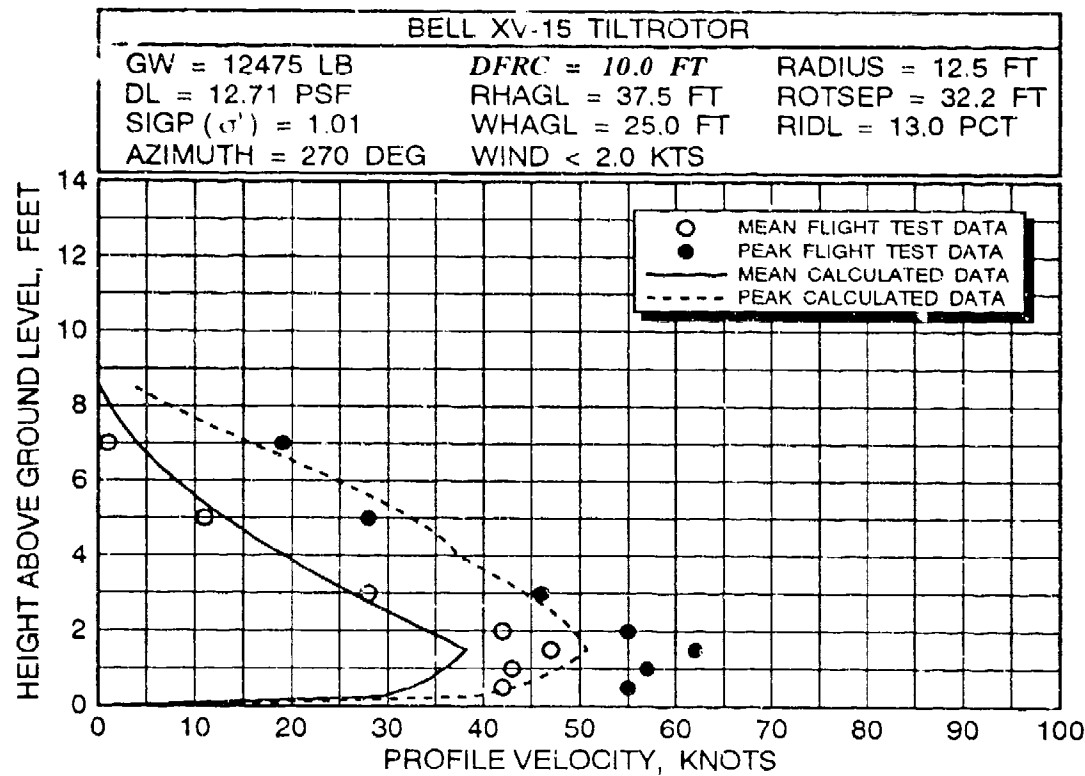


FIGURE 44 XV-15 MEAN/PEAK VELOCITY PROFILE CORRELATION ALONG THE 270- DEGREE AZIMUTH RADIAL AT AN AVERAGE GROSS WEIGHT OF 12,475 POUNDS AND A ROTOR HEIGHT OF 37.5 FEET

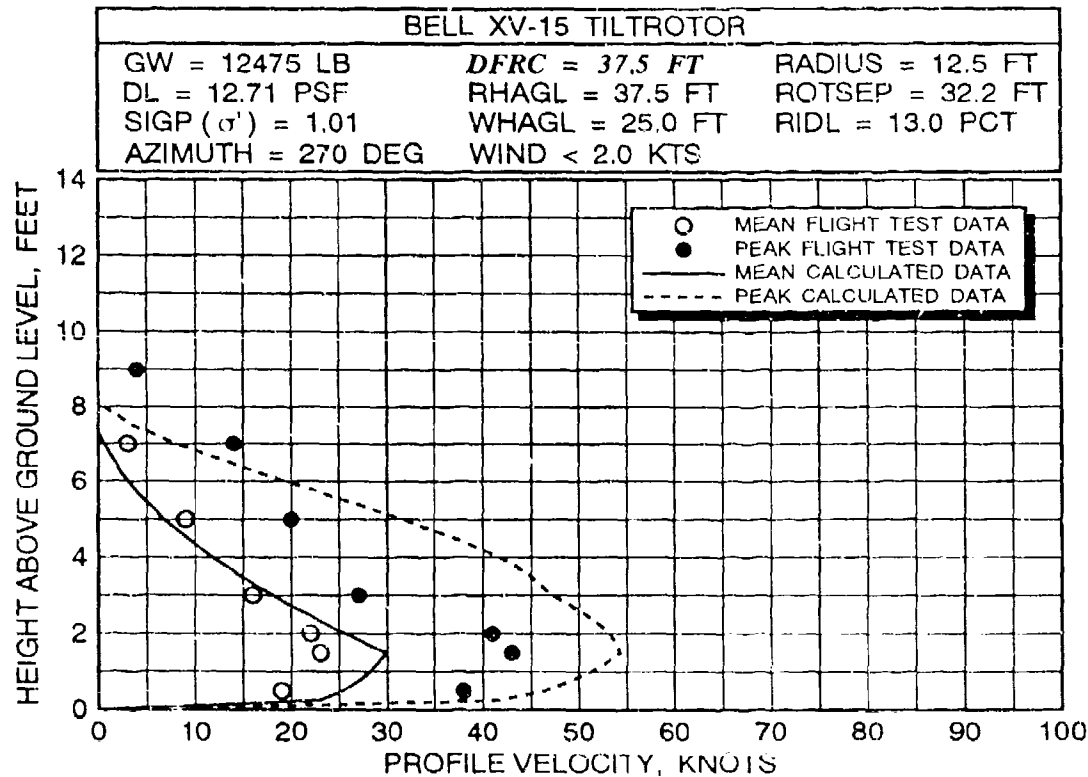
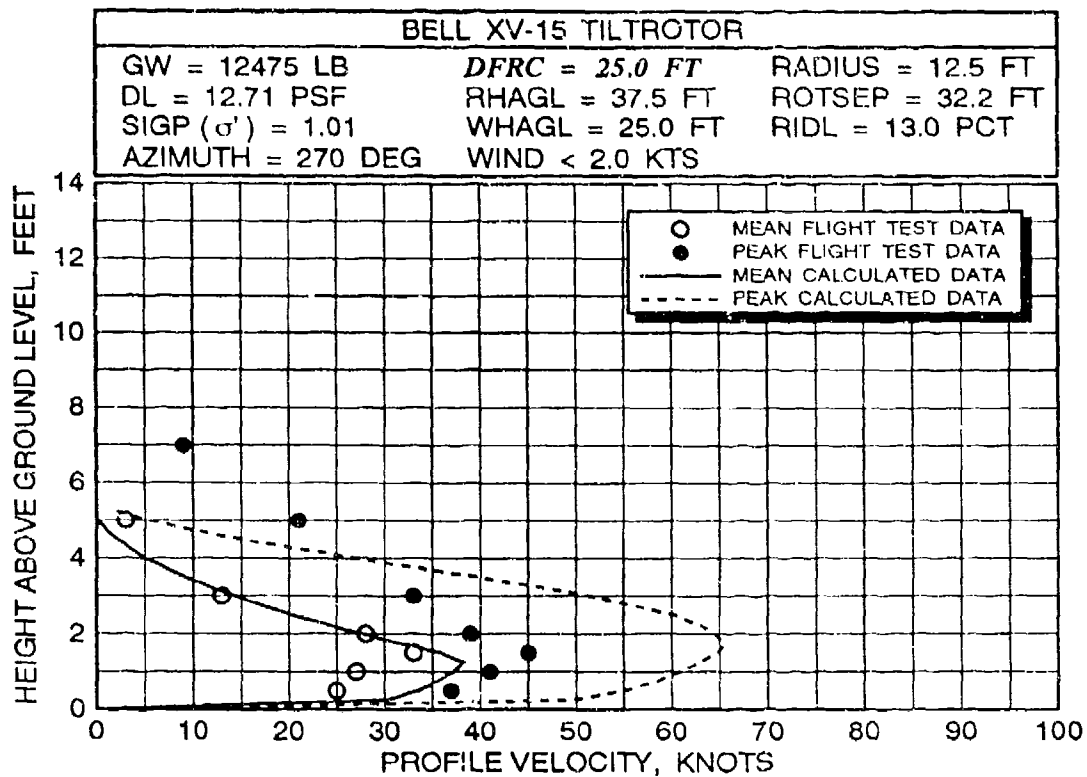


FIGURE 44 XV-15 MEAN/PEAK VELOCITY PROFILE CORRELATION ALONG THE 270- DEGREE AZIMUTH RADIAL AT AN AVERAGE GROSS WEIGHT OF 12,475 POUNDS AND A ROTOR HEIGHT OF 37.5 FEET (continued)

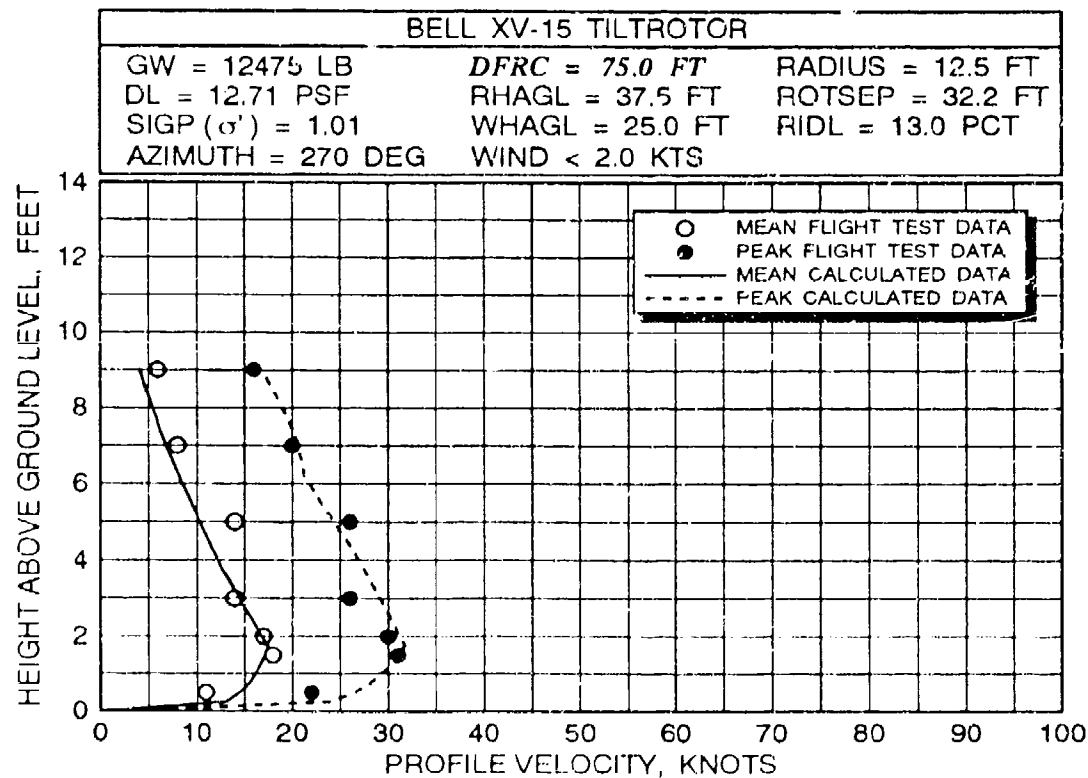
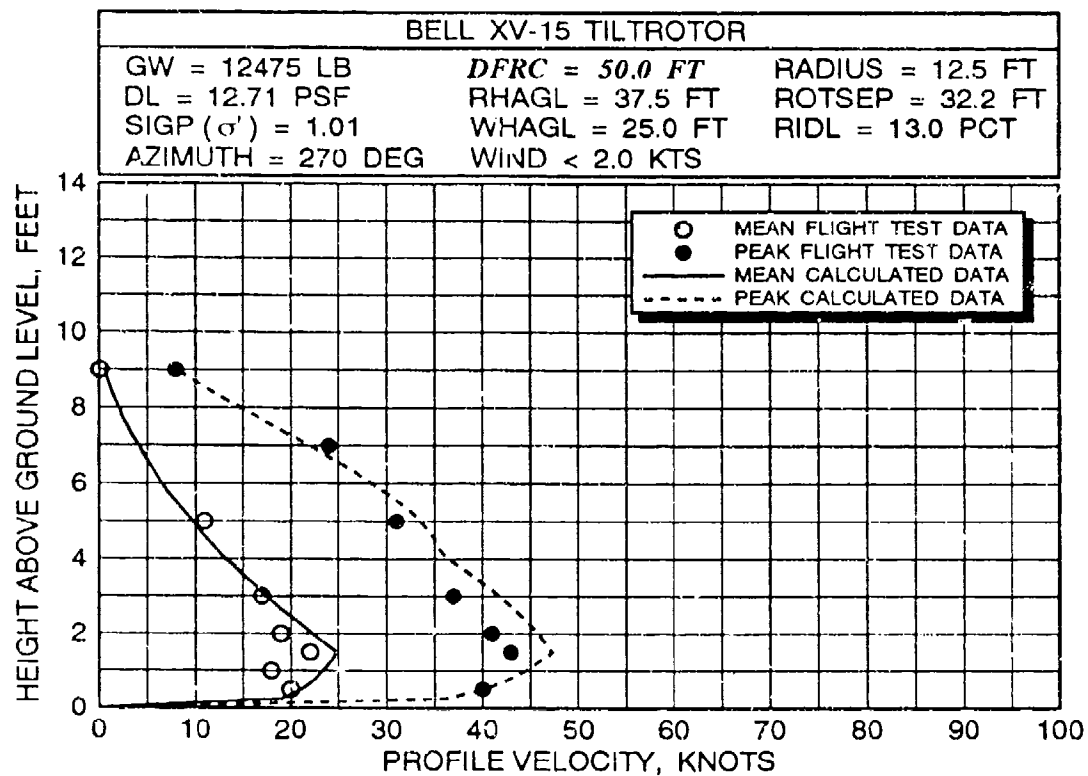


FIGURE 44 XV-15 MEAN/PEAK VELOCITY PROFILE CORRELATION ALONG THE 270- DEGREE AZIMUTH RADIAL AT AN AVERAGE GROSS WEIGHT OF 12,475 POUNDS AND A ROTOR HEIGHT OF 37.5 FEET (continued)

TABLE 4 EVALUATION MATRIX FOR XV-15 FLIGHT TEST/MATHEMATICAL MODEL DATA CORRELATION

FIGURE NUMBER	GROSS WEIGHT ¹ (lb)	DISK LOADING ¹ (lbs/ft ²)	ROTOR HEIGHT (feet)	AZIMUTH ANGLE (degree)	DISTANCE FROM LEFT ROTOR CENTER (DFRC) OR DISTANCE ALONG INTERACTION PLANE (DAIP) ²
44	12,475	12.71	37.5	270	10.0, 15.6, 25.0, 37.5, 50.0, 75.0
46	12,555	12.79	14.5, 37.5, 62.5	270	15.6
47	12,475	12.71	37.5	0	26.1, 31.7, 34.8, 41.1, 66.1, 99.1
48	12,475	12.71	37.5	180	26.1, 28.6, 31.7, 41.1, 66.1, 99.1
49	12,555	12.79	14.5, 37.5, 62.5	0	31.7
50	12,555	12.79	14.5, 37.5, 62.5	180	31.7

NOTES:

- (1) Even though care has been taken to calculate realistic average gross weights, the values are average values that could vary between 12,030 and 13,000 lbs at the extremes. Disk loadings are 12.71 lbs/ft² at 12,475 pounds and 12.79 lbs/ft² at 12,555 pounds.
- (2) The values of DFRC are applicable along only the 270-degree azimuth, whereas the values for DAIP are valid along only the 0- and 180-degree azimuths.
- (3) Atmospheric density ratio varied between 0.98 and 1.01 during testing.

Mean reverse flow velocities, as observed in measured data very close to the rotor, are not predicted at heights above ground level in excess of 5 to 7 feet. These velocities are due to vorticity and, at very low rotor heights, a tendency for rotor recirculation. Both of these effects are not modeled.

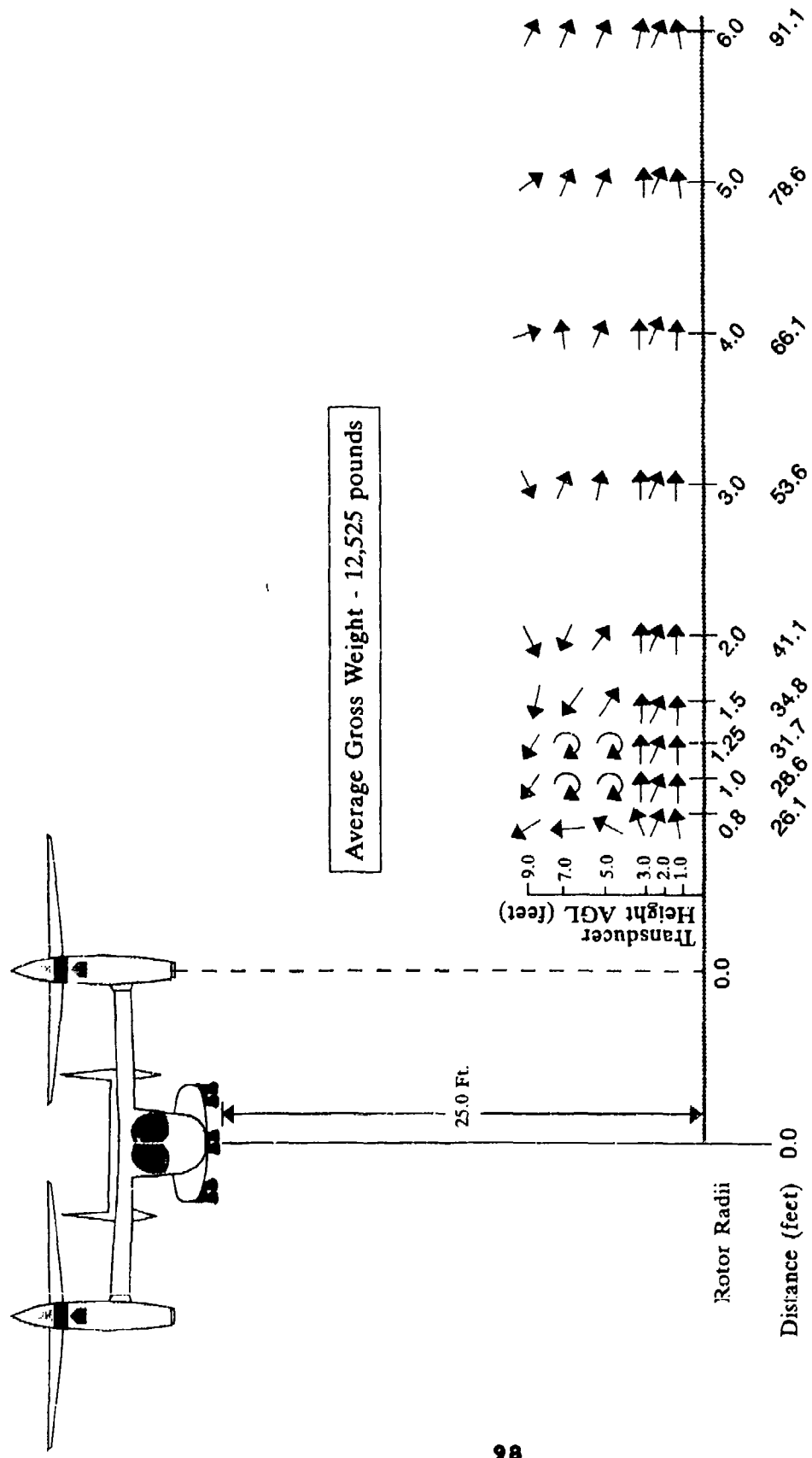
Figure 45, reproduced from reference 23, provides example direction of flow information for these portions of the flow field.

Data comparing velocity profiles at the 15.6-foot radial station as a function of a variation in rotor height (at 14.5-, 37.5-, and 62.5-feet RHAGL) are presented in figure 46. This limited comparison indicates that the calculated velocity profiles at the three rotor heights correlate quite well with the measured flight

test profiles. These results are particularly pleasing because this radial station is not at a particularly good distance for correlation. This is because the station is located extremely close to the tip of the rotor (within approximately 3 feet). Since correlation data as a function of rotor height are provided for only this one radial station, it must be assumed that the quality of correlation at other radial stations would be similar to that provided in figure 44.

Correlation of flight test and calculated data along the interaction plane (the plane perpendicular to and one-half the distance between the two rotors, or out the aircraft centerline along either the 0- or 180-degree azimuth) is presented in figures 47 and 48. It is important to note that the ROTWASH mathematical model does not take into account any fuselage characteristics that might affect results along either the 0- or 180-degree azimuths. The program assumes symmetry in the flow field for a zero wind hover at all positions equidistant from the line connecting the rotors. However, this assumption of symmetry is not necessarily validated by flight test data obtained in the presence of a real fuselage. A comparison of flight test velocity profiles at each of the interaction plane stations, particularly the 41.1-, 66.1-, and 91.1-foot positions, indicates that a distinct difference exists in the shape of the profiles. The reason for these differences is unknown at this time. Data correlated along the 0-degree azimuth indicate that the mathematical model closely predicts (or slightly overpredicts) the measured XV-15 velocity profiles. Likewise, a comparison of results along the 180-degree azimuth indicates a similar overprediction of velocity profiles, particularly at low profile heights, out to station positions slightly greater than 41.1 feet. At the 66.1- and 91.1-feet positions, correlation of the peak profiles is quite good, but the mean profiles are somewhat underpredicted.

Correlation for both the 0- and 180-degree azimuths as a function of rotor height at the 15.6-foot station position is presented in figures 49 and 50. In most cases, the magnitudes of the average calculated profile velocities compare quite well with measured velocities. However, the shapes of the calculated and measured velocity profiles do not compare as closely as would be desired, particularly at positions above 5-feet HAGL.



Source: Reference 23.

FIGURE 45 **XV-15** DOWNWASH FLOW FIELD VELOCITY VECTORS IN THE VERTICAL PLANE AT A 25.0 FOOT WHEEL HEIGHT ALONG THE 270 DEGREE AZIMUTH

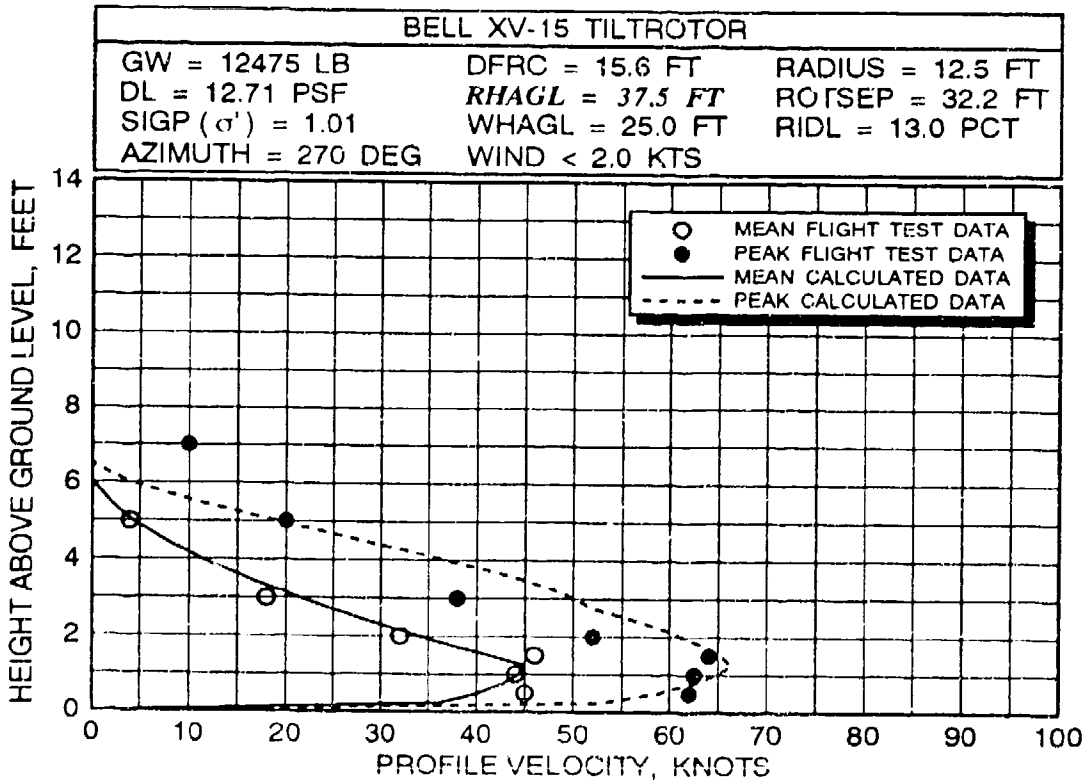
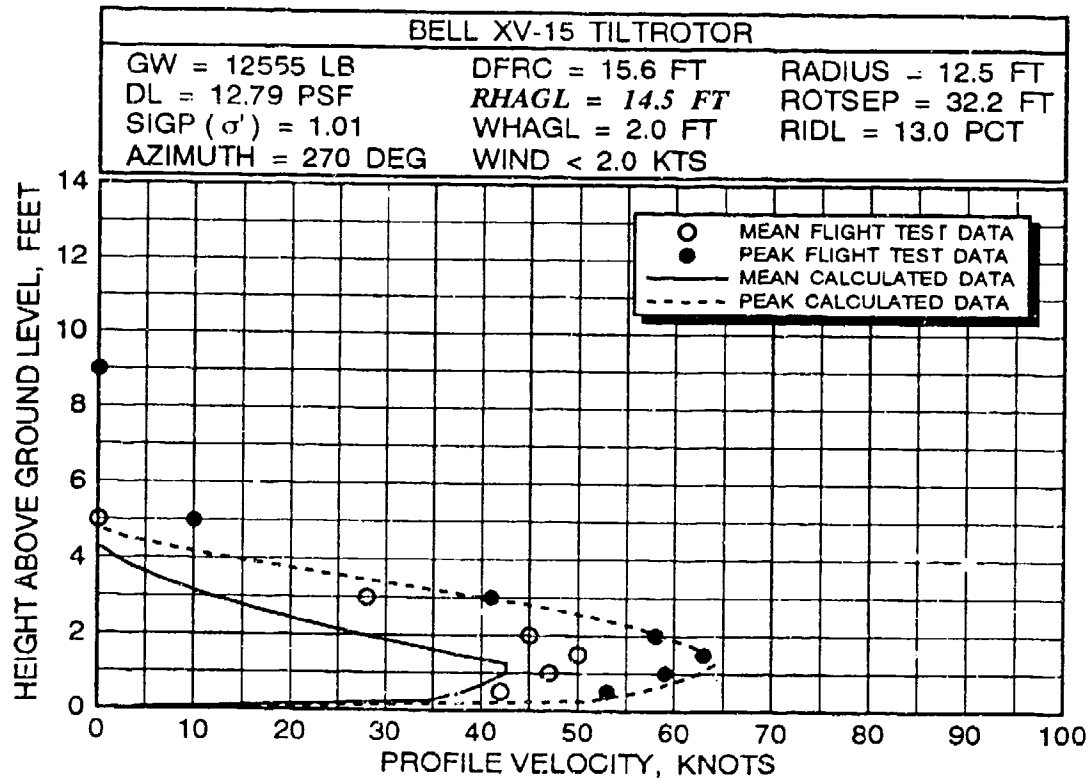
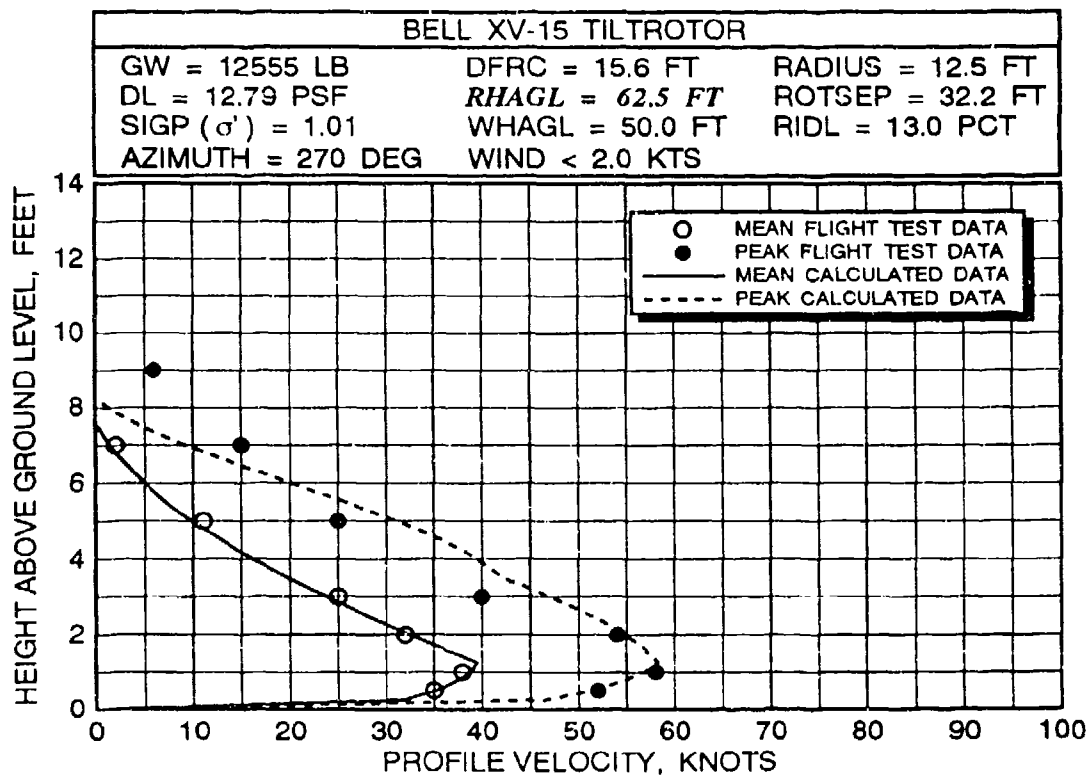


FIGURE 46 XV-15 MEAN/PEAK VELOCITY PROFILE CORRELATION ALONG THE 270-DEGREE AZIMUTH RADIAL AT THREE ROTOR HEIGHTS FOR AN AVERAGE GROSS WEIGHT BETWEEN 12,475 AND 12,555 POUNDS



**FIGURE 46 XV-15 MEAN/PEAK VELOCITY PROFILE CORRELATION
ALONG THE 270-DEGREE AZIMUTH RADIAL AT THREE
ROTOR HEIGHTS FOR AN AVERAGE GROSS WEIGHT BETWEEN
12,475 AND 12,555 POUNDS (continued)**

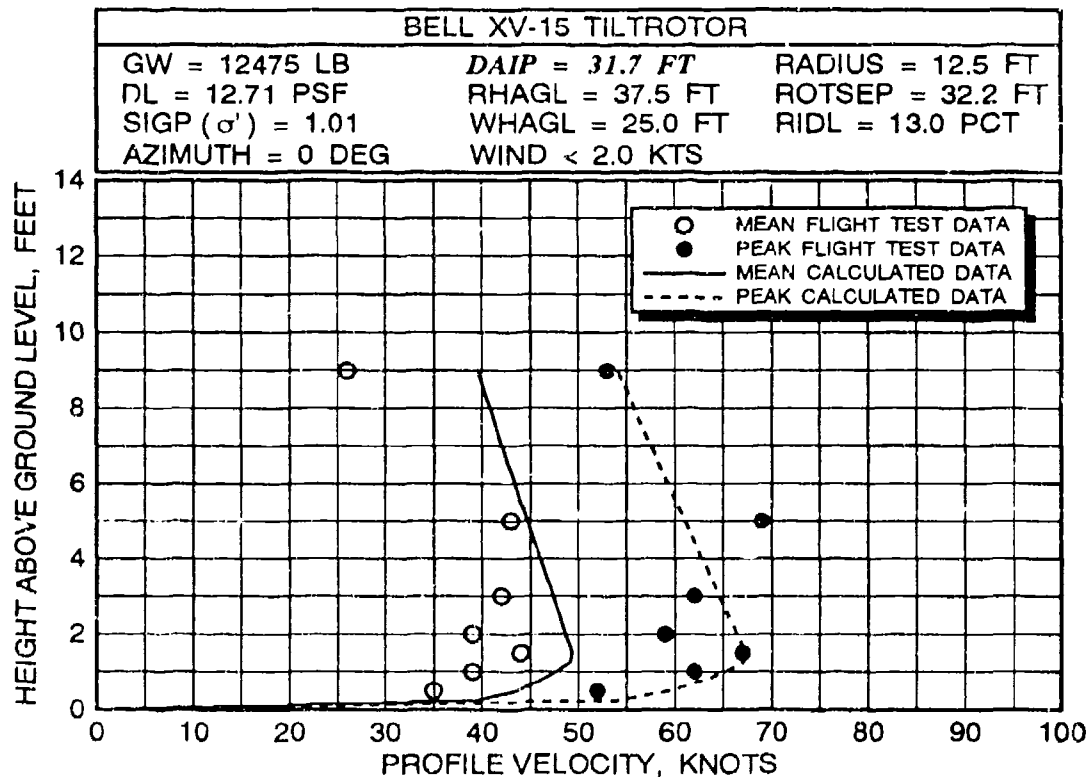
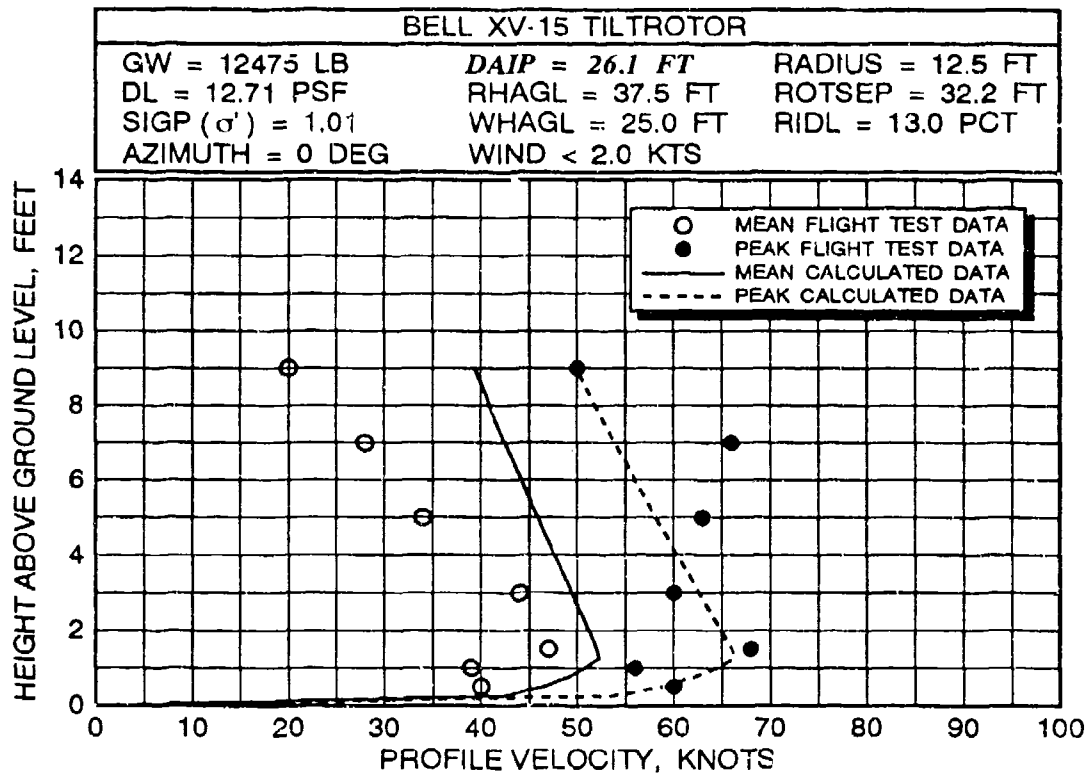


FIGURE 47 XV-15 MEAN/PEAK VELOCITY PROFILE CORRELATION ALONG THE 0-DEGREE AZIMUTH RADIAL AT AN AVERAGE GROSS WEIGHT OF 12,475 POUNDS AND A ROTOR HEIGHT OF 37.5 FEET

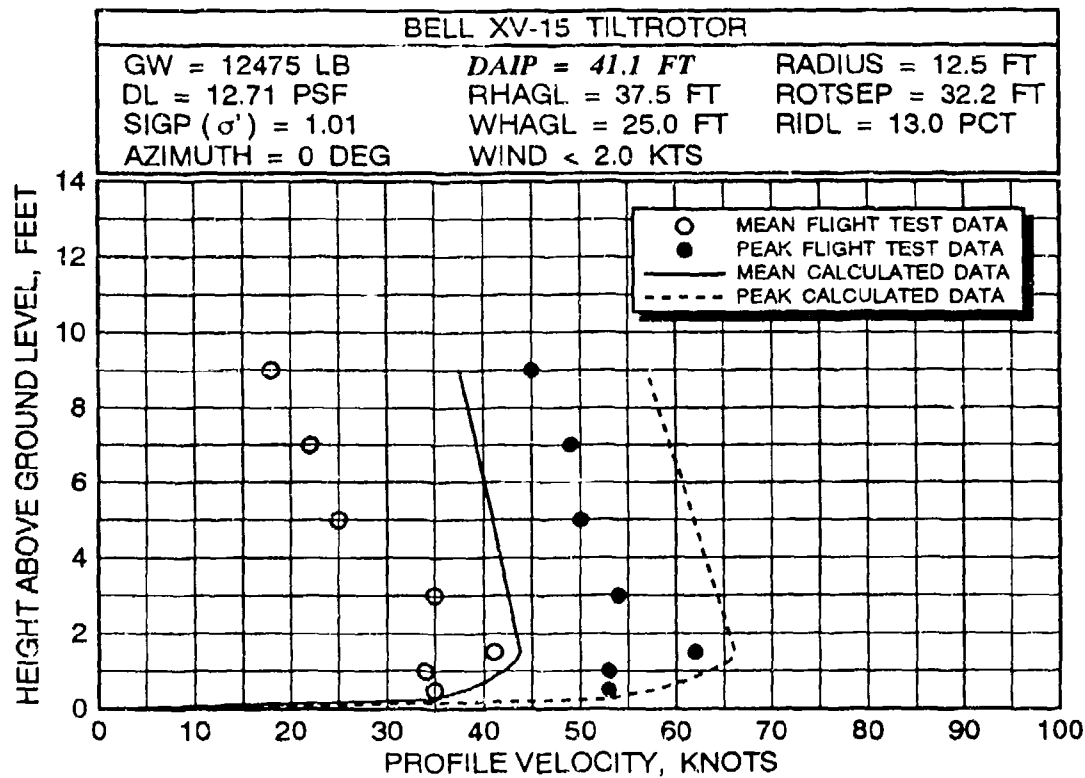
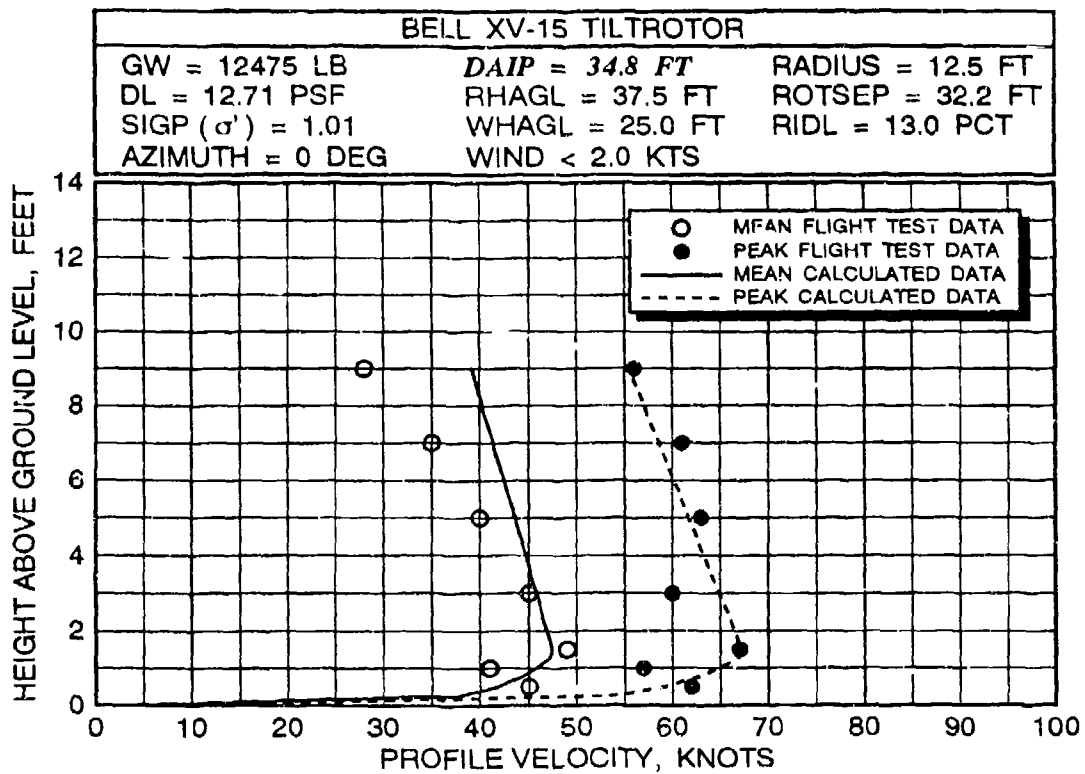


FIGURE 47 XV-15 MEAN/PEAK VELOCITY PROFILE CORRELATION ALONG THE 0-DEGREE AZIMUTH RADIAL AT AN AVERAGE GROSS WEIGHT OF 12,475 POUNDS AND A ROTOR HEIGHT OF 37.5 FEET (continued)

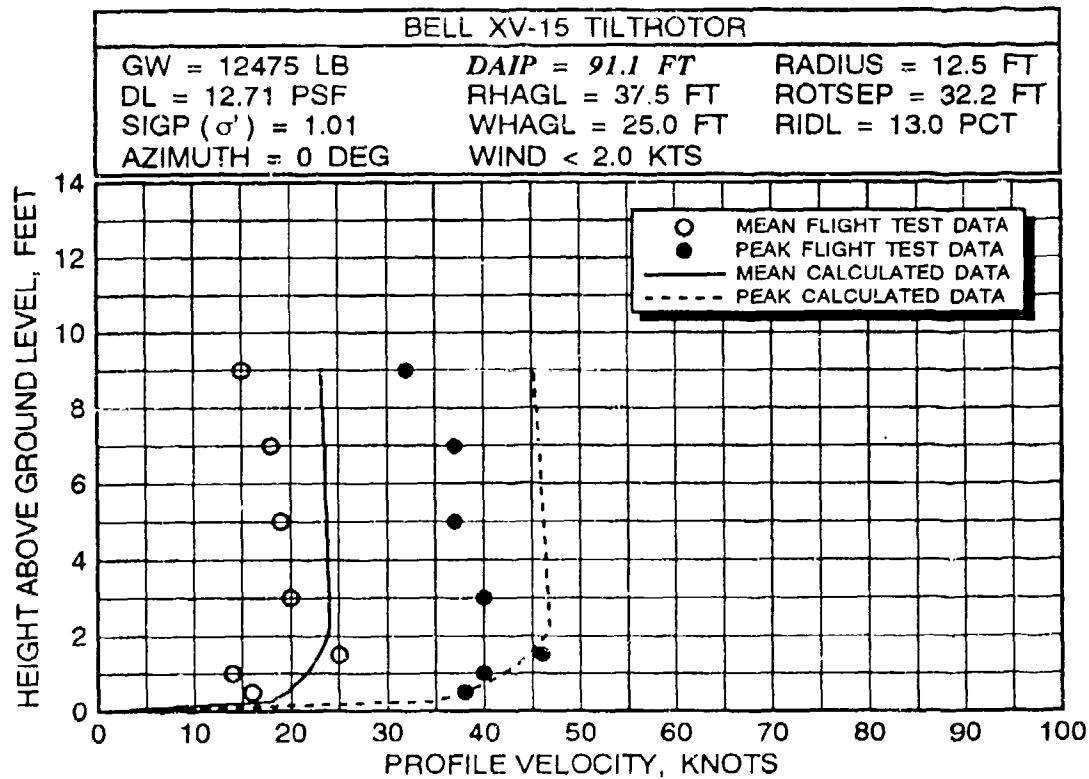
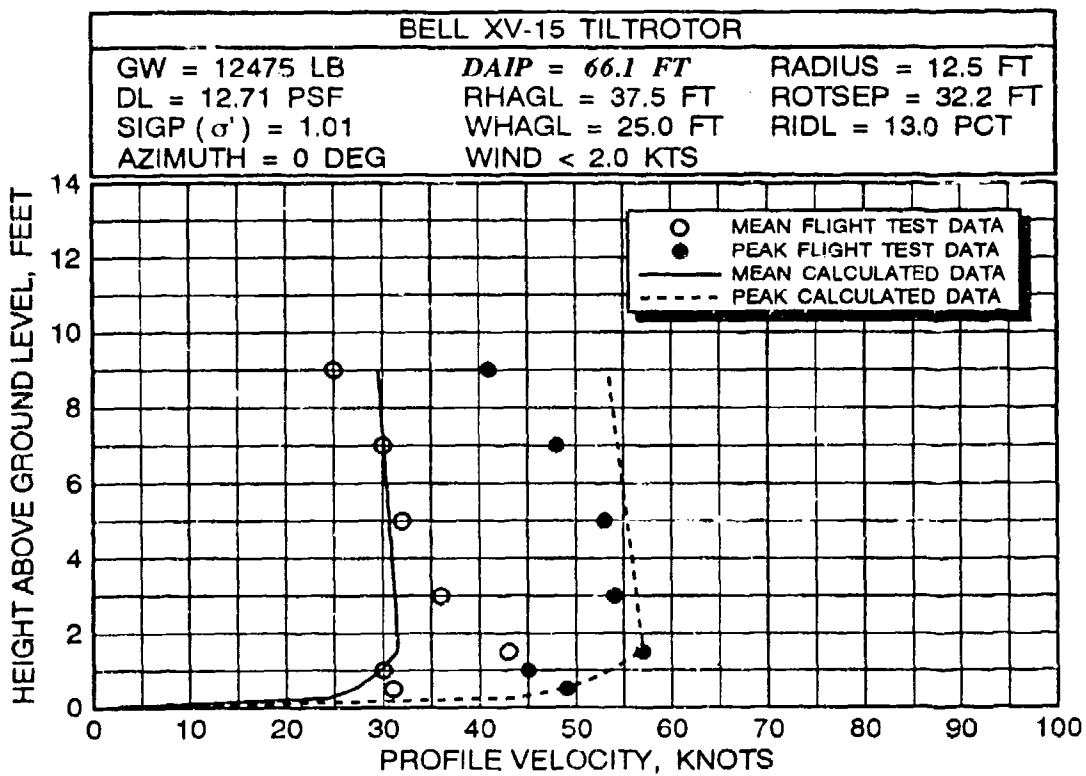


FIGURE 47 XV-15 MEAN/PEAK VELOCITY PROFILE CORRELATION ALONG THE 0-DEGREE AZIMUTH RADIAL AT AN AVERAGE GROSS WEIGHT OF 12,475 POUNDS AND A ROTOR HEIGHT OF 37.5 FEET (continued)

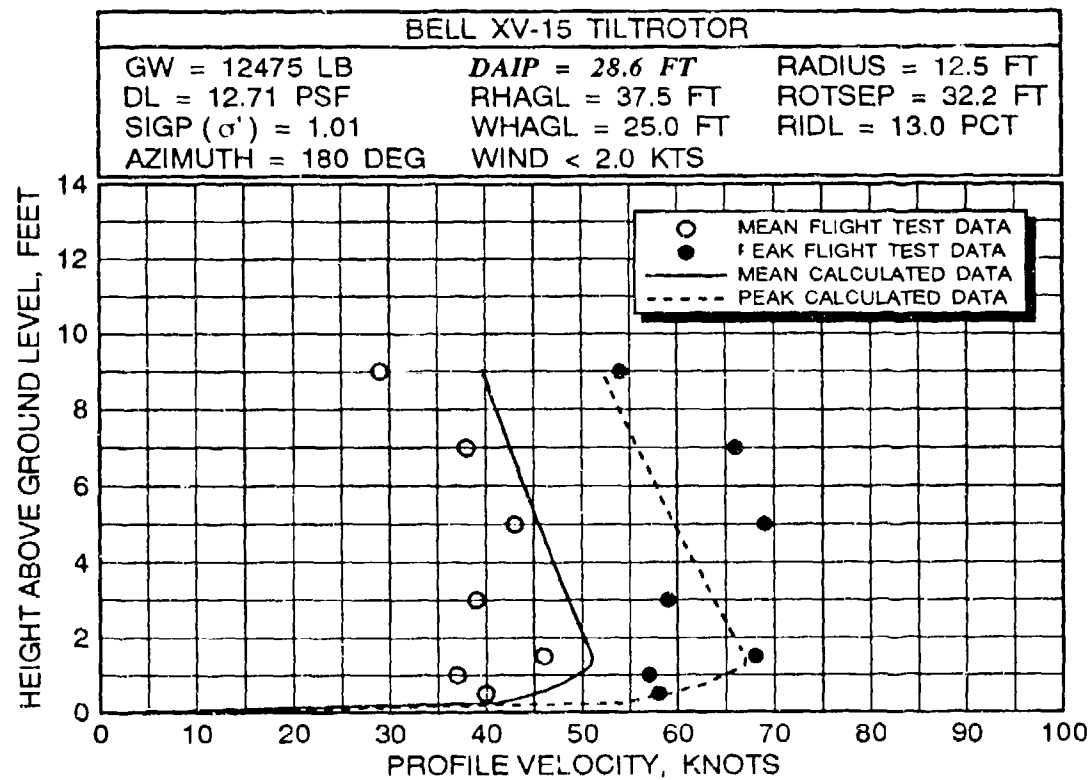
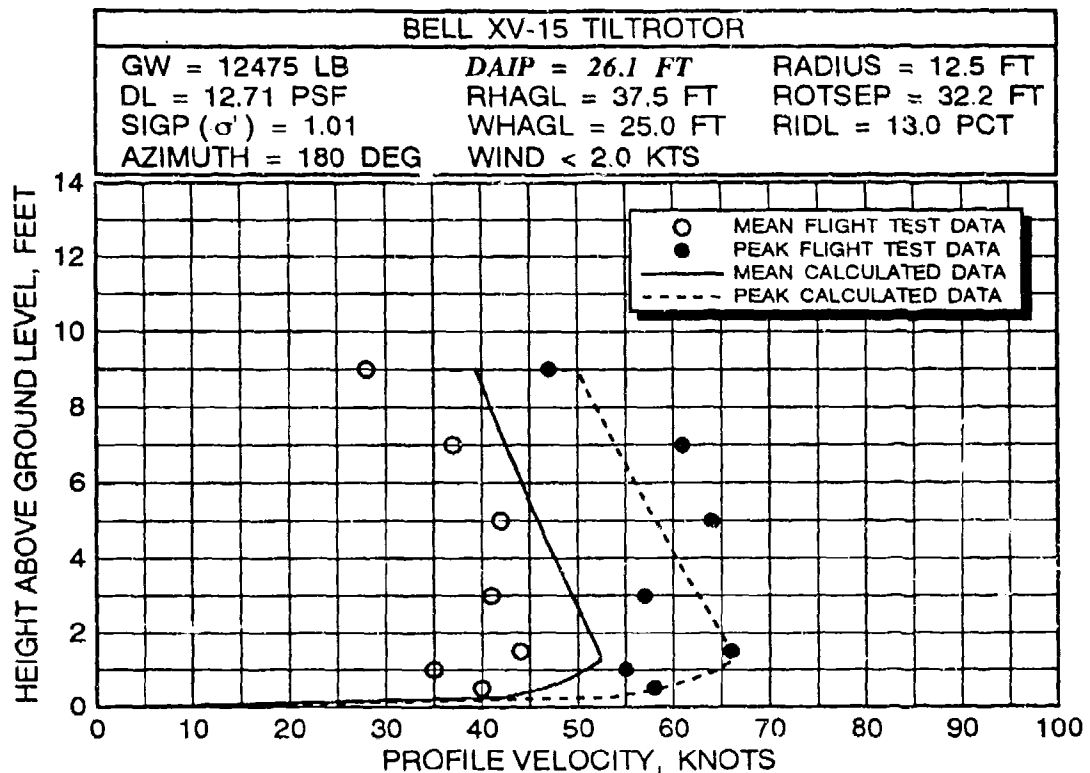


FIGURE 48 XV-15 MEAN/PEAK VELOCITY PROFILE CORRELATION ALONG THE 180-DEGREE AZIMUTH RADIAL AT AN AVERAGE GROSS WEIGHT OF 12,475 POUNDS AND A ROTOR HEIGHT OF 37.5 FEET

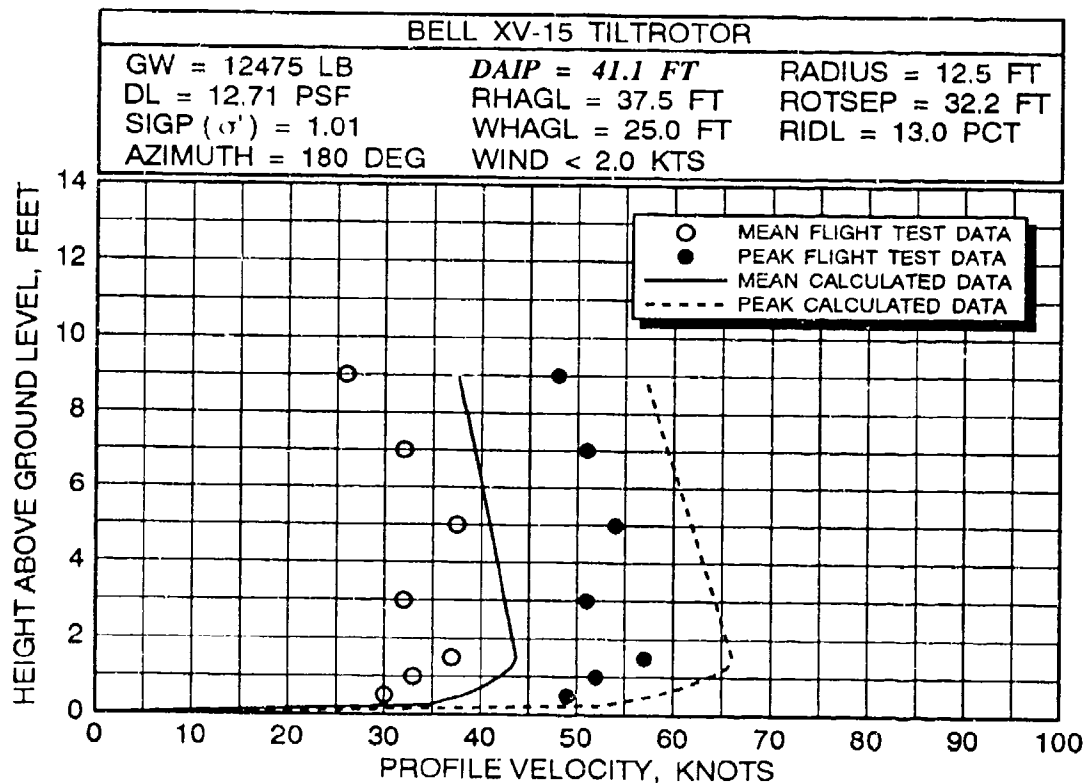
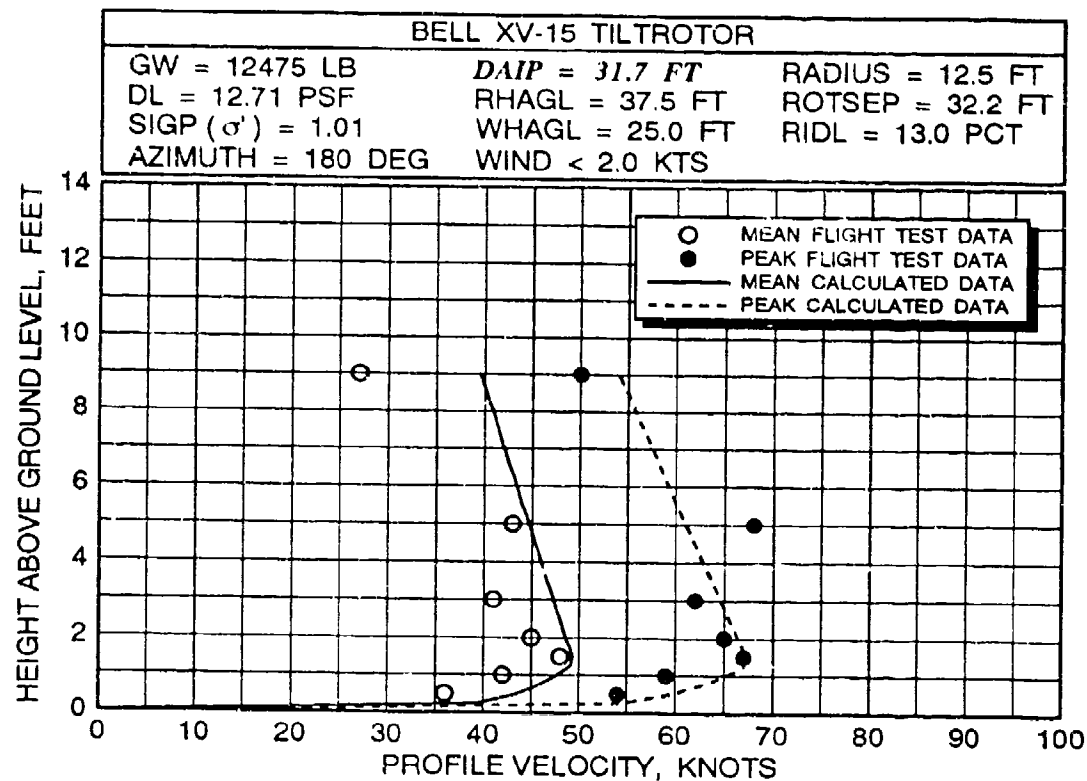


FIGURE 48 XV-15 MEAN/PEAK VELOCITY PROFILE CORRELATION ALONG THE 180-DEGREE AZIMUTH RADIAL AT AN AVERAGE GROSS WEIGHT OF 12,475 POUNDS AND A ROTOR HEIGHT OF 37.5 FEET (continued)

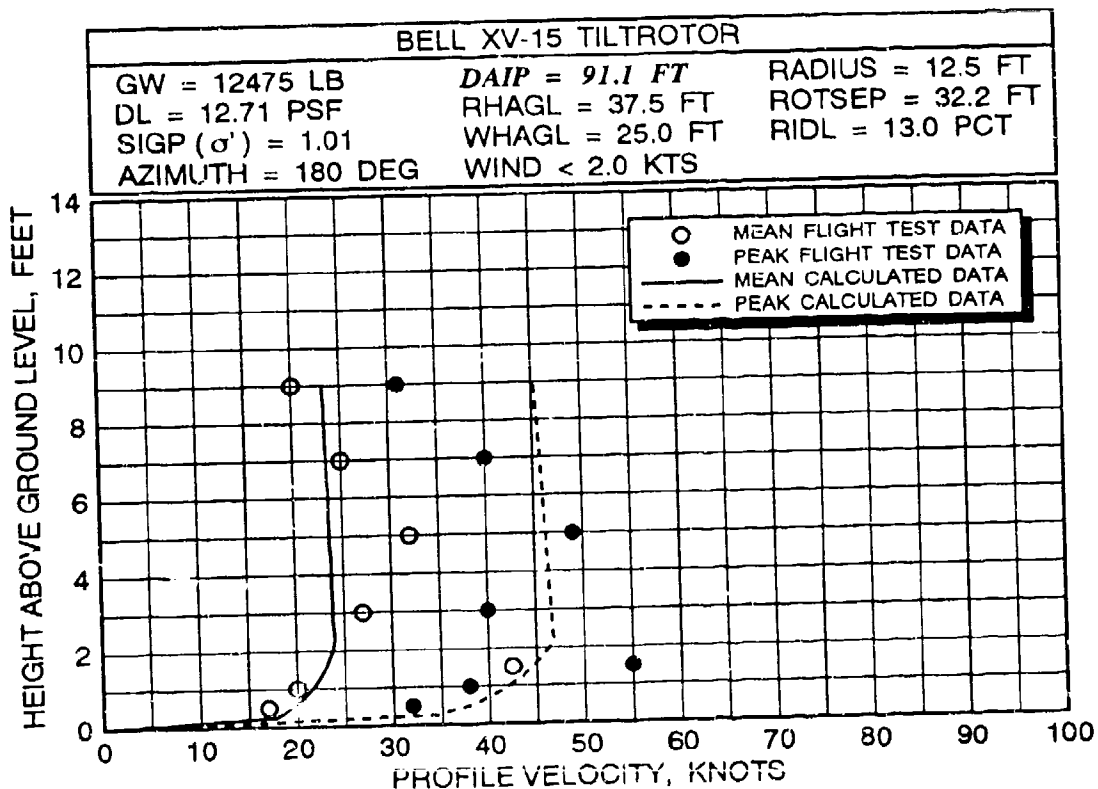
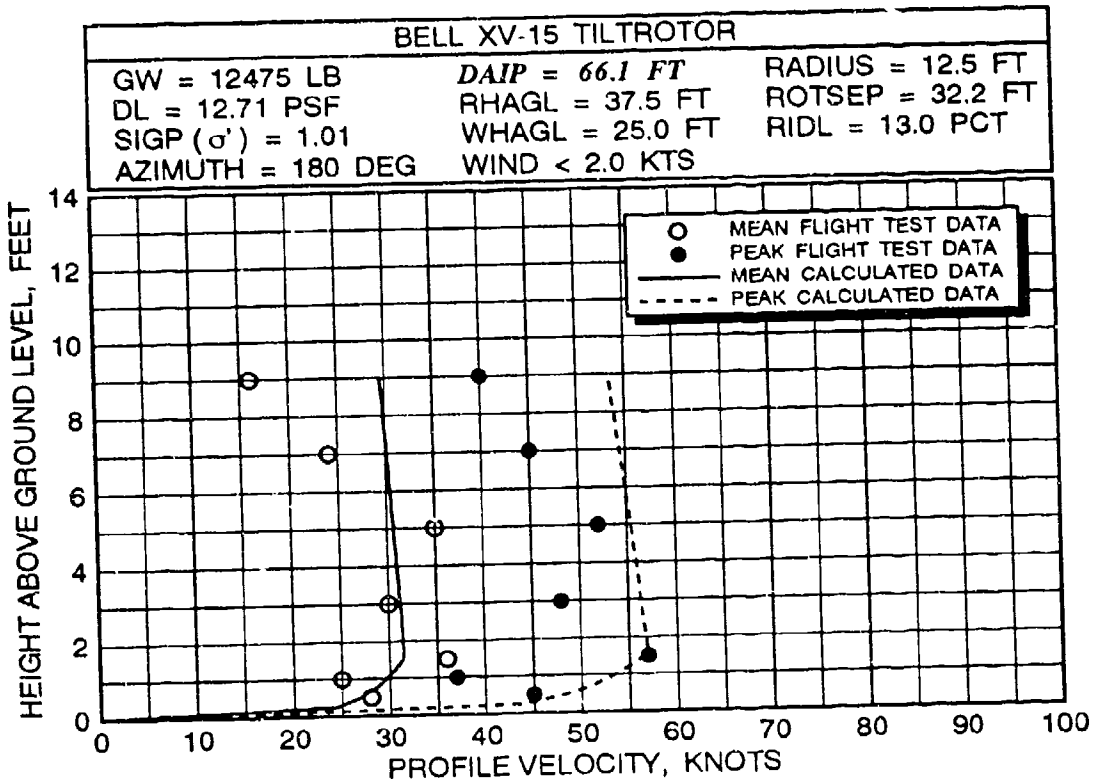


FIGURE 48 XV-15 MEAN/PEAK VELOCITY PROFILE CORRELATION ALONG THE 180-DEGREE AZIMUTH RADIAL AT AN AVERAGE GROSS WEIGHT OF 12,475 POUNDS AND A ROTOR HEIGHT OF 37.5 FEET (continued)

Overall, for the intended purposes, correlation of Bell XV-15 data appears quite good. Limitations associated with the mathematical model theory that were discussed with respect to the CH-53E can certainly be assumed to apply to an analysis of tiltrotors. It must also be noted that limitations and errors that are undocumented do exist in the procedures, instrumentation, and data reduction processes involved in measuring flight test data. The good correlation shown with the tiltrotor configuration also increases confidence for the quality of predictions for the more symmetrically balanced tandem rotor helicopter configurations, especially along the interaction plane.

3.3 MV-22 TILTROTOR VELOCITY PROFILE CORRELATION

The Bell-Boeing MV-22 is the first tiltrotor to go into production and weighs up to approximately 47,500 pounds in the vertical takeoff mode. A three view profile of this tiltrotor is presented in figure 51. Correlation with the MV-22 was conducted using the limited flight test data documented in reference 5. These flight test data were obtained at only one position with respect to the aircraft along the 0-degree azimuth (forward along the aircraft centerline) during a U.S. Navy preliminary flight evaluation. Later evaluations are planned to cover a large envelope of airspace around the aircraft at several rotor heights and gross weights (similar to the CH-53E and XV-15 evaluations). MV-22 specific input data parameters that are required to execute the ROTWASH analysis program were defined previously in table 2 (see page 68).

The velocity profile data measured for correlation are along the interaction plane at a distance of 57 feet from rotor center and are documented in figure 52. Gross weight during the test varied from a high of 40,300 pounds to a low of 39,350 pounds. Rotor heights above ground are 35.0, 46.0, and 68.0 feet. The component of ambient wind along the 0-degree azimuth where the data were measured was calculated as approximately 2.4 knots (unfortunately, the total ambient wind reached as high as 7 knots at times along the 250-degree radial). The atmospheric density ratio was approximately 1.015.

Correlation results presented in figure 52 indicate that at the 46-foot rotor height (wheel height of 25 feet), the calculated and measured mean velocity profiles compare quite closely. At sensor measurement positions below 4 feet, the measured profile velocities slightly exceed calculated velocities with the reverse occurring at heights above 4 feet. Peak velocity profile calculations are nearly identical with measured data at the 46-foot rotor height but are consistently less than measured data at the 35-foot height.

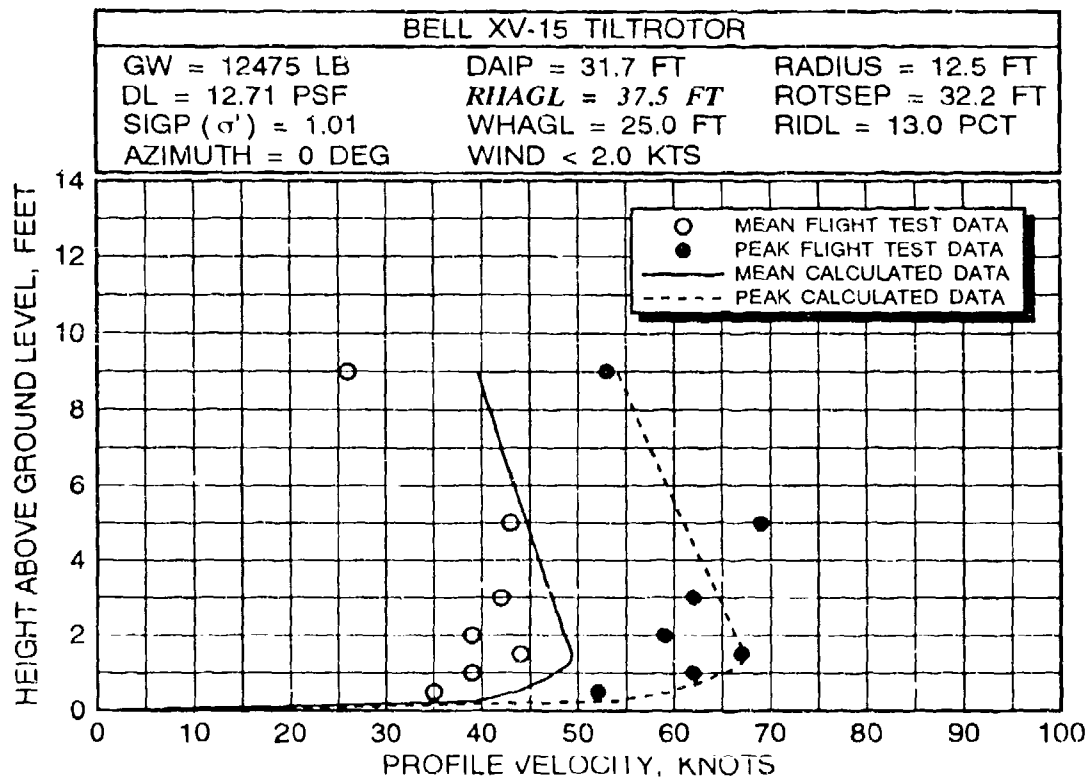
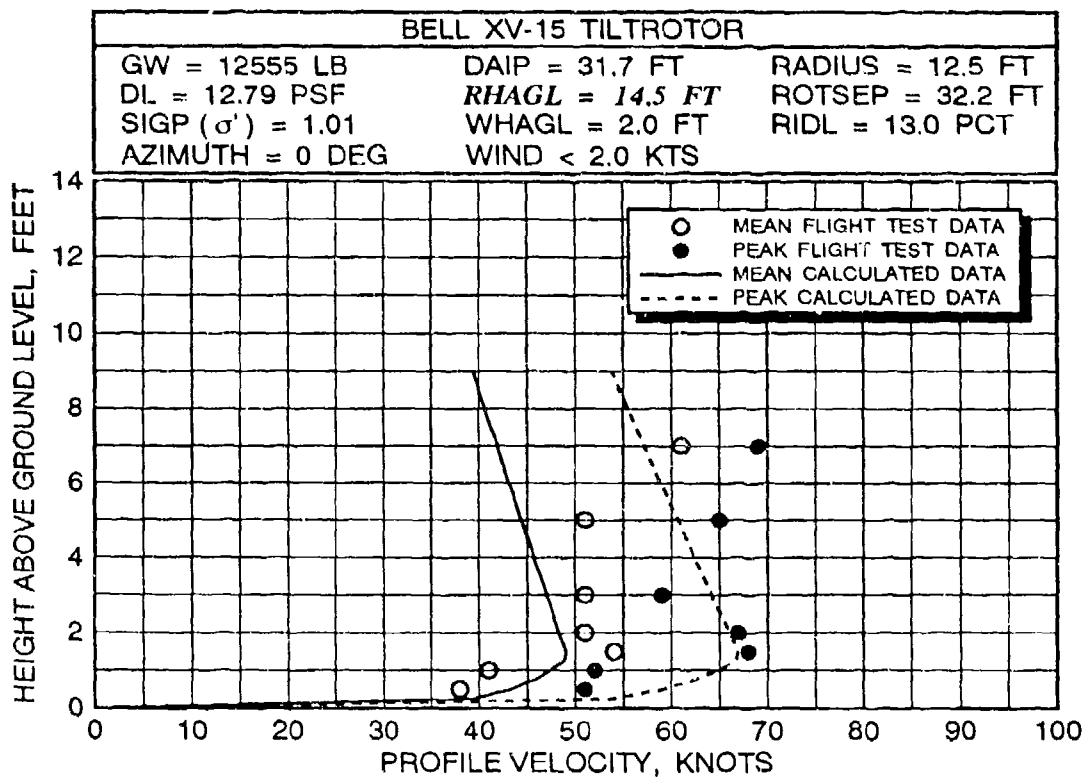


FIGURE 49 XV-15 MEAN/PEAK VELOCITY PROFILE CORRELATION ALONG THE 0- DEGREE AZIMUTH RADIAL AT THREE ROTOR HEIGHTS FOR AN AVERAGE GROSS WEIGHT BETWEEN 12,475 AND 12,555 POUNDS

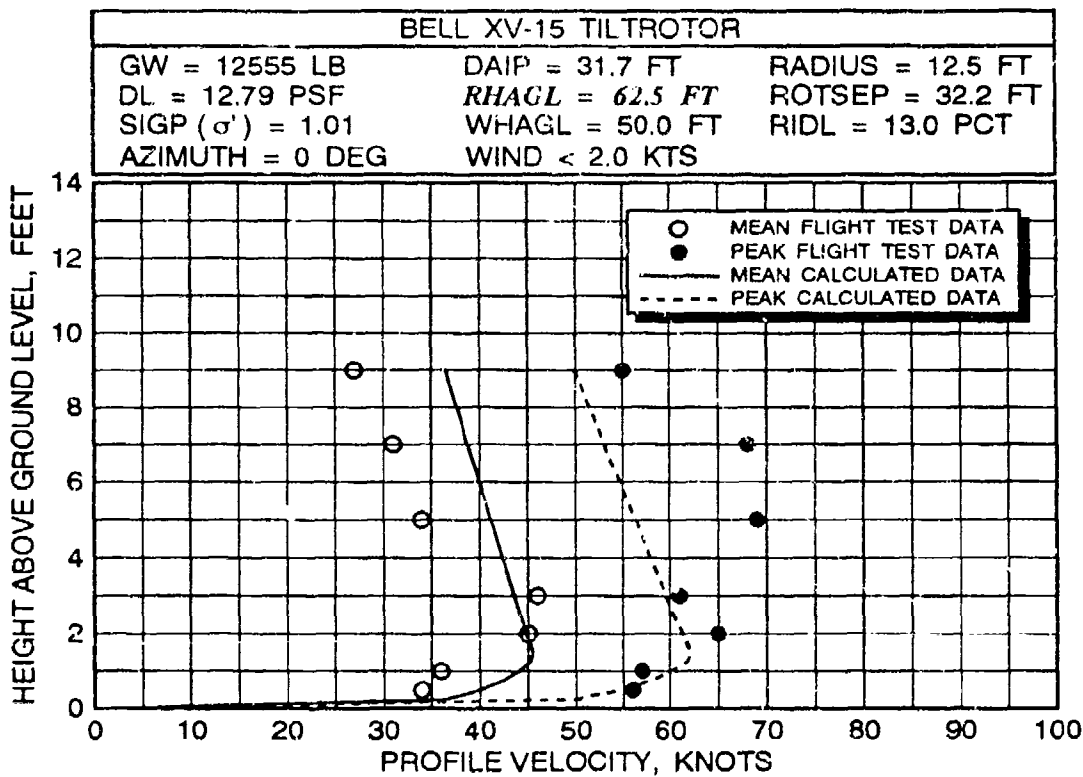


FIGURE 49 XV-15 MEAN/PEAK VELOCITY PROFILE CORRELATION ALONG THE 0- DEGREE AZIMUTH RADIAL AT THREE ROTOR HEIGHTS FOR AN AVERAGE GROSS WEIGHT BETWEEN 12,475 AND 12,555 POUNDS (continued)

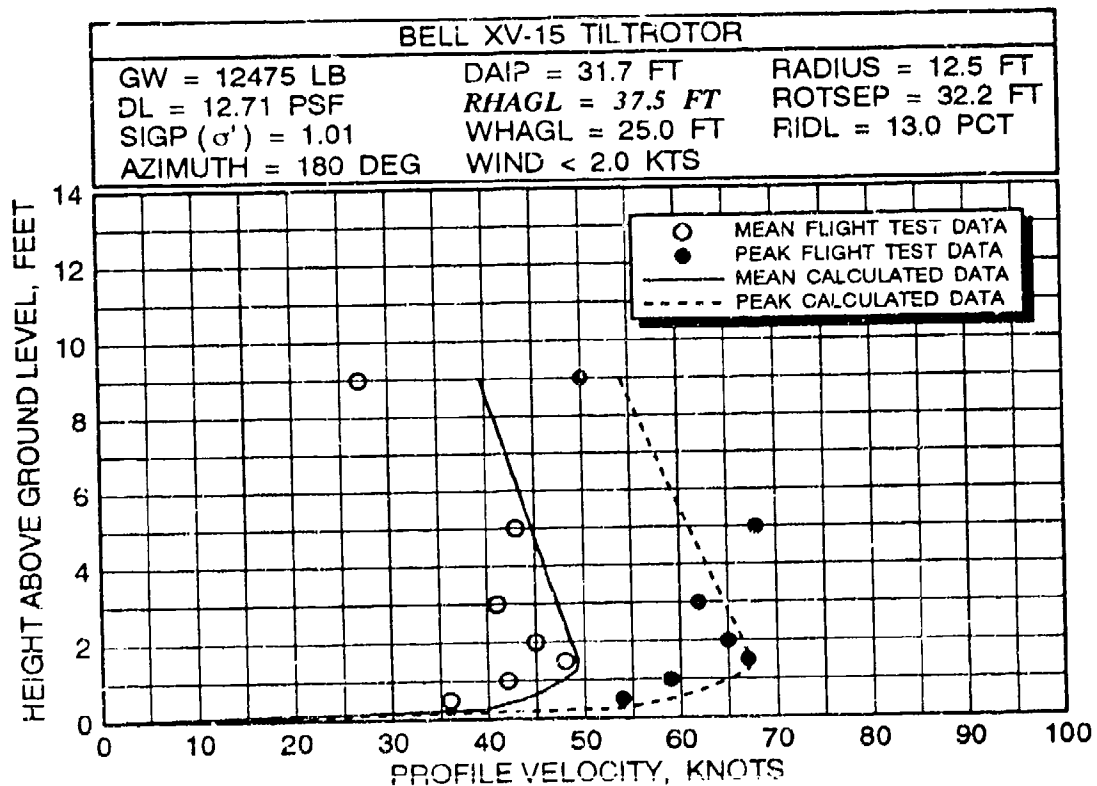
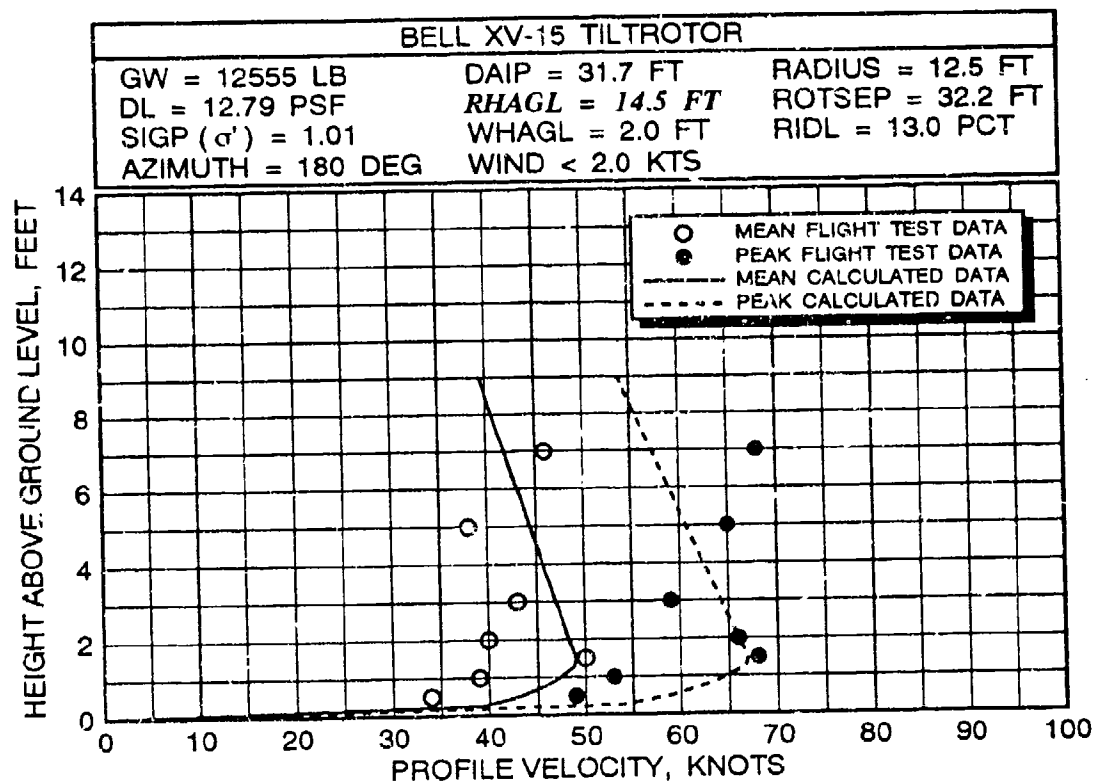


FIGURE 50 XV-15 MEAN/PEAK VELOCITY PROFILE CORRELATION ALONG THE 180- DEGREE AZIMUTH RADIAL AT THREE ROTOR HEIGHTS FOR AN AVERAGE GROSS WEIGHT BETWEEN 12,475 AND 12,555 POUNDS

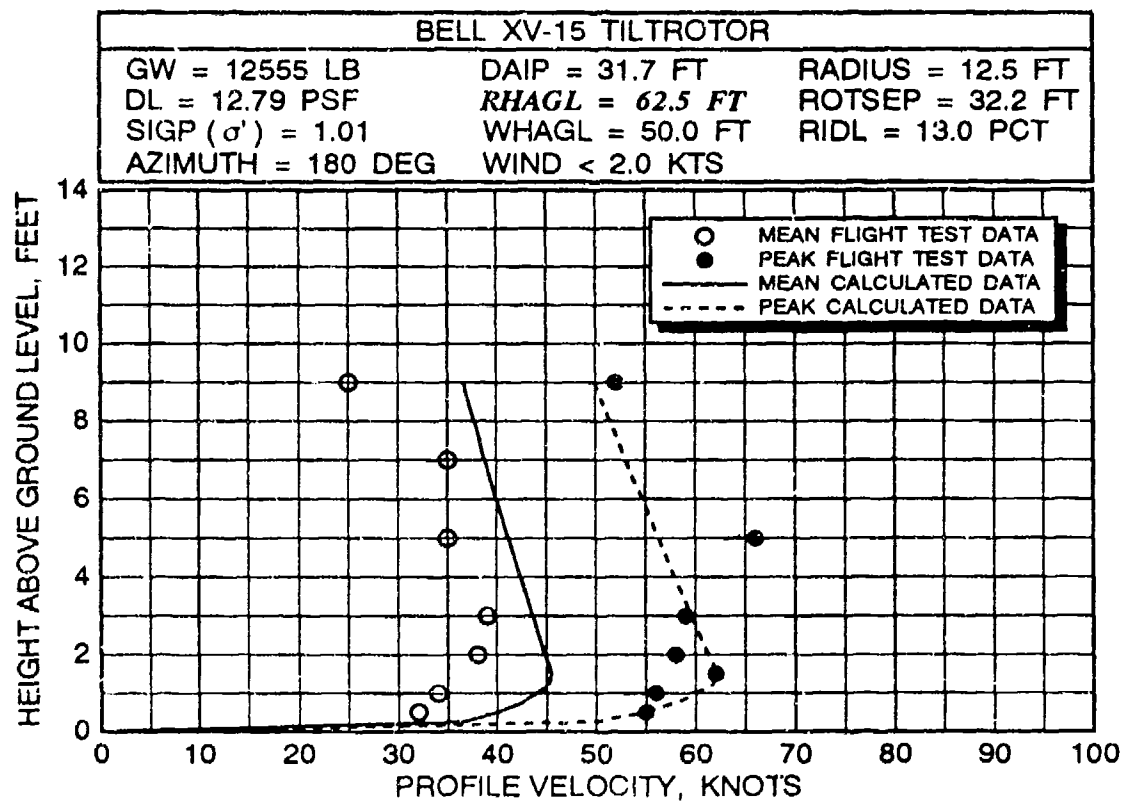


FIGURE 50 XV-15 MEAN/PEAK VELOCITY PROFILE CORRELATION ALONG THE 180- DEGREE AZIMUTH RADIAL AT THREE ROTOR HEIGHTS FOR AN AVERAGE GROSS WEIGHT BETWEEN 12,475 AND 12,555 POUNDS (continued)

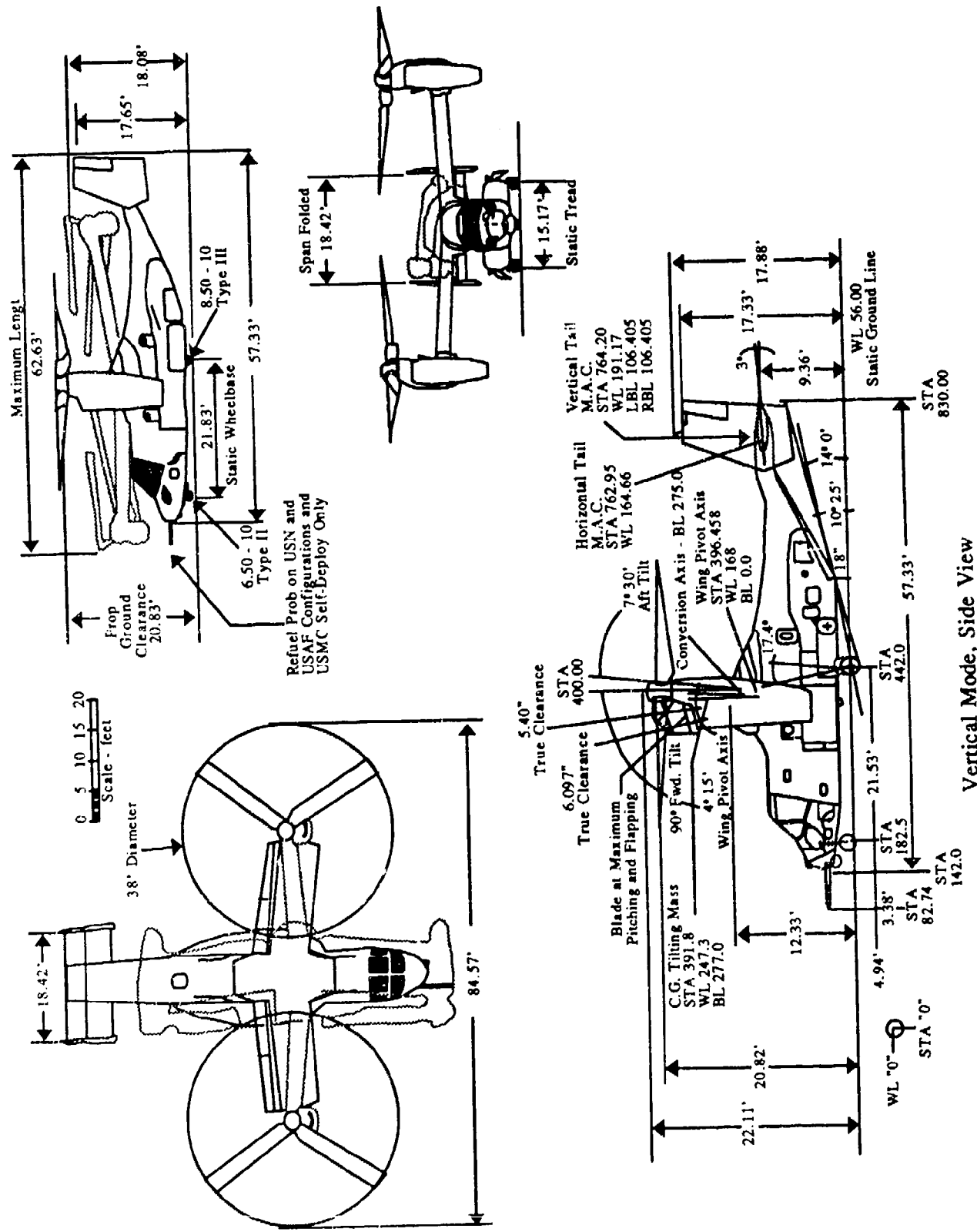


FIGURE 51 THREE-VIEW DRAWING OF THE BELL-BOEING MV-22

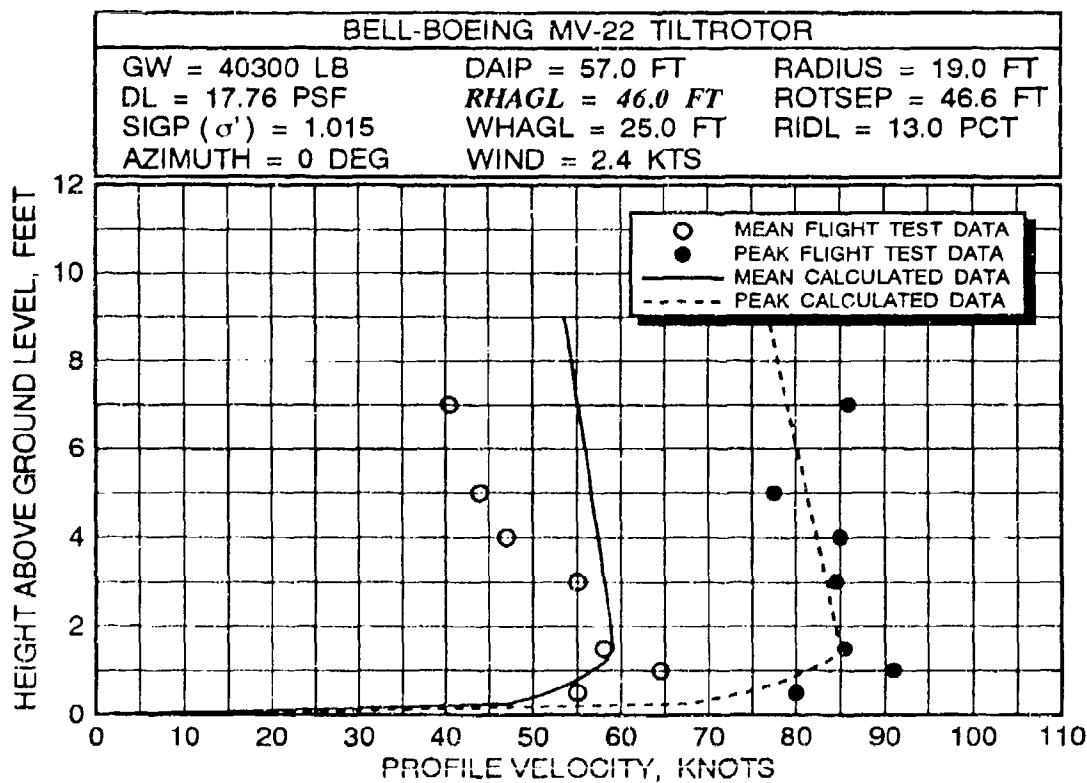
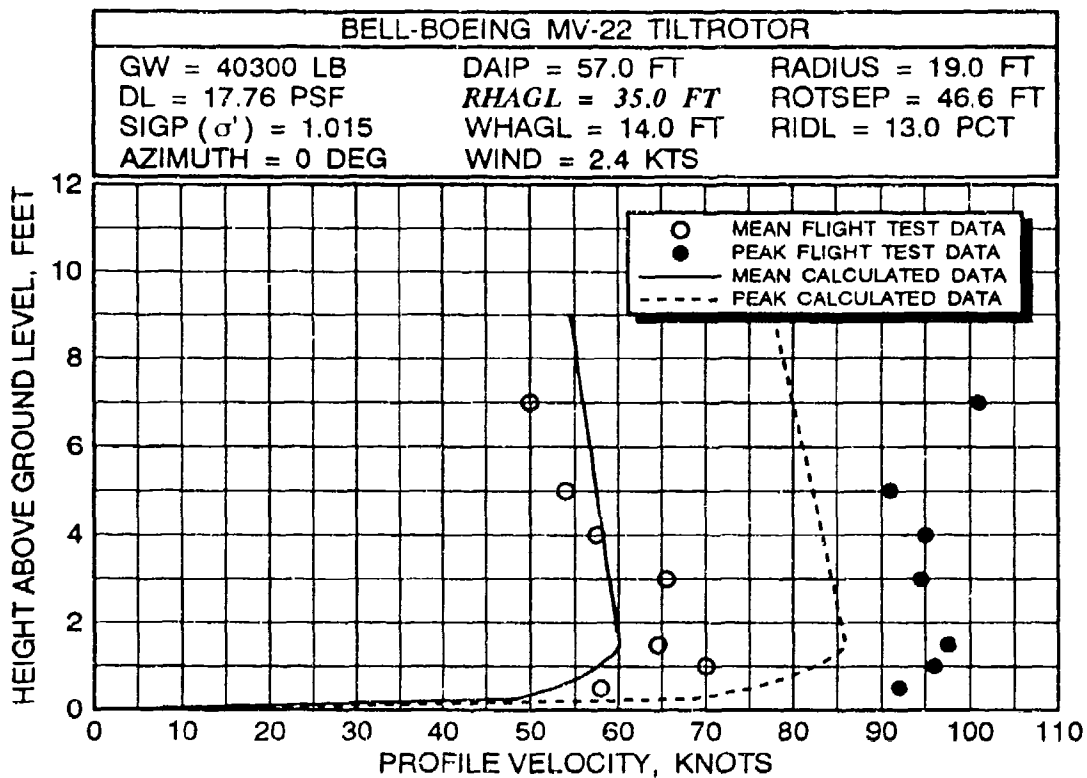


FIGURE 52 MV-22 MEAN/PEAK VELOCITY PROFILE CORRELATION AT 57 FEET ALONG THE 0-DEGREE AZIMUTH RADIAL AT THREE ROTOR HEIGHTS FOR AN AVERAGE GROSS WEIGHT OF 40,300 POUNDS

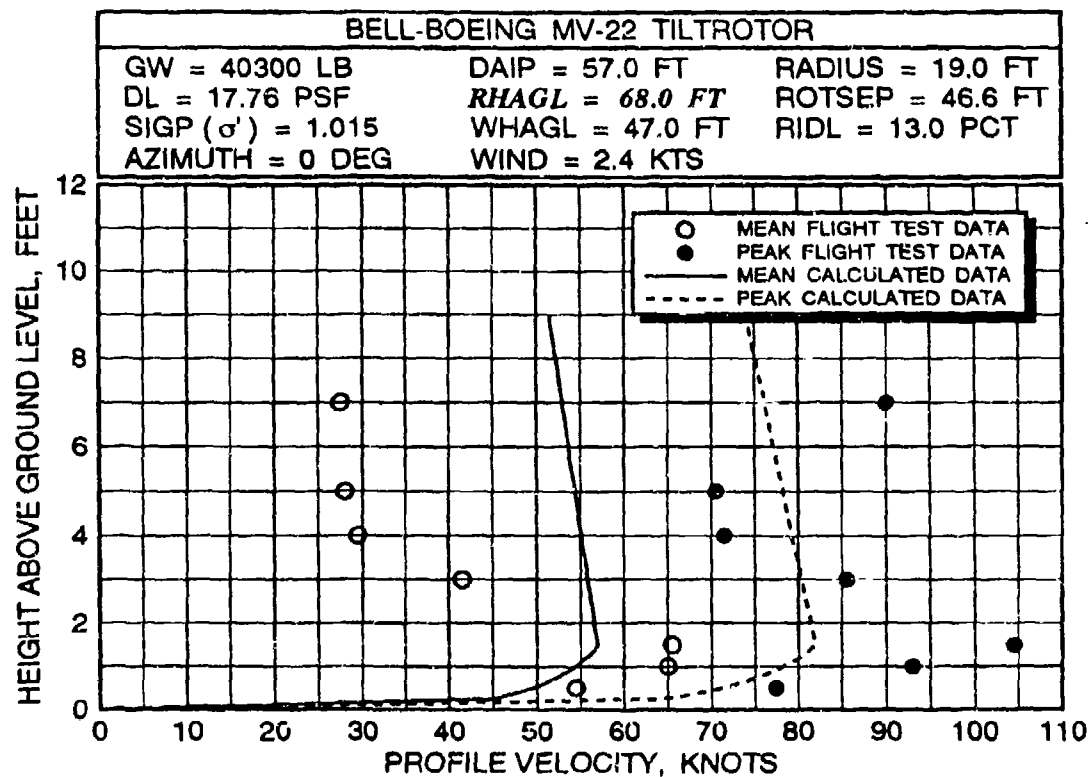


FIGURE 52 MV-22 MEAN/PEAK VELOCITY PROFILE CORRELATION AT 57 FEET ALONG THE 0-DEGREE AZIMUTH RADIAL AT THREE ROTOR HEIGHTS FOR AN AVERAGE GROSS WEIGHT OF 40,300 POUNDS (continued)

Correlation at the 68.0-foot rotor height for both the mean and peak profiles is much harder to quantify. This is due to the shape of the measured velocity profiles. While it would be desirable that correlation be more consistent among these three cases, they do provide excellent examples of the variability of the measured data for small changes in parameters, in this case only 33 feet of altitude. Also, based on other correlation work, the effect of the varying ambient wind during data acquisition could be extremely significant for these particular data.

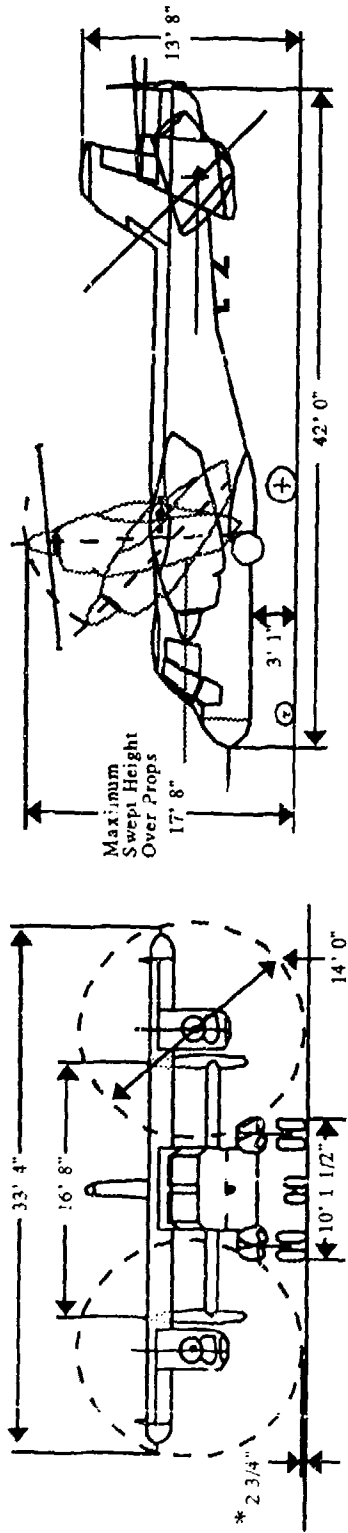
3.4 CL-84 TILTROTOR VELOCITY PROFILE CORRELATION

The Canadair CL-84 is a two-seat tiltwing concept demonstrator aircraft that was initially flown in 1965. The typical gross weight range of the aircraft for vertical takeoff operation varies between approximately 11,000 and 12,000 pounds. A three-view drawing of the CL-84 is provided as figure 53 for reference purposes. CL-84 specific input data parameters required to execute the ROTWASH analysis program were defined previously in table 2 (see page 68).

CL-84 flight test data used in the correlation analysis were obtained from reference 40. Four heights above ground level at three station positions were measured along the 0-, 180-, and 270-degree azimuths with respect to the nose of the tiltwing. Measured station positions were 20, 40, and 80 feet from the center of the aircraft. Sensor heights were 1.0, 2.0, 4.0, and 6.0 feet AGL. The data for the three station positions were also obtained for two rotor heights, 40.2- and 55.2-feet RHAGL (wheel heights of 25 and 40 feet). Unfortunately, only mean velocity profile data are documented in reference 40. During testing, winds were reported as 2 to 4 knots at the 55.2-foot rotor height. At 40.2-feet RHAGL, winds were reported up to 7 and 8 knots. Table 5 presents a matrix of the points tested.

CL-84 rotorwash test data are also documented in references 31 and 32. However, unlike the data in reference 40, these data were not obtained with an ion-beam deflection anemometer. Instead, these data were obtained with a mechanical type of anemometer. This type of anemometer has inertia in its rotating components causing the frequency response of the instrument to be significantly lowered in comparison to the ion-beam type. This inertia effect results in a reduced peak value of velocity being measured. Therefore, based on experience documented in reference 1 and more recently in reference 11 with respect to correlation of mechanical sensor data, no attempt was made to correlate peak velocity data with the ROTWASH program.

Correlation of flight test and calculated data as a function of DFRC is presented along the 270-degree azimuth in figure 54. These data are for a gross weight of approximately 11,540 pounds at a RHAGL of 55.2 feet. At a station position of 9.7 feet, the



* Prop Clearance at Normal
T.O. & Landing Wing Tilt
Angle (15°) is 28.25"

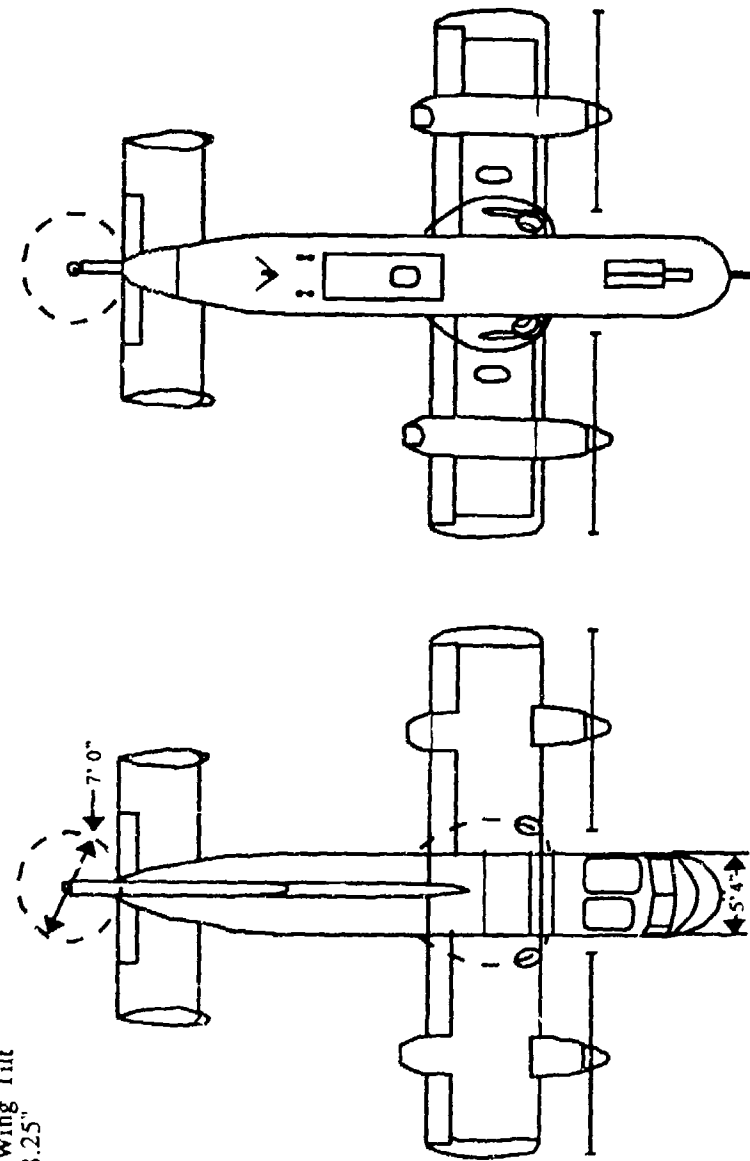


FIGURE 53 THREE-VIEW DRAWING OF THE CANADAIR CL-84

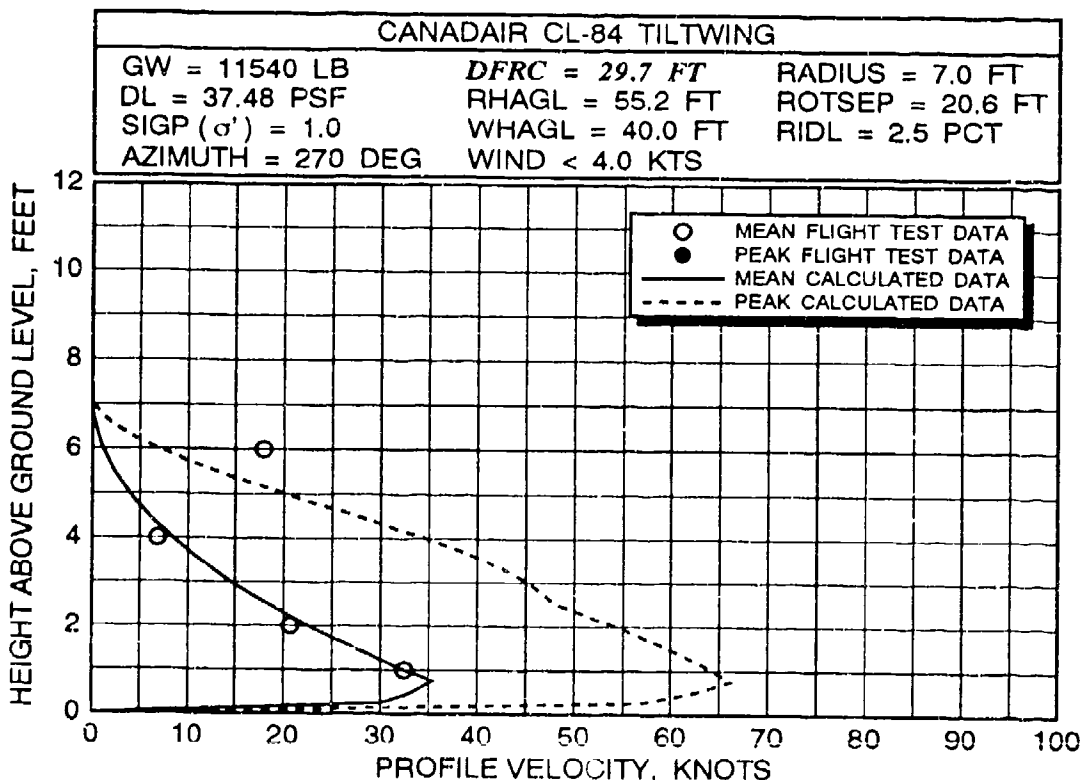
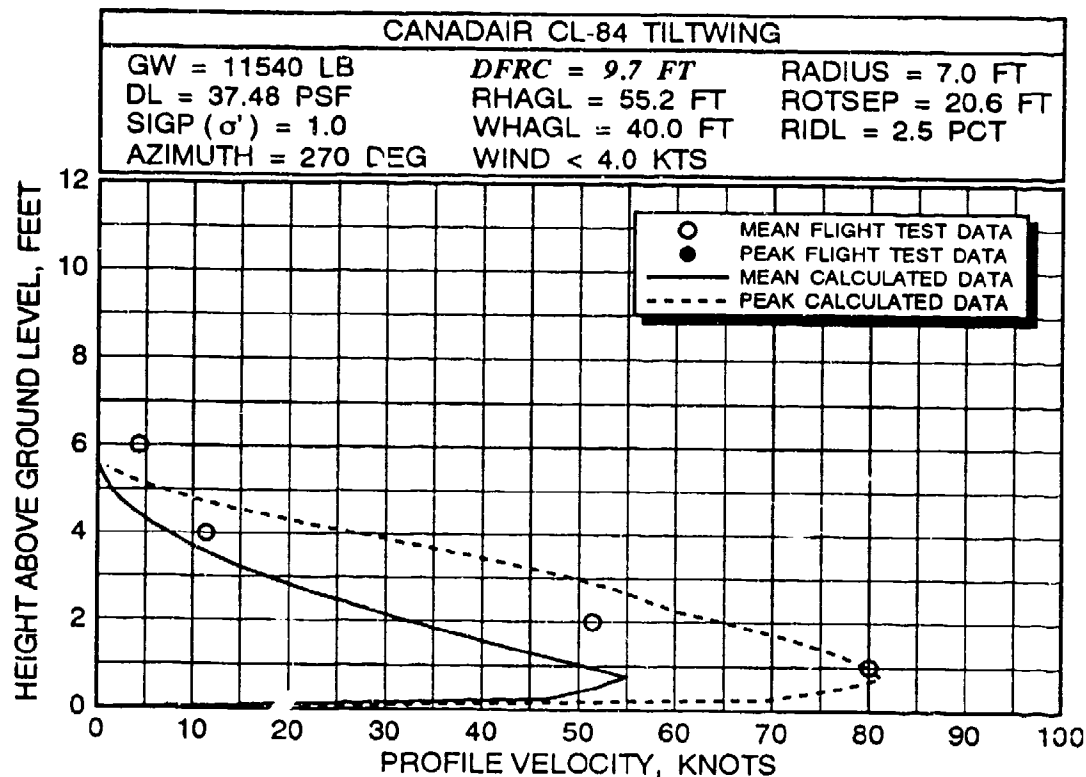


FIGURE 54 CL-84 MEAN VELOCITY PROFILE CORRELATION ALONG THE 270- DEGREE AZIMUTH RADIAL AT AN AVERAGE GROSS WEIGHT OF 11,540 POUNDS AND A ROTOR HEIGHT OF 55.2 FEET

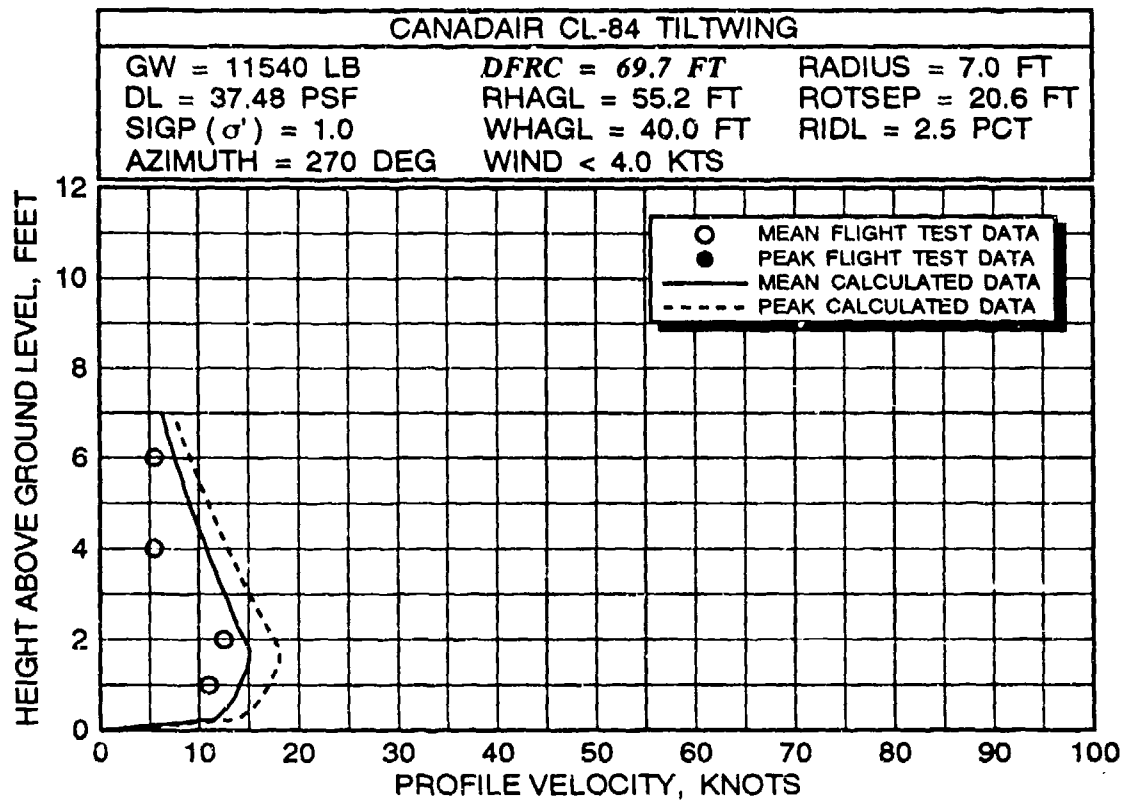


FIGURE 54 CL-84 MEAN VELOCITY PROFILE CORRELATION ALONG THE 270- DEGREE AZIMUTH RADIAL AT AN AVERAGE GROSS WEIGHT OF 11,540 POUNDS AND A ROTOR HEIGHT OF 55.2 FEET (continued)

TABLE 5 EVALUATION MATRIX FOR CL-84 FLIGHT TEST/MATHEMATICAL MODEL DATA CORRELATION

FIGURE NUMBER	GROSS WEIGHT ¹ (lb)	ROTOR HEIGHT (feet)	AZIMUTH ANGLE (degree)	DISTANCE FROM THE ROTOR CENTER (DFRC) OR DISTANCE ALONG THE INTERACTION PLANE (DAIP) ² (feet)
54	11,540	55.2	270	9.7, 29.7, 69.7
55	11,540	55.2	0, 180	20, 40, 80
56	11,270	40.2	270	9.7, 29.7, 69.7
57	11,270	40.2	0, 180	20, 40, 80

NOTES:

- (1) Even though care has been taken to calculate realistic average gross weights, actual gross weight values could vary between 11,000 and 12,000 pounds at the extremes. Disk loadings are 37.48 lbs/ft² at 11,540 pounds and 36.61 lbs/ft² at 11,270 pounds.
- (2) The values of DFRC are applicable along only the 270 degree azimuth, whereas the values for DAIP are valid only along the 0- and 180-degree azimuths.
- (3) Atmospheric density ratio, ambient windspeed/direction, wing incidence, and fuselage pitch attitude are either undefined or poorly defined with respect to the presented data.

maximum predicted mean velocity, at between 0.5 and 1.0 feet, is less than that of the measured value by 25 knots. This underprediction of mean velocity is not totally unexpected, however. At this station position, the rotor tip is located approximately 50 feet above and 2.7 feet laterally from the sensor. This same effect was observed in section 3.2 for the XV-15. At the 40- and 80-feet station positions (DFRC values of 29.7 and 69.7 feet respectively), correlation is substantially improved. Only one calculated mean velocity value is not within 3 to 5 knots of its corresponding measured value. This suspicious flight test value is at 29.7 feet at 6.0 feet AGL. When considering the trends of the other measured data, it is certainly possible that this measured point could be a bad point.

Data along the interaction plane for the same configuration are presented in figure 55. When these flight test data are compared with one another, 0 versus 180 degrees, it is interesting to observe the large differences in values for the same station positions. Theoretically, the measured values would be expected

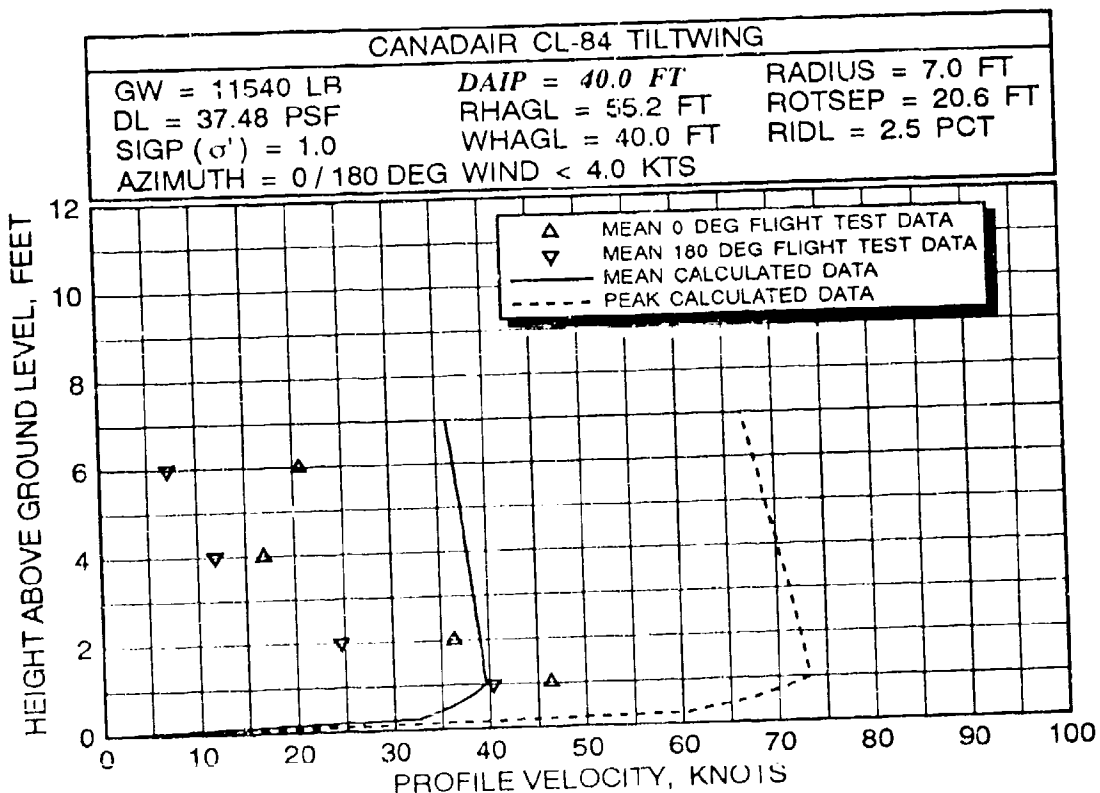
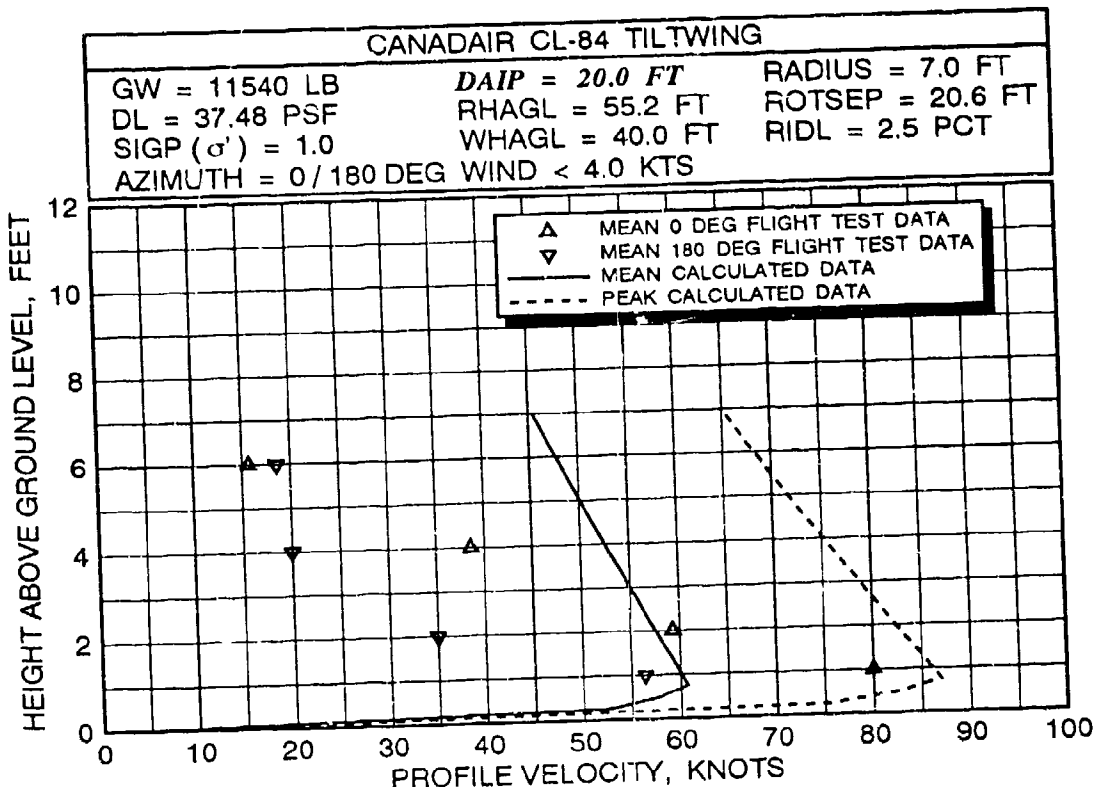


FIGURE 55 CL-84 MEAN VELOCITY PROFILE CORRELATION ALONG THE 0- AND 180-DEGREE AZIMUTH RADIALS AT AN AVERAGE GROSS WEIGHT OF 11,540 POUNDS AND A ROTOR HEIGHT OF 55.2 FEET

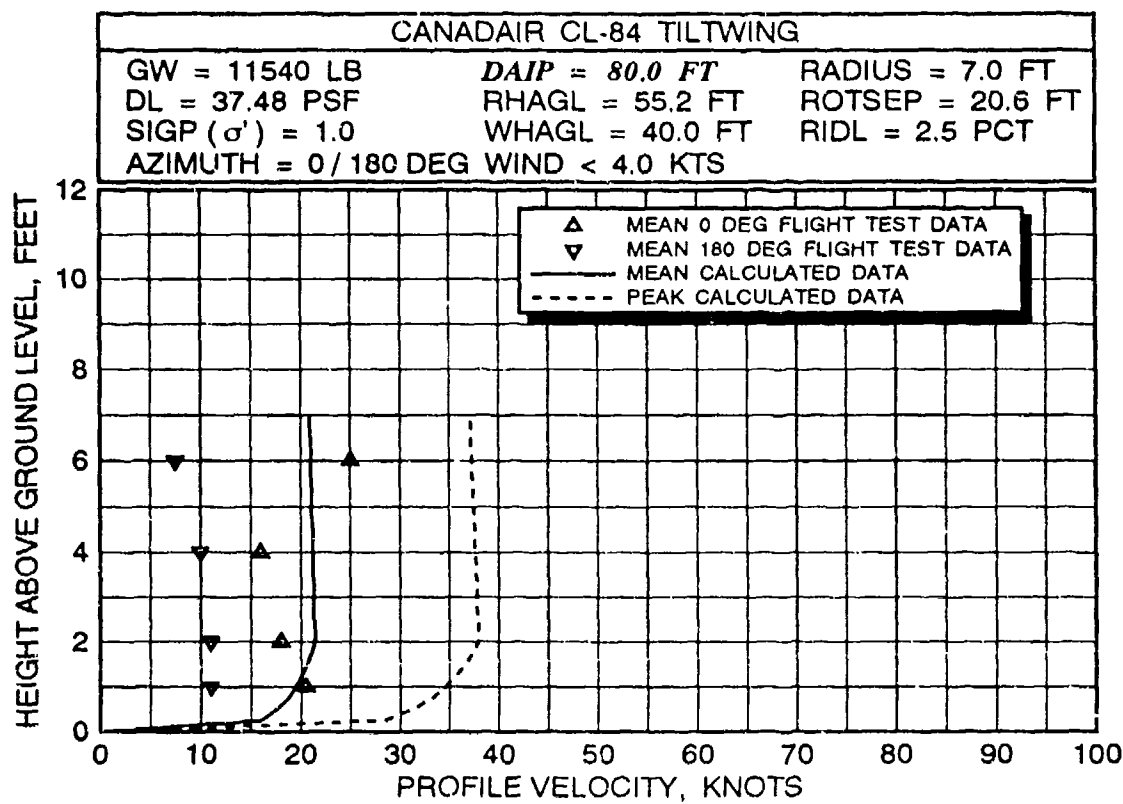


FIGURE 55 CL-84 MEAN VELOCITY PROFILE CORRELATION ALONG THE 0- AND 180-DEGREE AZIMUTH RADIALS AT AN AVERAGE GROSS WEIGHT OF 11,540 POUNDS AND A ROTOR HEIGHT OF 55.2 FEET (continued)

to be quite similar. In some cases, measured velocities differ by as much as 25 knots. Average differences are usually between 5 and 10 knots. Possible causes for these velocity variations can be attributed to the aft fuselage configuration, pitch control tail rotor, and the combinations of trim wing incidence and fuselage pitch attitude which are used (which were not documented in the flight test report). Two other important parameters, the ambient wind azimuth and the atmospheric density ratio, are also not documented in the report. However, any flow field effects due to these two parameters should have equally affected data along both azimuths. When compared at the 20-foot station position, calculated profile velocities at 3 to 6 feet HAGL significantly overpredict the measured velocity data. At the 40-foot position, correlation is improved; however, calculated mean profile velocities below 2 feet are underpredicted and velocities above 3 feet are overpredicted by 10 to 15 knots. Calculated mean velocity data at 80 feet compare quite well with the measured data. At this position, calculated data plot between the 0 and 180 degree measured data.

Data measured at a rotor height of 40.2 feet along all three azimuths are presented in figures 56 and 57. Along the 270-degree azimuth, figure 56, calculated data do not correlate with measured data as well as they did at the higher rotor height. At 9.7-feet DFRC, results are very similar to those at 40-feet HAGL. At 29.7 and 69.7 feet, calculated mean velocities continue to be less than measured mean velocities. Possible reasons for the degraded correlation could include weaknesses in the ROTWASH analysis model (such as corrections for high disk loading rotorcraft in ground effect). However, as mentioned previously, values for several important parameters are also unknown and not factored into the analysis. The ambient wind during measurement of these data was reported as 7 to 8 knots, and the azimuth of the wind vector with respect to the sensor azimuth was not reported. This effect, based upon limited data discussed in section 2.1.9, could be sufficient to shift the complete velocity profile by up to 15 knots. Other unknown parameters are discussed in the previous paragraph.

Along both the 0- and 180-degree azimuths, trends along the 270-degree azimuth are repeated. Calculated mean velocities tend to be 10 to 20 knots less than the measured velocities. The reported cross winds complicate correlation of these data, because the wing incidence has to be varied to maintain trim over the ground reference position (from 88 to 96 degrees along the 0- and 180-degree azimuths respectively, 90 degrees is vertical). Since corresponding values for trim pitch attitude are not reported with the wing incidence data, it is not possible to estimate the angle of the induced velocity vector with respect to the ground plane (which does not have to be perpendicular to the ground when influenced by the wind and partially trimmed by the pitch-axis tail rotor).

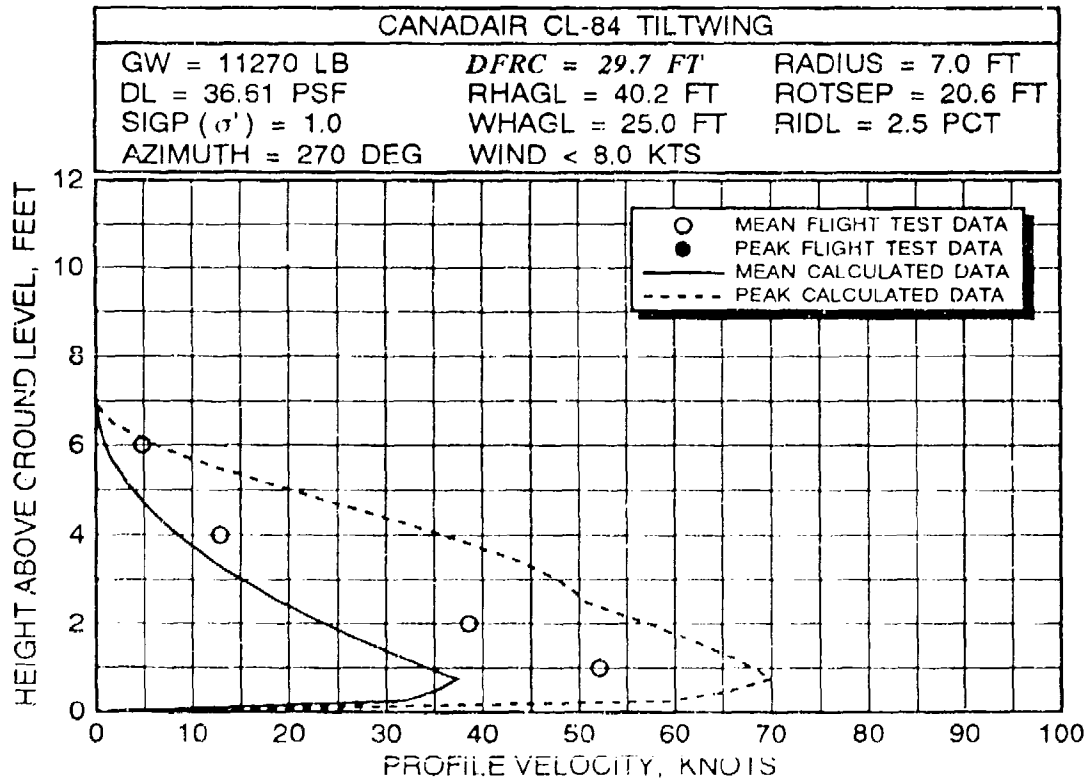
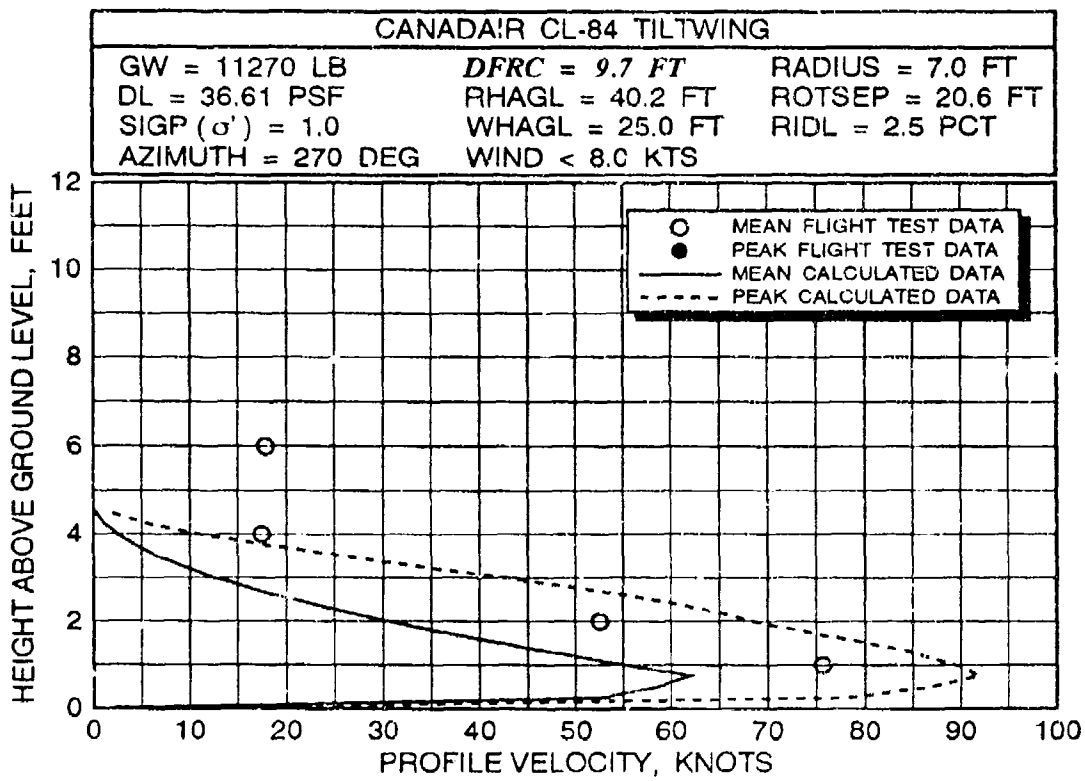


FIGURE 56 CL-84 MEAN VELOCITY PROFILE CORRELATION ALONG THE 270- DEGREE AZIMUTH RADIAL AT AN AVERAGE GROSS WEIGHT OF 11,270 POUNDS AND A ROTOR HEIGHT OF 40.2 FEET

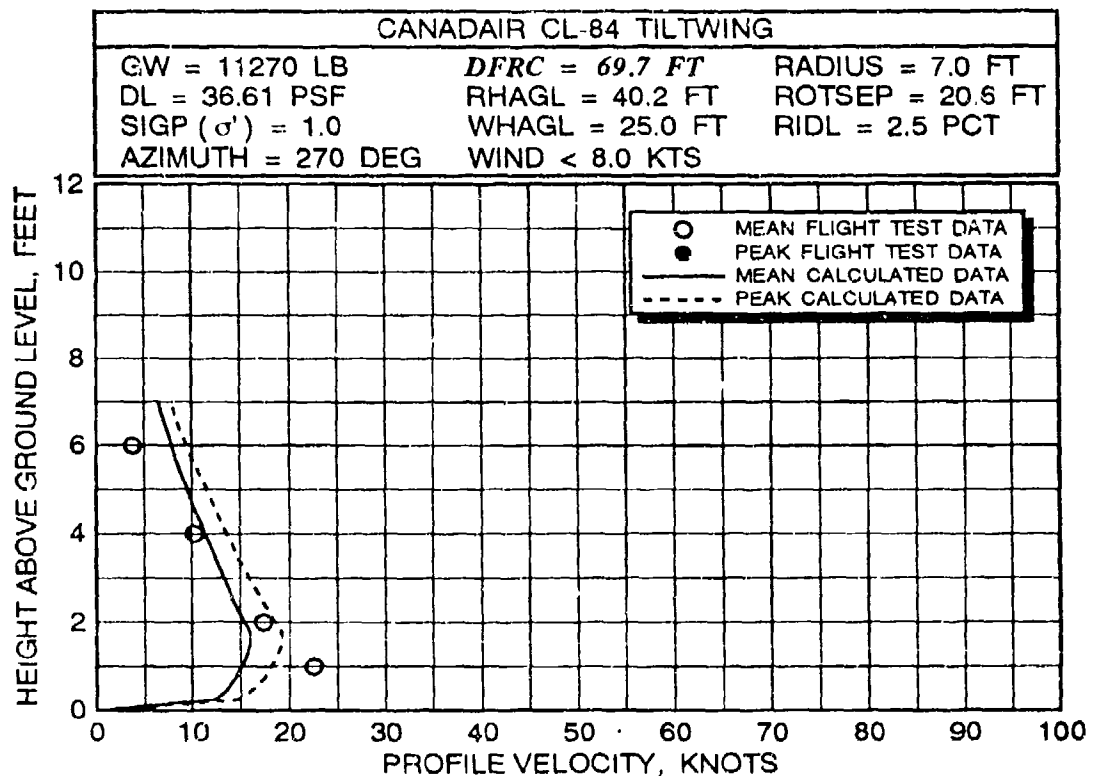


FIGURE 56 CL-84 MEAN VELOCITY PROFILE CORRELATION ALONG THE 270- DEGREE AZIMUTH RADIAL AT AN AVERAGE GROSS WEIGHT OF 11,270 POUNDS AND A ROTOR HEIGHT OF 40.2 FEET (continued)

In summary, if only the 55.2-foot rotor height data are taken into consideration, CL-84 correlation results are generally good. However, the lower quality of correlation at 40.2-feet RHAGL must be taken into account in any final evaluation. Significant uncertainties do exist at this lower rotor height for the values of several important parameters that are required as input to the ROTWASH program. These uncertainties make it virtually impossible to determine whether or not weaknesses in the mathematical model are the primary cause for poor correlation results.

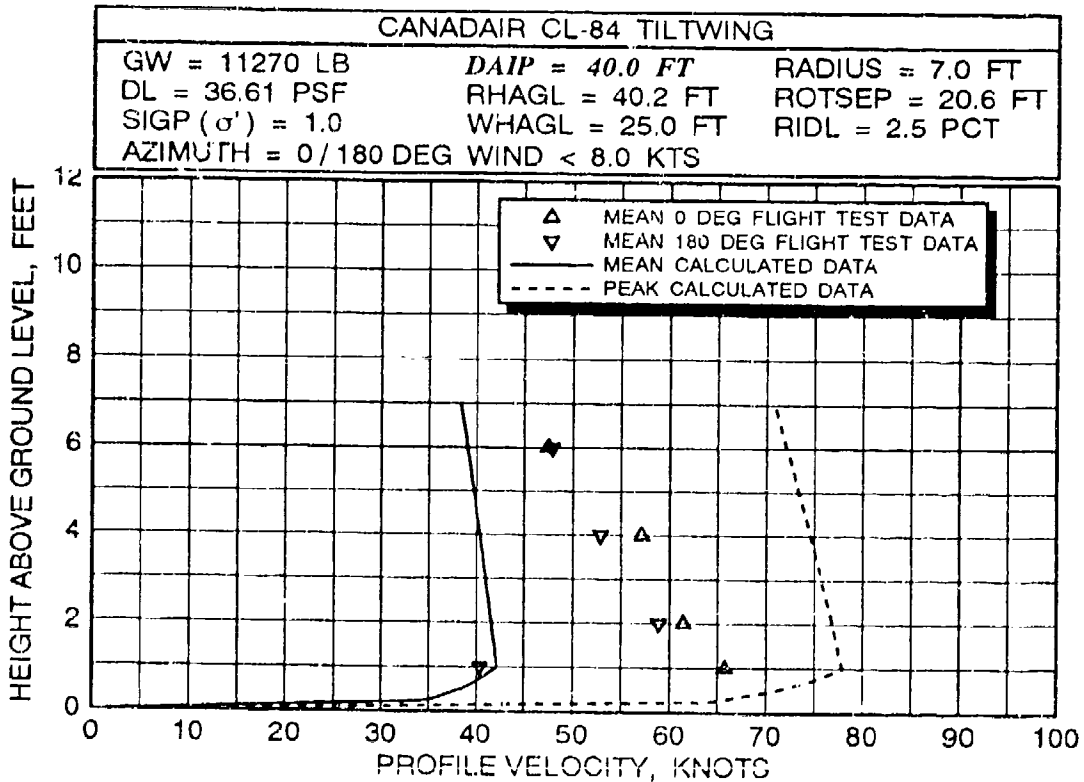
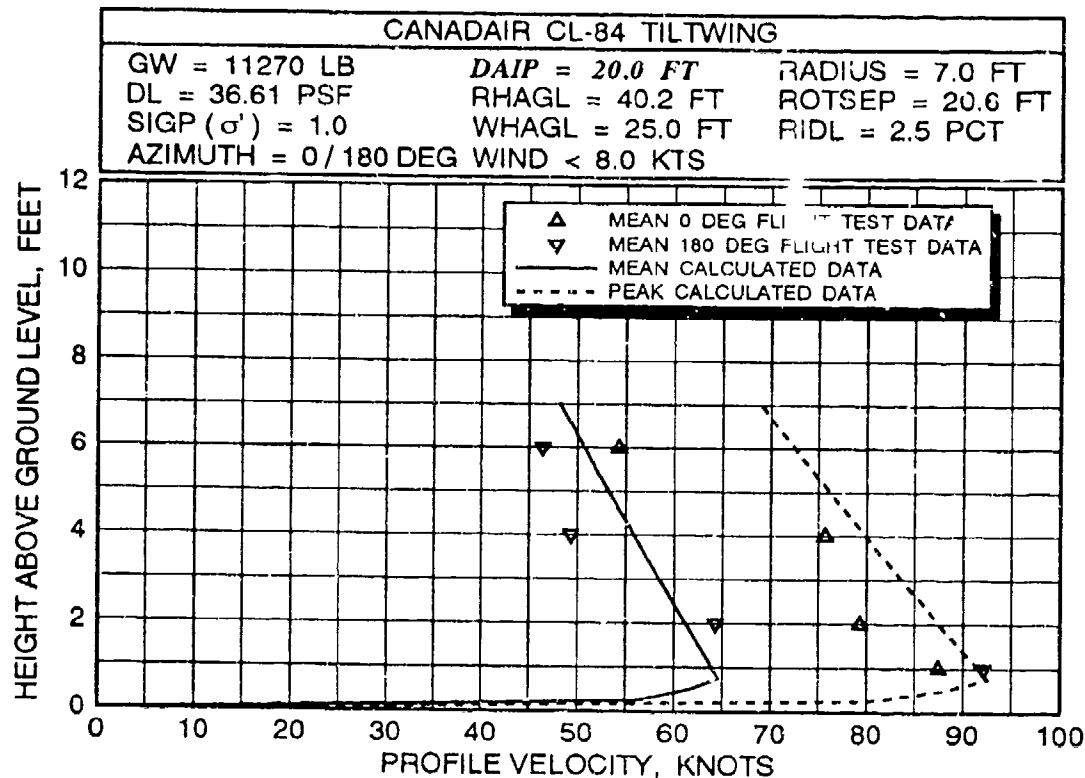


FIGURE 57 CL-84 MEAN VELOCITY PROFILE CORRELATION ALONG THE 0- AND 180-DEGREE AZIMUTH RADIALS AT AN AVERAGE GROSS WEIGHT OF 11,270 POUNDS AND A ROTOR HEIGHT OF 40.2 FEET

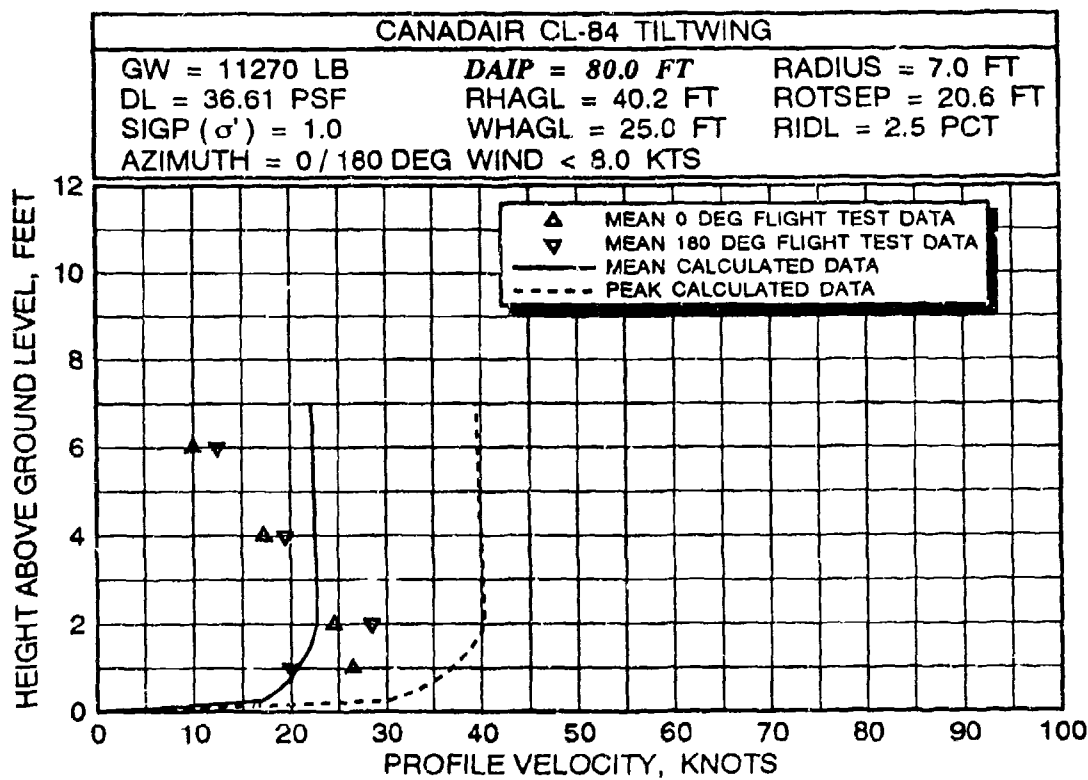


FIGURE 57 CL-84 MEAN VELOCITY PROFILE CORRELATION ALONG THE 0- AND 180-DEGREE AZIMUTH RADIALS AT AN AVERAGE GROSS WEIGHT OF 11,270 POUNDS AND A ROTOR HEIGHT OF 40.2 FEET (continued)

3.5 SH-60B HELICOPTER VELOCITY PROFILE CORRELATION

Limited flight test data for the Sikorsky SH-60B helicopter were obtained during a rotorwash sensor evaluation project and documented in reference 11. (Results from a comprehensive H-60 rotorwash test have just been published in reference 78, however, the wind has significant effects on some of these data.) The purpose of the experiment was to evaluate the performance of a cup and vane mechanical sensor in direct comparison with the ion-beam sensor. The flight test data were obtained at only one sensor height above ground, 1.5-feet AGL, and two radial stations in front of the helicopter (0-degree azimuth). These radial positions are 35 and 70 feet. Unfortunately, for correlation purposes, the ambient wind velocity varied up to 8 knots at an azimuth of 40 degrees to the nose of the helicopter during the test. Gross weight during the test varied from a high of 20,500 pounds to a low of 19,600 pounds. A three-view profile of the helicopter is presented in figure 58 for reference purposes. SH-60B specific input data parameters that are required to execute the ROTWASH analysis problem were defined previously in table 2 (see page 68).

The velocity profile data that were measured at a rotor height of 25 feet are documented in figure 59. The estimated component of ambient wind along the 0-degree azimuth is calculated as approximately 6.1 knots. These correlation results indicate that the ROTWASH wind model slightly overpredicts mean velocity data and both overpredicts (at 70 feet) and underpredicts (at 35 feet) peak velocity data. If the wind velocity is assumed to be 8 knots, the calculated data could be shifted to the left approximately 4 knots. Data at a rotor height of 15 feet are presented in figure 60. These correlation results are similar to the figure 59 results. Overall, for this extremely limited comparison, the mean velocities compare reasonably well. The calculated peak velocities average about 10 to 12 knots above or below measured test data. Reasons for the differences could be many. These reasons might include a weak wind effects model, use of an incorrect value for wind in calculations for the various data points, and the fact that the comparison was made along the 0-degree azimuth instead of the worst case 270-degree azimuth. This last reason could be important in that added engine and tail rotor mass flow effects are minimized. These effects are included in the empirical equations for peak velocity effects, since the equations are heavily based on CH-53E data from reference 24.

3.6 CORRELATION OF THE AMBIENT WIND, GROUND VORTEX, AND FORWARD FLIGHT MODELS

Mathematical models, as developed for the ambient wind, ground vortex, and forward flight effects, have each been developed using simple but sound theory. However, it is still important to note that limited flight test data are available for correlation

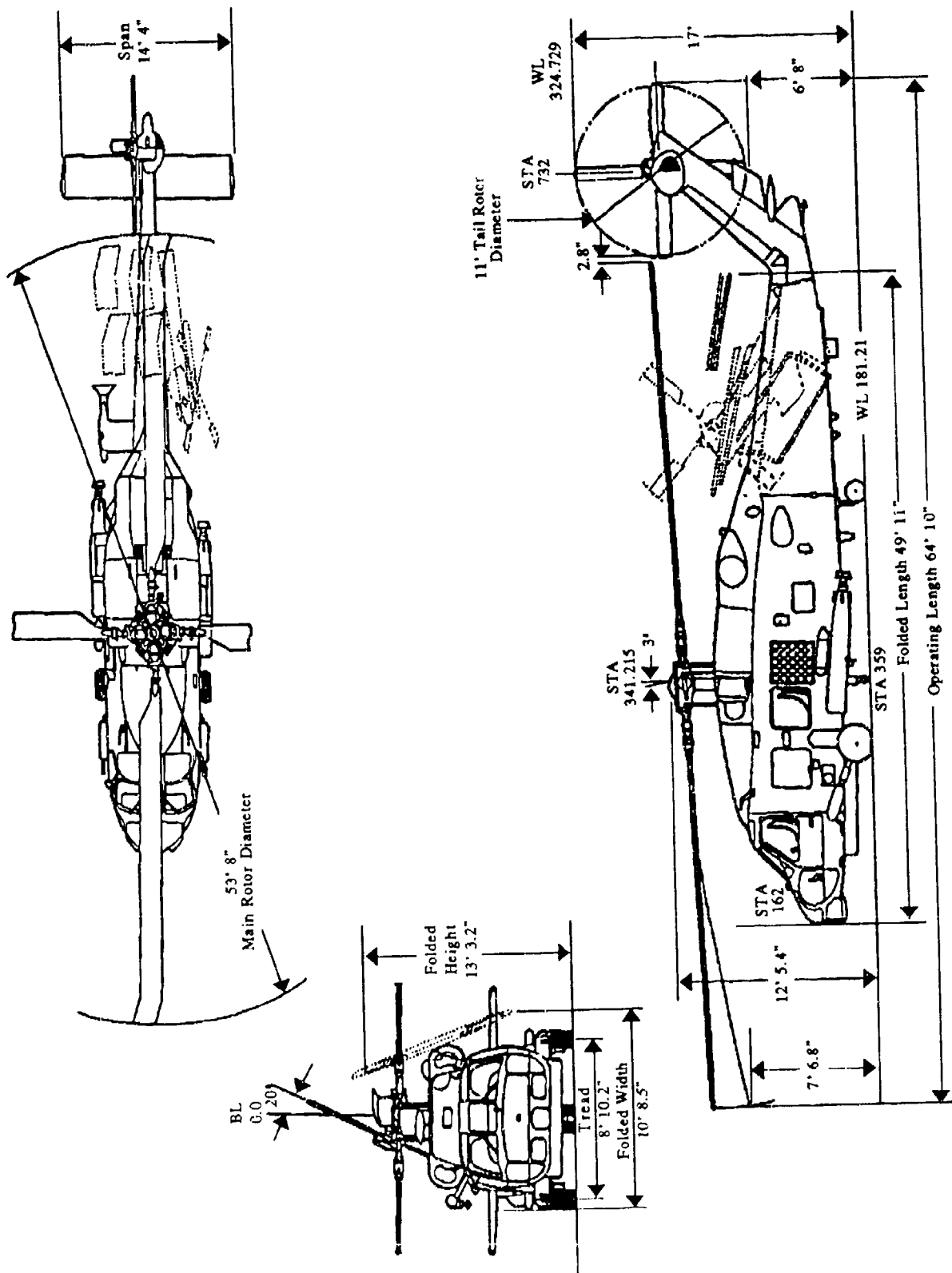


FIGURE 58 THREE-VIEW DRAWING OF THE SH-60B

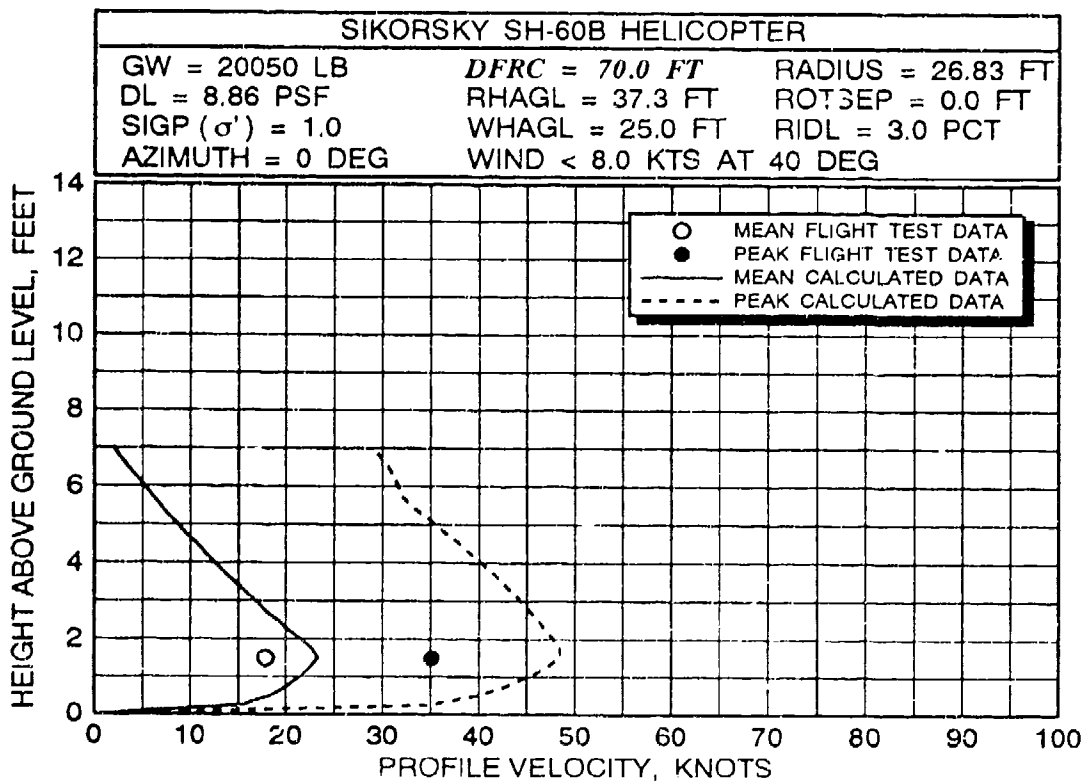
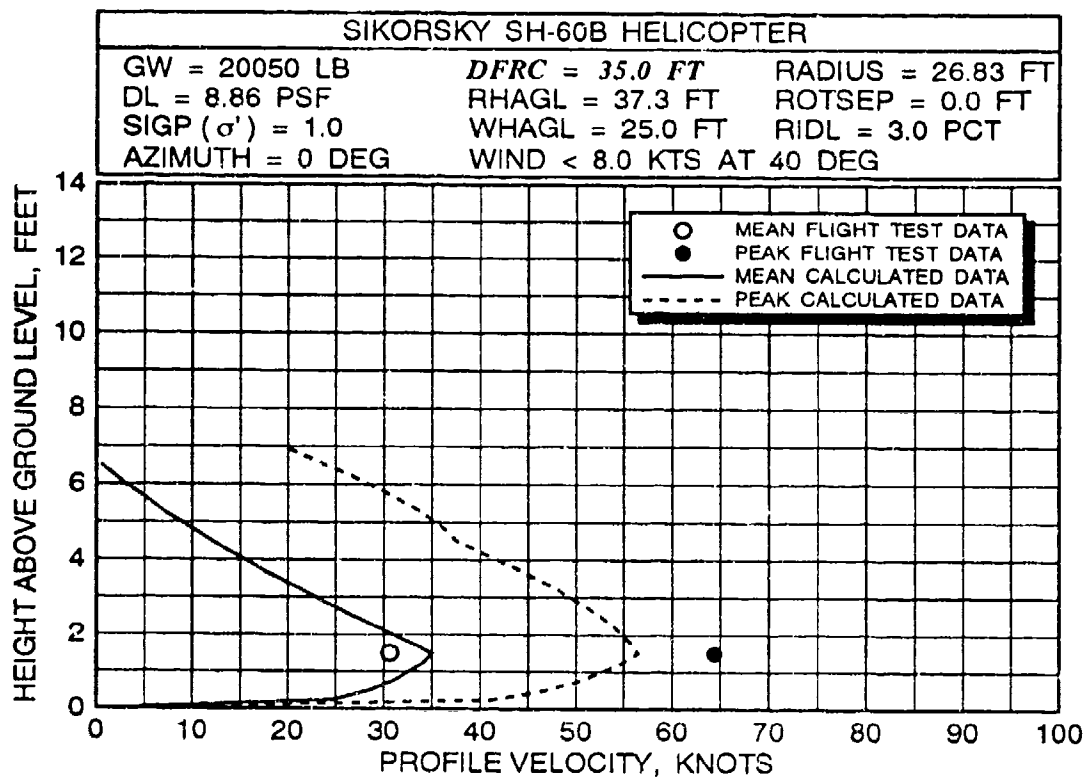


FIGURE 59 SH-60B MEAN/PEAK VELOCITY PROFILE CORRELATION ALONG THE 0-DEGREE AZIMUTH RADIAL AT A ROTOR HEIGHT OF 37.3 FEET

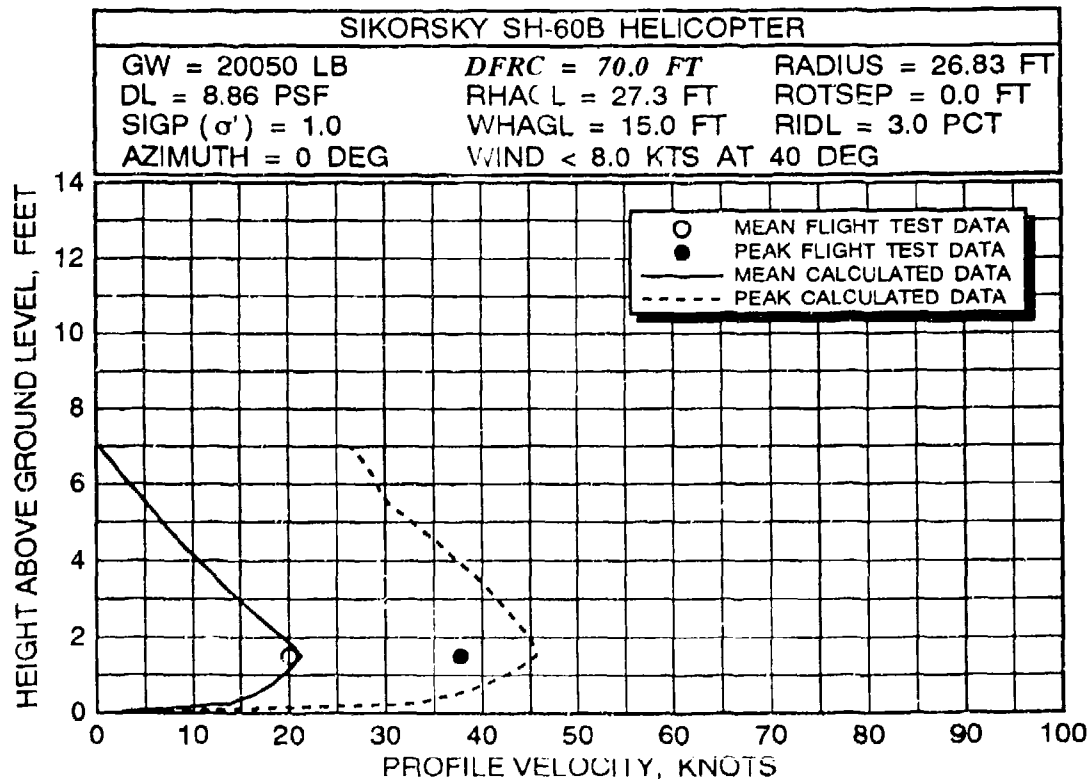
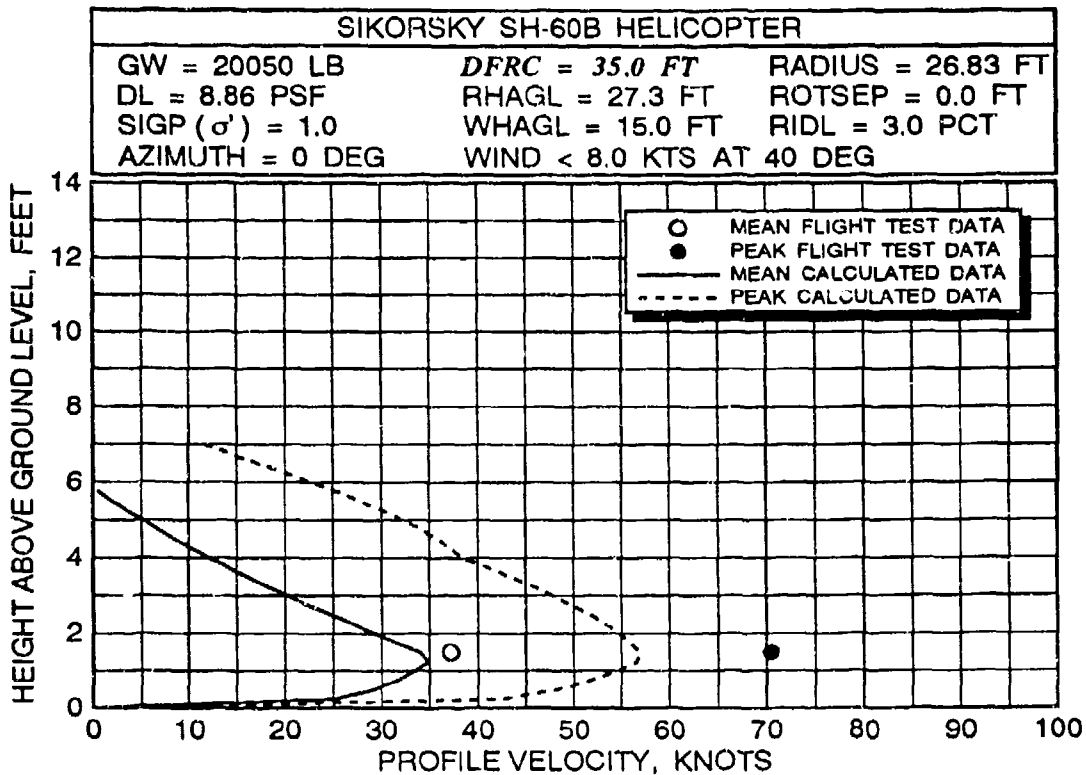


FIGURE 60 SH-60B MEAN/PEAK VELOCITY PROFILE CORRELATION ALONG THE 0- DEGREE AZIMUTH RADIAL AT A ROTOR HEIGHT OF 27.3 FEET

with the analytical results from these models. Test data that are available for correlation of the ambient wind effect are presented in sections 2.1.9 and 5.1. In the discussion in section 5.1, the data are presented in conjunction with correlation for overturning forces and moments as measured on personnel.

In the effort to locate flight test data for correlation with both the ground-vortex and the forward-flight trailing-vortex models, only limited flight test data were identified relating to trailing vortices. Therefore, no effort has been made to validate the ground vortex model other than that described in section 2.2 using the model data presented by Curtis and Sun. The trailing vortex flight test data that were identified for correlation purposes were obtained from reference 46 and some unpublished flight test data acquired by the FAA.

BELL UH-1H HELICOPTER

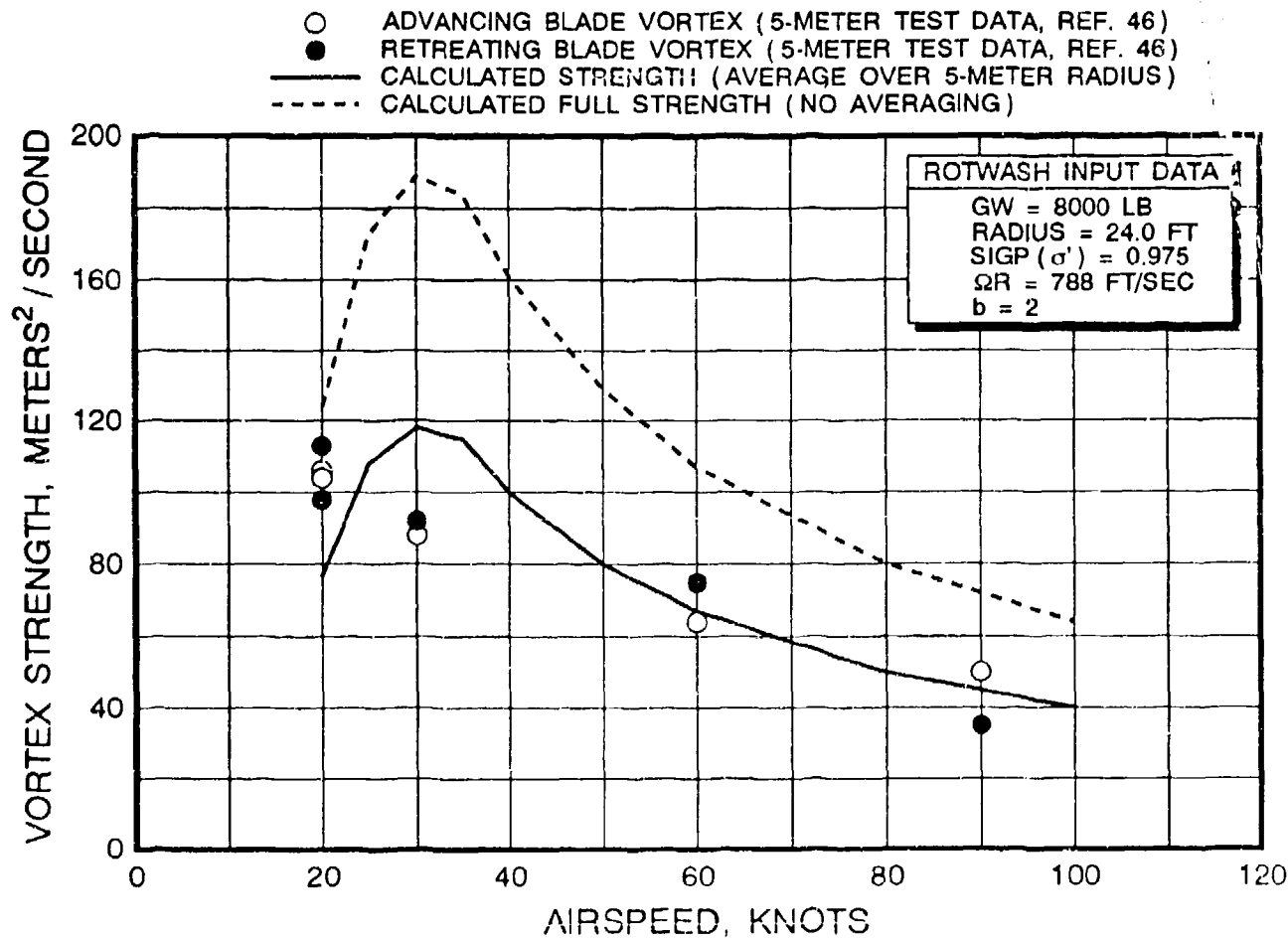


FIGURE 61 RELATION OF CALCULATED AND MEASURED UH-1H 5-METER WAKE-VORTEX STRENGTH AT AGE 20 SECONDS (APPROXIMATE) AS A FUNCTION OF AIRSPEED

SIKORSKY CH-54 HELICOPTER

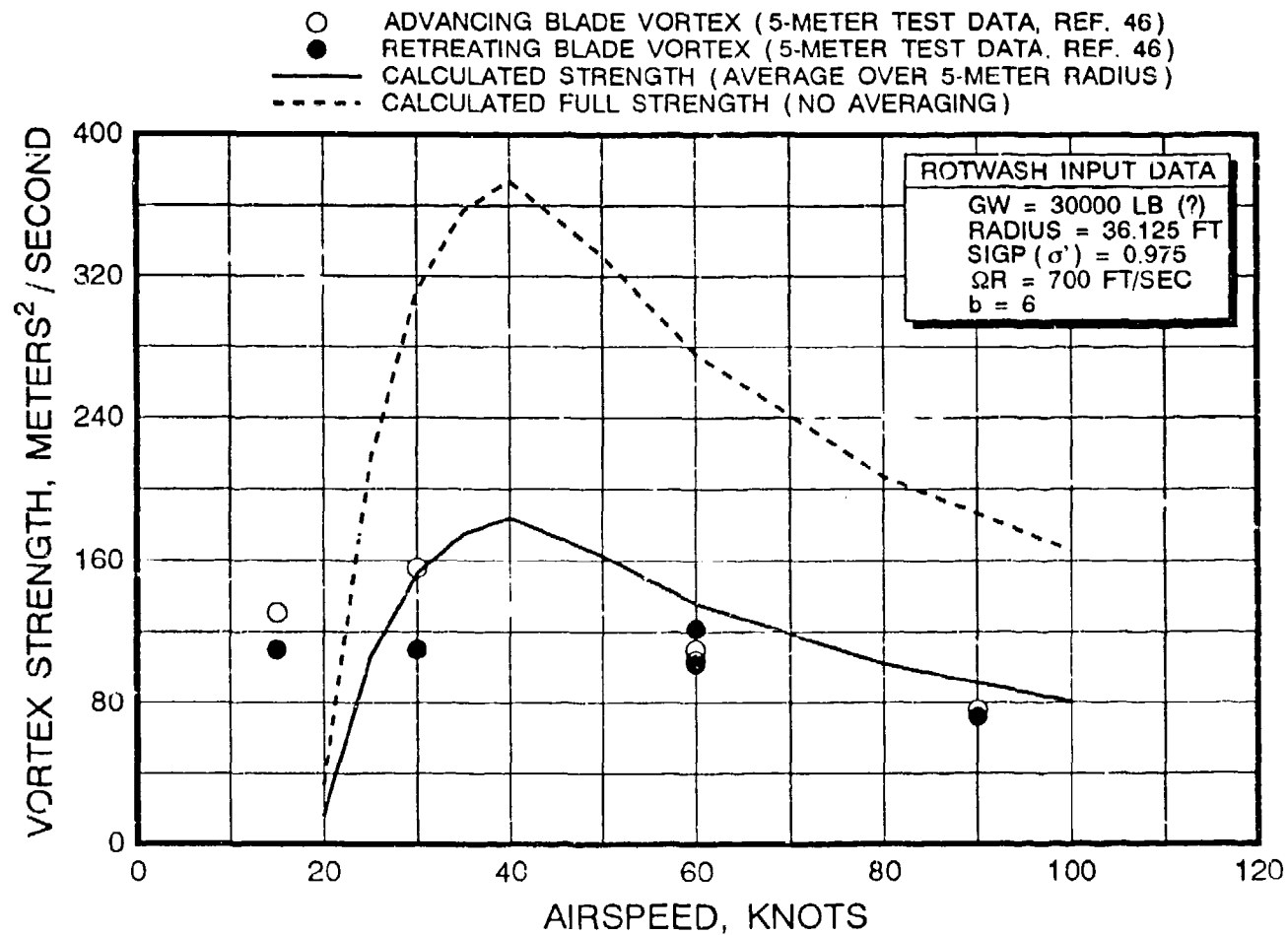


FIGURE 62 CORRELATION OF CALCULATED AND MEASURED CH-54 5-METER WAKE-VORTEX STRENGTH AT AGE 20 SECONDS (APPROXIMATE) AS A FUNCTION OF AIRSPEED

Data on trailing vortex strength acquired from reference 46 are presented in figures 61 and 62 as a function of airspeed for two helicopters. The helicopters are the UH-1H and the CH-54, respectively. The age of the measured vortex strength data is approximately 20 seconds, and the circulation is averaged to a radius of 5 meters. (This parameter estimates the vortex hazard to a fixed-wing airplane with a 5-meter semispan.)

The 5-meter averaged circulation presented in the figures, $\tilde{\gamma}_w(r)$, is less than the total circulation ($\tilde{\gamma}_w$) where by combining equations 58 and 59

$$\Gamma_w = \left(\frac{\pi R (\Omega R)^2 C_T}{2 V_f K_e} \right) (1.0 - (\chi - 8.0) (0.065)) \quad (60)$$

The averaged circulation is a function of the core radius (r_c) and is calculated using equation 61. This equation has been implemented in the ROTWASH model using a core radius that is assumed equal to 0.1 times the rotor diameter (or 0.2 times the rotor radius).

$$\Gamma'_w(r) / \Gamma_w = [1.0 - (r_c/r) \tan^{-1}(r/r_c)] \quad (61)$$

Results, as calculated using the ROTWASH model, are presented in figures 61 and 62 for both 5-meter averaged data (solid line) and uncorrected data or data averaged with a radius at infinity (dashed line). As can be observed, the infinity averaged data clearly overpredict vortex strength as measured in flight test (as would be expected).

The Bell UH-1H 5-meter averaged data correlate well with flight test data at 60 and 90 knots. At very low airspeeds, the calculated data are quite close in magnitude but shifted in airspeed. However, it is important to note that the flight test calibrated airspeeds were estimated by the pilot (reference 46) and many pitot static systems tend to underpredict calibrated airspeed by 5 knots at very low airspeeds. Therefore, it is quite possible that the test data could justifiably be shifted by at least 5 knots to the right. Strength data at these very low airspeeds also vary significantly in magnitude, because shed vorticity does not fully roll up into two distinct trailers. ROTWASH calculations at low airspeeds are predicted as influenced by the washout effect in equation 59 (section 2.3). Therefore, even if correlation is quite good, both the simple model and flight test data have to be considered suspect to some extent.

Sikorsky CH-54 5-meter average data correlate similarly to UH-1H data. However, two additional problems exist in correlating with these flight test data. The first problem results because there is uncertainty with respect to the helicopter gross weight during the tests. Calculated data are presented for an average gross weight of 30,000 pounds. However, there are indications that gross weight could have been in the 34,000 pound range. This would have the result of shifting the calculated 5-meter data up by 10 to 20 meters²/second at 50 knots and 5 to 10 meters²/second at higher airspeeds. The second problem exists in that all

ROTWASH calculations are made with the simplifying assumption that vortex strength does not decay with time. Therefore, the ROTWASH model only predicts initial peak vortex strength. The flight test data presented in reference 46 are plotted at a time of approximately 20 seconds. Several individual plots in this reference indicate that initial vortex strength could have been at least 10 to 15 percent greater in magnitude. One of these plots is presented later in this section.

Additional trailing vortex strength data have been acquired for the Sikorsky S-76, UH-60, and CH-53E from an unpublished source of flight test data. These strength data are presented in figures 63 through 65. The data are averaged over a radius of 5 meters, as were the reference 46 data. The starboard (or advancing blade) vortex strength was used in constructing each graph because analysis consistently indicated that this vortex was the stronger of the two. The age of the vortices is 10 to 15 seconds. This time span corresponds to the period immediately after rollup when minimal decay has occurred.

Correlation of ROTWASH predictions with the S-76 and UH-60 flight test data is quite good down to 50 knots. Between 30 and 50 knots, the calculated data either overpredict the test data or insufficient test data exist to make a good comparison. It is difficult to make this determination due to data scatter. Correlation of ROTWASH predictions with the CH-53E test data match extremely well down to 25 knots.

Figures 66 and 67 have been provided as examples of cross sections of velocity profiles that have been measured for trailing vortices from the UH-1H and the CH-54. The observed separations between the two vortices (one from each rotor tip), as measured in flight, are approximately 1.06 and 0.88 times the rotor diameter for the two helicopters, respectively. Given the accuracy of the experimental measurements, these values are consistent with the uniform rotor loading assumption made in equation 60, which would predict vortex separation equal to the rotor diameter.

As mentioned earlier, comparisons between the ROTWASH predicted data and the flight test data presented in figures 61 and 62 do not account for the vortex decay process. Figure 68 provides insight as to how the CH-54 5-meter averaged circulation decays as a function of time. The initial transient measured at the beginning of each run is believed to be related to the roll up process that becomes complete in about 6 to 10 seconds. Afterwards, vortex strength decays slowly. The approximately 20-second values chosen for correlation purposes in figures 61 and 62 should be reasonably representative of the initial vortex strengths at various airspeeds. However, in this particular case, the 5-meter peak strength appears to be as strong as 180 meters²/second at approximately 10 seconds. This value is

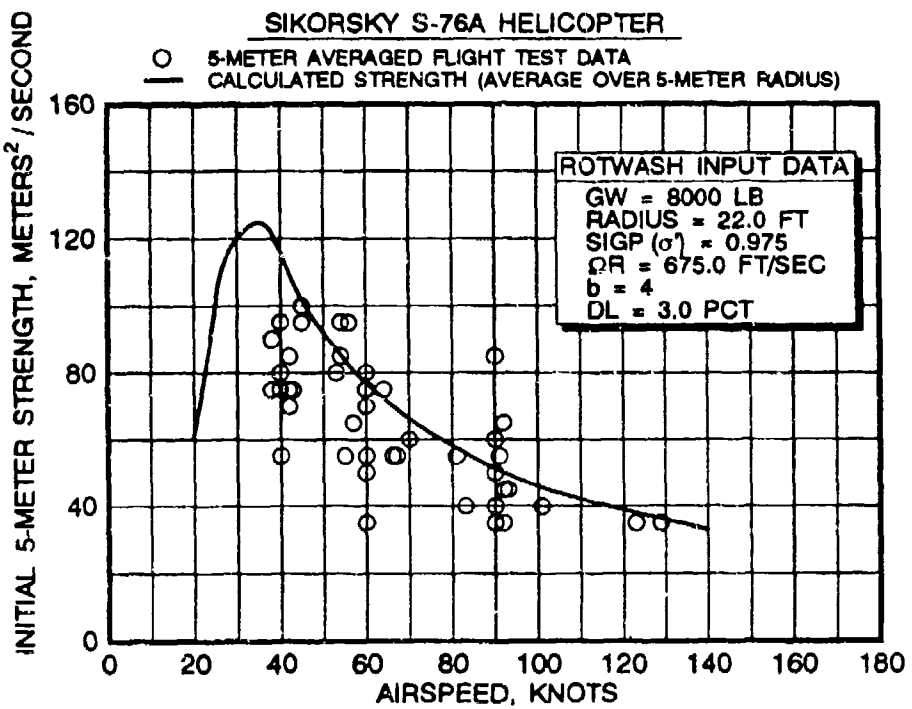


FIGURE 63 CORRELATION OF CALCULATED AND MEASURED S-76 5-METER WAKE VORTEX STRENGTH AS A FUNCTION OF AIRSPEED

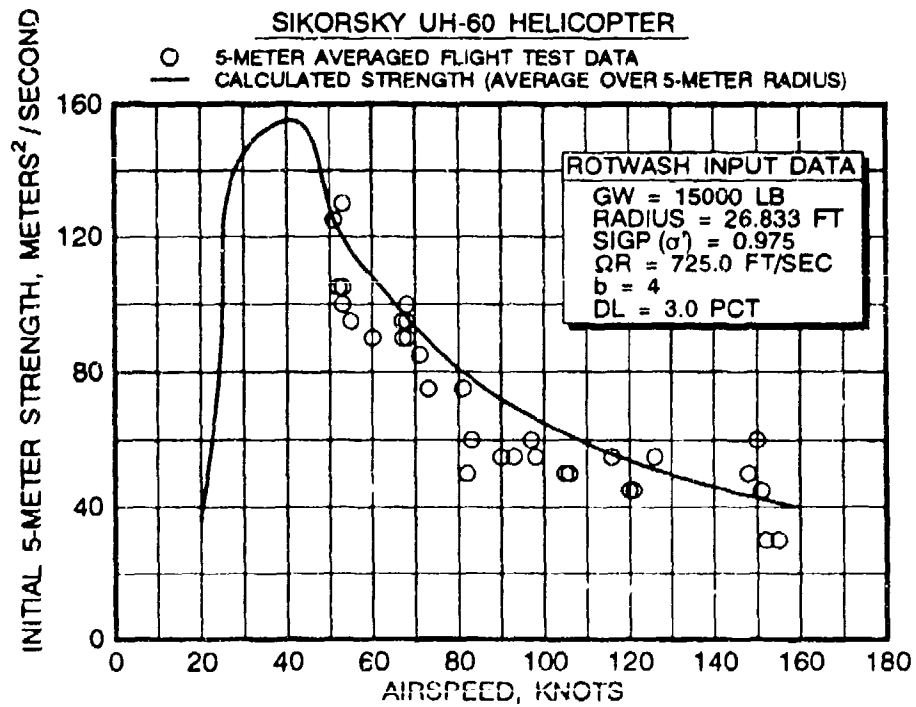


FIGURE 64 CORRELATION OF CALCULATED AND MEASURED UH-60 5-METER WAKE VORTEX STRENGTH AS A FUNCTION OF AIRSPEED

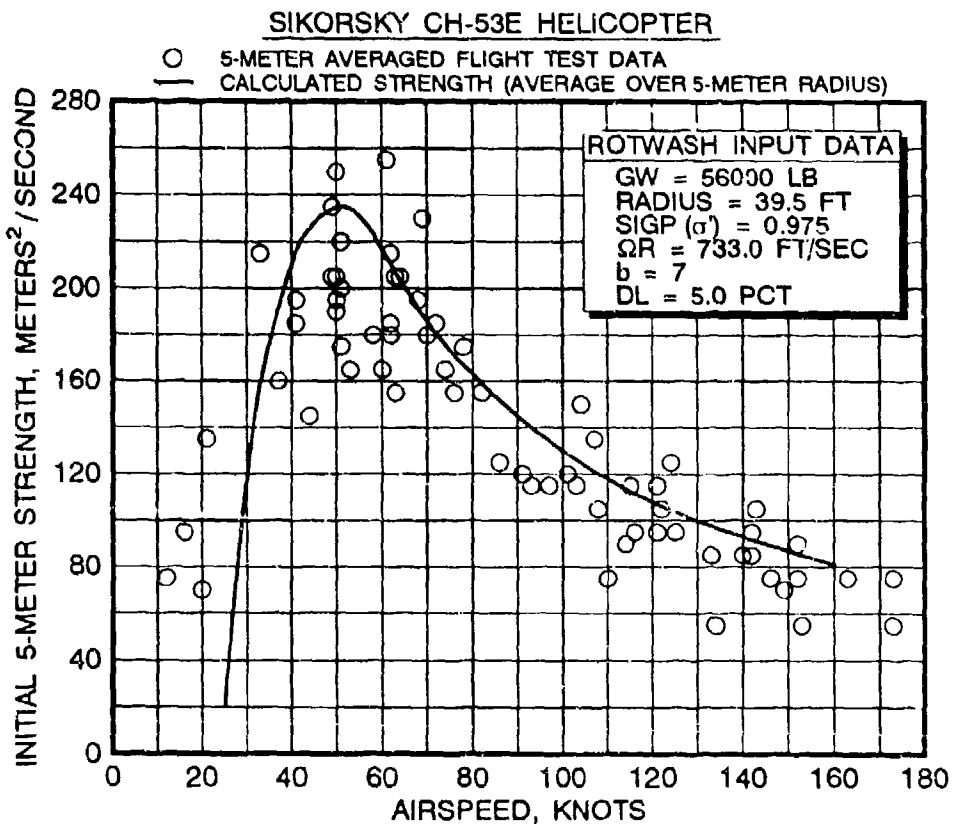
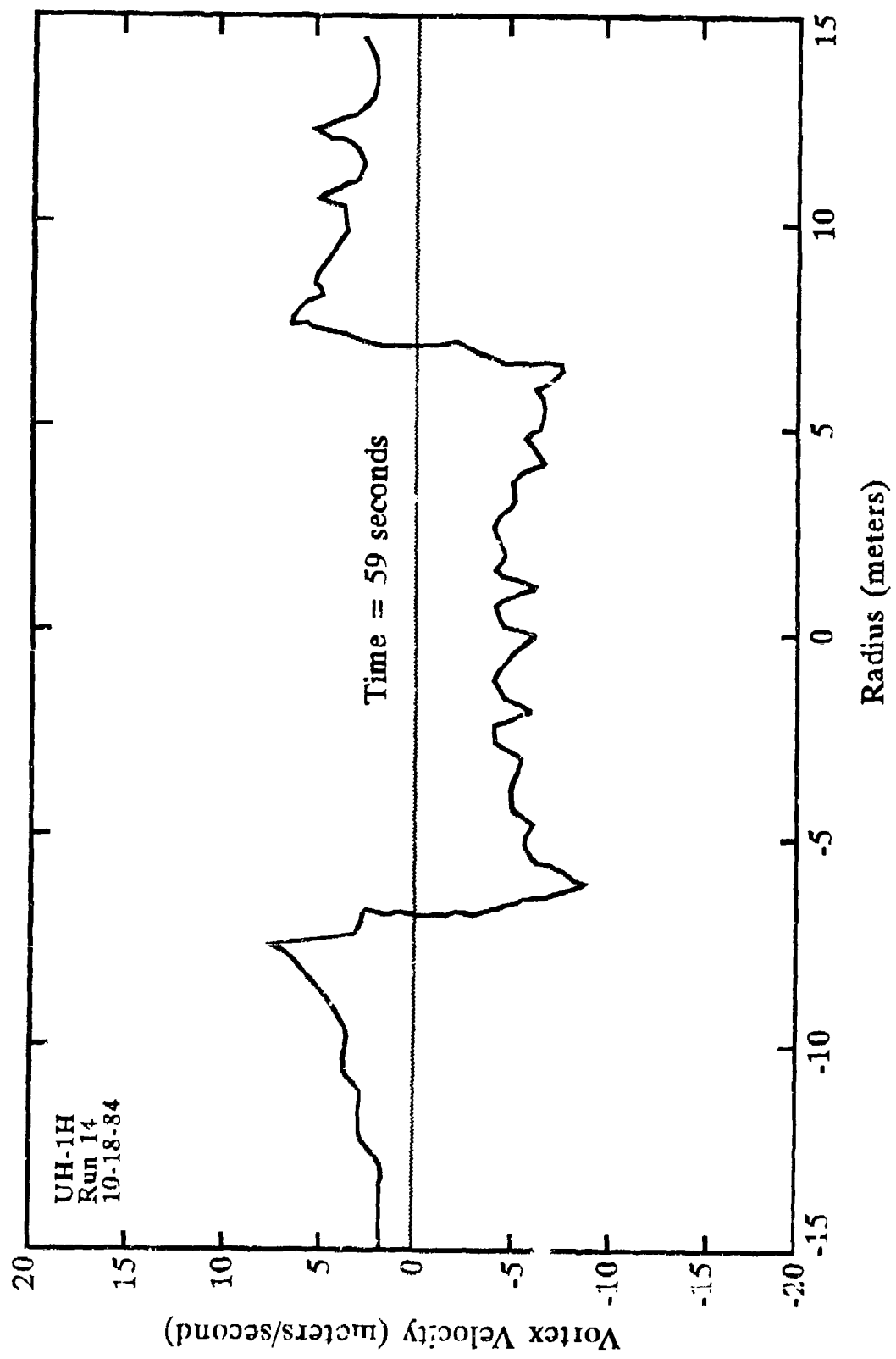


FIGURE 65 CORRELATION OF CALCULATED AND MEASURED CH-53E 5-METER WAKE VORTEX STRENGTH AS A FUNCTION OF AIRSPEED

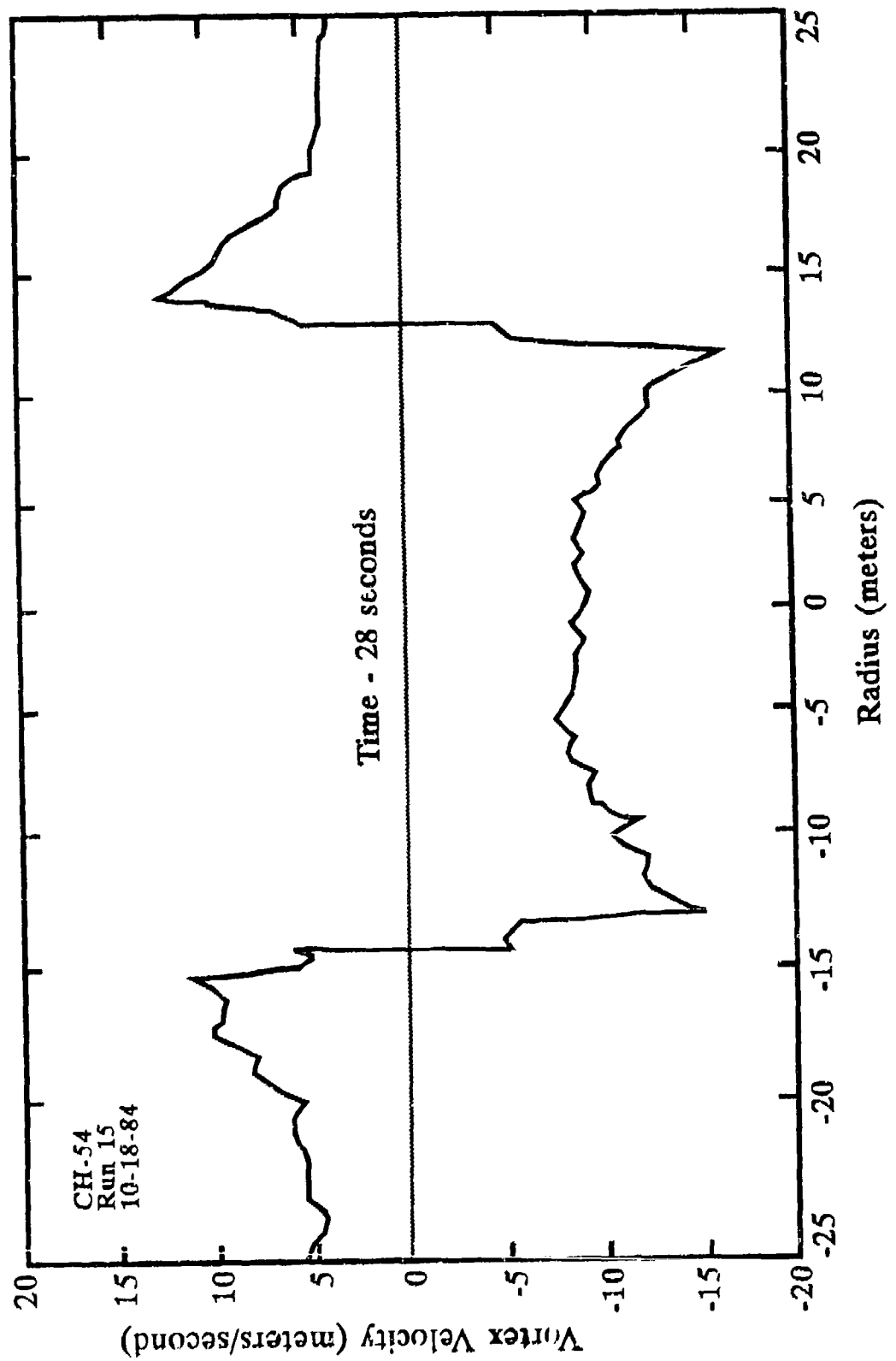
larger than the values provided in figure 62 that are documented in reference 46. However, it should be noted that figure 68 strength data may not include other unknown corrections that were applied to the figure 62 data.

In conclusion, it should again be emphasized that the wake vortex data presented in this section are preliminary data from an ongoing test program and are provided only for the purpose of gaining insight into the validity of using the ROTWASH mathematical model in hazard analysis. Until a more complete set of data runs for several helicopter types is measured, ROTWASH generated data should be used with caution.



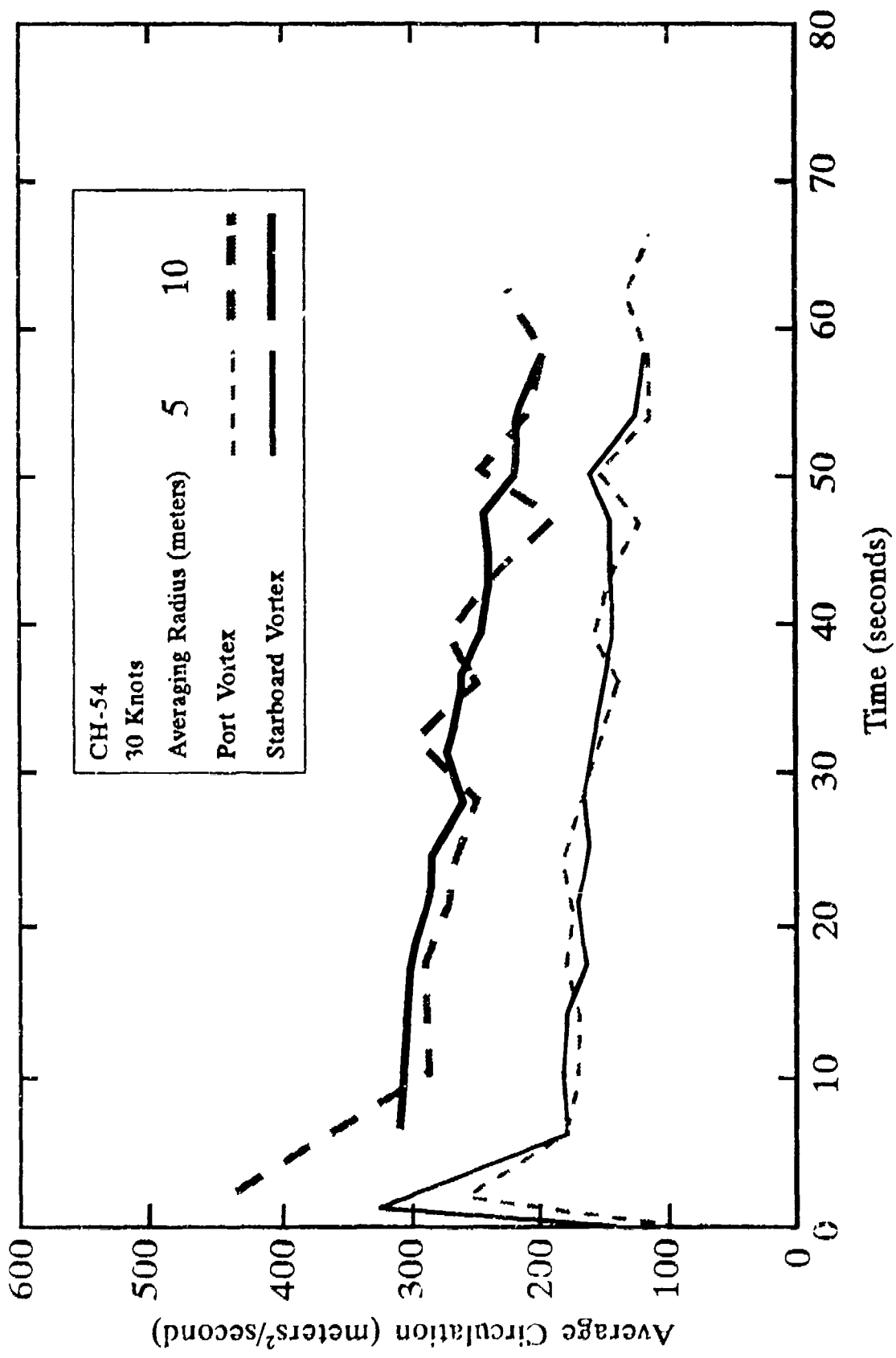
Source: Reference 46.

FIGURE 66 UH-1H WAKE-VORTEX PROFILE AT AGE 59 SECONDS



Source: Reference 46.

FIGURE 67 CH-54 WAKE-VORTEX PROFILE AT AGE 28 SECONDS



Source: Reference 46.

FIGURE 68 EXAMPLE OF CH-54 WAKE-VORTEX STRENGTH AS A FUNCTION OF TIME

4.0 DEVELOPMENT OF A MISHAP ANALYSIS METHODOLOGY

The first FAA-sponsored effort devoted to the development of a mathematical modeling and analysis methodology for rotorwash-related mishaps is documented in reference 1. This research effort, completed in 1986, provided the basis for additional work on tiltrotor and tiltwing configurations (reference 2), a further detailed analysis of several types of mishaps (reference 3), and the continued improvement of rotorwash analysis tools (reference 4). Each of these subsequent studies have contributed in different ways to strengthening the foundation for the eventual development of proposed separation guidelines for safe operation of rotorcraft at heliports and vertiports. However, the completion of additional research work, the acquisition of additional test data (references 5 through 11), and the use of additional research work in heliport/vertiport design and construction (references 12, 47, and 48) have resulted in several problems. The most serious of these problems has been the lack of an up-to-date handbook documenting:

1. the latest versions of various mishap analysis methods,
2. the most recently acquired examples of the types of mishaps that might be encountered (as well as up-to-date summaries of mishap data),
3. how mishap analysis methods should be utilized during the heliport/vertiport design process (with examples), and
4. limitations of the latest mishap analysis methods.

A primary goal of this report is to attempt to alleviate these problems. This is accomplished by consolidating the mishap analysis methodologies and results from previous research efforts, documenting recently acquired flight test and methodology validation data, and developing the requested handbook of heliport/vertiport design examples. The result of this effort is to provide the best possible tools to define rotorwash velocity thresholds that, when exceeded, increase the probability that mishaps will occur.

4.1 MANAGING THE MISHAP ANALYSIS EFFORT

In conducting an analysis of this type, the most important initial task is to somehow bound the research effort in order to make it more manageable. In order to accomplish this task, several assumptions had to be made early on in the effort. The first assumption was that the analytical effort should concentrate on "worst offender" types of rotorcraft. These include the most common types, light to medium classes (5,000 to 15,000 pounds), that are responsible for the majority of mishaps.

The second assumption is that mishaps having the highest frequency of occurrence in the past will occur more frequently in the future. These types of mishaps are also the ones that have the greatest potential for reduction in occurrence. Therefore, a list of the most common types of mishaps was carefully compiled from the literature and mishap data bases. Unique or spectacular mishaps not likely to reoccur in the future were eliminated from consideration.

A third assumption used to bound the effort was that any developed analysis methodology would justifiably be challenged by someone with the best of intentions at some future point in time. Therefore, a significant effort was made to validate analysis methods and results with experimental data and actual mishap data. This validation process was also used to minimize requirements for loosely defined safety factors on analysis results. In situations where safety factors are required, the safety factors are clearly identified and reasoning is provided for their assigned values.

The development of a methodology for classification and analysis of rotorwash-related mishaps is primarily a three-part process. This process involves:

1. identification of important types of mishaps,
2. mathematical modeling of the mishaps, and
3. evaluation of the analyzed mishaps to determine critical threshold values of rotorwash velocities.

A block diagram of this analysis methodology is presented in figure 69. The completion of each task provides the information required to initiate development of recommended safe separation guidelines. Separation guidelines can be developed between rotorcraft and ground personnel, ground vehicles, other rotorcraft or fixed-wing aircraft, ground structures, and equipment frequently found in the rotorcraft operational environment. However, it must be remembered that it is not a goal of this report to define formal rotorcraft separation guidelines. Instead, the goal is to develop background data and examples of analyses for heliport and vertiport design and to support future requirements for development of separation guidelines.

4.2 IDENTIFICATION OF MISHAPS FOR ANALYSIS

The first task of the three-part process presented in figure 69 involves the identification of rotorwash-related mishaps for potential analysis. In this report, a mishap is defined as the occurrence of an undesirable event that is known or believed to have been initiated by rotorwash. The amount of damage incurred

**IDENTIFICATION
TASK**

Identify Mishaps for Analysis

**MATHEMATICAL
MODELING
TASK**

Mathematically Model Mishaps

Mathematically Model Rotorcraft Rotorwash Flowfield Characteristics

**EVALUATION
TASK**

Evaluate Mishaps To Identify Critical Threshold Rotorwash Velocities

Improve Mathematical Models as Required Using Evaluation Results

Document Mishap Analysis Results

FIGURE 69 ANALYSIS METHODOLOGY FLOW CHART

may vary from minimal to complete destruction. Sources for identified mishaps include the military services (mishap databases from safety centers), government agencies, and rotorcraft operators. The majority of the sources used in this report were previously identified during the research efforts that resulted in the publication of references 1 and 3.

Each mishap identified for potential analysis was reviewed to ensure that an analysis would contribute to project goals. Mishaps were also prioritized so that mishaps believed to be the most important would be the ones that were analyzed first. Unique or spectacular mishaps were eliminated from consideration. In summarizing the mishap data that have been acquired, the following points can be briefly stated.

1. Numerous cases of personnel injury due to flying debris were reported (i.e., eye and internal injuries requiring medical evacuation).
2. Rotor blade strikes on tailbooms and tunnel covers (CH-47 tandems) occur quite frequently when rotorcraft fly next to other rotorcraft that have rotors operating at low rpm (independent of the number of rotor blades). In several cases, blade strikes even occurred when rotor blades were tied down. Drive shaft fairings, drive shafts, and main rotor blades were the most frequently damaged rotorcraft components.
3. Over 50 cases were identified that involved rotorcraft or fixed-wing doors being blown off their hinges by other rotorcraft (the majority of the identified cases were reported over a span of only several years by one source alone). Drive shaft covers and access panels were also frequently reported as being blown off or damaged (some were reported as being securely closed). Windows, canopies, and chin bubbles were often shattered when doors either separated from the vehicle or were damaged. Occasionally, personnel were severely injured.
4. Numerous cases of damage to fixed-wing aircraft were reported. Parked aircraft were reported to have been overturned when not tied down (usually one wing tip was severely damaged), rotated off tricycle gear onto their tails, "moved" or "spun around", and had damage inflicted to the empennage or control system.
5. Numerous flights by single rotorcraft (usually during hover, air taxi, takeoff, or landing) were reported that resulted in nearby rotorcraft being forced to crash, make hard landings, or incur transmission or engine overtorques. Formation flying was frequently

reported as being responsible for overtorques and loss of directional control.

6. The number of mishaps that reported rotor blade and airframe damage from rotorwash-blown foreign objects are too numerous to tabulate (in the hundreds as a minimum). In many cases the foreign object was never even identified. Impact noise, degraded flying qualities, or post-flight inspection usually provided the indication that damage had occurred.
7. Examples of the types of objects being blown around that either sustained or inflicted damage include:
 - a. empty 55-gallon oil drums, rotor blade box covers, packing cartons/boxes, and ammunition boxes,
 - b. maintenance stands (blown over or across the ground into other rotorcraft),
 - c. numerous rocks and round or jagged objects (struck equipment, broke glass and windshields),
 - d. metal landing pad planking,
 - e. dead tree branches and brush,
 - f. nylon, cloth, and plastic equipment bags or empty sand bags,
 - g. flare and personnel parachutes,
 - h. landing zone nylon and metal markers, and
 - i. sheet metal, corrugated metal, wood, and plastic panels.
8. Between 40 and 50 serious mishaps due to self-generated clouds of dust/dirt/debris (brownout), snow (whiteout), or water spray were reported. Foreign objects in these clouds, such as leaves, grass, corn husks, etc. were reported getting into rotors and engines. Severe mechanical damage, hard landings, and crashes were often reported as the final result.
9. Numerous tents and tarps were collapsed, blown away, or sucked into the rotor.
10. Camper shells were blown off trucks and motorcycles were overturned in nearby parking areas.

A collective review of these various types of mishaps resulted in the creation of a list of mishaps that warranted further

analytical review and study. Each of these types of mishaps was sorted into one of six defined groups to simplify the analysis and reporting process. These six groups are the basis for the subdivisions of section 5 that investigate mishaps involving:

1. injury to ground personnel,
2. damage to structures and ground vehicles,
3. damage to other rotorcraft,
4. damage to fixed-wing aircraft,
5. entrained object and debris hazards, and
6. water, dust, snow, and debris clouds.

The reader should note that the group titles and the number of mishaps mentioned within each group have no statistical meaning. As observed from the above summary list of mishap types, numerous other types of rotorwash-related mishaps have been reported in the literature. Statistical probabilities for the occurrence of any one specific type of rotorwash-related mishap can confidently be stated as unknown. No central clearinghouse exists for collection and reporting of these types of mishaps, because the offending rotorcraft rarely sustains damage and injuries to personnel are rarely life threatening. The military safety centers do the best job of collecting data; however, even their efforts rarely provide enough detailed information for subsequent mishap analysis efforts. This is partially due to the lower priority assigned to the investigation of these types of mishaps.

4.3 MATHEMATICAL MODELING OF MISHAPS

The mathematical modeling task described in figure 69 provides tools to understand the physics of mishaps and eventually to evaluate separation guidelines. As shown by the feedback loop, the modeling task is an inexact task and therefore iterative. Mathematical modeling of mishaps in the future will continue to be an iterative task because a large number of scenarios exist for most common types of mishaps. Also, mishaps identified in data bases and reports that are used to validate mathematical models are not controlled experiments. Therefore, detailed documentation of parameters such as wind, aircraft gross weight, mishap geometry, etc., is rarely available. If information of this type is provided, it is almost always someone's best recollection of events at a much later point in time. Most of the mishaps discussed in this report had to be studied iteratively several times. Therefore, results presented from this type of analysis must be qualified as an investigator's "best estimation" of conditions occurring at the time of the mishap. Mishap analysis results can rarely be presented as facts. This weakness in the analysis approach makes it

imperative that as many mishaps as possible be studied. Hopefully, a statistical significance can then become the basis for any reported results when separation guidelines are eventually proposed.

The mathematical models used in this effort are developed specifically for the mishaps being studied. Some of these models are modifications to previously developed models in cited literature and some are new developments. All rotorwash velocities estimated in the mishap analyses are calculated using version 2.1 of the rotorwash analysis computer program (ROTWASH). All generic analysis results similar to results originally presented in references 1 and 3 have also been updated using version 2.1 of the program. The version 2.1 user's guide is documented in appendix D.

4.4 EVALUATION OF MISHAP ANALYSIS RESULTS

The goal of the evaluation task in figure 69 is to identify critical threshold values of rotorwash velocity at which rotorwash mishaps are likely to occur. For some of the types of mishaps that are studied, this goal has been accomplished with a reasonably high level of confidence. These results should be most useful as background for any future development of separation guidelines. The quantity and quality of available data for several other types of mishaps do not support firm conclusions. The final output of the evaluation task is the documentation contained in this report. Documentation presented in section 5 focuses on a presentation format that includes:

1. an introduction to the type of mishap being investigated,
2. development of associated mathematical models, safety factors, and analysis procedures,
3. validation of mathematical models, and
4. a summary of results.

Work presented in sections 6.0 and 7.0 emphasizes "How To" design-oriented examples using the developed mathematical models. Recommendations for future research work to improve mathematical models and analysis procedures are provided in section 8.0.

5.0 ANALYSIS OF ROTORWASH RELATED HAZARDS

This section describes the approach, methods, and working equations required to implement a group of rotorwash-related hazard analysis models. These models are designed to be used as predictive tools in estimating and classifying potential rotorwash hazards as influenced by flight regime and rotorcraft configuration. Several of the models have been developed specifically for this study; others have been adapted from previous research efforts. Results calculated from these hazard models are used to define minimum safe separation distances among various rotorcraft of interest, various classifications of personnel, and other aircraft, structures, or vehicles. Each of the models is developed with emphasis on rotorcraft operations in close proximity to the ground. These mathematical models are also developed to be used in conjunction with the rotorwash flow field models developed in section 2.

Safety factors utilized with the hazard analysis models are also discussed in this section. When used, safety factors are provided in order to help assure that reasonable uncertainties are accounted for in the analysis process. A majority of these analytical modeling uncertainties are the result of one or both of the following factors:

1. unknown effects on the predictive accuracy of the downwash/outwash flow field models when used in conjunction with the hazard models (i.e., as affected by specific rotorcraft configuration, unsteady atmospheric conditions, and piloting technique), and
2. the hazard models themselves because few experimental and documented mishap data exist that can be used in correlating individual hazard analysis mathematical models.

In situations where use of a safety factor is deemed to be unreliable or where a refined estimate might significantly reduce the arbitrary impact of a safety factor, a recommendation for further research is provided along with a description of the type of experiment that is required (see section 8 for a summary of recommendations).

Validation results for each hazard analysis model are presented as often as possible through correlation with available flight test, model, or previous mishap data. The most extensive validation results are provided in association with the wall jet model in both single and twin-rotor configurations. Data used in these correlation analyses come primarily from flight test evaluations of the Sikorsky CH-53E, Bell XV-15, and Sikorsky S-61 (SH-3).

5.1 ROTORWASH OVERTURNING FORCE AND MOMENT EFFECTS ON PERSONNEL

In the development of any type of rotorwash-related separation criteria, the most important hazards are those that directly involve the safety and general welfare of people. Unlike buildings and equipment that can be repaired or replaced if damaged, a human that sustains serious injury (or death) precipitates a situation that will never be fully rectified, even in a court of law. Military research into personnel-related hazards has focused primarily on quantifying requirements and developing specifications and procedures for the use of protective gear. This work has generally been based upon the assumption that military personnel working in a rotorcraft downwash environment are generally male, weigh at least 130 pounds, and will receive at least some special hazard avoidance training. This research has also helped to quantify parameters that are associated with the prediction of overturning forces and moments on personnel.

Military-sponsored research that has been conducted to define what can be considered comfortable and uncomfortable to a full-size adult fully or partially immersed in a rotorwash flow field has been very limited in nature. Unfortunately, but understandably, none of this research has seriously examined the civilian side of the problem. Minimal work has been conducted to quantify what is unpleasant, uncomfortable, or dangerous to the untrained and therefore unsuspecting human (adult or child) that is suddenly either partially or fully immersed in a rotorwash flow field. Even less quantitative data exists to answer questions about what might happen to a person that is standing in or passing through such an environment while wearing a hat, carrying a purse or briefcase, or "towing" a startled and scared child.

While understandably not as complete as desired, the analyses presented in this section are nevertheless provided in order to attempt to answer some of the basic questions posed in the previous paragraph. Proposed research work that would provide information that will greatly enhance the database and significantly improve quantification of safety factors associated with the presented analyses is documented in section 8.

5.1.1 Background and Literature References

Personnel immersed in a rotorwash flow field are affected by a combination of factors such as the pressure forces generated by the horizontal velocity profile, the height of these forces above ground level, and the pulsating nature of the forces. It is difficult to analyze or to assess the direct effects of velocity profile data alone on personnel because:

1. velocity profile shape varies dramatically with height above ground, and
2. dynamic pressure created by rotorwash is a function of the velocity squared.

When comparing data for different flight conditions or types of rotorcraft, the variation in generated forces is far more meaningful from a hazard standpoint than the variation in velocity. Additionally, force data for various altitudes and gross weights generally correlate better than velocity data. This results from the fact that calculated force data somewhat filter variations in the measured peak velocity profile, whereas velocity data can only be compared directly for each corresponding height position.

Personnel forces and moments are easily calculated mathematically. However, significant procedural problems do arise when conducting the analysis itself. The first problem to be resolved is associated with choosing the "appropriate" velocity profile to convert to dynamic pressure. As has been mentioned previously, the outwash flow field is not a steady flow field by any stretch of the imagination. However, the choice of the experimentally measured peak velocity profile, instead of the statistically measured mean velocity profile, could be considered by some experimenters to be overly conservative.

A study of the literature (i.e., references 23, 24, and 44) indicates that use of the peak velocity profile in calculating overturning forces and moments and in quantification of safety standards is the correct choice. The literature also implies that hazardous overturning forces and moments should be termed "destabilizing" forces and moments for discussion purposes due to their highly oscillatory nature. Literature commentary refers to the personnel hazard as one where the forces on the human body eventually become large and oscillatory. At that point, personnel can no longer anticipate and react to position their body to move about and work safely without being unexpectedly knocked down or overturned. Development of a standard for quantification of these dynamic forces and moments is quite different from one that might be developed for simple overturning forces and moments while in a fixed body position or for avoiding injury when moving directly outward to escape a potentially hazardous outwash flow field.

Two laboratory experiments have been conducted in order to attempt to quantify limiting overturning force and moment values. Results from these experiments are presented in references 24 and 44. In reference 44, the test results quantify levels of unexpected uniform pressure distribution that will knock a person off balance. These results indicate that a sudden change in force over 400 milliseconds will cause at least limited disorientation and unbalance when the peak uniform velocity

profile creating the force is greater than 87 feet per second (51 knots). A uniform peak velocity profile of greater than 126 feet per second (75 knots) was determined to be sufficient to instantaneously unbalance and knock over a standing or walking man. However, since the research in reference 44 was an evaluation of a hazard that might occur following the loss of airliner cabin pressurization, it cannot be considered totally applicable to rotorwash related scenarios. As pointed out in the reference, "considerable judgment is necessary to successfully extend the experimental data beyond the limits for which it was intended." The data, however lacking, are nevertheless fully documented and referenceable.

Reference 24 provides a second source of experimental data to aid in quantification of practical limiting overturning force and moment values. However, before discussing this experiment, it is important to discuss another important factor. As mentioned previously, the first problem in the analysis process is to decide upon and justify use of either the mean or peak velocity profile to calculate forces. A second and perhaps an even more imposing problem is the establishment of analysis criteria for personnel. For example, what size, weight, and strength percentile is to be used to model a human being for evaluating the limiting overturning forces and moments? Clearly, the physiques of an average 7-year-old child, a 25-year-old 5-foot 6-inch woman, and a professional football player are vastly different, yet they are intimately connected with the ability of each individual to overcome rotorwash-generated forces and moments. Experimental data documented in reference 24 attempt to address this second problem for military personnel actively involved in rotorcraft operations.

Laboratory tests were conducted for the purpose of indirectly estimating a test subject's ability to work against rotorwash-generated wind forces. Each participant was tested to determine how much horizontal force could be pulled using a test fixture. This fixture consisted of a torso harness that distributed the load across the hips and chest to a line tied 3-feet above ground level (AGL). A weight, attached to the line, was lifted by the forward movement of the subject. Table 6 presents a list of the subject's weights and heights (percentiles are based on military statistics, not general population). Figure 70 presents a bar chart that indicates the amount of pull force that each individual was able to exert. The pull test data do not, of course, duplicate the dynamically applied downwash forces. However, dynamic forces were applied during the tests. These forces resulted because the slightest forward or reverse movement of the body or trunk caused the weight to move up or down. This movement of the weight required the subject to respond dynamically to the load acceleration. The limit of postural stability was taken to be the point that stability could no longer be maintained with some forward progress. These postural

stability limits are represented by the top of the black bars in figure 70.

TABLE 6 HEIGHT AND WEIGHT OF SUBJECTS USED IN DYNAMIC FORCE EVALUATION

SUBJECT NUMBER	HEIGHT		WEIGHT	
	INCHES	PERCENTILE	POUNDS	PERCENTILE
1	67	10th	133	2nd
2	73	90th	150	15th
3	74	95th	171	50th
4	74	95th	220	99th

Results from this postural stability laboratory experiment were used in the rotorwash evaluations of both the Sikorsky CH-53E and the Bell XV-15 (references 23 and 24). Fortunately, considerable qualitative comments (i.e., ability to safely conduct work tasks within the environment) were also obtained from the test subjects that aid in quantifying acceptable levels of rotorwash for civilian operations. Additional discussion with respect to this subject is presented in a later subsection.

5.1.2 Mathematical Modeling of Personnel

While direct measurement of overturning forces and moments would have been desired from the flight test experiments in references 23 and 24, it was, nevertheless, totally impractical. Therefore, "experimental" force and moment calculations had to be derived indirectly using human physical dimensions, aerodynamic coefficients, and experimentally measured mean or peak velocity profile data. In returning to the results of the first experiment (reference 44), it is possible to convert the 87 and 126 feet per second overturning velocity values into forces and moments. The "standardized" human that was assumed in this experiment had a drag coefficient (C_D) of 1.0 and was 6 feet tall and 1.1 feet wide. Using this model, the velocities convert to 60 pounds of force for purposes of unbalance and 125 pounds for purposes of disorientation. These force values convert to moments of approximately 180 and 375 foot-pounds, respectively (at a 3-foot application height). In comparing these forces with those presented in figure 70, the calculated values appear to be quite reasonable and certainly help to provide a more documentable basis for purposes of further evaluation.

The human aerodynamic mathematical model that has been developed for this study (and incorporated in the ROTWASH program contained in appendix E) relies heavily upon previous work. Compared with the model presented in references 23, 24, and 44 that assumes the

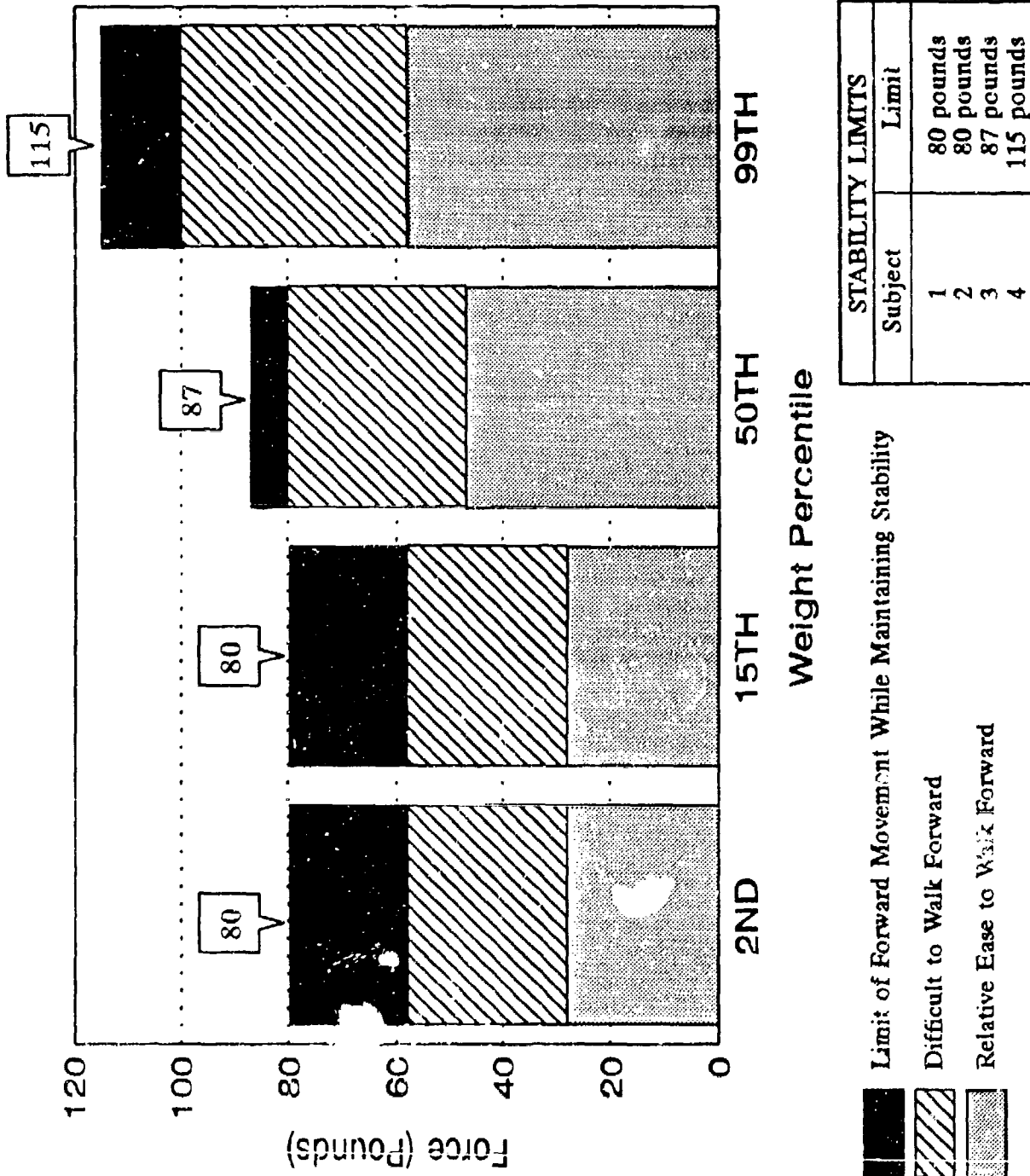


FIGURE 70 CAPABILITIES OF TEST SUBJECTS TO MOVE ABOUT WITH HORIZONTAL RESTRAINT LOADS APPLIED AT 3-FEET AGL

"standardized" human to be a slightly crouched person of 6 feet with a varying width and a coefficient of drag (C_D) of 1.0, other sources (i.e., reference 31) have assumed the "standardized" human to be an average of 1.0 foot wide. Hoerner, reference 49, points out that values for C_D can vary significantly for humans, from slightly less than 1.0 to as high as 1.3, especially for those wearing certain types of (bulkier) clothing. Therefore, two different "standardized" yet simple humans are used in conducting the civilian-related hazard analyses presented in this report. These personnel are defined as:

PARAMETER	PERSONNEL TYPE	
	L	S
Height, feet	6.0	4.0
Width, feet	1.1	0.8
C_D , -ND-	1.1	1.1

where the large or "L"-sized human is similar to those previously discussed, and the small or "S"-sized human is representative of a 7-year-old child of approximately 60 pounds. A C_D value of 1.1 (not 1.0) is utilized as a safety factor for both sizes in the hazard evaluation process (but not in the correlation effort with test data from references 23 and 24) in order to help account for any uncertainties in the analysis process.

Evaluations using the human aerodynamic models are made by first calculating the peak dynamic pressure at 0.5 feet increments up to the maximum height of the subject (figure 71). This can be expressed mathematically by evaluating the equation

$$Q_{pk} = 0.5 \rho_A V_{pk}^2 \quad (52)$$

where:

$$\begin{aligned} Q_{pk} &= \text{peak velocity dynamic pressure, lb/ft}^2 \\ \rho_A &= \text{atmospheric density, slugs/ft}^3 \\ V_{pk} &= \text{profile velocity, ft/sec} \end{aligned}$$

For an "L"-sized person, these pressure calculations are made at twelve vertical stations (Z_x) beginning at 0.25 feet and continuing in 0.5 feet increments up to 5.75 feet. Total force and moment are then calculated by summing each of the individual calculations made at the twelve vertical stations. The following equations are used in this process.

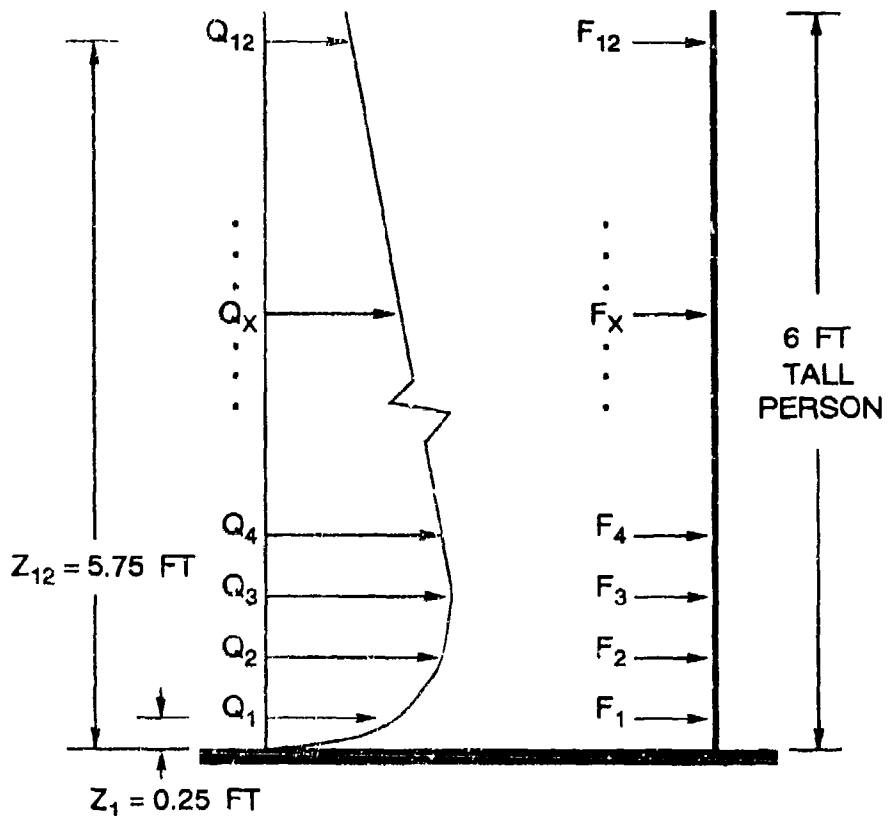


FIGURE 71 GRAPHICAL DEFINITION OF OVERTURNING FORCE AND MOMENT CALCULATION PROCEDURE

$$F_{pk} = \sum_{x=1}^{12} (Q_{pk_x}) (C_D) (W_h) (\Delta H) \quad (63)$$

$$M_{pk} = \sum_{x=1}^{12} (Q_{pk_x}) (Z_x) (C_D) (W_h) (\Delta H) \quad (64)$$

where:

C_D = human drag coefficient, -ND-

W_h = width of the human, ft

ΔH = incremental vertical height for evaluation, ft (in this case 0.5 ft)

In the case of the "S"-sized person, the same analysis methodology is used. However, the value of x is evaluated at only eight vertical stations (ending Z_x at 3.75 feet).

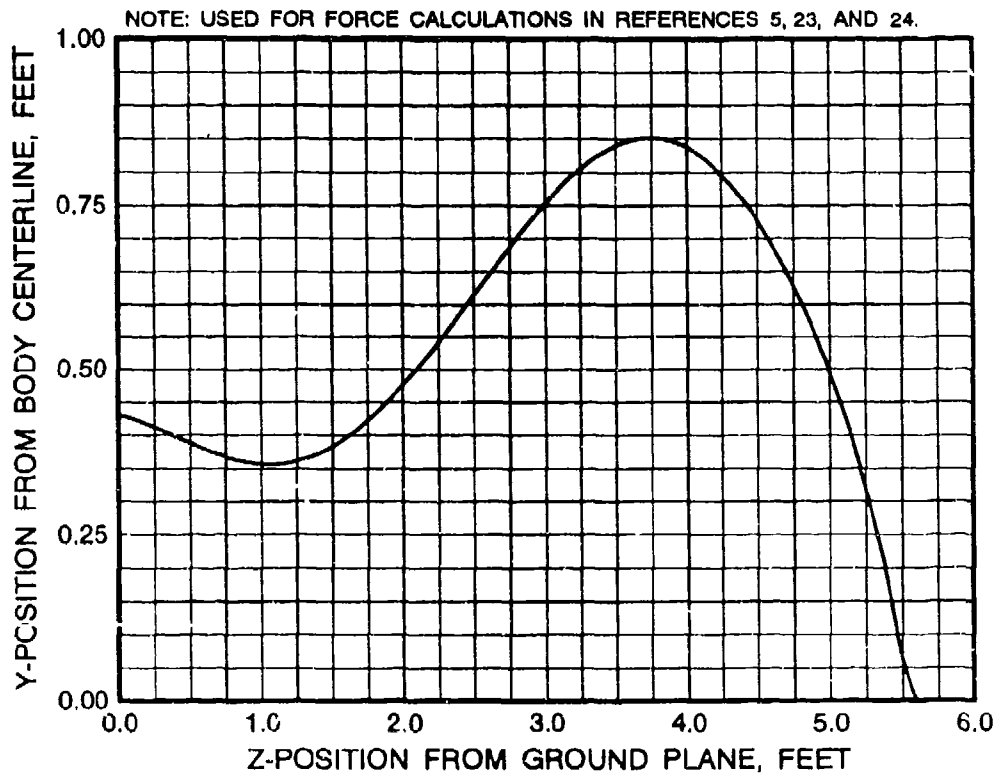
With definition of the personnel model now completed and with use of the section 2 rotorwash models, it is possible to evaluate potential personnel-related hazards. However, before this task is conducted, it is very important to correlate calculated data from the mathematical model with available flight test data to validate the analytical approach.

5.1.3 Quantitative Validation with Experimental Data

Experimental force and moment data, based on flight test velocity profiles, were identified from several sources for validation purposes. This database contains data for the CH-53E (reference 24), RH-53D (reference 24), XV-15 (reference 23), MV-22 (reference 5), CL-84 (references 31, 32, and 40), SH-3 (references 31, 32, and 41), and the HLH rotor (reference 29). In an effort to provide continuity with other correlation data used in this report and the rotorwash velocity data presented in section 3, CH-53E, XV-15, MV-22, and SH-3 data are used as validation data in this section.

Before discussion is presented on correlation of CH-53E results, it is important that the Naval Air Test Center's "standardized" human be documented. As stated in the previous section, the model used in references 23, 24, and 5 is based on a 6-foot human that is crouched into a 5.6-foot position. The width of the human also varies as a function of height. This model was developed by projecting the shadow of a reference 24 test subject in a rotorwash flow field position on a wall. After the profile was traced, an eleventh order polynomial equation was fitted to produce a curve of the shadow y-position edge from the shadow centerline as a function of shadow z-position above the ground. This curve is provided in figure 72. The associated drag coefficient (C_D) was assumed equal to 1.0 for calculation purposes. If 12 positions under this curve are integrated (and multiplied by 2 since a centerline reference is used) to obtain projected areas at the Z_1 through Z_{12} positions (see figure 71), then the ROTWASH program can use the projected areas listed in table 7 to make force and moment calculations. The values in this table are used only for correlation purposes with the CH-53E, XV-15, and MV-22 flight test data. The standardized "L" and "S" models presented in section 5.1.2 are used by the ROTWASH program for more uncertain civilian applications.

CH-53E overturning force data are presented in figures 73 through 75 for gross weights of 45,000, 56,000, and 70,000 pounds, respectively. Generally, prediction of the force distribution as a function of radial position is quite good at all three gross weights at the rotor height of 37 feet. Calculated force at approximately 60 feet or 1.5 times the rotor radius is overpredicted by 5 to 10 percent. However, this particular inaccuracy is not considered critical to the analysis because this region is extremely close to the rotor. As was noted in



Y-position equation is as follows:

$$\begin{aligned}
 Y_{POS} = & C_1 + C_2 (z_{POS}) + C_3 (z_{POS})^2 + C_4 (z_{POS})^3 \\
 & + C_5 (z_{POS})^4 + C_6 (z_{POS})^5 + C_7 (z_{POS})^6 \\
 & + C_8 (z_{POS})^7 + C_9 (z_{POS})^8 + C_{10} (z_{POS})^9 \\
 & + C_{11} (z_{POS})^{10}
 \end{aligned}$$

where:

C_1	=	0.430939	C_7	=	0.221653E-03
C_2	=	-0.0463972	C_8	=	-0.418444E-04
C_3	=	-0.139649	C_9	=	0.145194E-04
C_4	=	0.137545	C_{10}	=	-0.780009E-07
C_5	=	-0.0248764	C_{11}	=	-0.189822E-06
C_6	=	-0.549253E-03			

FIGURE 72 NAVAL AIR TEST CENTER "STANDARDIZED" HUMAN PROFILE FOR ROTORWASH APPLICATIONS

TABLE 7 PROJECTED AREAS USED IN CALCULATION OF HUMAN
OVERTURNING FORCES FOR CH-53E, XV-15, AND MV-22 FLIGHT TEST DATA

Z-POSITION, FEET	PROJECTED AREA (S_H), IN FEET ²	Z-POSITION, FEET	PROJECTED AREA (S_H), IN FEET ²
0.25	0.41	3.25	0.8
0.75	0.37	3.75	0.845
1.25	0.365	4.25	0.7875
1.75	0.42	4.75	0.625
2.25	0.5425	5.25	0.3
2.75	0.685	5.75	0.00625

Note: $S_H = (W_h)(\Delta H)$ in equations 62 and 63.

section 2, the mathematical model for the transition region (prior to formation of the wall jet) is considerably simplified. As distance increases, the calculated values are both greater and less than test data depending on gross weight and DFRC position. At rotor heights of 77 and 117 feet, the mathematical model generally overpredicts the experimentally measured force. This results from both overprediction of the maximum peak profile velocity and the prediction that profile velocities, up to 6 feet in height, vary in a more orderly profile shape than the flight test data. It is interesting to note that the correlation discrepancies are considerably less at the 70,000 pound (figure 75), or maximum gross weight condition, than they are at the lower gross weights (figures 73 and 74). This observation clearly indicates that the strength and shape of the experimentally measured flight test peak velocity profile varies with rotor height as well as disc loading for the CH-53E. The reasons for this phenomenon are not clearly understood at this time and warrant further research. Additional data for a smaller low disk loading helicopter, i.e., S-76 or UH-60, would be most desirable. Fortunately, the mathematical model, as empirically derived for prediction of the peak velocity profile, correlates well for the worst case condition (a CH-53E at the 70,000 pound max gross weight configuration).

The effect of wind on the peak forces generated by the CH-53E was, unfortunately, measured and documented only on the less hazardous upwind side at one radial position at gross weights of 45,000 and 56,000 pounds. Correlation with this less critical azimuth is presented in figures 76 and 77. Since the exact wind velocity is not known (reference 24 states 5 to 9 knots), an assumption of 7 knots is made for correlation purposes. Results at both gross weights show fairly good correlation at the 37 foot rotor height. Correlation is not as good at the 77 and 117 foot rotor heights (as would be expected from figures 73 through 75), because the

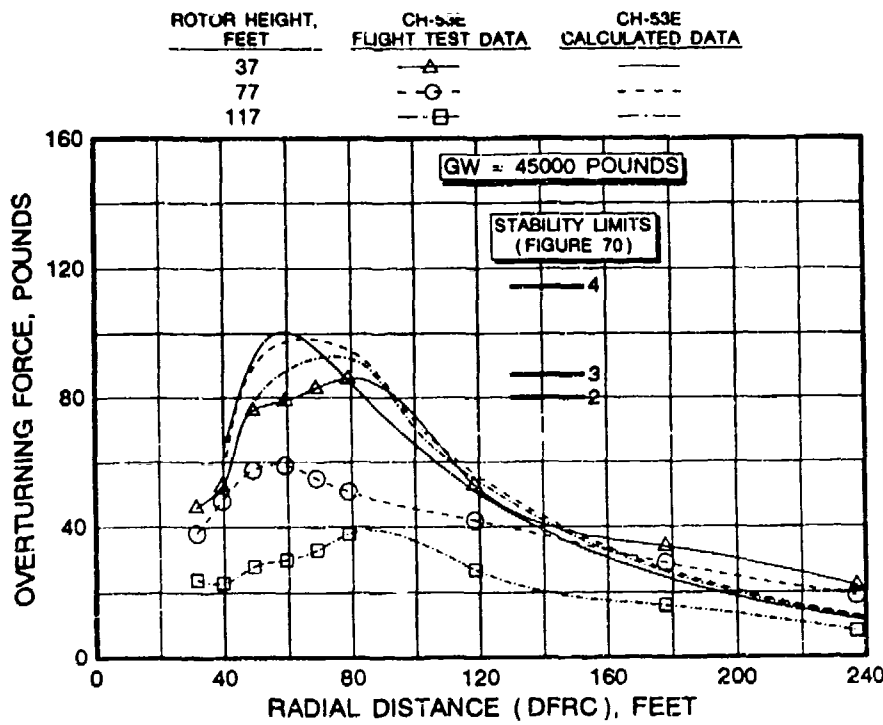


FIGURE 73 CORRELATION OF CH-53E HORIZONTAL OUTWASH FORCES AS A FUNCTION OF DISTANCE FROM THE ROTOR CENTER DURING HOVER AT 45,000 POUNDS GROSS WEIGHT

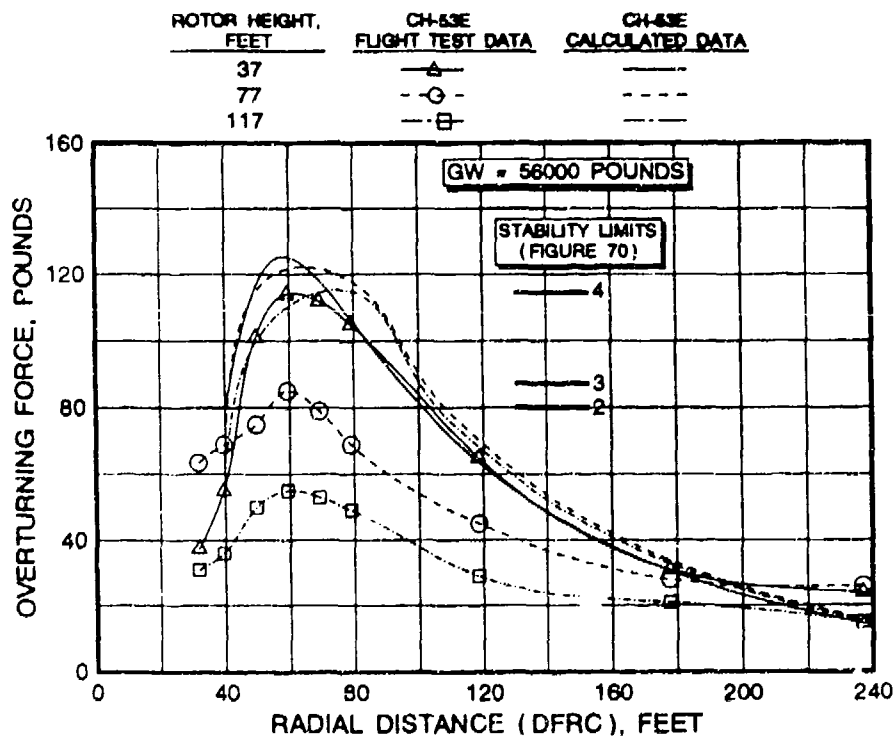


FIGURE 74 CORRELATION OF CH-53E HORIZONTAL OUTWASH FORCES AS A FUNCTION OF DISTANCE FROM THE ROTOR CENTER DURING HOVER AT 56,000 POUNDS GROSS WEIGHT

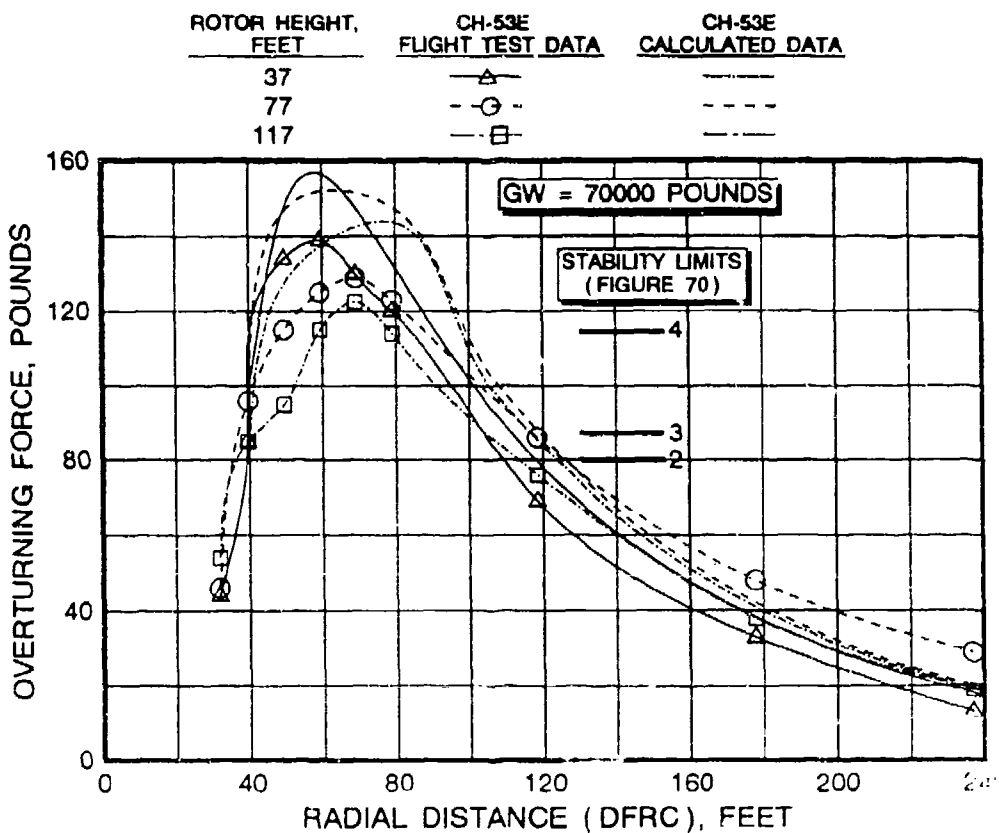


FIGURE 75 CORRELATION OF CH-53E HORIZONTAL OUTWASH FORCES AS A FUNCTION OF DISTANCE FROM THE ROTOR CENTER DURING HOVER AT 70,000 POUNDS GROSS WEIGHT

peak forces are overpredicted for the no-wind condition. If a lower wind speed value of 5 knots is used for correlation at the 37-foot height, calculated results are closer in value to the flight test data.

Experimentally measured XV-15 forces (reference 23) are presented at a rotor height of 37.5 feet at radial azimuths of 270 degrees (single-rotor radial) and 0 and 180 degrees (interaction plane) in figures 78 through 80, respectively. In general, correlation of these data indicates a tendency for the mathematical model to slightly overpredict the experimentally measured force data.

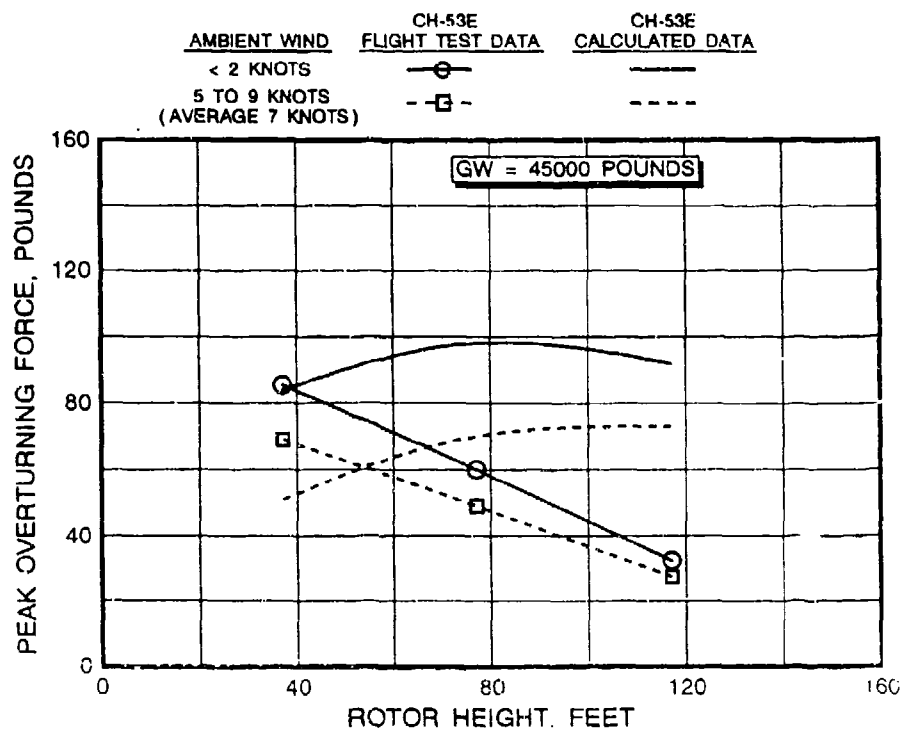


FIGURE 76 CORRELATION OF CH-53E HORIZONTAL OUTWASH FORCES AS A FUNCTION OF HOVER HEIGHT AT 45,000 POUNDS GROSS WEIGHT FOR TWO AMBIENT WIND CONDITIONS

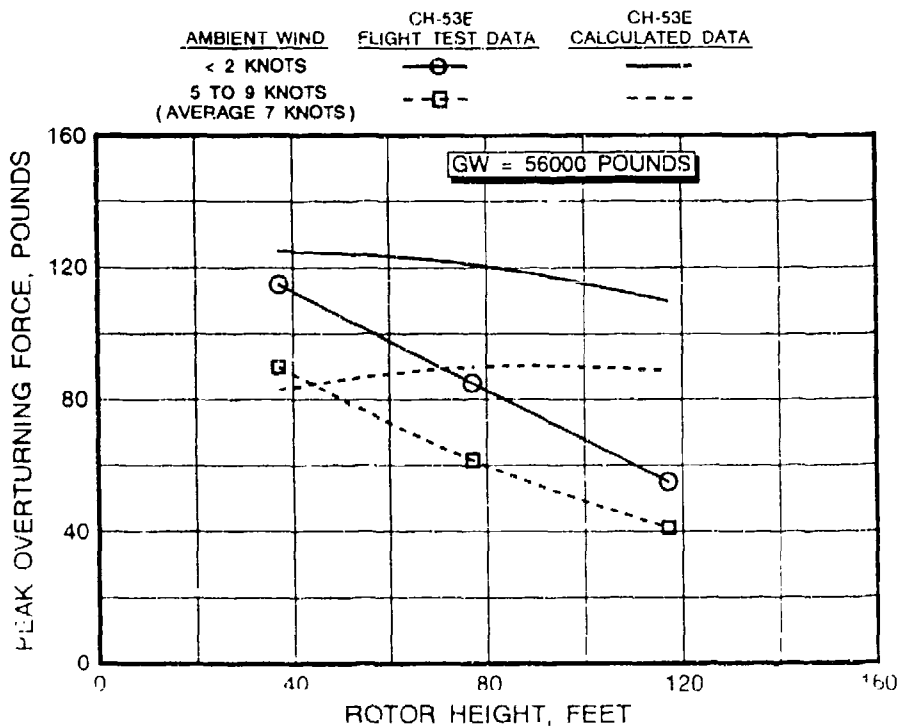


FIGURE 77 CORRELATION OF CH-53E HORIZONTAL OUTWASH FORCES AS A FUNCTION OF HOVER HEIGHT AT 56,000 POUNDS GROSS WEIGHT FOR TWO AMBIENT WIND CONDITIONS

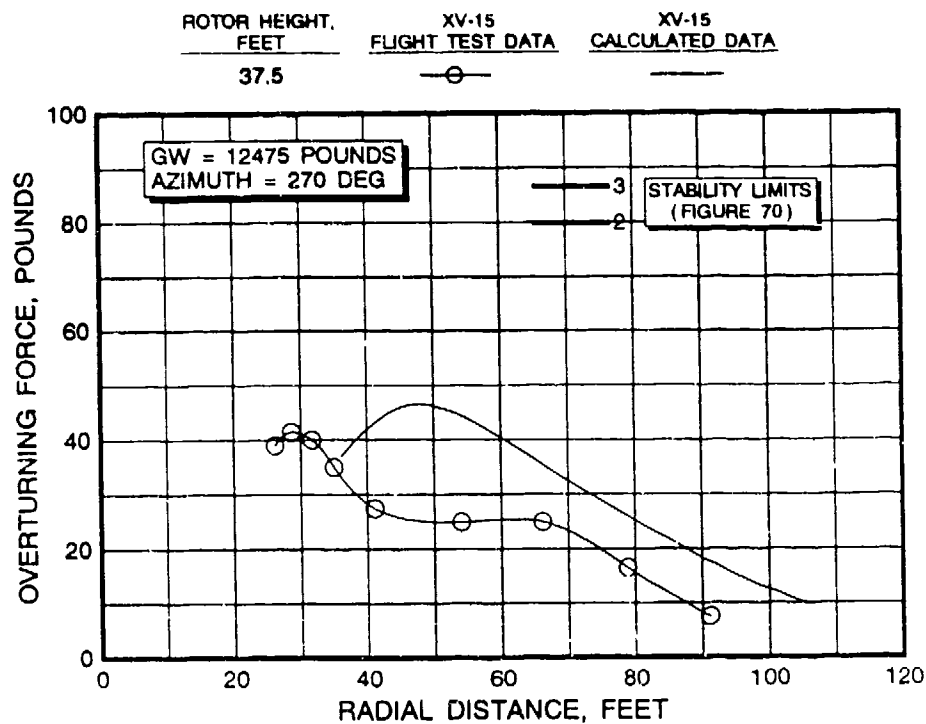


FIGURE 78 CORRELATION OF XV-15 HORIZONTAL OUTWASH FORCES AT 270 DEGREES DURING HOVER FOR A ROTOR HEIGHT OF 37.5 FEET AND A 12,475 POUND AVERAGE GROSS WEIGHT

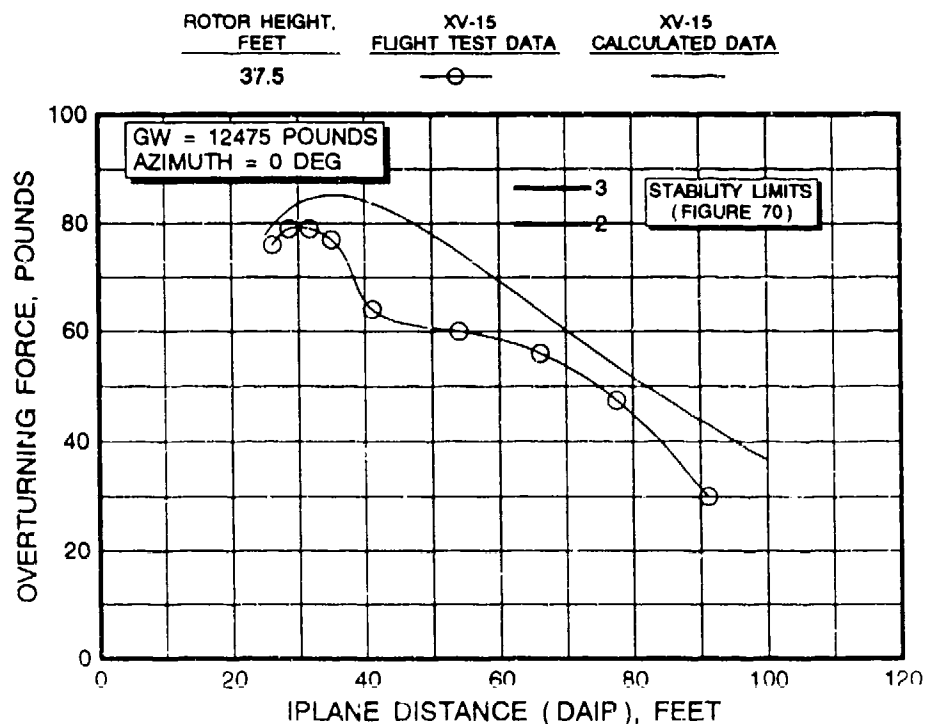


FIGURE 79 CORRELATION OF XV-15 HORIZONTAL OUTWASH FORCES AT 0 DEGREES DURING HOVER FOR A ROTOR HEIGHT OF 37.5 FEET AND A 12,475 POUND AVERAGE GROSS WEIGHT

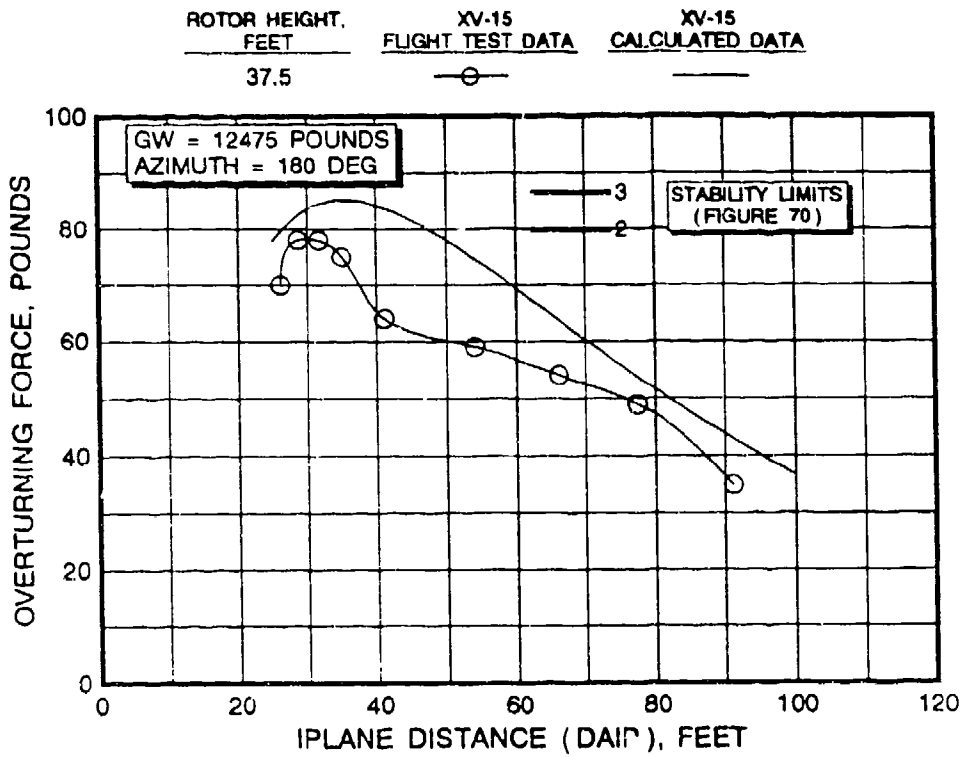


FIGURE 80 CORRELATION OF XV-15 HORIZONTAL OUTWASH FORCES AT 180 DEGREES DURING HOVER FOR A ROTOR HEIGHT OF 37.5 FEET AND A 12,475 POUND AVERAGE GROSS WEIGHT

The effect of ambient wind on XV-15 peak force along the 270-degree radial at 15.6 feet was measured at a rotor height of 24.5 feet on both the upwind and downwind sides. While these data essentially represent only a single data point, it is nevertheless another limited calibration of the mathematical model. Results from flight test indicate that the variation in peak force at 6 to 8 knots (downwind side) was 11 pounds (or 49 pounds total) above the no-wind value of approximately 38 pounds. On the upwind side, the measured peak force was approximately 2 pounds lower (or 36 pounds). The almost insignificant force reduction on the upwind side of the XV-15, when compared with the upwind side CH-53E data, does not provide data defining a consistent trend. Calculated data indicate that the variation should be from an increase to 60 pounds on the downwind side to a reduction to 25 pounds on the upwind side.

MV-22 force data (reference 5) were obtained at only one distance from the rotor along the interaction plane (57 feet DAIP). The peak force measured was 192 pounds at a gross weight of 40,300 pounds and a wheel height of 14 feet. The calculated value that compares with this data point is 144 pounds of overturning force (note that calculated peak velocities are less than the flight test data in figure 52). This value is approximately 48 pounds less and is clearly beyond the acceptable limits for both military and civilian purposes. It is interesting to note that a

later MV-22 test (DT-IIB) qualitatively indicates that force levels may be dramatically reduced when on board ship (with one rotor either partially or fully off the deck edge). Further research is planned at a later date to quantify this effect.

Correlation of peak force and moment data for the Sikorsky S-61 (SH-3), as measured experimentally (reference 31) at several station positions at rotor heights of 57 and 77 feet, is presented in figures 81 and 82. These data are based on a 6 foot by 1 foot human with a C_D of 1.0 on a cold day ($\sigma' = 1.1$, $\rho_A = 0.0026146$ slugs/feet³), which is slightly different from the previously described "Navy" human.

Results from this comparison for both forces and moments indicate that the data correlate reasonably well in the far field for an assumption that the ambient wind is approximately 3 knots. If the wind is assumed to be zero, calculated values overpredict the flight test data. However, these results should not be unexpected because a mechanical sensor was used to measure the velocities used to compute forces. Reference 11 documents that the use of such sensors results in lower than actual measurements of both velocities and forces. Commentary presented in reference 31 does not provide detailed information on the ambient wind velocity, gust levels, or direction other than a statement that the ambient wind varied from approximately 0 to 4 knots.

5.1.4 Qualitative Evaluation of Experimental Data

Quantitative data, as presented in the previous section, provide guidance for calculation and correlation of overturning forces and moments. However, these types of data do not provide guidance as to what may or may not be an acceptable level of rotorwash in association with civilian rotorcraft operations. Furthermore, definition of acceptable rotorwash levels for civilian operations is itself somewhat ill-defined. What may be acceptable and safe to an unprotected heliport ramp employee would be considerably different from that considered acceptable by an embarking business executive, a senior citizen, a disabled person, or a 7-year-old child. Therefore, before making an assumption that a certain level of overturning force or moment is acceptable for civilian operations, such as the 80 pound level in figure 70, it is important to review some of the available qualitative data that have been reported.

Qualitative comments provided by subjects 3 and 4 (figure 70) following the CH-53E test at the 45,000- and 56,000-pound gross weights agree well with quantitative predictions and the laboratory test results used to construct figure 70. At the 45,000-pound gross weight, subjects 3 and 4 experienced only minor difficulty while working in rotorwash at the 37-foot hover and no difficulty at the 77- and 117-foot hover heights. However, the forward movement of subject 3 was completely

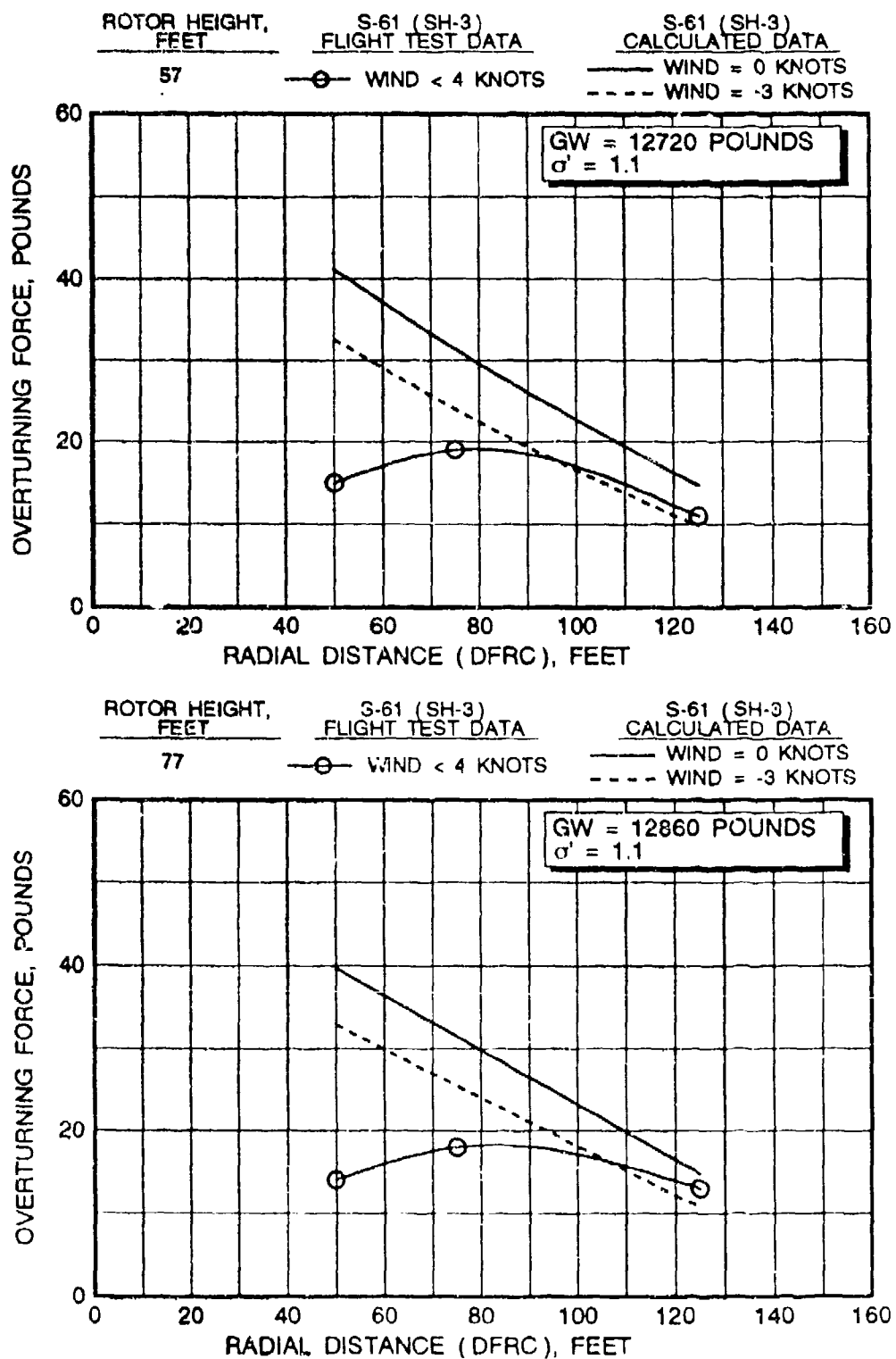


FIGURE 81 CORRELATION OF S-61 (SH-3) PEAK HORIZONTAL OUTWASH
 FORCES DURING HOVER AT ROTOR HEIGHTS OF 57 AND 77 FEET

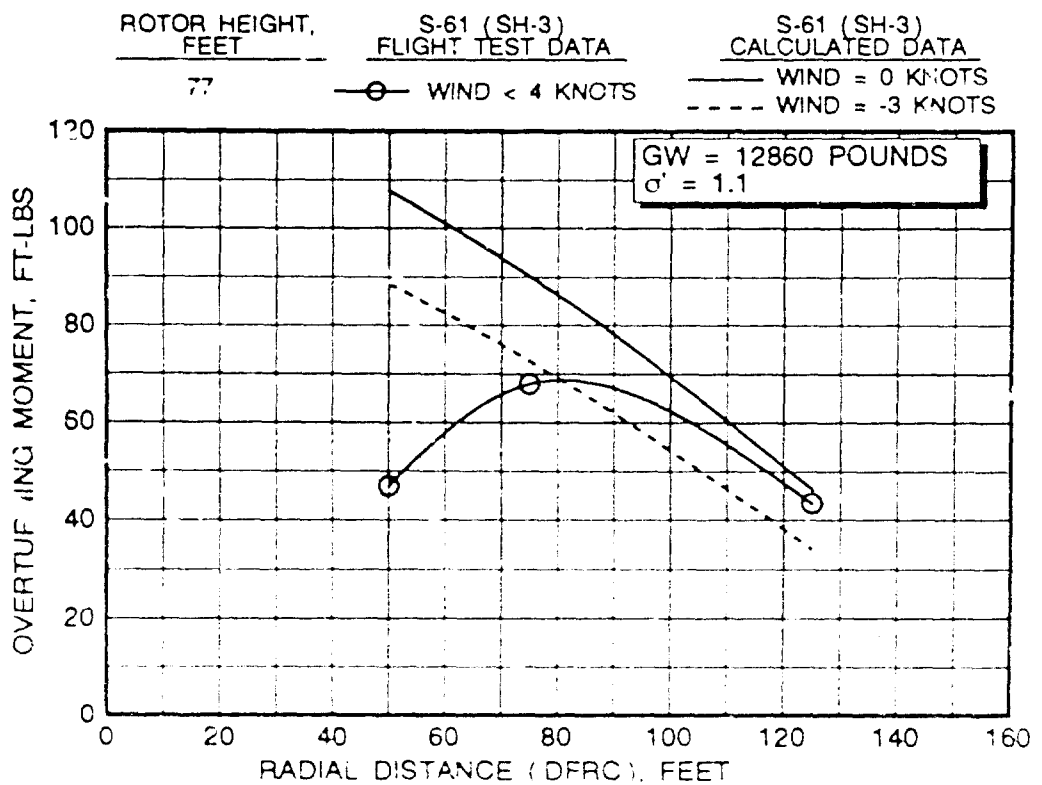
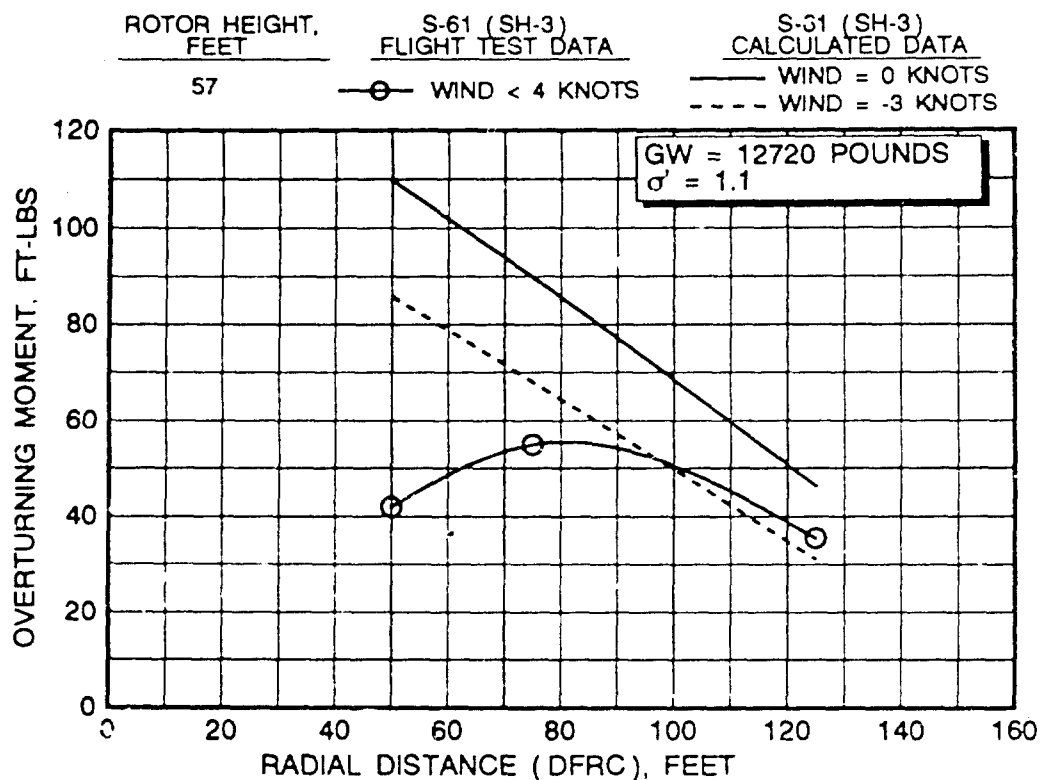


FIGURE 82 CORRELATION OF S-61 (SH-3) PEAK HORIZONTAL OUTWASH
MOMENTS DURING HOVER AT ROTOR HEIGHTS OF 57 AND 77 FEET

restrained near the position marked 80 feet (from the center of the test site) during the 37-foot hover at 56,000 pounds. During the 77-foot hover, subject 3 could maneuver in the peak force region with some difficulty. Subject 4 could maneuver in all regions of the flow field during the 56,000 pound test; however, he did experience difficulty while working in the peak force region during the 37-foot hover. Subject 4 also participated in a qualitative survey during the 70,000 pound gross weight evaluation. While he was able to completely penetrate the flow field at all three hover heights, he did experience great difficulty when moving in the peak force region, and postural stability could not be controlled.

Further work with the CH-53E at 42,625 and 50,664 pounds and with an RH-53D at 40,950 pounds was conducted along with the evaluation described in the previous paragraph (figure 83). Each of the four subjects listed in table 6 participated in the qualitative analysis portion of the test. Subjects 1, 2, and 3 indicated that the strength of the outwash flow fields for both helicopters made it difficult to maintain balance, and the forces were disorienting even at the lower disc loading (42,625 pounds) for the CH-53E. However, no major differences in the degree of difficulty required to maneuver in all three flow fields were reported. In general, all four subjects considered the RH-53D to have a more periodic and predictable pulsation, thus requiring continual compensation in order to maintain postural stability. Steady-state CH-53E flow field pulsations were not as easily identified. However, there were time periods between pulsations involving large gusts that were possibly caused by the automatic flight control system (AFCS). Compensation for these sudden unexpected gusts required even more caution and alertness.

During RH-53D and CH-53E tests at equivalent disc loadings (40,950 and 50,665 pounds, respectively), subjects 1 and 2 had to exert extreme effort, while maintaining only limited balance, in order to penetrate the maximum force region. Subject 3 could penetrate and maintain balance at these equivalent disc loading test points; however, subject 3 was unable to penetrate the maximum velocity region (80 feet from rotor center) during qualitative testing of the CH-53E at the 56,000-pound weight. Based on both of these sets of qualitative and quantitative data, it was concluded that the CH-53E is no more hazardous than the RH-53D at a similar disc loading. It is also indicated from the qualitative results that up to the 50,000-pound gross weight configuration, the flow fields are tolerable for trained military personnel. The CH-53E gross weight of 56,000 pounds (figure 74) presented difficulties to personnel over a wide range of weights and strengths that ranged from complete instability (very high hazard potential) to marginal instability (high hazard potential). It is therefore concluded that a CH-53E at a 50,000-pound gross weight produces the maximum forces and moments that personnel should be exposed to without restricting their di-

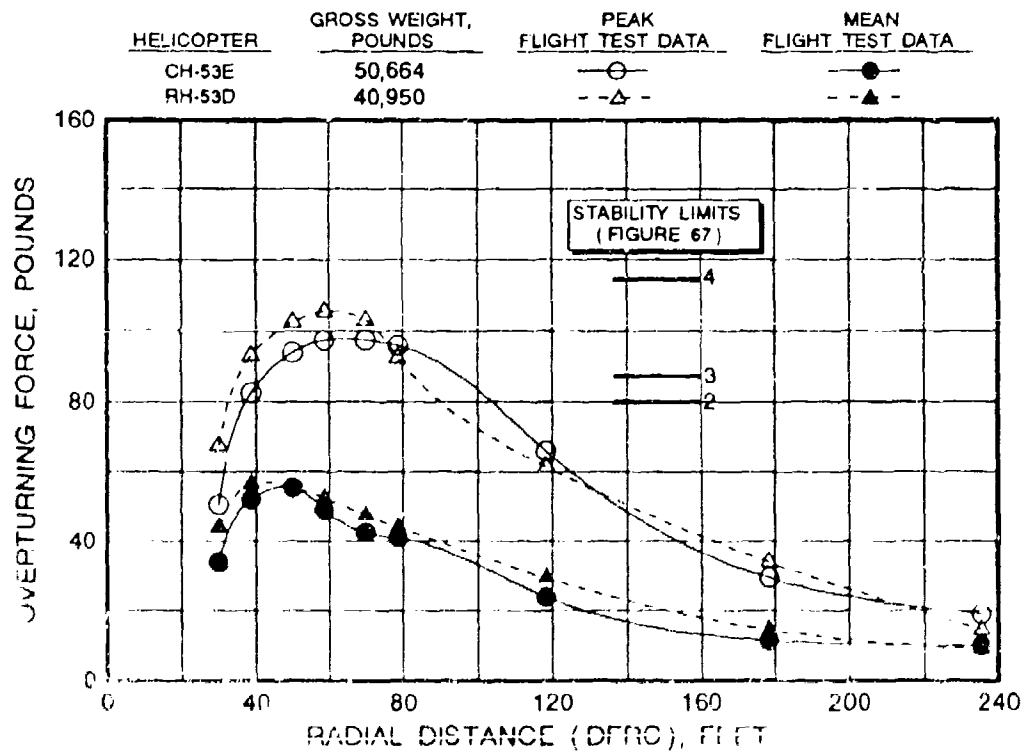
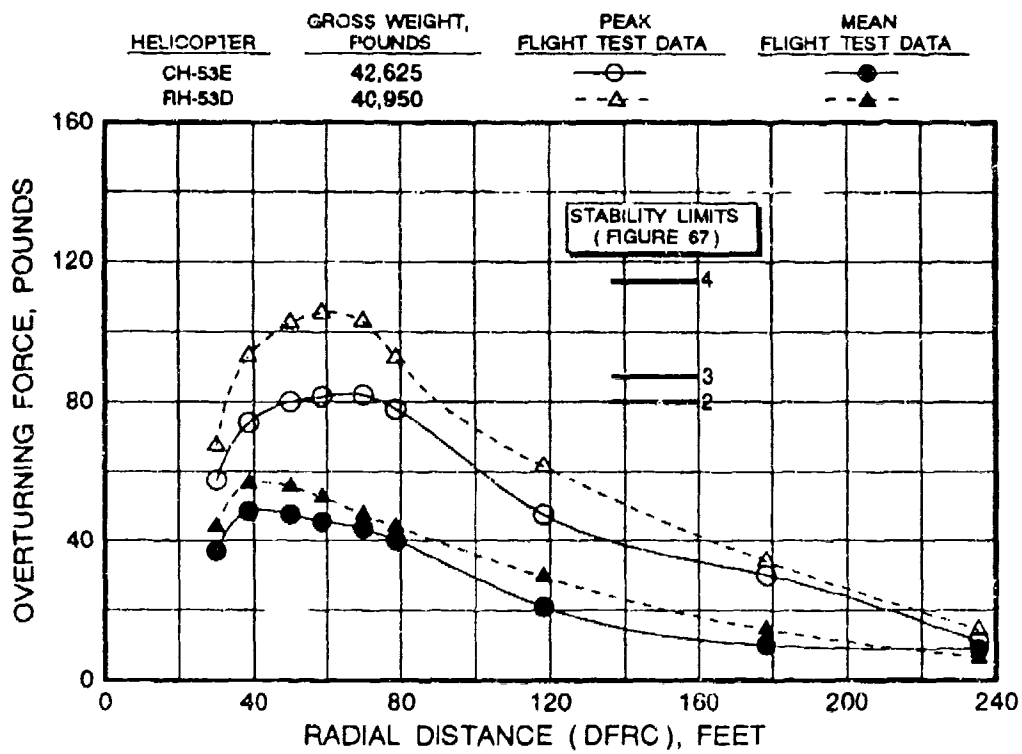


FIGURE 4-1 COMPARISON OF CH-53E AND RH-53D HORIZONTAL OUTWASH FOR F-3 ON TEST SUBJECTS AS A FUNCTION OF DISTANCE FROM THE FLOOR CENTER DURING HOVER AT A ROTOR HEIGHT OF 37 FEET

from the center of the rotorcraft. It is also important to note that qualitative observations by the subjects during the tests were made under optimum conditions; the only task required during these tests was to walk completely through the flow field. The ground surface was rough concrete (for best traction) and the helicopter was not moving so that the subjects could approach the flow field at their own pace. Therefore, for civilian purposes, one might conclude that the peak force levels (approximately 80 pounds) experienced at the lower CH-53E disc loading (42,625 pounds) are the maximum allowable (figure 83). This is because other variables would have to be taken into account when analyzing the rotorwash hazard potential as extrapolated to other classes of personnel. These variables would include factors such as age, size, weight, strength, endurance, and reflex response when subjected to the rotorwash. Environmental considerations such as the traction offered by the ground surface, loose foreign objects and grit, the difficulty of the task to be performed (in the flow field), and whether or not the rotorcraft is moving are also factors that require attention.

Qualitative tests were also conducted with the XV-15 (reference 23) at rotor heights of 37.5 and 62.5 feet using subject 4 (table 6 and figure 70). The path that test subject 4 traversed and the locations where he stood, both into and away from the flow direction, are sketched in figure 84. Test subject 4 reported no problems walking or standing under the XV-15 even though his forward movement was slightly impeded by the flow field. This test subject had the most difficulty along the 0- and 180-degree azimuths, and he noted that the flow magnitude was composed of frequent large wind gusts. Neither the test subject or observing test personnel noticed any differences in relative difficulty due to the variation in hover height. In summary, the limited qualitative observations are in good agreement with the quantitative force data as previously presented and correlated in figures 78 through 80. While no quantitative data were obtained under the XV-15 within a 26-foot circle (centered about the XV-15 center), test subjects indicated that forces in this area were extremely low. Observations by test observers and movies also indicated that velocities in this central region are relatively low in magnitude during a hover. Test personnel were observed to walk erect and relaxed in this region.

XV-15 outwash forces were also summarized in reference 23 by presenting the data in figures 78 through 80 as four regions that define distinct degrees of difficulty for personnel trying to maintain stability. These regions are described in figure 85. The degree of difficulty relative to each region, based on the quantitative criteria in figure 85, is presented in table 8. Based on these results (even though limited in scope), it can be assumed that the majority of regions III and IV present no significant problems to personnel walking, standing, or

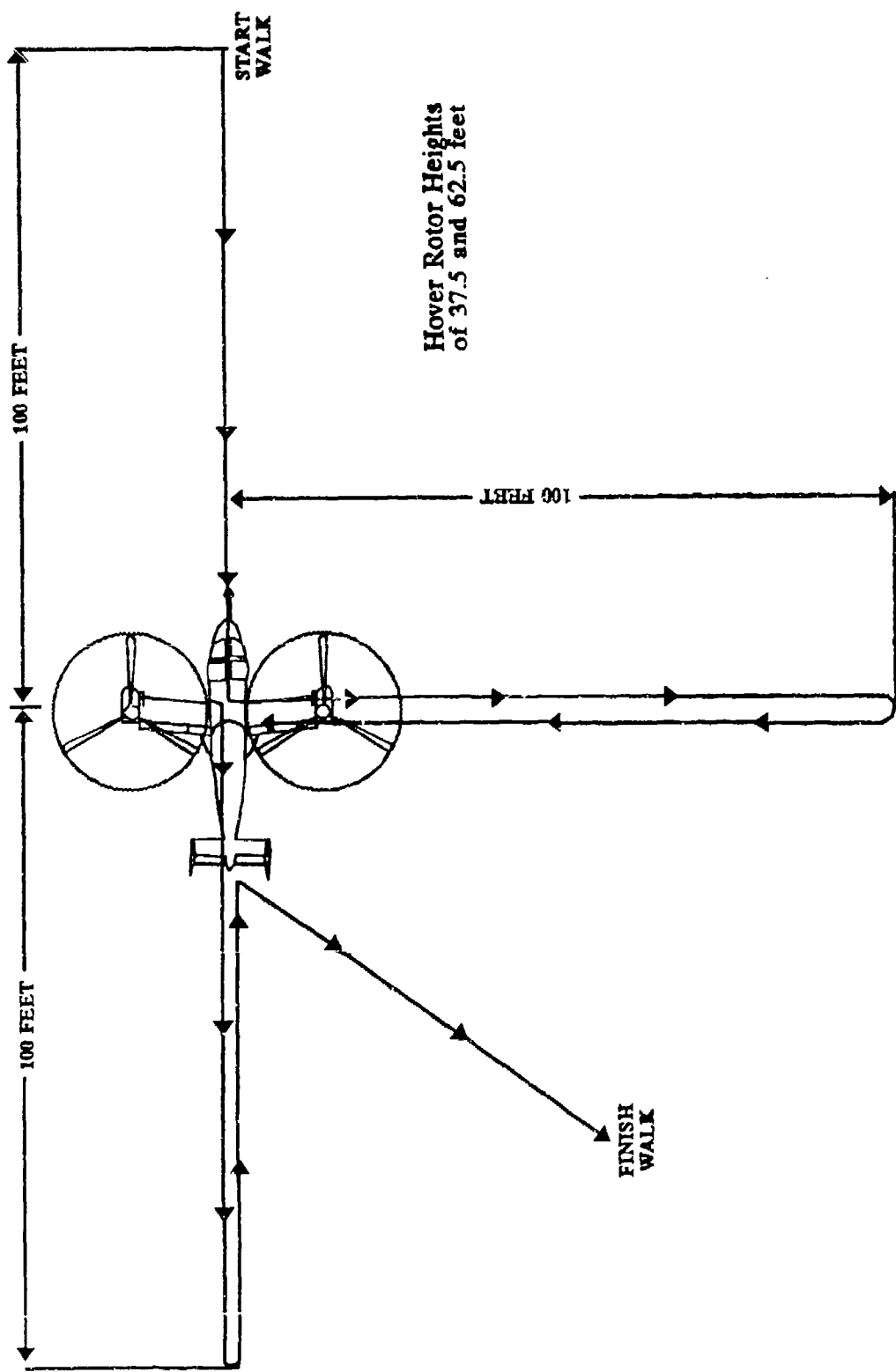
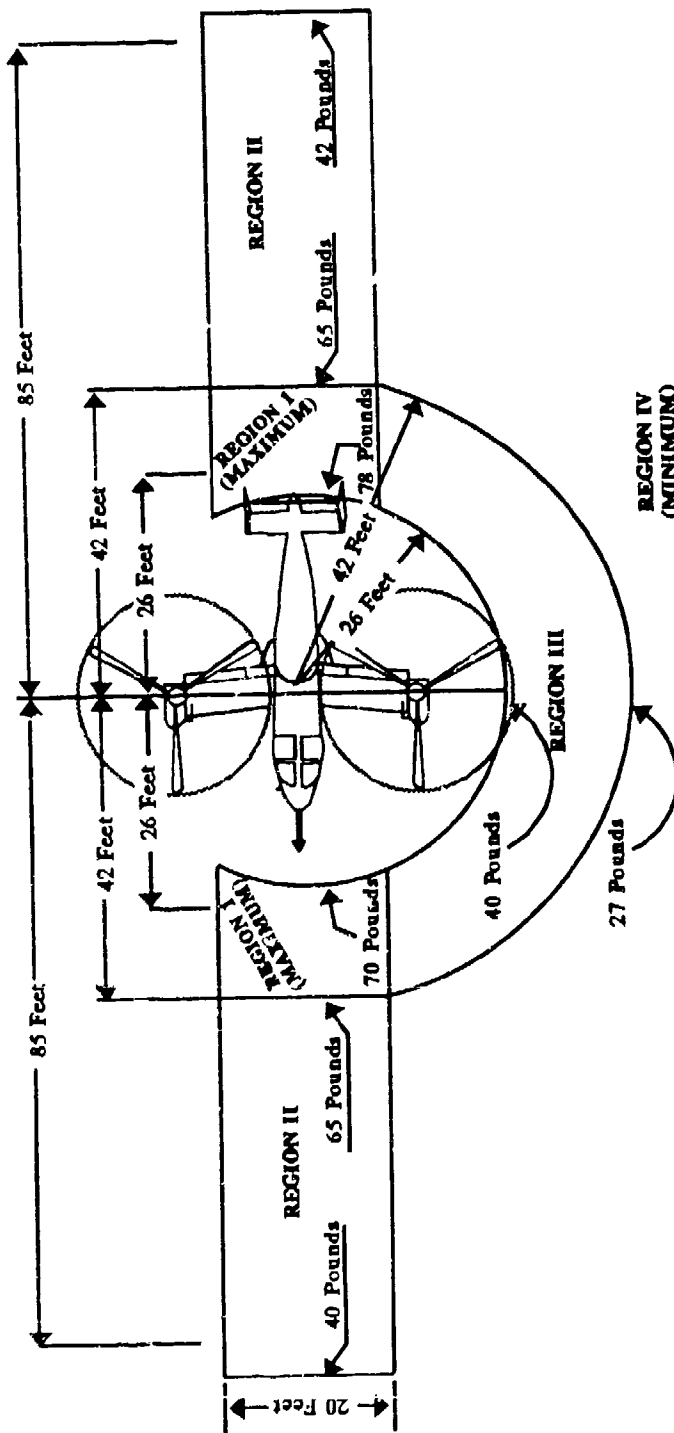


FIGURE 84 QUALITATIVE WALK THROUGH EVALUATION OF THE XV-15 ROTORWASH FLOW FIELD
AT ROTOR HOVER HEIGHTS OF 37.5 AND 62.5 FEET



NOTE: Description of level of force in each region is contained in Table 8.

FIGURE 85 REGIONS OF OVERTURNING FORCE GENERATED BY THE XV-15 ON GROUND PERSONNEL

TABLE 8 PERSONNEL LIMITATIONS IN XV-15 FLOW FIELD REGIONS

REGIONS ¹	WEIGHT (PERCENTILE ²), POUNDS		
	150 (25TH)	171 (75TH)	220 (99TH)
I	Exceeds stability limit, hazardous.	Difficult to walk through.	Slightly difficult to walk through.
II	Very difficult to walk through.	Slightly difficult to walk through.	No difficulty to walk through.
III	Moderately difficult to walk through.	No difficulty to walk through.	No difficulty to walk through.
IV	No difficulty to walk through.	No difficulty to walk through.	No difficulty to walk through.

Notes: (1) Regions defined in figure 85.
 (2) Reference 50.

performing limited work over the range of XV-15 test conditions. In contrast, regions I and II do have the potential to be hazardous to humans weighing less than 150 pounds (25th weight percentile). In studying these qualitative data further, it can be hypothesized that, for civilian operations, the level of outwash in region III would be a minimum limit. When quantifying this region, the values of force, as presented in figures 78 through 80, can be extracted. Forces in region III vary from a maximum of approximately 40 pounds at one rotor radius (12.5 feet) to a minimum of 27 pounds at 42 feet from the center of the XV-15. Likewise, forces in region IV vary from a maximum of 27 pounds to 0 pounds at large distances away from the XV-15.

Qualitative commentary from reference 31 for the Sikorsky S-61 (SH-3) indicates that the measured levels of rotorwash did not significantly impede the movement or working capabilities of any test subject. The buffeting of the outwash was random and of a low frequency. This helicopter was also not objectionably noisy and important conversations were able to be conducted without undue effort.

Even though it might be useful for documentation purposes to continue discussion of other qualitative results presented in the literature, any decision as to what is or is not an acceptable level of overturning force or moment would not be significantly affected. This is because each of the other studies are related in approach and methodology to those already discussed and were not designed to investigate civilian-oriented scenarios. Therefore, in the next subsection all quantitative and qualitative results that have been documented up to this point

are brought together to develop general guidelines. These guidelines are used in this report to evaluate values of overturning force and moment for various rotorcraft that have a potential to become involved in personnel-related mishaps.

5.1.5 Overturning Force and Moment Limits for Civilian Operations

Quantification of safe separation distances for civilian personnel requires the specification of hazardous force and moment levels. Results from the previous subsections are combined in figure 86 into a usable format for comparison purposes to start this task. This comparison is an expansion on the database presented in figure 70. Combining the data in figure 86 with the comments in table 8, one might propose the limits in table 9 as being safe for civilian operations.

TABLE 9 FORCE AND MOMENT GUIDELINES FOR CIVILIAN OPERATIONS

Personnel Classification	Force Limit, lb	Moment Limit, Ft-lb
I: Trained and protected ramp personnel frequently working in a rotorcraft downwash environment	80	260
II: Untrained and unprotected personnel rarely or not exposed to the rotorcraft downwash environment	40	120
III: Untrained and unprotected children likely to be walking without assistance from an adult in the rotorcraft downwash environment	30	60

While these limits are practical and reasonable, based on available data, there are by no means enough data to conclusively determine that these are the best limits that could be derived if the force and moment data base were more extensive. Therefore, the reader is referred to section 8 and a proposed experiment that, if conducted, would aid in further substantiating or modifying the proposed limiting values.

Limits specified for unaided children are derived from the extrapolation of table 6 and figure 86 data and are presented in figure 87. Several children were measured and weighed for this study in order to provide a rough estimate for developing the "S" type person (or 7-year-old child) model in section 5.1.2, as well as for aiding in the rough calculation of a force and moment

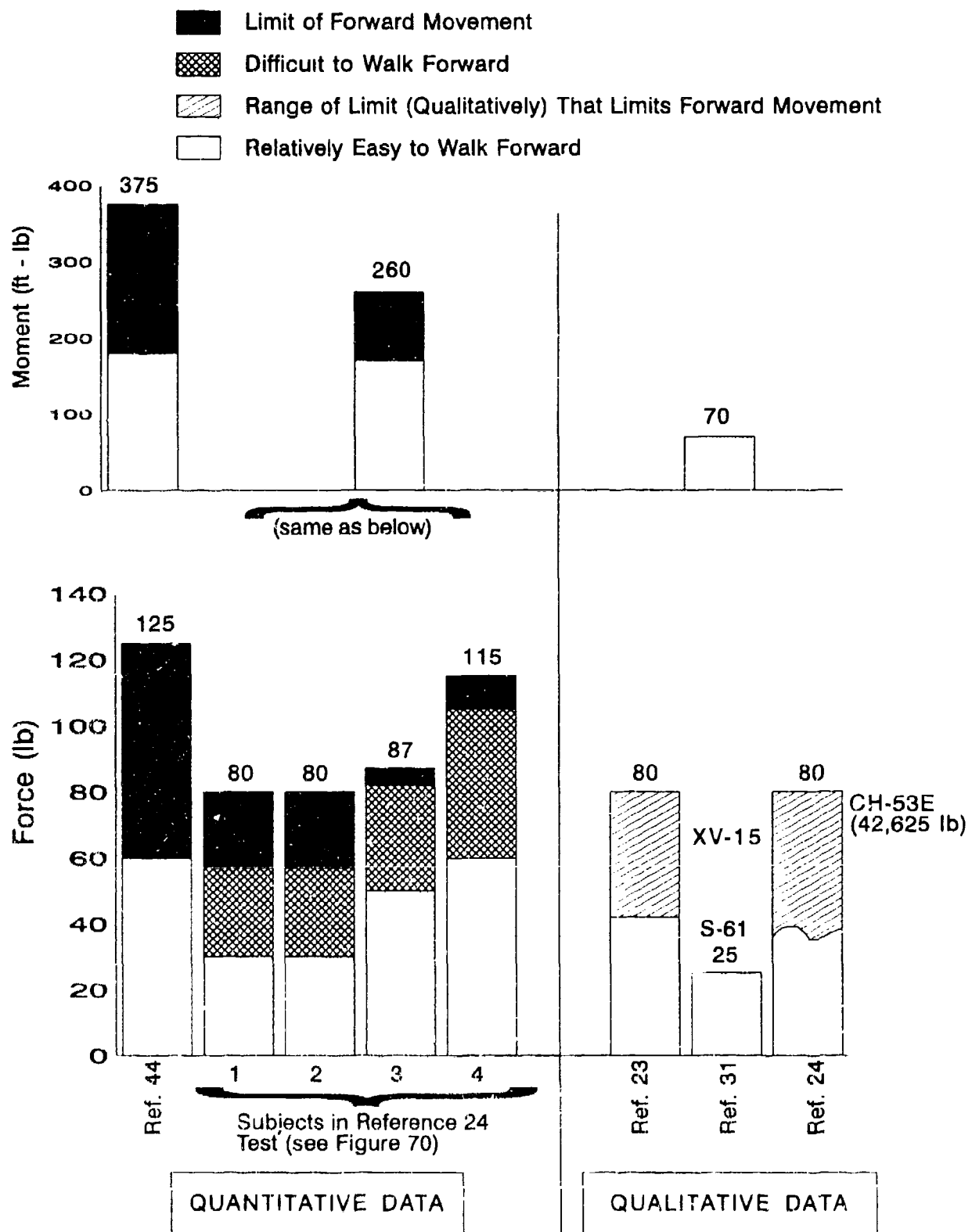


FIGURE 86 SUMMARY OF QUANTITATIVE AND QUALITATIVE DATA ON LIMITING VALUES OVERTURNING FORCE AND MOMENT

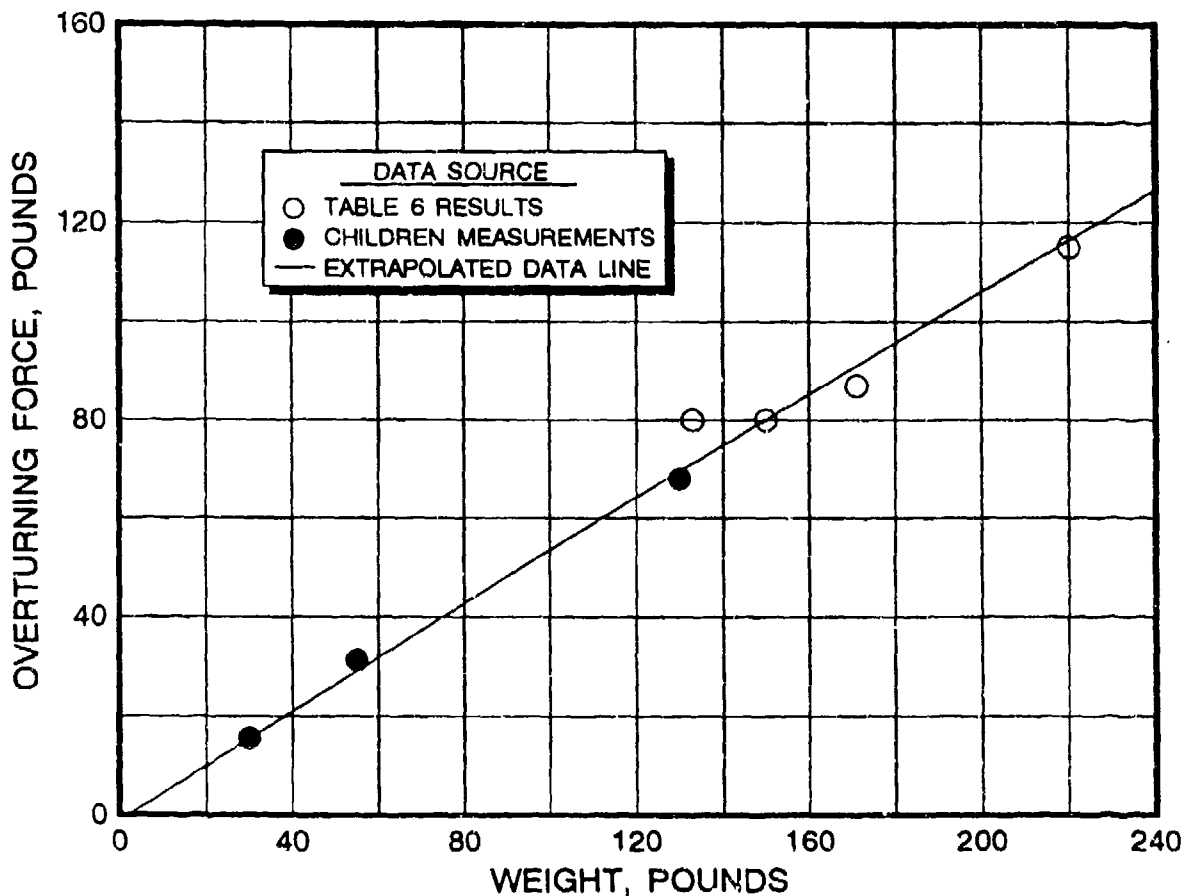


FIGURE 87 EXTRAPOLATION OF EXPERIMENTALLY MEASURED OVERTURNING FORCE DATA TO LIGHTER WEIGHT CLASSES OF PERSONNEL

limit. Based on the results presented in references 23 and 24, body weight is judged to be the most important scaling parameter for defining a force and moment limit. Moment calculations for an "S" type person are based on an application point of two feet versus the adult value of three feet.

5.1.6 Evaluation of Various Types of Rotorcraft Configurations

It quickly becomes obvious from a review of the personnel-related flight test data or the mathematics of the problem that as rotorcraft increase in size and/or disk loading, there is increased potential for generating hazardous levels of rotorwash. Therefore, the next step in this analysis effort is to:

1. identify specific types of rotorcraft that generate the greatest potential personnel-related hazards, and
2. index the characteristics of these rotorcraft into a usable format for preliminary hazard analysis screening.

This important task is accomplished in this report. However, for other reasons related to the report format, these results are presented in sections 6 and 7.2 as part of the "How To" design examples. These results are based on a composite review of the design characteristics of all rotorcraft presently in worldwide operation (as defined by table A-1 in appendix A).

5.1.7 Potential Overturning Force and Moment Hazards Due to Rotor Generated Trailing Vortices

A brief analysis was simultaneously conducted along with the outwash flow field analysis effort in order to determine if rotor-generated vortices (forward-flight trailing vortices or the ground vortex) present a hazard to personnel on the ground. These results are presented in this subsection using the mathematical models that were developed in sections 2.2 and 2.3.

The first task completed in this effort was simply a management task. A quick examination of the involved aerodynamics was conducted to evaluate whether or not a detailed analysis was warranted. This task was accomplished by first correlating the mathematical models with the UH-1H and CH-54 flight test data obtained from reference 46. These results are presented in section 3.6.

Based upon these correlation results for both the vortex strength and velocity profiles, it was determined that at least some further detailed analyses of the hazards were warranted. Three further assumptions were also made in order to better manage the analysis effort. The first of the assumptions was that airspeeds of less than 30 knots should not be evaluated, because the validity of the mathematical model is questionable at airspeeds lower than this value. A second, very conservative assumption was that the shed vortices would not decay or lose strength as a function of time after their formation. This assumption eliminated the need to predict vortex strength decay rates and location behind the rotorcraft. It was simply assumed that strong vortices would be laid down along the ground by the low-flying rotorcraft. The third assumption was that the maximum vortex-core rotational velocity would be approximately 1.6 times the centerline downwash velocity (as measured directly behind and along the centerline of the rotorcraft). This assumption, based on data like those presented in figures 66 and 67, eliminates the requirement to evaluate the calculated velocity field at numerous locations around the rotorcraft. This assumption also eliminated the need to model a detailed vortex core in order to estimate peak rotational velocity values in each vortex (for which more data would definitely be required).

Using the methodology described above, two rotorcraft configurations were initially evaluated for the trailing vortex hazard at airspeeds of 30 and 50 knots. The first of these configurations (M) weighed approximately 19,350 pounds and had a

rotor radius of 25 feet. The second (H) weighed approximately 73,390 pounds and had a rotor radius of 40 feet. Details on the calculations involved in the analysis are presented in the "How To" examples in section 7. Results for the estimated peak vortex velocities along the centerline of the pair of trailing vortices as well as in the core of each vortex are presented in table 10. As can be observed from these results, if the worst case hazard is that which is predicted at 50 knots, then the peak centerline downwash velocities for configurations "M" and "H" are 24 and 28 knots, respectively. Assuming that a "wall" of peak vortex core velocities of 38 to 45 knots respectively blows horizontal to the ground (which is a conservative assumption in itself), the wake vortices cannot be considered a significant hazard when compared to previously presented peak hover outwash profile velocities and dynamic pressures.

TABLE 10 TRAILING VORTEX AND GROUND VORTEX VELOCITY PROFILE EFFECTS ON GROUND PERSONNEL

SIZE CLASS	DISC LOADING (psf)	AIRSPEED, (kts)	CALCULATED PEAK CENTERLINE DOWNWASH, ft/sec (kts)	CALCULATED PEAK VORTEX CORE VELOCITY, ft/sec (kts)
M	9.6	30	26.6 (15.8)	42.6 (25.3)
		50	40.1 (23.8)	64.2 (38.1)
H	14.6	30	12.8 (7.6)	20.5 (12.3)
		50	47.2 (28.0)	75.5 (44.3)

These same "M" and "H" configurations were also evaluated for the ground vortex scenario. Safe separation guidelines derived for ground personnel were not significant to warrant further examination if the assumption is made that the rotorcraft could rapidly come to a hover. This resulted from the fact that the peak outwash profile would then become the predominant and characteristic flow field from which separation guidelines would have to be developed.

In conclusion, when considering each of the conservative assumptions applied to the analysis of the trailing vortices and the ground vortex, i.e.:

1. that substantial "profiles" of peak vortex velocities could strike personnel from an overturning or horizontal direction,
2. that the rotorcraft would fly a profile close to the ground and lay vortices directly on top of unsuspecting personnel,
3. that no vortex decay occurs with time or distance behind the rotorcraft, and

4. that the influence of the ground (less than 6 feet AGL where the personnel are) does not alter the nature of the hazardous velocities of the vortices;

then the velocities that are generated by the two example rotorcraft size classes are not significant for defining separation guidelines when compared to peak outwash velocity profiles generated by a wall jet in hover. Therefore, the logical conclusion would be to keep personnel away from the taxi or takeoff/landing paths using the same minimum separation distances that result from an analysis of hover rotorwash scenarios.

5.1.8 Summary of Personnel-Related Overturning Force and Moment Hazards

The previous sections have documented an analysis methodology for evaluating the hazard potential of overturning forces and moments on personnel that are exposed to rotorcraft downwash/outwash flow fields. This analysis methodology is based on correlation with both laboratory experiments and flight test results (both qualitative and quantitative) for several different rotorcraft. Safety factors are identified in the analyses whenever they are used to account for discussed uncertainties. Experiments are proposed in section 8 that would significantly improve the quantification of safety factors as well as limiting values for overturning forces and moments that are applied to unprotected and untrained civilian personnel. However, interim criteria are developed based on available data. These criteria are utilized in the presentation of separation guidelines for several classes of personnel in the "How To" examples in sections 6 and 7. Separation guidelines for all other types of rotorwash-related hazards are developed in the following sections.

5.2 ROTORWASH EFFECTS ON OTHER NEARBY ROTORCRAFT

The effect of rotorcraft outwash profiles on other nearby rotorcraft can generally be classified into one of three categories. These categories are hovering and taxiing rotorcraft and their effects on other:

1. parked and shutdown rotorcraft,
2. rotorcraft that have rotors turning while on the ground, and
3. rotorcraft hovering or taxiing nearby.

Historical records indicate that damage in these types of mishaps can vary from scratched paint to total destruction. Careful review of these records also quickly leads to a conclusion that many types of mishaps are not easily predicted or foreseen by pilots and that a detailed analysis of the many hazard/scenario combinations could easily take years. A majority of mishaps are unique and involve many complicating factors. Therefore, to better manage the analysis task, available mishap data were reviewed to identify the types of mishaps that had the highest frequencies of occurrence. The assumed hypothesis is that mishaps occurring in significant numbers in the historical records should also be the same types of mishaps that have the greatest potential to be reduced in frequency in the future. If these most common types of mishaps can be avoided through practical separation guidelines, it is hoped that many of the less common types of mishaps will also be reduced in frequency.

After a careful review of all available mishap data involving two or more rotorcraft, the types of mishaps occurring most frequently were found to include the following groups.

1. Doors or access panels of one rotorcraft were damaged by the dynamic pressure loads incurred from a passing rotorcraft's downwash. Often a plexiglass window or chin bubble was also shattered by any door that broke off at the hinges. Damage resulting from an incident such as this can easily run into many thousands of dollars.
2. The rotor blade of a stopped or low rpm rotor was induced by the passing rotorcraft's downwash to strike the tailboom or tail rotor driveshaft, thereby causing rotor blade, tailboom, and/or tail rotor driveshaft damage.
3. Rotorcraft flying too close to other rotorcraft were struck by downwash or trailing wake vortices. This type of "encountered turbulence" usually resulted in either a loss of tail rotor effectiveness or a loss of rotor lift due to the induced negative rotor angle-of-attack. The required collective inputs and engine torque used during recovery (if made at all) often resulted in overtorque of the rotor and drive train.

Each of these types of hazards will be examined to some level of detail in the following sections. Mishaps related to rotorcraft generated flying debris that subsequently struck another rotorcraft were also reported on numerous occasions in the mishap databases. However, discussion of this type of mishap is reserved for section 5.6.

5.2.1 Review of Mishap Data

A review of sources of available mishap data indicates that many operational incidents have occurred as the result of rotorwash from one rotorcraft impinging upon another. Also, as discussed in the previous section, three types of mishaps were found to be of particular interest. Approximate statistics for these three types of mishaps, identified in the literature for evaluation in this study, are summarized in table 11. It must be emphasized, as discussed in the notes of table 11, that these statistics do not imply that the listed numbers reflect the actual number of occurrences for these types of mishaps over any specified period of time. The statistics represent only the approximate number of mishaps that were "easily" identified in the literature for this study.

TABLE 11 MISHAP REPORTS INVOLVING
ROTORWASH INDUCED DAMAGE TO OTHER ROTORCRAFT

MISHAP TYPE	APPROXIMATE NUMBER OBTAINED WITH ONLY A BRIEF VERBAL SUMMARY	NUMBER OBTAINED WITH LIMITED DETAILED INFORMATION TO ENABLE SOME DETAILED ANALYSIS
Door, Access Panel Damage	50	13
Rotor Blade/Tailboom Strike Damage	20	1
Wake Induced Overtorque/Loss of Control	30	5

Notes:

1. These statistics are based on the approximate number of reported incidents to the U.S. Army Safety Center between January 1976 and April 1985, several high dollar damage reports from the FAA and NTSB, and several instances reported to Systems Control Technology, Inc. during an informal survey associated with reference 3.
2. These statistics cannot be interpreted as being representative of the actual number of worldwide occurrences of these types of mishaps over any specified period of time.

One of the significant problems that exists with these statistics is that in order to accommodate the legally imposed format for public reporting, the U.S. Army Safety Center must sanitize the mishap summaries. For example, the number of mishaps reviewed that involved damage to doors and cowlings totaled 28. Nine different types of helicopters were represented by this group, the smallest being the Bell 206 JetRanger, the largest being the Boeing CH-47, and the most numerous being the Bell UH-1. Of these 28 mishaps, 13 contained at least 1 quantitative fact that could be used in an analysis. The other 15 mishap summaries contained only qualitative information. None of the mishap reports provided details such as hover-taxi speed, whether or not low speed maneuvering occurred during the mishap (i.e., cyclic flare), or gross weight for the rotorwash-generating helicopter. This general lack of information dictates that assumptions be made in the analysis effort (more will be said on this subject in later sections). A representative example of one of the "quantitative" mishap summaries is presented below for informational purposes.

"The landing UH-1H terminated a normal approach to a lighted helipad. While performing a post flight inspection on the parked helicopter, the crew chief left the pilot's door unlatched. The rotorwash from a landing helicopter opened the pilot's door with sufficient velocity to fracture the right door hinges, damage the doorpost mount, and shatter the right chin bubble. The parking area was less than 120 feet from the helipad. The parking area was relocated. The ground crew failed to follow unit operating procedures while completing duties during the post flight inspection."

Unfortunately, it was not practical in the time available to try to research many of the mishaps by requesting information or specific details from the original mishap reports. It was also discovered in several of the cases where this was attempted that the original mishap reports were no longer available.

5.2.2 Analysis Methodology

The analysis methodology chosen and developed to define separation guidelines for the first two types of hazards described in table 11 relies on an indirect analysis approach. This approach might also be referred to as a "reverse engineering" approach. The effort required for a direct analysis (i.e., to calculate pressure and hinge loads as well as door accelerations in order to determine when door hinges will fail) is simply beyond the scope of available resources. Even if this method was to be utilized, a large body of experimental data would have to be made available (and it is not available) in order to verify the analyses, especially when one considers that each rotorcraft door or hinged access panel design is different.

With the indirect analysis approach, design details of doors and access panels are not important. Instead, each mishap is analyzed to determine the approximate rotorwash velocity values that were present at the time and location of the mishap (knowing that these velocity values definitely represent a hazard). If analysis of a large number of similar mishaps leads to identification of a statistically significant velocity value below which no mishaps occur, this limiting velocity is assumed to be the velocity at which some mishaps start to occur.

Assumptions that are required to use this approach are:

1. rotorwash characteristics can be mathematically estimated (with reasonable accuracy) for documented mishaps,
2. within a large group of similar mishaps being investigated, it is possible to identify common factors, and
3. when common factors are identified, operational procedures can be developed to reduce the probability that further mishaps will occur.

It should again be pointed out that the described analysis approach is not compatible with rigid scientific analysis procedures. However, detailed rotorcraft, crew, ground personnel, and atmospheric-related data immediately prior to, during, and subsequent to most mishaps are rarely obtained or reported. Therefore, this type of methodology is probably the best tool that will be available in the foreseeable future for the analysis of most types of rotorwash-related mishaps. Experiments are proposed in section 8 to enhance the data base with several scientifically controlled "mishaps." Subsequent to the acquisition of these types of data, guidelines as developed in the following sections will be fine-tuned and further documented.

5.2.3 Analysis Procedure

The first step in the analysis procedure was to develop a comprehensive list of the types of rotorcraft that were associated with the acquired mishap reports. Rotorwash characteristics were then calculated for each of these rotorcraft. This task was accomplished using the ROTWASH analysis program documented in this report (version 2.1). Rotorwash characteristics on the downwind side of the rotorcraft were calculated in hover for crosswind velocities of 0 and 9 knots at both the mid (one-half maximum payload) and maximum gross weights. The average atmospheric density ratio was assumed to be 0.95 and wheel heights for the various rotorcraft varied from 25 feet for the small rotorcraft to 40 feet for the Boeing CH-47 (approximately one rotor diameter above the ground). Table 12 and figure 23 summarize input data values that are used in calculating Bell UH-1H rotorwash characteristics. This type of

helicopter is used in several of the procedural example cases presented in this report.

TABLE 12 UH-1H INPUT DATA FOR THE ROTWASH ANALYSIS PROGRAM

PARAMETER	VALUE	UNITS
Number of Main Rotors	1	-ND-
Main Rotor Separation	0.0	ft
Rotor Radius	24.0	ft
Gross Weight	7400.0, 9500.0	lb
Rotor Height Above Ground	30.0	ft
Rotor Download on Fuselage	2.0	%
Tilt of Rotor Tip Path Plane	0.0	deg
Atmospheric Density Ratio	0.95	-ND-
Wind Velocity	0.0, 9.0	kts

All calculated rotorwash data were subsequently plotted in a special format. An example, using data for the UH-1H, is presented in figure 88. The radial distance from the center of the main rotor (in feet) is plotted on the independent or x-axis. The calculated peak profile rotorwash velocity (in knots) is plotted on the dependent or y-axis. The velocity data that are plotted in this format are derived from three vertical locations along the rotorwash profile, as shown in figure 89. These locations are at 4 feet, 8 feet, and at the height above ground level along the profile where the maximum peak velocity occurs (which increases in value as distance from the rotor increases). When plotted for both wind conditions and gross weights, these data form six bands stretching across the graph. The upper and lower range of values along each band represent the maximum and mid gross weight configurations, respectively. Below these plotted data are several pictures of small UH-1H helicopters. These helicopters are positioned along the independent axis so that the rotor tips are spaced one-half rotor diameter apart when the rotor blades are indexed perpendicular to the fuselage centerline. These pictures provide visual references with respect to spacing geometry when several helicopters operate in close proximity to one another. Position data derived from each individual mishap summary are then marked along the independent axis at estimated positions where damage was reported to have occurred. While some mishaps may be marked at a specific location, the majority of mishaps are assumed to occur within some range, i.e., 100 to 120 feet, as shown for the example hypothetical mishap labeled #1 in figure 88.

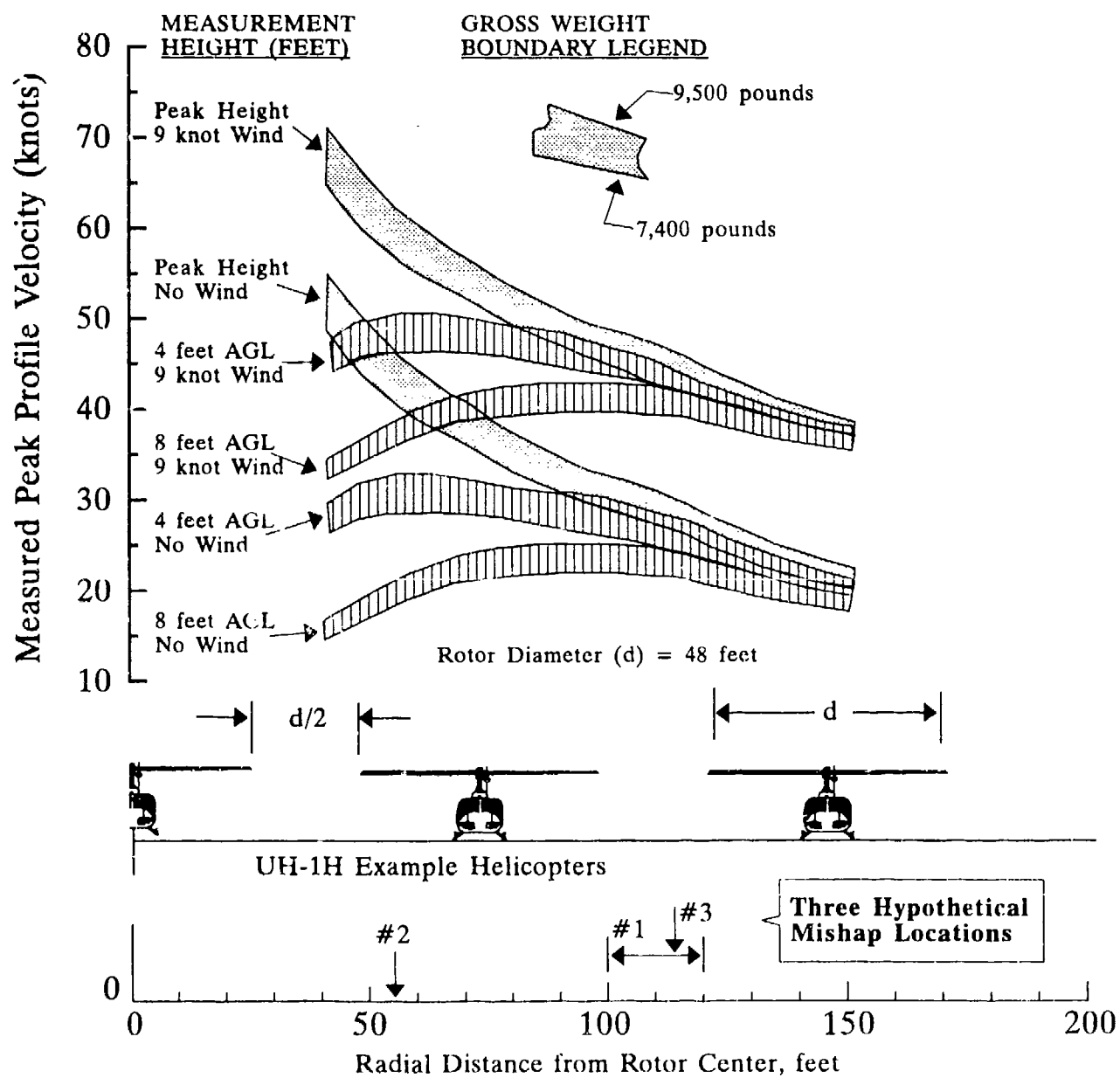


FIGURE 88 BELL UH-1H PREDICTION CHART FOR DOOR/AILERCASE PANEL AND ROTOR BLADE/TAILBOOM STRIKE MISHAPS

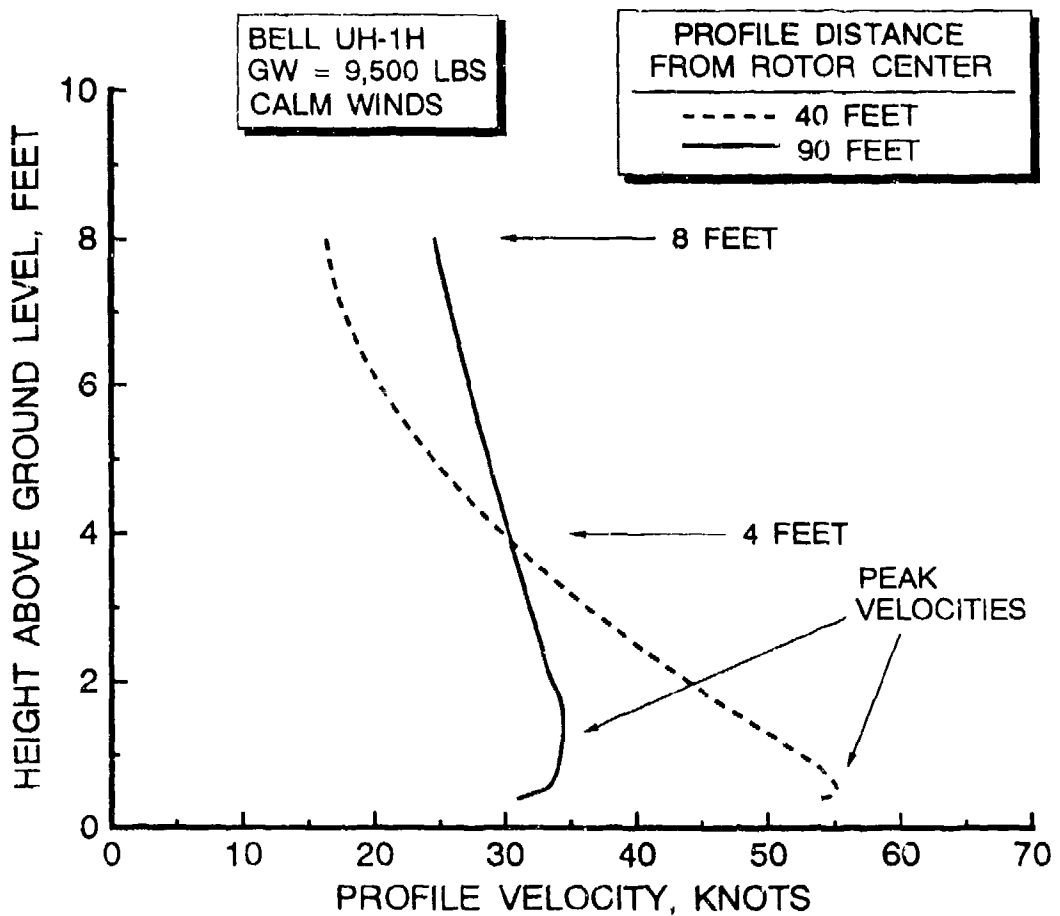


FIGURE 89 ROTORWASH VELOCITY PROFILE LOCATIONS PLOTTED IN THE DEVELOPMENT OF THE UH-1H ANALYSIS CHART PRESENTED AS FIGURE 88

Other information, such as wind limits for rotor startup and shutdown, were also plotted whenever they could be identified. For the OH-58, UH-1H, AH-1S, CH-46, and CH-47 (references 51 through 56), wind and gust spread limits during rotor startup or shutdown (based on flight test data) are documented in the pilot manual in order to insure that the rotor does not flap down and strike the fuselage at very low rpm. These limiting wind values were used as part of the technical basis for estimating and validating rotorwash peak velocity values that have the potential to result in rotor blade/tailboom strikes.

The next step in the analysis procedure was to estimate a minimum safe distance from each of the evaluated rotorcraft after each mishap was assigned an estimated location. At this distance (or range of positions), the associated bands of rotorwash velocity were noted. In the UH-1H example, hypothetical door/access panel mishaps #1 and #3 occurred in calm air at an average position of approximately 110 feet. The estimated peak rotorwash velocity at

this location at door height ($h_d < 4$ feet) is between 28 and 31 knots. With respect to rotor blade/tailboom strikes, other interesting results can be deduced from the chart. If a UH-1H was to land on the next pad (a distance of approximately 72 ft) with a crosswind of 9 knots, it is possible to have a rotorwash plus ambient wind velocity that is above the flight manual limit for rotor startup. At a radial distance of two pad spacings, the calculated total velocity values are below the pilot manual limits. Interestingly enough, no UH-1H blade/boom strikes were reported from the available mishap data sources at this separation distance (even when considering the non-quantitative, descriptive only accident reports).

The final step in the analysis procedure combined the estimated critical rotorwash values for each type of rotorcraft on one graph. At this point, the number of data points became sufficient to estimate the threshold value of rotorwash velocity that should be avoided. The results from this task are discussed in detail in the next section.

5.2.4 Analysis of Door and Cowling Related Mishaps

The desired result from the analysis in this section is to identify a threshold value of peak rotorwash velocity that, when not exceeded in close proximity to unlatched rotorcraft doors and cowlings, dramatically reduces the probability that a mishap might occur. Estimated peak rotorwash velocity ranges that should contain the threshold velocity value were developed using the procedures of section 5.2.3 and figure 88. These velocity ranges are summarized in figure 90 for the nine types of rotorcraft investigated. These estimated velocities range in value from 19 to 69 knots, depending on the height above ground and on whether the ambient wind is 0 or 9 knots. Both wind speed ranges are considered because only 1 mishap summary (of a total of 28) documented an estimated ambient wind value. Therefore, the assumption is that the ambient wind is between these values.

The choice of 9 knots as the upper ambient wind limit is based upon the assumption (see sections 2 and 3) that 9 knots may be close to the worst case scenario. Highly simplified sketches of the rotorwash flow fields for both 0- and 9-knot wind conditions are presented in figure 91. Rotorwash flow fields formed in crosswinds exceeding 9 knots are believed to be less severe. This condition results because it is known that rotor aerodynamics at airspeeds in excess of 10 to 15 knots do not support the formation of the same types of rotorwash flow field structures described in figure 91.

The second reason for the use of an ambient wind greater than 0 knots follows from the observation that the atmosphere is rarely calm (wind < 1 knot). Reference 57 notes that in the Cape Kennedy area, the atmospheric conditions at 10 meters AGL are

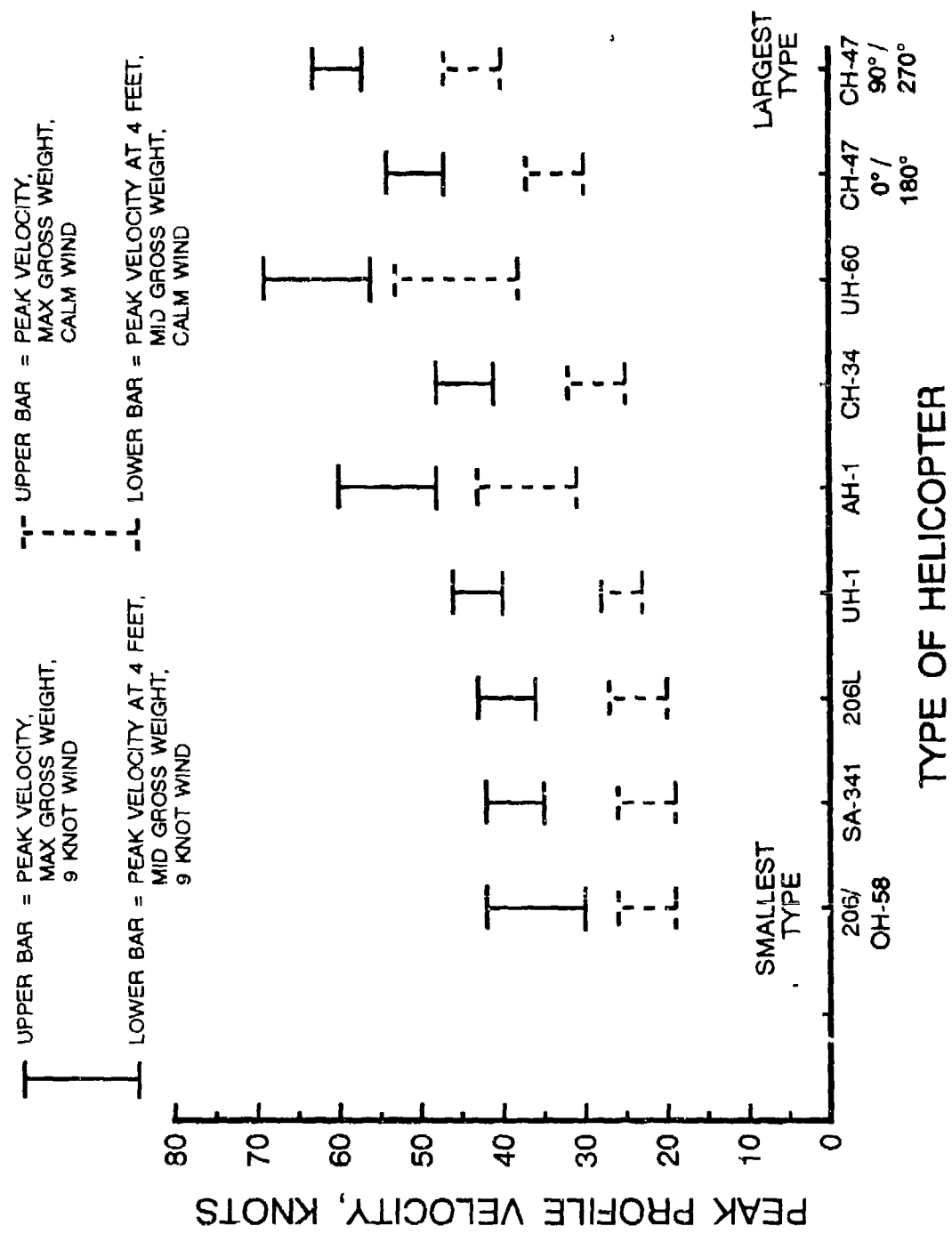


FIGURE 90 ESTIMATED THRESHOLD ROTORMASH VELOCITY RANGES FOR THE MISHAPS INVOLVING DOOR AND COWLING DAMAGE TO HELICOPTERS

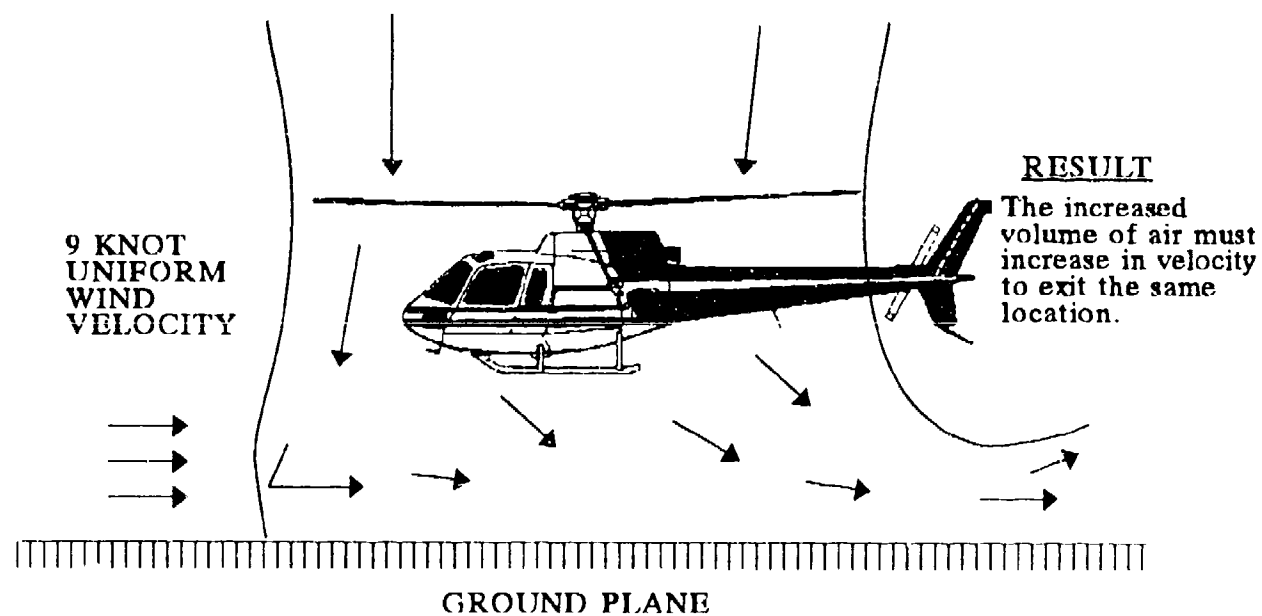
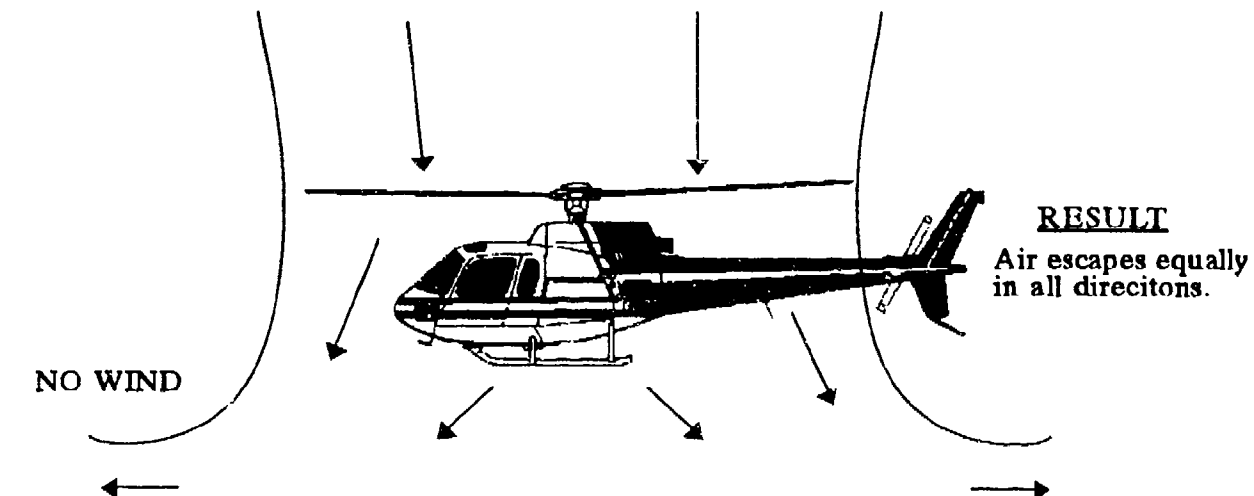


FIGURE 91 TYPICAL HOVER ROTORWASH FLOW PATTERN CHARACTERISTICS WITH AND WITHOUT WIND

calm only 4.5 percent of the time. This condition often occurs during early morning hours. If the mean ambient wind velocity values for each of the locations listed in table 13 (reproduced from reference 58) are added together, an average wind velocity of 8.5 knots (9.77 miles per hour) can be computed for the United States. The probability that the windspeed is between 8 and 12 miles per hour is greatest at 68 percent of the locations. While not statistically representative for the rest of the world, the likelihood of calm atmospheric conditions at any specific location is relatively small.

The top bar for each range of velocity values presented in figure 90 represents the estimated maximum peak profile velocity for the maximum gross weight. This maximum peak velocity varies in height above the ground as a function of position with respect to the center of the rotor. The lower bar represents the peak velocity estimated for the mid gross weight at a constant 4-foot height above ground level. The 4-foot height is in close proximity to the height above ground of most rotorcraft doors. One generally accepted approach for merging the available data and estimating one meaningful threshold value of rotorwash velocity is to use statistical methods. However, a question quickly arises on how the data should be defined for use in statistical calculations. This issue is further compounded when each of the assumptions used to derive these data are reviewed. As a result, it becomes obvious that rigorous scientific analysis methods cannot be used and subsequently defended with a high level of confidence.

The alternative analysis approach is to define a velocity range containing the unknown threshold value of rotorwash and assign a qualitative level of confidence to the range. An upper boundary defining the threshold velocity range can be estimated using figure 90 by connecting the maximum velocity values for the 9-knot data. A lower boundary can likewise be estimated by connecting the 4-foot velocity values for the 0-knot wind data. A set of mean values for each rotorcraft type can be calculated by adding these 2 values and dividing by 2. Results from the accomplishment of this task are presented in figure 92. The first observation obtained from these data is that threshold velocity ranges for 3 types of helicopters, the AH-1, UH-60, and CH-47 (at 90 degrees), are shifted toward higher velocities when compared with similar data from the remaining 6 helicopter types. A quick review of the 28 mishaps indicated that only 5 mishaps involved the AH-1, UH-60, and CH-47. The majority of these 5 mishap reports were also very poorly documented. Since use of these lesser quality data would result in separation guidelines for small helicopters being quite close to those for large helicopters (which is intuitively wrong), one must conclude that too few data exist for a proper analysis of the AH-1, UH-60, and CH-47 (at 90 degrees). If these suspect data are dropped from the analysis, the modified velocity boundaries are as presented in figure 93.

TABLE 13 ANNUAL PERCENTAGE FREQUENCY OF WIND
BY SPEED GROUPS AND THE MEAN WIND

STATE	STATION	Miles Per Hour									
		0- 3	4-7	8- 12	13- 18	19- 24	25- 31	32- 38	39- 46	47- +*	Mean Speed
AL	Birmingham	27	22	30	17	3	1	*	*	*	7.9
	Mobile	7	28	38	20	6	1	*	*	*	10.0
	Montgomery	31	29	27	12	2	*	*			6.9
AK	Anchorage	28	35	25	11	2	*	*	*		6.8
	Cold Bay	4	9	18	27	21	14	5	2	*	17.4
	Fairbanks	40	35	19	5	1	*	*	*		5.2
	King Salmon	11	20	30	24	10	4	1	*	*	11.4
AZ	Phoenix	38	36	20	5	1	*	*	*		5.4
	Tucson	18	35	30	14	3	1	*	*		8.1
AR	Little Rock	12	30	39	16	2	*	*	*		8.7
CA	Bakersfield	35	30	24	10	1	*	*			5.8
	Burbank	5	26	18	4	1	*	*	*		4.5
	Fresno	30	41	22	7	1	*	*			6.1
	Los Angeles	28	33	27	11	1	*	*			6.8
	Oakland	26	28	28	16	2	1	*	*	*	7.5
	Sacramento	15	28	31	18	5	1	*	*	*	9.3
	San Diego	28	38	28	6	*	*	*			6.3
	San Francisco	16	21	26	22	11	3	*	*	*	10.6
CO	Col. Springs	9	27	38	19	6	2	*	*	*	10.0
	Denver	11	27	34	22	5	2	*	*	*	10.0
CN	Hartford	13	26	32	24	6	1	*	*	*	9.8
DC	Washington	11	26	35	22	5	1	*	*	*	9.7
DE	Wilmington	15	31	30	19	4	1	*	*	*	8.8
FL	Jacksonville	10	33	35	18	3	*	*	*		8.9
	Miami	14	30	34	20	2	*	*	*	*	8.8
	Orlando	18	28	32	17	4	*	*	*		8.6
	Tallahassee	33	36	23	7	*	*				6.1
	Tampa	9	31	40	16	2	*	*	*	*	8.8
	W Palm Beach	9	22	36	27	6	1	*	*		10.5
GA	Atlanta	13	24	36	21	6	1	*	*		9.7
	Augusta	36	29	25	9	1	*	*			6.3
	Macon	10	26	46	16	2	*	*	*	*	8.9
	Savannah	12	34	37	14	3	*	*	*	*	8.4
HI	Hilo	7	34	43	15	2	*	*			8.7
	Honolulu	9	17	27	32	12	2	*	*	*	12.1

TABLE 13 ANNUAL PERCENTAGE FREQUENCY OF WIND
BY SPEED GROUPS AND THE MEAN WIND (Continued)

STATE	STATION	Miles Per Hour										Mean Speed
		0-3	4-7	8-12	13-18	19-24	25-31	32-38	39-46	47+		
ID	Boise	15	30	32	18	4	1	*	*			8.9
IL	(O'Hare)	8	22	33	27	6	2	*	*	*		12.1
	(Midway)	7	26	36	25	5	1	*	*	*		10.2
	Moline	14	23	32	24	7	2	*	*	*		10.0
	Springfield	7	22	28	27	12	3	1	*	*		12.0
IN	Evansville	19	23	32	21	5	1	*	*			9.1
	Fort Wayne	9	23	33	25	8	2	*	*	*		10.9
	Indianapolis	9	22	34	26	7	2	*	*	*		10.8
	South Bend	7	21	35	30	7	1	*	*			10.9
IA	Des Moines	3	17	38	29	10	3	1	*	*		12.1
	Sioux City	10	20	31	25	10	4	1	*	*		11.7
KS	Topeka	11	19	30	27	10	2	*	*	*		11.2
	Wichita	4	12	30	31	16	5	1	*	*		13.7
KY	Lexington	8	25	39	22	6	1	*	*			10.1
	Louisville	17	28	31	20	3	1	*	*			8.8
LA	Baton Rouge	17	29	34	17	3	*	*	*			8.3
	Lake Charles	19	31	29	17	4	1	*	*	*		8.5
	New Orleans	16	27	32	19	5	1	*	*	*		9.0
	Shreveport	12	26	37	21	4	1	*	*	*		9.5
ME	Portland	10	30	33	22	4	1	*	*	*		9.6
MD	Baltimore	7	24	39	22	6	2	*	*	*		10.4
MA	Boston	3	12	33	35	12	4	1	*	*		13.3
MI	Detroit City	8	23	37	26	5	1	*	*	*		10.3
	Flint	16	26	32	22	3	1	*	*	*		9.0
	Grand Rapids	14	23	32	25	5	1	*	*	*		9.8
MN	Duluth	6	15	33	31	11	4	1	*	*		12.6
	Minneapolis	8	21	34	28	9	2	*	*	*		11.2
MS	Jackson	33	25	26	14	2	*	*	*			7.1
MO	Kansas City	9	29	35	23	5	1	*				9.8
	St. Louis	10	29	36	21	3	1	*	*	*		9.3
	Springfield	4	13	34	32	13	3	1	*	*		12.9
MT	Great Falls	7	19	24	24	15	9	3	1	*		13.9
NE	Omaha	12	17	29	28	11	3	*	*			11.6
NV	Las Vegas	18	26	25	20	8	3	1	*	*		9.7
	Reno	52	20	13	10	4	1	*	*	*		5.9

TABLE 13 ANNUAL PERCENTAGE FREQUENCY OF WIND
BY SPEED GROUPS AND THE MEAN WIND (Continued)

STATE	STATION	Miles Per Hour										Mean Speed
		0-3	4-7	8-12	13-18	19-24	25-31	32-38	39-46	47+		
NJ	Newark	11	25	34	24	5	1	*	*	*		9.8
NM	Albuquerque	17	36	26	13	5	2	*	*	*		8.6
NY	Albany	23	24	27	21	4	1	*	*			8.6
	Binghamton	11	23	35	25	5	1	*	*	*		10.0
	Buffalo	5	17	34	27	13	3	1	*	*		12.4
	(Kennedy)	6	17	35	28	10	3	*	*	*		12.0
	(La Guardia)	6	15	30	31	12	4	1	*	*		12.9
	Rochester	8	22	34	25	9	2	1	*	*		11.2
	Syracuse	14	27	30	23	5	1	*	*	*		9.7
NC	Charlotte	20	32	31	14	2	*	*	*			7.9
	Greensboro	20	32	31	14	2	*	*	*	*		8.0
	Raleigh	18	33	34	14	2	*	*	*	*		7.7
	Winston-Salem	19	22	33	21	4	1	*	*			9.0
ND	Bismarck	14	20	27	24	12	3	1	*	*		11.2
	Fargo	4	13	28	31	15	7	2	*	*		14.4
OH	Akron-Canton	7	25	35	26	5	1	*	*	*		10.4
	Cincinnati	11	27	36	22	4	1	*	*	*		9.6
	Cleveland	7	18	35	29	9	2	*	*	*		11.6
	Columbus	26	23	29	18	4	1	*	*	*		8.2
	Dayton	8	25	36	23	6	2	*	*	*		10.3
	Youngstown	7	26	36	24	6	1	*	*	*		10.3
OK	Oklahoma City	2	11	34	34	13	6	1	*	*		14.0
	Tulsa	9	24	34	26	7	1	*	*	*		10.6
OR	Medford	47	31	14	6	2	*	*	*	*		4.6
	Portland	28	27	25	16	4	1	*	*	*		7.7
	Salem	25	32	28	13	2	*	*				7.1
PA	Harrisburg	28	31	25	13	3	1	*	*			7.3
	Philadelphia	11	27	35	21	5	1	*	*	*		9.6
	Pittsburgh	12	26	34	22	4	1	*	*			9.4
	Scranton	11	33	35	18	2	*	*	*			8.8
RI	Providence	11	20	32	28	7	2	*	*	*		10.7
SC	Charleston	12	28	35	19	4	1	*	*			9.2
	Columbia	25	35	26	12	2	*	*				7.0
SD	Huron	10	18	29	29	10	3	1	*	*		11.9
	Rapid City	15	22	28	21	10	4	1	*	*		11.0

TABLE 13 ANNUAL PERCENTAGE FREQUENCY OF WIND
BY SPEED GROUPS AND THE MEAN WIND (Continued)

STATE	STATION	Miles Per Hour										Mean Speed
		0-3	4-7	8-12	13-18	19-24	25-31	32-38	39-46	47+		
TN	Chattanooga	39	25	24	11	1	*	*				6.1
	Knoxville	29	29	25	12	4	1	*	*	*		7.5
	Memphis	14	26	34	20	5	1	*	*			9.4
	Nashville	27	31	23	14	2	*	*	*	*		7.2
TX	Amarillo	5	15	32	32	12	4	1	*	*		12.9
	Austin	13	25	34	23	5	1	*	*			9.7
	Brownsville	10	17	25	30	14	3	*	*	*		12.3
	Corpus Christi	11	16	26	33	12	2	*	*			11.9
	Dallas	9	21	32	28	9	1	*	*			11.0
	El Paso	10	22	32	22	9	4	1	*	*		11.3
	Ft. Worth	4	14	34	34	10	3	*	*	*		12.5
	Galveston	4	13	39	33	10	2	1	*	*		12.5
	Houston	6	18	36	28	10	2	*	*	*		11.8
	Laredo	6	15	32	34	12	1	*	*			12.3
	Lubbock	4	11	33	34	13	5	1	*	*		13.6
	Midland	9	22	38	16	4	1	*	*			10.1
	San Antonio	18	23	32	22	4	1	*	*			9.3
	Waco	3	14	36	35	10	2	*	*			12.5
	Wichita Falls	5	22	41	27	5	1	*	*	*		10.5
UT	Salt Lake City	12	33	36	14	4	1	*	*	*		8.7
VT	Burlington	24	24	28	22	2	*	*				8.3
VA	Norfolk	14	23	30	25	6	1	*	*	*		10.2
	Richmond	14	37	36	11	1	*	*	*			7.8
	Roanoke	31	22	23	17	5	2	*	*			8.3
WA	Seattle-Tacoma	13	16	35	26	8	2	*	*	*		10.7
	Spokane	17	38	27	14	3	1	*	*			8.1
WV	Charleston	29	37	25	8	1	*	*				6.2
WI	Green Bay	8	22	32	26	10	2	*	*	*		11.2
	Madison	15	22	30	23	7	2	*	*	*		10.1
	Milwaukee	8	17	31	30	11	3	1	*	*		12.1
WY	Casper	8	16	27	27	13	7	2	*	*		13.3
XX	Wake Island	1	6	27	48	17	2	*	*			14.6
PR	San Juan	15	28	27	25	4	*	*	*	*		9.1

One can assume in analyzing the figure 93 data that the probability of the threshold rotorwash value being near the lower boundary (mid gross weight, 4-foot height, 0-knot wind) is small because the wind is rarely calm. Also, the use of this boundary would result in the specification of large separation distances in the presence of ambient winds. These large separation distances would be highly restrictive to what presently appear to be very safe heliport operations. Likewise, the upper boundary (heavy gross weight, 9-knot wind) would appear not restrictive enough. This is because separation boundaries would be based on a large value of threshold velocity, the most liberal interpretation of available mishap data. Also, no proof exists that even the majority of the reported mishaps occurred in 9-knot crosswind conditions. Therefore, although based on data influenced by several key assumptions, a logical deduction is that the threshold rotorwash velocity value is between the lowest estimated mean value, approximately 30 knots, and the lowest estimated upper boundary value, approximately 40 knots.

The usefulness of any predictive methodology is only as good as its ability to correctly predict test cases. This statement is particularly true when a complex process is analyzed using a simplified model of the process. Unfortunately, no laboratory controlled test cases exist where a door/cowling mishap was intentionally planned, recorded, studied, and documented. However, limited flight data do exist in references 6 through 8 to provide clues to determine if rotorwash velocities of the predicted magnitudes exist in an operational environment for the smaller classes of helicopters. These data were obtained for approximately 14 different types of rotorcraft at approximately 20 inches above ground level at both the Wall Street and Indianapolis heliports. A total of 402 individual operational movements were recorded. This database included movements for three of the nine types of helicopters for which door and cowling-related mishap data were reported, the Bell 206, 206L, and UH-1. Accurate distances between the sensors and the helicopters as a function of time could not be recorded, because each helicopter was privately owned and therefore uninstrumented. However, rotorwash velocities recorded by the sensors are representative of typical operational rotorwash velocities. This is because the sensors were located in positions where other rotorcraft could have been parked.

Recorded velocity data in calm winds for the Bell 206, 206L, and UH-1 at both heliports frequently exceeded 30 knots as the helicopters flew by the sensors. It should be noted that these were mechanical sensors so actual peak rotorwash velocities were higher (as discussed earlier based on reference 11). The magnitudes of some of these measured velocity data (for all three types of helicopters) occasionally even exceeded the ROTWASH calculated peak velocities for 9 knots of wind. In some of these

ESTIMATED THRESHOLD VELOCITY BOUNDARIES

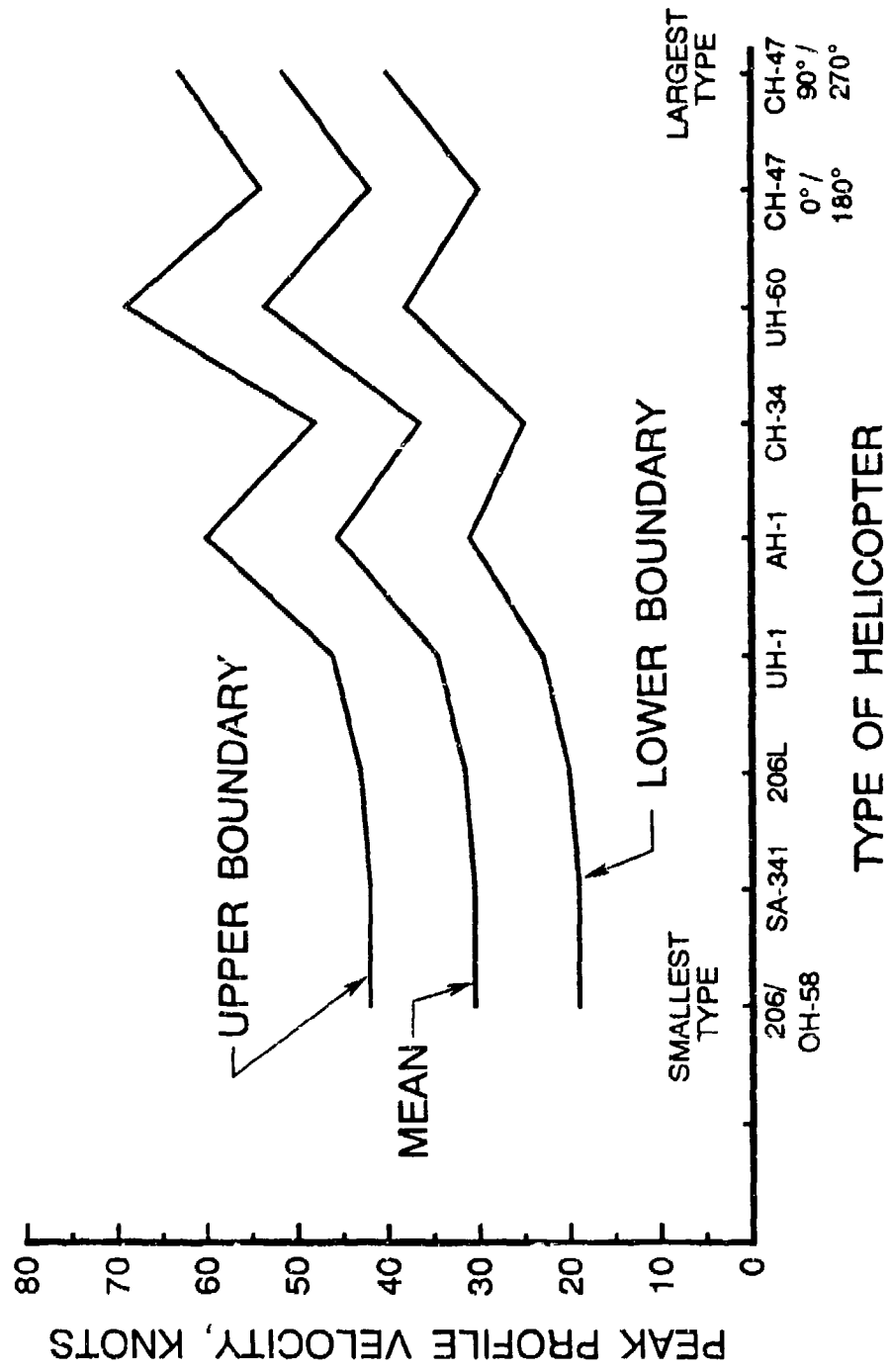


FIGURE 92 ESTIMATED THRESHOLD ROTORWASH VELOCITY MEAN VALUES AND RANGES FOR ALL HELICOPTER MISHAPS INVOLVING DOOR AND COWLING DAMAGE

ESTIMATED THRESHOLD VELOCITY BOUNDARIES

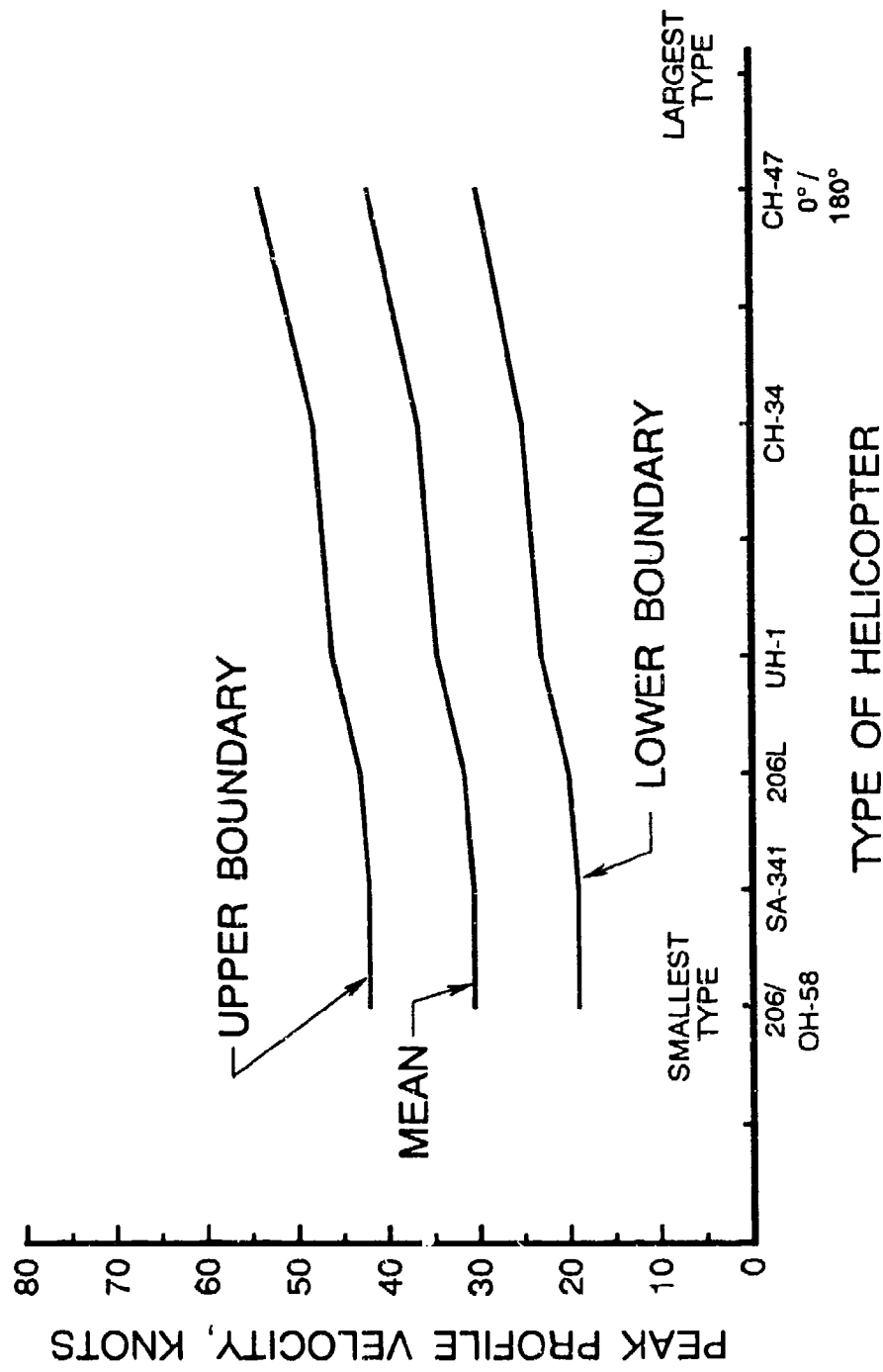


FIGURE 93 ESTIMATED THRESHOLD ROTORWASH VELOCITY MEAN VALUES AND RANGES USED IN THE FINAL ANALYSIS OF MISHAPS INVOLVING DOOR AND COWLING DAMAGE

cases, the measured peak velocities momentarily exceeded 85 knots (approximately 100 miles per hour). As an example, a recorded movement of a UH-1 at the Indianapolis Heliport is presented as figure 94 (reproduced directly from reference 8). Reasons for why these velocity values slightly exceed peak calculated values could include effects due to maneuvering and density altitude, as well as the ambient wind. It is generally accepted that peak rotorwash velocities directly in front of a helicopter during the final phase of a decelerating approach to hover are greater than those for the same helicopter after it is subsequently stabilized in hover. While these data do not necessarily provide specific insight into the reviewed mishaps, the data contained in references 6 through 8 do help support many of the assumptions inherent to the analysis. This is because:

1. rotorwash peak velocities measured in an operational environment vary significantly in magnitude for the same type of helicopter. Reasons for this documented fact include pilot technique, gross weight, and atmospheric conditions (to name only a few).
2. typical rotorwash peak velocity levels in close proximity to helicopters involved in the reported mishaps do significantly exceed the range in velocity that is expected to contain the threshold velocity value (if this observation was not confirmed by measured flight test data, doubts would exist with respect to the quality of the ROTWASH calculated velocity data and the validity of the whole analysis approach).

5.2.5 Analysis of Rotor Blade/Tailboom Strike Mishaps

Approximately twenty rotor blade/tailboom strike mishap summaries were reported in acquired documents, primarily for helicopters with two-bladed rotors. Unfortunately, only one mishap contained significant quantitative details. The typical mishap occurred when the rotor blade of a stopped (but not tied down) or low rpm main rotor was aerodynamically induced by a passing rotorcraft's downwash to strike a tailboom or tail rotor driveshaft. This type of mishap frequently resulted in damage to all three components of the helicopter.

Analysis of the 20 mishap reports was initiated by sorting them as a function of rotorcraft type and scenario. The division by scenario was based on whether or not the blades of the damaged helicopter were reported as being tied down or not. Separation distances, due to lack of detail in the reports, were generally estimated as being one, two, or three pads away. One pad to pad center distance is defined (as shown for the UH-1H in figure 88) to be three times the rotor radius in distance. Using these mishap data and velocity prediction charts for the Boeing CH-47

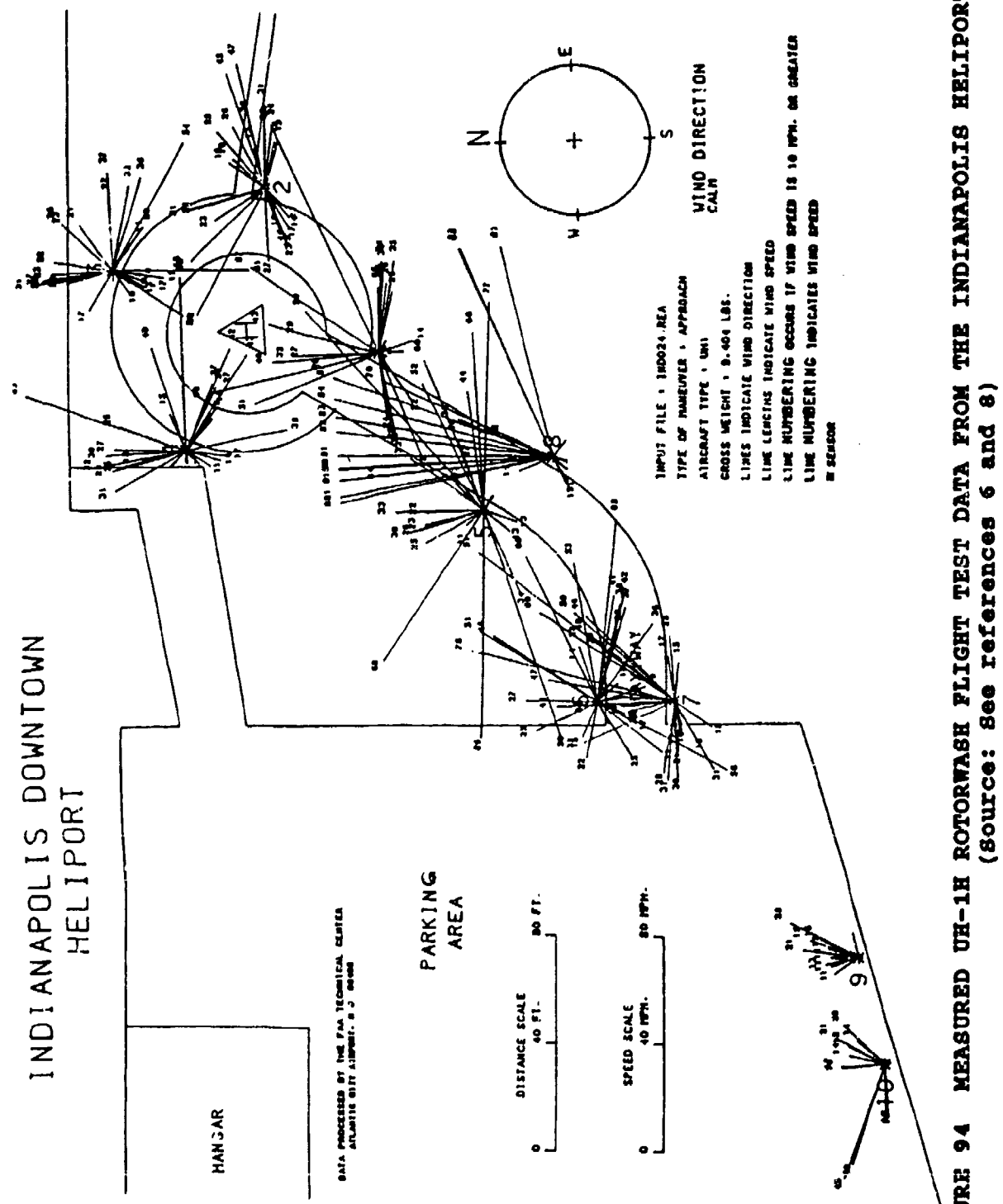


FIGURE 94 MEASURED UH-1H ROTORWASH FLIGHT TEST DATA FROM THE INDIANAPOLIS HELIPORT
(source: see references 6 and 8)

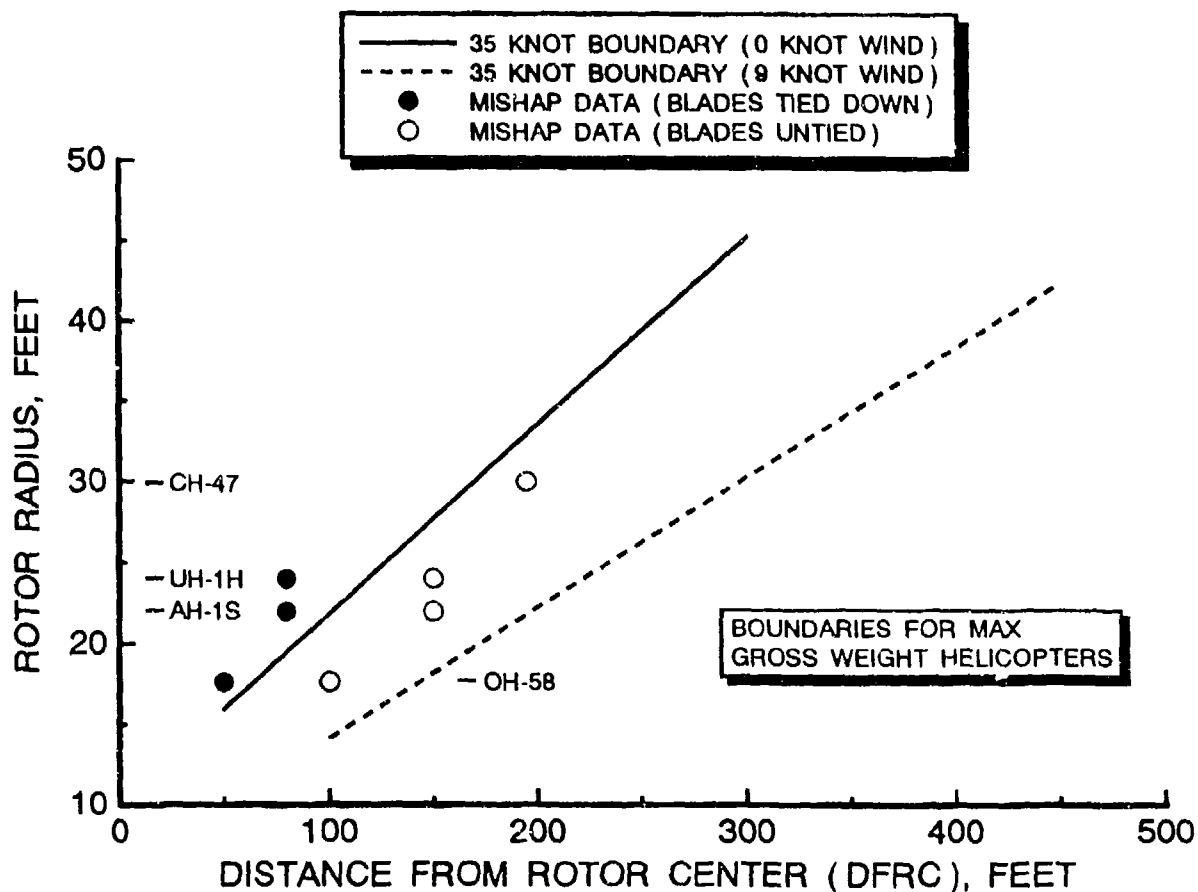


FIGURE 95 FIRST ESTIMATE SEPARATION DISTANCES REQUIRED TO AVOID ROTOR BLADE/TAILBOOM STRIKE MISHAPS

and the Bell UH-1, OH-58, and AH-1, the chart in figure 95 was constructed. This chart attempts to locate the estimated mishap separation distances (from the centers of the rotors of the helicopters involved) with respect to calculated lines that specify distances where the peak rotorwash velocity exceeds approximately 35 knots (for ambient wind values of 0 and 9 knots). It is quite interesting to observe that each of the estimated distances for mishaps involving untied rotor blades plot between the limiting lines. This indicates (only as a first estimate) that a critical peak velocity of approximately 35 knots is probably a reasonable estimate.

An additional piece of information that is available for an analysis of this mishap is the flight manual restriction (if one exists) on the maximum wind velocity allowed for rotor startup and shutdown. Wind velocities specified in flight manual restrictions for the CH-47, UH-1, AH-1, and OH-58 (references 57 through 56) were found to vary between 30 and 45 knots, depending

on how gusts were specified about a limiting mean wind velocity. Therefore, based on these restrictions, one could assume that the probability of a rotor blade/tailboom strike increases significantly when the peak velocity range of approximately 30 to 37 knots is exceeded (ambient or ambient wind plus rotorwash). Of course, this limit must be kept in perspective since the assumption is made that the rotor blades are not tied down and that the rotor is rotating at or below 10 to 20 percent of the operating rpm. Additional limited data appear to indicate that, if the rotor blades are tied down or the rotor is operating at a normal rpm, operation next to a departing or landing rotorcraft is generally safe on the next takeoff/landing pad (again, this assumes a separation of one rotor radius between rotor blade tips).

5.2.6 Evaluation of Rotorwash Hazards to Other Hovering or Taxiing Rotorcraft

The analysis of separation guidelines for rotorwash hazards involving other taxiing or hovering rotorcraft was by far the most difficult type of hazard that was examined. All but approximately five of the reported mishaps involved formation flight of helicopters where, during some part of the mission, one of the trailing helicopters got behind and below (instead of level with or above) or downwind and below the other helicopter(s) in the formation. In this position, the downwash and/or trailing vortices of the leading helicopter induced a sudden negative angle-of-attack or downdraft at the trailing helicopter's main rotor. This sudden change of flight environment resulted in the trailing rotorcraft being overtorqued or making a hard landing if close to the ground. These situations resulted because the pilot was required to pull in an excessive amount of collective in order to maintain altitude or avoid obstacles. The number of times that this or a similar scenario went unreported because the resulting mishap was narrowly avoided is unknown. Additional discussion on the particular scenario where a helicopter or fixed-wing aircraft flies through the well established trailing vortices of another helicopter will be presented in section 5.4.

The other type of reported hazard resulted in the loss of tail rotor effectiveness following the impingement of rotorwash from another nearby helicopter. In each of the three cases where this type of hazard was reported, gusty crosswinds in the 10- to 20-knot range were also reported. Lateral separation distances were reported to be between "right next to" and 100 meters away as well as below the helicopter that was generating the rotorwash.

A combined review of these types of mishaps leads to the conclusion that much more detailed analysis tools will be required in order to develop separation guidelines. Even then, it is questionable whether or not enough data exist to validate a

mathematical model. Therefore, as a rule of thumb, any type of low speed formation flight should be carefully controlled during normal operations in a heliport environment. Otherwise, using sparse available data, it must be assumed that if separation distances of the same magnitude are maintained between hovering or taxiing rotorcraft as those required for the door/access panel and rotor blade/tailboom strike hazards, then safe operations should be possible. This generalized recommendation should certainly be considered open for review as additional data become available following the completion of several ongoing FAA research efforts.

5.2.7 Conclusions from Analysis of Door/Cowling and Rotor Blade/Tailboom Strike-Related Mishaps

The previous sections have briefly evaluated the hazard potential where one rotorcraft (hovering or taxiing) generates a rotorwash flow field that impacts another hovering, taxiing, or parked rotorcraft (with the rotor stopped or slowly turning). Analysis results indicate that, given the time and resource constraints of this project, it was not possible to conduct a direct engineering analysis of each type of mishap. Instead, an indirect analysis approach was implemented using the reported mishap data. Guidelines, summarized in the following paragraphs, that are obtained from use of this analysis approach appear to be validated using available mishap and flight test data. Practical implementation of these guidelines in a detailed heliport design analysis is presented in the "How To" examples contained in sections 6 and 7.

Several general conclusions can be stated from analysis of the door and cowling-mishap summaries. Using presently available test data and analytical methods, it is impossible to specify and document a unique limiting peak rotorwash velocity value that, when not exceeded, is capable of preventing all door and cowling-related mishaps. Only a range of velocity values can be identified that have a high probability of containing the "critical value". This peak profile velocity range varies from 30 to 40 knots. Any further narrowing of this range to identify a specific threshold peak velocity value will require considerable additional data, both mishap data as well as data from planned flight test experiments. Even if a narrower range is eventually identified, the decision to document a specific threshold value as a guideline or standard would be a matter of judgment. This results from the fact that all scenarios cannot be evaluated. Also, any identified "absolutely safe" value may be economically too restrictive. It is therefore more practical to provide a higher threshold velocity value as a guideline through educational material and rely on common sense operation of rotorcraft by operators.

Likewise, based on the rotor blade/tailboom strike data, one could assume that the probability of a mishap increases

significantly when the peak rotorwash velocity range of approximately 30 to 37 knots is exceeded. Interestingly, this range of velocity values almost exactly matches the range that is estimated for door and cowling damage. Therefore, one could conclude that specification of guideline separation distances, based on a velocity range of 30 to 37 knots, is a technically justifiable approach to minimize several types of mishaps. However, this statement must not be considered as justification to reduce the need for improved mishap data, particularly if experimentally controlled data can be obtained.

A brief analysis was also conducted in order to evaluate the ground vortex and the very low-speed trailing vortex hazards as they might affect separation guidelines. Since these aerodynamic flow fields are localized and their movements with ambient winds are not clearly understood, it was not possible to develop and justify (and validate with confidence) any practical guidelines in addition to those that were developed in section 5.1. Additional discussion on the effects of well-developed helicopter trailing vortices at or above approximately 40 knots on other helicopter and fixed-wing aircraft is presented in section 5.4.

5.3 ROTORWASH EFFECTS ON FIXED-WING AIRCRAFT

The potentially hazardous effects of rotorwash on nearby fixed-wing aircraft can be grouped in one of two categories. The first of these categories includes aircraft that are parked with their engines turned off. These aircraft may or may not be tied down. The second category includes those aircraft with engines running that are parked, taxiing, or flying in close proximity to the ground. Seven mishaps were identified during this study that fitted into one of these categories. Even though two of the reviewed mishaps did not report the exact type of fixed-wing aircraft involved, it is believed that the aircraft were light, two to four seat, single-engine configurations. None of the reviewed mishaps specifically stated that larger fixed-wing aircraft types were involved. The lack of a large number of reported mishaps of this type does not necessarily indicate that this type of mishap rarely occurs. There are indications that existing mishap reporting systems often overlook mishaps when a parked fixed-wing aircraft without occupants is damaged and the offending undamaged helicopter exits the mishap area. Unfortunately, none of the reviewed mishap reports contained substantial detailed data for correlation using an analytical model. In spite of this problem, a simple analytical model is developed to study mishaps where rotorwash induces a fixed-wing aircraft (engine turned off) to roll over and damage one wing tip. This type of mishap had the largest number of reported incidents.

5.3.1 Mishaps Involving Fixed-Wing Aircraft With Engines Running

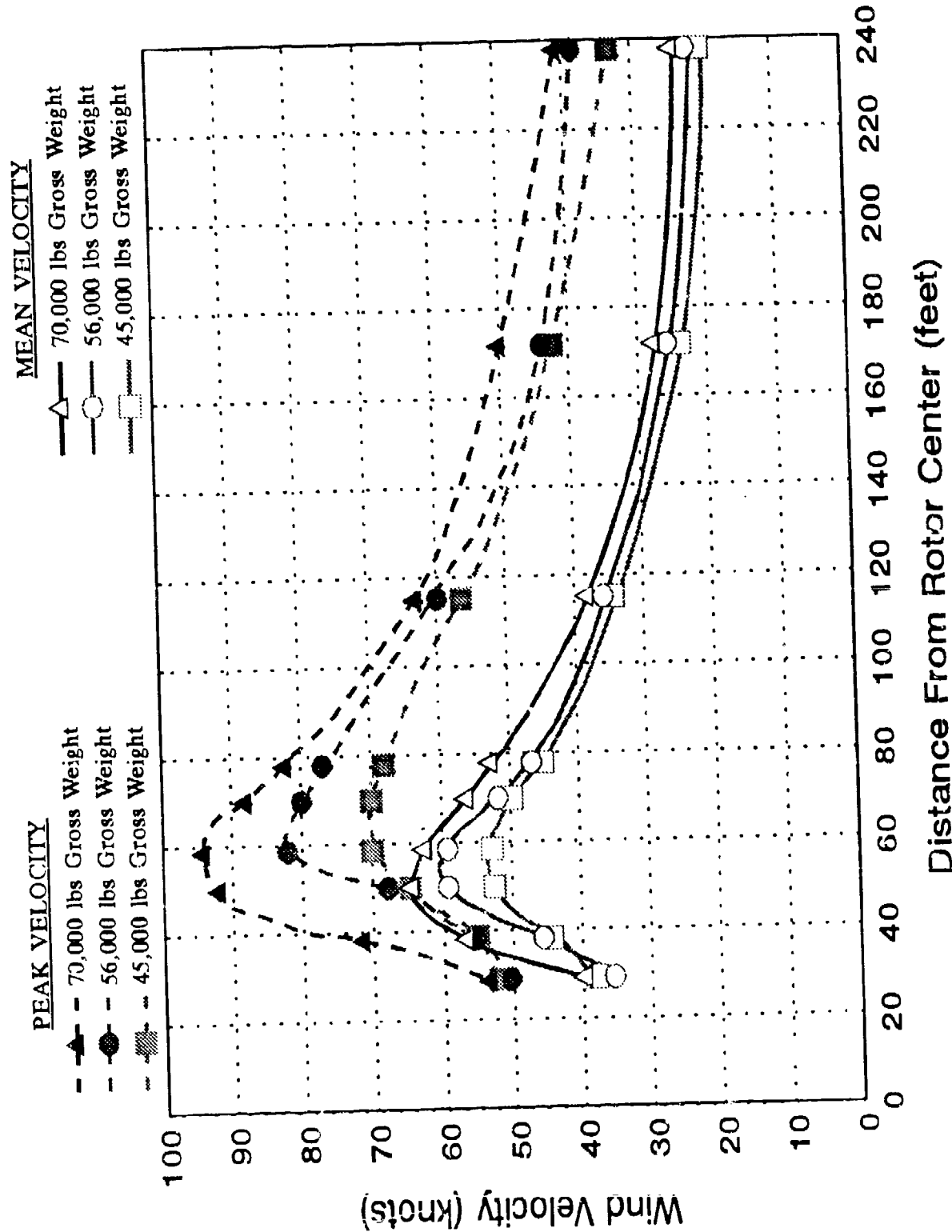
Three of the seven investigated mishaps involved fixed-wing aircraft with their engines running. Even though reported information was minimal (not enough for a detailed quantitative analysis), the mishap scenarios are most enlightening in a qualitative sense. It is believed that their documentation in this report may be useful in preventing similar mishaps in the future.

The first mishap in this category involved a tricycle gear Cessna 152 and a Sikorsky H-53 (the specific model of the H-53 was not identified). The Cessna taxied for takeoff with the intention of using runway 24 with an 8-knot wind. At the same time, the H-53 entered the landing pattern for the same runway. The Cessna then accepted the option to use runway 29 and was informed to stay clear of runway 24. The Cessna pilot taxied onto runway 29 at the intersection of the two runways, moved to takeoff position just beyond the intersection, and then braked to a stop with the tail pointed toward runway 24. The Cessna was cleared for takeoff and given the explanation that takeoff on runway 24 would have required a 3 minute wait to avoid wake turbulence from the H-53. The H-53 was then cleared to land on runway 24 behind the Cessna. As the H-53 passed by the Cessna, the tail lifted up and the airplane nosed over. Damage to the

Cessna was reported as substantial. The runways involved were reported to be 150 feet wide. Key unknown factors in the mishap are the specific model of H-53 (two or three engine version), the airspeed of the H-53, the exact distance between the two aircraft at the closest point, and whether or not the H-53 passed by in the air (at what altitude?) or on the ground. Without these pieces of information, a quantitative analysis is futile. However, if several assumptions are made, an estimate of the rotorwash velocities involved can be attempted.

If the H-53 was at a very low airspeed and almost on the ground when it passed the Cessna, one might assume that the H-53 was approaching hover. This is probably the worst case scenario from a rotorwash estimation standpoint. In this instance, peak profile velocity flight test data from reference 24 can be used to estimate the rotorwash velocities involved. These velocity data are presented in figure 96 (reproduced directly from reference 24). If the Cessna was between 100 and 200 feet away (which is highly probable), peak velocity values could have been between 40 and 60 knots. If the H-53 was flying at a low airspeed, such as 40 knots, the rotorwash flow field could have been composed of a trailing wake vortex structure. Data from reference 46 for a Sikorsky CH-54 (that has a rotor configuration almost identical to an H-53) are presented in figure 67 to provide insight into the wake velocities contained within this type of flowfield. These data correspond to a gross weight between 30,000 and 38,000 pounds at an airspeed of approximately 40 knots. Peak wake velocities measured at 28 seconds behind the CH-54 are between 15 and 20 meters per second (29 and 39 knots). It is reasonable to assume that these velocities could be increased by as much as 50 percent if the gross weight of the H-53 was greater than 38,000 pounds or if the wake data were measured within seconds after the helicopter passed by. In summary, if the Cessna 152 was struck by rotorwash flow fields of either type containing these estimated velocity values, there is little doubt that the aircraft could have been turned over (as was actually the case).

The second mishap in the category of aircraft with engines running occurred between a Sikorsky UH-60 helicopter and a tricycle gear Piper PA-28. The PA-28 landed at a gliderport and was either taxiing or holding position on the ground in an 8-knot wind when the UH-60 reportedly "swooped" down next to the PA-28. The UH-60 mistakenly intercepted the PA-28 as a drug smuggling aircraft and the officers on the helicopter were trying to make an arrest before the pilot could get away. No other details were given, other than substantial damage was incurred by the PA-28 and the government admitted their liability. Little can be learned from this mishap other than the fact that UH-60 series helicopters are clearly capable of overturning PA-28 size aircraft (which has a maximum gross weight of 2,150 pounds with four passengers; only the pilot was aboard in this incident).



Source: Reference 24.

FIGURE 96 MEASURED CH-53E PEAK PROFILE VELOCITIES AS A FUNCTION OF DISTANCE FROM THE ROTOR CENTER AT A HEIGHT OF 3 FEET FOR A HOVER WHEEL HEIGHT OF 20 FEET

The third reported mishap involved an unusual set of circumstances. In this mishap, a Cessna 152 and a helicopter were both destroyed while in the air. Analysis of this accident is clearly beyond the capabilities of available analytical tools. However, it is hoped that mention of the known factors in this mishap will someday help to prevent a similar incident. The Cessna was practicing takeoffs and landings with a student pilot and instructor on board. Winds were approximately 8 knots. As the Cessna entered the turn on final to runway 3, radio calls were made to a helicopter approaching the uncontrolled airport. These calls were apparently never heard by the helicopter pilot as he came to a hover near the taxiway parallel to runway 3. As the Cessna lifted off after the touch and go landing, it veered to the right and collided with the helicopter. The flight instructor survived the mid-air collision and stated that control of the Cessna was lost when it flew through rotor wake turbulence.

The lesson learned from this mishap is that even hovering rotorwash velocities can be dangerous to small aircraft that are flying at airspeeds where aerodynamic controls are quite effective. Therefore, specification of criteria for separation of rotorcraft and fixed-wing aircraft will have to take into account airborne separation distances from hovering rotorcraft. Unfortunately, at this time virtually no data exist, either analytically or experimentally obtained, that can be used to help define separation distances for this particular type of mishap scenario.

5.3.2 Mishaps Involving Fixed-Wing Aircraft With Engines Turned Off

Five mishaps were reviewed that involved fixed-wing aircraft on the ground with engines turned off. In three of the mishaps, the fixed-wing aircraft rotated about its longitudinal axis and one of the wing tips struck the ramp. In one instance, one side of the wing was tied down and the other side was untied. In a fourth mishap, the airplane rotated so that the empennage struck the ramp. The exact nature of the damage in the fifth incident was unreported. After a review of these mishap reports, the reader is left with the impression that a portion of the damaged aircraft becomes momentarily airborne before the aircraft suddenly and uncontrollably rotates about an axis and is damaged. Three of the mishaps involved Bell UH-1 helicopters and two involved Boeing CH-47s. Ambient winds appear to have been a contributing factor with rotorwash in at least four of the mishaps. Three mishaps reported winds in excess of 10 knots (however, direction of the wind was unclear). Reported damages in two of the mishaps, both involving wing tips, were \$200 and \$550, respectively. The three known damaged fixed wing aircraft were Cessna 150, 172, and 175 models. In several of the mishaps, undamaged fixed-wing aircraft were reportedly tied down next to the damaged aircraft. Unfortunately, documented details for all

five of the reported mishaps were insufficient to study each mishap analytically as a separate incident. However, the mishaps do provide guidance when studied as a group. Further discussion is presented on this subject in the next section.

5.3.3 Analytical Model for Overturning Fixed-Wing Aircraft

The analytical model developed to investigate fixed-wing overturning mishaps uses simple aerodynamic theory. The model is formulated for analysis of mishaps where fixed-wing aircraft roll about the fuselage and a wing tip strikes the ground. This modeling approach is a continuation of work originally developed and presented in reference 1. Mishaps where the empennage is lifted up and the nose strikes the ground are not modeled. Force and moment components utilized in the model are depicted graphically in figure 97.

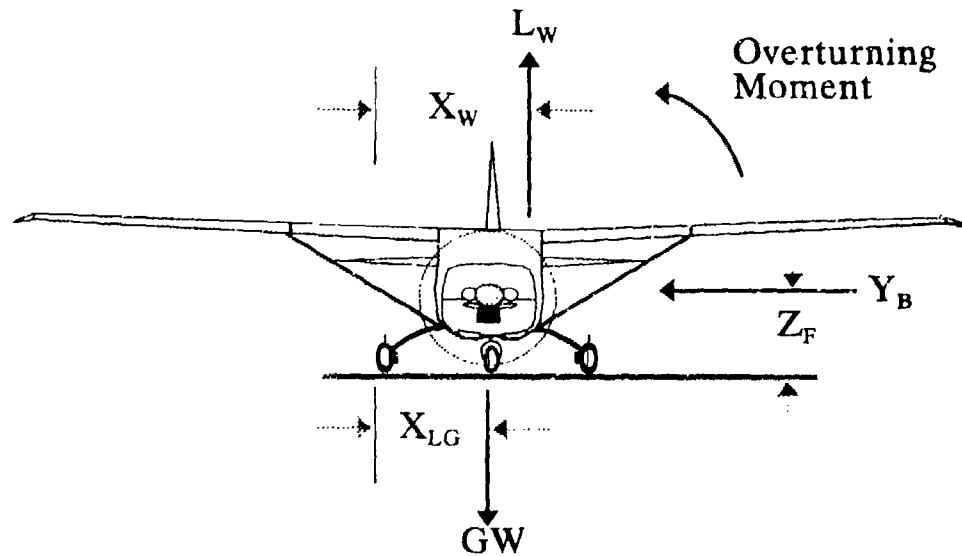


FIGURE 97 FORCES MODELED TO STUDY THE OVERTURNING OF LIGHT FIXED-WING AIRCRAFT

The mathematical model assumes that the fixed-wing aircraft is a small high-wing civilian type, such as a Piper PA-18 Cub or a Cessna 172. These two aircraft are representative of thousands of civilian aircraft that are flown in the United States. Mathematically, these aircraft are also the most susceptible to rotorwash-induced overturning moments.

The two primary aerodynamic components of the fixed-wing aircraft overturning moment are those that result from wing lift and body axis side-force (which is composed of wind axis side-force and drag components). The mathematical model uses low angle-of-attack wind tunnel data at sideslip angles up to 90 degrees from

a high-wing tricycle gear aircraft configuration (not built). The source for these unpublished data was identified during the reference 3 research effort. These data indicated that maximum rolling forces about the fuselage body axis existed at approximately 20 degrees of sideslip. The simple equation that equates the overturning aerodynamic moments to the stabilizing moment due to gross weight at the instant prior to overturning is:

$$(GW) (X_{LG}) = (L_W) (X_W) + (Y_B) (Z_F) \quad (65)$$

where:

GW = manufacturer's stated empty weight + 50 pounds

X_{LG} = moment arm of the gross weight about the landing gear (one-half the wheel stance), feet

L_W = wing lift, pounds

X_W = moment arm from the wheel to the point of application of the wing center of lift (this is conservatively estimated for a wing at a 20 degree yaw angle with a dihedral effect to be: $X_{LG} + (1/15)(b_W/2)$, where b_W is the wing span in feet), feet

Y_B = fuselage body-axis aerodynamic side-force, pounds

Z_F = vertical moment arm from the wheel to the point of application of the side-force on the aircraft fuselage, feet

It is important to note that this equation does not contain terms for forces created by the empennage (probably a conservative assumption). Also, no reduction in the landing gear pivot arm is accounted for if the rollover occurs along the line intersecting one main wheel and the tail or nose wheel (which is the more likely occurrence). The 50 pounds added to the gross weight term (GW) are provided to account for residual fluids and miscellaneous items aboard an aircraft over and above the manufacturer's stated empty weight.

In developing the equation further, it can be shown that the wing lift (L_W) and fuselage side-force (Y_B) terms can be expanded and substituted into equation 65 to obtain equation 69:

$$L_W = (C_L) (q) (S_W) \quad (66)$$

$$C_L = (a_{3d}) (\alpha_w) \quad (67)$$

$$Y_B = (C_{Y\beta}) (q) (S_w) \quad (68)$$

$$\alpha_w = \frac{(GW) (X_{LG}) - (C_{Y\beta}) (q) (S_w) (Z_p)}{(q) (S_w) (a_{3d}) (X_w)} \quad (69)$$

where:

α_w = wing angle-of-attack, degrees

$C_{Y\beta}$ = non-dimensional aerodynamic side-force coefficient

q = $(0.5) (\rho_A) (V^2)$ where ρ is the atmospheric density in slugs/feet³ and V is the air velocity in feet/second

S_w = wing area, feet²

a_{3d} = wing 3-dimensional lift curve slope (at a 20 degree sideslip angle), 1/degree

Once values are calculated for the constant aerodynamic and geometry terms, equation 69 can be evaluated. This task is accomplished by substituting a range of values for V , the air velocity. The resultant output is a graph of the minimum required wing angle-of-attack necessary to overturn the aircraft versus air velocity.

The data presented in figure 98 represent the estimated angle-of-attack values required to overturn a Piper PA-18 or Cessna 172 as a function of rotorwash peak velocity. Table 14 presents a summary of the input data values used to make these calculations. These results indicate that slightly lower values of rotorwash than were previously predicted in reference 1 may be capable of overturning light fixed-wing aircraft. At air velocities of approximately 40 knots, wing angle-of-attack values of only 6 to 8 degrees are required to overturn the aircraft. Angle-of-attack values of this magnitude are frequently measured in hover rotorwash flowfields. This is because the flowfields have a tendency to expand upward as the flow spreads out across the ground. Figure 99 presents measured flight test data (reproduced from reference 24) that confirm that the velocity vectors in a

TABLE 14 INPUT DATA VALUES FOR MODELED FIXED-WING AIRCRAFT

PARAMETER	PIPER PA-18 VALUE	CESSNA 172 VALUE	UNITS
Gross Weight (GW)	980	1,300	pounds
Moment Arm for Weight (X_{LG})	3.0	4.0	feet
Air Density (ρ)	0.00226	0.00226	slug/feet ³
Wing Area (S_W)	178.5	174	feet ²
3-d Lift Curve Slope (a_{3d})	0.072	0.072	1/degree
Side-Force Coefficient ($C_{Y\beta}$)	0.43	0.43	-ND-
Moment Arm for Lift (X_L)	3.18	4.18	feet
Moment Arm for Side-Force (Z_F)	3.0	6.0	feet

CRITICAL OVERTURNING ANGLES-OF-ATTACK

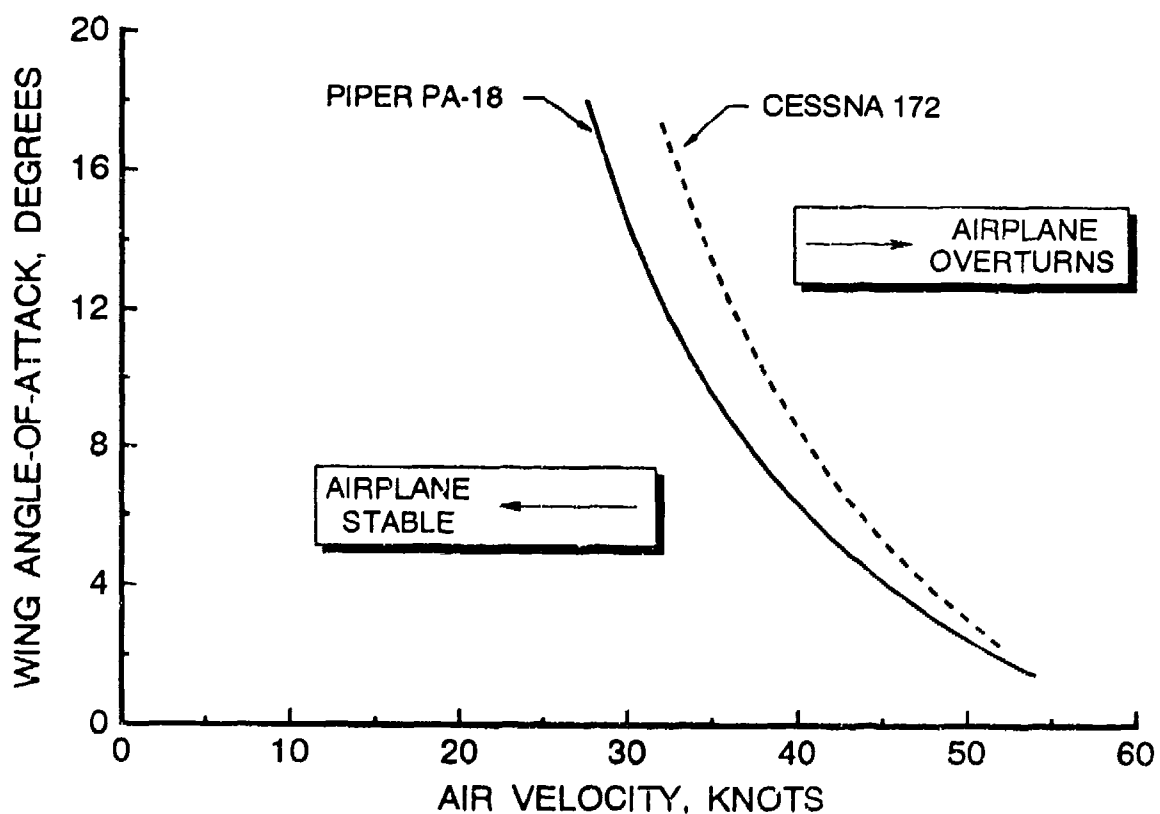


FIGURE 98 MINIMUM AIRSPEED/ANGLE-OF-ATTACK REQUIREMENTS FOR THE OVERTURNING OF LIGHT FIXED-WING AIRCRAFT

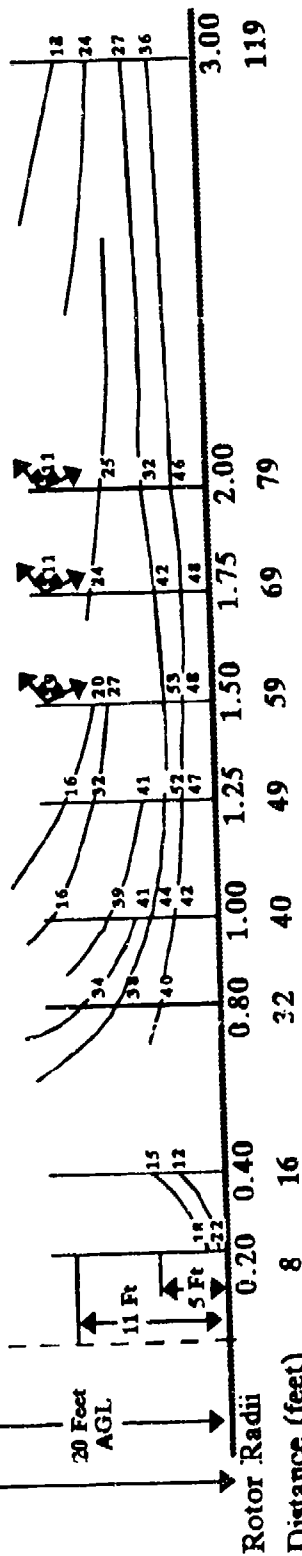
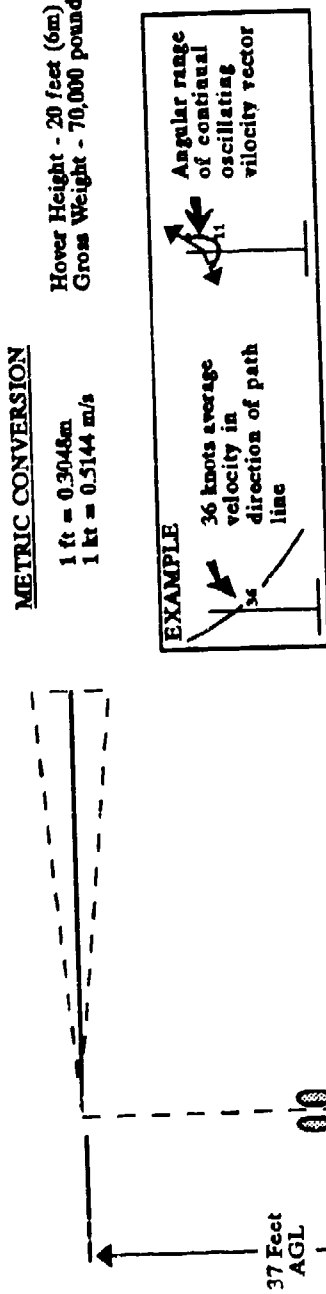
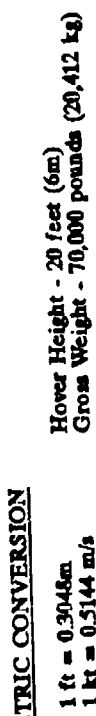


FIGURE 99 CH-53E ROTORWASH VELOCITY STREAMLINES

Source: Reference 24.

CH-53E rotorwash flowfield have an oscillatory upward component of velocity at a wheel height of 20 feet and a gross weight of 45,000 pounds.

The next logical step in the development of this analysis is to attempt a correlation of the model with actual mishap data. Unfortunately, as discussed earlier, the reported mishaps did not contain enough information for detailed analysis. In one mishap involving a Bell UH-1H that had just been refueled, the separation distance with the damaged Cessna 172 was reported as 100 to 130 feet.

However, a confusing factor in this mishap report was that the Cessna was reported upwind of the helicopter in winds gusting up to 30 knots. Simple calculations indicate that this reported piece of information is somewhat contradictory. Therefore, it is effectively impossible to define the type of flowfield to be used for any detailed analysis. If the Cessna had been reported downwind of the helicopter with 9 knot winds, then rotorwash velocities are predicted between approximately 35 and 40 knots at 8 feet AGL and higher at lower heights (see figure 88). These velocities are for a mid gross weight configuration (which could be slightly lower than those for a fully refueled helicopter). The estimated critical angle-of-attack at 40 knots is 8.5 degrees. Most Cessna aircraft have a 1- to 3-degree geometric angle-of-attack, a negative zero-lift-line offset (-2 to -3 degrees), as well as 1- to 2-degrees dihedral. Therefore, an effective angle-of-attack of 8.5 degrees could easily be obtained. It is important to note that the Piper PA-18 is clearly even more at risk. The geometric angle-of-attack for the wing on this aircraft is approximately 12+ degrees parked on the ramp because it is tail dragger configuration.

The only other mishap that reported a separation distance was one involving a Boeing CH-47 that had just refueled (probably indicating a mid to high gross weight). The exact type of civilian fixed-wing aircraft was not reported. The wind was described as 12 to 15 knots, and the CH-47 was directly upwind of the fixed-wing aircraft at approximately 225 feet. Estimated CH-47 rotorwash velocities at this distance are approximately 36 to 53 knots. This broad range of predicted velocities results because the CH-47's orientation with respect to the fixed-wing aircraft is unknown. Predicted velocities for tandem rotor configurations along the fuselage centerline are significantly lower than those predicted along a line at 90 degrees to the centerline. If the fixed-wing aircraft was similar to a Piper PA-18 or Cessna 172, the estimated critical angle-of-attack would be between approximately 1 and 10 degrees. This angle-of-attack range could easily be encountered in a rotorwash flow field for almost any type of light general aviation airplane.

One other mishap case was identified as involving a fixed-wing aircraft that incurred control system damage as a result of

rotorwash. A review of pilot manuals for numerous aircraft resulted in the discovery that tie-down requirements are not specified for prevention of this type of damage as a function of ambient wind. Owners are simply told to tie down their aircraft when not in use. Considering this fact, it must be assumed that the methodology that is used for predicting overturning moments will also be sufficient in predicting clearance to insure that control system damage will not occur. Too little information exists to develop a reliable model that would accurately predict structural damage for this type of hazard. In all probability, it would be very surprising if a limiting rotorwash velocity value (or recommended separation distance) resulting from an analysis would be less than the 30+ knots identified in the analysis of door/access panel mishaps.

5.3.4 Conclusions from the Analysis of Fixed-Wing Overturning Related Mishaps

Several different types of rotorcraft induced fixed-wing mishaps have been reviewed in this section. Analytical methods for the prediction of safe separation guidelines for several of these types of mishaps do not presently exist (i.e., for rotorwash lifting the tail of a fixed-wing aircraft). The most frequently reported mishap involves parked fixed-wing aircraft that are damaged near the wing tip after rotorwash rotates the aircraft about its fuselage. A simple methodology has been developed for an analysis of this mishap. This methodology estimates the wing angle-of-attack value required to overturn a light fixed-wing aircraft when the rotorwash velocity is specified. Two examples of the use of this methodology are discussed. Additional use of this methodology in an airport scenario is presented in the "How To" examples in sections 6 and 7.

Results from the overturning analysis indicate that if predicted critical angles-of-attack are less than 10 to 12 degrees (as a function of rotorwash velocity), then trends based on mishap data indicate that rotorcraft are probably too close to unsecured fixed-wing aircraft. Unfortunately, due to a lack of detailed information in the mishap reports, none of the reported mishaps could be used to conclusively validate this conclusion. Experiments designed to acquire validation data for this analysis methodology are outlined in section 8.

5.4 TRAILING WAKE VORTEX EFFECTS ON FIXED-WING AIRCRAFT AND ROTORCRAFT

As often occurs in the engineering world, if one searches for a certain combination of effects he often discovers that data are available for almost every combination but the combination that is desired. This thought certainly applies to the availability of flight test data from instrumented helicopters that have penetrated the trailing wake vortices of another helicopter. Excellent data are available for two light fixed-wing aircraft

penetrating the wakes of five helicopters, the UH-1H, S-76, UH-60, CH-47D, and CH-53E (reference 10). Flight test data are also available for the penetration of trailing vortices from a four-engine C-54 (or DC-4) transport by an instrumented Bell UH-1H. However, no flight test data are known to be available for a helicopter penetrating the trailing vortices of another helicopter.

Section 2.3 presented the mathematical modeling of the trailing wake structure of a helicopter. Section 3.6 presented correlation between calculated trailing wake vortex strength data and flight test data acquired from five different types of helicopters. The purpose of this section is to present a data summary that quantifies the known hazard generated by helicopters for fixed-wing aircraft and discusses the general effects of a helicopter on another helicopter. No attempt is made to develop mathematical model based predictions of minimum separation distances for two reasons. These reasons are:

1. Reference 10 provides excellent recommended flight-test-based separation guidelines for helicopters and fixed-wing airplanes based on real world test data. No calculated data could ever be expected to dramatically improve these recommendations.
2. The availability of helicopter on helicopter data is not sufficient in quality or quantity at this time to conclusively develop criteria similar to those developed for fixed-wing aircraft. With additional effort, some progress should be possible toward this goal, but it is certainly beyond the scope of available resources for this report.

Research conducted by the FAA and presented in reference 10 evaluated the effects of five helicopters on the Beechcraft T-34C trainer (a 4,300-pound low-wing monoplane) and the Bellanca 8KCAB Decathlon (an 1,800-pound high-wing monoplane). The aircraft were flown both parallel and into the helicopter wake and across the wake as described graphically in figure 100. The upset in bank angle, before the pilot could regain control, was measured as the aircraft encountered the wake. Summary plots of the results are presented in figures 101 through 104 for the UH-1H, UH-60, CH-47D, and CH-53E respectively (as reproduced from reference 10). Table 15 summarizes these data and recommends minimum IFR separation distances behind the helicopters. These separation distances are conservatively greater than the minimum distances at which the T-34C was upset with at least a 30-degree roll when encountering a vortex. The 30-degree roll limit is considered the maximum upset allowable for safe flight. If the data contained in table 15 are plotted as a function of maximum gross weight for each helicopter, as extracted from reference 10, then the relationships in figure 105 can be constructed. These relationships are clearly non-linear in nature.

TABLE 15 PROBE TEST SEPARATION DISTANCES

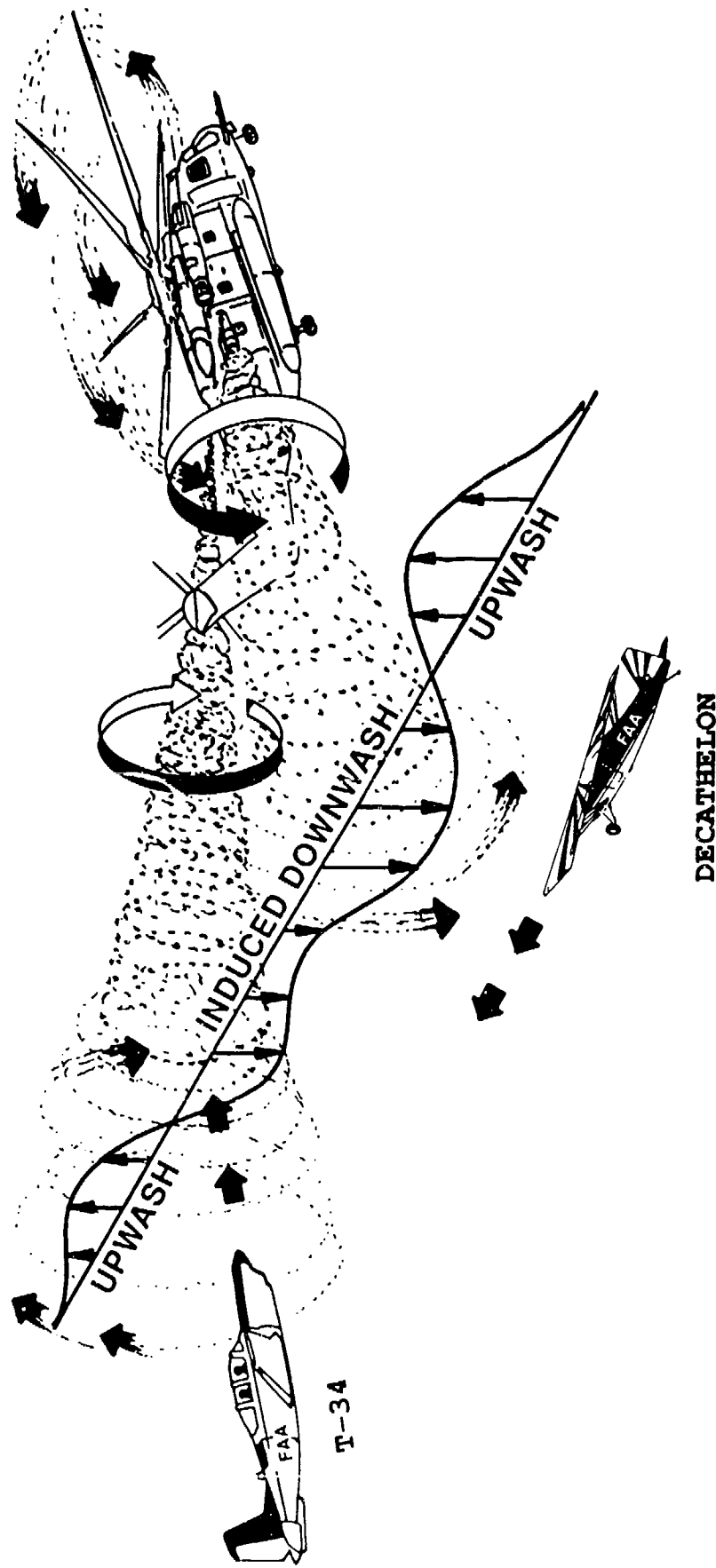
HELICOPTER	MAXIMUM DETECTABILITY DISTANCE (nm)	MAXIMUM DISTANCE 30 DEGREE UPSET (nm)	RECOMMENDED MINIMUM IFR SEPARATION (nm)
UH-1H	1.0	0.7	1.5
S-76A	1.0	0.7	1.5
UH-60	2.4	1.4	2.5
CH-47D	2.7	1.5	2.5
CH-53E	3.1	2.5	4.0

Research into the effects of fixed-wing aircraft trailing vortices on a helicopter was conducted by NASA in references 59 and 60. A Bell UH-1H was instrumented and flown behind a large four-engine C-54 (or DC-4) transport. Extensive data were acquired for helicopter response characteristics and structural loads. The C-54 was flown at 5,500 feet, 115 knots, and approximately 58,000 pounds. The UH-1H was flown at approximately 7,200 pounds at an airspeed of 60 knots. Penetrations of the C-54 wake were made over a range from 0.42 to 6.64 nautical miles behind the aircraft. The estimated strength of the trailing vortex was approximately $1,500 \text{ ft}^2/\text{sec}$ at a distance of 3 nautical miles.

Results from the flight test program indicated that the UH-1H never encountered any unsafe conditions, either in vehicle response or structural loads. The predominant helicopter vehicle response was in yaw. The range of separation distance from this particular fixed-wing aircraft did not dramatically affect measured results. By comparison, a small 2,200 pound fixed-wing airplane was flown into the same type of encounter at 90 knots. At a separation distance of 3.9 miles, the roll attitude upset for this airplane was still quite severe, whereas the UH-1H experienced minimal response.

The results from the UH-1H flight test effort would appear to indicate that helicopters are not significantly affected by trailing vortices. This appears to be a valid statement when compared with small-fixed wing aircraft under similar conditions. However, it must be emphasized that the UH-1H experiment is only one experiment for one combination of helicopter and fixed-wing transport. If a helicopter of another type were to fly into the wake of a large CH-53E or a Boeing 767, the results might be quite different. There is ample evidence to support this conclusion. The U.S. Army mishap data base information summarized in section 4.2 reported numerous cases of helicopter

T-34C ILLUSTRATES PARALLEL PROBE TECHNIQUE
DECATHELON ILLUSTRATES CROSS TRACK PROBE TECHNIQUE
(OBVIOUSLY CONDUCTED AT DIFFERENT TIMES BY EITHER AIRPLANE)



Source: Reference 10.

FIGURE 100 VORTEX PROBING TECHNIQUES

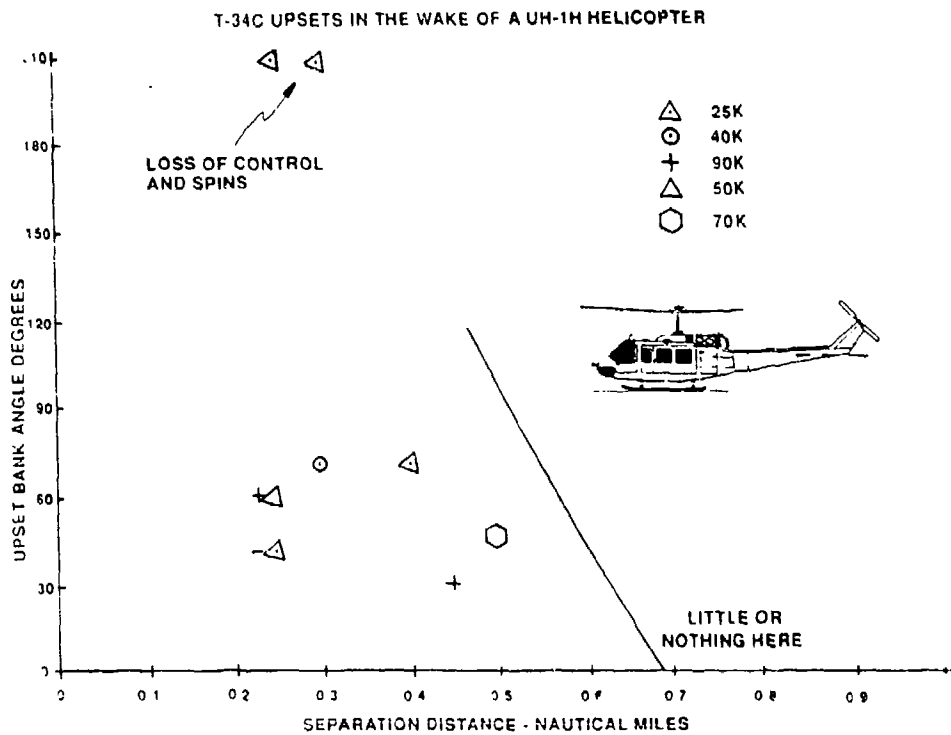


FIGURE 101 T-34C UPSETS IN THE WAKE OF A UH-1H HELICOPTER

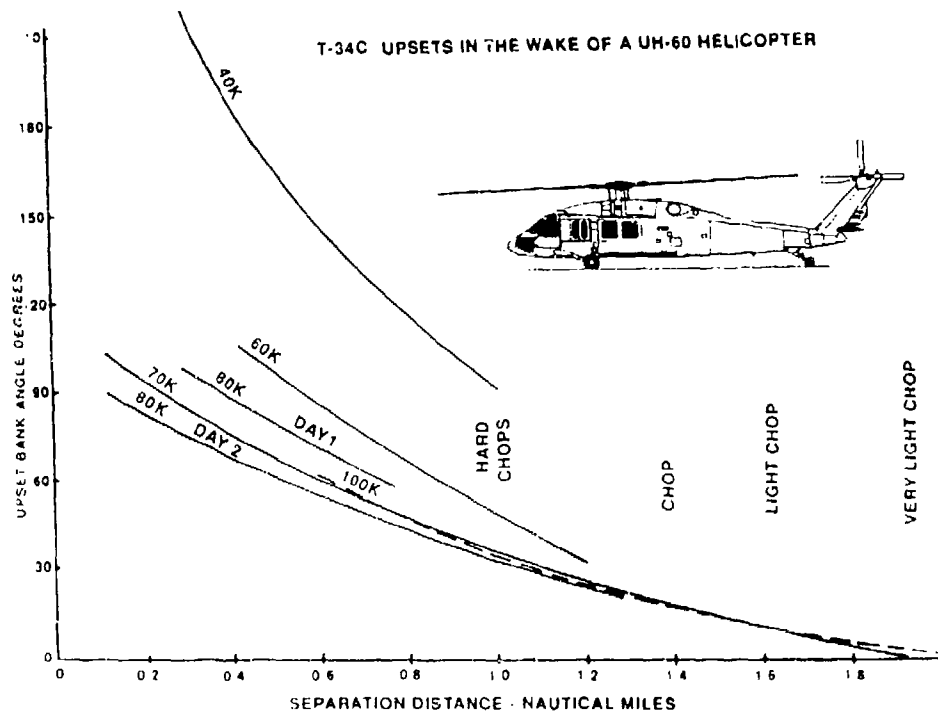
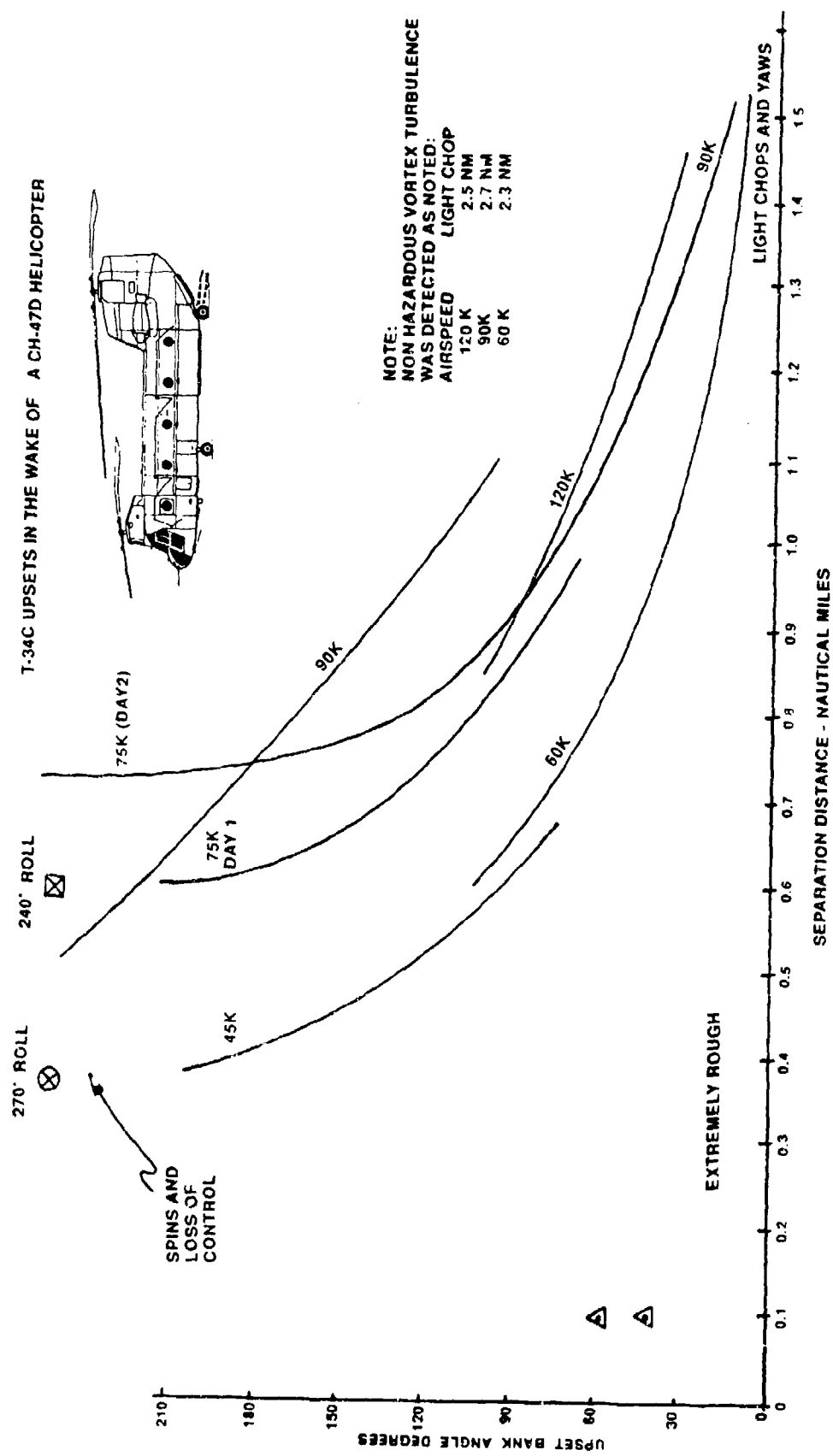


FIGURE 102 T-34C UPSETS IN THE WAKE OF A UH-60 HELICOPTER



Source: Reference 10.

FIGURE 103 T-34C UPSETS IN THE WAKE OF A CH-47D HELICOPTER

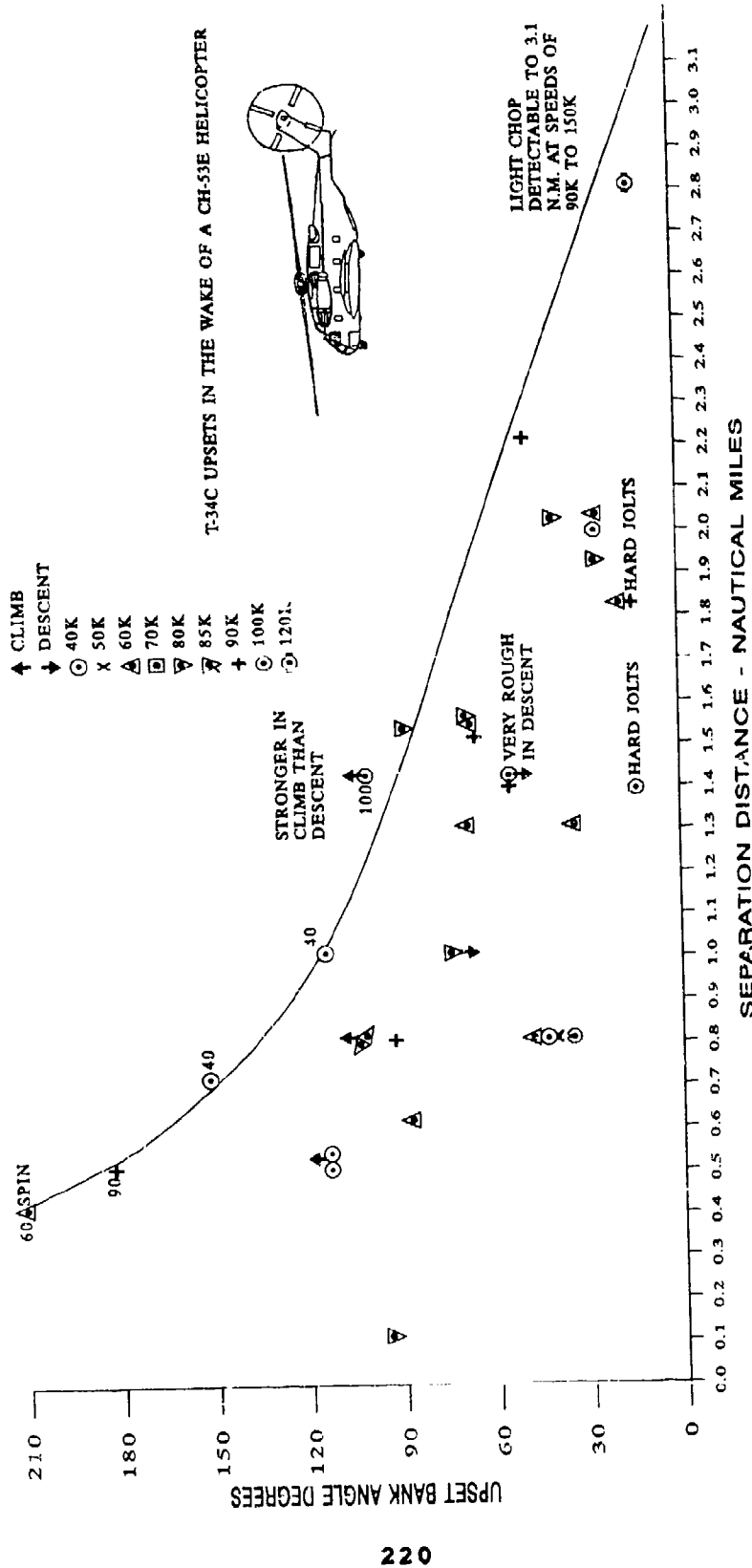


FIGURE 104 T-34C UPSETS IN THE WAKE OF A CH-33 HELICOPTER

Source: Reference 10.

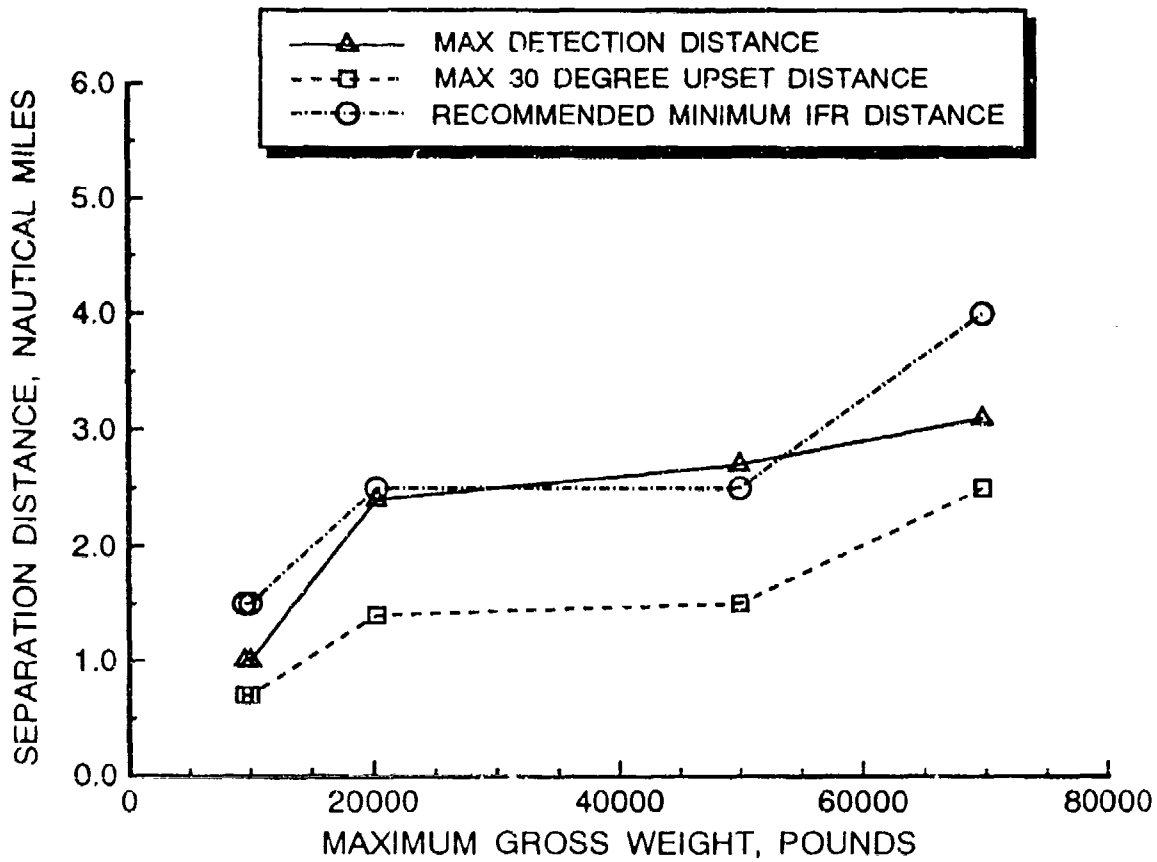


FIGURE 105 PROBE TEST SEPARATION DISTANCES

wakes being responsible for causing nearby or formation-flying rotorcraft to crash, make hard landings, or incur transmission or engine overtorques. Also, Curtiss reports in reference 61 that teetering rotor helicopters like the UH-1H are least susceptible to vortex encounters. His work indicates that high hinge offset rotors (i.e., the MBB-105 and BK-117) are affected significantly more in both vehicle response and structural loads. The work in this report is correlated with the UH-1H data from references 59 and 60.

In summary, it can be stated that small single-engine fixed-wing aircraft are at significant risk when encountering helicopter wake vortices. Fortunately, flight test-based separation guidelines, if implemented, exist to minimize the potential for mishaps. The risk to helicopters is less well quantified. Helicopters would appear to be safe if fixed-wing separation guidelines are followed. However, these guidelines are probably too restrictive. Therefore, to ascertain separation guidelines it would be useful to conduct research, both simulation and flight tests, to obtain additional data on several types of helicopters (i.e., as done for light fixed-wing aircraft).

5.5 ROTORWASH EFFECTS ON STRUCTURES

Rotorwash-related mishaps involving structures can usually be classified in one of two general categories. These include mishaps that:

1. directly result from outwash velocities (or dynamic pressure loadings), and
2. occur in a more indirect manner as the result of entrained particles and debris (e.g., rocks, sand, debris) that subsequently impact the structure.

The intent of this section is to investigate the first of these two types of mishaps. Discussion of impact damage from flying objects is reserved for section 5.7.

5.5.1 Literature Review of Peak Velocity Profile Effects on Structures

The effect of an oscillatory rotorwash velocity profile (and therefore the pressure loads) is considered important in heliport design, because buildings and other structures usually have to be located close to the takeoff/landing pad. This is particularly true in an urban area where the availability of real estate is usually quite limited and expensive. In reviewing the literature, it was discovered that one prior FAA-funded study, reference 62, was conducted in 1984 to investigate potential rotorwash effects on structures. Final results from that study agree in many aspects with the results of this research effort. However, because data are now available that were not available for use at that time, there are also areas where significant differences exist in the reported results. These differences affect the way in which recommended separation guidelines should be specified.

In conducting the reference 62 study, both model-scale and limited full-scale outwash profile data were used to develop a simple mathematical model to predict peak structural pressure loadings. Since the literature search was conducted solely through the National Technical Information Service (NTIS), the investigators identified only the full-scale and model data documented in references 27, 42, and 63 through 65. Unfortunately, none of the high quality work that was conducted by the U.S. Navy (references 23, 24, 29, and 40) was discovered, because these reports are not listed under NTIS. An attempt (reference 1) to correlate data from reference 42 with earlier versions of the mathematical models described in section 2 was thought to be successful after a brief comparison of CH-54A data with Navy CH-53E data (reference 24). However, when a more extensive correlation effort was attempted with the remaining reference 42 data, results were found to be very inconsistent and discouraging. Very early during this correlation effort, a

warning was issued by U.S. Navy personnel at Patuxent River Naval Air Station that this would probably occur. Therefore, the inconsistent results were not totally unexpected. The extremely inconsistent quality of these data was mentioned as the primary reason why the U.S. Navy tests were funded and why very accurate velocity measurement sensors and statistical data reduction techniques were used. In conclusion, while the analytical approach that was used in reference 62 was generally quite good, the results were contaminated by the poor experimental data that were available during development of the analytical procedure.

Results from the reference 62 study can generally be summarized by the data presented in figure 106. The curve of the ratio P_o/DL (total downwash pressure to rotorcraft disc loading (DL)) versus radial distance (x/R) was provided to enable calculations to be made quickly for the maximum expected pressure loading. The resulting calculations were then compared to the Uniform Building Code Design Requirements for wind loading as presented in figure 107. The only helicopter size category that was noted in the study as a possible hazard was the size category including large military helicopters such as the CH-53 and CH-54.

Rotorcraft such as the Bell 206L ($DL = 3.86$ pounds/feet² (psf)) and the Sikorsky S-76 ($DL = 6.77$ psf) were shown to produce maximum pressures of less than 8.5 psf and 14.9 psf, respectively, at radial distances of just a few feet beyond the tip of the rotor. These pressure values are clearly less than the 15 to 20 psf uniform loading design requirements indicated in figure 107. However, it must also be noted that this methodology did not include additional loading effects due to a combination of rotorwash plus ambient wind loads.

Conclusions presented in the reference 62 study indicated that both full-scale and model data revealed that maximum horizontal pressures might approach 2.0 to 2.2 times the rotorcraft disc loading. These peak pressure levels would then decrease quickly with increasing distance from the rotor hub. Peak rotorwash loads for the more common types of civilian helicopters (e.g., Bell 206L and Sikorsky S-76) would therefore be expected to be no more than 7 to 14 psf. Accordingly, since these pressure levels are well within uniform building code specifications, rotorwash-generated loads were deemed to be lower than code specified critical structural loading conditions. An extensive and impressive list of questionnaire responses from more than 90 operators was also evaluated and presented to substantiate this conclusion. The questionnaires indicated that operational problems associated with rotorwash were limited almost exclusively to the scattering of roof gravel and occasional instances where rooftop circulation vents ingested helicopter exhaust fumes.

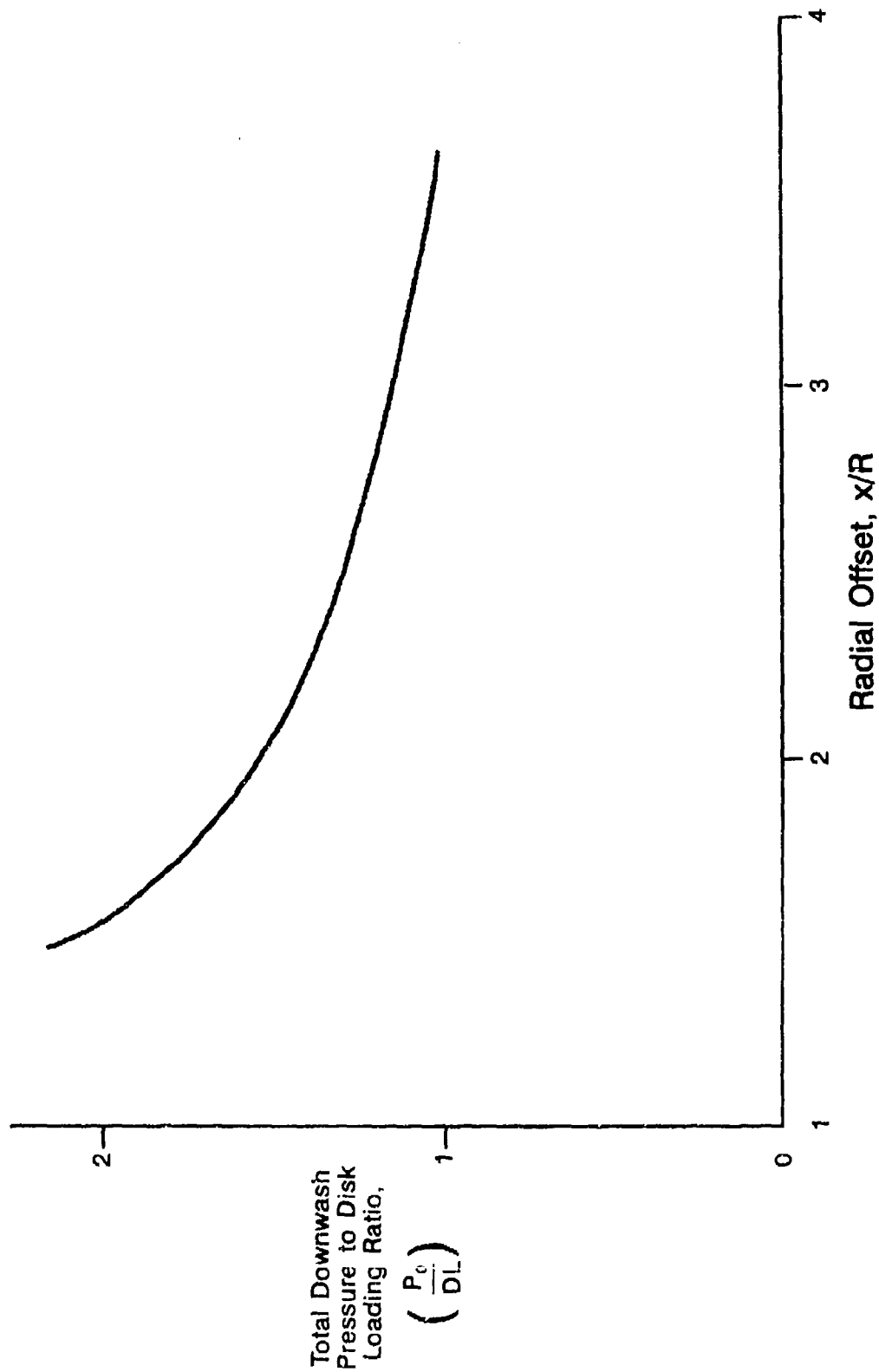


FIGURE 106 ROTORWASH GENERATED PRESSURE DISTRIBUTIONS RECOMMENDED FOR STRUCTURAL DESIGN AS A FUNCTION OF RADIAL OFFSET (from reference 62)

WIND PRESSURES FOR VARIOUS HEIGHT ZONES ABOVE GROUND*

HEIGHT ZONES (in feet)	WIND-PRESSURE-MAP AREAS (pounds per square foot)						
	20	25	30	35	40	45	50
Less than 30	15	20	25	25	30	35	40
30 to 49	20	25	30	35	40	45	50
50-99	25	30	40	45	50	55	60
100 to 499	30	40	45	55	60	70	75
500 to 1,199	35	45	55	60	70	80	90
1,200 and over	40	50	60	70	80	90	100

* See map. Wind pressure column in the table should be selected which is headed by a value corresponding to the minimum permissible, resultant wind pressure indicated for the particular locality.

The figures given are recommended as minimum. These requirements do not provide for tornadoes.

**MULTIPLYING FACTORS FOR WIND PRESSURES -
CHIMNEYS, TANKS, AND SOLID TOWERS**

HORIZONTAL CROSS SECTION	FACTOR
Square or rectangular	1.00
Hexagonal or octagonal	0.80
Round or elliptical	0.60

FIGURE 107 UNIFORM BUILDING CODE WIND LOADS

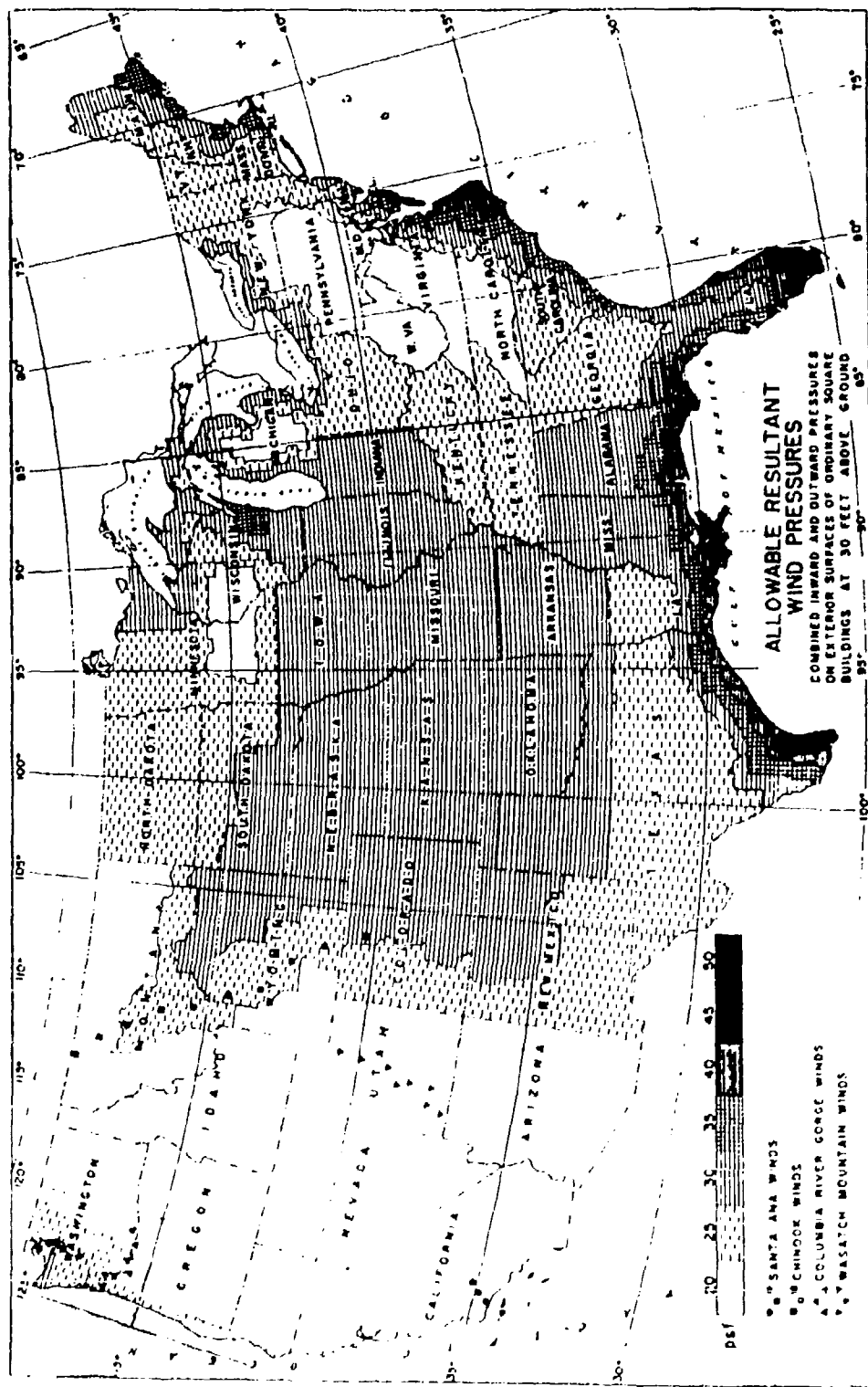


FIGURE 107 UNIFORM BUILDING CODE WIND LOADS (continued)

In 1990, subsequent to a design review in which both ambient wind and rotorwash-related hazards were discussed, a decision was made by the City of Dallas to authorize detailed studies of both of these effects prior to final design and construction of the Dallas Vertiport. This facility is shown in figure 108. Phase I is scheduled for completion in January 1994 as part of the expansion of the Dallas Convention Center. Key results from these studies are detailed in references 12 and 47.

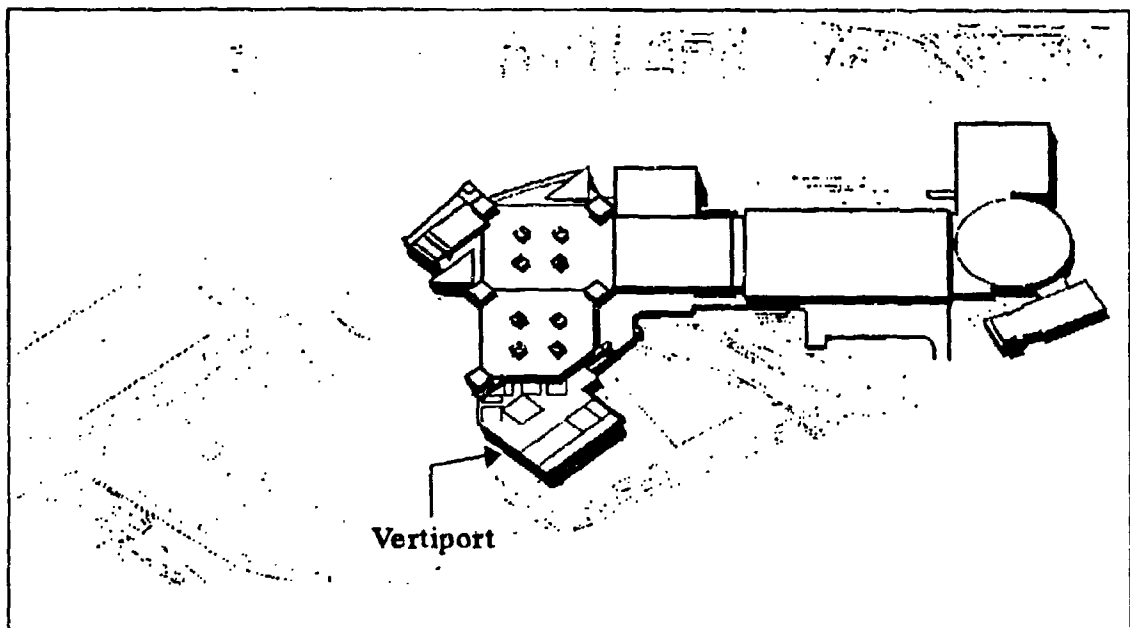
Reference 47 focuses on analytical predictions of rotorwash (using references 1 through 4 as background) for three rotorcraft, the Bell-Boeing V-22, the Bell 214ST, and the Sikorsky S-76. These rotorcraft were chosen as the three key design configurations for both structural loading and parking considerations. Reference 12 documents the wind engineering test of several scale models of the Dallas Vertiport. This test was conducted in the large wind engineering tunnel owned and operated by Cermak Peterka Peterson (CPP), Inc. of Fort Collins, CO. The largest of the scale models tested (1:136) used the work of reference 47 to calibrate two scaled rotorwash generators. An example of a dynamic pressure load that could conceptually occur with a large rotorcraft in an unusual operational situation is presented in figure 109 by converting the V-22 flight test data in figure 52a from units of knots to psf. The twin- and single-rotor configurations were moved about the vertiport to directly measure pressure loads at critical locations in both the landing/takeoff and parking areas.

Two aspects of the measured pressure loads were considered important:

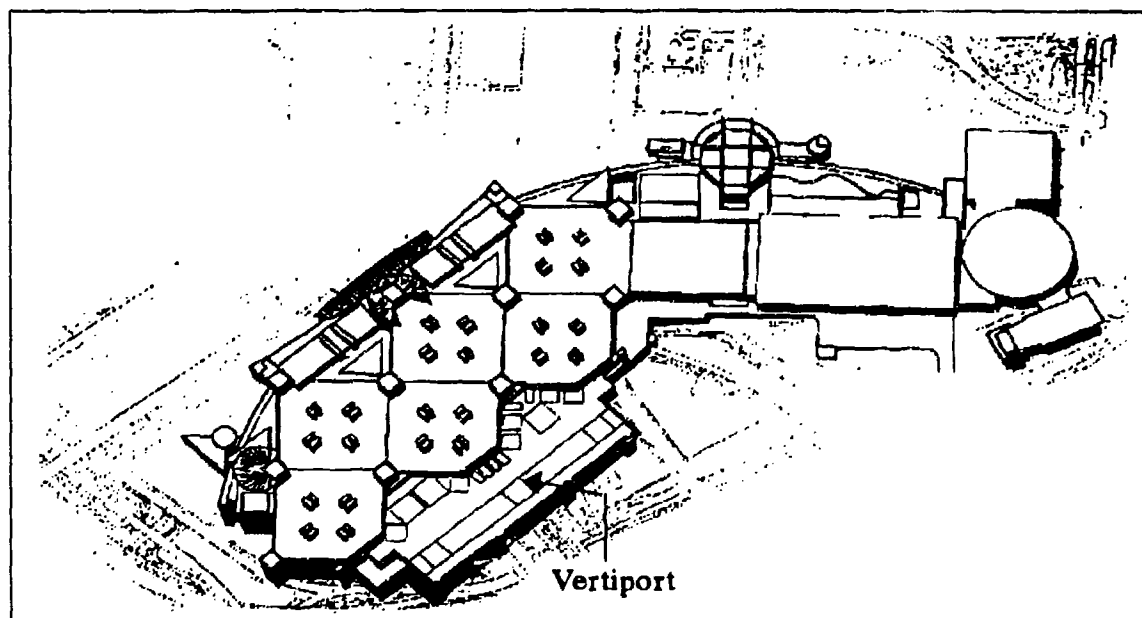
1. identification of any exceeded design loads due to rotorwash impingements on the structure, and
2. quantification of fatigue loads at magnitudes less than the limit design loads.

One key assumption made during the wind tunnel test was that the evaluated rotorcraft locations would be the worst case locations as shown in figure 110. This resulted from an acknowledgment by all involved that it was prudent to evaluate violations of operational procedures for structural design purposes even if it was believed that they would never occur. Operational procedures in this context refer to proposed limitations on the way rotorcraft would be allowed to air or ground taxi to avoid other types of rotorwash-related mishaps. The ambient wind was simulated at approximately 9 knots or 11.5 miles per hour so that worst case rotorwash atmospheric conditions would also be evaluated.

Phase I Layout



Phase II Layout



Source: Reference 73.

FIGURE 108 ARTISTS OVERHEAD SKETCHES OF THE DALLAS VERTIPORT

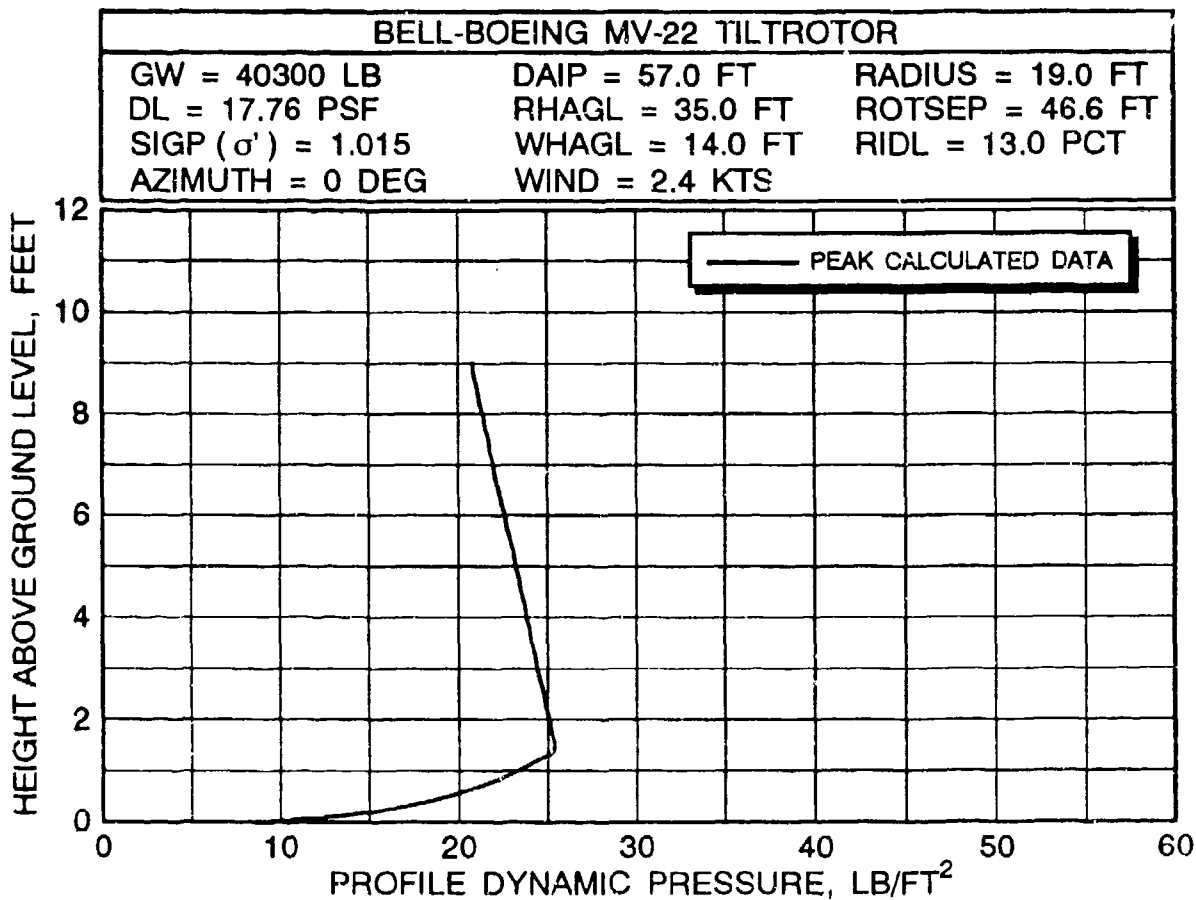
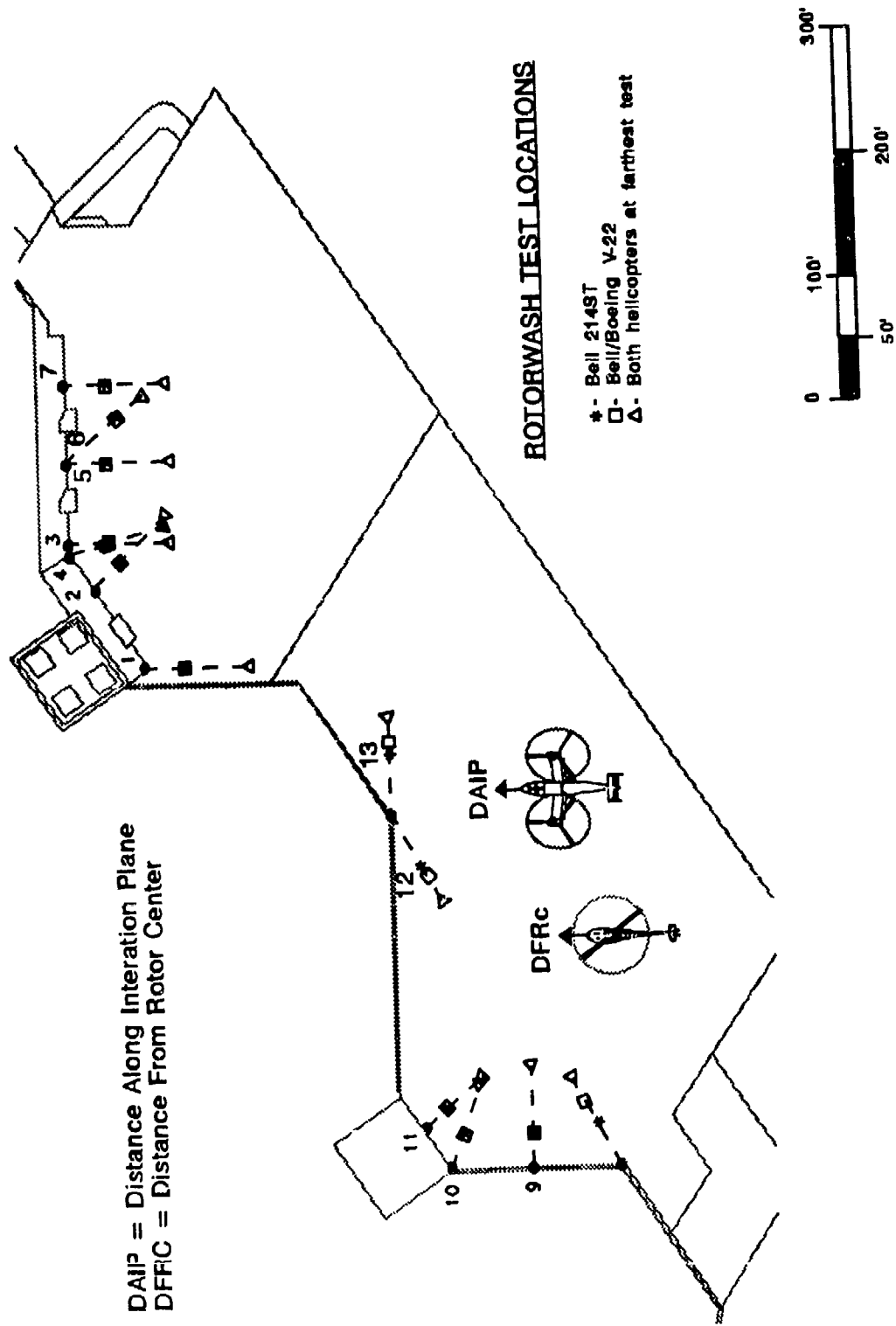


FIGURE 109 V-22 ROTORWASH FLIGHT TEST DATA CONVERTED FROM UNITS OF KNOTS TO PSF FOR STRUCTURAL DESIGN PURPOSES

The wind tunnel test results are most interesting because data of this type are not known to exist from any other source. A summary of these results is presented in table 16. Figure 111 identifies the critical locations in the table. As expected by CPP engineers, in each of the peak wall pressure comparisons and two of the four (but less critical) mean wall pressure comparisons, mathematically predicted results exceed measured test data. This occurs because the structure tends to integrate (or average) the effects of the rotorwash velocity profile over a finite height and width. Phrased another way, the structure is large enough to effect the shape and characteristics of the velocity profile. The mathematical model predictions do not consider the presence of any object large enough to significantly affect the flow field.



Source: Reference 12.

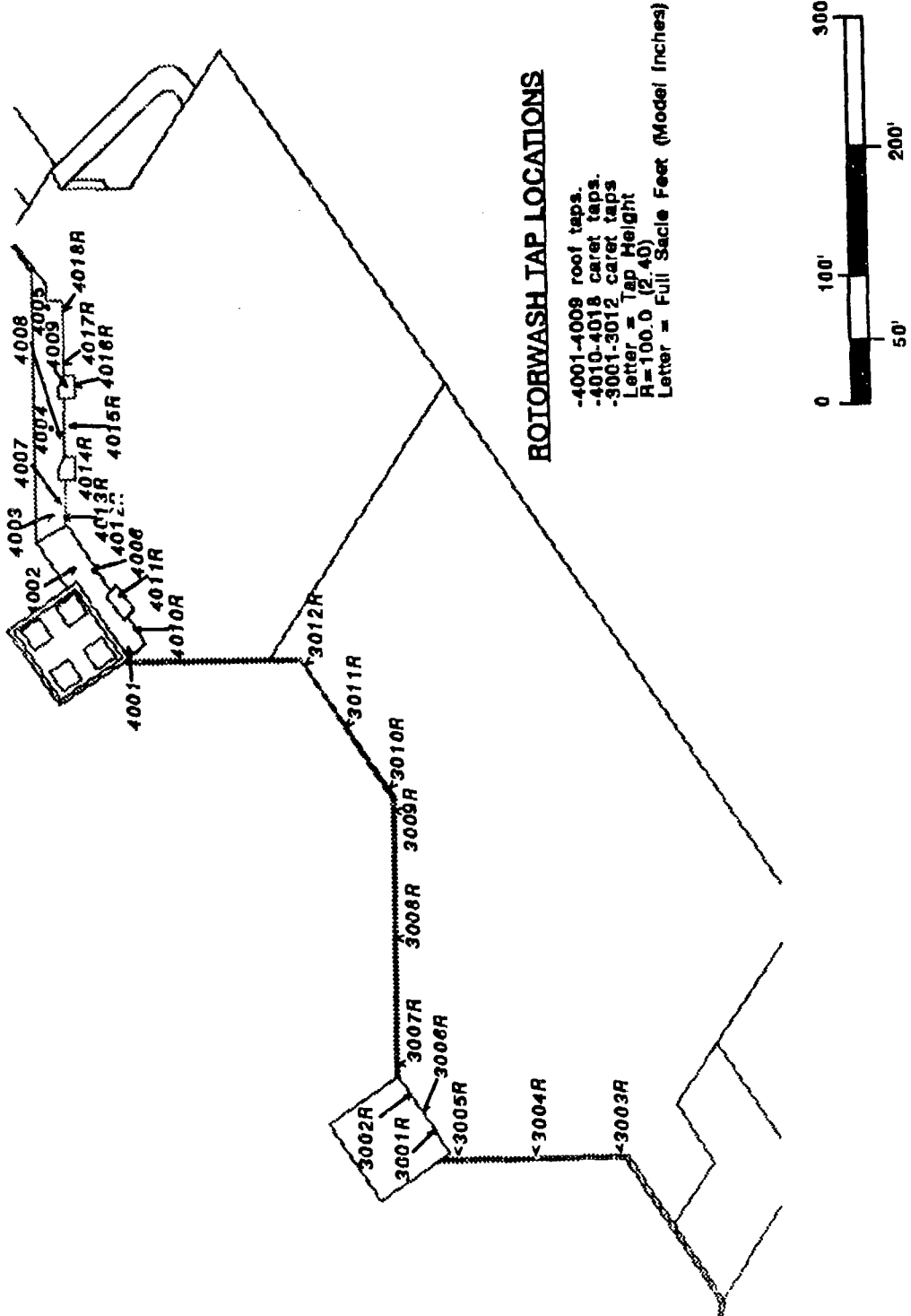
FIGURE 110 TEST LOCATIONS FOR ROTORCRAFT MODELS ON THE DALLAS VERTIPORT

TABLE 16 LARGEST PEAK AND MEAN PRESSURE MAGNITUDES
INDUCED BY ROTORCRAFT

Aircraft	Aircraft Location	Distance from Wall (feet)	Tap Number	Largest Peak or Mean Pressure (psf)	Predicted Pressure from Reference 47 (psf)
PEAK PRESSURES					
V-22	13	40	3011	33	40
V-22	5	100	4014	21	25
214ST	10	40	3005	21	26
214ST	8	100	3004	10	13
MEAN PRESSURES					
V-22	10	40	3006	19	27
V-22	5	100	4014	9	8
214ST	10	40	3005	12	15
214ST	13	100	3011	6	5

Conclusions from this wind tunnel test are summarized below as guidelines until additional data can be obtained. As would be expected with any first time experiment, lessons were learned that will result in acquisition of even better results whenever similar tests are conducted in the future. For example, improvements to the rotorwash-generating scale model used in the wind tunnel have already been identified. Also, full-scale pressure measurements on a specially designed test structure are being proposed to provide validation data for future wind tunnel tests as well as analytical structural design programs. General conclusions are listed below.

1. If operational procedures require the V-22 and other large rotorcraft to ground taxi to and from critical ramp locations (where rotor thrust levels are dramatically reduced), then high peak pressure loadings can be assumed to act only a few times during the structural life of building. Under these conditions building code requirements for aviation-related structures are sufficient for design purposes.
2. Pressure loads of 10 to 20+ psf for large skid gear helicopters such as the Bell 214ST should be considered frequent enough in occurrence to alert structural design engineers to the possibilities for fatigue damage over



Source: Reference 12

FIGURE 111 PRESSURE TAP LOCATIONS FOR ROTORWASH TEST OF THE DALLAS VERTIPORT

the lifetime of a facility. This is particularly true for openings in the structural walls containing windows, doors, and access panels. Fatigue damage at these locations can result in water damage over extended periods of time, as well as outright structural failure.

An example of a scenario that has not been analyzed in the literature that has an impact on structural-related separation guidelines is the situation where a sudden blast of rotorwash impacts a partially open or unlocked door or window, or one that is unexpectedly opened. No simple procedure is known to exist for analyzing this problem, especially when one considers the numerous types of doors and windows and installation orientations that are possible. It is possible that dampers may need to be required on all openings. Therefore, these types of potential hazards should be carefully identified in any preliminary structural design review so that procedures can be addressed to eliminate these types of potential problems.

5.5.2 Damage to Light Structures

Several mishaps and the operator survey results contained in reference 62 were reviewed for details involving rotorwash damage to light structures. One of the documented mishaps available for review, involving broken windows, is discussed in a later section since a personnel injury occurred. Two other mishaps, both involving tents, are discussed in the following paragraphs because they provide examples of mishaps that could have been avoided.

The first of the tent-related mishaps involved a large military Sikorsky CH-54L. Winds were reported to be only 3 knots. The helicopter picked up a 6,000-pound load and departed the area. As the helicopter passed through 50 feet AGL, the flight engineer observed one tent in a group of tents 300 feet away become airborne. This tent struck other tents and significant damage was later reported. The report also indicated that the tent may not have been tied down properly. No personnel injuries were reported; however, little doubt exists that they could have occurred. A mathematical analysis indicates that peak rotorwash-generated velocities at this distance were probably no greater than 25 to 30 knots.

The second reported mishap involved a much smaller helicopter, a Bell 206L. Mathematical modeling of this particular mishap was not possible because of the unknowns involved. However, very important lessons can be learned from this particular incident. The helicopter was making a standard approach to a marked helipad, and winds were less than 15 miles per hour. As the helicopter passed over the 8- to 10-foot high fence that surrounded the helipad area, a tent was blown down and totally destroyed. The skid height of the 206L as it passed over the

fence was 50 to 60 feet, and the pilot was adding power to arrest the helicopter's rate-of-descent. The tent was located just outside the fence in an RV park. Large warning signs were posted on the fence. Yet, on numerous occasions towels and other objects were observed drying on the fence. Fortunately, no people were injured in this mishap. The most disturbing aspect of this incident is that it was noted in the summary that this type of mishap occurs each year at this site.

Several lessons can be learned from these two incidents. One lesson is that tents are very susceptible to rotorwash. In the first mishap, the collapse was at 100 yards with only a 3-knot ambient wind. The critical threshold velocity in this mishap appears to be approximately 30 knots. In the second mishap, the most alarming fact is that a clearly hazardous scenario is being perpetuated on a permanent basis. Even though signs clearly warn campers of helicopter operations and potential hazards, lack of respect for these warnings has created a high probability that a serious injury will eventually occur. A second alarming aspect of this mishap becomes apparent if the long list of mishaps involving objects blown about by rotorwash is reviewed in section 5.7.1. A study of this list clearly indicates that the recreational vehicle (RV) park is a serious potential hazard to overflying rotorcraft. Therefore, the development of guidelines controlling the establishment of camping sites and the use of tents in close proximity to public-use heliports and vertiports should be a goal for the future. This may require zoning ordinances to prevent certain types of development immediately beyond fenced-off approach and departure zones.

5.5.3 Summary of Analysis Results

A brief analysis of the hazard potential of rotorwash-induced loads, as applied to buildings or structures, has been made and compared to available test data and uniform building code guidelines. Results indicate that these peak pressure loads do impact the heliport/vertiport design process and should be investigated for the limiting sizes of rotorcraft that are expected to operate from a particular facility. However, except for very large rotorcraft, it can be expected that in most cases the limit design requirements will be less severe than those imposed by high wind requirements in uniform building codes. Instead, the most important design issue will probably be related to fatigue characteristics. High frequency rotorcraft operations in close proximity to a structure can easily have the potential to induce localized peak loadings in the 10 to 20 PSF range. Many structural components associated with windows, doors, and access panels are at risk over extended periods of time when exposed to these types of repeated loadings and normal weathering effects. A good operational plan for how rotorcraft are operated in close proximity to structures is the best way to significantly reduce the impact of rotorwash-induced loads.

Even though a conservative position has been taken in this section with respect to rotorwash-induced loads, any projected separation guidelines resulting from a detailed analysis would not be expected to be severe. Examples of the development of guidelines are provided in the "How To" examples in sections 6 and 7. Graphs of the maximum expected pressure load for numerous types of rotorcraft as a function of distance from the rotor center are provided for design purposes. As will be shown by these graphs, the vast majority of rotorcraft in civilian use today are not capable of generating high structural loads even in crosswinds of up to 9 knots. Only large rotorcraft weighing in excess of 15,000 to 20,000 pounds should be restricted for structural reasons from hovering much less than 100 feet (or approximately three rotor radii) from buildings. Ironically, in the majority of situations, most pilots of large rotorcraft are inclined for other safety reasons to take off and land much farther away from buildings than structural limitations would require.

A brief mathematical model investigation of the affect of ground and disc edge vortices on structural design indicated that separation requirements would be less stringent than those required for the wall jet. Therefore, no results are presented for these types of forward flight related hazards. Good procedural common sense also suggests that rotorcraft operating in these flight regimes will be kept clear of structures for other safety reasons.

5.6 ROTORWASH EFFECTS ON GROUND VEHICLES

Rotorwash-related mishaps involving ground vehicles can usually be classified as one of three groups. The first group involves mishaps where objects are blown into vehicles. Damage can be caused by large objects (i.e., an oil drum), or small objects (such as gravel or sand) that result in scratched paint or broken glass. The reader is referred to section 5.7 for further discussion with respect to these types of mishaps. The second group of mishaps involves damage to camper shells (on pickup trucks) and automobile sunscreens (commonly found on hatchback models). The third group of mishaps involves damage to small vehicles (i.e., motorcycles).

5.6.1 Mishaps Involving Camper Shells and Automobile Sunscreens

Three mishaps involving damage to camper shells and automobile sunscreens were identified for possible analysis. In two of the mishaps, a Bell UH-1 overflew a parking lot and the camper shell was reported to have blown off the back of a pickup truck onto other cars. In one instance, the UH-1 was reported at approximately 25 to 30 feet above the parking lot. In the second mishap, the camper shell was reported to have been attached with 1/2 inch bolts without washers. No other significant details were provided. The only lesson that can be learned from these

two mishaps is that camper shells are susceptible to damage or destruction by rotorwash.

The mishap involving an automobile sunscreen occurred in a parking lot adjacent to a hospital helipad (helipad dimensions are 90 x 116 feet). The automobile was parked approximately 40 to 45 feet to the right of the helipad approach path. As a Sikorsky S-76 approached the pad for a landing, the sunscreen was blown up and off the rear window of the car. The sunscreen was reported to have been unlatched at the time (car not driveable) and the hinges were broken off during the mishap. The altitude of the S-76 when it slowly passed the car was reported at 40 to 50 feet AGL. Atmospheric conditions at the time are unknown.

Using the above reported information, a simple analysis of the mishap was conducted. If the wind was calm at the time of the incident, estimated peak rotorwash velocities, depending on the actual height above ground of the sunscreen, could have been between 45 and 55 knots (or slightly greater if a decelerating flare maneuver was made). This estimate also assumes that other cars were not parked between the damaged car and the helicopter (available analysis tools will not estimate velocities for complex scenarios). The predicted velocities could have been as high as 70 knots if the ambient wind was blowing at 9 knots toward the car from the direction of the S-76.

The most likely conclusion that can be made from this simple analysis is that the sunscreen was probably blown off by a lower rotorwash velocity (less than 55 knots). The unknown threshold velocity was probably generated when the helicopter was farther out on the approach path in the process of decelerating to a hover (comments said mishap occurred as helicopter approached). Even though too little information exists for development of quantitative separation guidelines, the mentioned distances should serve as a warning that even parked automobiles can be at risk at distances of less than 50 feet from the edge of a helipad.

5.6.2 Mishaps Involving Motorcycles

Two mishaps involving motorcycles were identified for analysis. Both mishaps involved unknown ambient winds and S-76 helicopters that were reported at mid gross weight. In the first mishap, the S-76 landed at a county park in a picnic area on an unprepared surface. While the S-76 was at 15 feet AGL, the motorcycle (type unknown) overturned at a distance of approximately 40 feet. The orientation of the motorcycle to the helicopter was not reported. In the second mishap, the S-76 landed at the same hospital helipad as was mentioned in the previous section. The overturned Harley-Davidson motorcycle was parked so that the left side of the motorcycle was pointed toward the passing helicopter. The distance between the helicopter and motorcycle was approximately 70 to 75 feet. The helicopter was reported at

40 to 50 feet AGL when it passed the motorcycle. Windshields and paint were damaged in both overturning mishaps.

The first task in the analysis of the motorcycle mishaps was to experimentally measure the overturning moments for a Harley-Davidson motorcycle. The smaller model Harley-Davidson was chosen to ensure that the measured moments were probably the lowest that would exist for this brand of motorcycle. The overturning moments were measured in the direction away from the kickstand, since the motorcycle overturns much easier in this direction, using a calibrated spring force gauge attached to a harness about the motorcycle. This direction is also the direction the Harley-Davidson reportedly overturned in the second mishap. The overturning moment measured with the front wheel turned toward the kickstand was approximately 117 foot-pounds. With the wheel turned away from the kickstand, the measured moment was considerably less, approximately 66 foot-pounds. Overturning moments for the numerous other types of motorcycles were not measured. However, it is quite probable that the critical moment values for some of these motorcycles are less than 66 foot-pounds.

The second task in the analysis was to develop a simple mathematical model to describe the mishap. In this model it is assumed that the overturning moment due to a component of the motorcycle weight (due to the tilt of the motorcycle on the kickstand) will be exactly counteracted at the instant of overturning by an applied aerodynamic moment. The simple equation describing this relationship is:

$$M_W = (Z_A) (F_A) \quad (70)$$

where,

M_W = measured motorcycle overturning moment, foot-pounds

Z_A = moment arm of the applied aerodynamic force, feet

F_A = applied aerodynamic force, pounds

This equation can be expanded to calculate the required overturning rotorwash velocity by substituting equation 71 into equation 70.

$$F_A = (S_M) (C_D) (0.5) (\rho_A) (V_C)^2 \quad (71)$$

The resulting equation is:

$$V_C = \sqrt{\frac{M_N}{(1.43)(Z_A)(\rho_A)(S_M)(C_D)}} \quad (72)$$

where,

V_C = critical overturning velocity, knots (the 1.68894 feet/second to knot conversion is included in the equation)

ρ_A = air density, slugs/feet³

S_M = projected side area of the motorcycle, feet²

C_D = motorcycle non-dimensional drag coefficient

Equation 72 was evaluated over a range of values for both the motorcycle drag coefficient and the length of the applied aerodynamic moment arm on the motorcycle. Exact values for these parameters are unknown for a Harley-Davidson. The value of the drag coefficient was varied from 0.25 to 1.0, and the length of the moment arm was varied from 2.3 to 2.9 feet. The air density used was 0.00226 slugs/feet³. A rough estimate of the projected side area, based on measurements of the motorcycle, was 17.5 square feet. Figure 112 presents a summary of the calculated results.

If the drag coefficient in figure 112 is assumed to be that for a solid flat plate, approximately 1.0, the critical velocity is predicted to be between 20 and 23 knots, depending on which moment arm is selected. At the other extreme, a drag coefficient of 0.25, the predicted critical velocity is 40 to 45 knots. The critical velocities for a drag coefficient of 0.5, probably the most realistic value, vary from 28 to 31 knots. One must keep in mind that the applied velocity in this case is a uniform velocity over the whole projected surface area.

The final analysis task for both reported mishaps is to estimate S-76 peak profile velocities at mid gross weight for both 0 and 9 knot winds. These peak velocities were estimated at 40 and 70 feet from the center of the rotor for the first and second mishaps, respectively. Results are presented in table 17.

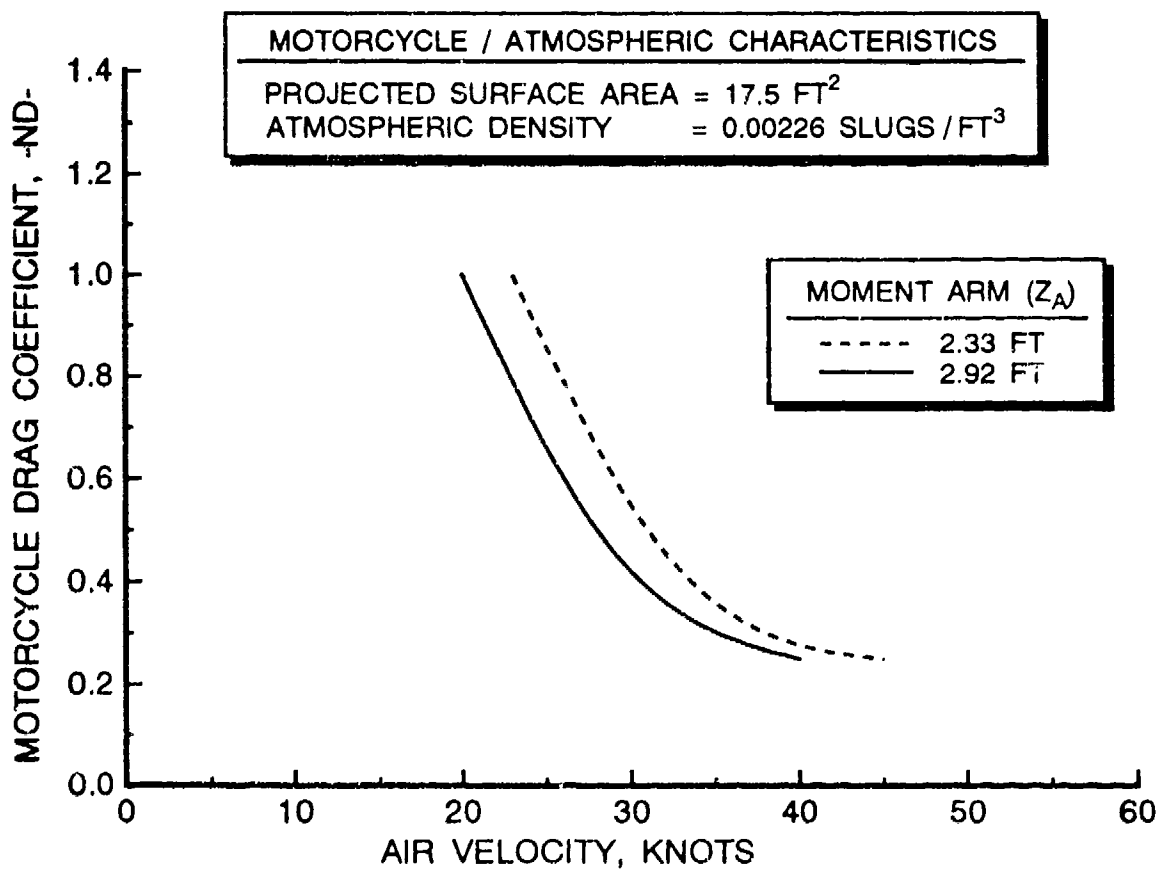


FIGURE 112 ESTIMATED THRESHOLD OVERTURNING VELOCITIES FOR A SMALL HARLEY-DAVIDSON MOTORCYCLE AS A FUNCTION OF DRAG COEFFICIENT AND APPLIED MOMENT ARM LENGTH

If the results presented in table 17 are compared to the calculated critical overturning moment velocities in figure 112, an evaluation of the two reported mishaps can be made. The reported position of the unknown type of motorcycle in the first mishap was 40 feet from the S-76 when it overturned. Calculated motorcycle overturning moment velocities are considerably exceeded by the estimated S-76 rotorwash velocities for all motorcycle drag coefficients equal to and greater than the 0.5 value. The required critical overturning velocity may even be exceeded in a 0 knot ambient wind with a flat plate drag coefficient approximately equal to 1.0. These results lead to one of four possible conclusions: either the analysis methodology or input data are incorrect; the motorcycle characteristics are much different than the measured Harley-Davidson characteristics; the motorcycle was parked in a different way than the methodology assumes; or it is always

TABLE 17 ESTIMATED SIKORSKY S-76 PEAK ROTORWASH
VELOCITIES AT 1.0 AND 3.5 FEET AGL

Distance From Rotor (feet)	Ambient Wind Velocity (knots)	Height Above Ground (feet)	Peak Rotorwash Velocity (ft/sec)
40	0	1.0	50
		3.5	31
40	9	1.0	67
		3.5	47
70	0	1.0	38
		3.5	32
70	9	1.0	54
		3.5	48

Note: S-76 Gross Weight = 8,000 lb

possible that the S-76 was farther away than 40 feet when the motorcycle actually toppled (perhaps the final separation distance was 40 feet?). If the motorcycle is a Harley-Davidson with the wheel pointed toward the kickstand, the overturning moment would be considerably higher. Also, if the motorcycle was parked at an angle to the rotorwash flow or another type of motorcycle, the projected side surface area might be considerably reduced. Unfortunately, the "what ifs" can continue forever. The key result is that straightforward calculations demonstrate that the rotorwash velocities were more than sufficient to topple a motorcycle.

The reported separation distance in the second mishap, which involved the Harley-Davidson, was 70 to 75 feet. The critical overturning velocity for a drag coefficient of 0.5 (28 to 31 knots) is just slightly exceeded by the calculated S-76 peak velocities for a 0 knot wind condition (32 to 38 knots). With the wind at 9 knots, the estimated S-76 velocities (48 to 54 knots) just slightly exceed the critical values required for the lowest evaluated drag coefficient (40 to 45 knots). Even though correlation is much improved for this mishap, the conclusions discussed in the previous paragraph are equally applicable to this particular scenario.

5.6.3 Conclusions from an Analysis of Mishaps Involving Ground Vehicles

Several conclusions can be reached from the analysis of mishaps involving rotorcraft and ground vehicles. First, there are clear implications that low altitude overflights of parking areas are always risky. Even if rocks and sand are not a hazard to paint, the probability that damage will occur to camper shells, hatchback sunscreens, and motorcycles is significant.

Unfortunately, threshold overturning velocities for motorcycles could not be conclusively determined in this analysis. More research will have to be devoted to this subject. However, indications do exist that point to the critical velocity being in the range of 30 to 40 knots. Recommendations from this analysis are listed below.

1. Motorcycle parking areas should always be located as far away from rotorcraft approach paths and landing areas as possible.
2. Signs directing camper shell equipped vehicles should be posted to caution owners to park away from approach and landing areas.
3. Automobiles should be provided general warnings that rotorcraft may overfly parking areas, causing sand, dirt, and debris to be blown about at high velocities. Any warnings should emphasize that all doors, windows, sunroofs, sunscreens, etc. be closed and secured.

5.7 ROTORWASH HAZARDS INVOLVING ENTRAINED OBJECTS AND DEBRIS

The creation of an environment in which particles, debris, or large objects are entrained and thrown about as projectiles in the rotorwash flowfield is one of the most serious rotorwash-related hazards that can be encountered. Unfortunately, as stated in reference 22, the prediction of particle or projectile velocity as a function of time and place becomes a monumental task if the effects of most variables are to be included. Furthermore, even if time were available to develop exact solutions, experimental data do not exist to correlate with most solutions. Therefore, one would expect that any methodology that is to be developed for the prediction of safe separation distances would have to be based on very general engineering theory (at most) and a lot of "good common sense."

5.7.1 Historical Data

The effort to develop a particle/projectile hazard avoidance methodology to estimate safe separation distances was initiated with a literature review of the subject. Unfortunately, little research was identified that has been devoted to this topic. Reference 21 states that "full scale experimental investigations with simulated or actual VTOL aircraft operating over sandy terrain with disc loadings as high as 50 psf have produced only superficial damage to the modern airframe." Calculations are provided to further substantiate this statement. Since rotorcraft, as defined in this study, typically operate at disc loadings of less than 20 psf, the assumption has been made that sand and small pebbles will not (in general) be a significant hazard to metal structures (i.e., helicopter airframes, ground equipment, hangers). However, it cannot be assumed that these

particles will not become hazardous to personnel or to certain other types of material (i.e., pitting of plastic windshields or paint erosion). Structures like rotating rotor blades where extremely high impact velocities occur are also at risk even though they may be constructed of metal or other substantial materials.

Operational mishap data reveal that objects or debris that have a large frontal area to weight ratio can become entrained in rotorwash along the ground and become a significant hazard. Examples obtained from U.S. Army mishap reports include:

1. sheet metal, corrugated metal, wood, or plastic panels (typically up to 3 square feet),
2. landing zone nylon/metal markers,
3. flare/personnel parachutes,
4. dead tree branches and brush,
5. nylon, cloth, and plastic equipment bags as well as empty sandbags,
6. metal landing pad planking,
7. numerous rocks and other round objects (hitting equipment, breaking glass and windshields),
8. maintenance stands (blown on their sides and along the ground prior to impacting other rotorcraft), and
9. rotor blade box covers, ammunition boxes, empty 55-gallon drums, and tents.

Clearly, it can be determined from this brief list that the potential is almost unlimited for many types of hazardous projectile impact in the heliport environment, particularly where personnel may be involved.

5.7.2 Energy Based Analysis Methodology

Discussion presented thus far has provided some qualitative information on various types of projectile-related hazards found in the heliport environment and their impact damage potential. One method for quantitative prediction of particle/projectile hazard potential was identified in the literature in reference 21. This method assumes a no-wind hover condition and is based on the definition of minimum energy levels that can injure personnel or damage various types of material. To fully understand the assumptions, limitations, and theory associated with this first-order estimation methodology (as described by the authors), reference 21 should be consulted. The lack of

correlated experimental data, a concern that the authors acknowledged in numerous paragraphs, is the greatest limitation to use of the methodology. The analysis methodology is basically a spreadsheet calculation approach augmented as necessary with charts for obtaining experimentally derived or analytical functions. As an aid to practical understanding of the use of the method, an example is presented in the following paragraphs.

The first step in using the analysis technique is to define the subject rotorcraft of interest along with the operational scenario. In this example, three rotorcraft size classes are defined for use in calculations. These classes, the S-, M-, and H-sized vehicles, define the upper limit of the numerous types of rotorcraft presently in production (more will be mentioned with respect to these size classes in section 6). Characteristics for these vehicles are as follows:

PARAMETER	ROTORCRAFT SIZE CLASSES		
	S	M	H
NUMBER OF ROTORS	1	1	1
ROTOR RADIUS, FEET	15.0	25.0	40.0
GROSS WEIGHT, LBS	4,730	19,350	73,390
DISK LOADING, PSF	6.7	9.86	14.6
FUSELAGE DOWNLOAD, PERCENT	1.5	2.5	5.0
HEIGHT ABOVE GROUND, FEET	30.0	30.0	30.0

These rotorcraft are evaluated at rotor heights above ground equal to approximately 30 feet. This rotor height generally insures that the maximum possible peak ground velocities are reached in the outwash flow.

The second step requires definition of the hazardous objects that are to be evaluated. Practically speaking, this task is almost impossible to accomplish when one considers the almost infinite variety of objects that exist in an airport or heliport environment. However, for the example in this section, several objects have been arbitrarily assumed. These objects are listed in table 18. After specification of each object type, the maximum drag area of each object must be calculated. An assumption of the procedure is that the largest projected surface area of the object is the one oriented in the direction of the flow field. Calculations must also be made for the size of the object's impact area (A_I). For a circular object, this surface area is the same as the drag area. For a rectangular object, this area is not well-defined. If the object impacts on a corner, there is much more potential for localized transfer of kinetic energy than there is if the impact area equals the

maximum drag area. In this example, the impact area is arbitrarily assumed to be equal to the smallest flat side of the object. The final preliminary calculation that is required is made for "insurance purposes." Each object should be evaluated to estimate the approximate minimum air velocity (V_{min}) required to produce enough drag force to lift the object's weight. This task is accomplished by evaluating the following equation for objects other than sand and water (see figure 113 for these particle types) where:

$$V_{min} = \sqrt{\frac{W_p}{0.5 \rho_A A_F C_D}} \quad (\text{feet/second}) \quad (73)$$

The variables in this equation are:

W_p = Particle weight (pounds)
 ρ_A = Atmospheric density (slugs/feet³)
 A_F = Maximum drag area (feet²)
 C_D = Drag coefficient (often assumed to be 1.0)

TABLE 18 CHARACTERISTICS OF AN ARBITRARY COLLECTION OF HAZARDOUS OBJECTS FOUND IN THE HELIPORT ENVIRONMENT

OBJECT TYPE	APPROXIMATE MASS, SLUGS	APPROXIMATE SIZE IN FEET	MAXIMUM DRAG AREA IN FT ²	IMPACT AREA IN FT ²
Sand (0.08mm)	5.0×10^{-11}	2.6×10^{-4} (diameter)	5.4×10^{-8}	5.4×10^{-8}
Sand (3mm)	2.65×10^{-6}	0.0099 (diameter)	7.6×10^{-5}	7.6×10^{-5}
Gravel	4.33×10^{-2}	0.25 (diameter)	4.9×10^{-5}	4.9×10^{-2}
Metal Lunch Box	0.031	$0.67 \times 0.58 \times 0.33$	0.39	0.19
Briefcase	0.25	$1.5 \times 1.16 \times 0.5$	1.74	0.58
Empty Barrel	1.24	2.0 (dia) \times 3.0 (hgt)	6.0	3.14

If the V_{min} value calculated in this step is equal to or greater than the predicted maximum velocities in the rotorwash flow field, the probability of the particle becoming completely airborne is minimal. In this example, the 0.25 feet or 3-inch diameter gravel will not become airborne for the S- and M-sized classes, because the required velocity to entrain and lift the particles is greater than 200 feet/second.
 (Note: 10^0 inches = 1 inch; 10^1 inches = 10 inches)

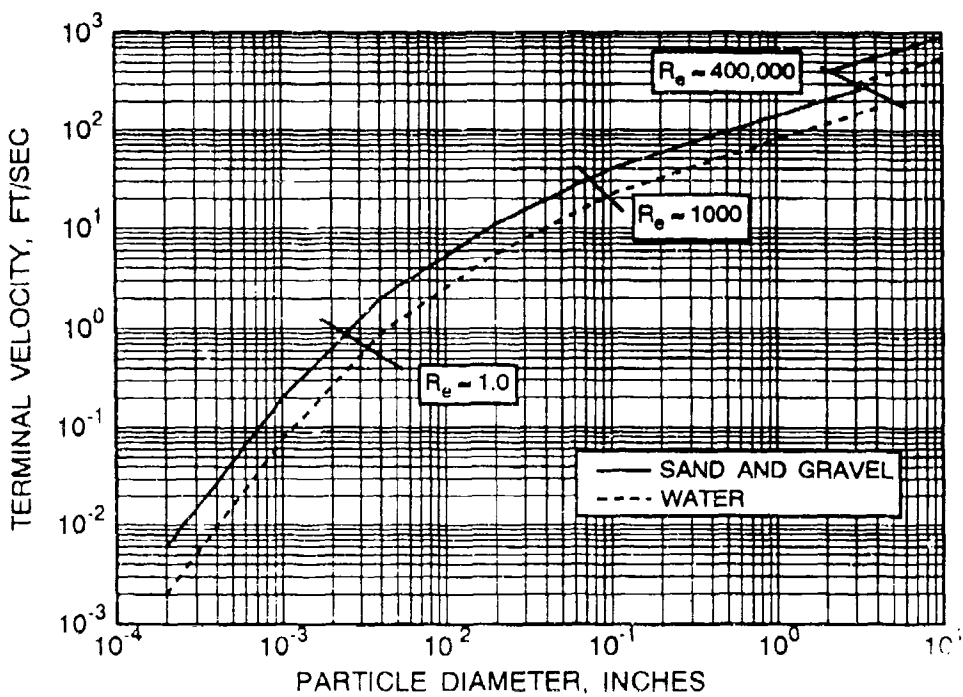


FIGURE 113 VARIATION OF PARTICLE TERMINAL VELOCITY WITH PARTICLE DIAMETER

Upon completion of the above preliminary calculations, the analysis methodology requires calculation of the size parameter (β), where:

$$\beta = \frac{4.24 R C_D \rho_A A_F}{m_p} \quad (74)$$

and

R = Rotor radius (feet)

m_p = Mass of the particle (slugs)

In this example, ρ_A is assumed equal to 0.0023769 slugs/feet³ and C_D is assumed equal to 1.0. The calculation of β is followed by calculation of the worst case particle velocity (V_p) that is described in figure 114 (figure 47 from reference 21) as:

$$V_p = \left(\sqrt{\frac{q_p}{\rho_A}} \right) \left(1 - \frac{1}{\sqrt{\beta+1}} \right) \quad (\text{feet/second}) \quad (75)$$

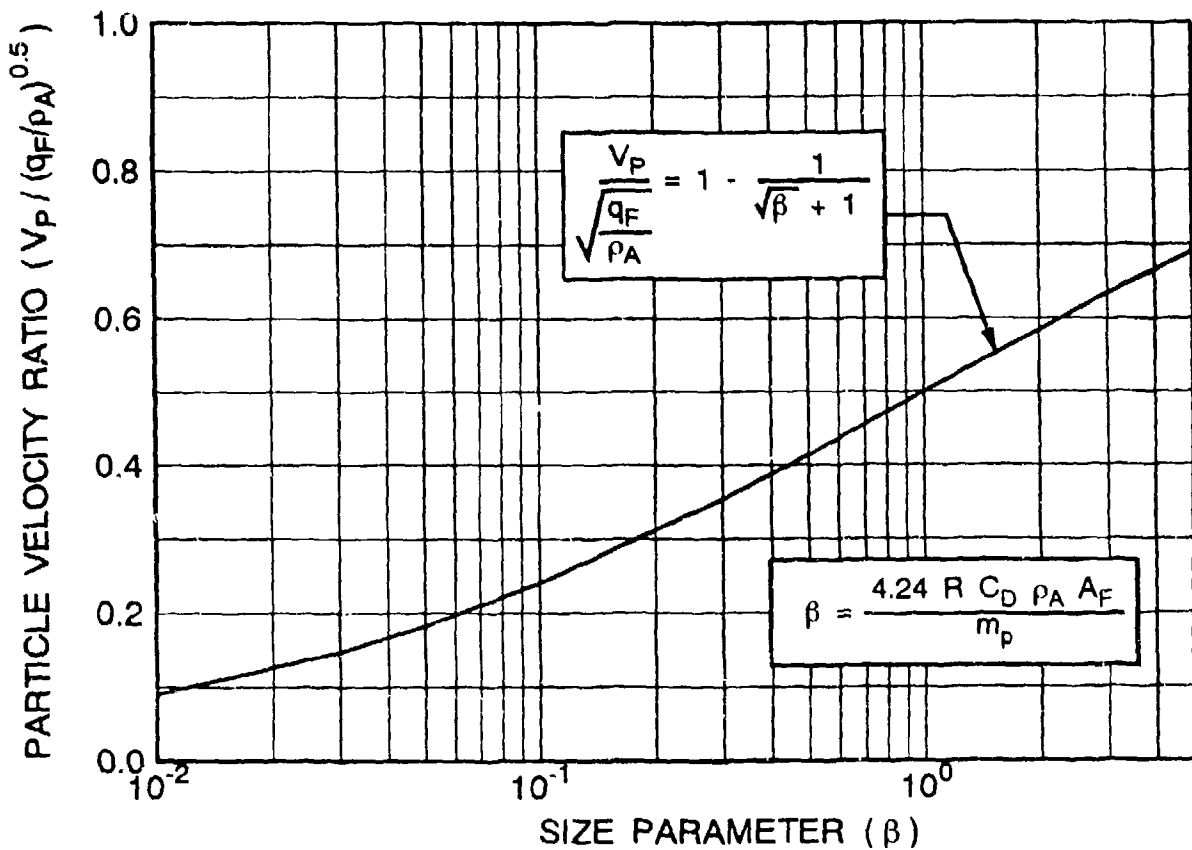


FIGURE 114 ENTRAINED PARTICLE VELOCITY RATIO AS A FUNCTION OF SIZE PARAMETER

The value for q_F is assumed for conservatism to be the maximum field dynamic pressure. For the three example rotorcraft configurations, this value is approximated using the mathematical models from section 3 and is presented in figure 115. The calculation of V_p is then used to compute the worst case impact energies and damage potential for the specific objects of interest. The energy of the object is the object's kinetic energy (E_p). This parameter is based on the object's density (ρ_p) and the square of the velocity (V_p).

$$E_p = 0.5 \rho_p V_p^2 \quad (\text{foot-pounds}) \quad (76)$$

Another value (E_p/A_I) can also be computed for the purpose of describing the actual localized energy that is released in an impact. The respective values that are associated with the six object types for β , V_p , E_p , and E_p/A_I are tabulated in table 19.

TABLE 19 CALCULATED VALUES FOR PARTICLE SIZE PARAMETER, VELOCITY, ENERGY, AND ENERGY-TO-IMPACT AREA RATIO FOR AN ARBITRARY COLLECTION OF OBJECTS

PARAMETER	OBJECT TYPE				
	Sand (0.08mm)	Sand (3 mm)	Gravel	Metal Lunch Box	Briefcase
β (-ND-)					
S Class	163	4.3	0.17	1.9	1.05
M Class	272	7.2	0.28	3.2	1.75
H Class	435	11.6	0.45	5.1	2.8
V_p (ft/sec)					
S Class	6	44	18	37	32
M Class	84	64	30	57	50
H Class	119	96	50	86	78
E_p (ft-lb)					
S Class	9.0×10^{-8}	2.6×10^{-3}	7	21	128
M Class	1.8×10^{-7}	5.4×10^{-3}	20		312
H Class	3.5×10^{-7}	1.2×10^{-2}	54		761
E_p/A_I (lb/ft)					
S Class	2	34	143	110	220
M Class	3	71	395	263	538
H Class	7	150	1102	605	1312
					1023

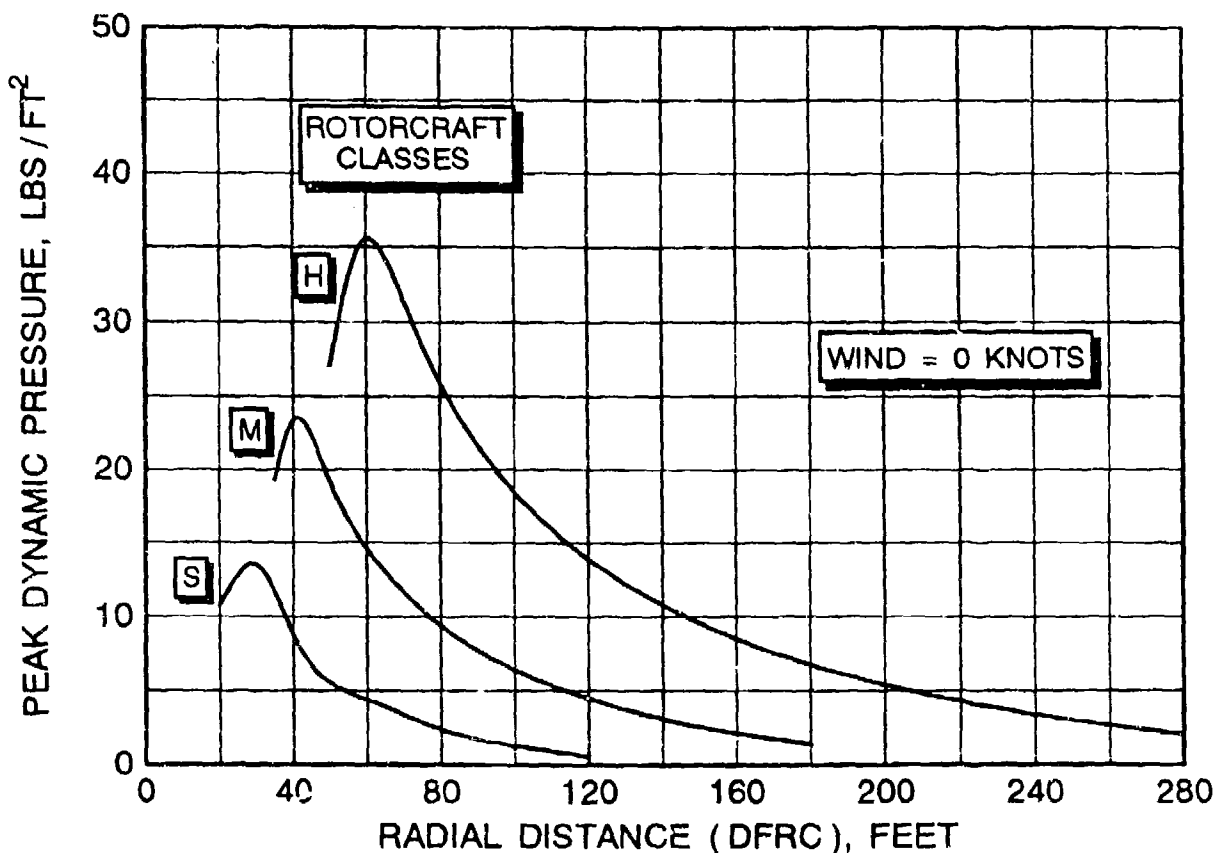


FIGURE 115 PEAK DYNAMIC PRESSURE AS A FUNCTION OF RADIAL DISTANCE FOR THE THREE EXAMPLE ROTORCRAFT CONFIGURATIONS

5.7.3 Available Test Data

As stated in the previous section, one of the weak points of the reference 21 methodology is the almost total lack of experimental data for correlation. In particular, very little can be said about the confidence level associated with calculation of the impact velocity, V_p , due to numerous factors. For example, impact velocity has been observed to be altered significantly by the way a rotorcraft approaches an object (i.e., from above versus laterally) and by the way an object is situated in a flow field. The interaction of ambient wind with objects and rotorwash is also ill-defined. Therefore, one area for future research (see section 8) must definitely be in the development of more experimental data for correlation purposes.

The small quantity of data that were identified for aiding in the development of separation guidelines were all taken from U.S. Army mishap reports. Several of these mishap summaries are listed below for the UH-1H and AH-1 helicopters in order to provide an example of the type of data available.

1. A UH-1H was parked on the medivac pad. Post flight of the aircraft revealed no discrepancies. Some hours later, the crew chief reported a broken plexiglass panel in the helicopter. The UH-1H that had been parked on the adjacent spot had hovered out during the intervening time period. Due to the high volume of loose rock found around the parking pads and in the sod hover lane, it is believed that the mishap was the result of rock debris thrown into the plexiglass.
2. During run-up and engine check, rotorwash blew a maintenance stand into the elevator of a nearby parked UH-1H. Locked wheels on the maintenance stand did not prevent it from being blown into the nearby helicopter.
3. After refueling at a civilian airport with a fixed refueling point, the pilot hovered his UH-1H out for takeoff. A 55-gallon garbage drum, located about 55 feet away from the helicopter, was blown about 20 feet into a parked car. Property damage to the car exceeded \$100.00.
4. A work stand was blown into a parked AH-1S during a blade tracking and alignment operation, damaging the helicopter. In addition to rotorwash, the ambient winds were gusting as high as 25 knots. The work stand had not been secured but it had been placed upon its side prior to the accident. Stands are recommended to be repositioned 100 feet from operating rotorcraft in the future.

If the assumption is made that spacing between UH-1H helicopters (summaries 1 and 2) is approximately one rotor radius when the blades are pointed toward the other helicopter (see figure 88), then the safe separation distance between the impact and the center of the "offending" rotorcraft is clearly greater than 72 feet due to simple geometry. A safe distance for avoidance of the barrel impact described in summary 3 is clearly greater than 75 feet. More will be discussed on this type of mishap in section 5.7.5. Lastly, the recommendation for safe separation of a maintenance stand (summary 4) is approximately 100 feet (several other summaries indicate that this value should clearly be in excess of 75 feet). While these data do not allow for correlation with any presented analytical method, they clearly aid in the application of "good judgment" to recommendations for safe separation guidelines.

5.7.4 Evaluation of Example Configurations Using Energy Methodology

The article/object characteristics used in the evaluation of the example rotorcraft configurations are summarized in table 19. The missing factor required for completion of the analysis is a definition for what should be considered hazardous. Values are

provided in section 5.1 for hazardous moments with respect to personnel that are evenly distributed across the body. These moment limits are 120 and 60 foot-pounds for personnel size classes "L" and "S", respectively. Different moment limits are appropriate when the forces are not evenly distributed.

Reference 44 states that the localized impact of projectiles on humans having energies in excess of 58 foot-pounds is incapacitating (this value can be reduced depending on numerous factors). This reference also provides information on the potential for damage to the human eye as defined for small particles (see figure 116). Almost without question, each of the particles/ objects being evaluated will result in damage to rotorcraft or aircraft if rotating components are struck, i.e., the rotor, engine, or propeller. The penetration potential of small particles to sheet metal of varying thicknesses can be estimated using data presented in figure 117.

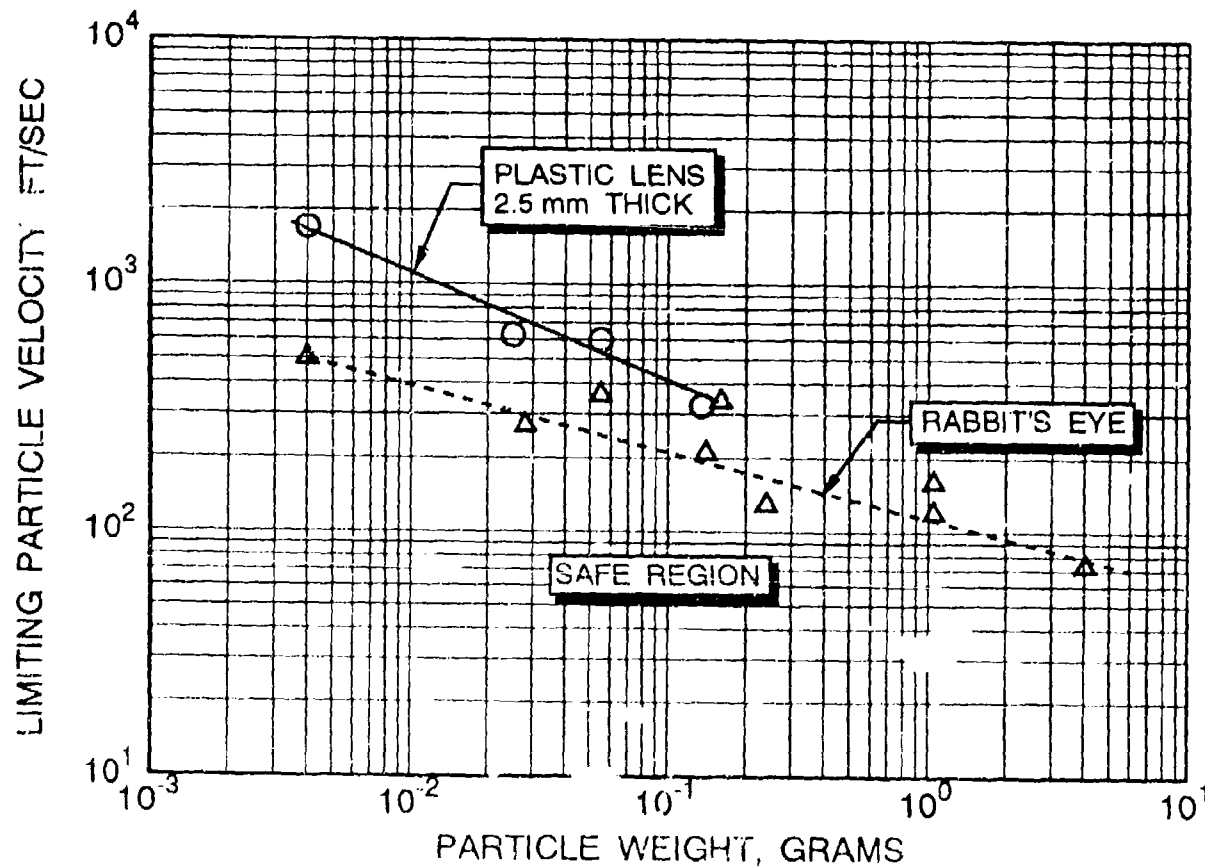


FIGURE 116 MAXIMUM PARTICLE VELOCITY AND WEIGHT LIMITS FOR EYE PROTECTION

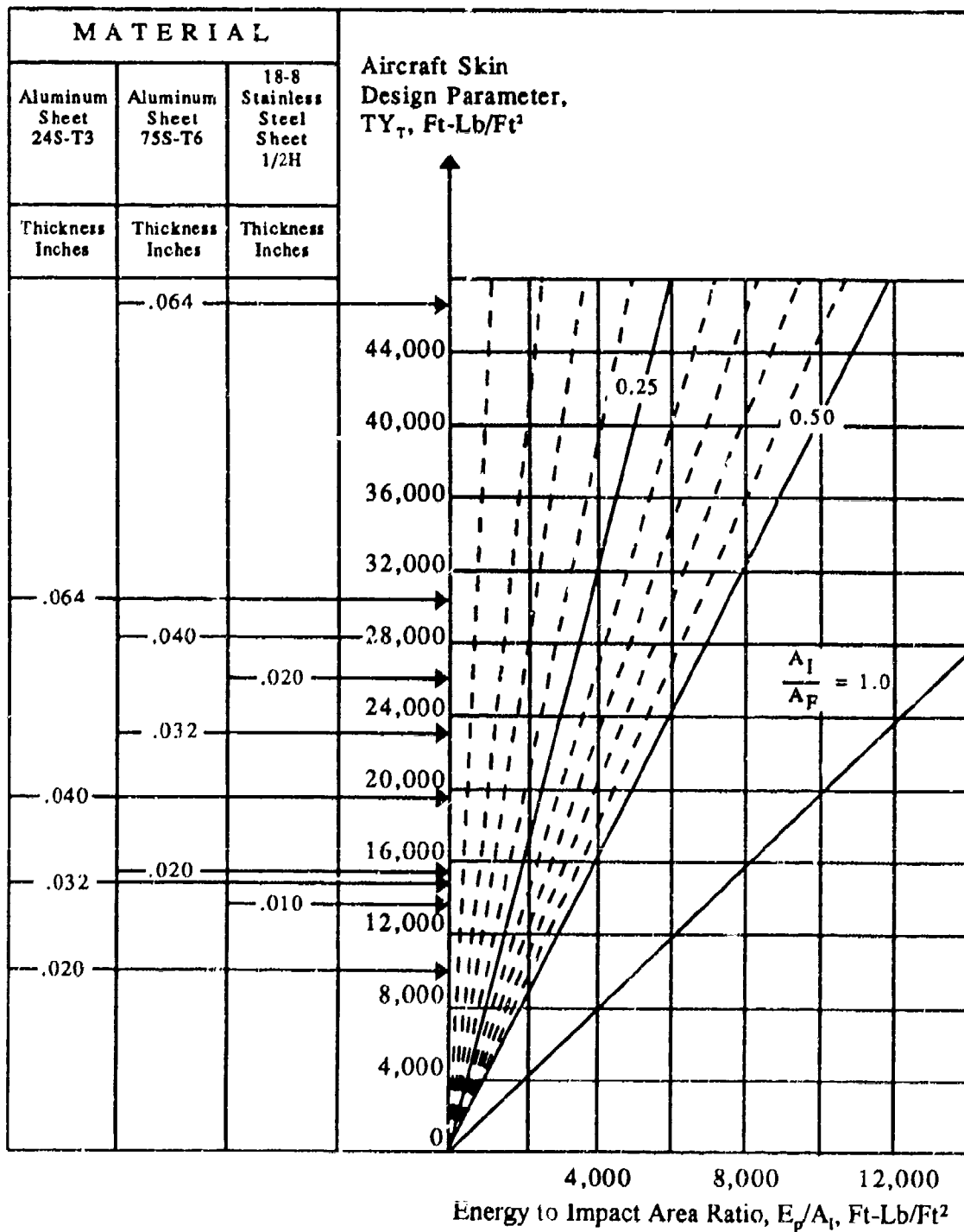


FIGURE 117 MINIMUM PARTICLE ENERGY REQUIRED FOR PENETRATION THROUGH AIRCRAFT SKIN

In further evaluating potential hazard impact on personnel, it can easily be demonstrated that the energies present in a flying lunch box, briefcase, or barrel are sufficient to injure personnel, particularly if struck by one of the object's corners. The UH-1H/AH-1 data (section 5.7.3) confirm this conclusion for rotorcraft configurations slightly smaller than the M-size class. The energy in 0.25-inch diameter gravel that results in a more localized release of energy on impact is certainly a hazard for H-sized rotorcraft based on the 58 foot-pound criteria. It would probably produce at least a bruise on personnel even for S-size rotorcraft if entrained in the flow field by some mechanism. The velocities of the two sizes of sand that vary from approximately 44 to 119 feet/second can be seen in figure 116 to be safe because the weight of the particles is less than 0.04 grams. The assumption that these particles are "safe" does not assume that they will not be bothersome to unprotected personnel. More discussion on this subject will be presented in section 5.8.

The potential for damage to sheet metal is evaluated using the data presented in figure 117. If the A_I/A_F and E_p/A_I ratios are evaluated, calculations indicate that none of the table 18 objects have the potential to actually pierce the aluminum sheets (however, energy levels required to dent or pit the metal are not known). It should be noted that if a barrel strikes on a sharp corner, it could release enough energy to do significantly more damage than just denting the metal.

The damage potential for each of the table 18 objects, except perhaps the smallest sand particle, is very significant if any rotating components are struck (i.e., rotor blade, propeller). Therefore, these types of impact must be avoided by insuring that these objects are not allowed in close proximity to any rotorcraft that has its rotor turning. Abrasion of rotating components will be discussed in greater detail in section 5.8.

The brief analysis presented in the previous paragraphs has primarily centered on providing general information on the damage potential of selected particles and objects. The important missing link up to this point is the lack of a safe separation distance associated with various particles and objects. The methodology, as stated in reference 21, is derived with the assumption that the airstream velocity is zero at three times the effective jet diameter from the vehicle. While this assumption is not true, as evidenced by flight test data, it is nevertheless a point at which most objects (particularly larger objects) will not be supported by a rotorwash flow field. This assumption is further supported by experimental data presented in reference 67 that states that large objects (i.e., rocks, dirt clods) are rarely propelled farther than 3.0 to 3.5 propeller diameters with twin-propeller VTOL aircraft (along the interaction plane). Certainly the impact energies of all objects should be significantly less at this distance than are calculated using this methodology. The effective jet diameter for rotorcraft is

approximately 0.707 times the actual rotor diameter, calculated using momentum theory. If this calculation is made for each of the three example rotorcraft configurations, safe separation guidelines from most large particles and objects might be proposed as follows:

TYPE CLASS	ROTOR RADIUS IN FEET	SAFE SEPARATION DISTANCE, FEET
S	15	65
M	25	110
H	40	170

In the case of the UH-1H and AH-1 data presented earlier, where the respective rotor radius values are 24 and 22 feet, the suggested separation guideline of approximately 110 feet certainly appears to be a reasonable value. The majority of the mishaps (see section 5.7.3) were hypothesized to occur around 75 feet. This guideline is also quite compatible with the recommended maintenance stand requirement for a 100-foot separation distance.

5.7.5 Mishaps Involving Oil Drums

Two mishaps involving oil drums were investigated as examples of mishaps that occur when rotorwash upsets large objects. These types of mishaps are serious because they usually occur unexpectedly and the large object mass can produce substantial damage. More often than not, these objects have large exposed surface areas and are the types of objects most people would not expect to be affected by rotorwash.

The first of the two analyzed mishaps involved the overturning of a 55-gallon oil drum by a Bell UH-1H at an airport refueling site. The drum was overturned and blown across the ground approximately 20 feet into a parked automobile. The UH-1H hover-taxied by the drum at a distance estimated to be 55 feet while repositioning for takeoff. The damage claim in this mishap was minor, only \$103.40, but it could have been much more serious had something or someone else been struck.

The second mishap involved a Bell 206L Long Ranger and an empty oil drum on an offshore drilling rig. The drum, which was supposed to have been tied down, was blown over and off the edge of the rig helipad during takeoff. The drum landed on a vessel that was making repairs to the rig. An undisclosed injury was subsequently reported for a crewman. Total damages, if any, were not disclosed.

5.7.5.1 Analytical Model of Mishaps Involving Oil Drums

The initial task in the analysis of these two mishaps was to acquire information on the amount of applied moment required to overturn an empty oil drum. Since information on this subject was not identified in any reference book or report, a simple experiment was conducted to measure the moment. The 55-gallon drums used in the experiment were located in a park on a grass surface and were being used as waste receptacles. The measured overturning force was applied to the top of the drum through a harness fitted around the drum. This force was measured with a calibrated spring force gauge and multiplied by the moment arm of 33 inches to obtain the overturning moment. Drums containing varying levels of refuse, as well as empty drums, were measured. The results are presented in figure 118. However, several items related to the experiment must be considered prior to use of the data. These items are listed below.

1. It was apparent during the experiment that the weight of the refuse in the drums had a significant impact on the results.

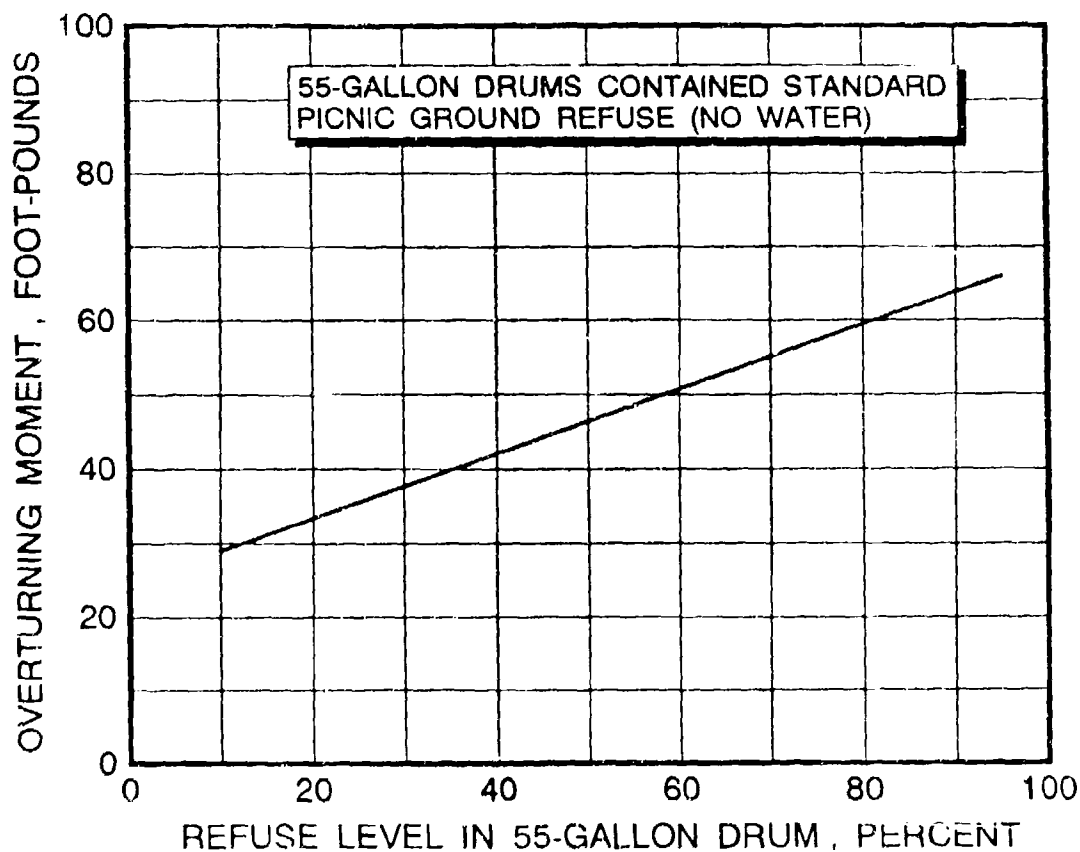


FIGURE 118 55-GALLON OIL DRUM OVERTURNING MOMENTS

2. Drums that were more than one-half full sometimes tended to slide across the grass and were not inclined to overturn as easily.
3. If water or oil had been contained in the bottom of the drums, which was not the case in this experiment, the fluid would have significantly increased the measured overturning moment. The drums would then have been more likely to slide before overturning if they were not constrained along the bottom edge.

The second analysis task was to estimate a generic velocity profile that would produce the required overturning moment for an empty oil drum, approximately 28 foot-pounds. This task was accomplished by dividing the drum into 17 equal segments and iteratively integrating calculated UH-1H velocity profiles from 0 to 33.5 inches until the calculated overturning moment exceeded the critical value. This procedure (and the equations involved) parallels the procedure specified in section 5.1 that is used to calculate the personnel overturning moments. The total projected drum surface area used in these calculations was approximately 5.3 square feet (this value is based on the maximum diameter of the drum and does not take into account the effect of the ridges along the side that slightly reduce the projected area). The coefficient of drag (C_D) was estimated as approximately 0.65 from reference 49. Air density used in the calculations was 95 percent of sea level standard day conditions. The approximate generic velocity profile found to produce the critical overturning moment value using the above values is documented in figure 119. The peak velocity along this profile is approximately 47 knots at a height of 8 to 10 inches above ground level and is reduced to approximately 38 knots at 33.5 inches. If a constant velocity profile is assumed for the sake of simplicity, the critical velocity is approximately 43 knots. With completion of this task, it was then possible to further analyze each of the two oil drum mishaps.

5.7.5.2 Analysis of Mishaps Involving Oil Drums

The distance at which critical velocity profile characteristics are exceeded for the mishap involving the UH-1H and the automobile is determined from figure 88. If the peak hover rotorwash velocity curve for a 0-knot wind is reviewed, the 47-knot threshold velocity is exceeded when the oil drum is less than 42 feet from the center of the rotor. Along the 9-knot wind curve, the peak velocity is exceeded at distances less than approximately 90 to 100 feet. These results tend to indicate that the ambient wind occurring during the mishap was probably less than 5 knots. Unfortunately, the actual ambient wind velocity was not recorded. It is also a bit presumptuous to assume that this analysis approach is so exact as to be capable

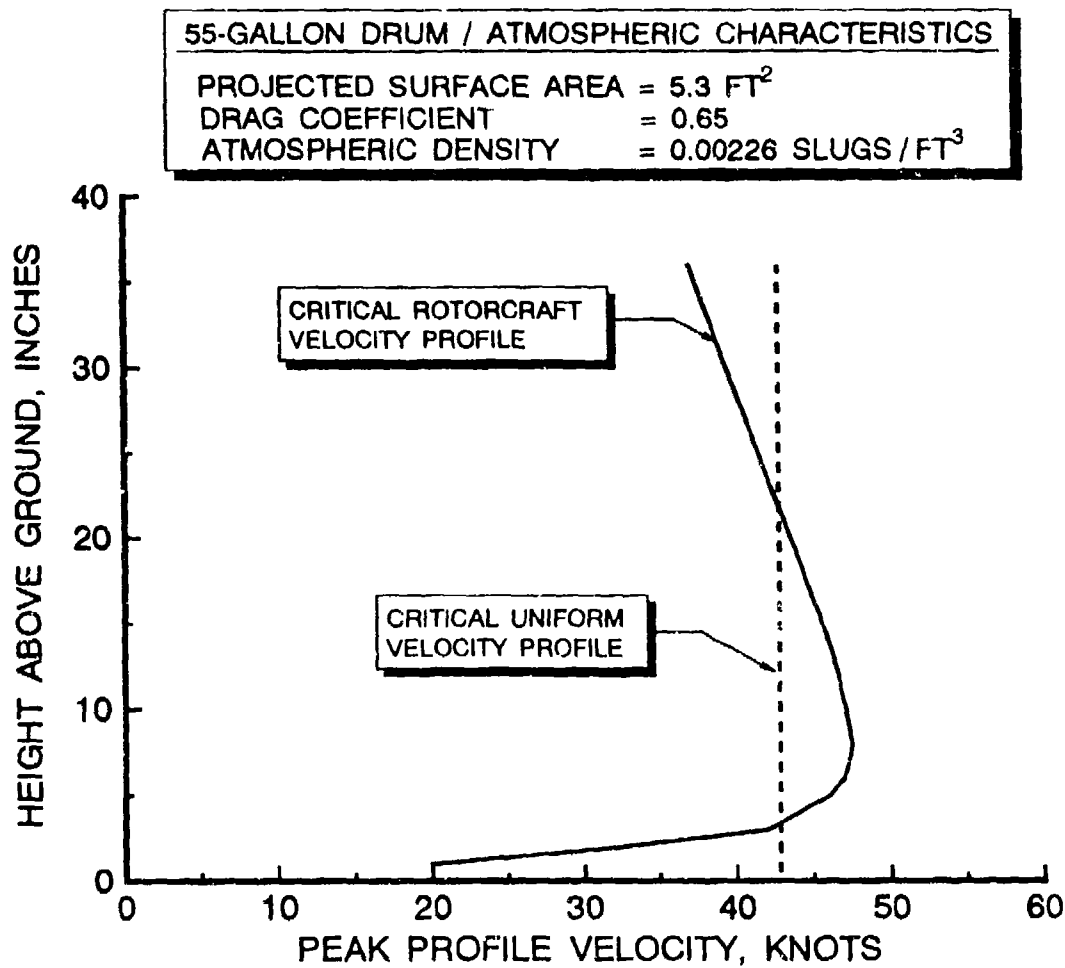


**FIGURE 119 GENERIC VELOCITY PROFILE CREATING THE MOMENT
REQUIRED TO OVERTURN A 55-GALLON OIL DRUM**

of predicting the actual wind conditions. However, when one considers the large number of unknowns related to the mishap (i.e., gross weight, actual distance to drum, wind direction and velocity, etc.), these results do indicate that the analysis appears capable of predicting quite reasonable results for this specific mishap.

The second reported mishap (see section 5.7.5) was analyzed in much the same way as the first. The most significant unknown in the description of this mishap was the distance between the oil drum and the 206L during takeoff. Since this information was not available, a search was initiated for as many photos as could be obtained on short notice of helicopters on oil rigs. Industry requirements for these types of helipads specify that the minimum dimension of the pad be no less than the diameter of the rotor of

the largest helicopter that will use the pad. In looking at the photographs, the helipads appeared, on average, to be approximately 1.25 times the diameter of most of the helicopter rotors. Also, many of the pads in the photographs showed Bell 212 helicopters somewhere in view. If the diameter of a Bell 212 rotor (48 feet) is multiplied by 1.25, the resulting pad minimum dimension would be exactly 60 feet. While this logic does not confirm the size of the pad in the 206L mishap, it does appear to make sense as a reasonable pad size. The diameter of the 206L rotor is 37 feet, and it would be unlikely that the critical dimension would be sized for such a small helicopter (pilot plus up to six passengers). Also, the pad obviously had to have enough extra room to safely accommodate other objects, such as the oil drum.

Assuming a pad size of 60 X 60 feet, if the 206L was centered on the pad, the oil drum would be approximately 30 feet from the center of the rotor or 12 feet from the tip of the rotor. If the helicopter was not centered on the pad, this distance could be increased by as much as 10 feet. A review of 206L rotorwash characteristics using a chart similar to figure 88 indicates that the oil drum will overturn if it is located within 45 feet of the center of the rotor in a 9-knot wind. The drum will also overturn at distances of up to 30 feet in a 5-knot wind. These estimates of the critical distance appear to be very reasonable in light of the few known facts about the mishap.

5.7.5.3 Conclusions for Mishaps Involving Oil Drums

Two conclusions result from the mishaps that have been analyzed in this section. The most important of the two conclusions is that objects which might normally be considered immovable by most civilian personnel and many pilots are, to the contrary, quite movable and potentially dangerous. This statement is justified by the fact that the mishaps did occur and were caused by light to medium class helicopters. Therefore, the rotorcraft community should devote their attention toward the prevention of similar types of "unlikely" mishaps.

A second conclusion is that the probability of occurrence for this type of mishap can be somewhat reliably predicted. This type of mishap is analyzed using simple analytical models that are based on the physics of the problem and straightforward assumptions. In mishaps involving empty oil drums, the critical rotorwash velocity is approximately 43 to 47 knots. This does not mean that the developed methodology is completely validated with sufficient experimental data to ensure that all similar mishaps can be prevented. Improvements to this methodology can be achieved if several carefully controlled experiments are conducted to acquire documented flight test data (see section 8).

5.7.6 Conclusions

A methodology has been developed and utilized in this section to roughly estimate the damage potential of various types of particles, flying objects, and debris. The very limited mishap data that are available do provide some guidelines as to the effectiveness of the analytical methods and indicate that the resulting proposed separation criteria are at least reasonable in many instances. Separation guidelines for the ground vortex and the trailing vortices are assumed to be less important when compared with hover scenarios due to the low velocities that were calculated in table 10. No method exists to compute their hazardous potential.

5.8 ROTORWASH-GENERATED PARTICULATE CLOUDS

Rotorwash-generated particulate clouds (i.e., dust, snow, water, and debris) have always been a serious concern to pilots. These clouds are a hazard to both the generating rotorcraft as well as other nearby rotorcraft and personnel. Particulate clouds most often inflict damage by "sandblasting" rotor blades (thus shortening their useful life) and producing engine foreign object damage that manifests itself as a sudden engine failure or as a slow degradation over time in maximum available engine power. The size and density of these clouds can also obstruct pilot vision. Vision limitations can result in hard landings, collisions with other obstacles (e.g., other rotorcraft in a formation or trees), and crashes. Between forty and fifty of the serious mishap summaries that were reported from the U.S. Army Safety Center database were related to this type of hazard. No record is available on the number of minor mishaps or "near misses."

In this analysis effort, the assumption is made that terrain conditions resulting in severe degradation of the pilot's visibility are totally unacceptable for public heliport use. Therefore, no effort is made to document mathematical methods that estimate parameters such as particulate cloud density or the degree of a pilot's impaired visibility for snow, sand, water, loose dirt, or other particulate matter in heavy concentrations. Readers that are interested in rotorcraft operation over unimproved terrain (as is the military) are referred to references 21, 22, 26, 68, 69, and 70 (also see appendix C listings).

The importance of particulate cloud analysis with respect to public heliports derives from the assumption that heliport operating surfaces will, from time to time, be covered with various low-thickness layers of sand, snow, water, or other particulate matter. Since these particulates will be "blown" by rotorwash, it is desirable to know approximate dimensions of the particulate clouds. Analysis results presented in this section are therefore directed toward methodology documentation and

estimation of the approximate particulate cloud boundaries for various types of common particulate matter. Detailed study of specific resulting hazards (e.g., engine damage) are discussed only in general terms. This is because cloud density and particulate size are extremely important to these types of hazard analysis estimations. General solutions are also impractical because each rotorcraft engine configuration is different and terrain can vary significantly in detailed particulate characteristics. In addition, limited public domain data exist to fully correlate any detailed analysis results.

5.8.1 Mathematical Modeling of Particulate Clouds

The mathematical model that is used in this report to predict three-dimensional particulate cloud boundaries as a function of terrain type was developed initially in reference 22 (also reference 25). It is the only method of its type that has been identified in the literature. However, Kuhn does provide guidelines in reference 26 for predicting the spray height of VTOL aircraft over water. A sketch of particulate cloud geometry, based on reference 22 methodology, is presented in figure 120. This method assumes that rotorwash impinges the ground directly under the hovering rotor (no ambient winds). As the wall jet forms and flows outward, the erosion and subsequent entrainment of particulate matter generates a cloud with boundaries of R_c and H_c . These boundaries, presented in figure 120, are the maximum cloud radius and cloud height, respectively. Rollup of the particulate cloud is brought about by a recirculating or tip vortex rollup mechanism that results from an interaction of the ground and the induced rotor flowfield.

Terrain erosion, as discussed in references 21, 22, and 25, is related to the maximum surface dynamic pressure in the wall jet such that an effective dynamic pressure is defined where:

$$q_s = \frac{q_{s_{\max}}}{\sqrt{K_T}} \quad (\text{pounds/ft}^2) \quad (77)$$

The terrain erosion factor, K_T , is dependent on terrain characteristics and is further defined in reference 22 as:

$$K_T = \frac{\bar{D}_p \rho_p}{D_w \rho_w} \quad (\text{non-dimensional}) \quad (78)$$

where the mean terrain particle size (\bar{D}_p) and density (ρ_p) are related to water droplet size (D_w) and density (ρ_w) as reported

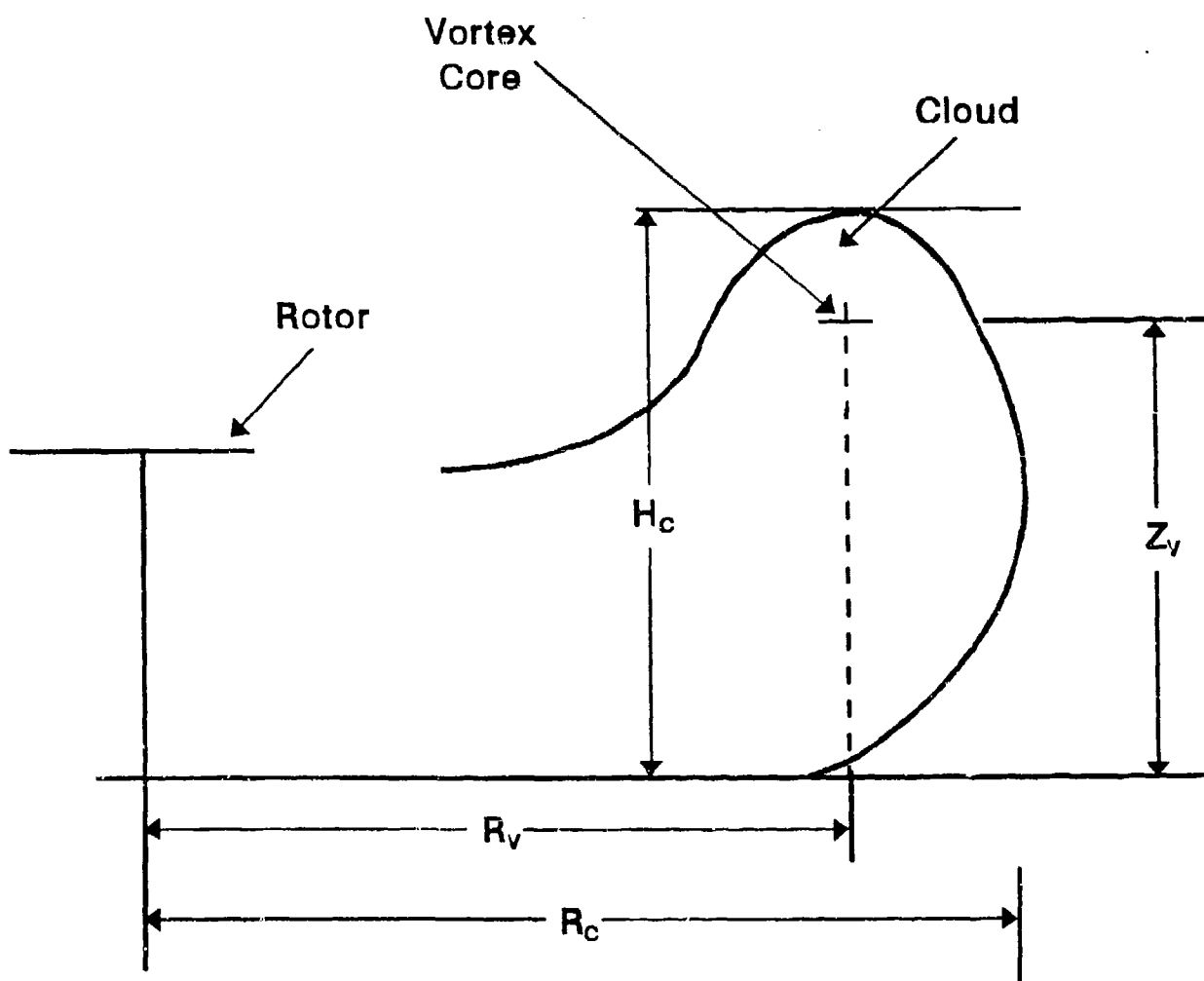


FIGURE 120 SCHEMATIC REPRESENTATION OF PARTICULATE CLOUD GEOMETRY

in references 21 and 22. Approximate values of K_T for various types of terrain are provided in figure 121 (as compiled from references 21, 22, and 68). It can further be shown that the particulate cloud radial boundary (R_C) can be approximated by the radial distance along the ground at which the effective surface dynamic pressure (equation 77) is approximately equal to 1.0 PSF. Using this information, equation 77, and equation 5a of section 2.1.3, which is restated here as:

$$\frac{U_M}{\bar{U}_M} = C_u \left(\frac{I}{R} \right)^{-1.143} \quad (79)$$

it can be shown that $R_C = r$ at $q_{seff} = 1.0$ PSF such that:

$$R_C = R \left(\frac{\sqrt{K_T}}{C_3 \frac{1}{2} \rho_A \bar{U}_M^2 C_u^2} \right)^{-0.437} \quad (\text{feet}) \quad (80)$$

where C_3 is a constant (added to improve correlation) that is equal to unity (1.0) for single-rotor helicopters and 2.2 for the interaction plane of twin-rotor rotorcraft.

The maximum height of a particulate cloud, H_C , is approximated by considering the path of the rotor blade tip vortices as they spread outward along the ground. A detailed analysis of the behavior of the vortex system can be made by replacing the continuous cylindrical vortex sheet with a finite number of discrete vortices. However, a step-by-step iterative procedure must then be applied to compute the motion of each ring vortex as it starts to expand along the ground.

In lieu of this process, which is complicated and time consuming, the researchers in references 21 and 22 decided to analyze the rollup process utilizing an analogy of the vortex sheet shed from the trailing edge of a lifting wing. The main difference between the flow mechanism of the cylindrical vortex sheet of a rotor and the vortex sheet of a lifting wing is that the former rolls up and forms a torus ring while the latter rolls up into two line vortices.

Using the analogy described above, which is discussed in detail in reference 22, conventional wing vortex theory is applied to predict approximately the effective center of the vortex core for a specific particle size or K_T . Figure 122 defines the nomenclature and coordinates for this vortex core that can be expressed as follows:

$$R_V = 0.785 R_C \quad (\text{feet}) \quad (81)$$

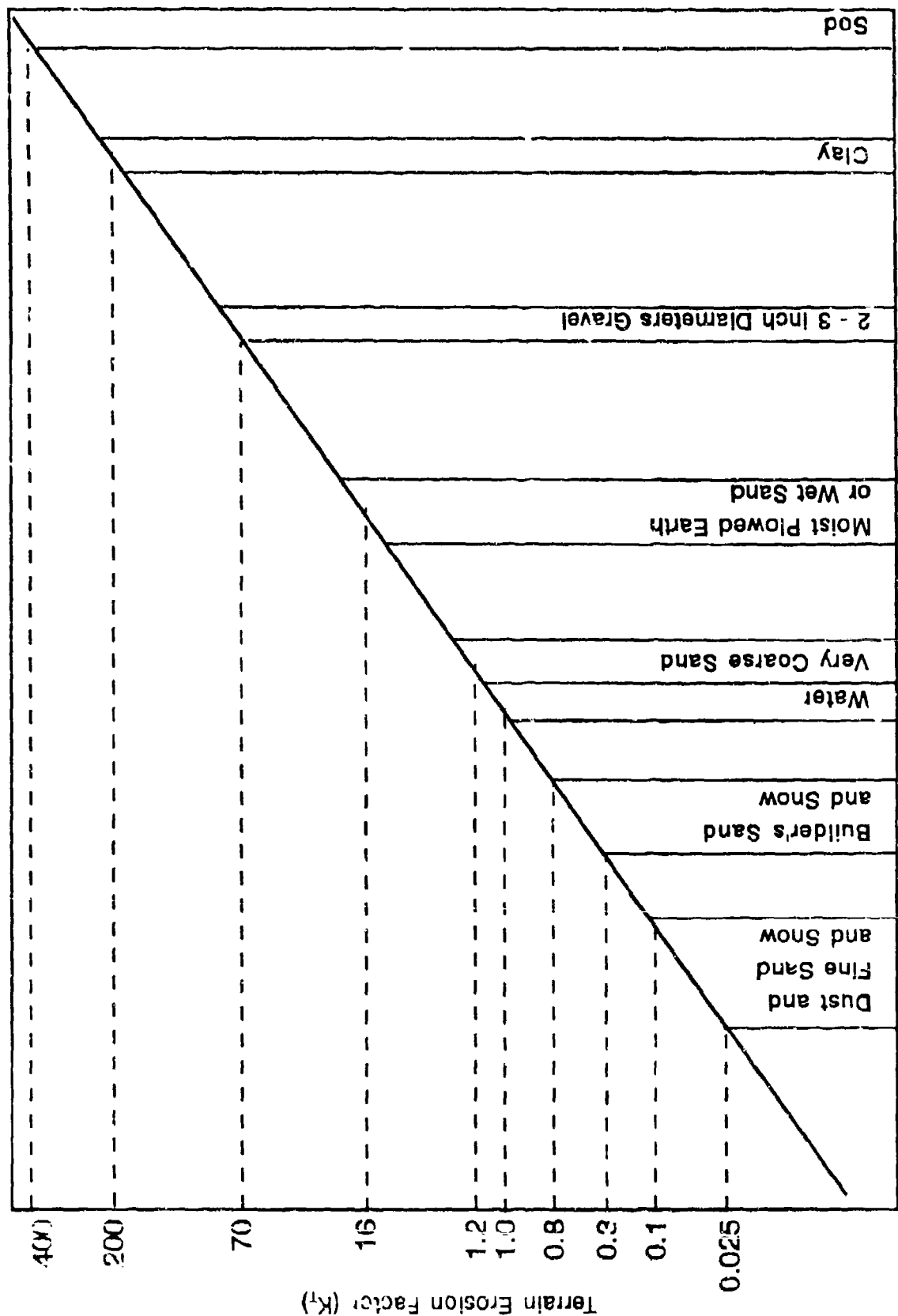


FIGURE 121 APPROXIMATE VALUES FOR THE TERRAIN EROSION FACTOR (K_t) AS IDENTIFIED IN THE LITERATURE

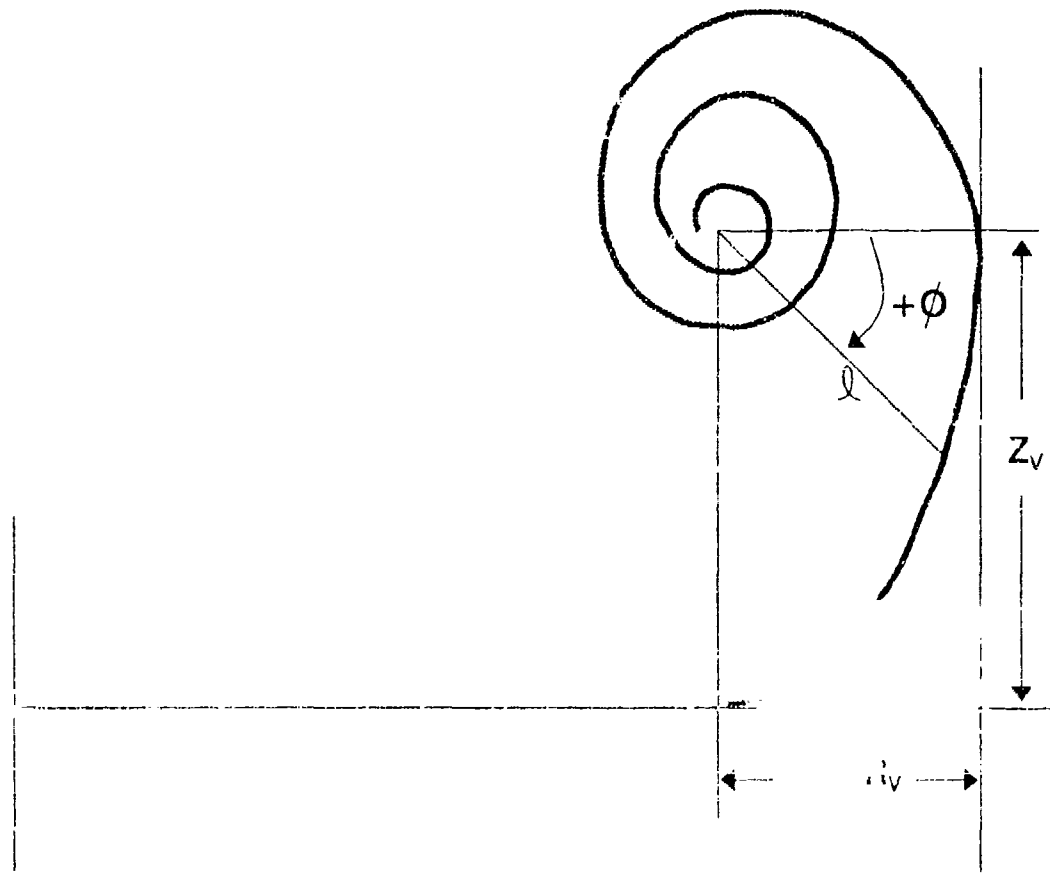


FIGURE 122 LOGARITHMIC SPIRAL REPRESENTATION OF VORTEX ROLLUP

$$Z_v = 0.329 R_c \quad (\text{feet}) \quad (82)$$

Once the "effective" center of the vortex core is defined, the cloud rollup is approximated by a logarithmic spiral relationship.

$$\ell = e^{A(\phi + \phi_0)} \quad (\text{feet}) \quad (83)$$

In this relationship, A and ϕ_0 are constants that are determined by applying the boundary conditions of $\phi = 0$ when $\ell = R_c - R_v$ and $\phi = \pi/2$ when $\ell = Z_v$. Solutions for these constants result in the following equations:

$$A = \frac{2}{\pi} \ln\left(\frac{Z_v}{R_c - R_v}\right) \quad (84)$$

$$\phi_0 = \frac{\pi}{2} \left(\frac{\ln(R_c - R_v)}{\ln(Z_v) - \ln(R_c - R_v)} \right) \quad (85)$$

It should be noted that the equation for ϕ_0 , typed as equation 35 in reference 22, was typed incorrectly and was rederived for this study. Knowing the radial location of the particulate cloud boundary (R_c) and the constants A and ϕ_0 , the vertical boundary is computed from the center of the vortex spiral by substituting $\phi = -\pi/2$ in equation 83. Thus,

$$\ell_v = e^{A(-\pi/2 + \phi_0)} \quad (\text{feet}) \quad (86)$$

The total particulate cloud height (H_c), as measured from the ground, is then provided by the following equation:

$$H_c = \ell_v + Z_v \quad (\text{feet}) \quad (87)$$

5.8.2 Validation of the Particulate Cloud Model

A review of the literature was conducted to identify data for validation of the particulate cloud model. As a result, three sources of test data were identified. The first source of data, references 22 and 68, is for a sand/dust cloud generated by the tandem rotor Vertol H-21 helicopter. The second source, reference 26, contains data for the spray height generated by a CH-53E. The third source, reference 71, provided data for the XV-15 tiltrotor while hovering over water. Unfortunately, no other flight test data (for helicopters, tiltrotors, or twin-

rotor tiltwings) were identified in the literature. Some limited data for the four-propeller Vought XC-142 and four-fan Bell X-22 were noted in references 22, 25, and 72. However, since the ROTWASH program does not model these configurations, they were excluded from evaluation. Several scale-model tests of limited usefulness were also identified. These results will be discussed as appropriate.

The flight test experiment involving the Vertol H-21 is developed in some detail in reference 22; however, for a full understanding of the experiment, reference 68 should be reviewed. The size distribution of the particles used in the experiment is provided as figure 35 in reference 22. This figure is reproduced in this report as figure 123 (the terrain sample data is from Ft. Yuma, Arizona). The authors in reference 22 make the assumption in their correlation case that approximately the 10th to 12th percentile size particle (by weight) should be used to compute the cloud boundaries. This assumption is significantly aided by the use of photographs, movies, and particle trap results from reference 68. This particle size is approximately 0.04 mm in diameter and is representative of extremely fine sand or dust. It should again be noted that the larger size particles have a higher computed K_T value and probably would not be found at the cloud boundaries. If these particles are used as input to the model, the predicted cloud size will be smaller and the effective center of the vortex core will be closer to the rotorcraft. Using the 0.04 mm size particle and a density (ρ_p) of approximately 92 lb/ft³ (sand), the value for K_T can be calculated as:

$$K_T = \frac{\bar{D}_p \rho_p}{D_w \rho_w} = \frac{(0.04 \text{ mm}) (92 \text{ lb/ft}^3)}{(2.54 \text{ mm}) (62.4 \text{ lb/ft}^3)} = 0.025 \quad (88)$$

If this K_T value is used, along with the ROTWASH H-21 input data (table 20), the particulate cloud boundaries (R_C and H_C) are estimated as presented in figure 124. These test data indicate the approximate boundary radius and height to be 190 feet and 95 feet, respectively. Both of these cloud boundary values are quite close to the mathematical model predictions.

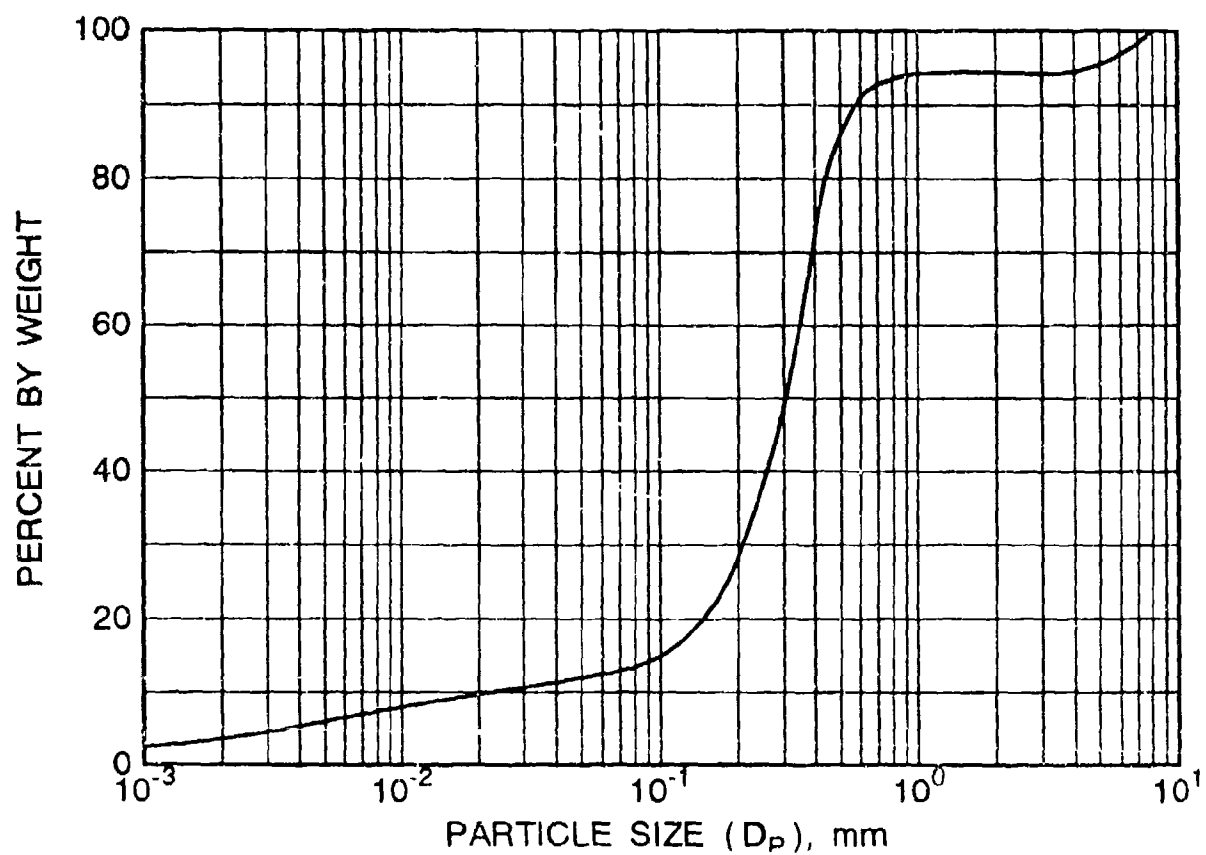


FIGURE 123 GROUND SAMPLE PARTICLE SIZE DISTRIBUTION

TABLE 20 INPUT DATA
FOR H-21, CH-53E, AND XV-15 CORRELATION CASES

ROTWASH INPUT PARAMETER	H-21	CH-53E	XV-15
Number of Rotors	2	1	2
Rotor Separation (feet)	42.0	0.0	32.2
Rotor Radius (feet)	22.0	39.5	12.5
Gross Weight (pounds)	13,000	41,000	12,500
Fuselage Download (%)	1.5	5.0	13.0
Rotor Height (feet)	17.0	102.0	62.5
Atmospheric Density Ratio	1.0	1.0	1.0
Ambient Wind (knots)	0.0	0.0	0.0

Limited particle data are also provided in reference 22 to guide in the estimation of where the cloud particle size boundaries might occur for particles larger than 0.04 mm. These test data are compared in figure 125 at 44 and 88 feet with calculated boundaries for particles varying from 0.5 mm to 2 mm. In a comparison of the non-interaction plane (NI) data, the 0.5 mm boundary seems to be quite close to what was measured as the maximum particle size at heights above ground of 5 and 10 feet (10 feet was the maximum height at which particle traps were located). The 2 mm particle boundary would appear to be conservative because 2 mm particles were trapped only at heights of less than 1 foot. Along the interaction plane (IPLANE), a comparison of test and calculated data yield similar results. However, before any final conclusions about the quality of correlation are reached, several aspects of the mathematical model deserve mention. First, it is important to remember that the theoretical assumption is made that all particles for a certain K_T are of the same size and that they do not collide in flight in the cloud. In addition, no loss of flowfield momentum due to particle transport is accounted for because particle cloud density is not assumed to be large enough to affect this parameter. These assumptions are rarely correct. In the real world, particle size distribution usually varies over a wide range (see figure 123 in reference 68). Also, collisions do take place, and these collisions reduce particle energy that might otherwise be utilized for further travel outward in the flowfield. If particle densities are large enough, the imparted momentum to the particles is also affected.

In conclusion, the presented H-21 test data are for only one terrain type and distribution. As a result, the data only permit one correlation point to actually be plotted. Should another terrain type be evaluated, the distances that the various particle sizes travel may be slightly increased or decreased. Ultimately, additional data are needed to fully validate the mathematical model.

The second source of data used for correlation is obtained from reference 26 for the CH-53E helicopter. The estimated gross weight and rotor hover height are 41,000 pounds and 102 feet, respectively. Other pertinent data are tabulated in the previously presented table 20. The reported spray height (H_C) is 68 feet. Unfortunately, no spray boundary (R_C) was reported. The calculated ROTWASH results for this test condition are 77 feet for spray height and 165 feet for the outer spray boundary. Considering the other unknowns in this case, correlation is quite good. The overprediction of the spray height is desirable because photographs used in the measurements tend to be misleading. More on this subject is discussed in the following paragraphs.

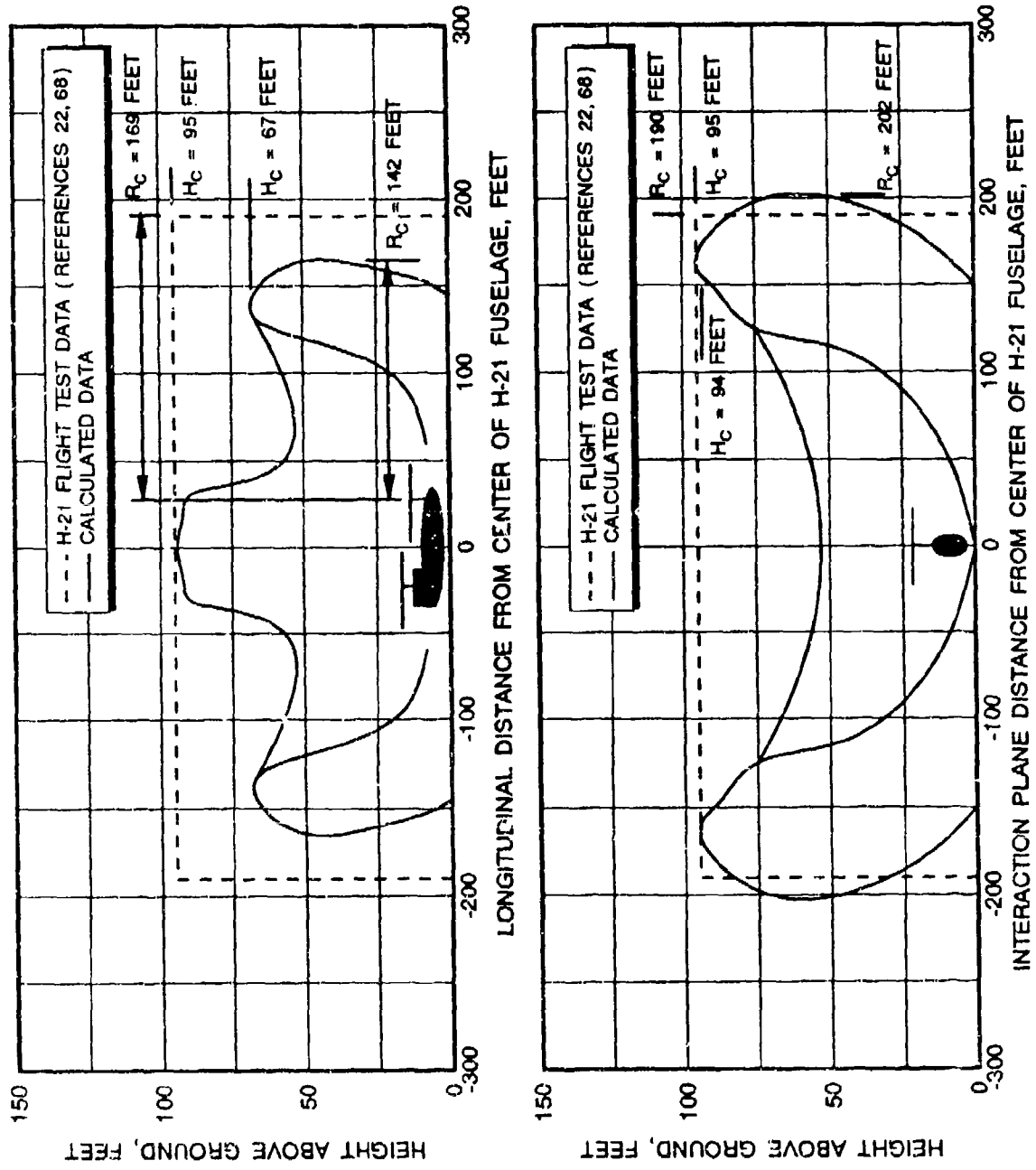
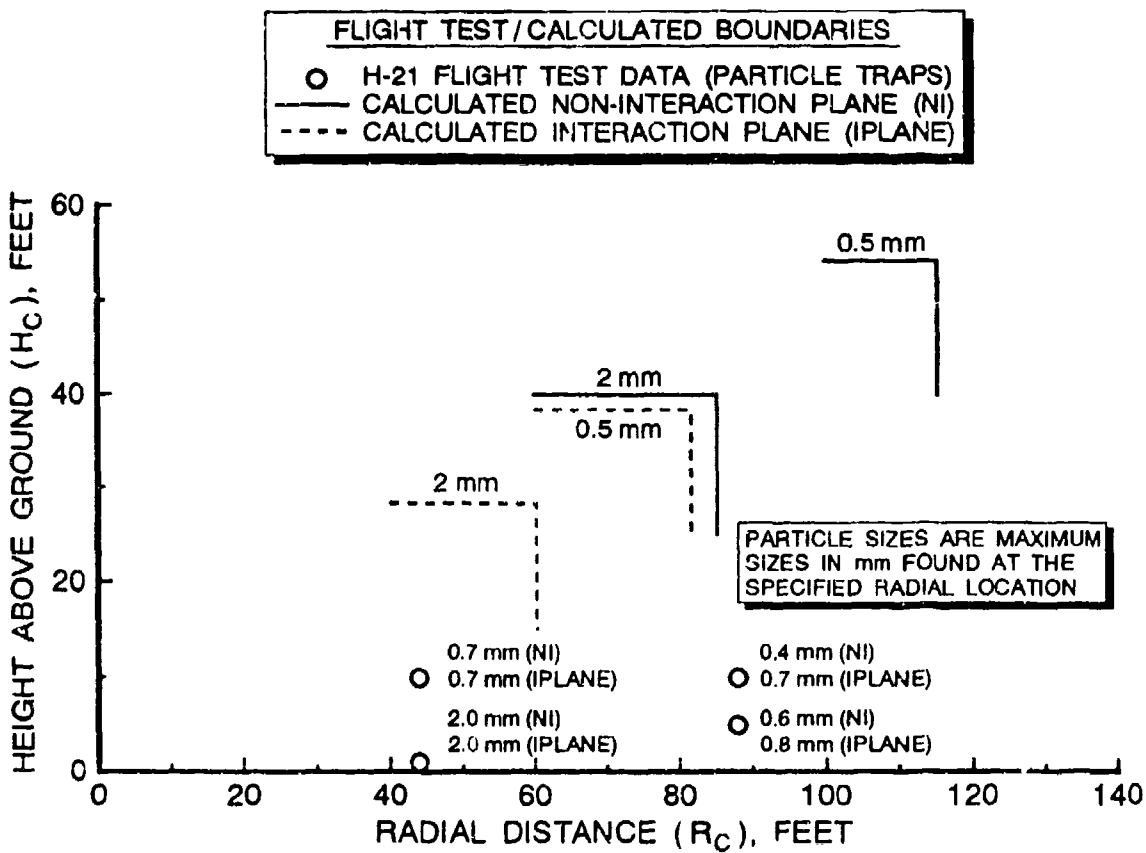


FIGURE 124 DUST CLOUD SIZE AND SHAPE FOR THE H-21 HELICOPTER



**FIGURE 125 H-21 PARTICLE CLOUD BOUNDARY COMPARISON
FOR PARTICLES RANGING FROM 0.5 mm TO 2.0 mm**

A third correlation attempt was conducted with XV-15 tiltrotor data that were obtained in 1983 in an over-the-water hover test (reference 71). In perfectly calm air (i.e., wind less than 5 knots) at a 62.5 foot rotor height, spray was observed from photographs to occur up to heights of approximately 3 feet. In gusty winds (12 to 20 knots), spray was observed up to approximately 20 feet. Using the input data from table 20 and a K_T equal to 1.0 (the value of 1.0 is assumed because water droplet diameter was not measured), the estimated spray height is 30 feet to the side and 42 feet fore and aft. These calculated results appear quite conservative, a discrepancy of 10 to 20 feet in spray height for the gusty wind case. However, it is important to note that in reference 70, it is stated that estimates of spray height made from photographs can be very misleading, even in controlled laboratory tests. This is due to the fine, as well as transparent, nature of spray particles when photographed in lower densities in air. Therefore, it would be believable that the XV-15 spray height data for the gusty wind conditions might approach 30 plus feet. The simplicity of the theory does not attempt to directly account for the effects of

light-to-medium winds. Therefore, it can only be assumed that some mild choppy wave action is necessary to help lift the spray up into the rotorwash flowfield and that this theory works for these types of environmental conditions. While this commentary might explain the gusty wind spray data, it does not explain the large discrepancy in the calm air results. Two methods exclusively devoted to prediction of spray height are presented in references 26 and 70. These highly empirical methods are recommended for anyone who is interested specifically in spray height calculations.

In summary, while the three discussed correlation cases provide fairly good validation for the reference 22 mathematical model, it is nevertheless risky to claim that the model is good for anything other than general estimation purposes. Use of this theory intuitively appears to be somewhat overpredictive of the cloud height (H_C) for the larger particle sizes. Should further correlation data be identified and similar correlation results be presented, then this statement of the method's accuracy can be modified accordingly.

5.8.3 Safety Concerns Associated With Particulate Clouds

In the previous section, the quantification of particulate cloud boundaries has been discussed in detail. However, no attempt was made to associate particulate cloud characteristics (i.e., particle size and velocity) with their potential for compromising safety. Discussion of this topic is the goal of this section. This discussion is mainly related to three subject areas that include:

1. personnel injury,
2. engine damage, and
3. abrasion of equipment and rotor blades.

The reader should not assume that these subject areas are necessarily the only ones of importance. Instead, it is hoped that discussion on these three subjects will be informative enough for the reader to apply the results to the solution of other problems.

Exposure of an unprotected human (or animal) to a particulate cloud for even a short period of time has the potential for serious injury. The most serious type of injury that has a high probability of occurrence is eye injury. Most other parts of the human body, particularly with clothing as protection, can safely withstand most particle impacts. While common sense would indicate that unprotected personnel (and particularly trained personnel) will instinctively close their eyes when subjected to uncomfortable levels of rotorwash, this assumption cannot be guaranteed. Therefore, the conservative assumption must be made that personnel and animals will sooner or later be "surprised" by rotorwash that contains dangerous sizes of particulate matter.

Reference 22 states as a guideline that winds above 59 knots can clearly be expected to cause damage to the unprotected eye. This statement must be qualified in that it assumes particles of a hazardous size or weight are contained in rotorwash.

Reference 21 provides an experimentally derived graph of particle weight versus particle velocity (steel particles) that is known to have caused corneal penetration of a rabbit's eyes. These data were presented earlier as figure 116. Unfortunately, the weight/velocity relationships that prevent abrasive damage and discomfort to the eye are not known.

Builder's sand particles, measured in reference 67, normally vary from about 0.003 to 0.05+ inches. Weights associated with these diameters are approximately 3.42×10^{-7} and 1.68×10^{-3} grams, respectively. If the conservative assumption is made that somehow the smallest particle of sand that can be hazardous (approximately 0.1 to 0.2 grams) will be entrained at the maximum rotorcraft outwash velocity and will strike and penetrate a human eye, then the diameter and K_T range for this size of sand particle is approximately 0.1 to 0.125 inches and 1.5 to 1.9 (non-dimensional, see equation 78), respectively. However, smaller particles may still be very bothersome. If the term bothersome is assumed to represent a scenario in which significant abrasion of equipment can take place over a period of time, then particle sizes in excess of 0.3 mm should be assumed to be hazardous. The approximate K_T value for sand particles of this size is 0.2.

Boundaries for trained personnel, or personnel wearing eye protection, cannot be accurately estimated using the presented techniques, particularly since hazardous particles may not even be present in substantial quantities in the typical heliport terrain environment. Also, boundaries for trained personnel may not even be relevant in that these personnel are usually required to work near rotorcraft (i.e., mechanic) even if hazardous rotorwash conditions exist. It is recommended that trained personnel wear eye protection at all times, particularly when working in close proximity to large rotorcraft. Reference 24 provides a graphic text description of the hazardous environment associated in working near the RH-53D and CH-53E rotorcraft.

In the case of engine and abrasive-related damage, a much longer duration exposure is usually required along with a significant particulate density in the flowfield. Engine and rotor blade abrasion damage can be looked at in two ways. If the engine and rotor are rotating, the particle velocities by themselves become unimportant. This is because the rotational velocities of engine components and rotor blades are well in excess of the velocities required for even static particles to inflict impact damage. Only particle presence in the flowfield is required. However, it should be noted that most modern rotorcraft turbine engines do have particle separators and all rotor blades have some type of a leading edge abrasion strip because of long term abrasion

concerns. These hardware features significantly reduce the hazard for rotorcraft operating in their own rotorwash environment. However, these protection features may not be assumed to be functioning for parked rotorcraft or parked/running fixed-wing rotating components (i.e., airplane propellers or executive jet engines). Therefore, a second way to study the problem is to assume that most endangered aircraft or rotorcraft are "parked" and that the main problem becomes one of equipment abrasion.

It is stated in reference 22 that significant compressor blade damage is caused by steady injection of large size particles (greater than 0.2 mm). Continued operation in this type of contaminated atmosphere will produce damage that will result in reduced engine-power-available and in increased fuel consumption. Table 21 provides test data from reference 22 that indicate that performance loss can be easily associated with accumulated weight of ingested sand and dust. For a 5 percent reduction in power-available, the associated engine endurance times in contaminated air can be shown to vary from 7.2 to 99 minutes. It is not the purpose of this study to estimate the mass flows that are associated with any particular terrain environment. However, it is important to note that rotorcraft should not necessarily be allowed to hover in close proximity to other rotating turbine engines for extended periods of time, particularly if large amounts of particulate matter are being blown about.

TABLE 21 RESULTS OF DUST INGESTION BY VARIOUS V/STOL ENGINES FOR A 5-PERCENT REDUCTION IN NORMAL RATED POWER

ENGINE TYPE	SAND INGESTED (LBS)	AIRFLOW (LBS/SEC)	ρ_p (LB/FT ³)	ENGINE ENDURANCE (MINUTES)
T-64(1)	29.0	24.5	7.7×10^{-5}	20.0
T-58(8)	24.0	12.4	34.1×10^{-5}	7.2
T-55L(5)	22.5	10.7	2.7×10^{-5}	99.0

Sand particle sizes of 0.2 mm equal a K_T of approximately 0.12 (non-dimensioned, see equation 78). Since significant particle densities are required to reach the mass flow rates described in table 21, one could assume that in civilian operations, normally conducted over "particle sparse" terrains, dust cloud hazards to engines and rotor blades should be minimal. This statement is reinforced by the fact that many modern rotorcraft engines do contain integral particle separators. Therefore, additional information needs to be known with respect to specific scenarios before further investigation can proceed.

If another rotorcraft, aircraft, or piece of equipment is parked near a rotorcraft that is generating a particulate cloud, abrasion can become a serious hazard. Very little information has been identified in the literature to define unacceptable levels of abrasion. Reference 22 states that severe abrasion of equipment will occur in winds greater than 35 knots if particle sizes in excess of 0.3 mm are present. Mild abrasion of equipment can occur in winds in excess of 14 knots for particle sizes in excess of 0.01 mm. K_T values for these sand particle sizes are equal to or below the value of 0.12. Calculations indicate that it is easy to generate large particle clouds containing particles of these sizes. However, it again becomes important to quantify the mass flow rates and exposure times that must be present to significantly impact on subject pieces of equipment. In the civil heliport environment, these mass flow rates should be quite low as long as concrete, asphalt, and well-maintained sod are the primary terrain types of choice.

5.8.4 Conclusions from an Analysis of Particulate Clouds

In summarizing the discussion associated with particulate clouds, it must be stated that an assumption has been made about the civilian heliport environment. The main components of this assumption are listed below.

1. No heliport terrain environment will be considered acceptable by the operators or the FAA if the pilot's vision is obstructed in any way due to high densities of particulate matter (i.e., dust, snow, sand).
2. Concrete, asphalt, and well-maintained sod are the terrain types that will be approved for heliport use.
3. Procedures will be implemented in the civil heliport environment to effectively separate untrained and unprotected personnel from those that are trained and familiar with working in the rotorwash environment (i.e., mechanics and ground handling personnel).

As long as these assumptions apply to the typical civil heliport scenario, particulate cloud-related hazards should not be a significant problem in defining practical separation guidelines. The "passing" rotorcraft will probably not inflict serious damage. One note of caution is appropriate: any practical separation guidelines must account for accidental deviations or course changes by the generating rotorcraft that may unexpectedly result in a safe separation distance becoming an unsafe distance. More on this subject is provided in the "How To" examples that are presented in sections 6 and 7.

If the above assumption is considered to be inappropriate for the way heliports are designed and used, it will be necessary to conduct a more detailed study of particulate cloud-related

hazards. This study will need to further validate the mathematical model and will also need to define the acceptable terrain types (in detail) over which rotorcraft operations will be conducted. These terrain types will need to be evaluated to determine what size particles can be eroded and at what mass flow rates the particles are distributed through the rotorcraft outwash flowfield. Until some of the uncertainties are further quantified by experiment, it is recommended that the conservative boundary defined by K_t equal to 0.3 be used as the boundary for unprotected and untrained personnel. This boundary equates more with what would probably be bothersome than what would cause serious physiological damage.

6.0 ROTORWASH ANALYSIS EXAMPLES - SCENARIO DEFINITION

One of the primary goals of this report is to provide a handbook of rotorwash analysis and design "How To" examples using the mathematical models and flight test data presented in sections 2 through 5. This goal is accomplished in sections 6 and 7 by evaluating a large hypothetical heliport (or vertiport) for potential design and operational problems that might result due to rotorwash. Two preliminary tasks that must be completed to meet this goal include definition of the:

1. hypothetical heliport/vertiport layout, and
2. the types of rotorcraft planned as users of the facility.

These two definitions are the focus of section 6, and the rotorwash design/analysis examples are the focus of section 7. The result of this effort is to provide rotorcraft engineers and heliport/vertiport designers practical examples for defining operationally oriented rotorwash velocity thresholds that, when exceeded, increase the probability that mishaps will occur.

6.1 DEFINITION OF THE VERTIPORT

Facilities built to support rotorcraft operations are generally unique and specifically designed for a particular location and function. A heliport can be defined as any area of land, water, or any structure used or intended to be used for the landing and takeoff of helicopters, and includes at least some additional facilities such as parking, terminal building, fuel, etc. If the additional facilities are not included, the landing/takeoff area is often referred to as a helipad or helistop. A vertiport meets the definition of a heliport with the added requirement that it be designed for takeoff and landing of tiltrotor, tiltwing, and other types of V/STOL aircraft. These facilities are generally the largest of the three types and may incorporate short runways or rollways for short takeoffs and landings (as an alternative to vertical takeoffs and landings).

As an aid to development of practical "How To" examples for the analysis of potential rotorwash-related problems, a hypothetical vertiport facility is defined in figure 126. This conceptual design is based upon a similar design described in reference 73. The vertiport contains a 400 by 150-foot rollway area that is bounded by water on one side and a parking area on the other side. The parking area contains short term parking for commuter operations (for V-22 size tiltrotor aircraft), as well as long term parking and service facilities. A terminal area is adjacent to the center section of the parking area for use by both the scheduled commuter passengers as well as corporate and military users. Both the rollway and parking areas are also elevated by

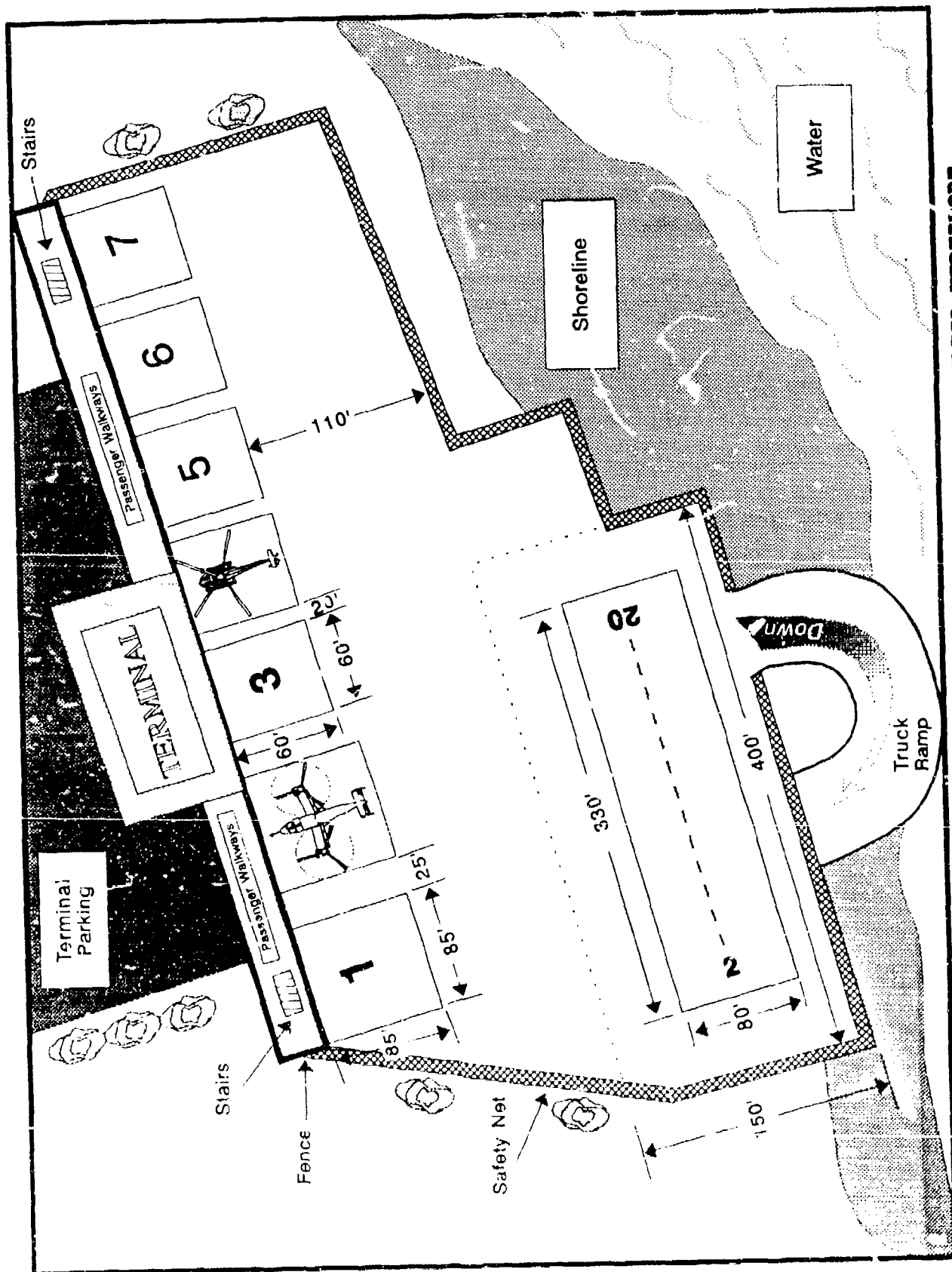


FIGURE 126 A CONCEPTUAL DESIGN FOR A FULL SERVICE ELEVATED VERTIPORT

30 feet with respect to the surrounding terrain and the surface of the water. A horizontal fence/safety net surrounds the parking and rollway areas, and a truck ramp curves up from ground level to the level of the rollway to permit vehicle access.

In section 7, this conceptual vertiport will be used as the facility component of the scenario in each of the rotorwash analysis and design examples. It should be noted that this conceptual vertiport is not based on any existing or known proposed facility.

6.2 DEFINITION OF THE DESIGN CLASSES OF ROTORCRAFT

Development of the "How To" examples also requires the definition of several critical types or size classes of rotorcraft. Figure 127 contains each of the rotorcraft types listed in appendix A plotted as a function of disk loading (DL) and rotor radius (R). Disk loading in this context is defined as:

$$DL = \frac{\text{Maximum Gross Weight}}{\pi R^2} = \frac{GW}{\pi R^2} \quad (89)$$

This parameter is important because the induced velocity (v_i) or downwash of a rotorcraft, the hazard in this study, is a direct function of the thrust (or gross weight plus airframe download) distributed over the surface area swept out by the rotor blades.

$$v_i = \sqrt{\frac{2 DL}{\rho_A}} \quad (\text{feet/second}) \quad (90)$$

As can be observed in figure 127, a line exists for the relationship of interest below which the majority of old, modern, and known future rotorcraft types are plotted. Two clear exceptions to this statement are the two tiltrotor configurations plotted at rotor radii of 12.5 and 19 feet (connected by the dashed TRDL line). If the two tiltrotor configurations are momentarily set aside, the upper boundary (defined by the solid SRDL line) can be redefined by five hypothetical rotorcraft of various sizes for analysis and design purposes (this concept for the development of size classes was first introduced in reference 1). These five hypothetical single main rotor configurations, known as the S, SM, M, MH, and H size classes, are described in detail in table 22. If the MT and HT tiltrotor configurations (XV-15 and V-22) are added to the group, a total of seven critical size classes are defined.

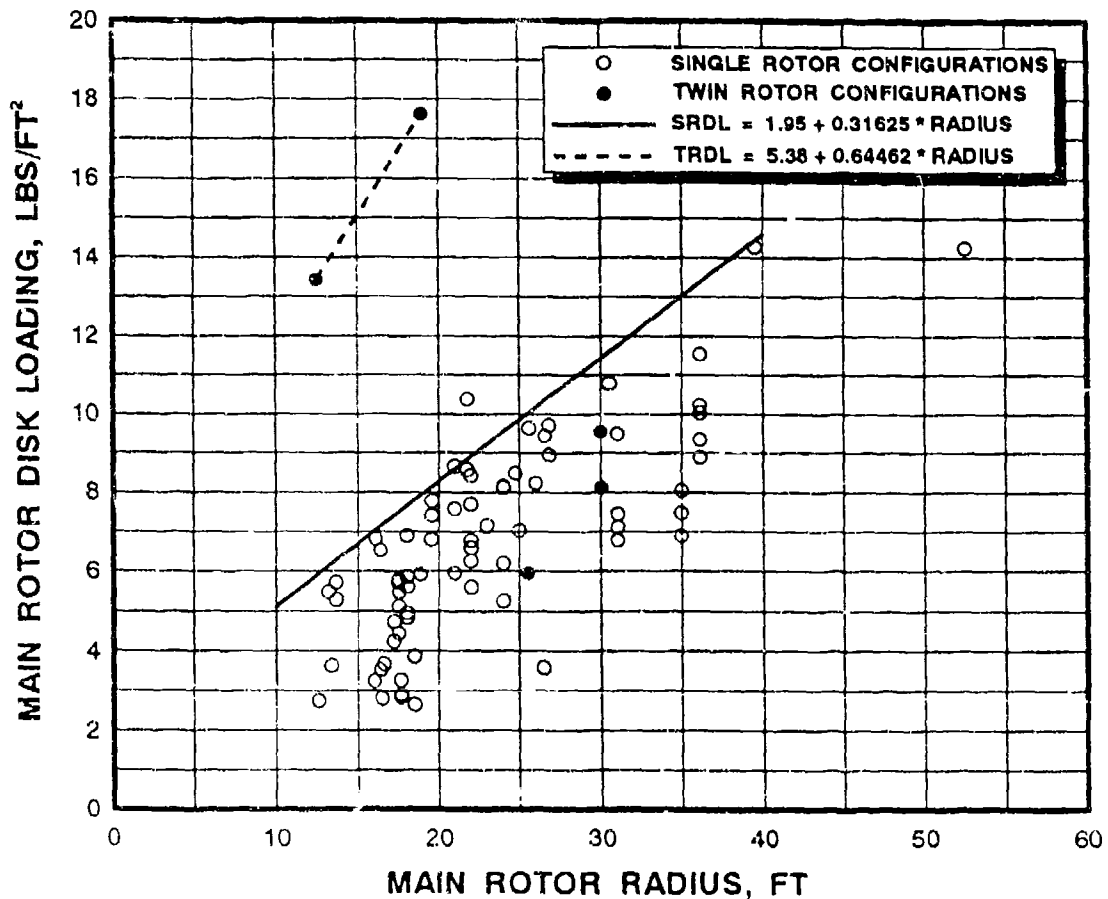


FIGURE 127 RELATIONSHIP OF ROTOR DISK LOADING TO ROTOR RADIUS

These seven classes of rotorcraft do not necessarily represent the most famous or popular types of rotorcraft in commercial or military service today. However, without identifying and using specific manufacturers' products as defined in appendix A, these size classes clearly include all of the most common types, particularly the light (S) to medium (M) classes that are responsible for the majority of reported rotorwash mishaps. Therefore, use of these hypothetical rotorcraft configurations results in the development of guidelines that are a clear indicator of whether or not rotorwash is a serious problem for a given operational scenario.

TABLE 22 CRITICAL ROTORCRAFT SIZE CLASSES FOR
"HOW TO" DESIGN AND ANALYSIS OPTIONS

CONFIGURATION PARAMETERS	CONFIGURATION IDENTIFIER						
	S	SM	M	MH	H	MT	HT
Number of Rotors	1	1	1	1	1	2	2
Rotor Radius (ft)	15.0	20.0	25.0	30.0	40.0	12.5	19.0
Maximum Gross Weight (lb)	4,730	10,400	19,350	32,340	73,390	13,200	40,000
Approximate Fuselage Download (percent)	1.5	1.5	2.5	3.5	5.0	13.0	10.0
Rotor Height Above Ground (ft)	10.0	12.5	15.0	17.5	20.0	12.5	20.0
Disk Loading (psf)	6.7	8.28	9.86	11.44	14.6	13.4	17.6
Rotor Separation (ft)	--	--	--	--	--	32.2	46.5

7.0 ROTORWASH ANALYSIS EXAMPLES - "HOW TO" APPLICATIONS

The rotorwash analysis "How To" examples presented in this section are designed to be instructional guides for anyone using the methodologies and data in this report. The goal of each example is to evaluate at least one design aspect of a large hypothetical heliport (or vertiport) for potential design and operational problems that might result due to rotorwash. The hypothetical vertiport design that is used in each of the examples is documented in the previous section (section 6). Each example uses version 2.1 of the rotorwash analysis computer program (ROTWASH) as the basis for calculations. A FORTRAN listing of this program is provided in appendix E.

Separation guidelines can be developed between rotorcraft and ground personnel, ground vehicles, other rotorcraft or fixed-wing aircraft, ground structures, and equipment frequently found in the rotorcraft operational environment. However, the reader must remember that it is not a goal of this report or these "How To" examples to define formal rotorcraft separation guidelines. The goal is to develop background data and examples of analyses for heliport and vertiport designers and rotorcraft engineers to support future requirements for the development of separation guidelines. The mathematical models are used only to demonstrate their usefulness as tools in better understanding some of the physics of rotorwash-related mishaps.

The examples that are presented in this section provide "How To" estimates for the following types of rotorwash calculations:

1. velocity/dynamic pressure profile curves,
2. personnel overturning forces and moments,
3. loadings on ground structures,
4. potential effects on parked rotorcraft,
5. overturning moments on light fixed-wing aircraft,
6. rotorwash velocities that entrain small objects and debris,
7. size of dust, debris, water spray, and snow clouds,
8. ground vortex strength, and
9. wake vortex strength.

7.1 VELOCITY/DYNAMIC PRESSURE PROFILE CURVES

The most important feature of the ROTWASH program is its capability to estimate rotorwash velocity and dynamic pressure

profiles as they expand outward along the ground from the rotor. Almost all of the other analysis features are completely dependent upon this key feature. In this "How To" example, the goal is to step through the process that is used to generate both velocity and dynamic pressure profile data. These profile data are then briefly compared with some of the available flight test data.

The example is initiated by referring to figure 128. Designers and future municipal operators of the conceptual vertiport have reviewed their design and made three major decisions. These three decisions are listed below.

1. Operationally, all rotorcraft with wheels will be required to ground taxi whenever they are not directly above the 400 x 150-foot section of rollway (bounded by points A, B, C and D on figure 128).
2. Because of uncertainty in the ability to control all emergency situations, the vertiport structure itself shall be designed to withstand the maximum rotorwash loads generated by large tiltrotor (HT) and heavy helicopter (H) configurations while hovering (defined in section 6) with a 5.0 knot worst azimuth crosswind condition (reduced from 9.0 knots to partially compensate for 3-dimensional and wind directional probability effects as discussed in section 5.5).
3. Operational rotorwash concerns at all points on the vertiport will be based upon air taxi operations of skid-equipped SM sized rotorcraft under worst case crosswind conditions (approximately a 9-knot wind condition).

It is important to note that these three decisions are not the only important ones required in the design of a vertiport; however, for this example these guidelines are sufficient.

Section 2.1 and more specifically figures 10 through 12 should be reviewed at this point if the reader is unfamiliar with the expected shape of rotorwash velocity and dynamic pressure profiles. Otherwise, the first analysis task is to define the peak rotorwash loads generated by the HT and H configurations. Design criteria are:

1. the HT and H configurations, in an emergency, are allowed to hover at maximum gross weight in the 85 x 85 foot parking locations to the left of the terminal building (see figure 128), and
2. the adverse design crosswind for these conditions is 5.0 knots.

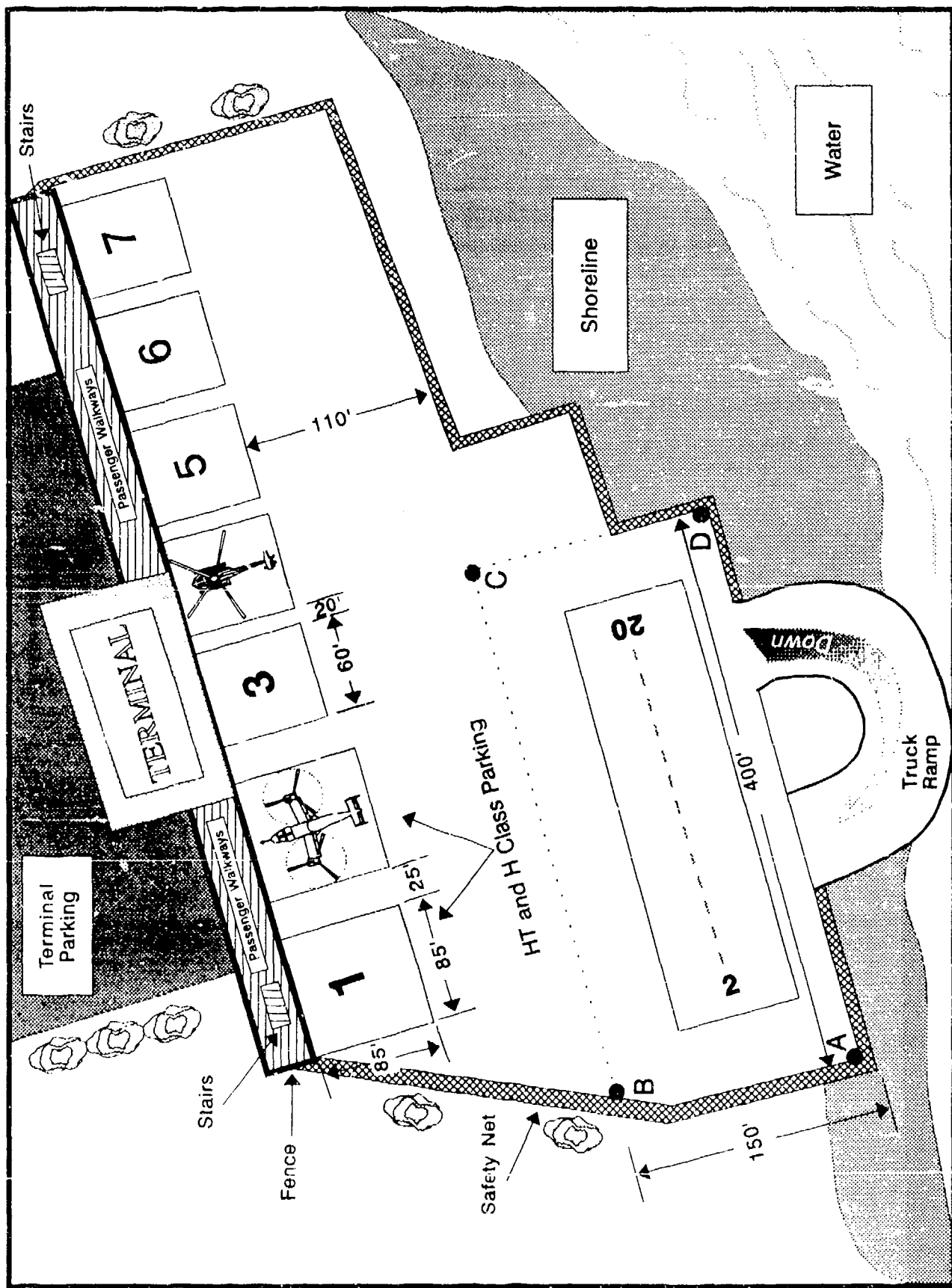


FIGURE 126 VERTIPOINT DESIGN DATA FOR EXAMPLE 7.1

The analysis process is initiated by executing the ROTWASH software, as described in the user's guide (appendix D), and entering the HT tiltrotor design values into the ROTWASH input data menu. These values (most are also listed in table 22) are:

HT CLASS TILTROTOR DESIGN DATA		
NUMBER OF ROTORS (1 OR 2)	2	-ND-
HUB TO HUB ROTOR SEPARATION	46.5	FT
ROTOR RADIUS	19.0	FT
GROSS WEIGHT	40,000	LB
FUSELAGE DOWNLOAD FACTOR	10.0	PCT
ROTOR HEIGHT ABOVE GROUND	46.0	FT
SHAFT TILT ANGLE (<20 DEG)	0.0	DEG
AIR DENSITY RATIO	1.0	-ND-
AMBIENT WIND (-10 TO 10 KT)	5.0	KT

Input values that have been assumed in this example are the atmospheric density ratio, which is equal to 1.0 (sea level standard conditions), and the rotor hover height, which is 46.0 feet (near out-of-ground effect).

As noted in section 2.1, the worst case tiltrotor velocity profile forms along the centerline axis of the aircraft (directly in front and aft). This axis is referred to as the interaction plane (IPLANE). Therefore, the IPLANE option is executed in the ROTWASH program. If a series of distances are evaluated along the IPLANE, graphs of peak profile velocity and dynamic pressure versus IPLANE distance can be developed, as shown in figure 129. An example profile at a distance of 57.0 feet along the IPLANE is presented in figure 130. The peak velocity chosen from this profile for plotting in figure 129 is the value of 87 knots at a height above ground level of 7.5 feet. After figure 129 is constructed, it appears that the IPLANE distance of approximately 40 to 50 feet produces the peak rotorwash velocity value for the given input data. The value of 50 feet is chosen for structural design purposes, because it is unlikely that the pilot would be comfortable at less than one rotor radius from surrounding objects during a hover (this equates to approximately 38 feet along the IPLANE). The peak velocity and dynamic pressure profiles for this location are presented in the tabular printout of figure 131 and the graphs of figure 132.

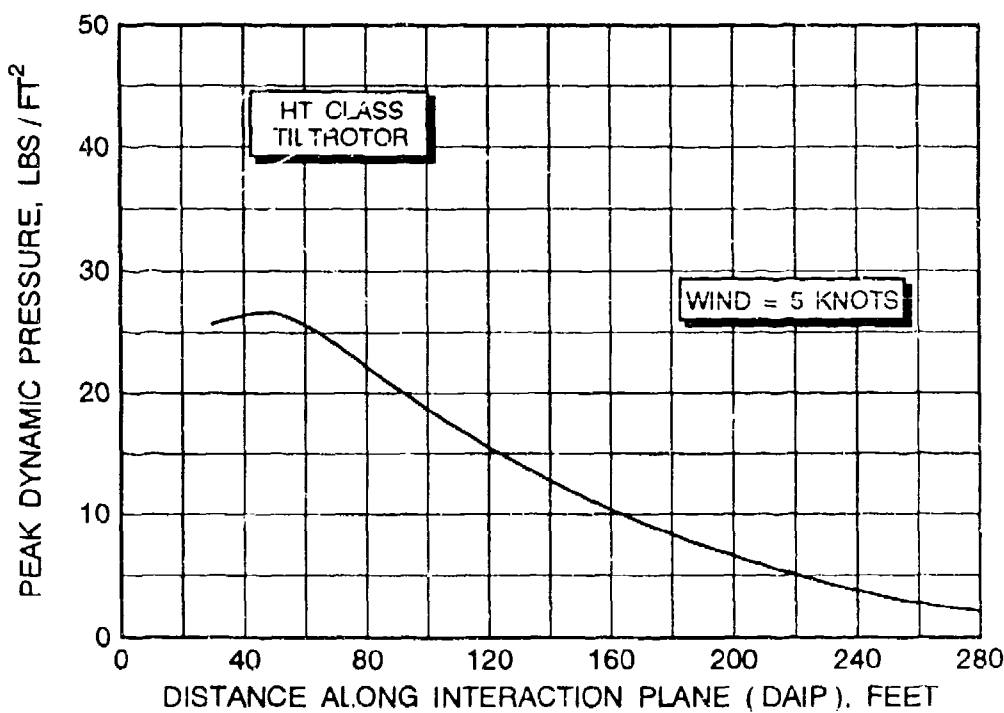
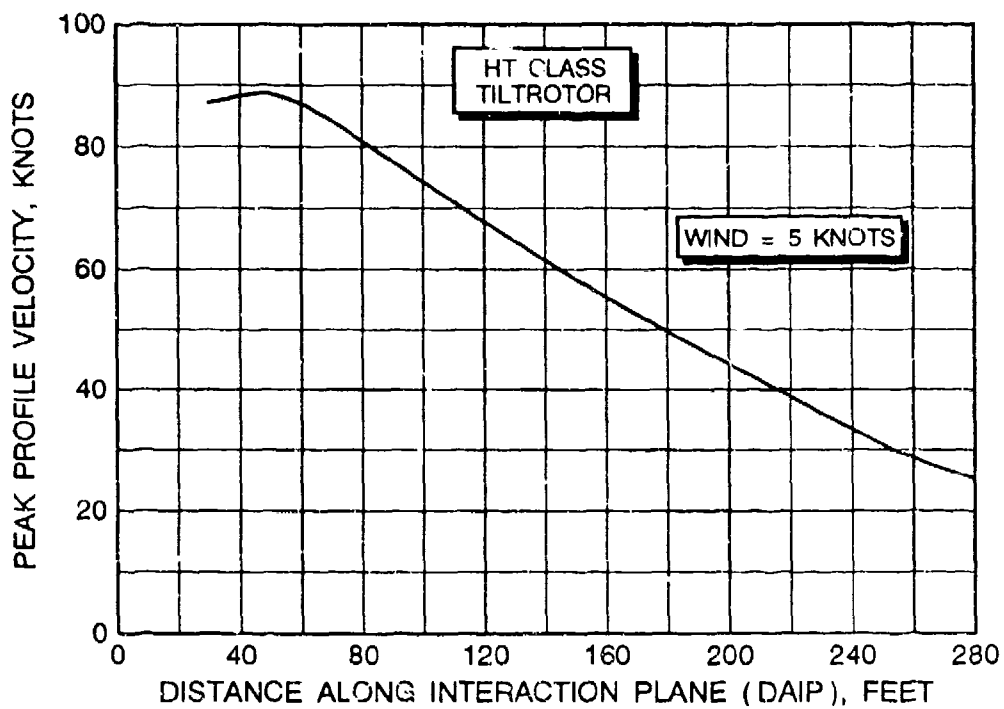


FIGURE 129 HT CONFIGURATION PEAK VELOCITY AND DYNAMIC PRESSURE VERSUS IPLANE DISTANCE

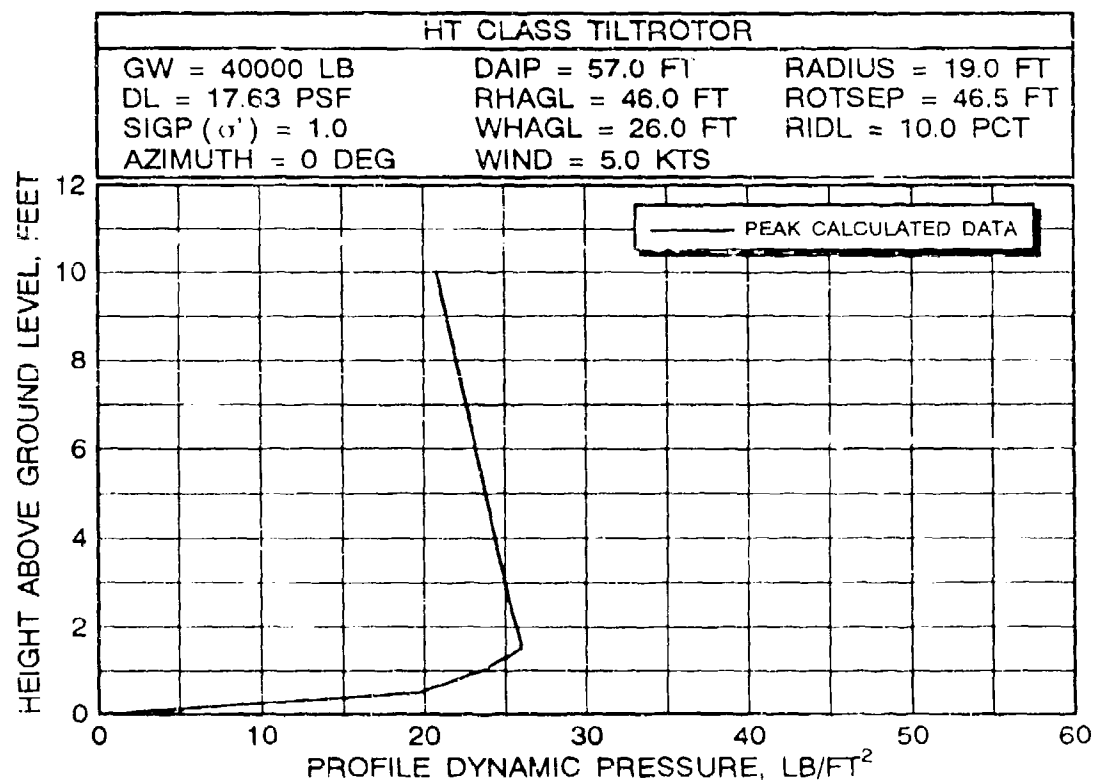
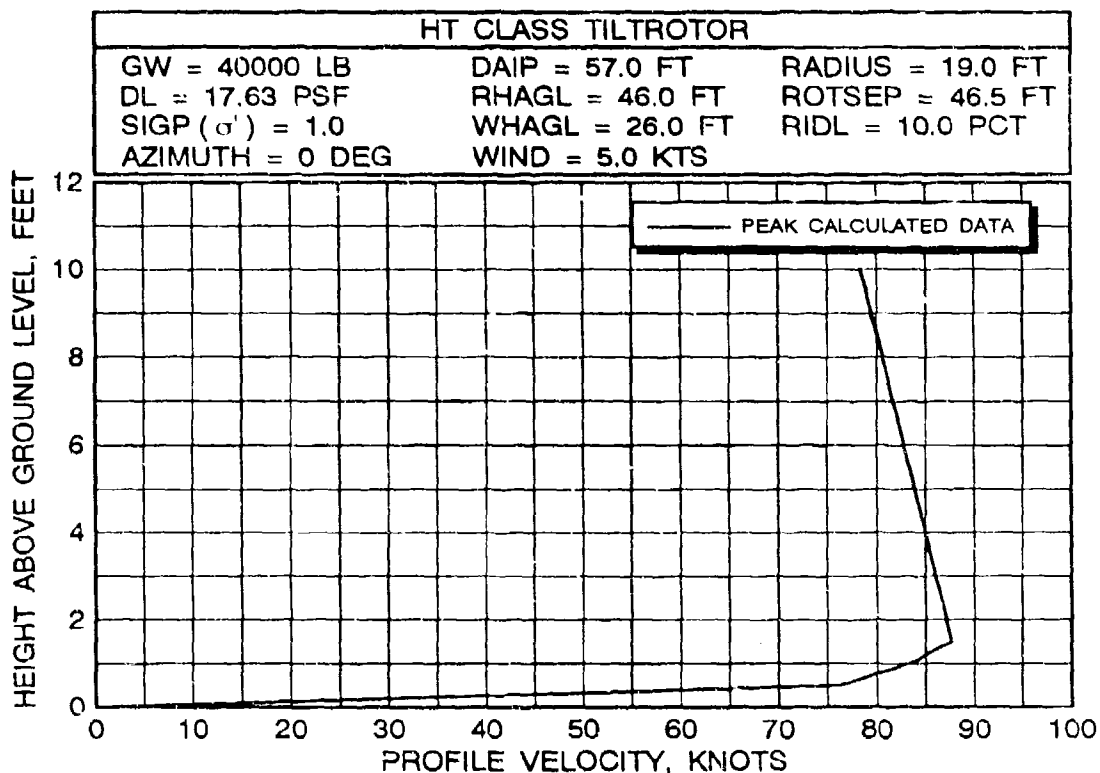


FIGURE 130 HT CONFIGURATION PEAK VELOCITY AND DYNAMIC PRESSURE PROFILES AT AN IPLANE DISTANCE OF 57 FEET

TWIN ROTOR INTERACTION PLANE VELOCITY PROFILE AT STATION = 50.0 FT

HEIGHT (FT)		MEAN VELOCITY (FPS)	MEAN VELOCITY (KN)	PEAK VELOCITY (FPS)	PEAK VELOCITY (KN)	MEAN Q (PSF)	PEAK Q (PSF)
.00	H	.000	.000	.000	.000	.000	.000
	V	.000	.000	.000	.000	.000	.000
.50	H	97.282	57.666	130.615	77.424	11.247	20.275
	V	41.043	24.329	56.876	33.714	2.002	3.844
1.00	H	105.905	62.777	142.563	84.507	13.329	24.154
	V	46.089	27.320	63.868	37.859	2.524	4.848
1.50	H	110.986	65.789	149.605	88.681	14.639	26.600
	V	49.554	29.374	68.671	40.706	2.918	5.604
2.00	H	110.189	65.316	148.500	88.026	14.430	26.208
	V	50.152	29.729	69.500	41.197	2.989	5.740
2.50	H	109.388	64.842	147.391	87.368	14.221	25.818
	V	50.733	30.073	70.305	41.674	3.059	5.874
3.00	H	108.585	64.366	146.278	86.709	14.013	25.429
	V	51.297	30.407	71.085	42.137	3.127	6.005
3.50	H	107.780	63.888	145.162	86.047	13.806	25.043
	V	51.843	30.731	71.842	42.586	3.194	6.134
4.00	H	106.973	63.410	144.044	85.384	13.600	24.659
	V	52.372	31.045	72.576	43.021	3.260	6.260
4.50	H	106.165	62.931	142.924	84.721	13.395	24.277
	V	52.885	31.348	73.286	43.442	3.324	6.383
5.00	H	105.356	62.451	141.803	84.056	13.192	23.897
	V	53.381	31.642	73.973	43.849	3.386	6.503
5.50	H	104.546	61.972	140.681	83.391	12.990	23.521
	V	53.860	31.926	74.637	44.243	3.448	6.621
6.00	H	103.737	61.492	139.559	82.726	12.789	23.147
	V	54.323	32.201	75.279	44.623	3.507	6.735
6.50	H	102.927	61.012	138.438	82.061	12.590	22.777
	V	54.770	32.466	75.899	44.990	3.565	6.846
7.00	H	102.119	60.533	137.317	81.397	12.393	22.409
	V	55.201	32.722	76.496	45.345	3.621	6.954
7.50	H	101.311	60.054	136.198	80.734	12.198	22.046
	V	55.617	32.968	77.072	45.686	3.676	7.060
8.00	H	100.505	59.576	135.080	80.071	12.005	21.685
	V	56.017	33.205	77.627	46.015	3.729	7.162
8.50	H	99.700	59.099	133.965	79.410	11.813	21.329
	V	56.403	33.434	78.161	46.331	3.781	7.260
9.00	H	98.897	58.623	132.852	78.751	11.624	20.976
	V	56.773	33.653	78.674	46.636	3.831	7.356
9.50	H	98.096	58.148	131.743	78.093	11.436	20.627
	V	57.129	33.864	79.167	46.928	3.879	7.449
10.00	H	97.298	57.675	130.637	77.437	11.251	20.282
	V	57.470	34.066	79.640	47.208	3.925	7.538

TYPE <C>ONTINUE, NEXT <P>OINT, <N>EW CASE, E<X>IT ==>

FIGURE 131 HT CONFIGURATION VELOCITY AND DYNAMIC PRESSURE PROFILE PRINTOUT AT AN IPLANE DISTANCE OF 50 FEET

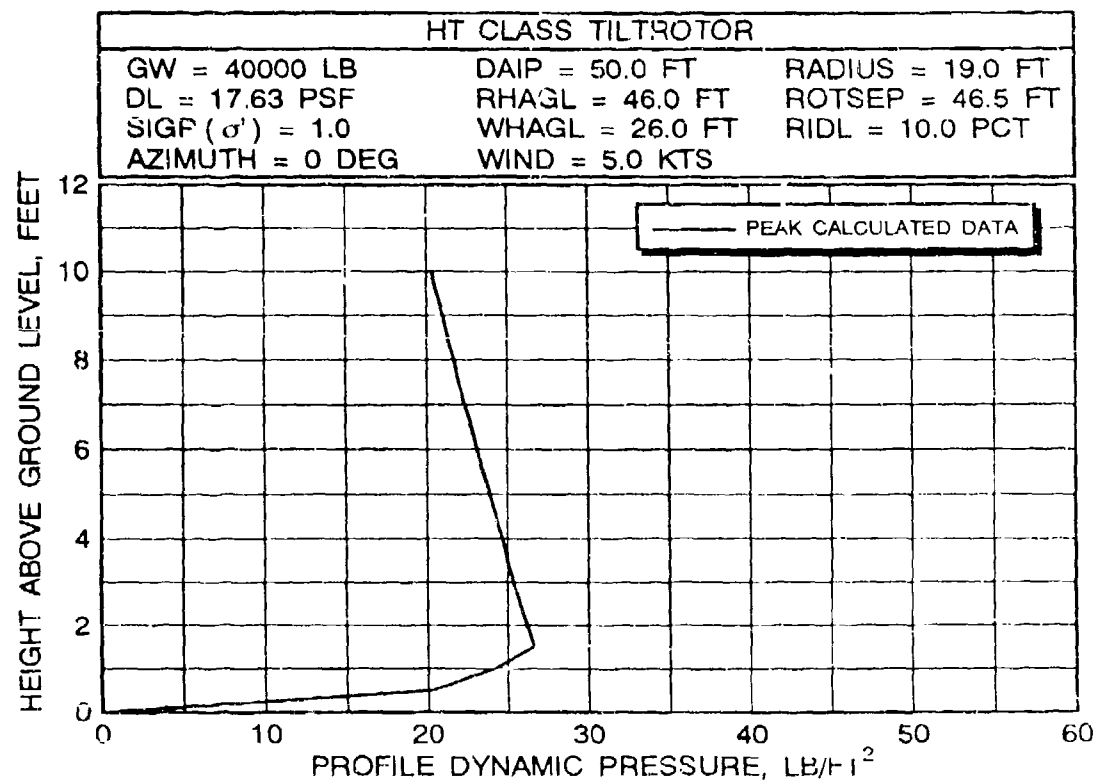
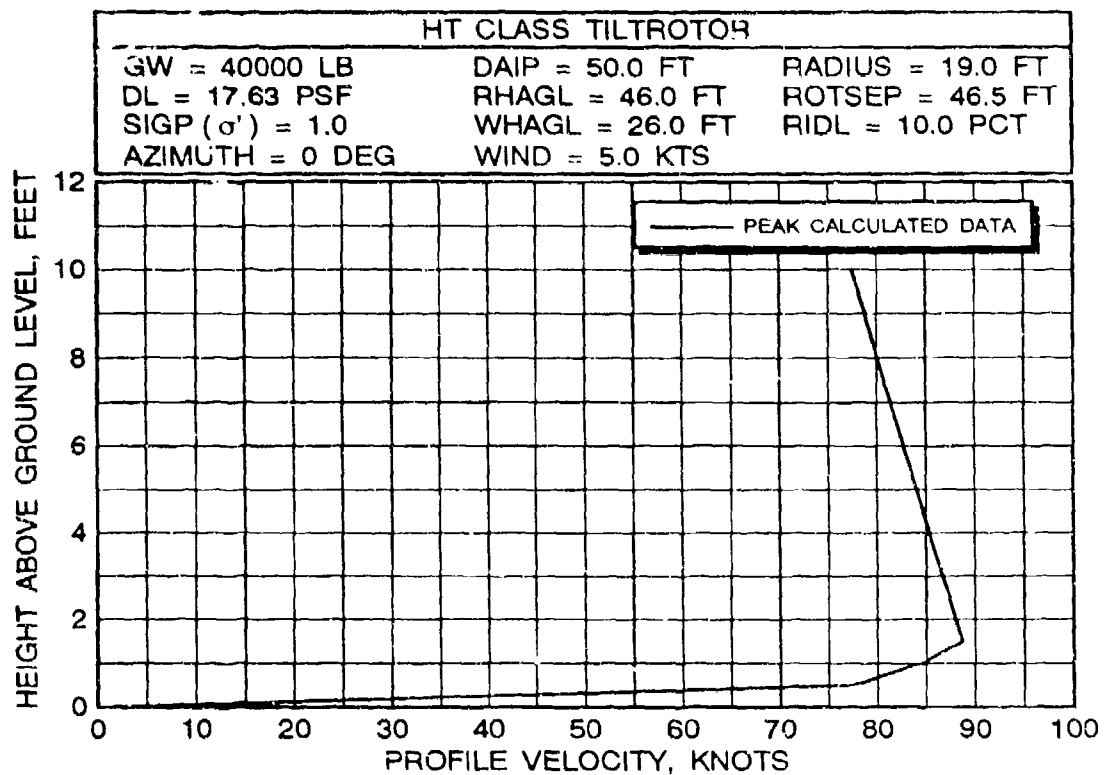


FIGURE 132 HT CONFIGURATION PEAK VELOCITY AND DYNAMIC PRESSURE PROFILES AT AN IPLANE DISTANCE OF 50 FEET

It is important to remember that detailed correlation or even an approximate comparison of any predicted design data with flight test data is very important whenever possible. In this instance, tabulation of the predicted profile at the IPLANE distance of 57 feet is presented for the user to compare the results with the correlated MV-22 data presented in figure 52. Even though flight test data are non-existent at the desired IPLANE position of 50 feet, the comparison of predicted results at the alternate IPLANE location is very close to available flight test data. Therefore, the designer has increased confidence that the design values are reasonably accurate.

The next step in the analysis is to define the loads generated by the H class helicopter configuration. The input data for this configuration as used in the example are:

H CLASS HELICOPTER DESIGN DATA		
NUMBER OF ROTORS (1 OR 2)	1	-ND-
HUB TO HUB ROTOR SEPARATION	0.0	FT
ROTOR RADIUS	40.0	FT
GROSS WEIGHT	73,390	LB
FUSELAGE DOWNLOAD FACTOR	5.0	PCT
ROTOR HEIGHT ABOVE GROUND	46.0	FT
SHAFT TILT ANGLE (<20 DEG)	0.0	DEG
AIR DENSITY RATIO	1.0	-ND-
AMBIENT WIND (-10 TO 10 KT)	5.0	KT

Identical values of density ratio and rotor height above ground level are used for consistency with the HT results. It should be noted that rotorwash velocities would be slightly higher at a higher rotor height, because 46.0 feet is in partial ground effect for the H configuration. However, since an emergency condition would not fit a high hover height scenario, the slightly lower loading should be more than appropriate for design purposes where a safety factor is applied.

Predictions of peak rotorwash velocities for the single-rotor helicopter configuration are made using the wall jet option in the ROTWASH program. Figure 133 presents the predicted H class peak profile velocities and dynamic pressures as a function of distance from the rotor center (DFRC). This range of distances is calculated by executing the wall jet option at 20-foot intervals (for vertical height increments along the profile of 0.5 feet) and picking off the peak and mean profile velocities

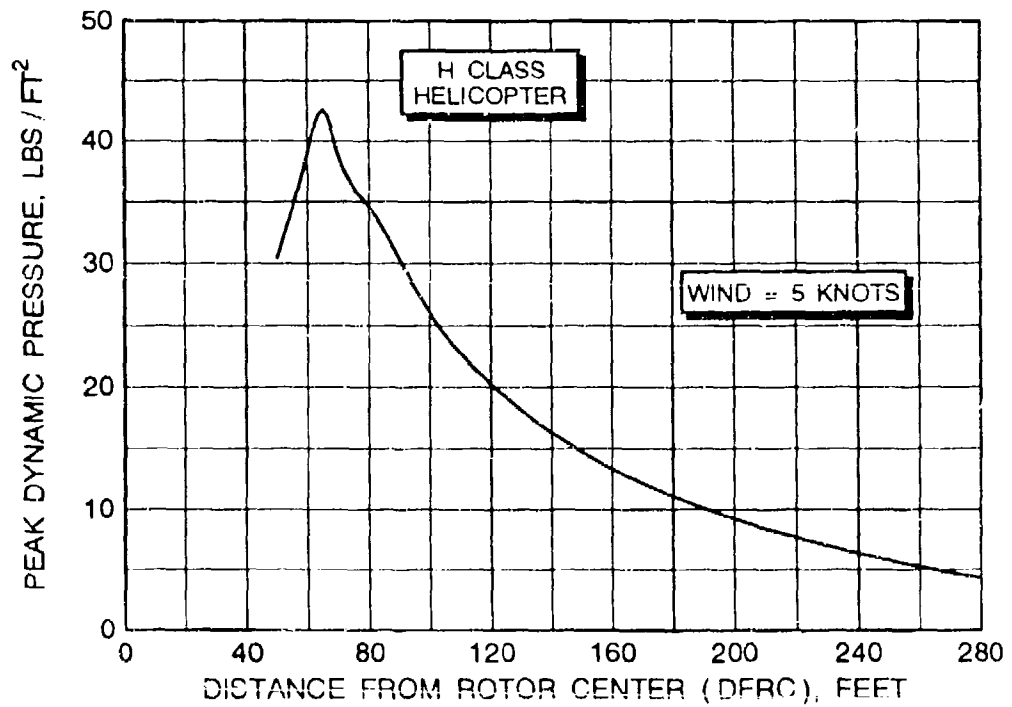
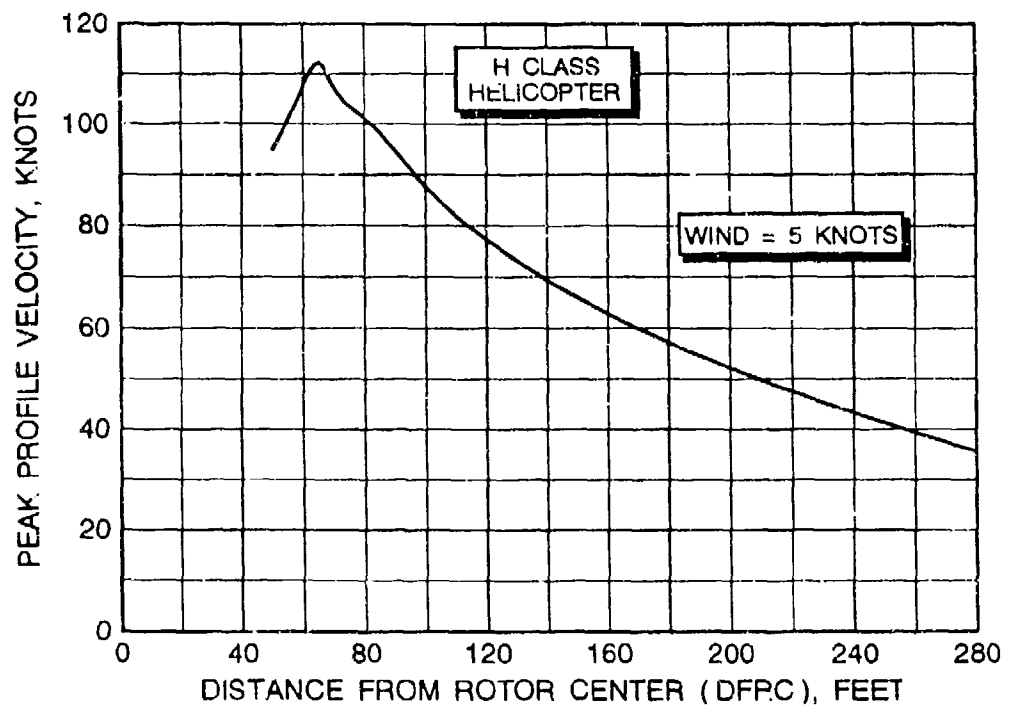


FIGURE 133 H CONFIGURATION PEAK VELOCITY AND DYNAMIC PRESSURE VERSUS DFRC DISTANCE

SINGLE ROTOR VELOCITY PROFILE AT RADIUS = 65.0 FT

PROFILE BOUNDARY HEIGHT = 13.54 FT
 HALF-VEL. HEIGHT = 5.41 FT
 MAX-VEL HEIGHT = 1.79 FT

HEIGHT (FT)	MEAN VELOCITY (FPS)	PEAK VELOCITY (FPS)	MEAN Q (PSF)	PEAK Q (PSF)
.00	.000	.000	.000	.000
.50	109.111	64.678	159.499	94.546
1.00	118.779	70.408	174.411	103.385
1.50	124.894	74.033	183.843	108.976
2.00	126.970	75.264	189.190	112.146
2.50	118.509	70.248	185.875	110.181
3.00	110.104	65.266	181.019	107.303
3.50	101.908	60.408	174.924	103.690
4.00	93.984	55.711	167.773	99.451
4.50	86.369	51.197	159.720	94.677
5.00	79.088	46.881	150.908	89.454
5.50	72.159	42.774	142.515	84.478
6.00	65.596	38.883	137.828	81.700
6.50	59.411	35.217	131.454	77.922
7.00	53.613	31.780	123.653	73.298
7.50	48.210	28.578	114.691	67.985
8.00	43.211	25.614	104.832	62.141
8.50	38.620	22.893	94.349	55.927
9.00	34.444	20.417	83.513	49.504
9.50	30.688	18.191	72.600	43.035
10.00	27.356	16.216	61.887	36.685

TYPE <C>ONTINUE, NEXT <P>OINT, <N>EW CASE, E<X>IT ==>

FIGURE 134 H CONFIGURATION VELOCITY AND DYNAMIC
 PRESSURE PROFILE PRINTOUT AT A DFRC DISTANCE OF 65 FEET

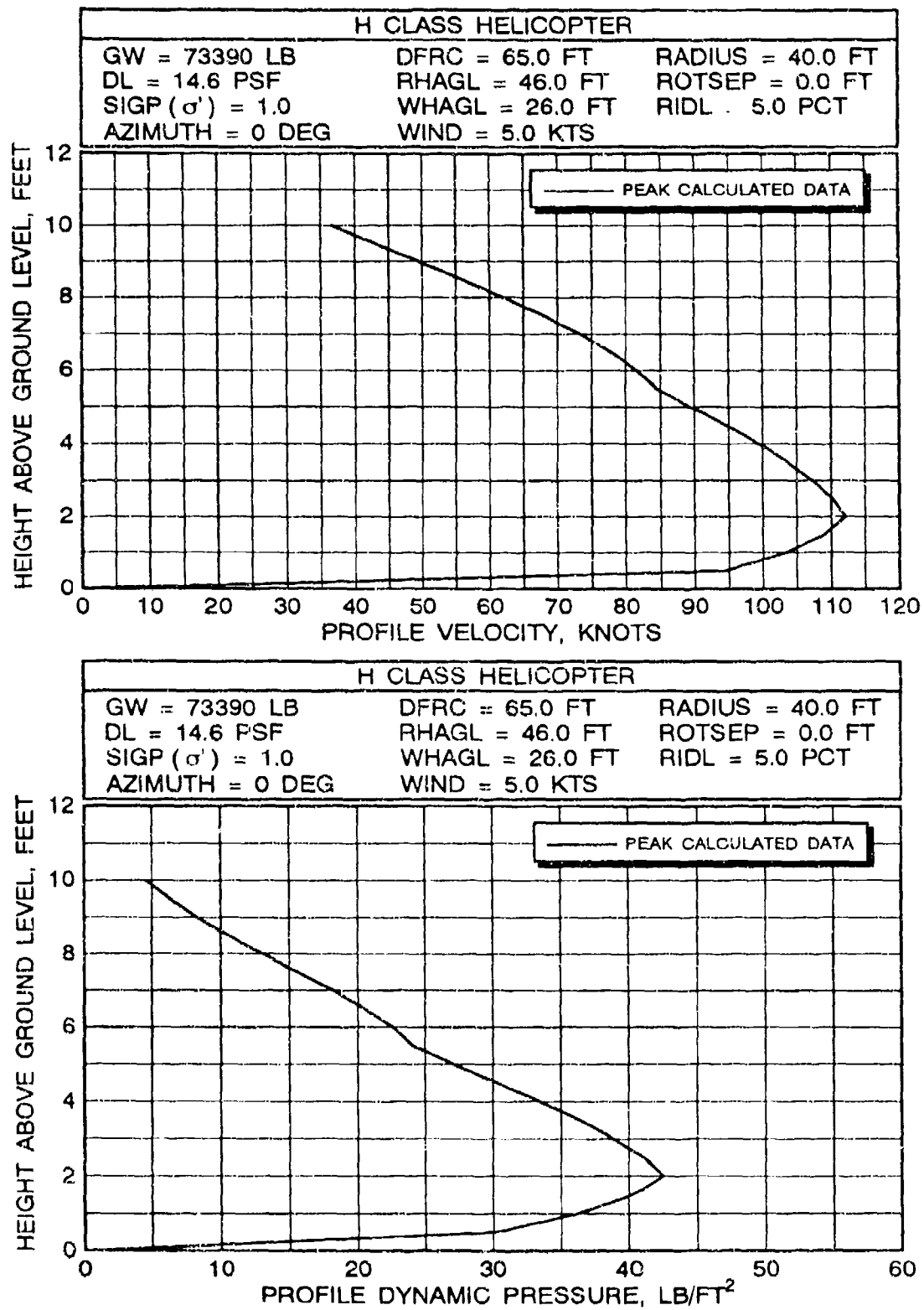


FIGURE 135 H CONFIGURATION PEAK VELOCITY AND DYNAMIC PRESSURE PROFILES AT A DFRC DISTANCE OF 65 FEET

from the tabular printout. Based on this figure, the distance at which the worst case peak velocity occurs is approximately 65 feet. The peak velocity and dynamic pressure profiles at this radial location are presented in the tabular printout of figure 134 and the graphs of figure 135. Correlation of predicted results with flight test data for this configuration is well represented by the CH-53E data that are presented in section 3.1 and appendix B (this is because the H class configuration is almost identical to the CH-53E at the 70,000 pound gross weight).

The definition of the worst case HT and H class peak velocity and dynamic pressure profiles provides the vertiport designer with data required for structural design purposes (meets decision #2 requirements, see section 7.1). More information on this subject will be presented in section 7.3.

Solutions to operational vertiport design issues, specified by decision #3 (see section 7.1), require velocity and dynamic pressure profile data of a slightly different nature. Therefore, the third task is to analyze the SM-sized configuration. Design criteria are listed below.

1. The SM configuration is a skid-equipped single main rotor helicopter. This helicopter is allowed to air taxi to any location on the vertiport ramp surface. Out-of-ground effect hover conditions are assumed possible at any location (this sets a minimum rotor height of approximately 40 feet).
2. The adverse design crosswind for these conditions is 9.0 knots.

The ROTWASH input data characteristics for the SM class are:

SM CLASS HELICOPTER DESIGN DATA		
NUMBER OF ROTORS (1 OR 2)	1	-ND-
HUB TO HUB ROTOR SEPARATION	0.0	FT
ROTOR RADIUS	20.0	FT
GROSS WEIGHT	10,400	LB
FUSELAGE DOWNLOAD FACTOR	1.5	PCT
ROTOR HEIGHT ABOVE GROUND	40.0	FT
SHAFT TILT ANGLE (<20 DEG)	0.0	DEG
AIR DENSITY RATIO	1.0	-ND-
AMBIENT WIND (-10 TO 10 KT)	9.0	KT

Using the wall jet option outlined in the user's guide, both mean and peak velocity and dynamic pressure profile data are obtained at 35, 40, 50, 70, 90, and 110 feet (DFRC). These data are presented in figures 136 and 137. Unfortunately, no specific flight test data exist for correlation with this particular size of rotorcraft. However, the generally good correlation of data with the CH-53E, XV-15, MV-22, and CL-84 in sections 2.1 through 2.4 and in appendix B provide confidence that the predicted SM class data are more than accurate enough for hazard analysis purposes. The availability of these profile data at a series of distances from the rotor center now make it possible to move on to an analysis of operationally related "How To" examples. These examples are presented in sections 7.2 through 7.7.

7.2 PERSONNEL OVERTURNING FORCES AND MOMENTS

The most serious types of mishaps are those that threaten the health and well-being of people. The most frequent types of rotorwash mishaps that threaten people are those that involve being knocked down by the impact of high velocity rotorwash and those where people are struck by blown objects. The "How To" example in this section focuses on the first of these two types of mishaps.

The physics and literature associated with mishaps involving people being knocked down by rotorwash are presented in section 5.1. Section 5.1.5 suggests safe overturning force and moment limits for three different classes of personnel. These limits, listed in table 23, are used as guidelines for avoiding potential mishaps in this conceptual design example. Decision #3 (see section 7.1) by the municipal operators and vertiport designers specifies that all operational rotorwash-related concerns be based on safe air taxi operations of the SM class helicopter for a 9 knot crosswind condition. Therefore, the first task at hand is to define the overturning force and moment characteristics of the SM sized rotorcraft. The second task involves an analysis of the vertiport design layout to determine if restrictions involving personnel have to be developed. A brief analysis will also be conducted to define the overturning force characteristics of the HT and H size rotorcraft.

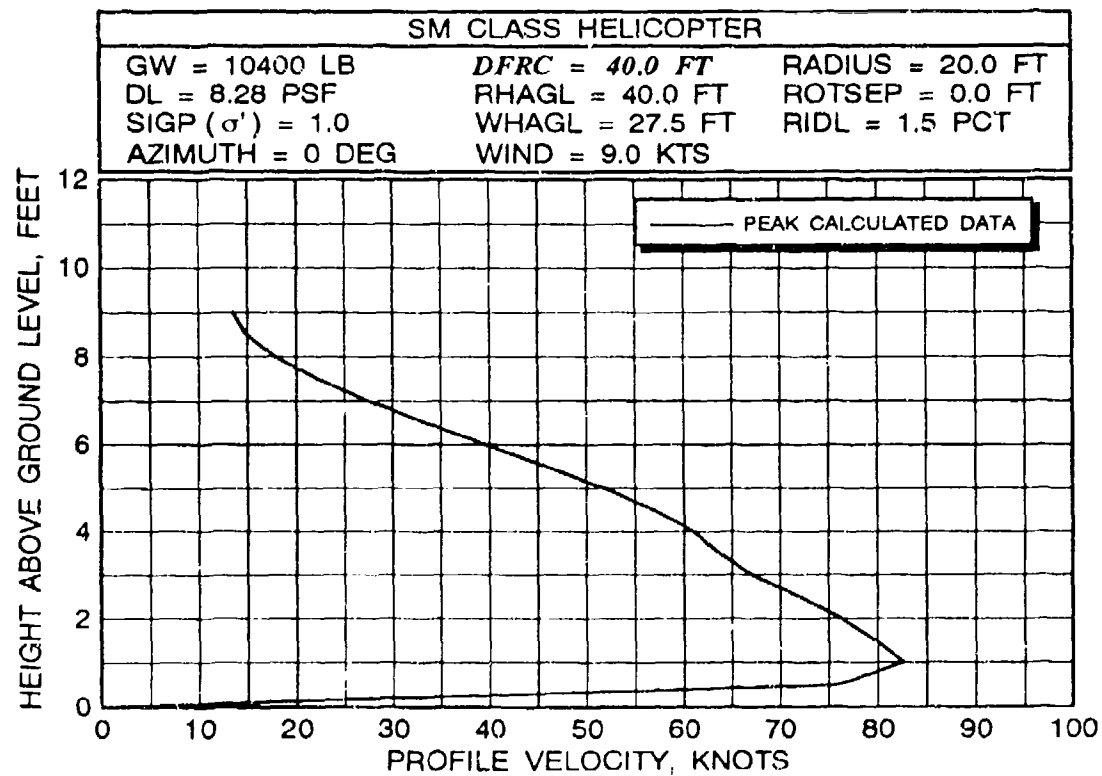
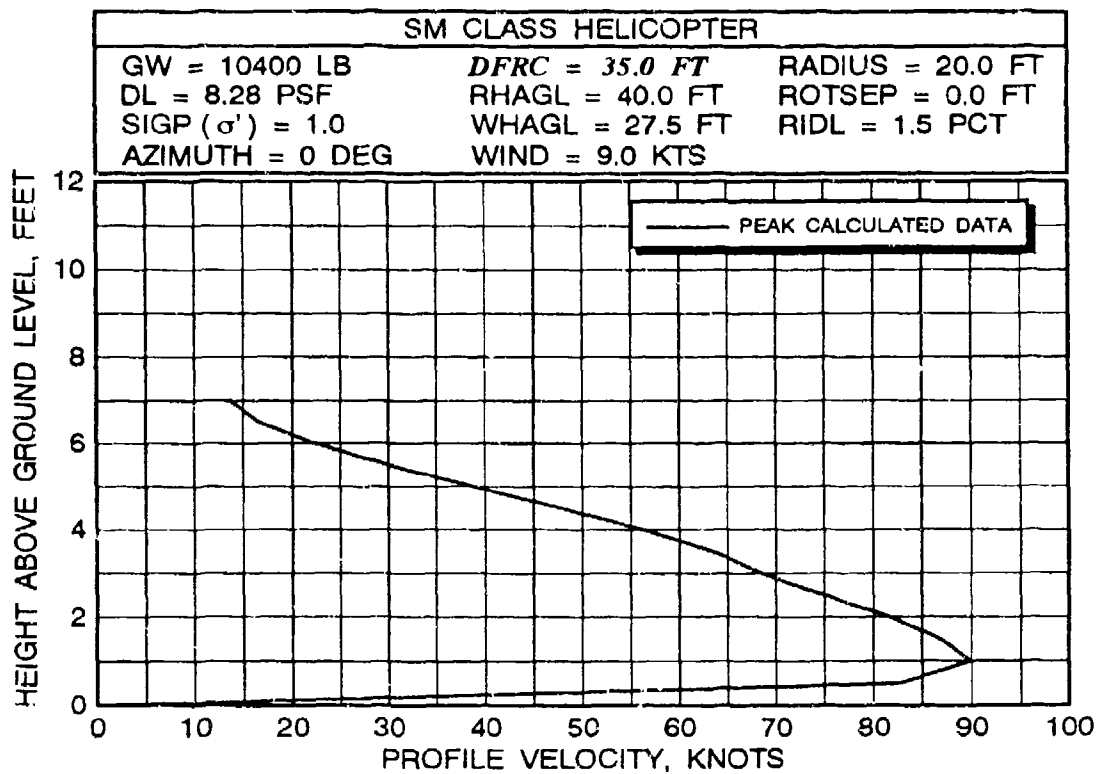


**FIGURE 136 SM CONFIGURATION PEAK VELOCITY
VERSUS HEIGHT ABOVE GROUND LEVEL**

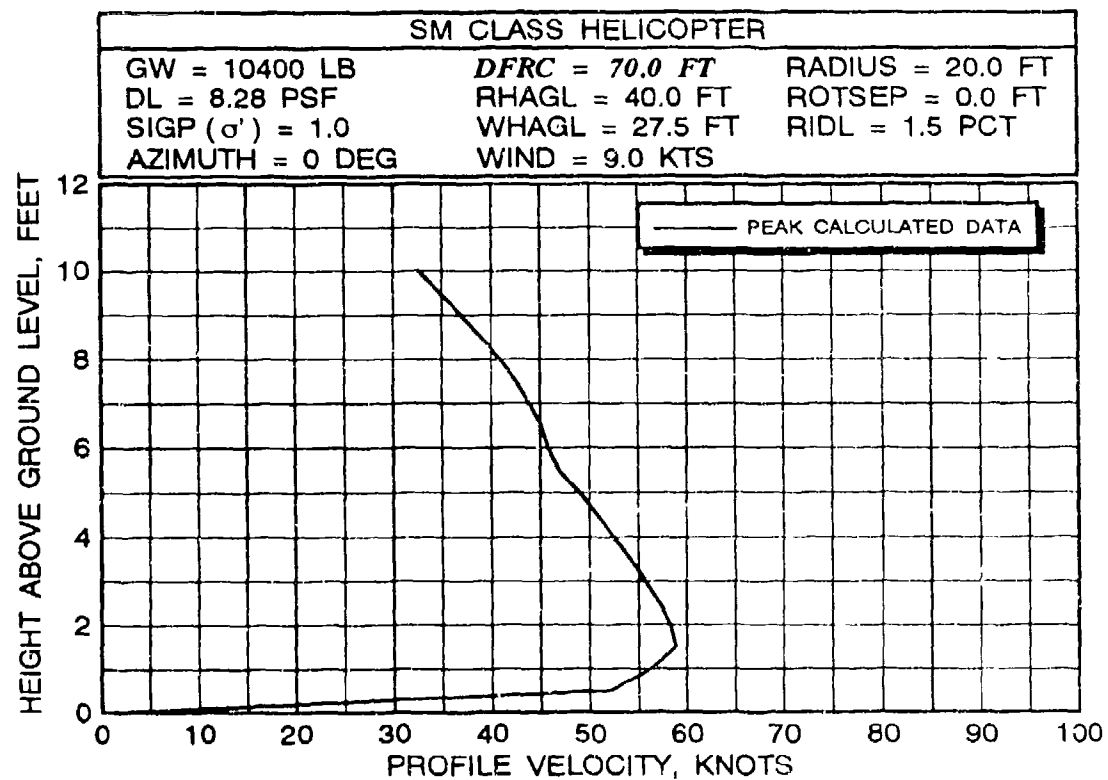
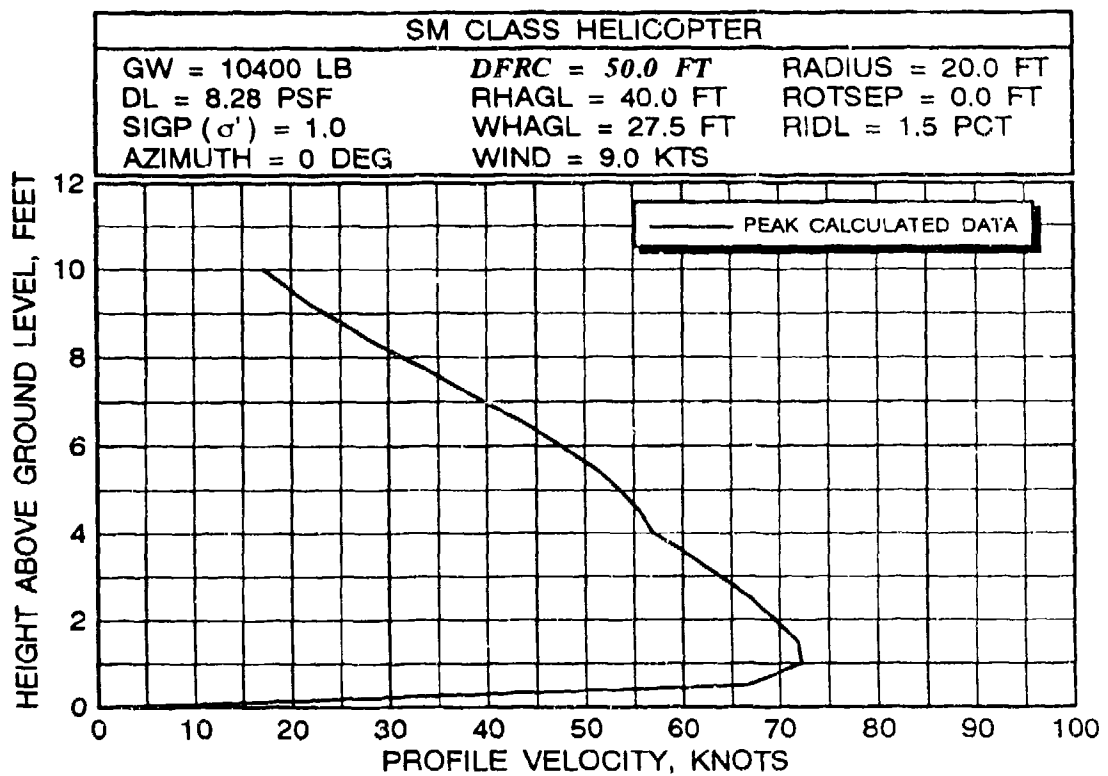


**FIGURE 136 SM CONFIGURATION PEAK VELOCITY
VERSUS HEIGHT ABOVE GROUND LEVEL (continued)**

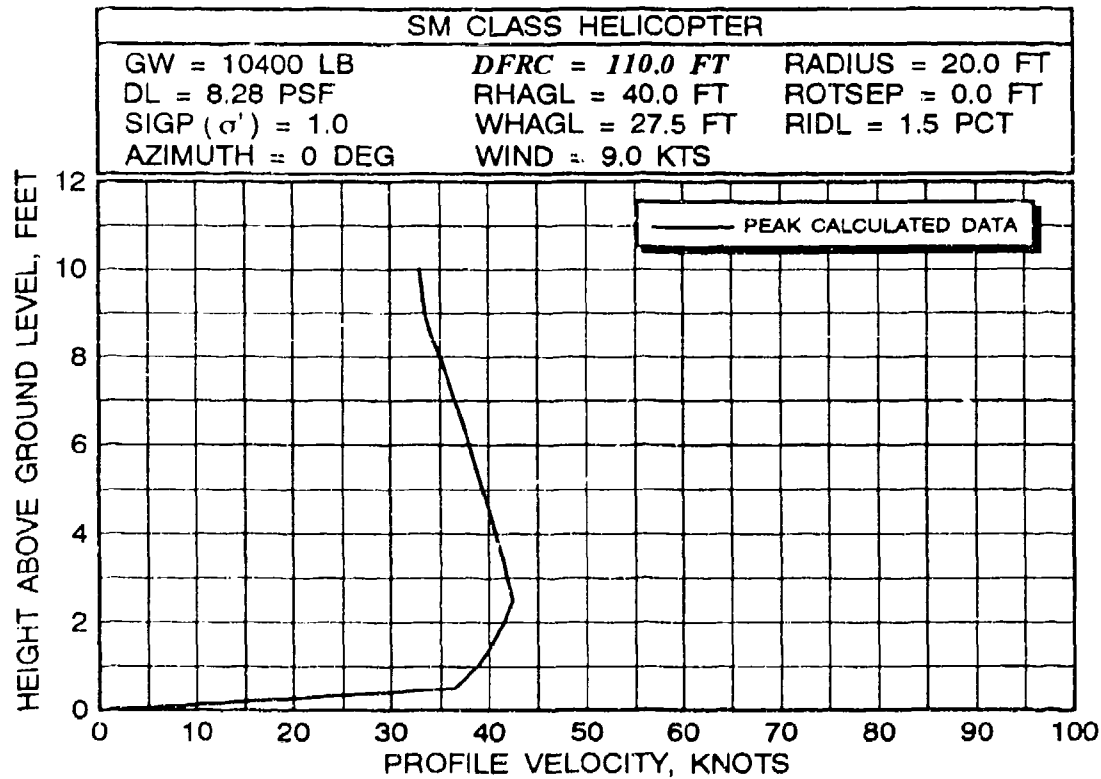
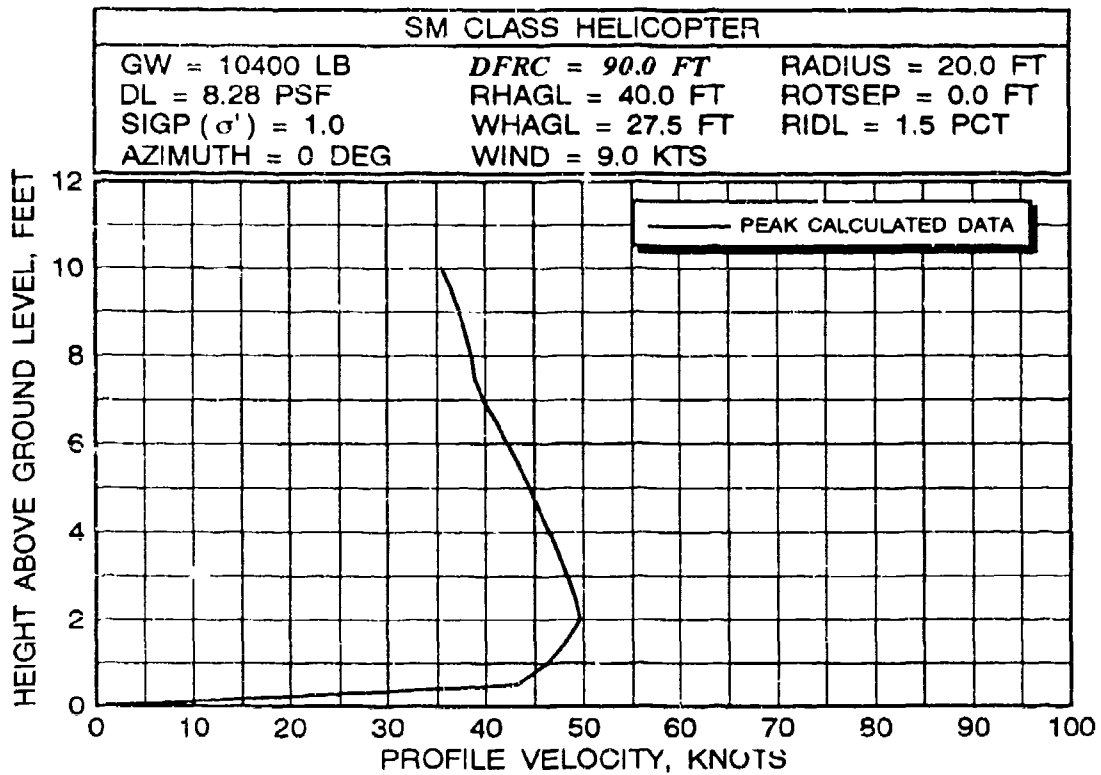


**FIGURE 136 SM CONFIGURATION PEAK VELOCITY
VERSUS HEIGHT ABOVE GROUND LEVEL (continued)**

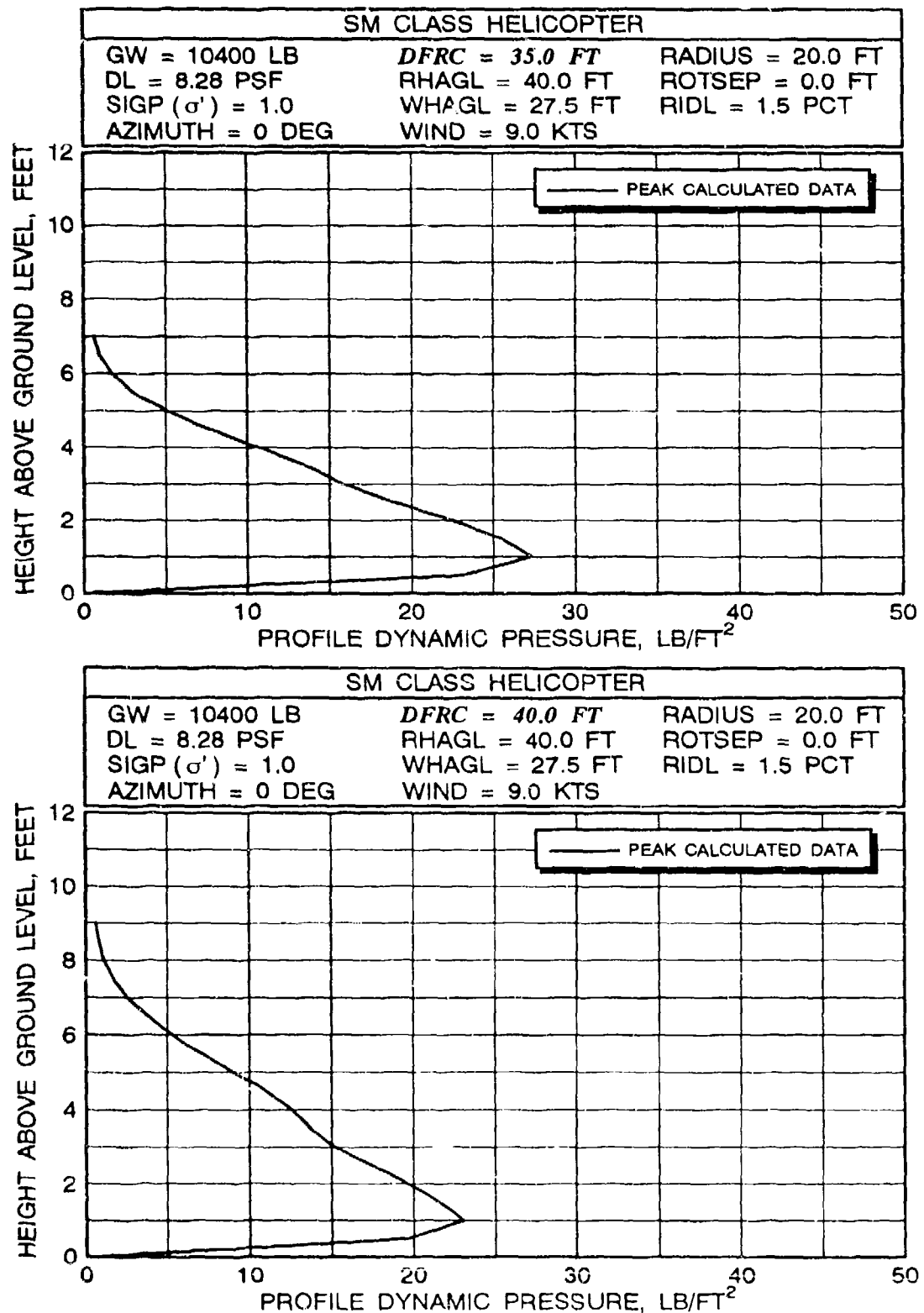


**FIGURE 137 SM CONFIGURATION PEAK DYNAMIC PRESSURE
VERSUS HEIGHT ABOVE GROUND LEVEL**

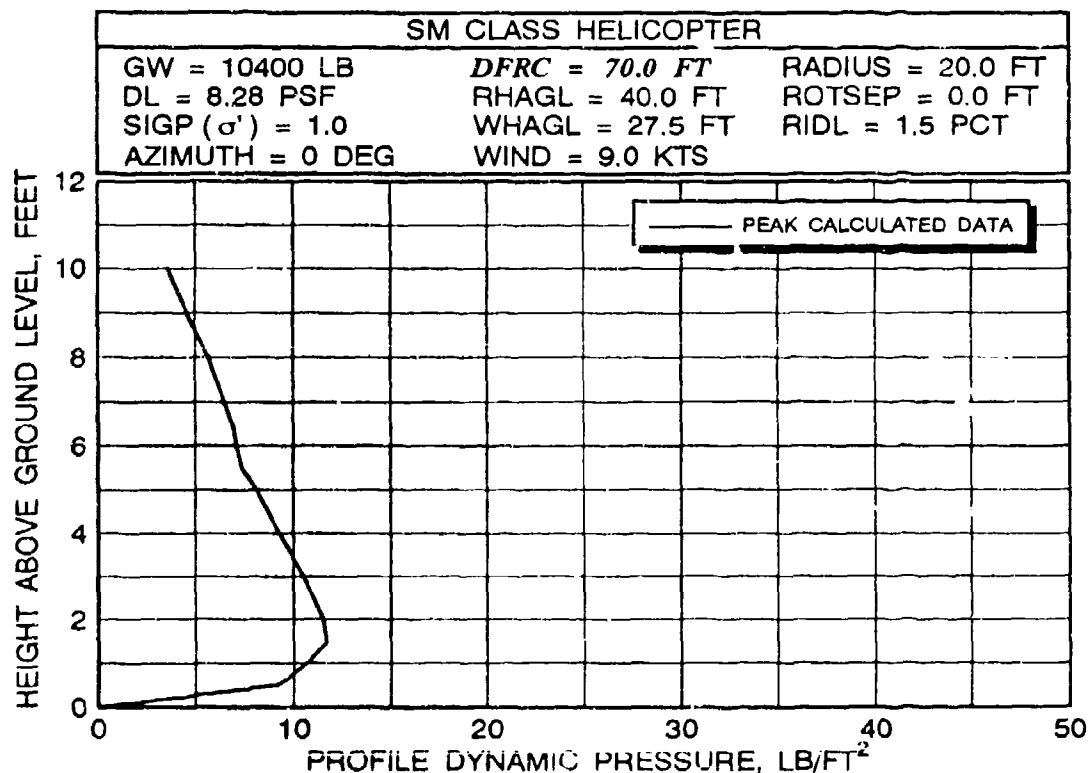
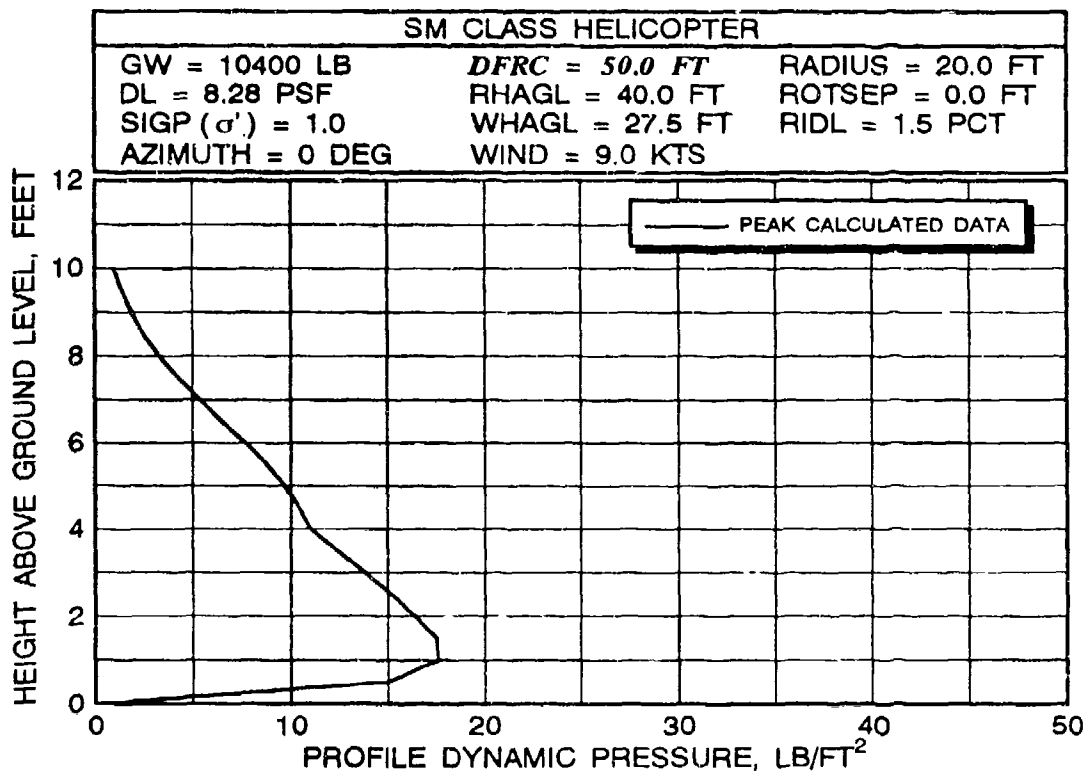
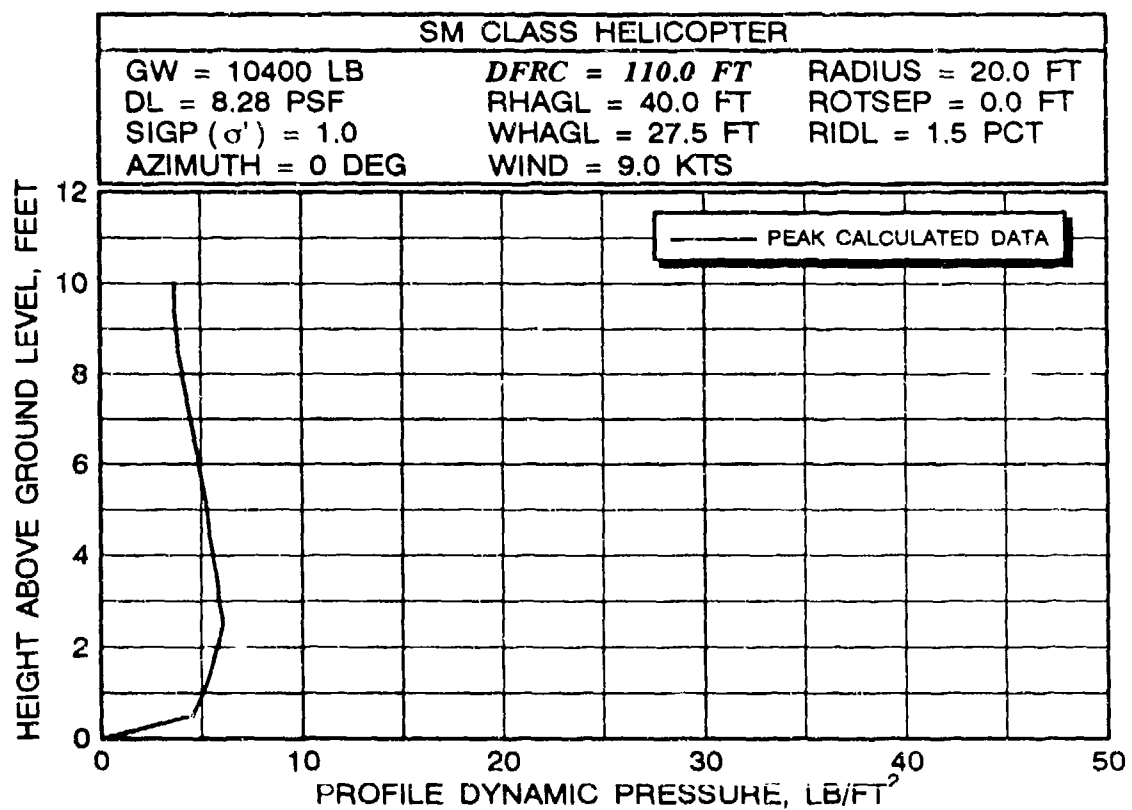
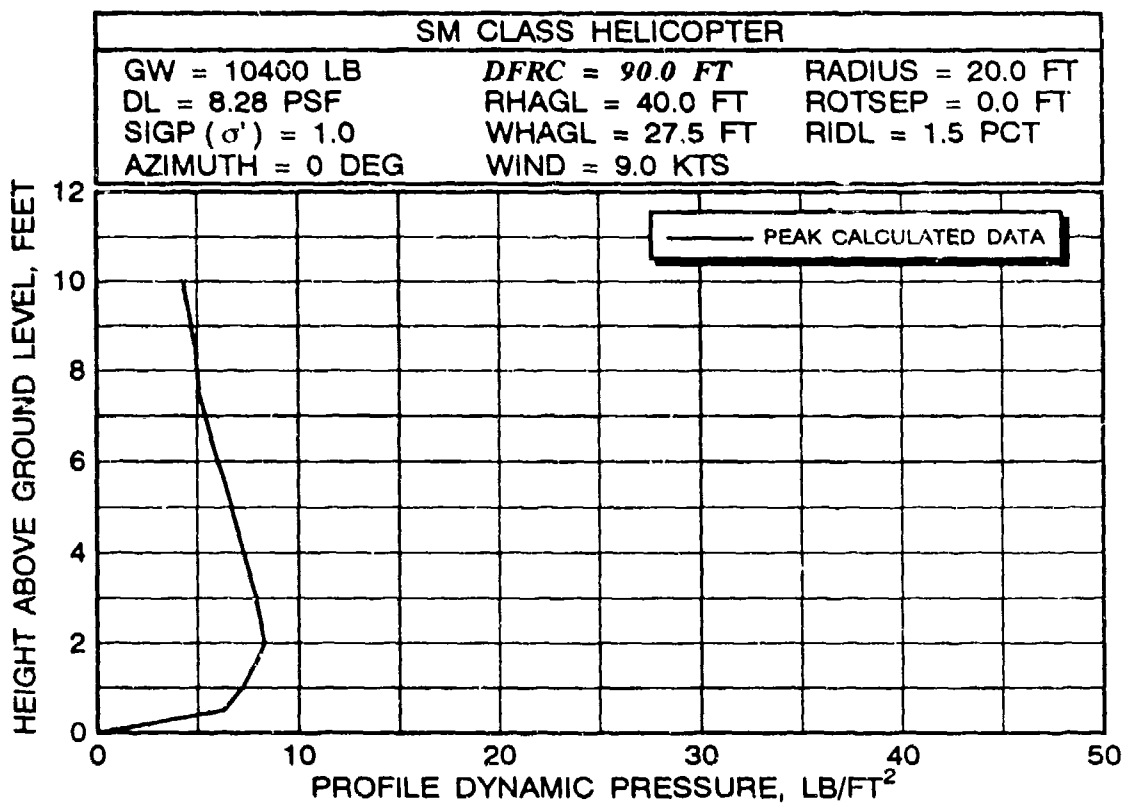


FIGURE 137 SM CONFIGURATION PEAK DYNAMIC PRESSURE VERSUS HEIGHT ABOVE GROUND LEVEL (continued)



**FIGURE 137 SM CONFIGURATION PEAK DYNAMIC PRESSURE
VERSUS HEIGHT ABOVE GROUND LEVEL (continued)**

TABLE 23 SUGGESTED FORCE AND MOMENT LIMITS ON PERSONNEL

PERSONNEL CLASSIFICATION	FORCE LIMIT, LBS	MOMENT LIMIT, FT-LBS
I Trained and protected ramp personnel frequently working in a rotorcraft downwash environment	80	260
II Untrained and unprotected personnel rarely or never exposed to a rotorcraft downwash environment	40	120
III Untrained and unprotected children likely to be walking without assistance from an adult in a rotorcraft downwash environment	30	60

Force and moment calculations on personnel are made by integrating SM class dynamic pressure profiles (figure 137) over the "L"- and "S"-sized personnel (6 and 4 feet in height respectively). Section 5.1.2 explains the mathematics of this process. This task is accomplished automatically using the ROTWASH program by choosing the OVERTURNING FORCE/MOMENT option on the hazard type menu. The user's guide in appendix D provides details on the mechanics of executing this option. If the SM class rotorcraft characteristics from table 22 are entered into the program and analyzed over a range of radial positions from 30 to 150 feet, the results in figure 138 are obtained. Force limits are exceeded for classes I through III (see table 23), respectively, at radial distances of less than 50, 95, and 115 feet, respectively, from the center of the rotor. These results have to be evaluated in the context of the vertiport design layout.

The basic dimensions of the vertiport landing and parking surfaces are presented in figure 126. The overturning force limit for trained and protected personnel is 80 pounds. Based on the data from figure 70, it is possible that for personnel not trying to sustain forward movement, the limit could be increased. This 80-pound limit is exceeded only at distances less than 50 feet (DFRC) under worst case conditions (9-knot wind) with the SM-sized helicopter. Since the vertiport is approximately 170 feet wide at its narrowest point (60 feet within the narrow parking space plus a ramp width of 110 feet to the safety net), trained personnel should be safe virtually everywhere on the vertiport. This assumes trained personnel are provided easy

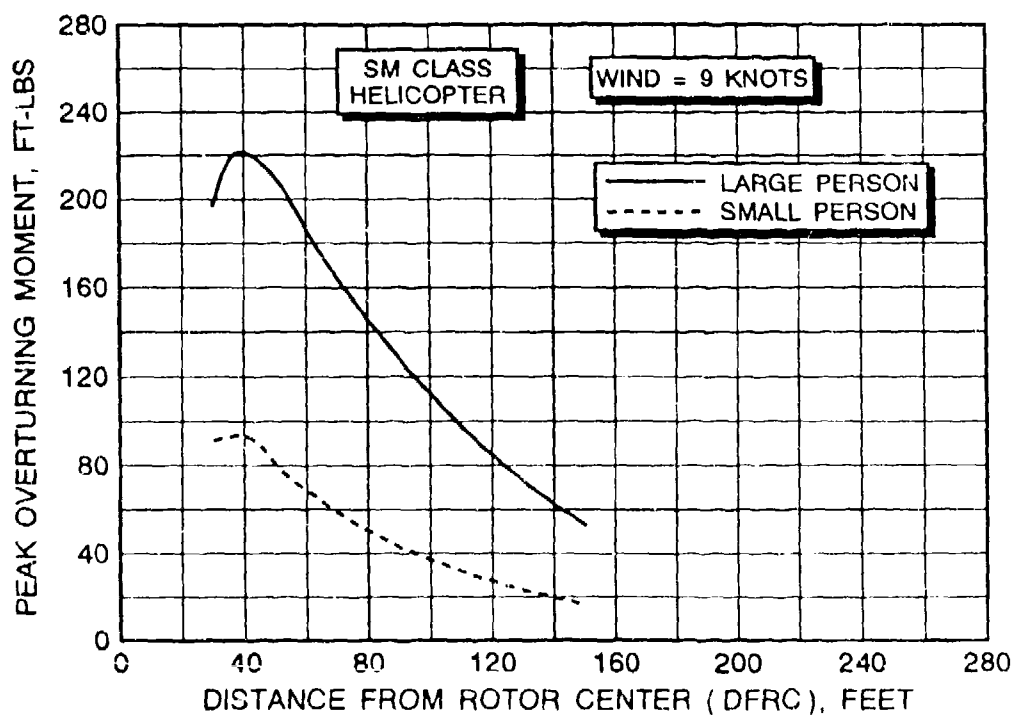
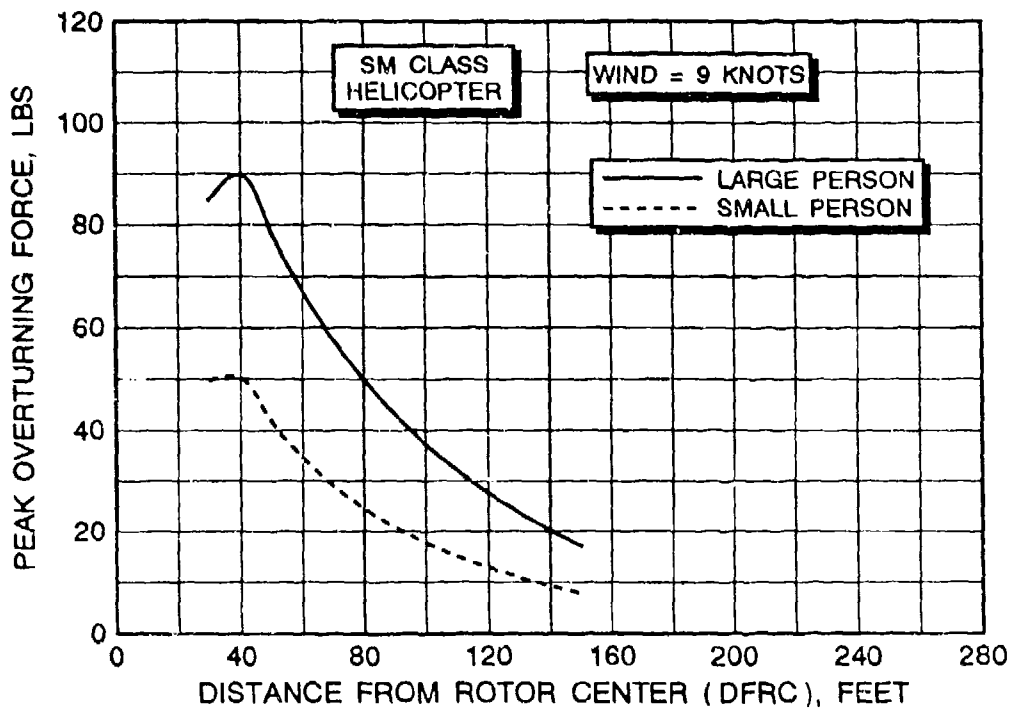


FIGURE 138 SM CONFIGURATION PEAK OVERTURNING FORCE AND MOMENT VERSUS DISTANCE FROM THE CENTER OF THE ROTOR

access to move about the surface as incoming SM helicopters transits to landing locations. Also, a prudent operational design feature would be to provide the rotorcraft a marked pathway to air taxi near the shoreline edge of the vertiport. This design feature, coupled with an operational procedure requiring use of the air taxi lane, would provide ground personnel prior knowledge of the transit route and provide a safe transit to touchdown. The air taxi lane will be discussed in more detail in a later section.

Untrained and unprotected personnel and children (classes II and III) exceed force limits at distances less than approximately 95 and 115 feet, respectively. These personnel classes also have no real reason to be on the vertiport surface unless entering or exiting a rotorcraft. If rotorcraft are required to air taxi near the shoreline area, these groups should be safe as long as they do not leave the passenger walkway or terminal areas. Therefore, a significant risk only occurs when untrained personnel stand and observe landings or departures immediately in front of a parking spot while on the walkway. One way to eliminate this risk is to build a solid fence or retaining wall separating the passenger walkway area from the rest of the vertiport surface. The purpose of this wall is to deflect rotorwash from the horizontal plane into the vertical plane and provide a safe place for personnel to walk. As a minimum, this "solid" wall should probably be about 4 feet high with a chain link fence up to at least 8 feet. Gates should be inserted at two or three locations on both sides of the terminal for easy access through the wall. The wall is also a good design feature for security within the vertiport operating area.

It has already been noted that HT and H class rotorcraft will be required to ground taxi from the rollway to either landing place numbers 1 or 2. This operational decision helps to insure that these large rotorwash-producing configurations do not interact with the rest of the vertiport users. However, to be thorough, overturning forces for the HT and H class rotorcraft under worst case conditions are calculated and presented in figure 139 for the 5-knot design condition included in decision #2 (see section 7.1). As can be seen, H class forces of 80 pounds can be obtained as far as 150 feet. If an assumption is made that 40 percent of a 73,390-pound takeoff weight is required to initiate a ground taxi after rollback, forces of 80 pounds are exceeded at a distance of approximately 65 feet. Along the interaction plane, the HT-class tiltrotor generates 70 pounds of force out to 50 feet. These calculations confirm several operational concerns:

1. Construction of a rotorwash deflecting wall for protection of all types of personnel on the walkway is a valid requirement. Use of enclosed paths (like jet-ways at an airport) would also be an option.

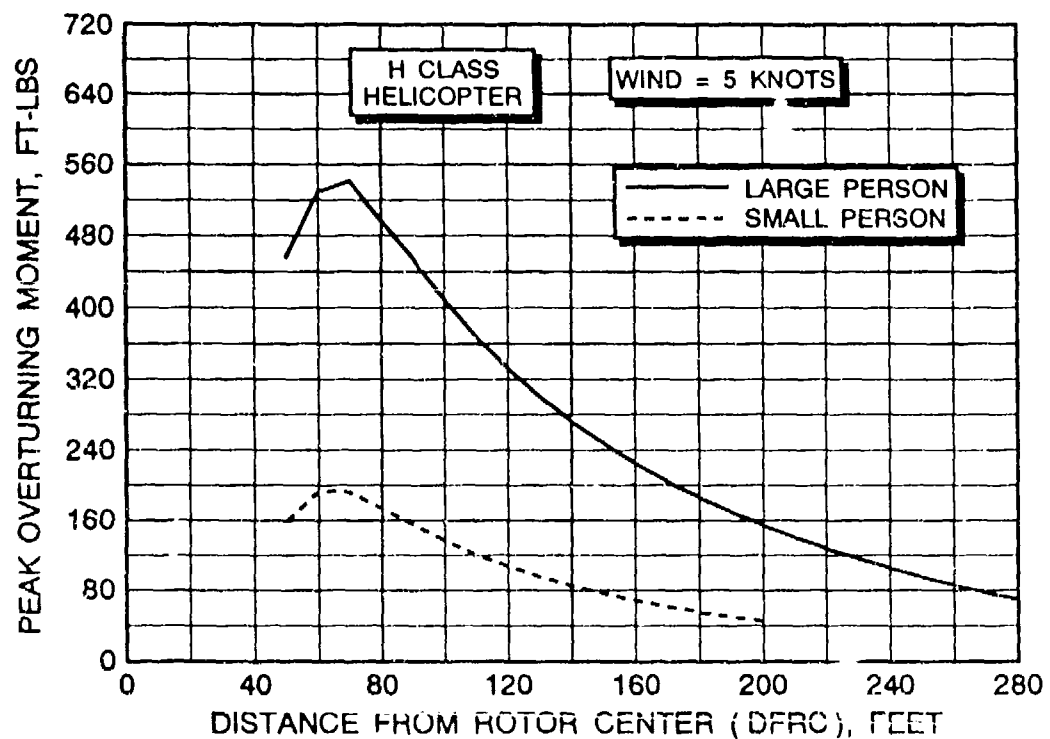
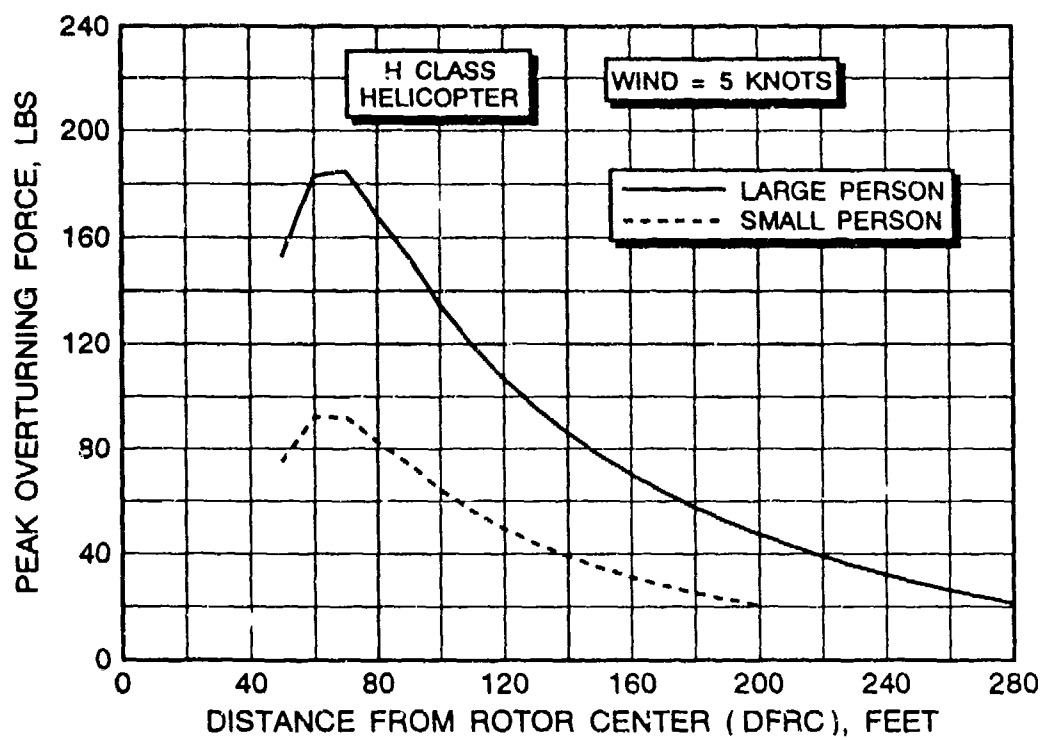


FIGURE 139 H CONFIGURATION PEAK OVERTURNING FORCE AND MOMENT VERSUS DISTANCE FROM THE CENTER OF THE ROTOR

2. All operations involving HT and H class rotorcraft under their own power need to be made to spots 1 and 2 with maximum clearance to spots 3 through 7.

In fairness to the SM, HT, and H class rotorcraft, it should again be pointed out that the above calculations are for worst case conditions related to this one conceptual design example. The suggested design features and operational restrictions should not be viewed as indicators that rotorwash will "damage everything along the pathways that large rotorcraft take." With further analysis, the clearances associated with the design example might very well be reduced or simplified in scope.

7.3 LOADINGS ON GROUND STRUCTURES

Design decision #2 (see section 7.1) states that the vertiport structure will be designed to withstand the maximum rotorwash loads generated by both the HT and H size configurations with a 5-knot worst azimuth crosswind condition. The mean dynamic pressure profiles for this design requirement were calculated in the section 7.1 example and presented in figures 132 and 135. The peak dynamic pressure loading for the HT class (figure 132) is approximately 27 psf at 2 feet above the ground. The peak loading for the H class (figure 135) is approximately 42 psf at 2 feet. These data provide a starting place for aiding the structural design engineer; however, peak loadings are not the only issue of importance to structure design.

Section 5.4.1 provides data from the uniform building codes that indicate that some parts of the United States only require design to distributed wind loads of 20 psf. Based on data from figures 132 and 135, this loading condition is probably exceeded at least over small areas of the structure. The caution in this statement comes from the fact that the data in the figures are generated for profiles that are freely flowing across open ground. Except for very small isolated structures (i.e., a human or a small sign), a structure can have a significant effect on altering the applied loading characteristics of a free-flowing profile. The general effect is to average or flatten out dynamic pressure loads in both the horizontal and vertical planes such that lower distributed loads are observed at the critical peak loading location along the profile. In the case of the H class, the profile load would tend to be reduced at the critical height of approximately 2 feet and increased at heights several feet above and below the critical height. The direction of the flow is also altered significantly, as the flow has to change direction to flow around the structure. The data in table 16 from the CPP wind tunnel test indicate that a 15 percent reduction in peak pressure loads due to three-dimensional effects is not unreasonable (It must also be noted that 5 knots instead of 9 knots of adverse crosswind has been used as the design criteria to account partially for this effect). Therefore, for this particular design example, it should be acceptable to assume

that the peak localized design load will probably not exceed 36 psf.

Even though design for rotorwash peak loading requirements is important, it may be even more important for the designer to consider fatigue loads. Data from figures 5, 6, 8, and 9 provide representative data on the typical magnitudes of rotorwash velocity variation and frequency content. If these data are applied to the dynamic pressure loading data of figures 132 and 135, then the designer must be prepared to design for large oscillatory loads at a frequency of 0.5 to 1.5 Hz. These oscillations could easily be in the 13 ± 10 psf range for the HT class and 20 ± 16 psf for the H class rotorcraft.

The final part of this example concerns the decision regarding application of various design loads. This task requires that figure 126 be reviewed. Clearly, any structure related to the terminal area and the passenger walkway areas should be designed to both the uniform peak loading value of 36 psf and the fatigue loads mentioned in the previous paragraphs. Until additional research is completed, any small isolated structural elements that are within several feet of a large flat surface should probably be designed to the peak loads presented in figures 132 and 135. Structural components below the rollway parking area that elevate the structure next to the shoreline are beyond the scope of this example for suggesting design criteria. However, the designer should be aware that blowing sand, water spray, and beach debris may produce damage to painted surfaces and hinder efforts to keep areas clean at these lower levels in the structure.

7.4 POTENTIAL EFFECTS ON PARKED ROTORCRAFT

Section 5.2 presents the background data and analysis results for mishaps involving rotorwash and other parked rotorcraft. Conclusions are presented in section 5.2.7 to justify the use of 30 to 37 knots as the critical threshold velocity range for rotorwash mishaps. This critical velocity range, when exceeded, applies to mishaps involving door and cowling damage, and rotor blade/tailboom strikes for both low RPM rotors and untied stopped rotors. In this example, the goal is to review the mishap potential of the SM class helicopter and suggest operational procedures to minimize the possibility of mishap occurrence.

If SM class mean/peak profile velocities are extracted from the six graphs in figure 136, the graph of peak profile velocity versus radial distance (DFRC) can be constructed as shown in figure 140. The critical peak velocity range of 30 to 37 knots for this configuration occurs at distances from approximately 125 to 155 feet under worst case, 9-knot ambient wind conditions. Operationally, this desired separation distance implies that hover air taxi of SM class helicopters should occur along a pathway close to the edge of the vertiport. A suggested line for

safety purposes would be 20 feet inboard of the safety net as shown in figure 141.

Being this near the edge of the vertiport should have another added advantage. Some as yet unpublished qualitative results from U.S. Navy operations aboard helicopter carriers indicate that drop-offs (from deck edge) near the tips of rotors may discourage the formation of rotorwash profiles across the deck in the same way that they would occur if the deck edge were not present. This effect, if it is valid, is particularly desirable for rotorcraft parking in spots 4 through 7.

Other operational considerations can also be suggested; however, before these are discussed the reader is reminded that the purpose of this design example is not to propose a mishap-proof vertiport design. Ultimately, the responsibility for safety has to remain in the hands of pilots and ground personnel. If a manned tower is included in the terminal facility, the tower operator can certainly influence the movement of large skid gear helicopters to minimize problems. Operational suggestions other than the use of the air taxi guideline painted on the surface of the deck include:

1. restrictions on air hover taxi maneuvers near parking spots where maintenance operations are underway,
2. restriction of maintenance operations to the use of parking spots at the end of the vertiport surface (i.e., spots 6 and 7), and
3. a policy where landings of large skid-equipped helicopters are made near the safety net, the helicopter is shut down, and tow tractors are used to move the helicopters to unoccupied parking locations.

Dissemination, enforcement, and wording associated with implementation of these types of guidelines, particularly in the absence of a tower operator, results in the creation of a different set of problems. Probably the most critical of these problems involves effective communication with pilots to tell them what is expected of them in operating their rotorcraft.

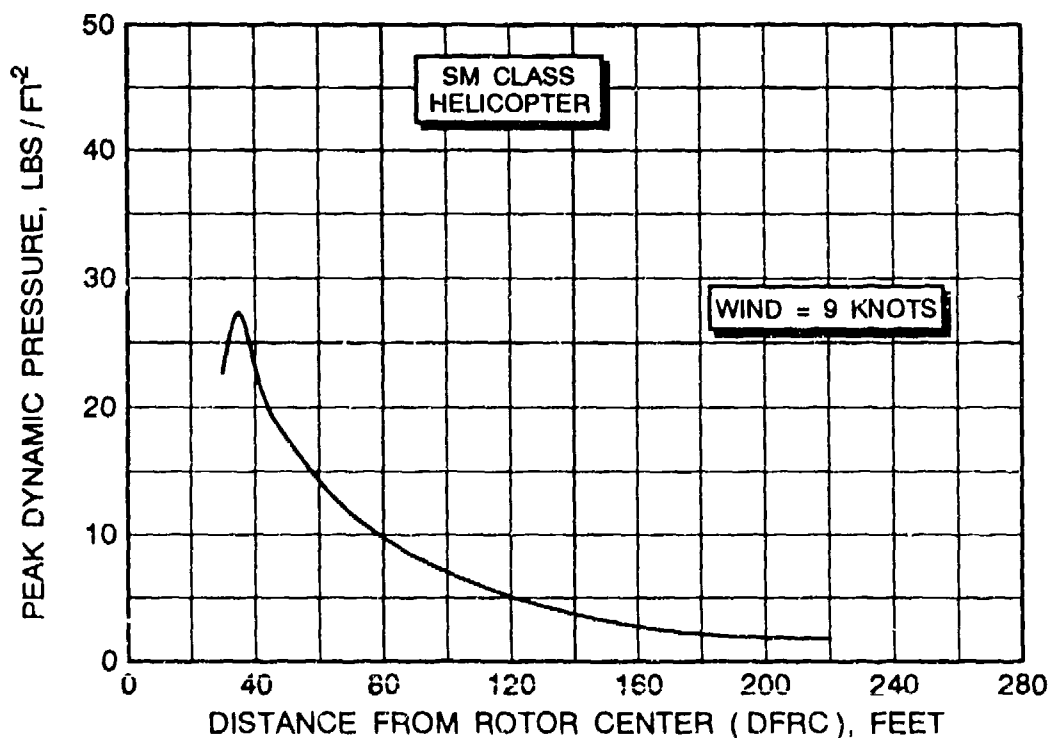
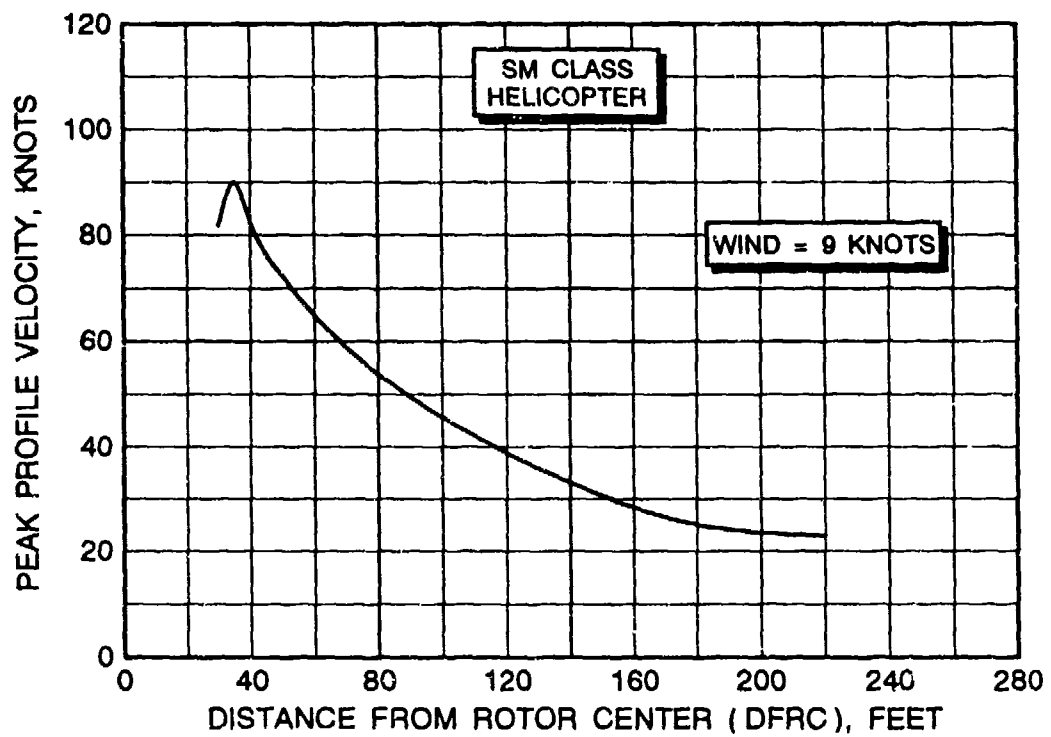
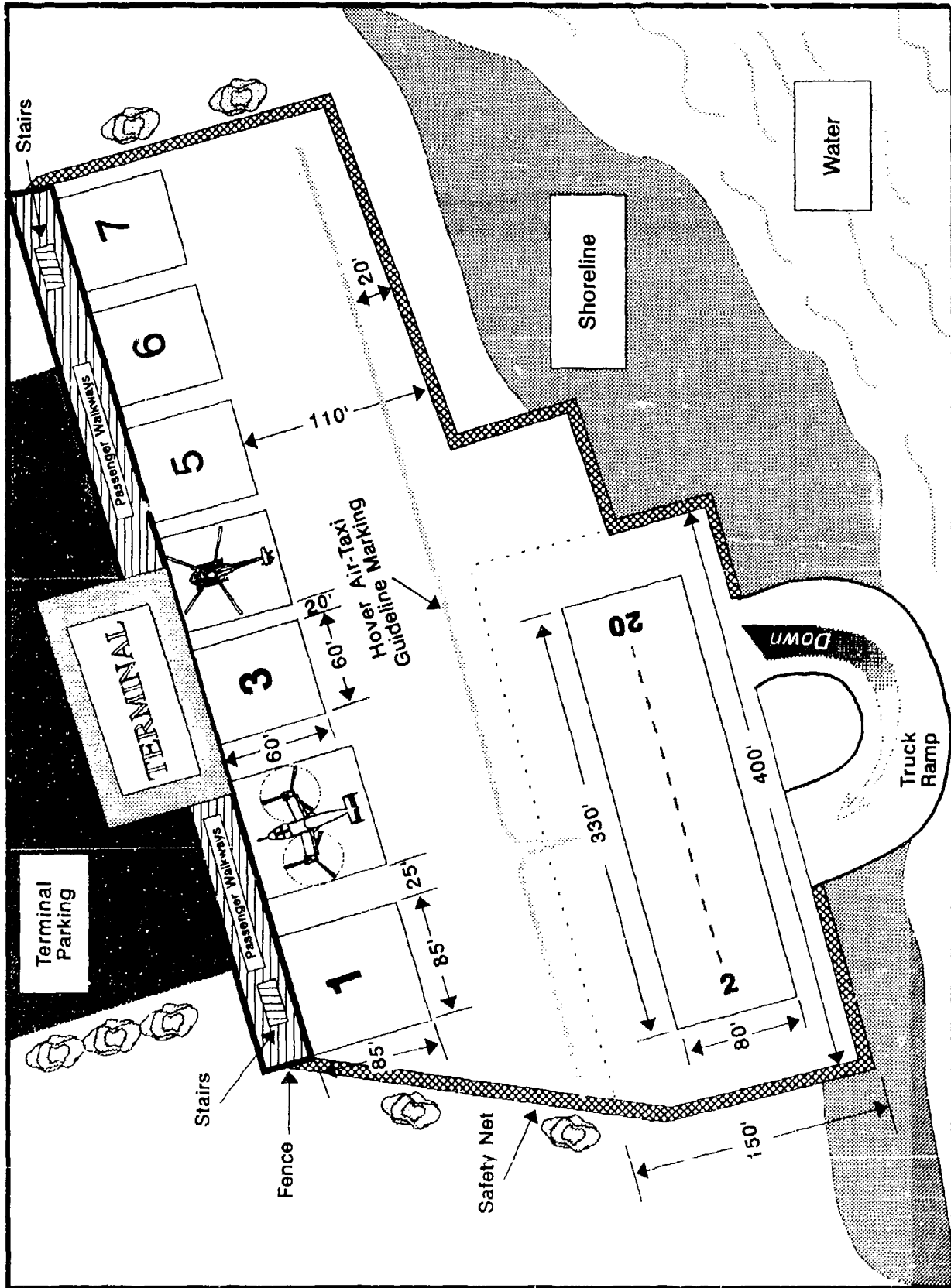


FIGURE 140 SM CONFIGURATION PEAK VELOCITY AND DYNAMIC PRESSURE VERSUS DISTANCE FROM THE CENTER OF THE ROTOR

FIGURE 14.1 VERTIPORT DESIGN DATA FOR EXAMPLE 7.4



7.5 OVERTURNING MOMENTS ON LIGHT FIXED-WING AIRCRAFT

Section 5.3 documents background data and analysis results for mishaps involving the overturning of light fixed-wing aircraft. Conclusions from this analysis imply that when critical angles-of-attack required to overturn the unsecured light aircraft are less than 10 to 12 degrees, the probability for overturning is significant. These critical angles-of-attack can easily be estimated for high-wing tail dragger configurations such as the Piper PA-18 Cub from peak velocity data.

Data presented in figure 98 represent the estimated critical angle-of-attack values required to overturn a Piper PA-18 or Cessna 172 as a function of rotorwash peak velocity. This chart can easily be modified to represent other light aircraft configurations using the defined equations. In using this chart to analyze overturning potential for the SM class helicopter, the data presented in figure 136 are all that are required. If the geometric angle-of-attack of the Piper PA-18 is assumed to be approximately 12+ degrees, the critical rotorwash velocity that should be avoided is approximately 35 knots (from figure 98). This value is exceeded for the SM class with a 9-knot worst azimuth wind at distances less than approximately 140 feet from the rotor center (figure 136). Analysis to any greater level of detail than has been described requires significantly more information about both the aircraft and the specific scenario involved. Therefore, the guideline resulting from this example would be that SM class rotorcraft should be separated from light fixed-wing aircraft at all times by at least 140 to 150 feet.

7.6 ENTRAINED OBJECTS AND DEBRIS

The type of mishap that often concerns many people when they think of rotorwash is one in which a stationary object suddenly becomes a dangerous flying projectile. This type of mishap is unexpected and people are usually unprotected from its consequences. Section 5.7 contains a long list of the many types of mishaps that have been encountered that involve flying objects and debris. Avoidance of many of these types of objects must simply be based upon experience, and the reader should review the historical data in section 5.7.1 in detail.

The number of "How To" examples that could be presented for this type of mishap are endless. Also, due to the nature of the dynamics of many types of projectiles, the analysis methodology varies depending on object type and scenario. "How To" examples for several different objects using an energy-based analysis methodology are presented in section 5.7.2. The reader is referred to these examples using the S, M, and H classes of rotorcraft. A guideline separation distance derived from work in this section is that all people and objects should be kept clear of passing rotorcraft by at least 3.0 to 3.5 times the effective jet diameter of the rotor. For a helicopter or tiltrotor, the

effective jet diameter is 0.707 times the rotor diameter. If applied to SM class rotorcraft in this example, all potential loose (or flying) objects should be kept at a minimum distance of 99 feet from the flight path of the SM class rotorcraft. This guideline does not insure that some of these large objects may not slide or roll across a smooth surface, only that most of the objects will not be airborne beyond this distance. Small objects such as sand particles are not included in this category and are covered in the next section.

Mishaps involving larger objects, such as empty oil drums, are more easily handled by traditional analysis methods. A "How To" example involving real world mishap data is presented in section 5.7.5 to predict the hazard potential for this specific object. The analysis predicts that a rotorwash peak velocity of 43 to 47 knots is sufficient to overturn an empty oil drum and produce a hazardous operational scenario. The SM class helicopter presented in this vertiport design scenario yields a peak rotorwash velocity exceeding this velocity threshold at distances less than 100 feet from the rotor center (refer to figure 140). It is interesting to note that this distance is quite close to the guideline separation distance mentioned in the previous paragraph.

The most important conclusion that the vertiport designer should gain from this section (and the historical background in section 5.7.1) is that the only safe object is:

1. an object that is securely tied down, or
2. a loose object that is removed from the vertiport environment.

Therefore, the most cost-effective solution becomes one in which unprotected and inexperienced people (with respect to the rotorwash environment) are kept clear of rotorcraft by security fences or protective walls that deflect rotorwash and objects blown across the ground.

7.7 PARTICULATE CLOUDS

Particulate cloud hazards (i.e., dust, sand, water spray, and snow clouds) are usually associated with rotorcraft operations from unimproved sites and have historically been of serious concern to the military services. Many cases are documented in the literature where a pilot has lost visual reference with the ground and crashed due to self-generated dust (brown out) or snow (white out) clouds. In commercial heliport and vertiport operations, this type of hazard is usually minimized because concrete and asphalt surfaces are generally used for takeoff and landing. However, a methodology has been developed to estimate the size of these clouds as a function of particle type

(estimates of visibility in these clouds are also available from references listed in section 5.8).

In this "How To" example, an investigation will be conducted to estimate the size of water spray clouds that might be generated by rotorcraft hovering over the water next to the vertiport (figure 126). It is assumed that the vertiport operators are concerned that the water spray clouds might be large enough to somehow effect long term operation and maintenance of the facility. The K_T factor associated with water that is used in the analysis methodology (see section 5.8.1) is 1.0 and is charted in figure 121 in comparison to other types of particles.

Calculations of the size of water spray clouds generated by the HT, H, and SM classes of rotorcraft are made using the particulate cloud option in the ROTWASH program. Input data parameters for these rotorcraft are entered into the program as discussed in section 7.1 for the velocity profile examples (using the input user's guide instructions provided in appendix D). The only other ROTWASH data entry is the K_T value on the "Cloud Option" menu. The K_T value of 1.0 for water is entered at this location (fine sand or snow would be 0.3 to 0.8).

ROTWASH output defining the estimated size of water spray clouds for each rotorcraft size class is tabulated in table 24. The reader is also referred to figures 120 and 124 for definitions of cloud dimensions and a visual reference of cloud shape characteristics. The estimated radial cloud dimension (R_C) varies from 82.5 to 209.9 feet for the SM and H helicopter classes, respectively. Estimated cloud height (H_C) varies from 38.7 to 98.6 feet for the same configurations. It should be noted that spray cloud dimensions along the interaction plane are larger for the HT class tiltrotor than they are out the non-interaction plane axis. Based on these results, one would expect that spray clouds for the SM class would not be a problem except to people or boaters on the beach next to the vertiport. However, spray clouds generated by the HT and H class vehicles may be large enough to be a nuisance, since with a slight wind the spray may cause the structure to be frequently coated with a thin film of water.

7.8 GROUND VORTEX STRENGTH

A ground vortex can be produced by a single rotor helicopter only over a narrow range of altitude, airspeed, and ambient wind conditions. Figure 25 provides a sketch of the typical characteristics associated with the formation of this flow field structure. The ROTWASH mathematical models that are available for estimation of ground vortex characteristics are still considered simplistic in nature. Therefore, as stated in section 2.2, these models should be used with caution. Only very limited experimental/flight test data exist for validation of the mathematical models.

TABLE 24 WATER SPRAY CLOUD SIZES GENERATED
BY HT, H, AND SM CLASS ROTORCRAFT¹

VEHICLE CLASS	R _C , FEET	R _V , FEET	Z _V , FEET	H _C , FEET	QSMAX ² , (IN psf)
SM (SR ³)	82.5	64.8	27.2	38.7	8.3
H (SR)	209.9	164.8	69.1	98.6	15.9
HT (SR ₄)	114.0	89.5	37.5	53.5	19.0
HT (IPLANE ⁵)	160.9	126.3	52.9	75.5	19.0

NOTES: 1. See figure 120 for dimensional definitions.
 2. See equation 77.
 3. SR - Single rotor.
 4. SR - Single rotor of a two rotor vehicle along the non-interaction plane).
 5. IPLANE - Interaction plane.

In this "How To" example, it is assumed that vertiport designers have a desire to define ground vortex velocities associated with the H class helicopter at a rotor height to rotor diameter ratio of 0.28 (a rotor height above the vertiport surface of 22 feet). Test data from figure 28 indicate that the worst case ground vortex strength should occur for a forward airspeed or crosswind condition of approximately 19 knots (if the aircraft is hovering in a fixed position above the vertiport surface) or at an advance ratio of approximately 0.043 in forward flight.

Ground vortex characteristics are computed using the ground vortex option in the ROTWASH program as described in the user's guide. H class helicopter design data are entered along with the following additional parameters:

ROTOR TIP SPEED	733.0 FT/SEC
NUMBER OF ROTOR BLADES	7.0
TRANSLATIONAL SPEED	19.0 KNOTS

It is important to note that the program requires that the wind speed be entered as a translational velocity of 19 knots even though our design example states that the helicopter is fixed with respect to ground position and a crosswind exists. The computer program always assumes wind velocity is zero and the helicopter is always slowly moving forward.

Ground vortex position calculations from the ROTWASH program are presented in figure 142. These results indicate that ground vortex position stabilizes at a location 63.8 feet in front of the helicopter at a height of 6.5 feet above ground level. It is important to note that the user must enter the strength ratio (Γ_g/Γ_{tip}) as part of the calculation process from figure 28 before the position is calculated. Details on this task are presented in both section 2.2 and the appendix D user's guide. Since the model does not calculate a core size, the user must be careful not to assume that rotorwash velocities calculated in the center of the ground vortex are real. A rough assumption made in this example is that the core radius is 7.5 percent of the rotor radius in size. Therefore, calculated velocities within a radius of 3 feet of the core position of the vortex can be assumed to be excessive. Figure 143 provides a tabular summary of the calculated x-, y-, and z-axis velocities from 0 to 8 feet at a position 3 feet in front of the vortex. Peak velocities in this summary are approximately 40 to 50 knots at a height of 3 to 7 feet above the ground plane. While these velocities are certainly significant, they are not the same magnitude as those generated by the wall jet for the same class of helicopter in a hover with less than 9-knot crosswinds. Therefore, for design purposes the ground vortex does not appear to be the type of flow field that generates upper limit design velocities.

7.9 WAKE VORTEX STRENGTH

The effect of trailing wake vortices on fixed-wing aircraft and helicopters that follow too closely behind a medium to large size helicopter can be significant. Section 2.3 provides an analysis methodology for quantifying the strength of helicopter trailing vortices, and figures 30 and 100 provide visual descriptions of the problem that must be solved. Section 3.6 presents correlation of five different types of helicopters (UH-1H, S-76, UH-60, CH-54, and CH-53E) with available flight test data in figures 61 through 65.

Several "How To" examples using the correlation data presented in section 3.6 are provided in the context of definition of suggested separation distances (discussed in detail in section 5.4). These data for the UH-1H, S-76, UH-60, and CH-53E make it possible to interpret suggested separation criteria for other types/classes of rotorcraft directly from table 15 and figure 105. Details on the velocities in the trailing wake can be obtained using the ROTWASH program. However, these results must be used with caution because no vortex decay model is presently included in the ROTWASH program. This means that all calculated field velocities are based on initial vortex strength. This can lead to overprediction of hazard potential if the program user is not thoroughly familiar with the mathematical model.

GROUND/DISK VORTEX INPUT DATA MENU
(FOR SINGLE MAIN ROTOR HELICOPTERS ONLY)

CODE	PARAMETER	VALUE	UNITS
A	ROTOR TIP SPEED	733.00	FPS
B	NUMBER OF ROTOR BLADES	7.00	--ND--
C	TRANSLATIONAL SPEED	19.00	KTS
D	XT POSITION	-66.80	FT
E	YT POSITION	.00	FT
F	ZT CALCULATION INCREMENT	1.00	FT
G	MAXIMUM CALCULATION HEIGHT	10.00	FT

ENTER DATA ENTRY CODE OR <RETURN> TO CONTINUE ==>

ROTOR HEIGHT ABOVE GROUND H/D	.2750
ADVANCE RATIO MU-STAR	.5644
ADVANCE RATIO MU	.0437

ENTER GROUND VORTEX STRENGTH RATIO
(SEE FIGURE D.20) ==> 5.0

GROUND VORTEX CORE POSITION

X-LOCATION (XXGV)	=	-63.80	FT
Y-LOCATION (ZZGV)	=	6.51	FT

GROUND VORTEX CIRCULATION = 1579.62 FT**2/SEC

PRESS <RETURN> TO CONTINUE

FIGURE 142 GROUND VORTEX POSITION CALCULATIONS

HEIGHT (FT)	MEAN VELOCITY			MEAN Q (PSF)
	(FPS)	(KN)		
.00	X -62.728	-37.183	4.676	
	Y .000	.000	.000	
	Z .000	.000	.000	
	T 62.728	37.183	4.676	
1.00	X -63.086	-37.395	4.730	
	Y .000	.000	.000	
	Z 7.543	4.472	.068	
	T 63.536	37.662	4.797	
2.00	X -63.950	-37.908	4.860	
	Y .000	.000	.000	
	Z 16.272	9.646	.315	
	T 65.988	39.116	5.175	
3.00	X -64.470	-38.216	4.940	
	Y .000	.000	.000	
	Z 27.541	16.326	.901	
	T 70.107	41.557	5.841	
4.00	X -62.407	-36.993	4.629	
	Y .000	.000	.000	
	Z 42.659	25.287	2.163	
	T 75.594	44.810	6.791	
5.00	X -53.151	-31.506	3.357	
	Y .000	.000	.000	
	Z 61.143	36.244	4.443	
	T 81.016	48.023	7.800	
6.00	X -31.877	-18.896	1.208	
	Y .000	.000	.000	
	Z 76.427	45.304	6.942	
	T 82.808	49.086	8.149	
7.00	X -3.420	-2.027	.014	
	Y .000	.000	.000	
	Z 77.121	45.715	7.068	
	T 77.196	45.760	7.082	
8.00	X 17.731	10.510	.374	
	Y .000	.000	.000	
	Z 63.116	37.413	4.734	
	T 65.559	38.861	5.108	

TYPE <C>CONTINUE, NEXT <P>POINT, <N>EW CASE, E<X>IT ==>

FIGURE 143 GROUND VORTEX VELOCITY FIELD CHARACTERISTICS

8.0 CONCLUSIONS AND RECOMMENDATIONS

A complete, in-depth analysis and review of rotorwash-related mishaps that occur in typical operational scenarios has been presented in this report. Several other key accomplishments have also been completed.

1. The known state of the art in rotorwash analysis methodologies through mid 1993 has been reviewed and documented. An extensive reference list on the subject of rotorwash has also been created.
2. The ROTWASH analysis program (as version 2.1) has been updated to account for improvements in prediction methodologies since version 2.0 was released (reference 4).
3. All known quality rotorwash-related flight test data available for analysis purposes have been reviewed, correlated with the ROTWASH model, and documented for future reference purposes. Also, data available from recent rotorwash sensor tests involving the ion-beam deflection anemometer and a more traditional mechanical anemometer have been reviewed and referenced.
4. A handbook of analysis examples has been created for the use of heliport and vertiport designers as well as other technical specialists interested in rotorwash-related issues.
5. The 30- to 40-knot velocity threshold hypothesis that was first discussed in reference 3 appears to be further validated by recent research work. This hypothesis simply states that the majority of rotorwash-related mishaps can be avoided if separation distances are maintained so that impacting rotorwash-generated velocities do not exceed 30 to 40 knots across the ground.

As with any field of research, there are areas where further work needs to be accomplished. This work will help to clarify unknowns in the present analysis state-of-the-art, reduce the need for large safety factors caused by unknown factors, and help improve safety for the rotorcraft industry and the flying public. Clearly, all guidelines or any future regulatory action on rotorcraft operations due to rotorwash-related safety issues must be crafted to enhance safety while considering economic impacts upon rotorcraft operators.

Recommendations for future research to meet these goals are listed below:

1. Additional rotorwash characteristics data need to be obtained through experimental means. These data have been detailed in the FAA test plans (references 74 through 76). These experiments are designed to enhance the database so that the effects of ambient wind, rotorcraft maneuvers near the ground, and rotor disk loading on rotorwash flow fields can be predicted more accurately.
2. Additional mishap data need to be obtained through experimental means. These data have also been detailed in FAA test plans (references 74 through 76). These experiments are designed to enhance the mishap database so that the effects of rotorwash on structures can be documented for validation of wind tunnel testing methods, and the effects of rotorwash on personnel, numerous types of objects, and other types of vehicles (e.g., motorcycles and light fixed-wing aircraft) can be documented for correlation with developed analytical methods.

As long as these test plans remain uncompleted, questions will continue to exist with respect to the definition of worst case scenarios in all rotorwash safety analyses.

LIST OF REFERENCES

1. Ferguson, S.W., and J.D. Kocurek, "Analysis and Recommendation of Separation Requirements for Rotorcraft Operation at Heliports and Airports," Systems Technology, Inc., STI Report TR-1224-1, September 1986.
2. Ferguson, S.W., "Evaluation of Rotorwash Characteristics for Tiltrotor and Tiltwing Aircraft in Hovering Flight," Federal Aviation Administration, Washington DC, Technical Report DOT/FAA/RD-90/16, December 1990.
3. Ferguson, S.W., "Analysis of Rotorwash Effects in Helicopter Mishaps," Federal Aviation Administration, Washington DC, Technical Report DOT/FAA/RD-90/17, May 1991.
4. Ferguson, S.W., and J.D. Kocurek, "Rotorwash Computer Model - User's Guide," Federal Aviation Administration, Washington DC, Technical Report DOT/FAA/RD-90/25, November 1991.
5. Meyerhoff, C. and D. Gorge, "Navy Developmental Test (DT-IIA) of the V-22 Aircraft - Contributory Rotor Downwash Report," Naval Air Test Center, ACS-CR-90-04, SY71A, Summer 1990.
6. Weiss, R.M.; J.G. Morrow; D. Gallagher; M. DiMeo; and S. Erlichman, "Analysis of Heliport Environmental Data: Indianapolis Downtown Heliport, Wall Street Heliport, Volume I Summary," Federal Aviation Administration, Technical Center, Atlantic City, NJ, Technical Report DOT/FAA/CT-TN87/54-I, October 1988.
7. Weiss, R.M.; J.G. Morrow; D. Gallagher; M. DiMeo; and S. Erlichman, "Analysis of Heliport Environmental Data: Indianapolis Downtown Heliport, Wall Street Heliport, Volume II Wall Street Heliport Data Plots," Federal Aviation Administration, Technical Center, Atlantic City, NJ, Technical Report DOT/FAA/CT-TN87/54-II, May 1989.
8. Weiss, R.M.; J.G. Morrow; D. Gallagher; M. DiMeo; and S. Erlichman, "Analysis of Heliport Environmental Data: Indianapolis Downtown Heliport, Wall Street Heliport, Volume III Indianapolis Downtown Heliport Data Plots," Federal Aviation Administration, Technical Center, Atlantic City, NJ, Technical Report DOT/FAA/CT-TN87/54-III, October 1989.
9. Weiss, R.M., "Analysis of Heliport Environmental Data; Intracoastal City," Federal Aviation Administration, Technical Center, Atlantic City, NJ, Technical Report DOT/FAA/CT-TN89/43, July 1990.

10. Tymczyszyn, J.J.; K.J. Biehl; and S.A. Teager, "Flight Test Investigation of the Wake Vortices Generated By Helicopters," Proceedings of the Aircraft Wake Vortices Conference - Volume 1 of 2, Washington DC, October 29-31, 1991, DOT/FAA/SD-92/1.1, June 1992.
11. Meyerhoff, C.; R.E. Lake; and D.N. Gordge, "Rotorwash Wind Sensor Evaluation," Technical Report DOT/FAA/RD-93/10, Federal Aviation Administration, Washington DC, August 1993.
12. Peterka, J.A., "Wind Tunnel Tests: Dallas Convention Center Expansion," Cermak Peterka Peterson, Inc., Fort Collins, CO, CPP Project 90-0666, June 1991.
13. Stanzione, K.A. and L.L. Oliver, "Downwash Design Criteria for VTOL Aircraft," Prepared by Praxis Technologies Corporation for the National Aeronautics and Space Administration, Contract NAS2-13395, January 1993.
14. Velkoff, H.R., "A Comparative Study of Downwash - Outflow Effects of Various VTOL Configurations as a Factor in the Design Selection Process," Advanced Systems Research and Analysis Office, U.S. Army Aviation and Troop Command, January 1993.
15. Anon., "Heliport Design," U. S. Department of Transportation, Federal Aviation Administration, Washington DC, Advisory Circular 150/5390-2, January 4, 1988.
16. Glauert, M.B., "The Wall Jet," Journal of Fluid Mechanics, Vol. 1, Part 6, December 1956, pp. 625-643.
17. Hohler, D.J., "An Analytical Method of Determining General Downwash Flow Field Parameters for V/STOL Aircraft," AFAPL-TR-66-90, November 1966.
18. Migdal, D.; W.G. Hill, Jr.; R.C. Jenkins; and M.J. Siclari, "VTOL in Ground Effect Flows for Closely Spaced Jets," NASA CR 152321, December 1979.
19. Ludwig, G.R. and W.G. Brady, "Theoretical and Experimental Studies of Impinging Uniform and Nonuniform Jets," TRECOM Technical Report 64-42, U. S. Army Transportation Research Command, Fort Eustis, VA, August 1964.
20. Watts, A., "V/STOL Downwash Impingement Study - Velocity Estimate," Canadair Aerodynamic Memorandum MAA-284-001, January 1969, Revised April 1971.

21. George, M.M., "Downwash Impingement Design Criteria for VTOL Aircraft," TRECOM Technical Report 64-48, U.S. Army Transportation Research Command, Fort Eustis, VA, August 1964.
22. George, M.; E. Kisielowski; and D.S. Douglas, "Investigation of the Downwash Environment Generated by V/STOL Aircraft Operating in Ground Effect," USAAVLABS Technical Report 68-52, July 1968.
23. Harris, D.J., and R.D. Simpson, "Technical Evaluation of the Rotor Downwash Flow Field of the XV-15 Tilt Rotor Research Aircraft," Naval Air Test Center Technical Report No. SY-14R-83, July 1983.
24. Harris, D.J., and R.D. Simpson, "CH-53E Helicopter Downwash Evaluation," Naval Air Test Center Technical Report No. SY-89R-78, August 1, 1978.
25. George, M.; J. Tang; S. Mills; and D. Douglas, "Downwash Environment for the Boeing Model 160 V/STOL Aircraft," Dynasciences Corporation Report DCR-268, January 1968.
26. Kuhn, R.E., "Height of Spray Produced By Vertical Takeoff and Landing (VTOL) Aircraft," David W. Taylor Naval Ship Research and Development Center Report DTNSRDC/ASED-79/04, April 1979.
27. Fradenburgh, E.A., "Flow Field Measurements for a Hovering Rotor Near the Ground," Fifth Annual Western Forum of the American Helicopter Society, Los Angeles, CA, September 1958.
28. Newsom, W.A., and L.P. Tosti, "Slipstream Flow Around Several Tilt-Wing VTOL Aircraft Models Operating Near Ground," NASA TN D-1382.
29. Harris, D.J., and R.D. Simpson, "Downwash Evaluation Under the U.S. Army Heavy Lift Helicopter Rotor. Final Report," Naval Air Test Center Technical Report No. SY-17R-76, March 16, 1976.
30. Morse, A., and H. Newhouse, "VTOL Downwash Impingement Study Surface Erosion Tests," U.S. Army Transportation Research Command, TREC TR 60-67, Ft. Eustis, VA, October 1960.
31. Anon., "A Comparison of Downwash and Outflow From a Tilt-Wing Aircraft and a Helicopter," Canadair Report RAG-084-107, February 1971.

32. Michaelsen, O.E., "A Comparison of Outflows From a Helicopter, Tilt Wing, and Jet Lift Hovering Aircraft," AIAA 8th Annual Meeting and Technical Display, Washington DC, AIAA Paper No. 71-992, October 25, 1971.
33. Curtiss, H.C., Jr.; Mao Sun; and E.J. Hanker, Jr., "Dynamic Phenomena in Ground Effect," AHS Paper No. A-83-39-76-0000, Presented at the 39th Forum of the American Helicopter Society, May 9-11, 1983.
34. Curtiss, H.C., Jr.; W. Erdman, and M. Sun, "Ground Effect Aerodynamics," Presented at the International Conference on Rotorcraft Basic Research, Research Triangle Park NC, February 19-21, 1985.
35. Sun, M., "A Study of Helicopter Rotor Aerodynamics in Ground Effect," Ph.D. Thesis, Princeton Mechanical and Aerodynamics Engineering Department, June 1983.
36. Cimbala, J.M.; D.R. Stinebring; A.L. Treaster; M.L. Billet; and M. M. Walters, "Experimental Investigation of a Jet Impinging on a Ground Plane in the Presence of a Cross Flow," Journal of Aircraft, Vol. 25, No. 10, October 1988, pp. 923-931.
37. Cimbala, J.M.; M.L. Billet; D.P. Gaublomme; and J.C. Oefelein, "Experiments on the Unsteadiness Associated With a Ground Vortex," Journal of Aircraft, Vol. 28, No. 4, April 1991, pp. 261-267.
38. Prouty, R.W., Helicopter Performance, Stability, and Control, Robert E. Krieger Publishing Company, Malabar, FL, 1990.
39. Gessow, A., and G.C. Myers, Aerodynamics of the Helicopter, Frederick Ungar Publishing Company, New York, NY, 1952.
40. Harris, D.J., and R.D. Simpson, "Tilt-Wing Vertical and Short Takeoff and Landing Downwash Evaluation," Naval Air Test Center Technical Report No. SY-52R-76, April 9, 1976.
41. Patton, W.G., and R.D. Simpson, "Investigation of SH- 3/HH-3 Helicopter Downwash Environment," Naval Air Test Center Report ST-197R-71, September 24, 1971.
42. Leese, G.W., and J.T. Knight, Jr., "Helicopter Downwash Data," Miscellaneous Paper S-74-17, U.S. Army Engineer Waterways Experiment Station, Vicksburg, Mississippi, June 1974.
43. O'Bryan, T.C., "An Investigation of the Effect of Downwash from a VTOL Aircraft and a Helicopter in the Ground Environment," NASA TN D-977, October 1961.

44. Shane, W.P., "Effects of Downwash Upon Man," U.S. Army Aeromedical Research Unit Report No. 68-3, November 1967.
45. Leese, G.W., "Helicopter Downwash Blast Effects Study," U.S. Army Engineer Waterways Experiment Station TR-3-664, Vicksburg, Mississippi, October 1964.
46. Burnham, D.C., and S.A. Teager, "Preliminary Measurements of Helicopter Wake-Vortex Velocity Profiles," DOT-TSC-FA527-PM-85-7, March 1985.
47. Ferguson, S.W., "Evaluation of Rotorwash Characteristics for the Bell/Boeing V-22, Bell 214ST, and Sikorsky S-76B," Prepared for JPJ Architects, Inc. and the City of Dallas Aviation Department, EMA Technical Report TR-91-1-1, February 1991.
48. Bennett, R., "Heliport Design for San Bernardino County Relocation Medical Center, Colton, CA," Prepared by Heliport Consultants, Westlake Village, CA, 1991.
49. Hoerner, Dr. S.F., Fluid Dynamic Drag, Published by Author, 1958.
50. Anon., Anthropometry of U.S. Military Personnel, Military Handbook DOD-HDBK-743, October 3, 1980.
51. Anon., Operators Manual. Army OH-58C Helicopter, Headquarters, Department of the Army, Technical Manual TM 55-1520-235-10, April 7, 1978.
52. Anon., Operators Manual. Army Models. UH-1D/H and EH-1H Helicopters, Headquarters, Department of the Army, Technical Manual TM 55-1520-210-10, May 18, 1979.
53. Anon., Operators Manual. Army AH-1S (Prod) Helicopter, Headquarters, Department of the Army, Technical Manual TM 55-1520-236-10, April 29, 1977.
54. Anon., Operators Manual. Army Model CH-47C Helicopter, Headquarters, Department of the Army, Technical Manual TM 55-1520-227-10-2, August 23, 1978.
55. Traasdahl, E.C., and S.A. Ruffa, "CH-46E/LHA Engage/Disengage Dynamic Interface Test," Naval Air Test Center Technical Report No. RW-58R-84, January 30, 1985.
56. Hurley, G.E.; C.W. Pitman; and L.L. Trick, "HH-46A/CV-64 Rotor Engage/Disengage Test," Naval Air Test Center Technical Report No. RW-55R-84, October 30, 1984.

57. Turner, R.E., and C.K. Hill, "Terrestrial Environment (Climatic) Criteria Guidelines for Use in Aerospace Vehicle Development," NASA Technical Memorandum 82473, June 1982.
58. Baldwin, J.L., "Climatic Atlas of the United States," Prepared by the Environmental Sciences Services Administration, U.S. Department of Commerce, June 1968.
59. Mantay, W.R.; G.T. Holbrook; R.L. Campbell; and R.L. Tomaine, "Helicopter Response to an Airplane's Trailing Vortex," Journal of Aircraft, Vol. 14, No. 4, April 1977, pp. 357-363.
60. Dunham, R.E.; G.T. Holbrook; W.R. Mantay; R.L. Campbell; and R.W. VanGunst, "Flight Test Experience of a Helicopter Encountering an Airplane Trailing Vortex," Presented at the 32nd Forum of the American Helicopter Society, Preprint 1063, May 1976.
61. Curtiss, H.C. and Z. Zhou, "The Response of Helicopters to Fixed Wing Aircraft Wake Encounters," Proceedings of Aircraft Wake Vortices Conference - Volume 1 of 2, Washington, D.C., October 29-31, 1991, DOT/FAA/SD-92/1.1, June 1992.
62. Schwartz, C.W.; M.W. Witczak; and R.B. Leahy, "Structural Design Guidelines for Heliports," Federal Aviation Administration, Washington D.C., Technical Report DOT/FAA/PM-84/23, October 1984.
63. Jenkins, B.Z., and A.S. Marks, "Rotor Downwash Velocities About the UH-1H Helicopter - Flight Test Measurements and Theoretical Calculations," Army Missile Research Development and Engineering Laboratory, Redstone Arsenal, Alabama, January 1975.
64. Leese, G.W., "UH-1H Downwash Velocity Measurements," Army Engineer Waterways Experiment Station, Vicksburg, Mississippi, August 1972.
65. Skujins, O., "An Experimental Investigation of Rotor Forces and Flow Field in the Vicinity of a Step Ground Plane," West Virginia University, Department of Aerospace Engineering, July 1970.
66. Basham, C. and Willis C., "A Summary Report: The Dallas Vertiport," Charles Willis & Associates, Inc., Arlington, TX, February 11, 1991.
67. O'Bryan, T.C., "An Experimental Study of the Effect of Downwash from a Twin Propeller VTOL Aircraft on Several Types of Ground Surfaces," NASA TN D-1239, May 1962.

68. Rogers, S.J., "Evaluation of the Dust Cloud Generated by Helicopter Rotor Downwash," USAAVLABS TR-67-81, March 1968.
69. Ebersole, J.F., "Obscuration by Helicopter-Produced Snow Clouds," Optical Engineering, Vol. 22, No. 1, January/February 1983.
70. Dyke, R.W., "An Investigation of the Over the Water Aspects of VTOL Airplanes at High Disk Loading," Curtis-Wright Corporation, VTOL Systems Group, Report No. 012-26, December 1963.
71. Schroers, L.G., Unpublished Data Obtained from the XV-15 Project Office, NASA Ames Research Center, 1985.
72. Marsh, K.R., "Research on VTOL Water Hover Effects, Including the Effects of Wind and Waves," LTV Aerospace Corporation, Report No. 2-55400/8R-6140, April 1968.
73. Mullins, Dr. B. Robert, et. al., "Southwest Region Vertiport Feasibility Study," University of Texas at Arlington, Report No. AE-91-02, July 1991.
74. Bolz, E.B., Ferguson, S.W., "Rotorwash Wind Effects Flight Test Plan," Federal Aviation Administration, Washington D.C., Technical Report FAA/RD-92/1-LR, September 1992.
75. Bolz, E.B., Ferguson, S.W., "Acceptable Rotorwash Personnel Thresholds Flight Test Plan," Federal Aviation Administration, Washington D.C., Technical Report FAA/RD-92/2-LR, September 1992.
76. Bolz, E.B., Ferguson, S.W., "S-76 Rotorwash Flight Test Plan," Federal Aviation Administration, Washington D.C., Technical Report FAA/RD-92/3-LR, September 1992.
77. Bolz, E.B., Ferguson, S.W., "XV-15 Rotorwash Flight Test Plan," Federal Aviation Administration, Washington D.C., Technical Report FAA/RD-92/4-LR, September 1992.
78. Meyerhoff, C.L.; Lake, Robert; and Peters, Lt. Dean, "H-60 Helicopter Rotor Downwash Wind Velocity Evaluation," Naval Air Warfare Center Report SY-3R-94, Patuxent River, MD, February 1994.

LIST OF ACRONYMS

AHS	American Helicopter Society
AFCS	automatic flight control system
AGL	above ground level
CPP	Certmak Peterka Peterson, Inc.
DAIP	distance along the interaction plane
DEG	degrees
DFAC	distance from aircraft center
DFRC	distance from the rotor center
dia	diameter
DL	disk loading
FAA	Federal Aviation Administration
FOD	foreign object damage
GW	gross weight
H	rotorcraft size class (see table 22)
HAGL	height above ground level
H/D	constant rotor height above ground divided by rotor diameter
HT	rotorcraft size class (see table 22)
IFR	instrument flight rules
IP	interaction plane
IPLANE	interaction plane
KT	knots
kts	knots
M	rotorcraft size class (see table 22)
MH	rotorcraft size class (see table 22)
MT	rotorcraft size class (see table 22)
ND	non-dimensional
NI	non-interaction plane
NTIS	National Technical Information Service
NTSB	National Transportation Safety Board
psf	pounds per square foot
R	radius
RHAGL	rotor height above ground level
RV	recreational vehicle
S	rotorcraft size class (see table 22)
SCT	Systems Control Technology, Inc.
SM	rotorcraft size class (see table 22)
SR	single-rotor
SRDL	single-rotor disk loading
TRDL	twin-rotor disk loading
Vmn	mean velocity
Vpk	peak velocity
V/STOL	vertical/short takeoff and landing
VTOL	vertical takeoff and landing
WHAGL	Wheel Height Above Ground Level